THE IMMUNOMODULATORY PROPERTIES OF EXTRACELLULAR VESICLES FROM PATHOGENS, IMMUNE CELLS AND NON-IMMUNE CELLS

EDITED BY: Ivan K. H. Poon, Christopher D. Gregory and Maria Kaparakis-Liaskos

PUBLISHED IN: Frontiers in Immunology

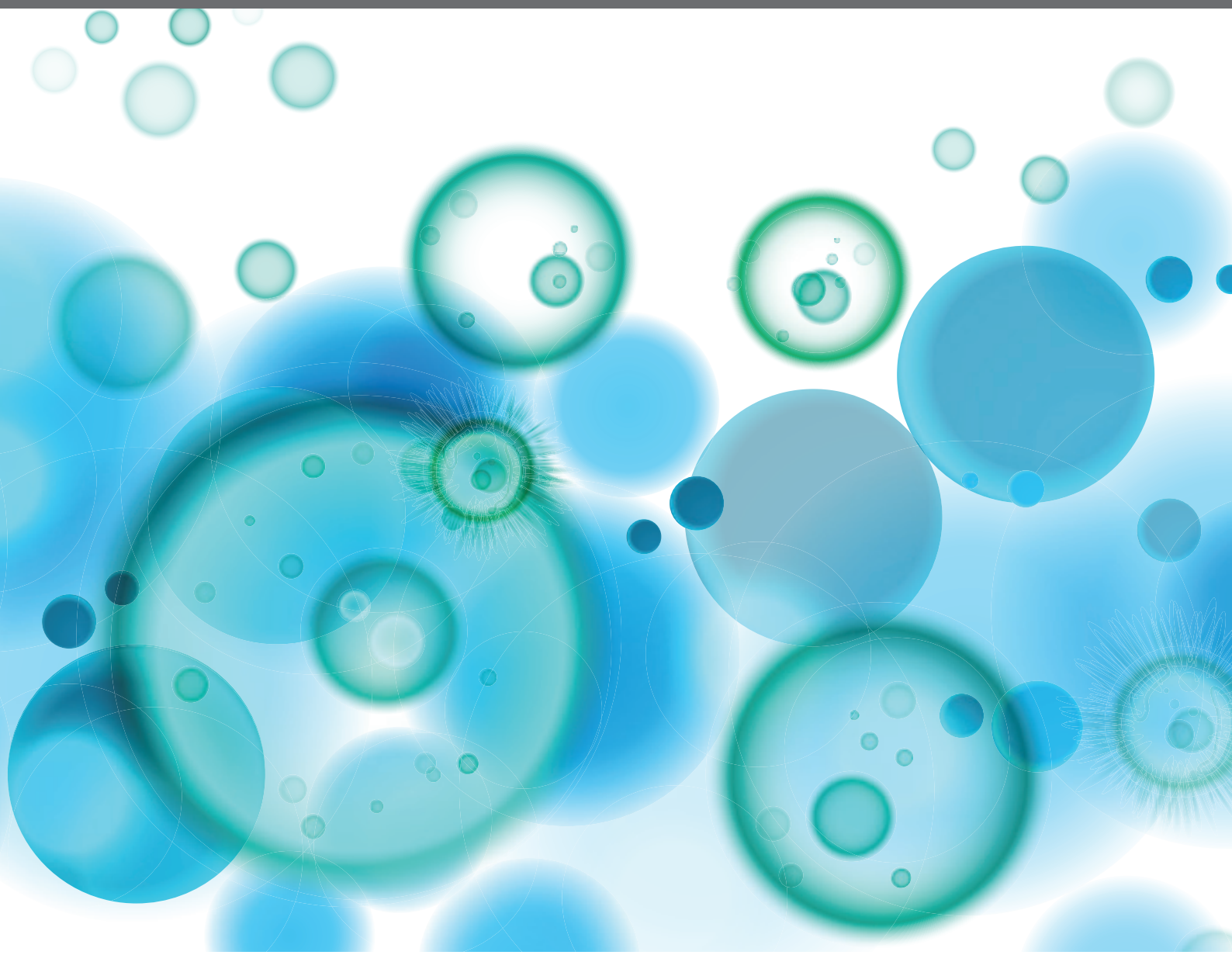

frontiers Research Topics

ISSN 1664-8714
ISBN 978-2-88945-754-0
DOI 10.3389/978-2-88945-754-0

About Frontiers

Frontiers is more than just an open-access publisher of scholarly articles: it is a pioneering approach to the world of academia, radically improving the way scholarly research is managed. The grand vision of Frontiers is a world where all people have an equal opportunity to seek, share and generate knowledge. Frontiers provides immediate and permanent online open access to all its publications, but this alone is not enough to realize our grand goals.

Frontiers Journal Series

The Frontiers Journal Series is a multi-tier and interdisciplinary set of open-access, online journals, promising a paradigm shift from the current review, selection and dissemination processes in academic publishing. All Frontiers journals are driven by researchers for researchers; therefore, they constitute a service to the scholarly community. At the same time, the Frontiers Journal Series operates on a revolutionary invention, the tiered publishing system, initially addressing specific communities of scholars, and gradually climbing up to broader public understanding, thus serving the interests of the lay society, too.

Dedication to Quality

Each Frontiers article is a landmark of the highest quality, thanks to genuinely collaborative interactions between authors and review editors, who include some of the world's best academicians. Research must be certified by peers before entering a stream of knowledge that may eventually reach the public - and shape society; therefore, Frontiers only applies the most rigorous and unbiased reviews.
Frontiers revolutionizes research publishing by freely delivering the most outstanding research, evaluated with no bias from both the academic and social point of view. By applying the most advanced information technologies, Frontiers is catapulting scholarly publishing into a new generation.

What are Frontiers Research Topics?

Frontiers Research Topics are very popular trademarks of the Frontiers Journals Series: they are collections of at least ten articles, all centered on a particular subject. With their unique mix of varied contributions from Original Research to Review Articles, Frontiers Research Topics unify the most influential researchers, the latest key findings and historical advances in a hot research area! Find out more on how to host your own Frontiers Research Topic or contribute to one as an author by contacting the Frontiers Editorial Office: researchtopics@frontiersin.org

THE IMMUNOMODULATORY PROPERTIES OF EXTRACELLULAR VESICLES FROM PATHOGENS, IMMUNE CELLS AND NON-IMMUNE CELLS

Topic Editors:
Ivan K. H. Poon, La Trobe University, Australia
Christopher D. Gregory, The University of Edinburgh, United Kingdom
Maria Kaparakis-Liaskos, La Trobe University, Australia

Citation: Poon, I. K. H., Gregory, C. D., Kaparakis-Liaskos, M., eds. (2019). The Immunomodulatory Properties of Extracellular Vesicles from Pathogens, Immune Cells and Non-Immune Cells. Lausanne: Frontiers Media. doi: 10.3389/978-2-88945-754-0

Table of Contents

CHAPTER 3

IMMUNOREGULATORY PROPERTIES OF EVs RELEASED FROM PATHOGENS

frontiers in Immunology

EDITORIAL
published: 19 December 2018
doi: 10.3389/fimmu.2018.03024

Editorial: The Immunomodulatory Properties of Extracellular Vesicles From Pathogens, Immune Cells, and Non-immune Cells

Ivan K. H. Poon[1,2]*, *Christopher D. Gregory*[3]* and *Maria Kaparakis-Liaskos*[2,4]*

[1] Department of Biochemistry and Genetics, La Trobe Institute for Molecular Science, La Trobe University, Melbourne, VIC, Australia, [2] Research Centre for Extracellular Vesicles, School of Molecular Sciences, La Trobe University, Melbourne, VIC, Australia, [3] The Queen's Medical Research Institute, University of Edinburgh Centre for Inflammation Research, Edinburgh, United Kingdom, [4] Department of Physiology, Anatomy and Microbiology, School of Life Sciences, La Trobe University, Melbourne, VIC, Australia

Keywords: apoptotic cells, apoptotic bodies, bacterial membrane vesicles, exosomes, extracellular vesicles, immunomodulatory, microvesicles, tumor cells

Editorial on the Research Topic

The Immunomodulatory Properties of Extracellular Vesicles From Pathogens, Immune Cells, and Non-immune Cells

OPEN ACCESS

Edited and reviewed by:
Herman Waldmann,
University of Oxford, United Kingdom

***Correspondence:**
Ivan K. H. Poon
i.poon@latrobe.edu.au
Christopher D. Gregory
chris.gregory@ed.ac.uk
Maria Kaparakis-Liaskos
m.liaskos@latrobe.edu.au

Specialty section:
This article was submitted to Immunological Tolerance and Regulation, a section of the journal Frontiers in Immunology

Received: *09 November 2018*
Accepted: *06 December 2018*
Published: *19 December 2018*

Citation:
Poon IKH, Gregory CD and Kaparakis-Liaskos M (2018) Editorial: The Immunomodulatory Properties of Extracellular Vesicles From Pathogens, Immune Cells, and Non-immune Cells. Front. Immunol. 9:3024. doi: 10.3389/fimmu.2018.03024

INTRODUCTION

Intercellular communication is key for immune regulation and extracellular vesicles (EVs) are emerging as important mediators of this process. EVs like exosomes, microvesicles, and apoptotic bodies are membrane-bound vesicles that can be released by both immune and non-immune cells. Although different types of EVs vary greatly in their size (~30 nm to 5 μm in diameter) and mechanism of formation, it is now well-established that the cellular constituents in/on EVs (e.g., antigens, cytokines, membrane proteins, and microRNAs) can regulate a variety of immune responses. Besides mammalian cells, bacteria, fungi, and parasites can also release membrane vesicles to modulate host immune responses. In this research topic, a collection of primary research and review papers explored the immunoregulatory properties of EVs released from immune cells, tumor cells, apoptotic cells as well as pathogens.

IMMUNOREGULATORY PROPERTIES OF EVS RELEASED FROM GRANULOCYTES AND MACROPHAGES

EVs can be released from a variety of cell types, in particular by immune cells to regulate immune responses (1). In this research topic, small and large EVs (<220 nm and >220 nm, respectively) generated from granulocytes were described by Danesh et al. to exhibit immunostimulatory properties on monocytic cells. Interestingly, the authors also observed a positive association between the levels of $CD66b^{+}$ granulocyte-derived EVs with mortality in intensive care unit patients. In another study in this research topic, Alvarez-Jimenez et al. described the ability of EVs generated from *Mycobacterium tuberculosis*-infected neutrophils (~100–700 nm) to promote the release of proinflammatory cytokines from macrophages and removal of intracellular *M. tuberculosis* via an autophagy-dependent mechanism. Furthermore, Singhto et al. examined the role of macrophage-derived EVs (~50–80 nm) in the context of kidney stone pathogenesis. The

authors described the proteomic profile of macrophage-derived EVs following calcium oxalate monohydrate crystals (a type of crystal that is more pathogenic in kidney stone disease) treatment, and how these EVs could modulate a variety of immune cell functions *in vitro*. Collectively, these studies highlight the immunomodulatory properties of EVs generated from immune cells.

IMMUNOREGULATORY PROPERTIES OF EVS RELEASED FROM TUMOUR AND APOPTOTIC CELLS

Tumor cells can play a key role in establishing a microenvironment that favors their growth, and a variety of soluble factors released from tumor cells including VEGF and IL-10 have been shown to facilitate this process (2). Similarly, tumor cell-derived exosomes and microvesicles have also been reported to contribute to the establishment of tumor microenvironment (3, 4). In this research topic, Dörsam et al. reported the ability of EVs (∼130 nm) generated from Hodgkin lymphoma to promote recipient fibroblasts to exhibit a cancer-associated fibroblast phenotype, resulting in the release of pro-inflammatory cytokines, growth factors and pro-angiogenic factors that could facilitate a tumor supportive environment. In another research article, Dionisi et al. explored a different concept and demonstrated the ability of tumor (Burkitt's lymphoma)-derived microvesicles (3 predominant EV populations of ∼105, 175, and 285 nm) carrying tumor antigens to enhance cross-processing ability of clinical grade dendritic cells and facilitate activation of $CD8^+$ T cells. These findings suggest the potential use of tumor cell-derived microvesicles to promote the efficacy of dendritic cell-based vaccines for anti-tumor immunotherapy.

In addition to EVs released from healthy/viable tumor cells, two reviews by Gregory and Dransfield and Muhsin-Sharafaldine and McLellan discussed the recent literature on the ability EVs released from apoptotic tumor cells to modulate tumor growth and anti-tumor immunity. Firstly, Gregory and Dransfield described the heterogeneity of apoptotic cell-derived EVs in terms of size and content, as well as their mechanism of formation. The authors also discussed how EVs could facilitate intercellular communication in the tumor microenvironment and regulate tumor growth, metastasis, drug resistance, and anti-tumor immunity. However, the importance of EVs generated from apoptotic cells (ApoEVs), in particular from dying tumor cells, in modulating the tumor microenvironment remains to be fully defined. Muhsin-Sharafaldine and McLellan also discussed how ApoEVs generated from tumor cells could exhibit immunosuppressive or immunostimulatory properties depending on the experimental context. In particular, how $CD169^+$ macrophages in the lymph node could play a key role in interacting with tumor cell-derived ApoEVs and regulate anti-tumor immunity, as well as how the exposure of phosphatidylserine on tumor cell-derived ApoEVs (e.g., generated after chemo-/radio-therapy) could promote tumor growth through activation of the extrinsic coagulation cascade. It should be noted that in additional to tumor cell-derived ApoEVs, ApoEVs released from a range of untransformed cells during apoptosis could also exhibit immunoregulatory properties. Another review by Caruso & Poon discussed how ApoEVs generated from a range of cell types could modulate immune responses by regulating the efficient clearance of apoptotic cells, antigen presentation, as well as trafficking of cytokines, damage-associated molecular patterns and pathogens. Caruso and Poon also highlighted the variation in nomenclature and isolation/characterization methods used in a range of ApoEV studies.

IMMUNOREGULATORY PROPERTIES OF EVS RELEASED FROM PATHOGENS

In additional to the importance of EVs in mediating intercellular communication in higher organisms, it is also well-established that a variety of pathogens can release membrane vesicles to modulate host immunity (5), with three research articles in this research topic exploring this area of research. First, Turner et al. examined the mechanism underpinning the entry of Gram-negative bacterial derived outer membrane vesicles (OMVs) into host cells. The authors described the size of OMV being a key determining factor for OMV cargo composition and their host cell entry, with smaller OMVs (20–100 nm) and larger OMVs (90–450 nm) entering host epithelial cells via caveolin-mediated endocytosis and macropinocytosis/endocytosis, respectively. Second, Eichenberger et al. performed proteomic and RNA-seq analysis on parasite (*Nippostrongylus brasiliensis*)-derived EVs (60–160 nm), as well as demonstrated the ability of parasite-derived EVs to suppress inflammation in a murine model of colitis. Lastly, Ofir-Birin et al. described the use of imaging flow cytometry to monitor malaria parasites (*Plasmodium falciparum*)-derived EVs, their uptake into host monocytes, as well as the subsequent translocation of phosphorylated IRF3 into the nucleus in monocytes.

AFTERWORD

The field of EVs is a rapidly growing area of research, with the identification of new types of EVs, expansion on the cell types or organisms that could release EVs and their functions, as well as the development of novel approaches to study EVs. This research topic has covered a number of cutting-edge discoveries in this field. Lastly, we would like to thank all the authors for their contribution to this research topic and the referees for their prompt and in-depth reviews.

AUTHOR CONTRIBUTIONS

All authors listed have made a substantial, direct and intellectual contribution to the work, and approved it for publication.

REFERENCES

1. Robbins PD, Morelli AE. Regulation of immune responses by extracellular vesicles. *Nat Rev Immunol*. (2014) 14:195–208. doi: 10.1038/nri3622
2. Landskron G, De la Fuente M, Thuwajit P, Thuwajit C, Hermoso MA. Chronic inflammation and cytokines in the tumor microenvironment. *J Immunol Res*. (2014) 2014:149185. doi: 10.1155/2014/149185
3. Milane L, Singh A, Mattheolabakis G, Suresh M, Amiji MM. Exosome mediated communication within the tumor microenvironment. *J Control Release* (2015) 219:278–94. doi: 10.1016/j.jconrel.2015.06.029
4. D'Souza-Schorey C, Clancy JW. Tumor-derived microvesicles: shedding light on novel microenvironment modulators and prospective cancer biomarkers. *Genes Dev*. (2012) 26:1287–99. doi: 10.1101/gad.192351.112
5. Kuipers ME, Hokke CH, Smits HH, Nolte-'t Hoen ENM. Pathogen-derived extracellular vesicle-associated molecules that affect the host immune system: an overview. *Front Microbiol*. (2018) 9:2182. doi: 10.3389/fmicb.2018.02182

Conflict of Interest Statement: The authors declare that the research was conducted in the absence of any commercial or financial relationships that could be construed as a potential conflict of interest.

frontiers in Immunology

ORIGINAL RESEARCH
published: 08 May 2018
doi: 10.3389/fimmu.2018.00956

Granulocyte-Derived Extracellular Vesicles Activate Monocytes and Are Associated With Mortality in Intensive Care Unit Patients

*Ali Danesh[1,2], Heather C. Inglis[1], Mohamed Abdel-Mohsen[1,2†], Xutao Deng[1,2], Avril Adelman[3], Kenneth B. Schechtman[3,4], John W. Heitman[1], Ryan Vilardi[5], Avani Shah[1], Sheila M. Keating[1,2], Mitchell J. Cohen[5†], Evan S. Jacobs[1], Satish K. Pillai[1,2], Jacques Lacroix[6], Philip C. Spinella[7] and Philip J. Norris[1,2,8]**

[1] Blood Systems Research Institute, San Francisco, CA, United States, [2] Department of Laboratory Medicine, University of California, San Francisco, San Francisco, CA, United States, [3] Division of Biostatistics, Washington University School of Medicine in St. Louis, St. Louis, MO, United States, [4] Department of Medicine, Washington University School of Medicine in St. Louis, St. Louis, MO, United States, [5] Department of Surgery, University of California, San Francisco, San Francisco, CA, United States, [6] Centre Hospitalier Universitaire (CHU) Sainte-Justine, Université de Montréal, Montreal, QC, Canada, [7] Department of Pediatrics, Washington University School of Medicine in St. Louis, St. Louis, MO, United States, [8] Department of Medicine, University of California, San Francisco, San Francisco, CA, United States

To understand how extracellular vesicle (EV) subtypes differentially activate monocytes, a series of *in vitro* studies were performed. We found that plasma-EVs biased monocytes toward an M1 profile. Culturing monocytes with granulocyte-, monocyte-, and endothelial-EVs induced several pro-inflammatory cytokines. By contrast, platelet-EVs induced TGF-β and GM-CSF, and red blood cell (RBC)-EVs did not activate monocytes *in vitro*. The scavenger receptor CD36 was important for binding of RBC-EVs to monocytes, while blockade of CD36, CD163, CD206, TLR1, TLR2, and TLR4 did not affect binding of plasma-EVs to monocytes *in vitro*. To identify mortality risk factors, multiple soluble factors and EV subtypes were measured in patients' plasma at intensive care unit admission. Of 43 coagulation factors and cytokines measured, two were significantly associated with mortality, tissue plasminogen activator and cystatin C. Of 14 cellular markers quantified on EVs, 4 were early predictors of mortality, including the granulocyte marker CD66b. In conclusion, granulocyte-EVs have potent pro-inflammatory effects on monocytes *in vitro*. Furthermore, correlation of early granulocyte-EV levels with mortality in critically ill patients provides a potential target for intervention in management of the pro-inflammatory cascade associated with critical illness.

Keywords: extracellular vesicles, monocytes, granulocytes, exosomes, microvesicles, mortality, intensive care unit, receptor

OPEN ACCESS

Edited by:
Ivan Poon,
La Trobe University,
Australia

Reviewed by:
Amy Alexandra Baxter,
La Trobe University,
Australia
Sho Morioka,
University of Virginia,
United States

***Correspondence:**
Philip J. Norris
pnorris@bloodsystems.org

†Present address:
Mohamed Abdel-Mohsen,
The Wistar Institute,
Philadelphia, PA, United States;
Mitchell J. Cohen,
The University of Colorado,
Denver, CO, United States

Specialty section:
This article was submitted to Immunological Tolerance and Regulation, a section of the journal Frontiers in Immunology

Received: *28 December 2017*
Accepted: *17 April 2018*
Published: *08 May 2018*

Citation:
Danesh A, Inglis HC, Abdel-Mohsen M, Deng X, Adelman A, Schechtman KB, Heitman JW, Vilardi R, Shah A, Keating SM, Cohen MJ, Jacobs ES, Pillai SK, Lacroix J, Spinella PC and Norris PJ (2018) Granulocyte-Derived Extracellular Vesicles Activate Monocytes and Are Associated With Mortality in Intensive Care Unit Patients. Front. Immunol. 9:956. doi: 10.3389/fimmu.2018.00956

INTRODUCTION

Extracellular vesicles (EVs) are double membrane vesicles that can be released from virtually all cell types under physiological and pathological conditions and may be detected in blood and other body fluids (1, 2). The role of EVs in cell–cell communication and immunity is a new area in biology and medicine, and immunosuppressive and immunostimulatory roles have been attributed to EVs (3–6). We previously showed that EVs from stored leukoreduced blood are heterogeneous and

originate from multiple cell types. We observed that monocytes bind to and engulf EVs, and T cell response modulation by EVs is indirect and mediated *via* monocyte activation (7). Red blood cell (RBC)-EVs have been described as immunosuppressive or immunostimulatory in separate studies (8, 9). The literature is also conflicting on the stimulatory vs. suppressive effect of platelet-EVs on monocytes and macrophages (10, 11).

Understanding how EV subtypes interact with immune cells would better allow their manipulation in disease states, as several mechanisms of uptake have been described for EVs. EV surface proteins can play an important role in EV uptake, as treatment of EVs with proteinase K decreases the uptake of EVs by ovarian cancer cells (12). Phagocytosis, clathrin-mediated endocytosis, caveolin-mediated endocytosis, and membrane fusion are suggested mechanisms for EV uptake (13). It is believed that adhesion molecules, integrins, and lectins play a role in EV uptake (13–15). Proteoglycans such as heparin sulfate may also play a role in EV uptake, as treatment of cells with a heparin sulfate mimetic reduces EV uptake (16). The role of TLRs in EV uptake has also been studied, and the data in the literature on TLRs are conflicting (17, 18). In general, EV uptake can involve several receptors (12, 19–24). The role of scavenger receptors in EV uptake is not well studied, but it has been shown that endothelial-EVs bind to the scavenger receptor CD36 on platelets and contribute to thrombosis in mice (25).

Increased levels of particular EV subtypes have been associated with specific diseases, and EV subtypes may serve as novel biomarkers. The plasma level of $CD31^+$ EVs is associated with increased risk of cardiovascular death (26). Tissue factor (CD142)-positive EVs derived from endothelial cells and monocytes in sickle cell disease contribute to thrombin generation and coagulation (27). In a study of critically ill patients, the ratio of platelet-EVs to platelet count was associated with mortality, primarily driven by an inverse relationship between platelet count and mortality (28). In critically ill burn patients, white blood cell (WBC)- and granulocyte-EVs at intensive care unit (ICU) admission are associated with subsequent mortality (29).

Using RNA sequencing and global transcriptomic analyses, here we show that plasma-EVs bias primary monocytes toward an M1 profile, which leads to generation of a dominant inflammatory response. We also show that whether EVs induce pro- or anti-inflammatory responses in monocytes depends on their cell of origin. Finally, we demonstrate that a group of scavenger receptors were regulated in monocytes stimulated with EVs, and that RBC-EVs bind monocytes at least in part *via* the scavenger receptor CD36. We enrolled a subset of 100 critically ill subjects from three of the clinical sites participating in the Age of BLood Evaluation (ABLE) trial and measured a broad array of immune and coagulation parameters to determine if the age of blood transfused affected these parameters, and secondarily whether any of the parameters predicted subsequent mortality (30). We showed that in addition to cystatin C and tissue plasminogen activator (TPA), EVs expressing CD66b (granulocyte), CD15 (granulocyte and monocyte), CD11b (adhesion molecule), and CD62P (activated platelets and endothelial cells) are early predictors of mortality in ICU patients.

MATERIALS AND METHODS

Study Samples

For *in vitro* experiments Trima filters (discarded byproducts of platelet apheresis) were used to generate large stocks of stored peripheral blood mononuclear cells (PBMCs). Fresh blood from six healthy donors was used for isolation of granulocytes to generate pure granulocyte-EVs. To purify RBC- and platelet-EVs, RBC units and platelet units were washed by automation and stored for 21 and 5 days, respectively. All filters and units were de-identified and acquired from Blood Centers of the Pacific (BCP). All study protocols were approved by the University of California, San Francisco Committees on Human Research.

Samples from the ABLE study were used for *ex vivo* experiments. ABLE was a multicenter, randomized, controlled clinical trial that studied the effect of RBC unit storage time in 1,430 critically ill patients who received RBC transfusion. PBMC samples from a subset of 100 patients in the ABLE trial were collected pre-transfusion and on days 2, 6, 28, and 180 post-transfusion. ABLE sites participating in this study included The Ottawa Hospital (General and Civic campuses) and the Institut de Cardiologie et de Pneumologie de Québec, Université Laval. All patients from the ABLE trial were eligible to participate, with the exception of those with history of bone marrow transplantation. Plasma samples were used for measurement of EVs, cytokines, growth factors, and coagulation factors. In addition, clinical data were collected in the ABLE trial, including mortality and multiorgan dysfunction syndrome score. Samples were collected under informed consent and IRB approval in accordance with the Declaration of Helsinki. A group of 48 healthy control subjects was enrolled at Blood Systems Research Institute, with a blood sample collected at a single time point for analysis of EV subtypes in peripheral blood.

Sample Processing

Plasma-EVs were isolated from ACD-treated blood using differential centrifugation. Plasma was separated at 1,000 *g* from cells and spun at 13,000 *g* to make platelet-free plasma (PFP). Six mL of PFP were added to 30 mL phosphate-buffered saline and spun for 1 h at 100,000 *g*. EV pellets were resuspended in 1 mL RPMI and stored at −80°C. Purified EVs were used for functional experiments.

For measurement of EV subtypes in peripheral blood, whole blood from 48 donors was collected in a citrate tube. Tubes were centrifuged at 2,500 *g*, and plasma was stored in 0.5 mL aliquots at −80°C until testing. Whole blood was collected in EDTA tubes from ABLE study subjects on day 0 (before transfusion) and on days 2, 6, and 28 after the first RBC transfusion. Collection tubes were centrifuged at 1,000 *g* to separate cells from plasma, and plasma was centrifuged at 13,000 *g* for removal of platelets and large fragments of cells. Aliquots of 0.5 mL PFP were stored at −80°C until testing.

Generation of Pure EV Subtypes Based on Their Cell of Origin

Pure RBC-, platelet-, monocyte-, granulocyte-, and endothelial-EVs were prepared for functional experiments. Monocytes were

isolated from PBMCs of healthy donors by double negative selection using an EasySep Human Monocyte Enrichment Without CD16 Depletion Kit (Stemcell Technologies), and they were cultured at 1 million cells/mL for 2 days to generate monocyte-EVs in the culture supernatant. Whole blood was treated with HetaSep (Stemcell Technologies) to sediment RBCs and isolate leukocytes. Granulocytes were isolated from leukocytes by double negative selection using an EasySep Human Pan-Granulocyte Isolation Kit (Stemcell Technologies) and were cultured at 1 million cells/mL for 24 h to generate granulocyte-EVs. Washed leukoreduced RBC units were stored for 21 days in CP2D plus AS3 storage solution at 4°C to generate pure RBC-EVs. Platelet units were washed and stored for 5 days on a shaker at 25°C to generate platelet-EVs. Human umbilical vein endothelial cells (University of California, San Francisco Cell Culture Facility) were cultured to 90% confluence for 1 week to generate endothelial-EVs. EV subtypes were isolated from monocyte, granulocyte, and endothelial cell culture supernatants, and from stored RBC units and stored platelets by differential centrifugation as described earlier, followed by storage at −80°C.

Characterization of EVs

To characterize EVs from patients, PFP samples were stained and acquired as previously described (31) using 14 different fluorochrome-conjugated monoclonal antibodies in three separate panels, including CD235a-FITC, CD62P-APC, CD3-PerCP/Cy5.5, CD19-Alexa/700, CD28-FITC, CD16-V450, CD62L-APC, CD11b-PE/Cy7, CD66-PE (BioLegend), CD15-FITC (ExAlpha), CD152-APC, CD14-APC/Cy7, CD108a-PE, and CD41a-PerCP/Cy5.5 (BD Biosciences). In normal donor samples CD142-PE (BioLegend) and CD154-APC (BD Biosciences) were substituted for CD14 and CD152, respectively. To reduce the background staining and as the size of small EVs fall below the detection limit of flow cytometer, stained EVs were diluted in PBS and were centrifuged for 5 min at 500 *g* using 0.22 μm Ultrafree MC-GV Centrifugal Filter Units (Millipore). Flow through (small EVs and unbound antibodies) was discarded, and stained large EVs were harvested in PBS from the top of the filter. Data were acquired using an LSR II flow cytometer (BD Biosciences). FSC/SSC voltages were set to the highest values that excluded the majority of background noise (i.e., just below the voltage threshold at which event rate surpassed 5 events/s while running a tube of PBS alone). Typically, this threshold occurred at FSC and SSC voltages of around 500–600 and 300–350, respectively. Gates were set using beads sized 100, 200, 240, 500, and 1,000 nm (Megamix-Plus SSC; BioCytex), and EVs were collected from the threshold to the 1,000 nm gate based on SSC. Analysis was performed using FlowJo 7.6.5 software (Tree Star).

Isolation of PBMCs and Purification of Monocytes

Whole blood or leukocytes trapped in TRIMA filters were overlaid on Ficoll-Paque (Sigma-Aldrich) and centrifuged for 30 min at 600 *g*. PBMC layers were harvested followed by washing and cryopreservation in fetal bovine serum (FBS) containing 10% DMSO. Isolation of monocytes from PBMCs was performed by double negative selection from PBMCs using the EasySep Human Monocyte Enrichment Without CD16 Depletion Kit (Stemcell Technologies).

Stimulation of Monocytes With EVs

Extracellular vesicles were counted using Trucount Absolute Counting Tubes (BD Biosciences). To each Trucount™ tube, 50 μL sample and 350 μL PBS were added and samples were read immediately on the flow cytometer. EV concentrations were calculated using the following equation:

$$\text{EVs}/\mu\text{L} = \left[\text{EV region events} / \text{bead region events}\right] \times \left[\text{Trucount}^{\text{™}}\ \text{beads} / \mu\text{L of sample added}\right].$$

One million monocytes were cultured in 1 mL of 10% inactivated exosome-free FBS (SBI) in RPMI (containing 10 mM *N*-2-hydroxyethylpiperazine-*N*′-2-ethanesulfonic acid, 100 U/mL penicillin G, and 100 mg/mL streptomycin) in the presence or absence of one million plasma-EVs in a 5% CO_2 incubator at 37°C for 1, 3, and 24 h. Each experiment was performed in duplicate wells, and cell culture supernatants (0.3 mL) were harvested for cytokine assays and cells were added to 0.7 mL QIAzol Lysis Reagent (Qiagen) for total RNA isolation. For experiments using individual EV subtypes, 1 million monocytes were cultured with 1 million EVs of a given subtype (RBC-, platelet-, monocyte-, endothelial-, and granulocyte-EVs) for 24 h, and supernatants were harvested for cytokine assays. For some experiments EVs were fractionated by size. Briefly, EVs were centrifuged at 500 *g* using 0.22 μm Ultrafree MC-GV Centrifugal Filter Units (Millipore) to separate small and large EVs (enriched for exosomes and MVs, respectively). The small EVs (<220 nm) were collected in the flow through, and the large EVs (>220 nm) were recovered from the top of the filter. Each fraction was incubated with monocytes for 16 h followed by permeabilization of cells using Cytofix/Cytoperm Kit (BD Biosciences) and intracellular staining for TNF-α (-V421 labeled, BioLegend).

Gene Expression Profiling With High Throughput Sequencing

Total RNA from monocytes, EVs, and PBMC positive controls was extracted using the miRNeasy Mini Kit (Qiagen) with the optional on-column DNAse treatment step. RNA was quantified using a NanoDrop ND-1000 Spectrophotometer (NanoDrop Technologies) and integrity was assessed using an Agilent 2100 Bioanalyzer (Agilent Technologies). For RNA-Seq experiments cDNA was generated using the Illumina TruSeq Stranded mRNA Library Prep Kit (Illumina Technologies), and 400 ng of total RNA was used as input. Single-read sequencing was performed using the Illumina HiSeq 2000 instrument to obtain 30–50 million single reads of 51 nucleotides. RNA-Seq data were preprocessed by adaptor trimming and low quality 3′-tail trimming (Phred > 20). The preprocessed reads were mapped using Tophat to the reference genome hg19. Gene level expression quantification in FPKM (Fragments Per Kilobase of transcript per Million mapped reads) was calculated using Cufflinks suite including Cufflinks, Cuffmerge, Cuffquant, and Cuffnorm. Significant changes in

transcript expression were quantified by *t*-test, which were adjusted by false discovery rate (FDR < 0.05). Gene annotations and GO terms were extracted from BioMart using the Bioconductor/biomaRt package.

Intracellular Cytokine Assays and TLR Blocking Antibodies

Intracellular staining of monocytes for detection of TNF-α was performed after stimulation of 1 million/mL monocytes with EVs as previously described (7). To test the efficacy of anti-TLR neutralizing antibodies, one million PBMCs were treated with 1 μg/mL TLR1, TLR2, or TLR4 antibodies for 1 h, and then stimulated with TLR agonists (InvivoGen) for 16 h. Synthetic tripalmitoylated lipopeptide Pam3CysSerLys4 (Pam3CSK4, 20 ng/mL) was used as a TLR1 and TLR2 agonist, and LPS (5 ng/mL) was used as a TLR4 agonist. Finally, cells were stained with CD14-APC/Cy7 antibody (BioLegend) before permeabilization, then washed and stained for TNF-α, and run on the flow cytometer.

Measurement of Cytokines in Supernatant of Monocytes Stimulated With EVs

A Milliplex MAP Kit (Millipore) was used to measure the level of 13 cytokines and growth factors in culture supernatants of monocytes stimulated with plasma-EVs (GM-CSF, IFNγ, IL-10, IL-12p70, IL-13, IL-1β, IL-2, IL-4, IL-5, IL-6, IL-7, IL-8, and TNF-α). A second Milliplex MAP kit from the same manufacturer was used to measure the level of 12 cytokines in supernatants of monocytes stimulated with EV subtypes (IFNγ, IL-10, sCD40L, IL-1RA, IL-1α, IL-1β, IL-6, MIP-1α, TNF-α, MIG, GM-CSF, and TGF-β). A Bio-Plex 200 instrument (Bio-Rad) was used for data acquisition.

Cell Surface Expression of Scavenger Receptors and TLRs

Cell surface expression of scavenger receptors CD36, CD163, and CD206, and cell surface expression of TLR1, TLR2 and TLR4 on monocytes were assessed by staining PBMCs with CD14-PerCP/Cy5.5, CD36-PE, CD163-APC, CD206-Alexa Fluor 488, TLR2-PE, TLR4-APC (BioLegend), and TLR1-FITC (Invivogen) fluorochrome-conjugated antibodies according to the manufacturers' instructions. Samples were fixed in 2% paraformaldehyde solution and were run on the flow cytometer. Percent expression of scavenger receptors and MFI of TLRs were measured after gating on $CD14^+$ monocytes.

EV–Monocyte Binding Assay

Plasma-EVs, aged RBC-EVs, or EV subtypes were stained with PKH26 Red Fluorescent Cell Linker Dye (Sigma-Aldrich). EVs were washed twice with 10% exosome-free FBS in RPMI to quench the unbound dye. Recombinant annexin V (BD Biosciences) or functional grade blocking monoclonal antibodies against phosphatidylserine (PS) (Millipore), CD36 (Stemcell Technologies), CD163, CD206 (BioLegend), TLR1 (Invivogen), TLR2, and TLR4 (BioLegend) were used at multiple concentrations (0.01–2.0 μg/mL) to block EV–monocyte binding. In some experiments, EVs were incubated with annexin V or anti-PS antibody. In other experiments PBMCs were incubated with monoclonal antibodies against CD36, CD163, CD206, TLR1, TLR2, or TLR4 in a 5% CO_2 incubator at 37°C for 1 h. PBMCs (500,000) were cultured with EVs, in a final volume of 0.5 mL for 24 h. PBMCs were stained with CD14-PerCP/Cy5.5 (BioLegend) and were fixed in 2% paraformaldehyde solution. PBMCs were subject to flow cytometry, and percent binding of monocytes to EVs was measured by gating on $CD14^+$ cells.

Measurement of Cytokines and Coagulation Factors

PFP from 100 ABLE study subjects was analyzed for levels of immune and coagulation markers. To determine the inflammatory and coagulation profile of PFP, a total of 43 different markers were measured, including 16 coagulation factors: prothrombin time, partial thromboplastin time, D-dimer concentration, factor II, factor V, factor VII, factor VIII/40, factor IX/20, factor X, antithrombin III, protein C, fibrinogen concentration, thrombomodulin, endothelial cell protein C receptor, TPA, and plasminogen activator inhibitor type-1 (PAI-1). The markers of coagulation were analyzed on a Stago or Dade Behring-Siemens device. Coagulation factors Va, VIIIa, VII, as well as antithrombin III, prothrombin time, partial thromboplastin time, TPA, D-dimer, and protein C were measured on a Diagnostica Stago™ coagulation analyzer. Concentrations of prothrombin fragments 1 + 2, soluble thrombomodulin, PAI-1, soluble endothelial protein C receptor, and cytokines were measured using commercially available ELISA kits. In addition, 27 cytokines were measured using Milliplex MAP kit (Millipore): GM-CSF, IL-12p70, IL-17A, IL-1β, IL-2, IL-21, IL-23, IL-6, IL-7, IL-8, ITAC, MIP-1α, MIP-1β, TNF-α, EGF, FGF, IFN-γ, IP-10, VEGF, β2-microglobulin, cystatin C, myeloperoxidase, PAI-1, PDGF-AB/BB, RANTES, sICAM-1, and sVCAM–1. A Bio-Plex 200 instrument (Bio-Rad) was used for cytokines data acquisition.

Data Analysis

Supervised gene analysis was performed on all genes that were mapped by high throughput sequencing and used in this paper. FDRs were computed using the Benjamini–Hochberg procedure to adjust for multiple comparisons in the RNA-Seq data. The heat maps were generated using standardized *Z*-scores. GraphPad Prism v.6 was used for ANOVA and *t*-test analyses as noted in the figure legends. The significance of predictors of mortality was based on Cox regression analyses. The distribution of the data was analyzed, and for analytes with non-normally distributed data, values were log-transformed before analysis.

RESULTS

EV Exposure Initiates an M1 Phenotype Gene Expression Program

To better understand how EVs affect human immune cells, we performed transcriptomic analyses using RNA-Seq on monocytes at baseline and longitudinally after exposure to EVs derived from PFP. It has been shown that monocytes and monocyte-derived macrophages internalize EVs, which leads to

their activation (11, 32, 33). Our prior work demonstrated that monocytes ingest EVs found in stored RBC units (7), therefore we focused our studies on this population of immune cells. It has been shown that several genes are expressed differentially during the process of monocyte polarization to M1 and M2 profiles, and that the M1 phenotype has pro-inflammatory effects, while the M2 phenotype possesses anti-inflammatory properties (34). We analyzed 53 genes that have been described as associated with the M1 profile and 43 genes associated with the M2 profile (34). From M1-associated genes, the mRNA of 19 genes were significantly upregulated at 3 and/or 24 h, including *NAMPT*, *IL15RA*, *VCAN*, *CHI3L2*, *IL7R*, *IL2RA*, *PTX3*, *SLC2A6*, *BIRC3*, *SPHK1*, *TNF*, *EDN1*, *BCL2A1*, *CCR7*, *CCL20*, *IL6*, *INHBA*, *PFKFB3*, and *SLC7A5* (**Figure 1A**). Three genes were downregulated at 1 and/or 3 h, including *SLC31A2*, *PSMB9*, and *PSAM2*. Analysis of M2 genes showed that the majority of M2-biasing genes with significant changes after EV exposure were downregulated (**Figure 1B**). We found that mRNA of 19 genes were downregulated, most notably at 3 h post EV exposure, including *MSR1*, *CXCR4*, *CD302*, *GAS7*, *TPST2*, *CD36*, *MS4A6A*, *LTA4H*, *TLR5*, *SLC38A6*, *SLEC10A*, *LIPA*, *MS4A4A*, *SLCO2B1*, *LPAR6*, *TGFBI*, *ADK*, *HS3ST1*, and *HEXB*. Only four M2-associated genes were upregulated, including

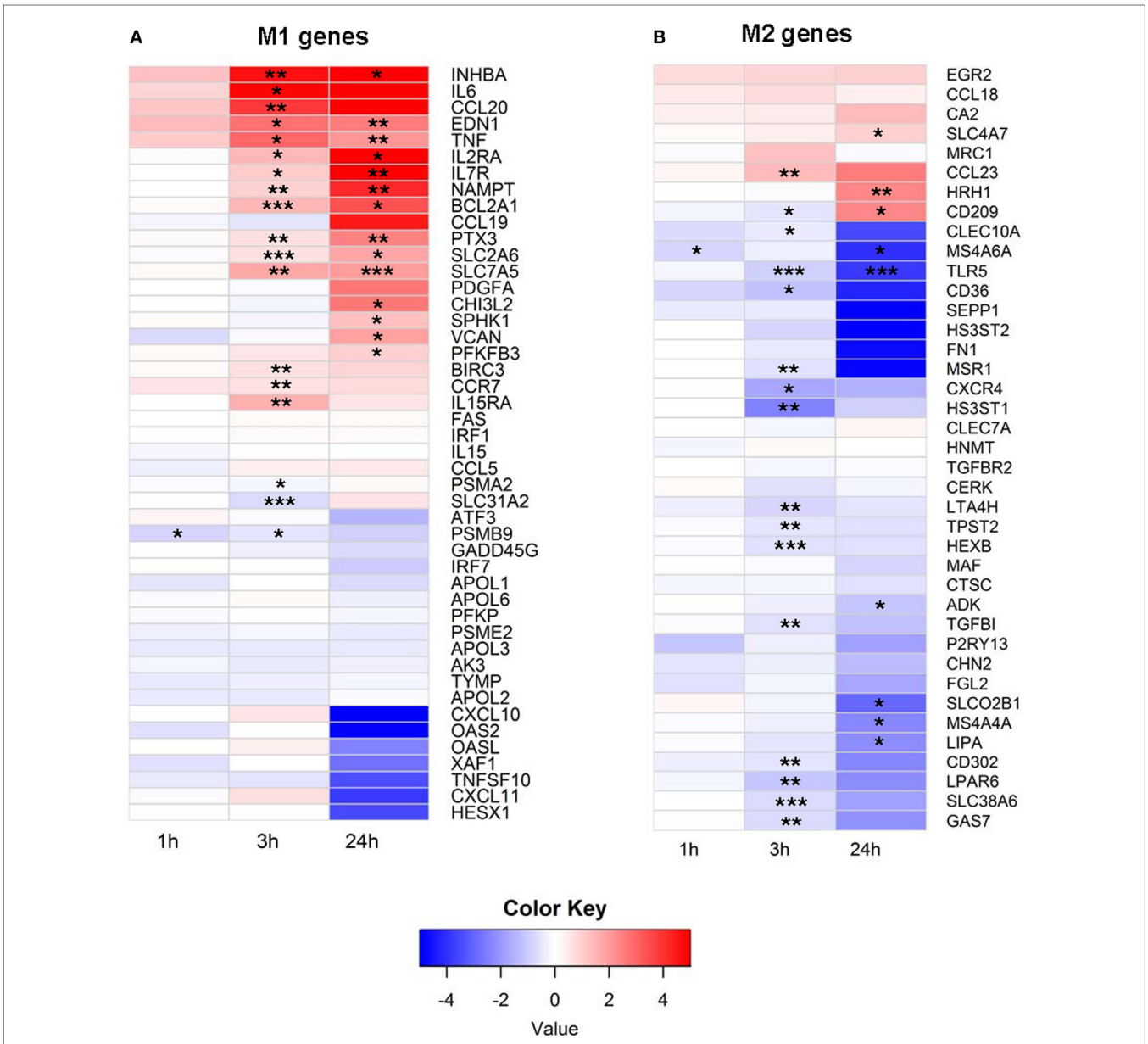

FIGURE 1 | **(A)** M1 and **(B)** M2 mRNA expression profile of extracellular vesicle (EV)-exposed monocytes. Monocytes were purified from peripheral blood mononuclear cells of five healthy donors and were cultured unstimulated or stimulated with plasma-EVs from five other healthy donors for 0, 1, 3, and 24 h. mRNA expression was determined by RNA-Seq and analyzed longitudinally for a panel of previously described M1 and M2-associated genes. Results for EV-incubated conditions were normalized to matched, unstimulated conditions at each time point and $\log_2$-transformed (*$p < 0.05$, **$p < 0.01$, and ***$p < 0.001$).

SLC4A7, *CD209*, *CCL23*, and *HRH1*. In summary, exposure of primary monocytes to EVs from plasma of healthy donors led to predominant upregulation of M1-associated genes (19 up and 3 down) and downregulation of M2-associated genes (4 up and 19 down), and the different regulation pattern of M1 and M2-associated genes was significant ($p < 0.0001$, Fisher's exact test).

Effector Molecules Induced in Monocytes Exposed to EVs

The RNA-Seq data were next analyzed to examine expression of cytokines and growth factors in more detail. From 36 known interleukins, message for 27 was detectable by high throughput sequencing. The mRNA expression of 14 interleukins and interleukin receptors was significantly upregulated at 3 and/or 24 h (**Figure 2A**). We next looked at the gene expression of chemokines and found 24 mRNA transcripts that were detectable. Expression of 17 chemokines changed significantly, with the majority upregulated at 3 and/or 24 h (**Figure 2B**). In contrast to interleukins and chemokines, most interferon transcripts were not detectable, and of the five that were, none showed significant changes after EV exposure (**Figure 2C**).

To determine whether the changes in cytokine mRNA levels measured after monocyte exposure to EVs translated to changes in protein levels, the supernatants from the same stimulated monocytes were tested using a multiplex cytokine assay. The levels

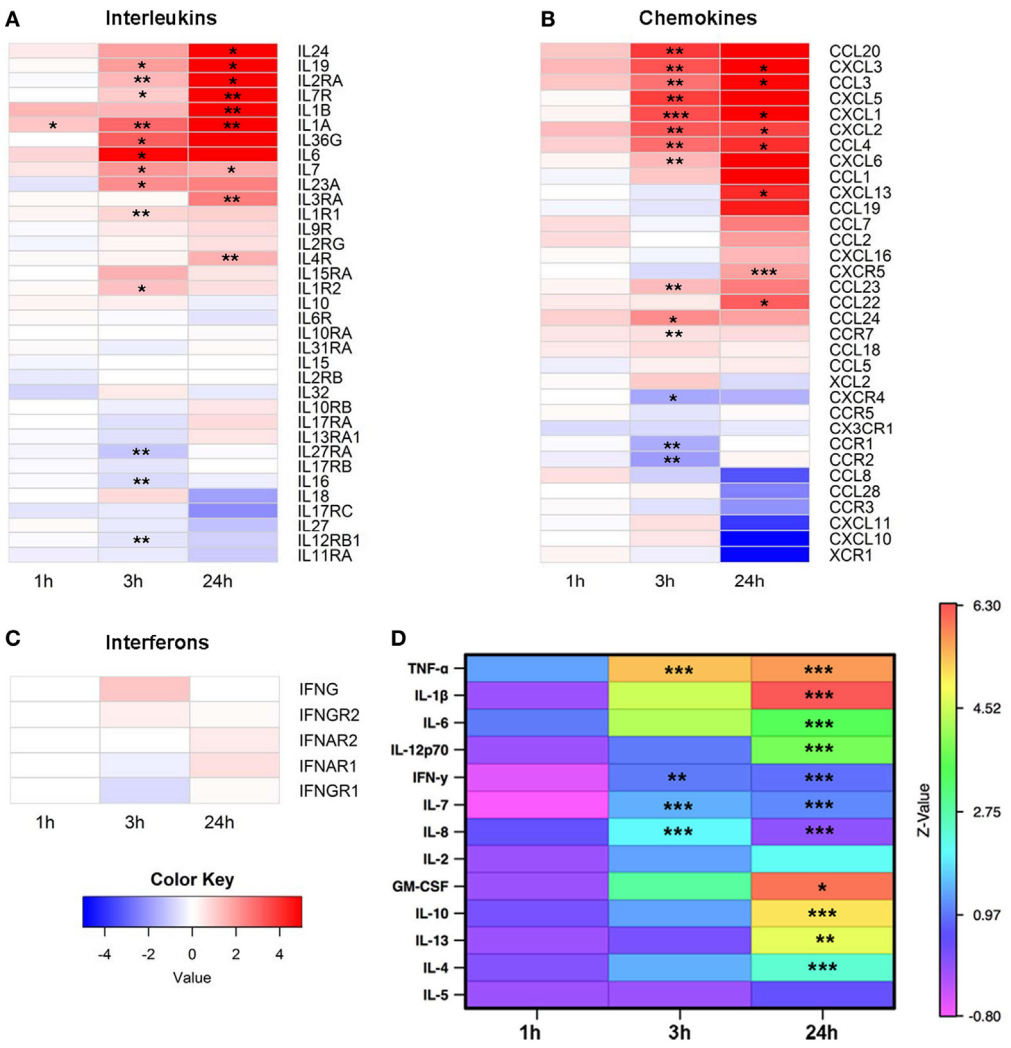

FIGURE 2 | Expression of cytokines, chemokines, and growth factors. Monocytes were purified from peripheral blood mononuclear cells of five healthy donors and were cultured unstimulated or stimulated with plasma-EVs from five other healthy donors for 0, 1, 3, and 24 h. Supervised gene analysis was performed, and significant changes in transcript expression quantified by *t*-test, which were adjusted by false discovery rate (<0.05). **(A)** Of the panel of genes for interleukins or their receptors, expression of 14 was significantly upregulated and of 3 was downregulated at 3 and/or 24 h in monocytes stimulated with EVs compared with paired unstimulated samples. **(B)** Of the chemokines and their receptors, expression of 14 was significantly upregulated and of 3 was downregulated at 3 and/or 24 h. **(C)** mRNA expression of most interferons was not detectable, and of the detectable messages none was significantly different from unstimulated monocytes. **(D)** Supernatants were collected from the same cultures used for mRNA expression analysis. Results for stimulated conditions were normalized to unstimulated data and $\log_2$-transformed to show log-fold increase after stimulation (*$p < 0.05$, **$p < 0.01$, and ***$p < 0.001$).

of nine pro-inflammatory and four anti-inflammatory cytokines were measured at 0, 1, 3, and 24 h intervals in the supernatant of monocytes that were unstimulated or incubated with EVs isolated from normal donor plasma, and values were reported as a ratio of EV-exposed to unstimulated conditions at each time point (**Figure 2D**). Of the cytokines in the panel, mRNA levels of *TNF* and *IL7* were elevated at 3 and 24 h after EV exposure, and mRNA from *IL1B* was elevated at 24 h. Protein levels of all these analytes were significantly elevated and concordant with the mRNA expression data, with the exception that *IL6* mRNA was significantly elevated at 3 h while the elevation in IL-6 protein did not reach significance until 24 h. In addition, there were two cytokines with elevated protein levels at 3 h (IFN-γ and IL-8) and seven cytokines or growth factors with elevated protein levels at 24 h that were either not significantly elevated or not detected in the mRNA analysis (*IL-12p70*, IFN-γ, *IL-8*, *GM-CSF*, *IL-10*, *IL-13*, and *IL-4*). Examination of the mRNA and protein expression data of four representative cytokines revealed similar patterns between mRNA and protein expression for TNF-α, IL-1β, and IL-6, while increases in IL-10 were detectable at the protein but not mRNA expression level (Figure S1 in Supplementary Material). To determine whether EV-derived mRNA contributed to the signal in the RNA-Seq experiments, RNA was quantified in the monocyte preparations as well as separate PBMC, EV, and blank well conditions. Monocyte and PBMC controls showed peaks consistent with both small and mRNA species, while RNA was not detectable in EV preparations (Figures S2A,B in Supplementary Material). Overall, these data demonstrate that EVs found in healthy human plasma bias purified monocytes to a pro-inflammatory, M1 phenotype.

EV Cell of Origin Determines Effect of EVs on Monocytes

To better discriminate which EVs in plasma affect monocyte phenotype, we tested EVs derived from purified cell populations. Monocytes were stimulated with smaller EVs (<220 nm, enriched for exosomes) and larger EVs (>220 nm, enriched for microvesicles) derived from granulocyte- and platelet-EVs for 16 h and monitored for TNF-α production. While both small and large EV fractions of granulocyte-EVs led to production of TNF-α, neither the small nor the large EV fractions of platelet-EVs induced the production of this pro-inflammatory cytokine (**Figure 3A**).

To more comprehensively measure EV subtype effects, purified monocytes were stimulated with RBC-, platelet-, monocyte-, endothelial-, or granulocyte-EVs, and a panel of 12 cytokines was measured in cell culture supernatants. Granulocyte-EVs were the most pro-inflammatory, inducing significant increases in monocyte secretion of TNF-α, IL-1β, IL-6, MIP-1α, and GM-CSF (**Figure 3B**). Stimulation of monocytes with monocyte-EVs led to a significant increase in TNF-α, IL-6, and MIP-1α, and endothelial-EVs induced IL-6 and MIP-1α secretion. Stimulation of monocytes with platelet-EVs led to a significant increase of TGF-β production. Analysis of all 12 cytokines revealed EV-induced changes in IL-10 and IL-1RA as well. Stimulation of monocytes with RBC-EVs did not change the secretion of cytokines that we measured (**Figure 3C**). In general, culturing monocytes with pure granulocyte-, monocyte-, and endothelial-EVs induced the secretion of several pro-inflammatory cytokines, in contrast to platelet- and RBC-EVs.

Gene Regulation and Cell Surface Expression of Scavenger Receptors

The role of scavenger receptors in EV uptake is an area of active investigation (25, 35, 36). The mRNA expression of 24 scavenger receptors was measured by RNA-Seq to determine if these receptors are regulated in monocytes after plasma-EV exposure. The mRNA expression of scavenger receptors *SRA-1* (*CD204*), *SRI-1* (*CD163*), *CD280*, *SRI-2* (*CD163L1*), *SRB-2* (*CD36*), and *SRJ-1* was downregulated, and the mRNA expression of *SRF-1*, and *CD209* was upregulated compared with the time-matched unstimulated condition (Figure S3A in Supplementary Material).

Several scavenger receptors were selected for analysis of protein expression and requirement for EV–monocyte binding. It has been shown that the scavenger receptor CD36 plays a role in thrombosis in mice by binding to endothelial-EVs (25). Monocytes express the scavenger receptor CD163, which binds to hemoglobin and haptoglobin-hemoglobin complex (37). As RBC-EVs are loaded with hemoglobin (38), we thought CD163 may play a role in EV binding. The mRNA expression of *CD206*, a receptor on monocytes that binds to mannose residues on bacteria (39), did not change in the RNA-Seq data, so this gene was included as a control (Figure S3B in Supplementary Material). To validate the mRNA findings, the cell surface expression of these receptors was determined. CD36 expression was decreased significantly 3 h after stimulation of monocytes with plasma-EVs. Expression of CD163 on the monocyte cell surface was decreased significantly at 3 and 24 h. Incubation of monocytes with plasma-EVs did not significantly change surface CD206 expression (Figure S3C in Supplementary Material). The surface expression of the scavenger receptors on monocytes was largely consistent with the mRNA expression data, with decreases seen after incubation with EVs.

Gene Regulation and Cell Surface Expression of Toll-Like Receptors

The expression of *TLR1*, *TLR2*, and *TLR4* mRNA was examined after exposure to plasma-EVs, as TLRs have been proposed as potential receptors for EVs (17, 18). The mRNA expression of *TLR1* was downregulated at 3 h and upregulated at 24 h. The mRNA expression of *TLR2* was upregulated at 3 and 24 h time points. Expression of *TLR4* mRNA was downregulated at 3 h (Figure S3D in Supplementary Material). The surface expression of the TLR receptors was not concordant with the gene expression data. TLR1 surface expression did not differ after exposure to plasma-EVs, while TLR2 and TLR4 surface expression dropped at 3 h after EV exposure (Figure S3E in Supplementary Material).

Dependence of EV–Monocyte Binding on Scavenger Receptors and Toll-Like Receptors

Plasma-EVs were incubated with PBMCs for 24 h with or without the addition of annexin V or antibodies to phosphatidyl serine or

several scavenger receptors. Blocking phosphatidyl serine, CD36, CD163, or CD206 did not affect EV–monocyte binding (**Figure 4A**). Similarly, blockade of TLR1, TLR2, or TLR4 had no effect on EV–monocyte binding (**Figure 4B**). To ensure that the TLR antibodies had blocking activity, PBMCs from two subjects were activated with LPS or Pam3CSK4 and incubated with TLR4 or TLR1/2 antibodies, respectively. Monocyte TNF-α production was decreased 30–80% by the TLR antibodies (Figure S4A in Supplementary Material).

In addition to testing the ability of plasma-EVs to bind to monocytes, EVs derived from packed RBC units stored for

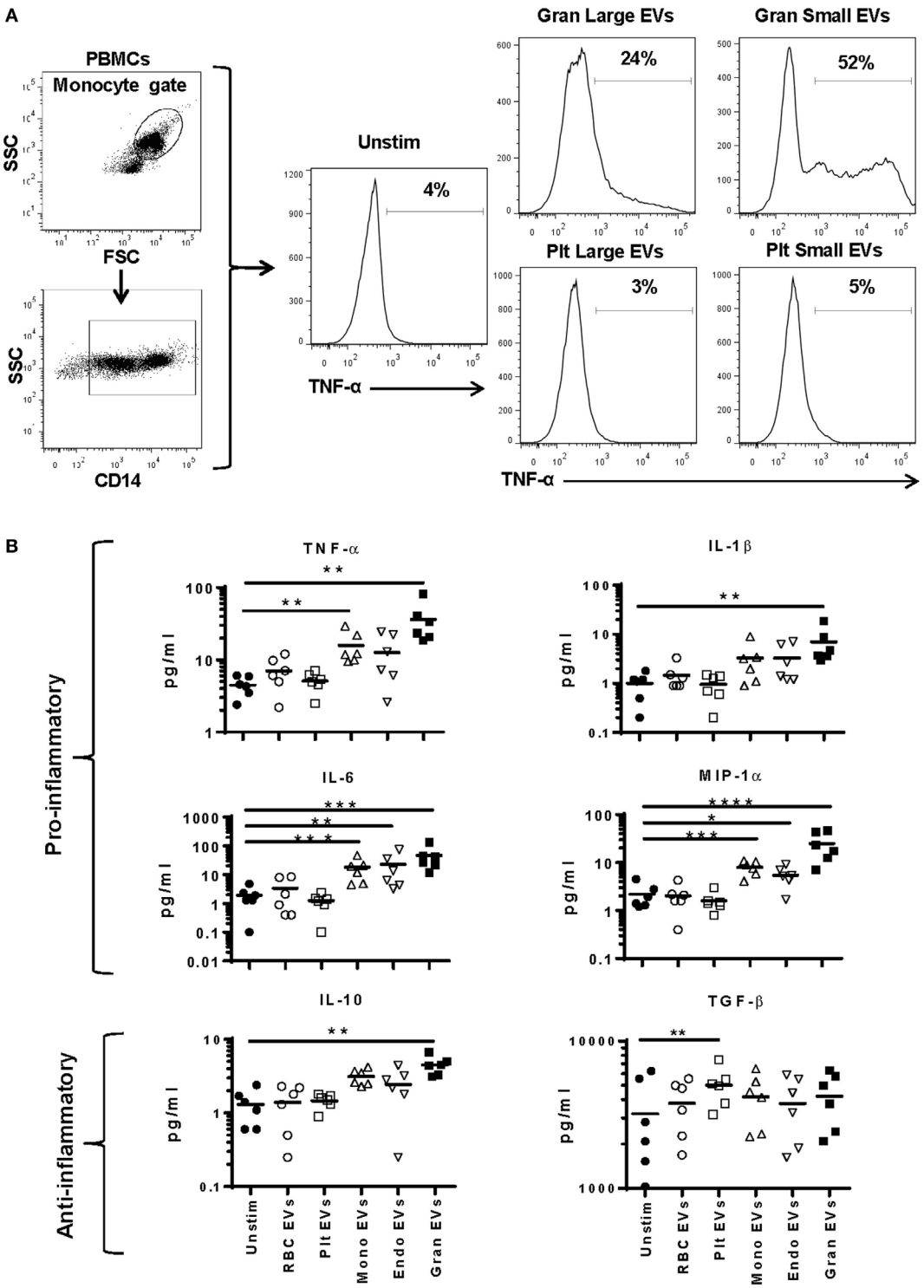

FIGURE 3 | Continued

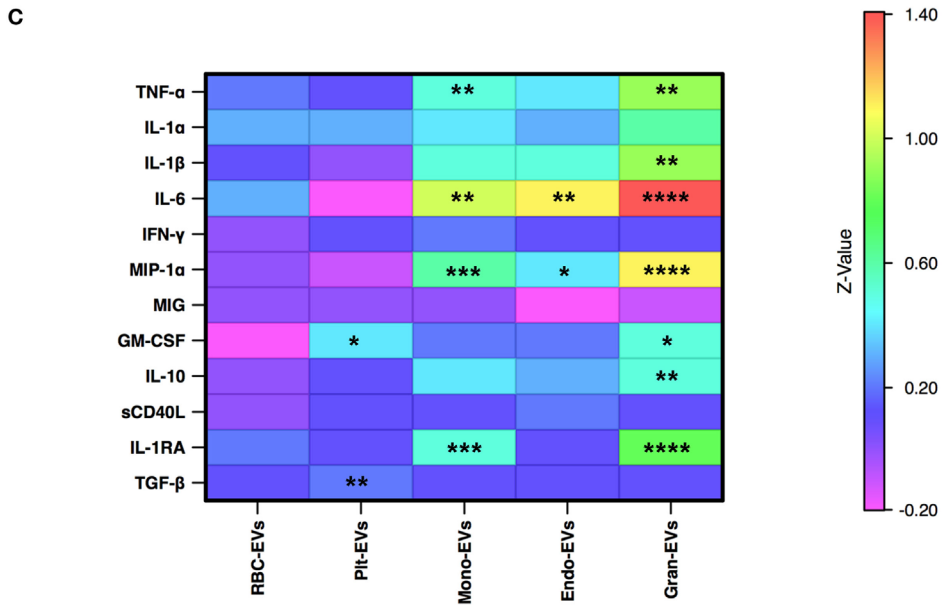

FIGURE 3 | Cytokine secretion by monocytes stimulated with subtypes of extracellular vesicles (EVs). Monocytes from peripheral blood mononuclear cells of six healthy donors were purified by negative selection. Six replicates of red blood cell-, platelet-, monocyte-, endothelial-, and granulocyte-EVs were prepared as described in the "Materials and Methods" section. Monocytes were cultured unstimulated or incubated with noted EV subtypes for 24 h. **(A)** Two independent experiments were run with small (enriched for exosomes) and large (enriched for MVs) fractions of granulocyte- and platelet-EVs, and the percentage of monocytes that produced TNF-α was measured by intracellular staining. Representative data showing intracellular cytokine staining of monocytes incubated with small and large fractions of granulocyte- and platelet-EVs. **(B)** Supernatants were collected at 24 h and were tested using a multiplex cytokine assay for 12 cytokines. Data were analyzed by ANOVA, and each condition was compared with the control condition using a Dunnett's post-test. Data are shown for 6 of the 12 cytokines tested. **(C)** The $\log_{10}$ ratio of cytokines induced by incubating monocytes with five subtypes of EVs over the control condition is summarized in a heat map for all 12 cytokines (*$p < 0.05$, **$p < 0.01$, and ***$p < 0.001$).

42 days were examined for their binding capacity to monocytes. As we previously published, the predominant EV subtype in these preparations was RBC-derived (7). Incubation of RBC unit-EVs with annexin V or anti-phosphatidyl serine antibody before incubation with monocytes significantly reduced binding to monocytes. Incubation of monocytes with anti-CD36 antibody also significantly reduced binding to RBC unit-EVs (**Figure 4C**).

Based on the data that CD36 blockade decreased interaction of RBC unit- but not plasma-EVs with monocytes, the binding capacity of, monocyte-, granulocyte-, RBC-, and platelet-EVs to primary monocytes was tested with or without monoclonal antibody blockade of scavenger receptor CD36. A representative titration of antibody is shown for purified RBC-EVs and monocytes (Figure S4B in Supplementary Material). Inhibition of binding of platelet-, granulocyte-, and monocyte-EVs to primary monocytes in PBMC cultures was tested, and none showed significant inhibition after incubation with anti-CD36 antibody. These data show that CD36 is important in the binding of RBC-EVs to monocytes, but not for EVs derived from platelets, granulocytes, or monocytes (**Figure 4D**).

Cellular Origin of EVs in Healthy Subjects

The plasma EV profile in 48 healthy subjects (42% male, median age 46) was examined using a panel of markers to identify EVs bearing markers of endothelial cells (CD142, CD62P), platelets (CD41a, CD62P), RBCs (CD235a, CD108a), and multiple WBC populations. Flow plots gated on EVs (events <1 μm by forward and side scatter, **Figure 5A**) revealed that the RBC marker CD235a and platelet marker CD41a were found on separate populations, while the RBC activation marker CD108a was only found on EVs also positive for CD235a (**Figure 5B**). Similarly, EVs bearing the granulocyte marker CD66b were a separate population from those bearing CD62P (P-selectin), while those bearing the adhesion molecule CD11b were found almost exclusively on the granulocyte-EVs (**Figure 5C**). Platelet-EVs were more numerous than those derived from any other cell type measured, and those bearing CD142 (tissue factor) were rarely detected (**Figure 5D**). To characterize WBC-EVs, various cell lineage and activation markers were examined (**Figure 5E**). EVs bearing markers of T cells (CD3), B cells (CD19), monocyte/NK cells (CD16), and granulocytes (CD66b) were all detected. The adhesion molecule CD15 was detected at higher levels than the adhesion molecule CD62L (L-selectin), though overall there were insignificant differences in expression of various WBC markers on EVs in healthy subjects. These data demonstrate that EVs from different cell subtypes can be distinguished by flow cytometry and that WBC-EVs are present at low-level in healthy subjects' plasma.

Predictors of Mortality in Critically Ill Patients

As part of the ABLE study to analyze the effect of RBC unit storage on clinical outcomes in transfused, critically ill patients (30),

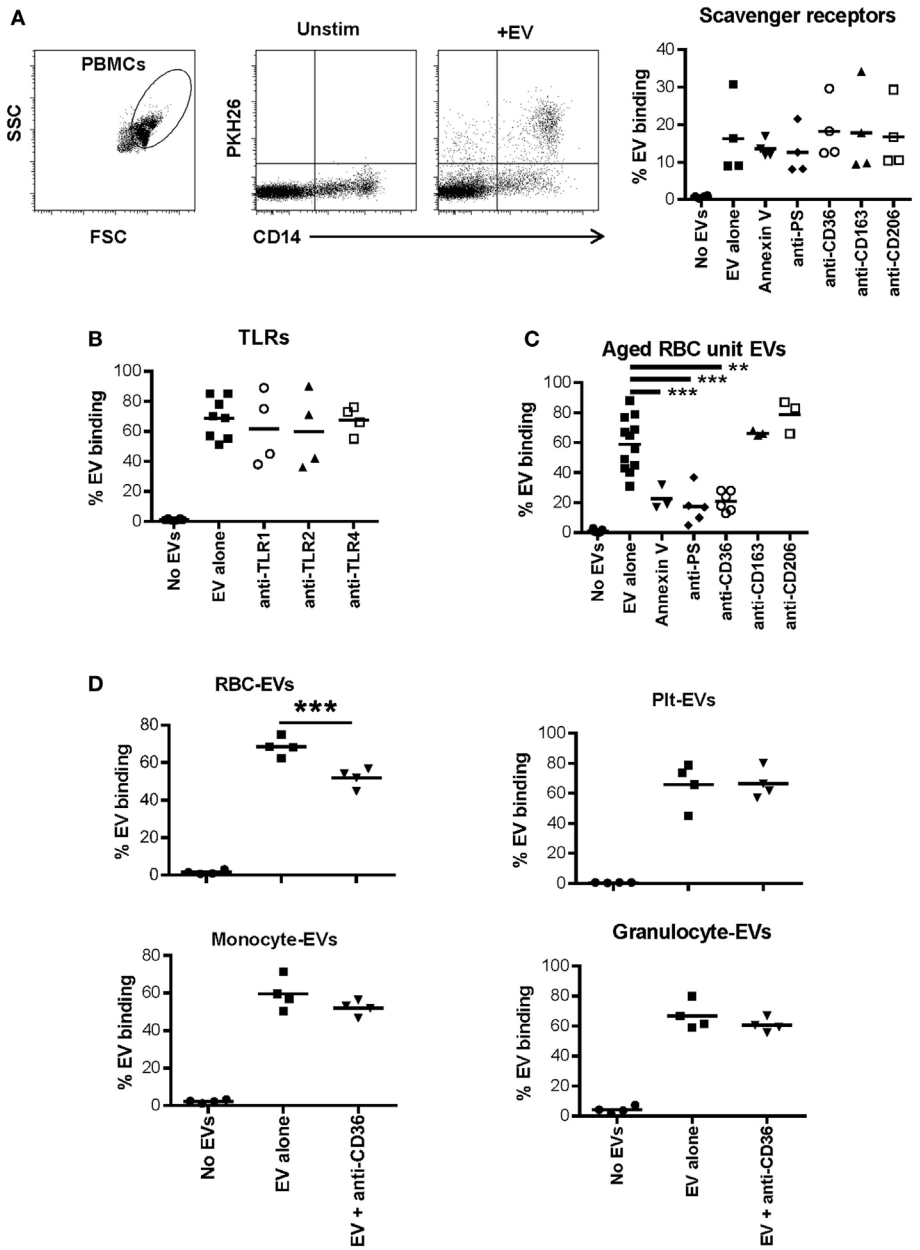

FIGURE 4 | Role of scavenger receptors and TLRs in extracellular vesicle (EV)-monocyte binding. Peripheral blood mononuclear cells (PBMCs) (500,000) from 4 healthy donors were cultured unstimulated or incubated with 100 µL of PKH26 labeled EVs derived from plasma of 4 other healthy donors for 24 h. **(A)** PBMCs were incubated with EVs alone, or EVs pre-incubated with annexin V (1.0 µg/mL) or anti-phosphatidylserine (PS) antibody (1.0 µg/mL) for 1 h and added to PBMCs, or PBMCs were pre-incubated for 1 h with other antibodies noted on the *x*-axis at 1.0 µg/mL and added to PBMCs. After 24 h cells were stained with anti-CD14 and monocyte-EV binding was analyzed. **(B)** PBMCs were pre-incubated for 1 h with the noted TLR antagonists before incubation with EVs for 24 h as above. **(C)** PBMCs were incubated with EVs derived from red blood cell (RBC) units stored for 42 days, and binding inhibitors were added as above. **(D)** Binding of EVs derived from four different purified cell types to monocytes was assessed with or without pre-incubation of PBMCs with anti-CD36 antibody. EV binding inhibition conditions were compared with the EV alone condition by ANOVA with Dunnett's post-test **(A–C)** or by *t*-test **(D)** (*$p < 0.05$, **$p < 0.01$, and ***$p < 0.001$).

serial samples were collected from 100 subjects randomized to receive RBC units that had been stored for a shorter or longer period. These subjects were 95% medical admissions, were 50% female, and had a median age of 67. These samples were tested for an array of 16 coagulation, 27 cytokine, 3 immune cell, and 14 EV markers. The ABLE study found no effect of RBC unit storage age on mortality or other clinical outcomes, and the longitudinal analysis of the relationship of these markers with RBC unit age is the subject of a manuscript in preparation. For this study, we analyzed the 100 subjects in aggregate to determine if immune or coagulation markers in samples collected at ICU admission, pre-transfusion predicted subsequent 28-day mortality, which

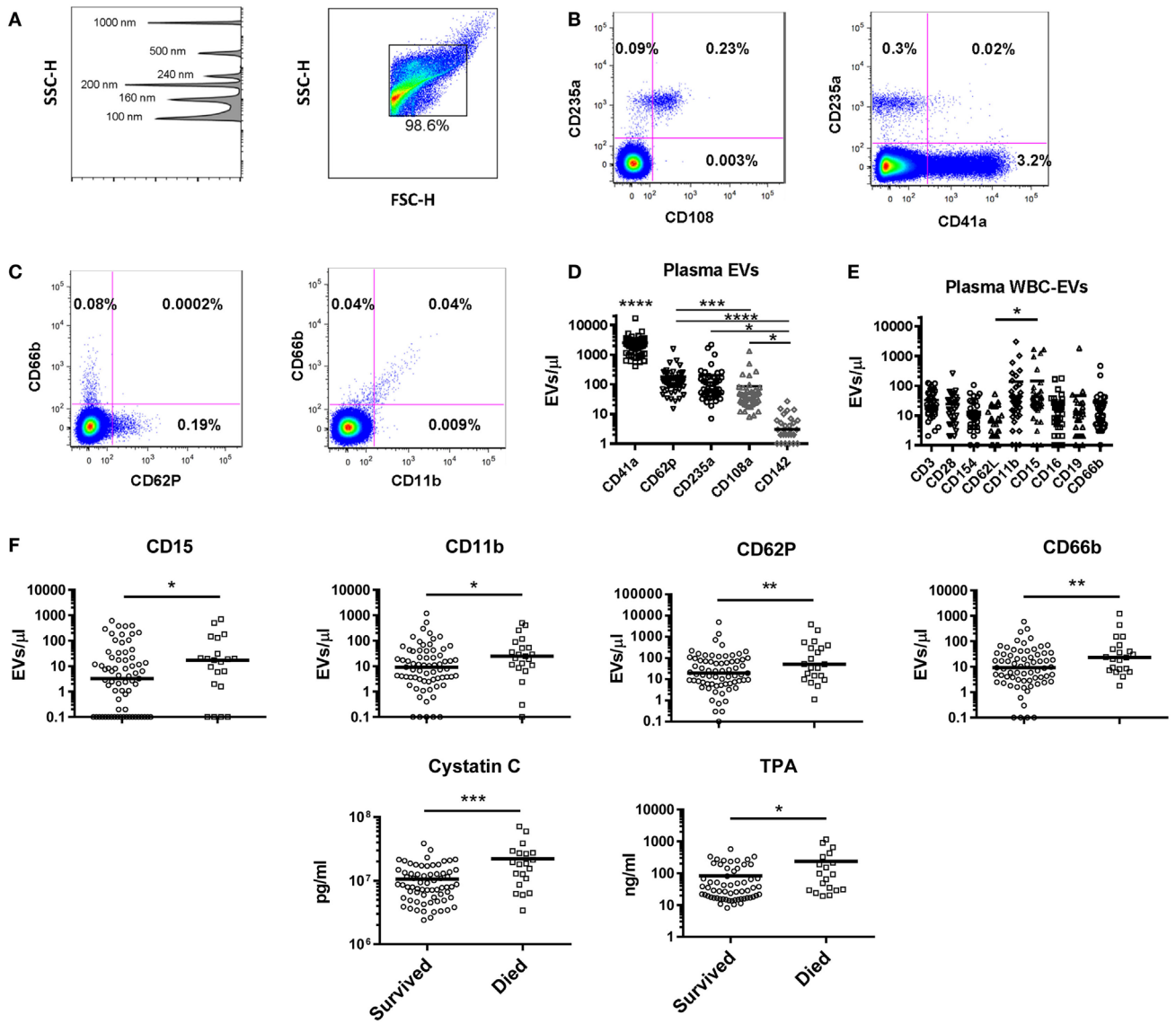

FIGURE 5 | Extracellular vesicles (EVs) in healthy controls and as predictors of mortality in intensive care unit patients. **(A)** Gating strategy for EVs shows detection of beads sized 100–1,000 nm on the SSC channel in the left panel, and gating of EVs in the right panel. Representative flow cytometry plots for **(B)** red blood cell (RBC) and **(C)** granulocyte markers are shown. **(D)** Levels of EVs were measured in 48 healthy control subjects using a panel of markers to identify EVs derived from platelets (CD41a and CD62P), RBCs (CD235a and CD108a), and endothelial cells (CD142). $CD41a^+$ EVs were significantly more abundant than all other populations ($p < 0.0001$); all other significant differences are noted on the graph. **(E)** White blood cell (WBC)-EVs were characterized based on cell of origin (CD3, CD16, CD19, CD66b) and expression of co-stimulatory (CD28 and CD154), and adhesion molecules (CD62L, CD11b, and CD15). **(F)** Of 62 parameters measured at baseline in 100 critically ill subjects, the 6 associated with 28-day mortality are shown, including EVs expressing four markers (CD15, CD11b, CD62P, and CD66b) (*$p < 0.05$, **$p < 0.01$, ***$p < 0.001$, and ****$p < 0.0001$).

was 22% in these subjects (**Table 1**). Elevated levels of six factors upon intensive care unit (ICU) admission were associated with subsequent mortality: cystatin C, TPA, and EVs bearing the markers CD15, CD11b, CD62P, or CD66b (**Figure 5F**).

DISCUSSION

In this article, we show that plasma-EVs biased primary monocytes toward an M1 profile and led to secretion of inflammatory mediators. Inspection of EVs from purified cell populations revealed that monocyte-, granulocyte-, and endothelial-EVs drove a pro-inflammatory monocyte response, with granulocyte-EVs inducing the broadest and highest magnitude response. In addition, platelet-EVs were the only population to induce monocyte production of the anti-inflammatory cytokine TGF-β, and RBC-EVs did not regulate cytokines and chemokines that we measured. The scavenger receptor CD36 is a potential receptor for RBC-EVs but not for the other EV subtypes tested. Finally, we showed that $CD66b^+$ granulocyte-EVs are early predictors of mortality in ICU patients.

Knowing that plasma-EVs are comprised of a heterogeneous mix of subtypes derived from distinct cells of origin (40–42), and to better understand which EVs in plasma bias monocytes to a pro-inflammatory phenotype, EVs were prepared from purified cell populations using routine procedures in a blood bank setting (RBC- and platelet-EVs), or by culturing unstimulated cells (monocyte-, granulocyte-, and endothelial-EVs) to avoid the effect of mitogens on EV cargo (43). Granulocyte-EVs were found to be the most potent pro-inflammatory agents of the EV subtypes studied, followed by monocyte- and endothelial-EVs in pro-inflammatory activity in our in vitro assays. Granulocyte-EVs have also been described to augment or suppress immune response (42, 43). Eken et al. have reported that EVs released by granulocytes induce a MerTK-dependent anti-inflammatory pathway in monocyte-derived macrophages (44). One difference between that study and the current work is that they stimulated purified granulocytes with fMLP to generate EVs. This stimulation could have affected the EV cargo and composition compared with EVs that are released during physiologic conditions or from granulocytes that were not stimulated (45). In contrast to the pro-inflammatory EVs, platelet-EVs induced TGF-β secretion by monocytes. TGF-β is a multifunctional cytokine with a dominant immunosuppressive activity. While it plays a positive role in tissue repair and in the control of autoimmune and infectious diseases, its upregulation may increase the growth of tumor cells (46). Platelet-EVs may have therapeutic value in tissue repair and downregulating the immune system in autoimmune diseases.

After demonstrating that plasma-EVs activated monocytes, we searched for antibodies that could block EV–monocyte binding. The RNA-Seq data showed the downregulation of a cluster of scavenger receptors on monocytes followed by their stimulation with total EVs. Two well-known scavenger receptors that were downregulated (*CD36* and *CD163*) and one whose gene transcription did not change (*CD206*) were selected for functional studies. Blockade of these receptors did not affect the binding of plasma-EVs to monocytes, though anti-CD36 antibody blocked RBC-EV binding to monocytes. A prior study has shown that endothelial-EVs bind to the scavenger receptor CD36 on platelets and contribute to thrombosis in mice (25). We found that the scavenger receptors CD36 and CD163 were downregulated on the cell surface of monocytes stimulated with plasma-EVs; however, a binding inhibition assay showed that only CD36 was involved in RBC-EV binding to monocytes. Given the relative lack of effect of RBC-EVs in our monocyte stimulation assays,

TABLE 1 | Baseline predictors of mortality.

Coagulation			Cytokines			Extracellular vesicles		
Parameter	***p* Value**	**HR (cb)**	**Parameter**	***p* Value**	**HR (cb)**	**Parameter**	***p* Value**	**HR (cb)**
PT	0.33	1.02 (0.97–1.08)	GM-CSF	0.059	0.70 (0.48–1.01)	EV concentration	0.83	1.04 (0.74–1.45)
PTT	0.085	1.01 (0.999–1.017)	IFN-γ	0.84	0.97 (0.73–1.29)	Annexin V	0.85	0.98 (0.80–1.20)
D-dimer	0.7	1.04 (0.86–1.25)	IL-10	0.84	1.03 (0.77–1.37)	CD3	0.78	1.04 (0.79–1.37)
Factor II	0.28	0.99 (0.97–1.01)	IL-12p70	0.84	1.06 (0.58–1.96)	CD14	0.56	1.06 (0.88–1.27)
Factor V	0.21	0.99 (0.98–1.004)	IL-17A	0.3	0.81 (0.54–1.21)	CD16	0.62	0.93 (0.70–1.24)
Factor VII	0.28	0.75 (0.45–1.26)	IL-1β	0.89	1.06 (0.45–2.49)	CD19	0.8	0.97 (0.76–1.24)
Factor VIII40	0.63	1.00 (0.998–1.003)	IL-2	0.62	0.85 (0.45–1.61)	CD28	0.22	1.11 (0.94–1.31)
Factor IX	0.96	1.00 (0.99–1.01)	IL-21	0.31	0.73 (0.40–1.34)	CD152	0.59	0.93 (0.72–1.21)
Factor X	0.95	0.99 (0.98–1.01)	IL-23	0.84	0.98 (0.78–1.22)	CD41a	0.32	1.12 (0.89–1.41)
ATIII	0.74	1.03 (0.88–1.20)	IL-6	0.62	0.92 (0.67–1.27)	CD62L	0.091	1.22 (0.97–1.55)
PC	0.18	0.90 (0.78–1.05)	IL-7	0.69	1.01 (0.94–1.09)	CD108a	0.71	0.94 (0.70–1.28)
FIB	0.26	0.99 (0.98–1.01)	IL-8	0.62	1.10 (0.75–1.61)	CD235a	0.98	1.00 (0.76–1.31)
TM	0.69	1.18 (0.51–2.73)	ITAC	0.92	0.98 (0.70–1.38)	CD11b	**0.01**	1.44 (1.09–1.91)
ECPR	0.72	1.01 (0.94–1.10)	MIP-1α	0.19	0.73 (0.46–1.17)	CD15	**0.021**	1.25 (1.03–1.52)
TPA	**0.011**	1.57 (1.10–2.22)	MIP-1β	0.24	0.70 (0.38–1.26)	CD62P	**0.008**	1.34 (1.08–1.66)
PAI-1	0.27	1.14 (0.93–1.44)	TNF-α	0.81	1.06 (0.67–1.67)	CD66b	**0.001**	1.60 (1.20–2.15)
			EGF	0.82	1.03 (0.77–1.39)			
			FGF	0.82	0.97 (0.72–1.30)	*Cellular immunity*		
			VEGF	0.29	1.10 (0.92–1.31)	Treg	0.098	1.25 (0.96–1.63)
			β2-Microglobulin	0.28	1.12 (0.91–1.31)	CD4-IL-7	0.21	2.30 (0.63–8.37)
			Cystatin C	**<0.0001**	1.04 (1.02–1.07)	CD8-IFN-γ	0.3	0.98 (0.94–1.02)
			MPO	0.26	1.19 (0.88–1.59)			
			PDFG AB/BB	0.59	1.05 (0.88–1.26)			
			RANTES	0.47	0.91 (0.70–1.18)			
			sICAM-1	0.57	1.01 (0.98–1.04)			
			sVCAM-1	0.084	1.02 (1.00–1.04)			

HR, hazard ratio; cb, confidence bound; PAI-1, plasminogen activator inhibitor type-1; TPA, tissue plasminogen activator; EV, extracellular vesicle.
Significant values in bold.
HRs reflect the change in the hazard that is associated with one unit of change in particular variables except as noted below.
10 units of change: GM-CSF, IFN-γ, IL-10, IL-23, IL-6, IL-8, ITAC, EGF, FGF, and VEGF.
100 units of change: PDFG AA/BB, CD3, CD14, CD16, CD19, CD28, CD152, CD62L, CD108a, CD11b, CD15, and CD66b.
1,000 units of change: RANTES, CD235a, CD62P, and annexin V.
10,000 units of change: MPO, sICAM-1, CD41a, and EV concentration.
1 million units of change: cystatin C.
10 million units of change: β2-microglobulin.

it is unclear how effective CD36 blockade would be in regulating immune changes potentially induced by transfusions rich in RBC-EVs, though other investigators have described RBC-EVs as having immune suppressive activity (9). Blockade of CD9, CD81, CD54, CD11a, CD51, and CD61 is reported to reduce EV uptake by dendritic cells (22). The interaction of lectin family members such as CD205 and CD209 has also been studied, and their blockade leads to reduced EV uptake (21, 23). In general, EV uptake cannot be prevented completely by blockade of one receptor, suggesting that several receptors are involved (12, 19, 21–24). TLRs have also been described to play a role in EV uptake. We tested antibodies against TLR1, TLR2, and TLR4, and they did not block EV–monocyte binding. It has been shown that tumor-exosomes control the expansion of myeloid-derived suppressor cells through TLR2 and not TLR4, which leads to secretion of IL-6 and suppression of $CD8^+$ T cells (18). However, it was found in another study that stimulation of the monocytic cell line THP1 with tumor-exosomes induced TNF-α, IL-1β, and IL-6 through TLR2 and TLR4 signaling (17).

In our *ex vivo* study on plasma samples from ICU patients, a panel of 43 cytokines and coagulation factors was examined, and only TPA and cystatin C were associated with mortality risk (47–52). TPA is involved with fibrinolysis and has been reported to be a marker for subsequent mortality in subjects hospitalized for acute dyspnea (50). Its significant release by endothelial cells after traumatic injury has been shown to result in excessive bleeding and hyperfibrinolysis, which are known risk factors for mortality (48, 49). Cystatin C is a cysteine protease inhibitor that plays a role in catabolism of proteins, and it has been widely described as being associated with mortality risk in various disease states (47, 51, 52). In addition, 4 of the 14 EV markers tested were associated with increased death risk in this population of critically ill patients who primarily presented with medical as opposed to surgical diagnoses (30). The existing literature is relatively scarce describing the prognostic potential of EVs as predictors of mortality. Our results indicate that CD66b, CD15, CD11b, and CD62P EVs were predictors of mortality in our cohort of patients. Of these, CD66b is the most specific and is a marker for granulocytes (53). CD15 is expressed on granulocytes and monocytes (54), and given that levels of the monocyte markers CD14 and CD16 were not associated with risk of death, it is likely that the CD15 EVs arose from granulocytes rather than monocytes. CD11b is expressed on many cell types including granulocytes, monocytes, and lymphocytes (55), so while elevated CD11b-expressing EVs is consistent with a granulocyte cell of origin, this marker is not specific. CD62P is an endothelial and platelet marker (56), and in this study EVs bearing the platelet marker CD41a were not associated with mortality risk. CD41a-expressing EVs have been reported to be positively or negatively associated with mortality in prior studies (57–59). Endothelial-EV markers were not measured in this study, though it is possible that CD62P EVs were derived from endothelial cells. The upregulation of endothelial-EVs has been described in patients with systemic inflammation due to sickle cell disease (27). Given the exploratory nature of the large panel of analytes studied, correlations were not corrected for multiple comparisons. The pattern of predominantly granulocyte-EVs correlating with mortality risk is suggestive that the correlations were not random, though future studies will be needed to confirm the association. Of note, WBC- and granulocyte-EVs were recently reported to be associated with subsequent mortality in a population of critically ill burn patients, increasing confidence in the validity of the association (29). Our data are consistent with a model in which EVs from various cell types signal circulating monocytes, which can synthesize these

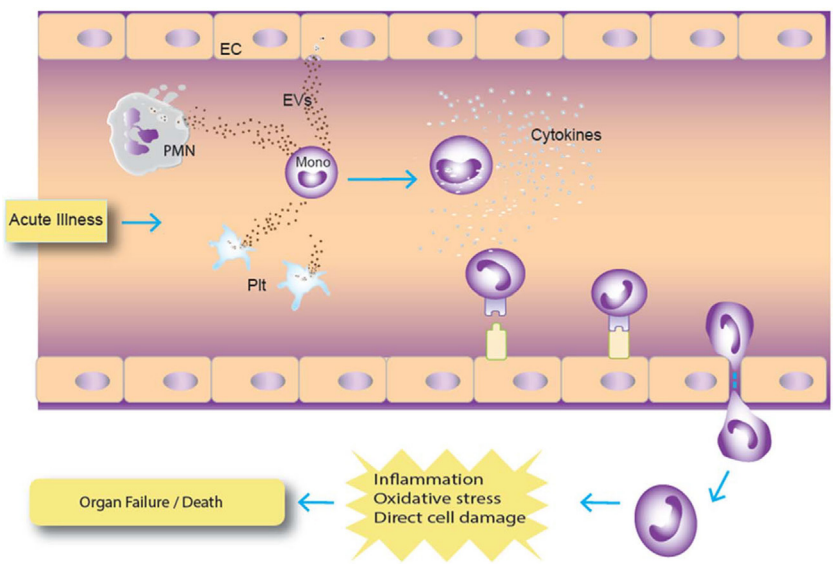

FIGURE 6 | Hypothetical model of extracellular vesicle (EV) interaction with monocytes. In this model, acute infection results in augmented release of EVs from cells, particularly granulocytes, which are ingested by monocytes. Activated monocytes can then differentiate and migrate to tissues, which can increase tissue inflammation and damage. Abbreviations: PMN, polymorphonuclear cell (granulocyte); Plt, platelet.

signals to become activated and potentially participate in tissue damage (**Figure 6**).

Here, we have shown by gene expression analysis that incubation of monocytes with EVs polarized monocytes toward a pro-inflammatory state. Of five EV subtypes that were tested, monocyte-, endothelial-, and granulocyte-EVs induced production of pro-inflammatory cytokines in monocytes, and granulocyte-EVs were the most potent inflammation trigger. Platelet-EVs induced production of the anti-inflammatory cytokine TGF-β and GM-CSF, and RBC-EVs did not regulate cytokines and chemokines that were measured. We demonstrated a role for the scavenger receptor CD36 in the binding of RBC-EVs to monocytes. Finally, we have shown granulocyte-EVs (expressing CD66b) were early predictors of mortality in ICU patients. Characterization of anti-inflammatory subtypes of EVs may have therapeutic applications in inflammatory diseases including critical illness, and pro-inflammatory EVs could potentially be harnessed as vaccine adjuvants or targeted for blockade to reduce inflammation during critical illness.

ETHICS STATEMENT

This study was carried out in accordance with the recommendations of the University of California, San Francisco Institutional Review Board with written informed consent from all subjects. All subjects gave written informed consent in accordance with the Declaration of Helsinki. The protocol was approved by the University of California, San Francisco Institutional Review Board.

AUTHOR CONTRIBUTIONS

AD designed, performed, and analyzed the *in vitro* experiments, designed the EV panels for patient samples, and wrote the manuscript. HI, RV, SK, JH, PS, and MC designed and/or performed analysis of patient samples. JL and PS provided clinical samples. MA-M, EJ, and SP assisted with design of laboratory methods. XD, AA, and KS designed and performed statistical analyses. PN designed and oversaw the project and wrote the manuscript.

ACKNOWLEDGMENTS

We thank the study coordinators at each clinical site, Irene Watpool, Tracy McArdle, and Marie-Claude Ferlan. We also thank Anne Eickelberg for graphic art support in creating **Figure 6** and Lani Montalvo for assistance with RNA quantification.

FUNDING

This work was supported by contracts from the Department of Defense W81SWH-10-1-0023, W81XWH-1-0028 and the National Institutes of Health, National Heart, Lung, and Blood Institute grants RO1 HL095470 and U01 HL072268.

SUPPLEMENTARY MATERIAL

The Supplementary Material for this article can be found online at https://www.frontiersin.org/articles/10.3389/fimmu.2018.00956/full#supplementary-material.

REFERENCES

1. Admyre C, Johansson SM, Qazi KR, Filen JJ, Lahesmaa R, Norman M, et al. Exosomes with immune modulatory features are present in human breast milk. *J Immunol* (2007) 179:1969–78. doi:10.4049/jimmunol.179.3.1969
2. Angelillo-Scherrer A. Leukocyte-derived microparticles in vascular homeostasis. *Circ Res* (2012) 110:356–69. doi:10.1161/CIRCRESAHA.110.233403
3. Gasper-Smith N, Crossman DM, Whitesides JF, Mensali N, Ottinger JS, Plonk SG, et al. Induction of plasma (TRAIL), TNFR-2, Fas ligand, and plasma microparticles after human immunodeficiency virus type 1 (HIV-1) transmission: implications for HIV-1 vaccine design. *J Virol* (2008) 82:7700–10. doi:10.1128/JVI.00605-08
4. Kolowos W, Gaipl US, Sheriff A, Voll RE, Heyder P, Kern P, et al. Microparticles shed from different antigen-presenting cells display an individual pattern of surface molecules and a distinct potential of allogeneic T-cell activation. *Scand J Immunol* (2005) 61:226–33. doi:10.1111/j.1365-3083.2005.01551.x
5. Rozmyslowicz T, Majka M, Kijowski J, Murphy SL, Conover DO, Poncz M, et al. Platelet- and megakaryocyte-derived microparticles transfer CXCR4 receptor to CXCR4-null cells and make them susceptible to infection by X4-HIV. *AIDS* (2003) 17:33–42. doi:10.1097/00002030-200301030-00006
6. Sheng H, Hassanali S, Nugent C, Wen L, Hamilton-Williams E, Dias P, et al. Insulinoma-released exosomes or microparticles are immunostimulatory and can activate autoreactive T cells spontaneously developed in nonobese diabetic mice. *J Immunol* (2011) 187:1591–600. doi:10.4049/jimmunol.1100231
7. Danesh A, Inglis HC, Jackman RP, Wu S, Deng X, Muench MO, et al. Exosomes from red blood cell units bind to monocytes and induce proinflammatory cytokines, boosting T-cell responses in vitro. *Blood* (2014) 123:687–96. doi:10.1182/blood-2013-10-530469
8. Camus SM, De Moraes JA, Bonnin P, Abbyad P, Le Jeune S, Lionnet F, et al. Circulating cell membrane microparticles transfer heme to endothelial cells and trigger vasoocclusions in sickle cell disease. *Blood* (2015) 125:3805–14. doi:10.1182/blood-2014-07-589283
9. Sadallah S, Eken C, Schifferli JA. Erythrocyte-derived ectosomes have immunosuppressive properties. *J Leukoc Biol* (2008) 84:1316–25. doi:10.1189/jlb.0108013
10. Barry OP, Pratico D, Savani RC, FitzGerald GA. Modulation of monocyte-endothelial cell interactions by platelet microparticles. *J Clin Invest* (1998) 102:136–44. doi:10.1172/JCI2592
11. Sadallah S, Eken C, Martin PJ, Schifferli JA. Microparticles (ectosomes) shed by stored human platelets downregulate macrophages and modify the development of dendritic cells. *J Immunol* (2011) 186:6543–52. doi:10.4049/jimmunol.1002788
12. Escrevente C, Keller S, Altevogt P, Costa J. Interaction and uptake of exosomes by ovarian cancer cells. *BMC Cancer* (2011) 11:108. doi:10.1186/1471-2407-11-108
13. Mulcahy LA, Pink RC, Carter DR. Routes and mechanisms of extracellular vesicle uptake. *J Extracell Vesicles* (2014) 3:24641–54. doi:10.3402/jev.v3.24641
14. Nazarenko I, Rana S, Baumann A, McAlear J, Hellwig A, Trendelenburg M, et al. Cell surface tetraspanin Tspan8 contributes to molecular pathways of exosome-induced endothelial cell activation. *Cancer Res* (2010) 70:1668–78. doi:10.1158/0008-5472.CAN-09-2470
15. Rana S, Yue S, Stadel D, Zoller M. Toward tailored exosomes: the exosomal tetraspanin web contributes to target cell selection. *Int J Biochem Cell Biol* (2012) 44:1574–84. doi:10.1016/j.biocel.2012.06.018
16. Christianson HC, Svensson KJ, van Kuppevelt TH, Li JP, Belting M. Cancer cell exosomes depend on cell-surface heparan sulfate proteoglycans for their internalization and functional activity. *Proc Natl Acad Sci U S A* (2013) 110:17380–5. doi:10.1073/pnas.1304266110
17. Bretz NP, Ridinger J, Rupp AK, Rimbach K, Keller S, Rupp C, et al. Body fluid exosomes promote secretion of inflammatory cytokines in monocytic cells via toll-like receptor signaling. *J Biol Chem* (2013) 288:36691–702. doi:10.1074/jbc.M113.512806

18. Chalmin F, Ladoire S, Mignot G, Vincent J, Bruchard M, Remy-Martin JP, et al. Membrane-associated Hsp72 from tumor-derived exosomes mediates STAT3-dependent immunosuppressive function of mouse and human myeloid-derived suppressor cells. *J Clin Invest* (2010) 120:457–71. doi:10.1172/JCI40483
19. Barres C, Blanc L, Bette-Bobillo P, Andre S, Mamoun R, Gabius HJ, et al. Galectin-5 is bound onto the surface of rat reticulocyte exosomes and modulates vesicle uptake by macrophages. *Blood* (2010) 115:696–705. doi:10.1182/blood-2009-07-231449
20. Feng D, Zhao WL, Ye YY, Bai XC, Liu RQ, Chang LF, et al. Cellular internalization of exosomes occurs through phagocytosis. *Traffic* (2010) 11:675–87. doi:10.1111/j.1600-0854.2010.01041.x
21. Hao S, Bai O, Li F, Yuan J, Laferte S, Xiang J. Mature dendritic cells pulsed with exosomes stimulate efficient cytotoxic T-lymphocyte responses and antitumour immunity. *Immunology* (2007) 120:90–102. doi:10.1111/j.1365-2567.2006.02483.x
22. Morelli AE, Larregina AT, Shufesky WJ, Sullivan ML, Stolz DB, Papworth GD, et al. Endocytosis, intracellular sorting, and processing of exosomes by dendritic cells. *Blood* (2004) 104:3257–66. doi:10.1182/blood-2004-03-0824
23. Obregon C, Rothen-Rutishauser B, Gerber P, Gehr P, Nicod LP. Active uptake of dendritic cell-derived exovesicles by epithelial cells induces the release of inflammatory mediators through a TNF-alpha-mediated pathway. *Am J Pathol* (2009) 175:696–705. doi:10.2353/ajpath.2009.080716
24. Tian T, Wang Y, Wang H, Zhu Z, Xiao Z. Visualizing of the cellular uptake and intracellular trafficking of exosomes by live-cell microscopy. *J Cell Biochem* (2010) 111:488–96. doi:10.1002/jcb.22733
25. Ghosh A, Li W, Febbraio M, Espinola RG, McCrae KR, Cockrell E, et al. Platelet CD36 mediates interactions with endothelial cell-derived microparticles and contributes to thrombosis in mice. *J Clin Invest* (2008) 118:1934–43. doi:10.1172/JCI34904
26. Sinning JM, Losch J, Walenta K, Bohm M, Nickenig G, Werner N. Circulating $CD31^+$/annexin V^+ microparticles correlate with cardiovascular outcomes. *Eur Heart J* (2011) 32:2034–41. doi:10.1093/eurheartj/ehq478
27. Shet AS, Aras O, Gupta K, Hass MJ, Rausch DJ, Saba N, et al. Sickle blood contains tissue factor-positive microparticles derived from endothelial cells and monocytes. *Blood* (2003) 102:2678–83. doi:10.1182/blood-2003-03-0693
28. Ohuchi M, Fujino K, Kishimoto T, Yamane T, Hamamoto T, Tabata T, et al. Association of the plasma platelet-derived microparticles to platelet count ratio with hospital mortality and disseminated intravascular coagulopathy in critically ill patients. *J Atheroscler Thromb* (2015) 22:773–82. doi:10.5551/jat.29439
29. O'Dea KP, Porter JR, Tirlapur N, Katbeh U, Singh S, Handy JM, et al. Circulating microvesicles are elevated acutely following major burns injury and associated with clinical severity. *PLoS One* (2016) 11:e0167801. doi:10.1371/journal.pone.0167801
30. Lacroix J, Hébert PC, Fergusson DA, Tinmouth A, Cook DJ, Marshall JC, et al. Age of transfused blood in critically ill adults. *N Engl J Med* (2015) 372:1410–8. doi:10.1056/NEJMoa1500704
31. Inglis HC, Danesh A, Shah A, Lacroix J, Spinella PC, Norris PJ. Techniques to improve detection and analysis of extracellular vesicles using flow cytometry. *Cytometry A* (2015) 87:1052–63. doi:10.1002/cyto.a.22649
32. Baj-Krzyworzeka M, Baran J, Weglarczyk K, Szatanek R, Szaflarska A, Siedlar M, et al. Tumour-derived microvesicles (TMV) mimic the effect of tumour cells on monocyte subpopulations. *Anticancer Res* (2010) 30:3515–9.
33. Vasina EM, Cauwenberghs S, Feijge MA, Heemskerk JW, Weber C, Koenen RR. Microparticles from apoptotic platelets promote resident macrophage differentiation. *Cell Death Dis* (2011) 2:e211. doi:10.1038/cddis.2011.94
34. Martinez FO, Gordon S, Locati M, Mantovani A. Transcriptional profiling of the human monocyte-to-macrophage differentiation and polarization: new molecules and patterns of gene expression. *J Immunol* (2006) 177:7303–11. doi:10.4049/jimmunol.177.10.7303
35. Etzerodt A, Berg RM, Plovsing RR, Andersen MN, Bebien M, Habbeddine M, et al. Soluble ectodomain CD163 and extracellular vesicle-associated CD163 are two differently regulated forms of 'soluble CD163' in plasma. *Sci Rep* (2017) 7:40286. doi:10.1038/srep40286
36. Schiller M, Parcina M, Heyder P, Foermer S, Ostrop J, Leo A, et al. Induction of type I IFN is a physiological immune reaction to apoptotic cell-derived membrane microparticles. *J Immunol* (2012) 189:1747–56. doi:10.4049/jimmunol.1100631
37. Graversen JH, Madsen M, Moestrup SK. CD163: a signal receptor scavenging haptoglobin-hemoglobin complexes from plasma. *Int J Biochem Cell Biol* (2002) 34:309–14. doi:10.1016/S1357-2725(01)00144-3
38. Liu C, Zhao W, Christ GJ, Gladwin MT, Kim-Shapiro DB. Nitric oxide scavenging by red cell microparticles. *Free Radic Biol Med* (2013) 65:1164–73. doi:10.1016/j.freeradbiomed.2013.09.002
39. Moseman AP, Moseman EA, Schworer S, Smirnova I, Volkova T, von Andrian U, et al. Mannose receptor 1 mediates cellular uptake and endosomal delivery of CpG-motif containing oligodeoxynucleotides. *J Immunol* (2013) 191:5615–24. doi:10.4049/jimmunol.1301438
40. Mathivanan S, Ji H, Simpson RJ. Exosomes: extracellular organelles important in intercellular communication. *J Proteomics* (2010) 73:1907–20. doi:10.1016/j.jprot.2010.06.006
41. Piccin A, Murphy WG, Smith OP. Circulating microparticles: pathophysiology and clinical implications. *Blood Rev* (2007) 21:157–71. doi:10.1016/j.blre.2006.09.001
42. Sadallah S, Eken C, Schifferli JA. Ectosomes as immunomodulators. *Semin Immunopathol* (2011) 33:487–95. doi:10.1007/s00281-010-0232-x
43. Johnson BL III, Kuethe JW, Caldwell CC. Neutrophil derived microvesicles: emerging role of a key mediator to the immune response. *Endocr Metab Immune Disord Drug Targets* (2014) 14:210–7. doi:10.2174/1871530314666140722083717
44. Eken C, Sadallah S, Martin PJ, Treves S, Schifferli JA. Ectosomes of polymorphonuclear neutrophils activate multiple signaling pathways in macrophages. *Immunobiology* (2013) 218:382–92. doi:10.1016/j.imbio.2012.05.021
45. Dalli J, Montero-Melendez T, Norling LV, Yin X, Hinds C, Haskard D, et al. Heterogeneity in neutrophil microparticles reveals distinct proteome and functional properties. *Mol Cell Proteomics* (2013) 12:2205–19. doi:10.1074/mcp.M113.028589
46. Akdis M, Aab A, Altunbulakli C, Azkur K, Costa RA, Crameri R, et al. Interleukins (from IL-1 to IL-38), interferons, transforming growth factor beta, and TNF-alpha: receptors, functions, and roles in diseases. *J Allergy Clin Immunol* (2016) 138(4):984–1010. doi:10.1016/j.jaci.2016.06.033
47. Bell M, Granath F, Martensson J, Lofberg E, Ekbom A, Martling CR, et al. Cystatin C is correlated with mortality in patients with and without acute kidney injury. *Nephrol Dial Transplant* (2009) 24:3096–102. doi:10.1093/ndt/gfp196
48. Cardenas JC, Matijevic N, Baer LA, Holcomb JB, Cotton BA, Wade CE. Elevated tissue plasminogen activator and reduced plasminogen activator inhibitor promote hyperfibrinolysis in trauma patients. *Shock* (2014) 41:514–21. doi:10.1097/SHK.0000000000000161
49. Chapman MP, Moore EE, Moore HB, Gonzalez E, Gamboni F, Chandler JG, et al. Overwhelming tPA release, not PAI-1 degradation, is responsible for hyperfibrinolysis in severely injured trauma patients. *J Trauma Acute Care Surg* (2016) 80:16–23; discussion 23–15. doi:10.1097/TA.0000000000000885
50. Lund N, Gransbo K, Wernersson C, Melander O. Cardiometabolic biomarkers are predictors of readmission and death in patients hospitalized for acute dyspnea. *Am J Emerg Med* (2017) 35:610–4. doi:10.1016/j.ajem.2016.12.048
51. Senturk GO, Unluer EE, Vandenberk N, Yavasi O, Eroglu O, Surum N, et al. The prognostic value of cystatin C compared with trauma scores in multiple blunt trauma: a prospective cohort study. *J Emerg Med* (2013) 44:1070–6. doi:10.1016/j.jemermed.2012.11.037
52. Yang S, Song L, Zhao L, Dong P, Lai L, Wang H. Predictive value of cystatin C in people with suspected or established coronary artery disease: a meta-analysis. *Atherosclerosis* (2017) 263:60–7. doi:10.1016/j.atherosclerosis.2017.05.025
53. Skubitz KM, Campbell KD, Ahmed K, Skubitz AP. CD66 family members are associated with tyrosine kinase activity in human neutrophils. *J Immunol* (1995) 155:5382–90.
54. Larsen E, Palabrica T, Sajer S, Gilbert GE, Wagner DD, Furie BC, et al. PADGEM-dependent adhesion of platelets to monocytes and neutrophils is mediated by a lineage-specific carbohydrate, LNF III (CD15). *Cell* (1990) 63:467–74. doi:10.1016/0092-8674(90)90443-I
55. Mazzone A, Ricevuti G. Leukocyte CD11/CD18 integrins: biological and clinical relevance. *Haematologica* (1995) 80:161–75.

56. McEver RP. Regulation of function and expression of P-selectin. *Agents Actions Suppl* (1995) 47:117–9.
57. Curry N, Raja A, Beavis J, Stanworth S, Harrison P. Levels of procoagulant microvesicles are elevated after traumatic injury and platelet microvesicles are negatively correlated with mortality. *J Extracell Vesicles* (2014) 3:25625. doi:10.3402/jev.v3.25625
58. Jacoby RC, Owings JT, Holmes J, Battistella FD, Gosselin RC, Paglieroni TG. Platelet activation and function after trauma. *J Trauma* (2001) 51:639–47. doi:10.1097/00005373-200110000-00003
59. Matijevic N, Wang YW, Holcomb JB, Kozar R, Cardenas JC, Wade CE. Microvesicle phenotypes are associated with transfusion requirements and mortality in subjects with severe injuries. *J Extracell Vesicles* (2015) 4:29338. doi:10.3402/jev.v4.29338

Conflict of Interest Statement: The authors declare that the research was conducted in the absence of any commercial or financial relationships that could be construed as a potential conflict of interest.

The reviewer AB and handling Editor declared their shared affiliation.

frontiers in Immunology

ORIGINAL RESEARCH
published: 19 February 2018
doi: 10.3389/fimmu.2018.00272

Extracellular Vesicles Released from *Mycobacterium tuberculosis*-Infected Neutrophils Promote Macrophage Autophagy and Decrease Intracellular Mycobacterial Survival

Violeta D. Alvarez-Jiménez[1], Kahiry Leyva-Paredes[1], Mariano García-Martínez[1], Luis Vázquez-Flores[1], Víctor Gabriel García-Paredes[1], Marcia Campillo-Navarro[1,2], Israel Romo-Cruz[3], Víctor Hugo Rosales-García[4,5], Jessica Castañeda-Casimiro[1], Sirenia González-Pozos[5], José Manuel Hernández[3], Carlos Wong-Baeza[6], Blanca Estela García-Pérez[1], Vianney Ortiz-Navarrete[7], Sergio Estrada-Parra[1], Jeanet Serafín-López[1], Isabel Wong-Baeza[1], Rommel Chacón-Salinas[1,8] and Iris Estrada-García[1]**

[1] Departamento de Inmunología, Escuela Nacional de Ciencias Biológicas (ENCB), Instituto Politécnico Nacional (IPN), Mexico City, Mexico, [2] Departamento de Fisiología y Farmacología, Facultad de Medicina Veterinaria y Zootecnia, Universidad Nacional Autónoma de México (UNAM), Mexico City, Mexico, [3] Departamento de Biología Celular, Centro de Investigación y de Estudios Avanzados del Instituto Politécnico Nacional (CINVESTAV-IPN), Mexico City, Mexico, [4] Laboratorio de Citometría de Flujo de Diagnóstico Molecular de Leucemias y Terapia Celular SA. De CV. (DILETEC), Mexico City, Mexico, [5] Laboratorios Nacionales de Servicios Experimentales (LANSE), Centro de Investigación y de Estudios Avanzados del Instituto Politécnico Nacional (CINVESTAV-IPN), Mexico City, Mexico, [6] Departamento de Bioquímica, Escuela Nacional de Ciencias Biológicas (ENCB), Instituto Politécnico Nacional (IPN), Mexico City, Mexico, [7] Departamento de Biomedicina Molecular, Centro de Investigación y de Estudios Avanzados del Instituto Politécnico Nacional (CINVESTAV-IPN), Mexico City, Mexico, [8] Unidad de Desarrollo e Investigación en Bioprocesos (UDIBI), Escuela Nacional de Ciencias Biológicas (ENCB), Instituto Politécnico Nacional (IPN), Mexico City, Mexico

OPEN ACCESS

Edited by:
Christopher Gregory, University of Edinburgh, United Kingdom

Reviewed by:
Maria Cecilia G. Marcondes, San Diego Biomedical Research Institute, United States
Bruce Milne Hall, University of New South Wales, Australia

***Correspondence:**
Rommel Chacón-Salinas
rommelchacons@yahoo.com.mx;
Iris Estrada-García
iestrada5@hotmail.com

Specialty section:
This article was submitted to Immunological Tolerance and Regulation, a section of the journal Frontiers in Immunology

Received: *03 November 2017*
Accepted: *30 January 2018*
Published: *19 February 2018*

Citation:
Alvarez-Jiménez VD, Leyva-Paredes K, García-Martínez M, Vázquez-Flores L, García-Paredes VG, Campillo-Navarro M, Romo-Cruz I, Rosales-García VH, Castañeda-Casimiro J, González-Pozos S, Hernández JM, Wong-Baeza C, García-Pérez BE, Ortiz-Navarrete V, Estrada-Parra S, Serafín-López J, Wong-Baeza I, Chacón-Salinas R and Estrada-García I (2018) Extracellular Vesicles Released from Mycobacterium tuberculosis-Infected Neutrophils Promote Macrophage Autophagy and Decrease Intracellular Mycobacterial Survival. Front. Immunol. 9:272. doi: 10.3389/fimmu.2018.00272

Tuberculosis is an infectious disease caused by *Mycobacterium tuberculosis* (Mtb). In the lungs, macrophages and neutrophils are the first immune cells that have contact with the infecting mycobacteria. Neutrophils are phagocytic cells that kill microorganisms through several mechanisms, which include the lytic enzymes and antimicrobial peptides that are found in their lysosomes, and the production of reactive oxygen species. Neutrophils also release extracellular vesicles (EVs) (100–1,000 nm in diameter) to the extracellular milieu; these EVs consist of a lipid bilayer surrounding a hydrophilic core and participate in intercellular communication. We previously demonstrated that human neutrophils infected *in vitro* with Mtb H37Rv release EVs (EV-TB), but the effect of these EVs on other cells relevant for the control of Mtb infection, such as macrophages, has not been completely analyzed. In this study, we characterized the EVs produced by non-stimulated human neutrophils (EV-NS), and the EVs produced by neutrophils stimulated with an activator (PMA), a peptide derived from bacterial proteins (fMLF) or Mtb, and observed that the four EVs differed in their size. Ligands for toll-like receptor (TLR) 2/6 were detected in EV-TB, and these EVs favored a modest increase in the expression of the co-stimulatory molecules CD80, a

higher expression of CD86, and the production of higher amounts of TNF-α and IL-6, and of lower amounts of TGF-β, in autologous human macrophages, compared with the other EVs. EV-TB reduced the amount of intracellular Mtb in macrophages, and increased superoxide anion production in these cells. TLR2/6 ligation and superoxide anion production are known inducers of autophagy; accordingly, we found that EV-TB induced higher expression of the autophagy-related marker LC3-II in macrophages, and the co-localization of LC3-II with Mtb inside infected macrophages. The intracellular mycobacterial load increased when autophagy was inhibited with wortmannin in these cells. In conclusion, our results demonstrate that neutrophils produce different EVs in response to diverse activators, and that EV-TB activate macrophages and promote the clearance of intracellular Mtb through early superoxide anion production and autophagy induction, which is a novel role for neutrophil-derived EVs in the immune response to Mtb.

Keywords: extracellular vesicles, neutrophils, tuberculosis, macrophage, autophagy

INTRODUCTION

Tuberculosis is an infectious disease that causes more than a million deaths per year worldwide. The infection with *Mycobacterium tuberculosis* (Mtb) is transmitted by aerosols, and macrophages are the first immune cells that have contact with Mtb in lung alveoli, through their toll-like receptors (TLRs), NOD-like receptors, and C-type lectin-like receptors (1). The binding of these receptors with their ligands induces Mtb phagocytosis and the production of pro-inflammatory cytokines, including TNF-α, IL-6, IL-8, and IL-1β, which promote activation and migration of other immune cells, such as neutrophils, to the infected site (2, 3). Neutrophils are the most abundant phagocytic cells of the innate immune system and are crucial for the immune response to Mtb, since the absence of neutrophils accelerates death in Mtb-infected mice (4). Patients with active pulmonary tuberculosis present abundant neutrophils in sputum samples and bronchoalveolar lavages, which indicates that these cells are relevant during human infection with Mtb (5). Neutrophils phagocytose Mtb and kill them in the phagolysosome, which contains several antimicrobial molecules, such as myeloperoxidase, neutral proteinases (mainly cathepsin G, elastase, and proteinase 3), bactericidal/permeability-increasing protein and defensins (6, 7). In addition, neutrophils are able to trap Mtb in neutrophil extracellular traps (NETs), although they are unable to eliminate the mycobacteria (8). Moreover, neutrophils cooperate with other cellular elements of the immune response, such as dendritic cells (DCs), which mount T cell responses to mycobacteria (9).

Neutrophils participate in several intercellular communication networks. One of these networks has attracted interest in recent years and involves the release of extracellular vesicles (EVs) to the extracellular milieu. Human neutrophil-derived EVs were first described when these cells were incubated with sublytic doses of complement (10). The EVs that are released by neutrophils are formed by a lipid bilayer with trans-membrane proteins, which limits an internal milieu with hydrophilic components; this membrane is derived from the neutrophil cellular membrane, so these EVs are classified as ectosomes. Neutrophil-derived EVs have phosphatidylserine in the outer layer of their membranes, and also contain CR1/CD35, LFA-1/CD11a, CD11b, FcγRIII/CD16, L-selectin, HLA class I, CD66b, DAF/CD55, and CD59 (11); their diameter ranges from 100 to 1,000 nm, and they participate in intercellular communication, modulating several biological processes (12). For example, neutrophil-derived EVs decrease the phagocytic capacity and the expression of CD80 and CD86 and increase the expression of TGF-β1, in immature DCs, thus promoting a low T cell-activating capacity in mature DCs (13). Neutrophil ectosomes contain the enzymes myeloperoxidase, elastase, matrix metalloproteinase 9 and proteinase 3, which suggests that neutrophil-derived ectosomes are "ecto-organelles" with antimicrobial activity against opsonized microorganisms in the extracellular milieu (14). In fact, recent studies showed that neutrophil-derived EVs contain antimicrobial proteins from the neutrophil granules, and that these EVs form integrin-dependent aggregates with *Staphylococcus aureus*, impairing bacterial growth (15). Our group demonstrated for the first time that human neutrophils infected *in vitro* with Mtb H37Rv release EVs with a diameter of 500–1,000 nm, and that these EVs express CD35, phosphatidylserine, gp91Phox, Rab5, Rab7, and a subunit of cytochrome b555 (16). However, the effect of these EVs on other cells that are present at the infected site, such as macrophages, is not completely understood. Therefore, we investigated the effect of EVs derived from Mtb-infected neutrophils on human macrophages. In this study, we characterized the EVs released by non-stimulated human neutrophils ("spontaneous" EVs), and those released by neutrophils stimulated with an activator (PMA), a peptide derived from bacterial proteins (fMLF) or an intracellular pathogen (Mtb), in terms of their size and heterogeneity and their TLR-ligand content. We also evaluated the ability of these different types of EVs to affect cytokine, superoxide anion and NO production, and the expression of costimulatory molecules on macrophages, and determined if the EVs altered the intracellular growth of Mtb and the cellular mechanism involved in this intracellular killing of Mtb.

MATERIALS AND METHODS

Mtb Culture

Mycobacterium tuberculosis H37Rv (Mtb) TMC 102 strain was grown in Middlebrook 7H9 (BD BBL, NJ, USA) with 10% glycerol and 10% OADC (BD BBL, NJ, USA) for 4 weeks at 37°C, until the logarithmic phase was reached. Bacteria were harvested by centrifugation and stored in DMEM (Gibco, CA, USA) with 10% FCS (Gibco) at −70°C.

Preparation of Human Neutrophil and Macrophage Cultures

Peripheral blood was obtained by venipuncture from healthy volunteers, which signed an informed consent form. This study was approved by the Bioethics Committee of ENCB-IPN (CEI-ENCB 114 011/2013). Fifteen milliliters of peripheral blood were collected in tubes with heparin (BD Vacutainer). Neutrophils were separated by gradient centrifugation on Histopaque 1119-Percoll (Sigma-Aldrich, MO, USA), according to Aga et al. (17). All neutrophil cultures had purity and viability of at least 98%. Monocytes were separated by gradient centrifugation on Histopaque 1077 (Sigma-Aldrich). To obtain macrophages, monocytes were resuspended in RPMI (Gibco) with penicillin (100 U/ml), streptomycin (100 µg/ml), and L-glutamine (2 mM), and placed in 24-well culture plates (2×10^6 cells/well) at 37°C and 5% CO_2 for 2 h. Wells were washed three times with warm RPMI and cultured in RPMI with 10% FCS at 37°C and 5% CO_2 overnight. GM-CSF (5 ng/ml, PeproTech, NJ, USA) was added on days 1 and 3, and after 7–10 days, macrophage differentiation was confirmed by flow cytometry analysis. The cells were stained with anti-CD14/APC (clone: HCD14), anti-CD11b/PB (clone: 3.9), HLA-DR/FITC (clone: L243), and anti-CD86/PE-Cy7 (clone: IT2.2) (all from BioLegend, CA, USA); macrophages were CD14+ CD11b+ HLA-DR+ CD86+ (data not shown). Data were analyzed on a BD LSR Fortessa with BD FACSDiva software v. 6.0; data were analyzed with FlowJo software v.7.6 (FlowJo LLC, OR, USA). The neutrophils and the macrophages in each experiment were derived from the same donor.

Production, Concentration, and Characterization of Neutrophil-Derived EVs

Neutrophils (10×10^6 cells/ml in DMEM) were stimulated with 10 nM phorbol 12-myristate 13-acetate (PMA) (Sigma-Aldrich), or with 1 µM *N*-formylmethionyl-leucyl-phenylalanine synthetic peptide (fMLF) (Sigma-Aldrich), or with Mtb at a multiplicity of infection (MOI) of 10 viable bacteria per cell. Neutrophils were incubated at 37°C and 5% CO_2 for the indicated times. To determine if neutrophil apoptosis is induced under these conditions, apoptosis was evaluated after 30 min of stimulation with PMA, fMLF or Mtb; dexamethasone (100 ng/ml) (Chinoin, Mexico) was used as positive control. Neutrophils were then stained with annexin V/APC (BioLegend) and propidium iodide (BioLegend) and analyzed by flow cytometry. To concentrate EVs from culture supernatants, the supernatants (from neutrophils stimulated with PMA, fMLF, or Mtb, or from non-stimulated neutrophils) were centrifuged, sequentially, at $300 \times g$ for 10 min, $2{,}000 \times g$ for 10 min and ultra-centrifuged at $160{,}000 \times g$ for 60 min in an SW40Ti rotor (Beckman Coulter, CA, USA). The concentrated EVs were resuspended in 50 µl of 0.2 µm-filtered PBS. EVs were stored for no more than 24 h at 4°C before performing the experiments. Determination of the protein concentration in EVs: EVs were lysed with 0.2% SDS and analyzed with the micro-bicinchoninic acid method (ThermoFisher Scientific, MA, USA), according to the manufacturer's protocol. For all the experiments, the EV suspensions were adjusted to 30 µg of protein per ml of 0.2 µm-filtered PBS. *Analysis of EVs by flow cytometry*: neutrophils were incubated for 10 min with CellVue Jade (Polysciences, PA, USA), a dye that binds phospholipids, and washed with 0.2% BSA in 0.2 µm filtered PBS. The released EVs with the different stimuli (30 µg) were incubated with 5 µl of antihuman CD35/PE (clone: E11) (BioLegend), 5 µl of annexin V/PE-Cy7 (BioLegend), or 5 µl of anti-mouse IgG/PE (isotype control, BioLegend) at 4°C for 1 h. The samples were stored at 4°C until acquisition. EVs were acquired on low flow speed, at a rate of less than 50 events per second on a flow cytometer CytoFLEX S (Beckman Coulter). Basal fluorescence was set with 0.2 µm-filtered PBS (to evaluate electronic noise). To set an acceptable forward-scatter (FSC) range suitable for discriminating electronic noise from EVs, we employed Megamix-Plus FSC beads (BioCytex, Marseille, France), which have different sizes (0.1, 0.3, 0.5, and 0.9 µm.) and are recommended for daily standardization for microparticle measurement on the CytoFLEX (18). The threshold was set to limit the analysis to CellVue Jade-positive events. EVs were detected using violet side scatter (VSSC), which has a greater sensitivity to detect small events; FSC and VSSC scales were set in logarithmic mode, with a threshold of 200 arbitrary units for FSC, and the EV gate was set using microbeads (Megamix-Plus). At least 50,000 total events were acquired for each sample, and the data were analyzed with Kaluza Software 1.3v (Beckman Coulter). *Analysis of EVs by nanoparticle tracking analysis (NTA)*: EVs were resuspended in 1 ml of 0.2 µm-filtered PBS, and analyzed in a NanoSight NS 300 (Malvern Instruments Ltd., Malvern, UK). Latex spheres of 100, 200, and 400 nm (Malvern Instruments) were used to calibrate the equipment. Analysis of EVs by transmission electron microscopy (TEM): EVs were obtained as previously described, with an extra centrifugation of $10{,}000 \times g$ for 30 min before ultra-centrifugation at $160{,}000 \times g$ to improve TEM images. After ultra-centrifugation, EVs were resuspended in 0.2 µm-filtered PBS and fixed with 1% glutaraldehyde for 20 min. The sample was then absorbed for 2 min on a nickel mesh grid, previously shaded with polyvinyl formal and carbon. After washing, EVs were stained with 2% uranyl acetate, and the mesh grid was observed in a JEM 1400 electron microscope (JEOL USA Inc., MA, USA).

Detection of TLR ligands in EVs: 2×10^5 HEK cells, stably transfected with human TLR2/6, 4, or 5 (InvivoGen, CA, USA), were stimulated with EVs (30 µg of total protein) that were produced by non-stimulated neutrophils (EV-NS), or by neutrophils stimulated with PMA (EV-PMA), fMLF (EV-fMLF), or Mtb (EV-TB) for 30 min. As positive controls, cells were stimulated with

Zymosan (InvivoGen, 10 μg/ml) for TLR2/6 activation, lipopolysaccharide (LPS) from *Escherichia coli* O111:B4 (InvivoGen, 10 μg/ml) for TLR4 activation, and flagellin from *Salmonella typhimurium* (InvivoGen, 10 μg/ml) for TLR5 activation. After 24 h, supernatants were collected, and IL-8 was quantified by ELISA (BioLegend), according to the manufacturer's protocol.

Cytokine Production and Activation of Macrophages in Response to Neutrophil-Derived EVs

Extracellular vesicles (30 μg total protein/ml), which were produced by non-stimulated neutrophils (EV-NS), or by neutrophils stimulated with PMA (EV-PMA), fMLF (EV-fMLF), or Mtb (EV-TB) for 30 min, were used to stimulate macrophages (2×10^5) for 24 h. As controls, the macrophages were left with medium alone (NS) or were infected with Mtb (2×10^6). After this incubation, the supernatants were collected, centrifuged at $400 \times g$ at 4°C and stored at −20°C until analysis. IL-1β, IL-6, IL-10, and TNF-α were measured with a cytometric bead array (BD), and TGF-β was measured with an ELISA Kit (BioLegend), according to the manufacturer's protocol. In the same experiments, macrophages (detached from the culture plate with cold PBS) were washed and centrifuged at $400 \times g$ at 4°C, and stained with anti-CD14/APC, Lin1 (anti-CD3, CD14, CD16, CD19, CD20 and CD56)/FITC, anti-HLA-DR/FITC, anti-CD1a/PE, anti-CD11c/PB, anti-CD80/PE-Cy5, anti-CD86/PE-Cy7, and the corresponding isotype controls (BioLegend), for 15 min at 4°C. Cells were then washed with 1% BSA in PBS and analyzed by flow cytometry.

Determination of Mtb CFU in Mtb-Infected Macrophages (IM)

Macrophages (2×10^5) were plated in triplicates on 24-well plates, infected with Mtb (2×10^6) for 2 h at 37°C, washed three times with HBSS, and treated with 8 μg/ml amikacin for 2 h (to eliminate extracellular Mtb). Cells were then washed three times with HBSS and stimulated with EVs (30 μg of total protein per ml) for 4 h. Cells were washed with PBS and incubated for 24 or 48 h. The cells were then lysed with 0.2% SDS for 5 min, and the lysis was stopped with 500 μl of 5% albumin. In some experiments, 50 μg/ml rapamycin (Sigma-Aldrich) was added instead of EVs to induce autophagy, and 150 nM wortmannin (Sigma-Aldrich) was added after EV treatment as an autophagy inhibitor.

Intracellular CFU were determined by serial dilutions in PBS, which were plated on Middlebrook-7H10 agar supplemented with glycerol and OADC. Agar plates were incubated at 37°C for 2 weeks. For each time point in each repetition of the experiment, CFU were determined from three different wells.

Quantification of Superoxide Anion and NO in Mtb-IM

Macrophages (2×10^5) were infected with Mtb (2×10^6) for 2 h. After this incubation, the cells were washed with PBS, treated with 8 μg/ml amikacin for 2 h, and incubated with EVs (EV-NS, EV-PMA, EV-fMLF, or EV-TB) for 4 h. To quantify superoxide anion, cells were washed with PBS and incubated for 15, 30, and 45 min and 1–6 h, in the presence of nitro blue tetrazolium (Sigma-Aldrich), as previously reported (19). NO was quantified using the Griess reagent (Promega, WI, USA), at 1, 2, 4, and 6 h, according to the manufacturer's protocol. In some cases, NADPH oxidase was inhibited with diphenyliodonium chloride (DPI) (Sigma-Aldrich) before the stimulus with EVs.

Detection of the Autophagy Marker LC3-II in Macrophages

To determine if EVs induce LC3-II expression, macrophages (2×10^5) were incubated with EVs (EV-NS, EV-PMA, EV-fMLF, or EV-TB) (30 μg/ml) for 4 h. As a positive control for autophagy induction, macrophages were treated with 5 μg/ml of peptidoglycan (Sigma-Aldrich) for 4 h. The cells were then stained with anti-LC3-II (goat anti-MAP LC3 α/β, Santa Cruz Biotechnology, Inc., Midland, ON, Canada) (green) and DAPI (Vector Laboratories, CA, USA) (blue) and examined in a confocal microscope (LSM5 Pascal, Zeiss, Oberkochen, Germany) to determine LC3-II mean fluorescence intensity (MFI). At least 100 cells from each condition were analyzed, and the MFI of LC3-II was calculated using Zeiss LSM image Browser software v.4.2 (Informer Technologies, Inc., Madrid, Spain). To determine if EVs induce the co-localization of LC3-II with Mtb, macrophages (2×10^5) were infected with Mtb (2×10^6) previously stained with CellVue Maroon (Polysciences). After this incubation, the cells were washed with PBS and left untreated (IM), or were incubated with EVs (EV-NS, EV-PMA, EV-fMLF, or EV-TB) for 4 h. The cells were fixed with 4% paraformaldehyde for 20 min at 4°C. Cells were then permeabilized and blocked for 30 min with 4% BSA and 0.25% SDS/Triton X-100, and incubated with primary (goat anti-MAP LC3 α/β) and secondary (donkey anti-goat IgG/FITC, Santa Cruz Biotechnology) antibodies. The slides were mounted with VECTASHIELD with DAPI (Vector Laboratories, CA, USA) and examined in an inverted confocal microscope (LSM5 Pascal, Zeiss). At least 50 cells from each condition were counted, and the percentage of cells with LC3-II+ puncta (autophagosomes) was calculated.

Ethical Statement

This human study was approved by the Bioethics Committee of Escuela Nacional de Ciencias Biológicas from the Instituto Poltécnico Nacional (CEI-ENCB 011/2013). All written informed consents were received from participants before inclusion in this study.

Statistical Analysis

Cytokine, superoxide anion, and NO concentrations, and Mtb CFU were compared with ANOVA, followed by Tukey's test. All other results were compared with Kruskal–Wallis test with Dunn's posttest. The analysis were performed using GraphPad Prism v. 5.0 (GraphPad Software, CA, USA), and significance was set at $P < 0.05$.

RESULTS

Human Neutrophils Produce EVs with Different Physical Characteristics and TLR-Ligand Content in Response to Mtb, PMA and fMLF

Previous studies (20, 21) had reported that monocytes, platelets and endothelial cells release EVs in response to different activators, from bacterial products like LPS to cellular stress. In this study, we compared the EVs produced by non-stimulated human neutrophils ("spontaneous" EVs, EV-NS) to the EVs produced by neutrophils stimulated with an activator (PMA), a peptide derived from bacterial proteins (fMLF) or an intracellular pathogen (Mtb).

Figure 1A shows the flow cytometry analysis of these EVs. The gating strategy includes the calibration of the cytometer with beads of different sizes (a) to allow the differentiation of EVs from the electronic noise, the EVs were acquired in a highly sensitive cytometer for analysis of microvesicles, the EVs were analyzed as single events and CellVue Jade-positive events (c). Since this is a dye that binds phospholipids, the positive events correspond to structures that contain a lipid membrane. The gate in the fourth panel (**Figures 1A–D**) shows homogenous population of EVs that express CD35 and phosphatidylserine (annexin V+), which have been previously described as markers of ectosomes (21).

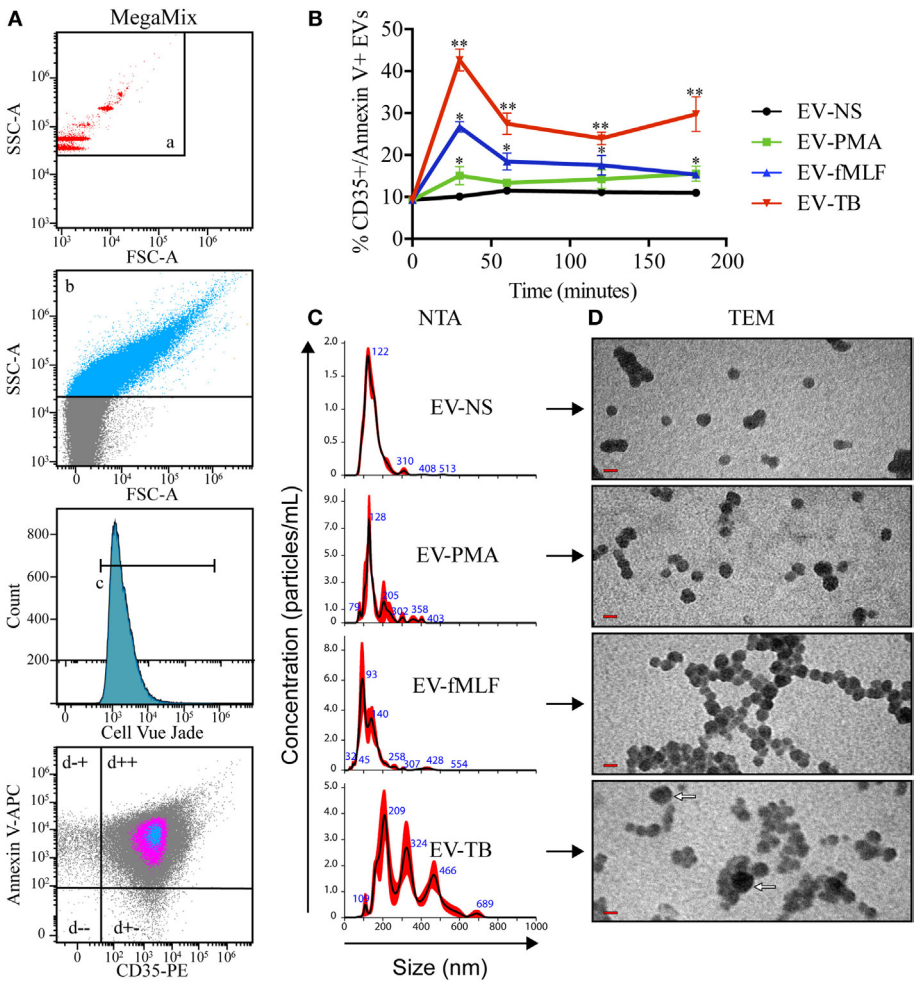

FIGURE 1 | Neutrophil extracellular vesicles (EVs) that are induced by *Mycobacterium tuberculosis* (Mtb) have different characteristics than neutrophil EVs induced by PMA or fMLF. EVs were derived from neutrophils that were left with medium alone (EV-NS) or stimulated with PMA (EV-PMA), fMLF (EV-fMLF), or with Mtb (EV-TB) for the indicated times. **(A)** Gating strategy for the flow cytometry analysis of EVs. (a) Side scatter (SSC-A) of MegaMix® beads of different sizes, which allowed the differentiation of EVs from the electronic noise. (b) SSC-A of neutrophil-derived EVs, (c) EVs derived from neutrophils stained with CellVue Jade, and (d) analysis of the expression of CD35 and annexin V on neutrophil-derived EVs. **(B)** Percentage of CD35+, annexin V+ EVs derived from neutrophils activated with different stimuli. Data points represent mean and SEM from four independent experiments and were analyzed (at each time point) with Kruskal–Wallis test with Dunn's posttest. Asterisks on the graph represent significant differences between EV-NS and EV-PMA, EV-fMLF, or EV-TB (*$P < 0.05$ and **$P < 0.01$). **(C)** Nanoparticle tracking analysis (NTA) of EVs derived from neutrophils activated with different stimuli. Three measurements were made from each sample. A result representative of four independent experiments is shown. **(D)** Transmission electron microscopy (TEM) of EVs derived from neutrophil activated with different stimuli. The red bars indicate 100 nm, and the white arrows indicate the largest EVs. The images are representative of three independent experiments.

Figure 1B shows the percentage of CD35+/annexin V+ EVs among EVs that were produced by non-stimulated neutrophils (EV-NS), or by neutrophils stimulated with PMA (EV-PMA), fMLF (EV-fMLF) or Mtb (EV-TB) for the indicated times. At 30 min, the percentage of CD35+/annexin V+ EVs is higher in EV-TB than in EV-NS. EV-TB continued to be more abundant at 180 min; however, at this time point the neutrophils are positive for both annexin V and propidium iodide, and the EVs are likely to contain apoptotic bodies. For all the subsequent experiments, EVs were concentrated from the supernatants of neutrophils stimulated with PMA, fMLF or Mtb for 30 min, when neutrophils are not apoptotic or necrotic (Figure S1 in Supplementary Material).

Figure 1C shows the size distribution of the four types of EVs (EV-NS, EV-PMA, EV-fMLF, and EV-TB), as determined by NTA. EV-TB are more heterogeneous than the other EVs, and most of the vesicles in the EV-TB preparation are larger in diameter than 200 nm (100–700 nm). Most of the vesicles in the EV-NS preparation have a diameter of 100–200 nm, while the vesicles in the EV-PMA preparation have a diameter of 100–300 nm, and those in the EV-fMLF have a diameter of 100–200 nm. EV-TB have only vesicles with higher concentration of particles/ml than EV-NS, EV-PMA, and EV-fMLF (Videos S1–S4 in Supplementary Material). TEM shows dense spheres in the four types of EVs; EV-NS contains the smallest vesicles (50–100 nm), compared with EV-PMA and EV-fMLF, whose vesicles are larger than 200 nm. EV-fMLF contains a larger proportion of aggregated vesicles, compared with other EVs.

Because we observed a heterogeneity in EVs depending on the stimulus that induced their release, and previous studies have described a difference in the protein content of different EVs, which carry information from the parent cell (22), we tested whether EV-TB contain ligands for TLRs. We observed that EV-TB induced the highest activation of HEK cells stably transfected with human TLR2/6 (**Figure 2A**). No ligands for TLR4 and 5 were detected in all the EV tested (**Figures 2B,C**). These results indicate that neutrophils stimulated with Mtb release EVs with intrinsic physical characteristics, which are different from the physical characteristics of EVs induced by different signals, and that EV-TB have the ability to differentially interact with innate immune receptors.

EV-TB Induce the Production of Pro-inflammatory Cytokines and the Expression of Costimulatory Molecules by Human Macrophages

Toll-like receptor 2/6 plays an important role in the recognition of mycobacterial lipopeptides by inducing the production of pro-inflammatory cytokines (23), so we decided to evaluate the production of cytokines on macrophages stimulated with EV-NS, EV-PMA, EV-fMLF, or EV-TB for 24 h. As expected, EV-TB induced the highest production of TNF-α, IL-6, and IL-10, and the lowest amounts of TGF-β in macrophages, compared with the other EVs (**Figure 3**). By contrast, EV-TB were unable to induce IL-1β (**Figure 3C**). Because TLR activation also leads to an increase in costimulatory molecules and MHC class II proteins in macrophages (24), we tested whether different EVs induced a different expression of these molecules on macrophages. We observed that EV-TB induced the highest expression of the costimulatory molecule CD86 on macrophages, compared with the expression induced by other EVs, while CD80 expression was significantly increased by EV-TB, compared with EV-PMA and EV-fMLF. No changes were observed in the expression levels of

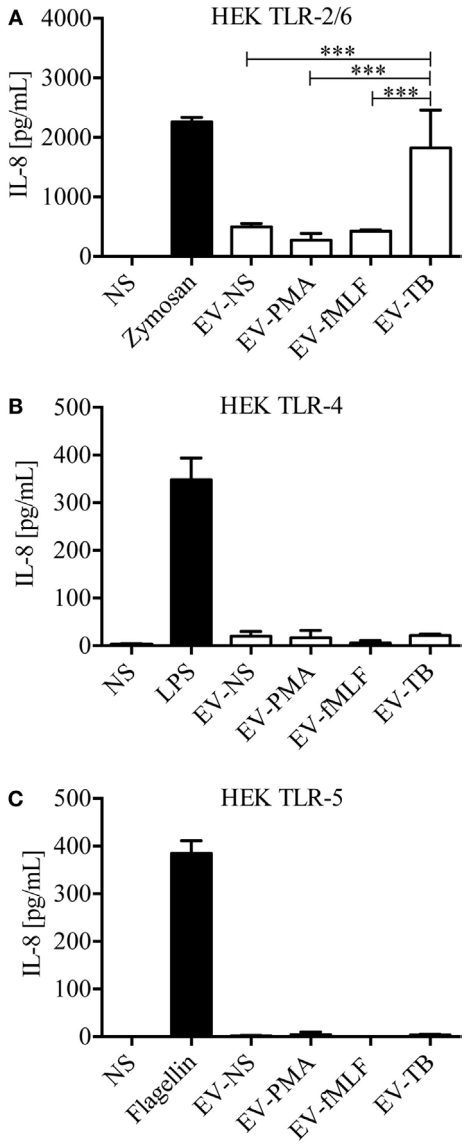

FIGURE 2 | Extracellular vesicles (EVs) derived from *Mycobacterium tuberculosis* (Mtb)-infected neutrophils (EV-TB) contain ligands for toll-like receptors (TLR) 2/6. HEK cells expressing TLR2/6 **(A)**, TLR4 **(B)**, or TLR5 **(C)** were stimulated with EVs that were produced by non-stimulated neutrophils (EV-NS) or by neutrophils stimulated with PMA (EV-PMA), fMLF (EV-fMLF), or Mtb (EV-TB) for 30 min. Zymosan (TLR 2/6), lipopolysaccharide (LPS) (TLR4) and flagellin (TLR5) were used as positive controls, as indicated, and non-stimulated cells were used as negative controls (NS). After 24 h, supernatants were collected, and IL-8 was quantified. Data points represent mean and SD from three independent experiments and were analyzed with one-way ANOVA followed by Tukey's test (***$P < 0.001$).

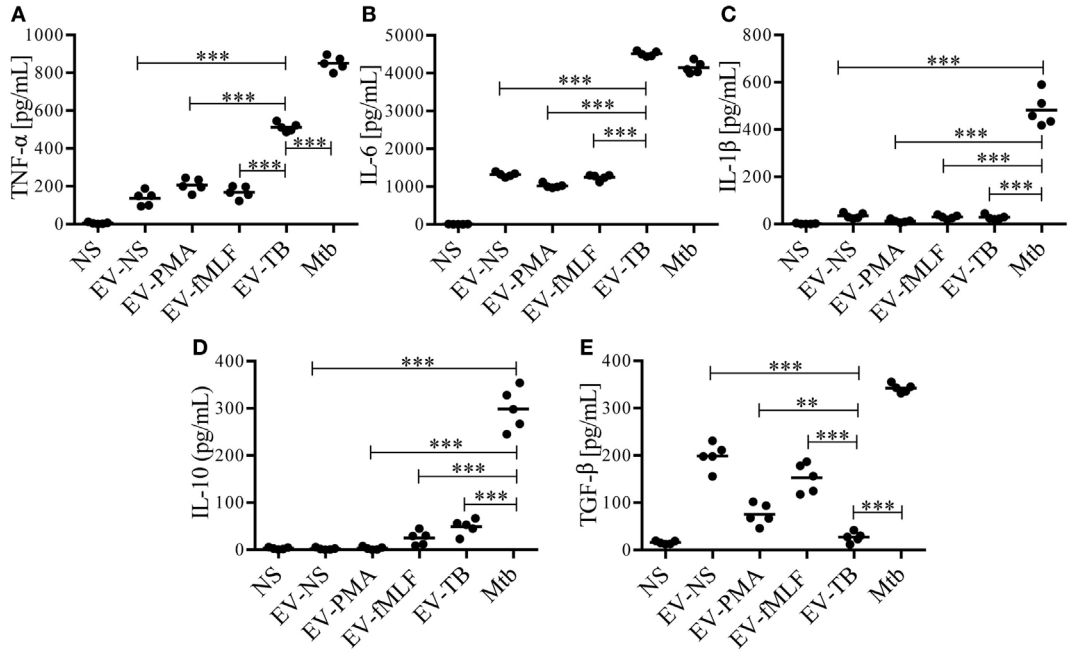

FIGURE 3 | Neutrophil-derived extracellular vesicles (EVs) that are induced by *Mycobacterium tuberculosis* (Mtb) induce the production of TNF-α and IL-6 and IL-10 by macrophages. Macrophages were stimulated for 24 h with EVs that were produced by non-stimulated neutrophils (EV-NS), or by neutrophils stimulated with PMA (EV-PMA), fMLF (EV-fMLF), or Mtb (EV-TB) for 30 min. As controls, the macrophages were left with medium alone (NS) or were infected with Mtb. TNF-α **(A)**, IL-6 **(B)**, IL-1β **(C)**, IL-10 **(D)**, and TGF-β **(E)** were measured in the supernatants. The graphs represent the results obtained with cells from five different healthy volunteers and were analyzed with one-way ANOVA followed by Tukey's test (*$P < 0.05$, **$P < 0.01$, and ***$P < 0.001$).

HLA-DR (**Figure 4**). These data indicate that EV-TB differentially regulate macrophage activation, when compared with other neutrophil-derived EVs.

EV-TB Reduce the Amount of Intracellular Mtb and Increase Superoxide Anion Production and Autophagy in Human Macrophages

Since EV-TB induced the production of pro-inflammatory cytokines and the expression of costimulatory molecules by macrophages, we investigated if these activated macrophages were able to eliminate intracellular Mtb. Macrophages were infected with Mtb for 2 h and then stimulated with EV-NS, EV-PMA, EV-fMLF, or EV-TB and incubated for 24 or 48 h, before CFU determination.

Figure 5 shows that EV-TB induced a significant decrease in the amount of intracellular Mtb at 24 and 48 h after EV treatment, compared with the other neutrophil-derived EVs.

To investigate the mechanism that allowed macrophages to kill intracellular Mtb, we first focused on superoxide anion and NO production, because they have been implied in controlling intracellular Mtb (25, 26). Superoxide anion and NO were measured in Mtb-IM that were treated with the four EVs. EV-TB induced the highest modulation of superoxide anion when compared with the other EVs at 30 min after EV-TB treatment (**Figure 6A**) this peak could be attributed to the activity of NADPH oxidase, because DPI inhibited this increase in superoxide anion production (**Figure 6C**). By contrast, neither of the neutrophil-derived EVs modified NO production in the Mtb-IM (**Figure 6B**). TLR2/6 ligands and reactive oxygen species (ROS) production are well-known signals that induce autophagy (27, 28), and autophagy is a crucial mechanism to inhibit Mtb survival in macrophages (29), so we investigated if EV-TB were efficient at inducing autophagy in macrophages. We found that EV-TB induced the highest LC3-II expression, compared with macrophages treated with other EVs (**Figure 7A**). Moreover, EV-TB induced the co-localization of the autophagy marker LC3-II with Mtb in macrophages that internalized Mtb (**Figures 7B,C**), suggesting that autophagy could contribute to EV-TB-induced Mtb elimination. To test this hypothesis, we treated macrophages with wortmannin, an autophagy inhibitor (30), and evaluated intracellular viable Mtb. We observed that Mtb-IM stimulated with EV-TB and treated with this inhibitor showed a full recovery of mycobacterial survival (**Figure 7D**). By contrast, IM that were treated with rapamycin, an autophagy inductor (31), showed a decreased survival of intracellular Mtb (**Figure 7D**). Taken as a whole, our results indicate that Mtb activates neutrophils to release EVs with unique physical and biological properties, which are different to those of the EVs induced by other activation pathways in neutrophils. Moreover, EV-TB have the ability to activate macrophages, promoting the control of Mtb intracellular survival through autophagy.

DISCUSSION

Neutrophils display different effector mechanisms in response to Mtb infection, including phagocytosis and the induction of

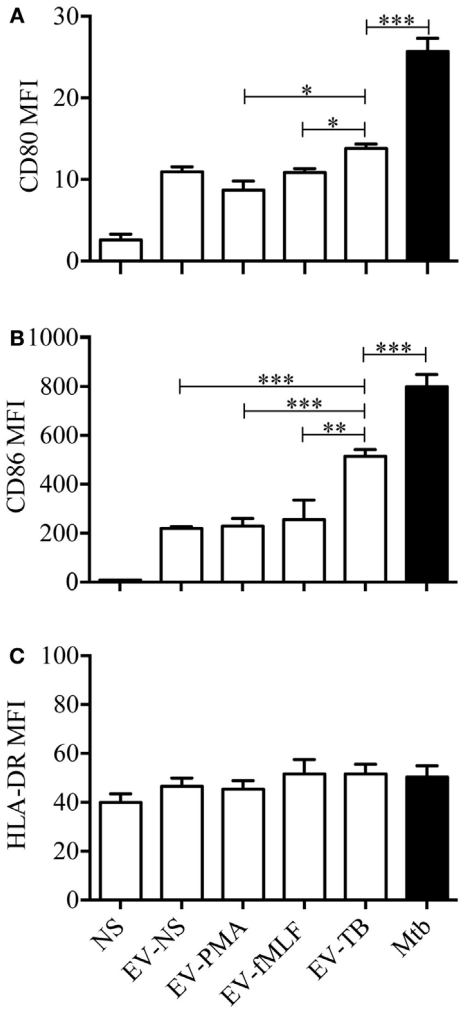

FIGURE 4 | Effect of neutrophil-derived extracellular vesicles (EVs) on the expression of costimulatory molecules in macrophages. Macrophages were stimulated for 24 h with EVs that were produced by non-stimulated neutrophils (EV-NS), or by neutrophils stimulated with PMA (EV-PMA), fMLF (EV-fMLF), or *Mycobacterium tuberculosis* (Mtb) (EV-TB) for 30 min. As controls, the macrophages were left with medium alone (NS) or were infected with Mtb. The expression of CD80 **(A)**, CD86 **(B)**, and HLA-DR **(C)** was analyzed by flow cytometry. The graphs represent the results obtained with cells from five different healthy volunteers, and were analyzed with Kruskal–Wallis test and Dunn's posttest (*$P < 0.05$, **$P < 0.01$, and ***$P < 0.001$).

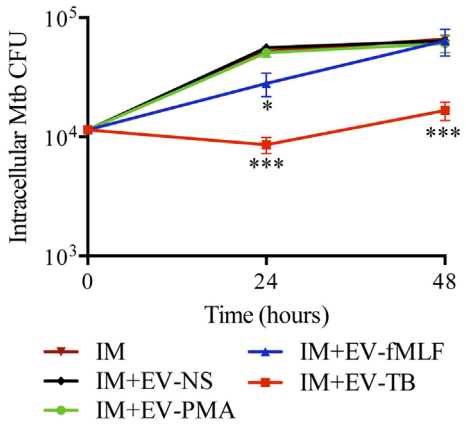

FIGURE 5 | EV-TB reduce the amount of intracellular *Mycobacterium tuberculosis* (Mtb) in macrophages. Macrophages were infected with Mtb at a multiplicity of infection (MOI) of 10 for 2 h. Extracellular bacteria were eliminated with amikacin, and the cells were left untreated (IM) or stimulated with the four types of extracellular vesicles (EVs). The EVs were produced by non-stimulated neutrophils (EV-NS), or by neutrophils stimulated with PMA (EV-PMA), fMLF (EV-fMLF), or Mtb at an MOI of 10 (EV-TB) for 30 min. After 4 h of stimulation with EVs, macrophages were washed with PBS and incubated for a total of 24 and 48 h after infection. Finally, IM were lysed, and intracellular bacteria were evaluated through CFU by performing serial dilutions of macrophage lysates. Data points represent the mean and SD from three independent experiments and were analyzed (at each time point) with one-way ANOVA followed by Tukey's test. Asterisks on the graph represent significant differences between IM and IM plus each EV (*$P < 0.05$, **$P < 0.01$, and ***$P < 0.001$). Abbreviation: IM, infected macrophages.

NETs. In this work, we described another mechanism that is deployed by neutrophils and allows intercellular communication with macrophages through EV release. Previous studies have reported that EVs released from activated neutrophils can regulate the functions of macrophages and DCs (13, 20). In this study, we characterized the EVs that are produced by neutrophils, spontaneously (EV-NS), and in response to PMA (EV-PMA), fMLF (EV-fMLF), or Mtb (EV-TB). All our experiments were performed in an autologous system, which means that the neutrophils used to produce the EVs and the monocyte-derived macrophages were from the same donor. In this system, we detected the release of EVs that express CD35 and phosphatidylserine, which binds annexin V, after neutrophil stimulation with PMA, fMLF or Mtb. However, EV-TB contained a higher percentage of CD35+/annexin V+ EVs after 30 min, compared with EV-NS. These results indicate that vesiculation occurs at the earliest stages of neutrophil activation and it occurs independently from apoptosis, since we did not detect apoptotic neutrophils at this time point. In addition to these CD35+/annexin V+ vesicles, EV-NS, EV-PMA, EV-fMLF, and EV-TB also contained annexin V- vesicles, and previous studies indicate that these vesicles could have an incomplete translocation of phosphatidylserine to the outer layer of their membranes, caused by inactivation of the "scramblase" enzyme (32). The EVs that were released spontaneously from neutrophils (EV-NS) had different physical characteristics than the EVs that were released by activated neutrophils, and different stimuli induced the production of EVs that also differed in their physical characteristics and TLR-ligand content. EV-TB were the most heterogeneous in size, EV-NS were the smallest of the four EVs, and EV-fMLF contained a larger proportion of aggregated vesicles, compared with other EVs, which may indicate that EV-fMLF contain a larger proportion of adhesion molecules, as has been observed previously (33). Mtb is recognized by the innate immune system through several PRRs, including TLR2/1, TLR2/6, TLR4, TLR5, and possibly TLR8, which has been implicated in the recognition of mycobacterial cell wall-associated glycolipids (34). We found no detectable ligands for TLR2/6, TLR4, or TLR5 in EV-NS, EV-PMA, and EV-fMLF, which suggests that these EVs

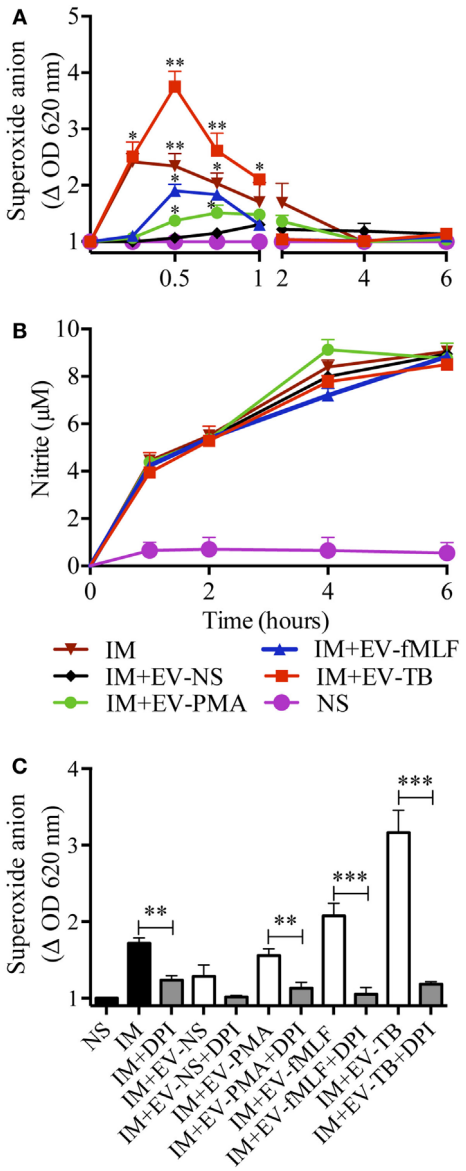

FIGURE 6 | EV-TB induce the production of superoxide anion in *Mycobacterium tuberculosis* (Mtb)-IM. Macrophages were infected with Mtb for 2 h. Extracellular bacteria were eliminated, and macrophages were left untreated (IM), or incubated with extracellular vesicles (EVs) (EV-NS, EV-PMA, EV-fMLF, or EV-TB) for 4 h. Un-IM were used as negative controls (NS). **(A)** Superoxide anion was measured with the nitro blue tetrazolium method. The graph represents the change in optical density at 620 nm ± SD of stimulated cells, compared with untreated cells. **(B)** NO was measured with the Griess method. Data from three independent experiments were analyzed (at each time point) with one-way ANOVA followed by Tukey's test. Asterisks on the graph represent significant differences between IM and IM plus each EV and the bar in the superoxide anion graph represent significant differences between EV-TB and each EV. **(C)** NADPH oxidase inhibition with DPI. The graph represents the change in optical density at 620 nm ± SD of stimulated cells, compared with untreated cells. Results were obtained with cells from three different healthy volunteers and were analyzed with one-way ANOVA followed by Tukey's test (*$P < 0.05$, **$P < 0.01$, and ***$P < 0.001$). Abbreviation: IM, infected macrophages.

do not carry damage-associated molecular patterns or alarmins that could activate these receptors. EV-TB contained ligands for TLR2/6, which is not unexpected, since several components of Mtb are known TLR2/6 ligands, including lipoarabinomannan (ManLAM), lipomannan, phosphatidylinositol mannoside, and the 19 and 38 kDa lipoproteins (35, 36). This indicates that mycobacterial components reach neutrophil-derived EVs in as little as 30 min after infection; the "sorting" mechanism responsible for this effect has not yet been described. Bhatnagar et al. reported that exosomes derived from Mtb-IM could induce a pro-inflammatory response in macrophages (37); this response could be caused by one or more of the 40 mycobacterial components that are transported in these vesicles, including the TLR2/6 ligand ManLAM (38). However, other studies report that exosomes derived from Mtb-IM have immune-suppressing effects, but these effects are attributed to the miRNAs that are transported in these exosomes, which interfere with the translation of genes involved in cellular activation and inflammation (39).

We observed that EV-TB induced the production of higher amounts of TNF-α and IL-6, and the expression of higher levels of costimulatory molecules in macrophages, compared with the other EVs; these results correlate with a significant decrease in intracellular Mtb CFU in Mtb-IM after EV treatment. TNF-α and IL-6 are well-known macrophage activators, which increase the production of superoxide anion, NO, antimicrobial peptides, and other antimicrobial molecules. In fact, EV-TB induced the production of higher amounts of superoxide anion, with a peak at 30 min after EV-TB treatment, compared with the other EVs. It has been reported that EVs have a direct antimicrobial effect: they can be considered "ecto-organelles" that contain a high concentration of proteolytic enzymes from neutrophils granules (14). Timár et al. reported that neutrophil-derived EVs contain lactoferrin and myeloperoxidase, and directly eliminate *S. aureus*; this bactericidal effect is independent of NET formation (15). However, another study reported that EVs derived from Mtb-infected neutrophils interfere with the antibacterial activity of human macrophages against virulent Mtb (40), in contrast with our results. The difference in outcome could be explained by the differences in the MOI for neutrophil infection, the time allotted for EV release by neutrophils, the amount of EVs used for macrophage activation, the duration of Mtb infection in macrophages and the protocol for obtaining EVs; for instance, Duarte et al. used a different centrifugation protocol, that could lead to the enrichment of different types of EVs.

Autophagy is a highly conserved mechanism that delivers proteins or whole organelles to lysosomes for degradation. The induction of autophagy in Mtb-IM results in increased fusion of Mtb-containing and LC3-II-expressing autophagosomes with lysosomes, which leads to increased bactericidal activity (29). Autophagy can be induced by ROS (27) and also by TLR activation (41). Mycobacterial lipoprotein LpqH induces autophagy through TLR2, and TLR2 stimulation with the mycobacterial lipoprotein LpqH robustly induces antibacterial autophagy through the activation of vitamin D receptor signaling and the induction of cathelicidin synthesis (27). Here, we report that EV-TB induced the expression of the autophagy-related marker

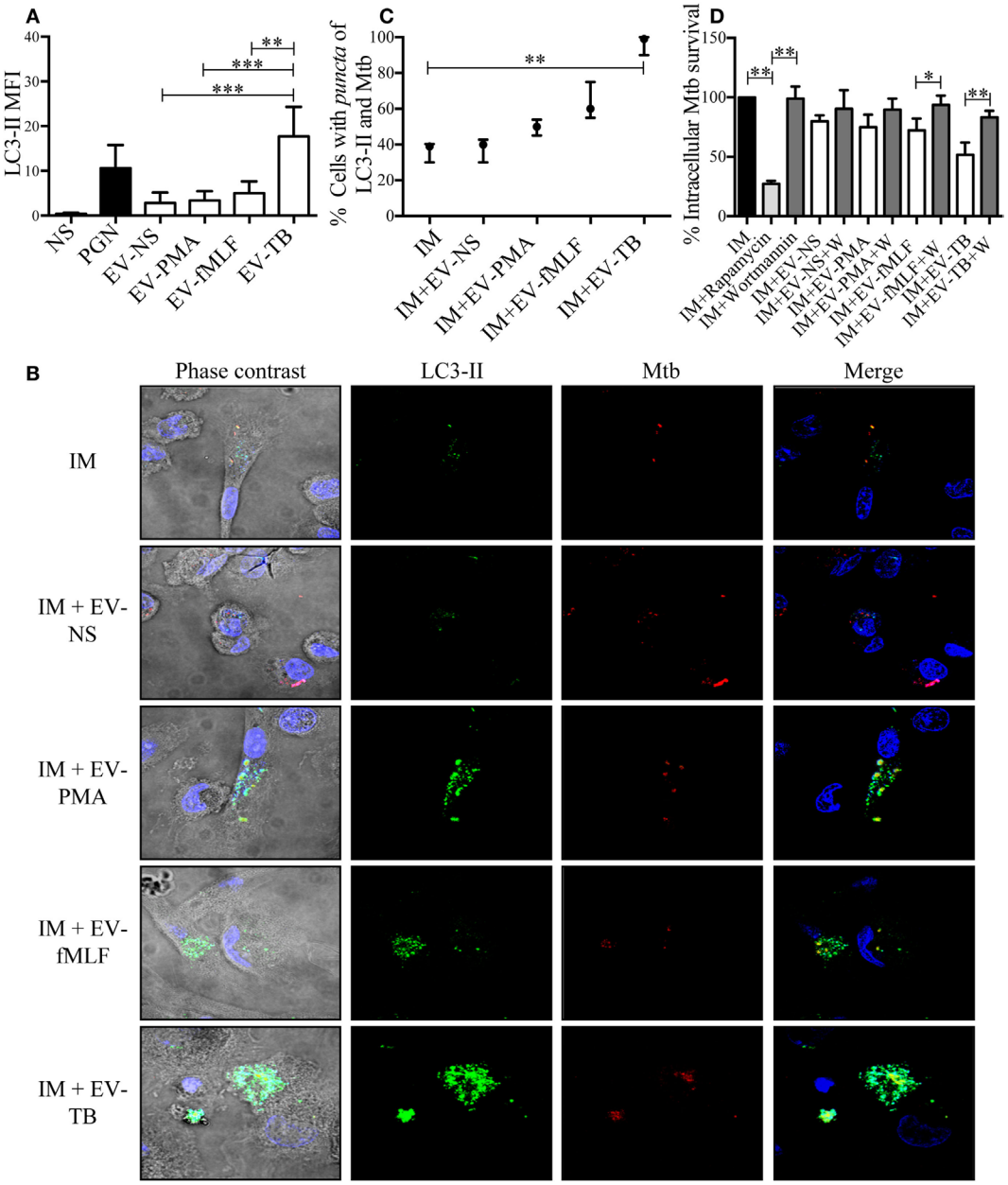

FIGURE 7 | EV-TB-induced autophagy contributes to *Mycobacterium tuberculosis* (Mtb) elimination in Mtb-IM. **(A)** Macrophages were incubated with extracellular vesicles (EVs) (EV-NS, EV-PMA, EV-fMLF, or EV-TB) for 4 h. Non-stimulated cells were used as negative control (NS). As a positive control for autophagy induction, macrophages were treated with peptidoglycan (PGN) for 4 h. The cells were then stained with anti-LC3-II (green) and DAPI (blue) and examined in a confocal microscope to determine LC3-II mean fluorescence intensity (MFI). Data points represent the mean and SEM from three independent experiments and were analyzed with Kruskal–Wallis test and Dunn's posttest (*$P < 0.05$ and **$P < 0.01$). **(B)** Macrophages were infected with Mtb previously stained with CellVue Maroon (red) for 15 min. After this incubation, the cells were left untreated (IM), or were incubated with EVs (EV-NS, EV-PMA, EV-fMLF, or EV-TB) for 4 h. The cells were then stained with anti-LC3-II (green) and DAPI (blue) and examined in a confocal microscope. The images are representative of three independent experiments. **(C)** Percentage of cells with co-localization of LC3-II and Mtb was calculated. The medians with the interquartile ranges are shown ($n = 3$) and were analyzed with Kruskal–Wallis test and Dunn's posttest (**$P < 0.01$). **(D)** Percentage of intracellular Mtb survival. Macrophages were infected with Mtb for 2 h. Extracellular bacteria were eliminated, and cells were incubated with EVs (EV-NS, EV-PMA, EV-fMLF, or EV-TB) for 4 h, with or without wortmannin (autophagy inhibitor); IM were also treated with rapamycin (autophagy positive control) or wortmannin. The cells were washed with PBS and incubated for 4 h. The cells were then lysed, and intracellular bacteria were evaluated through CFU by performing serial dilutions of macrophage lysates. The percentage of Mtb survival was calculated for each condition, with Mtb-IM considered as 100%. Data points represent the mean and SEM from three independent experiments and were analyzed with Kruskal–Wallis test and Dunn's posttest (*$P < 0.05$, **$P < 0.01$, and ***$P < 0.001$). Abbreviation: IM, infected macrophages.

LC3-II in macrophages, and the co-localization of LC3-II with Mtb inside these macrophages. These results suggest that autophagy is a key mechanism through which EV-TB reduce intracellular Mtb in macrophages. In fact, we found that blocking autophagy in Mtb-IM (using the autophagy inhibitor wortmannin) increases the survival of Mtb. We detected TLR2/6 ligands in EV-TB, which could be the autophagy inducers in our model. The induction of autophagy inhibits IL-1β secretion by degrading pro-IL-1β (42), and in our experiments, EV-TB were unable to induce a significant amount of IL-1β, which coincides with an increase in LC3-II expression in macrophages. However, Mtb is not completely eliminated from EV-TB treated macrophages; the ability of Mtb to persist inside macrophages is well documented. In particular, Mtb can block autophagosome maturation to create a replication niche; Mtb upregulates miR-155 in an ESAT6-dependent manner to avoid elimination and to promote infection in macrophages (43), and Mtb also induces miR-33 to inhibit autophagy and to reprogram the host lipid metabolism to enable its intracellular survival (44). In conclusion, our study demonstrated that neutrophils produce EVs in response to different activators, and that these EVs differ in their physical characteristics and TLR-ligand content. Furthermore, these EVs can modulate the response of other cells of the innate immune system. In particular, EV-TB activate macrophages and promote the clearance of intracellular Mtb through high production of superoxide anion and autophagy. Whether superoxide anion is enough to confer resistance needs to be clarified in future works. To the best of our knowledge, this phenomenon represents a new mechanism by which neutrophils participate in the control of Mtb infection.

ETHICS STATEMENT

This human study was approved by the Bioethics Committee of Escuela Nacional de Ciencias Biológicas from the Instituto Poltécnico Nacional (CEI-ENCB 011/2013). All written informed consents were received from participants before inclusion in this study.

AUTHOR CONTRIBUTIONS

VA-J, KL-P, MG-M, LV-F, VG-P, MC-N, IR-C, VR-G, JC-C, and SG-P performed experiments and analyzed data; VA-J, KL-P, BG-P, VR-G, JM-H, SG-P, and VO-N analyzed and interpreted data; VA-J, CW-B, SE-P, JS-L, IW-B, RC-S, and IE-G interpreted data, drafted the manuscript, and contributed with intellectual content; RC-S and IE-G designed and supervised the study and obtained funding. All the authors critically revised and approved the final version of this manuscript.

FUNDING

This work was supported by grants from Consejo Nacional de Ciencia y Tecnología (CONACyT), México (SEP-CONACyT 105278 and 221002 to IE-G and SEP-CONACYT 157100 to RC-S), and from Secretaría de Investigación y Posgrado, Instituto Politécnico Nacional (SIP-IPN, 20180537), México.

SUPPLEMENTARY MATERIAL

The Supplementary Material for this article can be found online at http://www.frontiersin.org/articles/10.3389/fimmu.2018.00272/full#supplementary-material.

FIGURE S1 | Percentage of live neutrophils after 30 and 180 min of treatment with PMA, fMLF, or *Mycobacterium tuberculosis* (Mtb). Neutrophils were left with medium alone or were stimulated with PMA, fMLF, or with Mtb for 30 min **(A)** or for 180 min **(B)**. Neutrophils were stained with annexin V/PE-Cy7 and propidium iodide and analyzed by flow cytometry. The graph represents live (annexin V−/PI−) and apoptotic/dead neutrophils (annexin V+/PI+, annexin V+/PI−, and annexin V−/PI+) for each condition.

VIDEOS S1–S4 | EV-TB have higher concentration of particles per milliliter than other extracellular vesicles (EVs). EV-NS, as well as EV-PMA, EV-fMLF, and EV-TB (produced by neutrophils after 30 min) were analyzed by nanoparticle tracking analysis; non-stimulated cells (Video 1), stimulated with PMA (Video 2), fMLF (Video 3), or with *Mycobacterium tuberculosis* (Video 4). The videos show 10 s of Brownian movement from EVs, the data were correlated with particle concentration.

REFERENCES

1. Schafer G, Jacobs M, Wilkinson RJ, Brown GD. Non-opsonic recognition of *Mycobacterium tuberculosis* by phagocytes. *J Innate Immun* (2009) 1(3):231–43. doi:10.1159/000173703
2. Tsao TC, Hong J, Huang C, Yang P, Liao SK, Chang KS. Increased TNF-alpha, IL-1 beta and IL-6 levels in the bronchoalveolar lavage fluid with the upregulation of their mRNA in macrophages lavaged from patients with active pulmonary tuberculosis. *Tuber Lung Dis* (1999) 79(5):279–85. doi:10.1054/tuld.1999.0215
3. D'Avila H, Roque NR, Cardoso RM, Castro-Faria-Neto HC, Melo RC, Bozza PT. Neutrophils recruited to the site of *Mycobacterium bovis* BCG infection undergo apoptosis and modulate lipid body biogenesis and prostaglandin E production by macrophages. *Cell Microbiol* (2008) 10(12):2589–604. doi:10.1111/j.1462-5822.2008.01233.x
4. Eruslanov EB, Lyadova IV, Kondratieva TK, Majorov KB, Scheglov IV, Orlova MO, et al. Neutrophil responses to *Mycobacterium tuberculosis* infection in genetically susceptible and resistant mice. *Infect Immun* (2005) 73(3):1744–53. doi:10.1128/IAI.73.3.1744-1753.2005
5. Eum SY, Kong JH, Hong MS, Lee YJ, Kim JH, Hwang SH, et al. Neutrophils are the predominant infected phagocytic cells in the airways of patients with active pulmonary TB. *Chest* (2010) 137(1):122–8. doi:10.1378/chest.09-0903
6. Jones GS, Amirault HJ, Andersen BR. Killing of *Mycobacterium tuberculosis* by neutrophils: a nonoxidative process. *J Infect Dis* (1990) 162(3):700–4. doi:10.1093/infdis/162.3.700
7. Jena P, Mohanty S, Mohanty T, Kallert S, Morgelin M, Lindstrom T, et al. Azurophil granule proteins constitute the major mycobactericidal proteins in human neutrophils and enhance the killing of mycobacteria in macrophages. *PLoS One* (2012) 7(12):e50345. doi:10.1371/journal.pone.0050345
8. Ramos-Kichik V, Mondragon-Flores R, Mondragon-Castelan M, Gonzalez-Pozos S, Muniz-Hernandez S, Rojas-Espinosa O, et al. Neutrophil extracellular traps are induced by *Mycobacterium tuberculosis*. *Tuberculosis (Edinb)* (2009) 89(1):29–37. doi:10.1016/j.tube.2008.09.009
9. Morel C, Badell E, Abadie V, Robledo M, Setterblad N, Gluckman JC, et al. *Mycobacterium bovis* BCG-infected neutrophils and dendritic cells cooperate to induce specific T cell responses in humans and mice. *Eur J Immunol* (2008) 38(2):437–47. doi:10.1002/eji.200737905
10. Stein JM, Luzio JP. Ectocytosis caused by sublytic 452 autologous complement attack on human neutrophils. The sorting of endogenous plasma-membrane proteins and lipids into shed vesicles. *Biochem J* (1991) 274(Pt 2):381–6. doi:10.1042/bj2740381
11. Gasser O, Hess C, Miot S, Deon C, Sanchez JC, Schifferli JA. Characterisation and properties of ectosomes released by human polymorphonuclear neutrophils. *Exp Cell Res* (2003) 285(2):243–57. doi:10.1016/S0014-4827(03)00055-7

12. Nusse O, Lindau M. The dynamics of exocytosis in human neutrophils. *J Cell Biol* (1988) 107(6 Pt 1):2117–23. doi:10.1083/jcb.107.6.2117
13. Eken C, Sadallah S, Martin PJ, Treves S, Schifferli JA. Ectosomes of polymorphonuclear neutrophils activate multiple signaling pathways in macrophages. *Immunobiology* (2013) 218(3):382–92. doi:10.1016/j.imbio.2012.05.021
14. Hess C, Sadallah S, Hefti A, Landmann R, Schifferli JA. Ectosomes released by human neutrophils are specialized functional units. *J Immunol* (1999) 163(8):4564–73.
15. Timár CI, Lorincz AM, Csepanyi-Komi R, Valyi-Nagy A, Nagy G, Buzas EI, et al. Antibacterial effect of microvesicles released from human neutrophilic granulocytes. *Blood* (2013) 121(3):510–8. doi:10.1182/blood-2012-05-431114
16. Gonzalez-Cano P, Mondragon-Flores R, Sanchez-Torres LE, Gonzalez-Pozos S, Silva-Miranda M, Monroy-Ostria A, et al. *Mycobacterium tuberculosis* H37Rv induces ectosome release in human polymorphonuclear neutrophils. *Tuberculosis (Edinb)* (2010) 90(2):125–34. doi:10.1016/j.tube.2010.01.002
17. Aga E, Katschinski DM, van Zandbergen G, Laufs H, Hansen B, Muller K, et al. Inhibition of the spontaneous apoptosis of neutrophil granulocytes by the intracellular parasite *Leishmania major*. *J Immunol* (2002) 169(2):898–905. doi:10.4049/jimmunol.169.2.898
18. Spittler A. *Set-Up of the CytoFLEX for Extracellular Vesicle Measurement*. Medical University of Vienna (2016). Available from: http://molbiol.ru/forums/index.php?act=Attach&type=post&id=235071
19. Campillo-Navarro M, Leyva-Paredes K, Donis-Maturano L, Gonzalez-Jimenez M, Paredes-Vivas Y, Cerbulo-Vazquez A, et al. Listeria monocytogenes induces mast cell extracellular traps. *Immunobiology* (2017) 222(2):432–9. doi:10.1016/j.imbio.2016.08.006
20. Eken C, Gasser O, Zenhaeusern G, Oehri I, Hess C, Schifferli JA. Polymorphonuclear neutrophil-derived ectosomes interfere with the maturation of monocyte-derived dendritic cells. *J Immunol* (2008) 180(2):817–24. doi:10.4049/jimmunol.180.2.817
21. Nomura S, Tandon NN, Nakamura T, Cone J, Fukuhara S, Kambayashi J. High-shear-stress induced activation of platelets and microparticles enhances expression of cell adhesion molecules in THP-1 and endothelial cells. *Atherosclerosis* (2001) 158(2):277–87. doi:10.1016/S0021-9150(01)00433-6
22. Dalli J, Montero-Melendez T, Norling LV, Yin X, Hinds C, Haskard D, et al. Heterogeneity in neutrophil microparticles reveals distinct proteome and functional properties. *Mol Cell Proteomics* (2013) 12(8):2205–19. doi:10.1074/mcp.M113.028589
23. Marinho FA, de Paula RR, Mendes AC, de Almeida LA, Gomes MT, Carvalho NB, et al. Toll-like receptor 6 senses *Mycobacterium avium* and is required for efficient control of mycobacterial infection. *Eur J Immunol* (2013) 43(9):2373–85. doi:10.1002/eji.201243208
24. Sieling PA, Chung W, Duong BT, Godowski PJ, Modlin RL. Toll-like receptor 2 ligands as adjuvants for human Th1 responses. *J Immunol* (2003) 170(1):194–200. doi:10.4049/jimmunol.170.1.194
25. MacMicking JD, North RJ, LaCourse R, Mudgett JS, Shah SK, Nathan CF. Identification of nitric oxide synthase as a protective locus against tuberculosis. *Proc Natl Acad Sci U S A* (1997) 94(10):5243–8. doi:10.1073/pnas.94.10.5243
26. Lee PP, Chan KW, Jiang L, Chen T, Li C, Lee TL, et al. Susceptibility to mycobacterial infections in children with X-linked chronic granulomatous disease: a review of 17 patients living in a region endemic for tuberculosis. *Pediatr Infect Dis J* (2008) 27(3):224–30. doi:10.1097/INF.0b013e31815b494c
27. Shin DM, Yuk JM, Lee HM, Lee SH, Son JW, Harding CV, et al. Mycobacterial lipoprotein activates autophagy via TLR2/1/CD14 and a functional vitamin D receptor signalling. *Cell Microbiol* (2010) 12(11):1648–65. doi:10.1111/j.1462-5822.2010.01497.x
28. Vural A, Kehrl JH. Autophagy in macrophages: impacting inflammation and bacterial infection. *Scientifica (Cairo)* (2014) 2014:825463. doi:10.1155/2014/825463
29. Gutierrez MG, Master SS, Singh SB, Taylor GA, Colombo MI, Deretic V. Autophagy is a defense mechanism inhibiting BCG and *Mycobacterium tuberculosis* survival in infected macrophages. *Cell* (2004) 119(6):753–66. doi:10.1016/j.cell.2004.11.038
30. Blommaart EF, Krause U, Schellens JP, Vreeling-Sindelarova H, Meijer AJ. The phosphatidylinositol 3-kinase inhibitors wortmannin and LY294002 inhibit autophagy in isolated rat hepatocytes. *Eur J Biochem* (1997) 243(1–2):240–6. doi:10.1111/j.1432-1033.1997.0240a.x
31. Jung CH, Jun CB, Ro SH, Kim YM, Otto NM, Cao J, et al. ULK-Atg13-FIP200 complexes mediate mTOR signaling to the autophagy machinery. *Mol Biol Cell* (2009) 20(7):1992–2003. doi:10.1091/mbc.E08-12-1249
32. Scott RE, Maercklein PB. Plasma membrane vesiculation in 3T3 and SV3T3 cells. II. Factors affecting the process of vesiculation. *J Cell Sci* (1979) 35:245–52.
33. Fujimi S, Ogura H, Tanaka H, Koh T, Hosotsubo H, Nakamori Y, et al. Increased production of leukocyte microparticles with enhanced expression of adhesion molecules from activated polymorphonuclear leukocytes in severely injured patients. *J Trauma* (2003) 54(1):114–9; discussion 9–20. doi:10.1097/01.TA.0000046317.49507.F2
34. Means TK, Jones BW, Schromm AB, Shurtleff BA, Smith JA, Keane J, et al. Differential effects of a toll-like receptor antagonist on *Mycobacterium tuberculosis*-induced macrophage responses. *J Immunol* (2001) 166(6):4074–82. doi:10.4049/jimmunol.166.6.4074
35. Jones BW, Means TK, Heldwein KA, Keen MA, Hill PJ, Belisle JT, et al. Different toll-like receptor agonists induce distinct macrophage responses. *J Leukoc Biol* (2001) 69(6):1036–44. doi:10.1189/jlb.69.6.1036
36. Thoma-Uszynski S, Stenger S, Takeuchi O, Ochoa MT, Engele M, Sieling PA, et al. Induction of direct antimicrobial activity through mammalian toll-like receptors. *Science* (2001) 291(5508):1544–7. doi:10.1126/science.291.5508.1544
37. Bhatnagar S, Shinagawa K, Castellino FJ, Schorey JS. Exosomes released from macrophages infected with intracellular pathogens stimulate a proinflammatory response in vitro and in vivo. *Blood* (2007) 110(9):3234–44. doi:10.1182/blood-2007-03-079152
38. Giri PK, Kruh NA, Dobos KM, Schorey JS. Proteomic analysis identifies highly antigenic proteins in exosomes from *M. tuberculosis*-infected and culture filtrate protein-treated macrophages. *Proteomics* (2010) 10(17):3190–202. doi:10.1002/pmic.200900840
39. Singh PP, Li L, Schorey JS. Exosomal RNA from *Mycobacterium tuberculosis*-infected cells is functional in recipient macrophages. *Traffic* (2015) 16(6):555–71. doi:10.1111/tra.12278
40. Duarte TA, Noronha-Dutra AA, Nery JS, Ribeiro SB, Pitanga TN, Lapa ESJR, et al. *Mycobacterium tuberculosis*-induced neutrophil ectosomes decrease macrophage activation. *Tuberculosis (Edinb)* (2012) 92(3):218–25. doi:10.1016/j.tube.2012.02.007
41. Sanjuan MA, Dillon CP, Tait SW, Moshiach S, Dorsey F, Connell S, et al. Toll-like receptor signalling in macrophages links the autophagy pathway to phagocytosis. *Nature* (2007) 450(7173):1253–7. doi:10.1038/nature06421
42. Harris J, Hartman M, Roche C, Zeng SG, O'Shea A, Sharp FA, et al. Autophagy controls IL-1beta secretion by targeting pro-IL-1beta for degradation. *J Biol Chem* (2011) 11:9587–97. doi:10.1074/jbc.M110.202911
43. Kumar R, Halder P, Sahu SK, Kumar M, Kumari M, Jana K, et al. Identification of a novel role of ESAT-6-dependent miR-155 induction during infection of macrophages with *Mycobacterium tuberculosis*. *Cell Microbiol* (2012) 14(10):1620–31. doi:10.1111/j.1462-5822.2012.01827.x
44. Ouimet M, Koster S, Sakowski E, Ramkhelawon B, van Solingen C, Oldebeken S, et al. *Mycobacterium tuberculosis* induces the miR-33 locus to reprogram autophagy and host lipid metabolism. *Nat Immunol* (2016) 17(6):677–86. doi:10.1038/ni.3434

Conflict of Interest Statement: The authors declare that the research was conducted in the absence of any commercial or financial relationships that could be construed as a potential conflict of interest.

frontiers in Immunology

ORIGINAL RESEARCH
published: 27 February 2018
doi: 10.3389/fimmu.2018.00316

Roles of Macrophage Exosomes in Immune Response to Calcium Oxalate Monohydrate Crystals

*Nilubon Singhto[1,2], Rattiyaporn Kanlaya[1,3], Angkhana Nilnumkhum[1,3] and Visith Thongboonkerd[1,3]**

[1] Medical Proteomics Unit, Office for Research and Development, Faculty of Medicine Siriraj Hospital, Mahidol University, Bangkok, Thailand, [2] Immunology Graduate Program, Department of Immunology, Faculty of Medicine Siriraj Hospital, Mahidol University, Bangkok, Thailand, [3] Center for Research in Complex Systems Science, Mahidol University, Bangkok, Thailand

In kidney stone disease, macrophages secrete various mediators *via* classical secretory pathway and cause renal interstitial inflammation. However, whether their extracellular vesicles, particularly exosomes, are involved in kidney stone pathogenesis remained unknown. This study investigated alterations in exosomal proteome of U937-derived macrophages (by phorbol-12-myristate-13-acetate activation) after exposure to calcium oxalate monohydrate (COM) crystals for 16-h using 2-DE-based proteomics approach. Six significantly altered proteins in COM-treated exosomes were successfully identified by nanoscale liquid chromatography–electrospray ionization–electron transfer dissociation tandem mass spectrometry as proteins involved mainly in immune processes, including T-cell activation and homeostasis, Fcγ receptor-mediated phagocytosis, interferon-γ (IFN-γ) regulation, and cell migration/movement. The decreased heat shock protein 90-beta (HSP90β) and increased vimentin were confirmed by Western blotting. ELISA showed that the COM-treated macrophages produced greater level of interleukin-1β (IL-1β), one of the markers for inflammasome activation. Functional studies demonstrated that COM-treated exosomes enhanced monocyte and T-cell migration, monocyte activation and macrophage phagocytic activity, but on the other hand, reduced T-cell activation. In addition, COM-treated exosomes enhanced production of proinflammatory cytokine IL-8 by monocytes that could be restored to its basal level by small-interfering RNA targeting on vimentin (si-Vimentin). Moreover, si-Vimentin could also abolish effects of COM-treated exosomes on monocyte and T-cell migration as well as macrophage phagocytic activity. These findings provided some implications to the immune response during kidney stone pathogenesis *via* exosomal pathway of macrophages after exposure to COM crystals.

Keywords: calcium oxalate, calcium oxalate monohydrate, inflammasome, inflammation, kidney stone, migration, phagocytosis

OPEN ACCESS

Edited by:
Ivan Poon,
La Trobe University, Australia

Reviewed by:
Sho Morioka,
University of Virginia, United States
Christian Kurts,
University of Bonn, Germany

***Correspondence:**
Visith Thongboonkerd
thongboonkerd@dr.com,
vthongbo@yahoo.com

Specialty section:
This article was submitted to Immunological Tolerance and Regulation, a section of the journal Frontiers in Immunology

Received: *10 November 2017*
Accepted: *05 February 2018*
Published: *27 February 2018*

Citation:
Singhto N, Kanlaya R, Nilnumkhum A and Thongboonkerd V (2018) Roles of Macrophage Exosomes in Immune Response to Calcium Oxalate Monohydrate Crystals. Front. Immunol. 9:316. doi: 10.3389/fimmu.2018.00316

INTRODUCTION

During an initial phase of kidney stone formation, the causative chemical crystals, such as calcium oxalate (CaOx), can be deposited in the renal interstitium, where macrophages are recruited to eliminate these crystals *via* phagocytosis (1–3). Between the two common hydrated forms of CaOx crystals, calcium oxalate monohydrate (COM) crystals are predominantly found in clinical stones,

whereas CaOx dihydrate (COD) crystals can be also found but with smaller proportion (4). Due to differences in adhesive capability, binding kinetics, atomic lattice, and surface ionic pattern, COM crystals are more pathogenic during the kidney stone pathogenesis than COD crystals, which can be also found in the normal urine of healthy individuals (5–9).

Several lines of evidence have shown that macrophages exposed to COM crystals increase secretion of reactive oxygen species (ROS), chemokines, proinflammatory cytokines, and several fibrotic factors to promote renal interstitial inflammation in kidney stone disease (10–12). The COM-phagocytosed macrophages can activate NACHT, leucine-rich repeat (LRR), and pyrin domain-containing protein 3 (NLRP3), which is the central molecule triggering vascular permeability, leukocyte recruitment, complement activation, and inflammatory mediator production (13, 14). NLRP3-inflammasome-activated macrophages can secrete several proinflammatory cytokines, including interleukin-1β (IL-1β), IL-6, and IL-18, which serve as the amplification loop factors to activate tubulointerstitial damage by stimulating the recruited inflammatory cells (15, 16). Additionally, macrophages exposed to naturally occurred kidney stone fragments secrete greater levels of several chemokines, particularly macrophage inhibitory protein-1, monocyte chemoattractant protein-1, and interleukin-8 (IL-8) (17). These chemokines consequently enhance recruitment of various immune cells, i.e., monocytes, macrophages, neutrophils, dendritic cells, and T-cells into the inflammatory locale (18).

In addition to these inflammatory/proinflammatory mediators, macrophages can also secrete nanovesicles with a discrete diameter of approximately 30–100 nm, namely "exosomes," which play pivotal roles in intercellular communications and multibiological functions (19). Nevertheless, whether exposure to COM crystals causes any alterations in macrophage exosomes remained unknown. This study thus aimed to investigate alterations in exosomal proteins after macrophages were exposed to COM crystals using a proteomics approach followed by validation of expression data as well as several functional assays to address functional significance of exosomes derived from COM-treated macrophages in relation to kidney stone pathogenesis, particularly during an induction phase of renal interstitial inflammation.

MATERIALS AND METHODS

COM Crystal Preparation

Calcium oxalate monohydrate crystals were prepared as described previously (20, 21). Briefly, 10 mM $CaCl_2.2H_2O$ was mixed with 1.0 mM $Na_2C_2O_4$ (1:1 v/v) to make their final concentrations to 5 and 0.5 mM, respectively, in a buffer containing 10 mM Tris-HCl and 90 mM NaCl (pH 7.4). After incubation at 25°C overnight, COM crystals were harvested by a centrifugation at 2,000 *g* for 5 min. The supernatant was discarded, whereas COM crystals were washed three times with methanol. After another centrifugation at 2,000 *g* for 5 min, methanol was discarded and the crystals were air-dried overnight at 25°C. The typical morphology of COM crystals was examined under an inverted phase-contrast light microscope (model ECLIPSE Ti-S, Nikon; Tokyo, Japan).

Cell Culture and Macrophage Differentiation

U937 human monocytic cell line and Jurkat T-cell line were cultivated and maintained in complete RPMI 1640 medium (Gibco; Grand Island, NY, USA) supplemented with 10% (v/v) heat-inactivated fetal bovine serum (FBS) (Gibco), 100 U/ml penicillin G and 100 mg/ml streptomycin (Sigma, St. Louis, MO, USA).

Macrophages were derived from U937 human monocytic cell line using phorbol 12-myristate 13-acetate (PMA) (Fluka, St. Louis, MO, USA) for differentiation as previously described (22). Briefly, U937 monocytic cells at a density of 1×10^6 cells/ml were treated with 100 ng/ml PMA for 48 h (induction phase) and then vigorously washed three times with ice-cold PBS to remove PMA and non-adherent cells, whereas the adherent cells were further maintained as aforementioned for 48 h (recovery phase). The characteristics of macrophages were observed under an inverted phase-contrast microscope (Nikon ECLIPSE Ti-S) as previously described (22).

COM Crystal Treatment

The COM crystals were decontaminated by exposure to UV light for 30 min prior to incubation with the cells. After recovery phase, U937-derived macrophages (10×10^6 cells/flask) were vigorously washed five times with ice-cold PBS to remove serum-containing medium and further cultivated in serum-free medium with or without 100 μg/ml COM crystals for 16 h, which was the optimal time-point defined for studying macrophage secretome as previously reported (22) ($n = 5$ independent culture flasks per group; a total of 10 independent cultures were subjected to 2-DE analysis, whereas three independent biological replicates were used for other experiments). After 16-h incubation, the culture supernatants were harvested and further subjected to exosome isolation as detailed below.

Exosome Isolation by Microfiltration and Differential Centrifugation

The controlled and COM-treated macrophage supernatants were filtrated through 0.22-μm cellulose acetate membrane (Sartorius Stedim Biotech GmbH, Goettingen, Germany) to remove cell debris and apoptotic bodies. Microvesicles and/or larger vesicles were further removed by centrifugation at 10,000 *g* and 25°C for 30 min. Exosomes were then isolated from the remaining supernatants by ultracentrifugation at 100,000 *g* and 25°C for 90 min using an ultracentrifuge (Sorvall, Langenselbold, Germany). The isolated exosomal pellets were washed twice with PBS and resuspended in 2% (w/v) paraformaldehyde or a lysis buffer (based on experiments described below).

Examination of Exosome Morphology by Transmission Electron Microscopy (TEM)

Exosomes were resuspended in 2% (w/v) paraformaldehyde and loaded onto carbon-Formvar-coated copper grids. The samples were left on the grids for 20 min to adsorb and form monolayers. The remaining samples were washed three times with PBS. The

grids were then fixed with 50 µl of 2% (v/v) glutaraldehyde for 5 min and subsequently washed eight times with distilled water. The grids were contrasted with 50 µl of 4% (v/v) uranyl acetate (pH 7.0) for 5 min and the excess fluid was then removed by filter paper. Finally, the grids were loaded onto a transmission electron microscope (Tecnai G2 TEM Series, Hillsboro, OR, USA) with an accelerating voltage set at 80 kV with a magnification of 250,000×.

Exosomal Protein Extraction

Exosomes were resuspended in a 2-D lysis buffer containing 7 M urea, 2 M thiourea, 4% 3-[(3-cholamidopropyl)-dimethyl-ammonio]-1-propanesulfonate (CHAPS), 120 mM dithiothreitol (DTT), 2% ampholytes (pH 3–10), and 40 mM Tris-HCl and incubated at 4°C for 30 min. Protein concentrations were measured by the Bradford's method using Bio-Rad protein assay (Bio-Rad, Milano, Italy).

Western Blotting

Equal amount of exosomal proteins (20 µg/sample) from each sample were mixed with 2× Laemmli's buffer (to make the final concentration of 1× Laemmli's buffer) and resolved by 12% SDS-PAGE at 150 V for approximately 2 h using SE260 mini-Vertical electrophoresis unit (GE Healthcare; Uppsala, Sweden). After the completion of SDS-PAGE, the resolved proteins were transferred onto a nitrocellulose membrane (Whatman, Dassel, Germany) using a semidry transfer apparatus (GE Healthcare) at 85 mA for 1.5 h. Non-specific bindings were blocked with 5% skim milk in PBS at 25°C for 1 h. The membrane was incubated with mouse monoclonal anti-heat shock protein 70 (anti-HSP70), anti-Rab5, anti-HSP90β, anti-vimentin, or rabbit polyclonal anti-Rab7 antibody (all were purchased from Santa Cruz Biotechnology, Santa Cruz, CA, USA and were diluted 1:1,000 in 1% skim milk/PBS) at 4°C overnight. After washing with PBS three times, the membrane was incubated with corresponding secondary antibody conjugated with horseradish peroxidase (1:2,000 in 1% skim milk/PBS; DAKO Glostrup, Denmark) at 25°C for 1 h. Immunoreactive bands were developed by SuperSignal West Pico chemiluminescence substrate (Pierce Biotechnology, Rockford, IL, USA) and were then visualized by autoradiogram.

2-DE and Staining

Exosomal proteins derived from each culture flask were resolved in each 2-D gel as previously described (21, 23) (60 µg total protein/each sample/gel; $n = 5$ gels/group; a total of 10 gels were analyzed). Each protein sample was premixed with a rehydration buffer containing 7 M urea, 2 M thiourea, 2% CHAPS, 120 mM DTT, 40 mM Tris-base, 2% ampholytes (pH 3–10), and a trace of bromophenol blue to make a final volume of 150 µl. The mixture was rehydrated onto an Immobiline DryStrip (nonlinear pH gradient of 3–10, 7 cm long) (GE Healthcare, Uppsala, Sweden) at 25°C for 10–15 h. The first dimensional separation or isoelectric focusing (IEF) was performed in Ettan IPGphor III IEF System (GE Healthcare) at 20°C, using a stepwise mode to reach 9,083 Vh with a limiting current of 50 mA/strip. The IPG strips were then incubated for 15 min in equilibration buffer I containing 6 M urea, 130 mM DTT, 112 mM Tris-base, 4% SDS, 30% glycerol, and 0.002% bromophenol blue following by another 15 min in equilibration buffer II containing similar compositions as of buffer I, but DTT was replaced with 135 mM iodoacetamide. The equilibrated IPG strips were subjected to the second dimensional separation in 12.5% SDS-polyacrylamide gel using SE260 Mini-Vertical Electrophoresis Unit (GE Healthcare) at 20 µA/gel for approximately 1.5 h. Thereafter, the resolved proteins were stained with Deep Purple protein fluorescence dye (GE Healthcare) and visualized by using Typhoon 9200 laser scanner (GE Healthcare).

Spot Matching and Quantitative Intensity Analysis

Protein spots visualized in 2-DE gels were analyzed using ImageMaster 2D Platinum software (GE Healthcare). Parameters used for spot detection were (i) minimal area = 10 pixels; smooth factor = 2.0 and (ii) saliency = 200. A reference gel was created from an actual gel with the greatest number of protein spots and additional spots that were present in other gels were also combined to produce a single artificial reference gel with all protein spots present in all gels. The reference gel was then used for matching the corresponding protein spots across different gels. Background subtraction was performed and the intensity volume of each spot was normalized with total intensity volume (summation of the intensity volumes obtained from all spots within the same 2-D gel). Differentially expressed protein spots that reached statistically significant threshold ($P < 0.05$) were subjected to in-gel tryptic digestion and identification by mass spectrometry.

In-gel Tryptic Digestion

In-gel tryptic digestion was performed following protocol described previously (24, 25). Briefly, the protein spots with significantly differential levels were excised from 2-D gels, washed with 1 ml deionized water, and then destained with 100 µl of 100 mM NH_4HCO_3 at 25°C for 15 min. Thereafter, 100 µl acetonitrile (ACN) was added and incubated at 25°C for 15 min. After removing the solvent, the gel pieces were dried in a SpeedVac concentrator (Savant; Holbrook, NY, USA) and rehydrated with 50 µl of 10 mM DTT in 100 mM NH_4HCO_3 at 56°C for 30 min using a heat box. After removing the reducing buffer, the gel pieces were incubated with 50 µl of 55 mM iodoacetamide in 100 mM NH_4HCO_3 at 25°C for 20 min in the dark. The buffer was then removed, whereas the gel pieces were incubated with 100 µl of 50 mM NH_4HCO_3 at 25°C for 15 min. Thereafter, 100 µl ACN was added and incubated at 25°C for 15 min. After removing the solvent, the gel pieces were dried in a SpeedVac concentrator, and then incubated with a minimal volume (just to cover gel pieces) of 12 ng/µl sequencing grade modified trypsin (Promega, Madison, WI, USA) in 50 mM NH_4HCO_3 in a ThermoMixer® C (Eppendorf, Hauppauge, NY, USA) at 37°C for 16–18 h. The digestion reaction was stopped by incubation with 100 µl of 5% formic acid/ACN (1:2 vol/vol) at 37°C for 15 min. The digested peptide mixtures were collected using a pipette with gel loader tip, transferred into a fresh tube, dried by a SpeedVac concentrator, and subjected to MS/MS analysis.

Identification of Proteins by Nanoscale Liquid Chromatography–Electrospray Ionization–Electron Transfer Dissociation Tandem Mass Spectrometry (nanoLC-ESI-ETD MS/MS)

Separation of the digested peptides was performed using EASY-nLC II (Bruker Daltonics, Bremen, Germany) as previously described (26, 27). Briefly, peptides were loaded from a cooled (7°C) autosampler into an in-house, 3-cm-long pre-column containing 5-µm C18 resin (Dr. Maisch GmbH, Ammerbuch, Germany) and then to an in-house, 10-cm-long analytical column packed with 3-µm C18 resin (Dr. Maisch GmbH) using mobile phase A (0.1% formic acid). The peptides were then separated by mobile phase B (ACN/0.1% formic acid) gradient elution with three steps as follows: 0–35% for 30 min, 35–80% for 10 min, and then 80% for 10 min at a flow rate of 300 nl/min. Peptide sequences were then analyzed by amaZon speed ETD (Bruker Daltonics) with ESI nanosprayer ion source (spray capillary: fused silica with outer diameter of 90 µm and inner diameter of 20 µm) controlled by HyStar version 3.2 and trapControl version 7.1. Mass spectrometric parameters were set as follows: electrospray voltage = 4,500 V, high-voltage end-plate offset = 500 V, nebulizer gas = 0.55 bar, dry gas = 5.0 l/min, and dry temperature = 150°C. Precursors were scanned from 400 to 2,200 *m/z* range with enhanced resolution mode (speed = 8,100 *m/z*/s), ion charge control (ICC) target = 200,000, maximal accumulation time = 50 ms. The three most intense signals in every MS scan were selected for MS/MS analysis, whereas singly charged ions were excluded. For MS/MS experiment, fragmented peptides from 150 to 3,000 *m/z* range were scanned with XtremeScan mode (speed = 52,000 *m/z*/sec), ICC target = 200,000, maximal accumulation time = 100 ms. Mass spectra were deconvoluted *via* DataAnalysis version 4.0 SP5 (BrukerDaltonics) to *.mgf* file. Mascot software version 2.4.0 (Matrix Science; London, UK) was used to search MS/MS spectra against NCBI database of mammalian with the following standard Mascot parameters for CID: Enzyme = trypsin, maximal number of missed cleavages = 1, peptide tolerance = ± 1.2 Da, MS/MS tolerance = ± 0.6 Da, fixed modification = carbamidomethyl (C), variable modification = oxidation (M), charge states = 2+ and 3+, and instrument type = ESI-Trap.

Effect of COM Crystals on Inflammasome Activation

To evaluate the effect of COM crystal treatment on inflammasome activation, the culture supernatants derived from the controlled and COM-treated macrophages (2×10^6 cells/well) were collected, clarified by centrifugation at 300 *g*, and then subjected to indirect ELISA to measure level of IL-1β, one of the markers of inflammasome activation. Briefly, the clarified culture supernatant was concentrated by vacuum concentrator until completely dried. Thereafter, the samples were resuspended in 50 µl coating buffer (15 mM Na_2CO_3 and 30 mM $NaHCO_3$; pH 9.4) and then coated onto 96-well ELISA plate (Nunc, Roskilde, Denmark) at 4°C overnight. After washing with a washing buffer [0.05% (v/v) Tween-20/PBS], non-specific bindings were blocked by 1%BSA/PBS at 25°C for 2 h. After another wash, 100 µl of hamster monoclonal anti-IL-1β primary antibody (Santa Cruz Biotechnology) (diluted 1:50 in 0.1% BSA/PBS) was added and incubated at 25°C for 2 h. After another wash, the corresponding secondary antibody conjugated with horseradish peroxidase (diluted 1:100 in 0.1% BSA/PBS) was added and further incubated at 25°C for 2 h in the dark. The plate was then washed and added with 100 µl substrate solution (1.5 mM ortho-phenylenediamine dihydrochloride in 35 mM citric acid and 0.012% H_2O_2; pH 5.5). The reaction was allowed for 15 min in the dark before 50 µl of stop reaction solution (2 M H_2SO_4) was added. Finally, the absorbance (optical density) of the sample was measured at λ492 nm using an ELISA plate reader (Biochrom Ltd., Cambridge, UK).

Effects of COM-Treated vs. Controlled Exosomes on Monocyte and T-Cell Migration

Effects of exosomes derived from untreated (controlled exosomes) vs. COM-treated macrophages (COM-treated exosomes) on the migratory ability of monocytes and T-cells were evaluated using transwell culture plates with 5-µm pore size (Corning Life Sciences; Tewksbury, MA, USA) following protocol described previously with slight modification (3). Briefly, a total of 2×10^5 cells/well of U937 monocytes and Jurkat T-cells were cocultivated with 30 µg intact controlled or COM-treated exosomes at the upper chamber of transwell containing serum-free medium. To provide chemoattractant gradient, the medium at the lower chamber was supplemented with 10% FBS. After 24-h incubation, numbers of monocytes and T-cells migrated from upper to lower chambers were observed under an inverted phase-contrast light microscope (Nikon ECLIPSE Ti-S) and counted from at least 10 low-power fields (LPF) using ImageJ software (version 1.50f) (http://imagej.nih.gov/ij).

Effects of COM-Treated vs. Controlled Exosomes on Monocyte and T-Cell Activation

To evaluate effects of exosomes derived from untreated (controlled exosomes) vs. COM-treated macrophages (COM-treated exosomes) on monocyte and T-cell activation, flow cytometric analyses of markers for activated monocytes (CD11b) and T-cells (CD69) were performed. Following the migration assay as described above, the migrated cells at lower chamber of transwell were fixed with 2% (w/v) paraformaldehyde at 25°C for 15 min. Non-specific bindings were blocked with 5% (w/v) BSA in PBS and the cells were incubated with 1 µg/10^6 cells mouse monoclonal anti-CD11b or anti-CD69 antibody (both were from Santa Cruz biotechnology and were diluted in 1% BSA/PBS) at 25°C for 1 h. Thereafter, the cells were incubated with rabbit anti-mouse IgG conjugated with Alexa 488 (Molecular probe, Invitrogen; Eugene, OR, USA) (1:2,000 in 1%BSA/PBS) at 25°C for 1 h. The cells were then washed twice with ice-cold PBS and further analyzed by a flow cytometer (FACaliburs, Becton Dickinson Immunocytometry System, San Jose, CA, USA). IgG1 isotype antibody was used as the negative control.

Effects of COM-Treated vs. Controlled Exosomes on Macrophage Phagocytic Activity

To evaluate effects of exosomes derived from untreated (controlled exosomes) vs. COM-treated macrophages (COM-treated exosomes) on phagocytic activity, macrophages (2×10^5 cells/well) were incubated with 30 μg of intact controlled or COM-treated exosomes for 24 h. Thereafter, approximately 2×10^7 cells of *Saccharomyces cerevisiae* were cocultured with macrophages for 1 h. Phagocytic cells (macrophages containing at least one internalized yeast) were examined under an inverted phase-contrast light microscope (Nikon ECLIPSE Ti-S) and phagocytic activities were calculated from at least 10 high-power fields (HPF) using the following formulas.

Formula 1:

Percentage of phagocytic cells =
(Number of phagocytic cells in each HPF/
Total number of macrophages in each HPF) ×100.

Formula 2:

Phagocytic index = Percentage of phagocytic cells in each HPF
× Average number of internalized yeasts per cell.

Knockdown of Vimentin by Small-Interfering RNA (siRNA)

To further validate functional significance of the COM-treated exosomes in immune response, vimentin whose level was significantly increased in the COM-treated exosomes was selected as the target to be knocked down by siRNA technique. Briefly, macrophages (10×10^6 cells/flask) were transfected with 60 pmol of siRNA targeting on vimentin (si-Vimentin) or the controlled siRNA (si-Control) mixed with transfection reagent in the transfection medium (Santa Cruz Biotechnology) according to the manufacturer's protocol. After 6-h incubation in a humidified incubator with 5% CO_2 at 37°C, the transfection medium was removed and replaced with complete RPMI 1640 medium supplemented with 10% (v/v) heat-inactivated FBS and the cells were further incubated for 18 h. At 24-h post-transfection, the si-Control-transfected and si-Vimentin-transfected cells were subjected to COM crystal treatment as described earlier in the non-transfected cells (incubated in serum-free medium with or without 100 μg/ml COM crystals for 16 h). Confirmation of vimentin knockdown in the siRNA-transfected macrophages was performed by immunofluorescence staining as described below, whereas the culture supernatants were collected and subjected to exosome isolation as described above.

Immunofluorescence Staining

After COM treatment, the si-Control-transfected and si-Vimentin-transfected macrophages were adhered on a coverslip, fixed by 4% (v/v) paraformaldehyde/PBS at 25°C for 15 min, and then permeabilized with 0.2% Triton X-100/PBS at 25°C for 15 min. After washing, the cells were incubated at 4°C overnight with mouse monoclonal anti-vimentin antibody (Santa Cruz Biotechnology) (diluted 1:50 in 1% BSA/PBS). After washing, the cells were incubated with corresponding secondary antibody conjugated with Alexa Fluor 488 (Invitrogen) (diluted 1:2,000 in 1% BSA/PBS) at 25°C for 1 h. Finally, the cells were extensively washed with PBS and mounted onto a glass slide using 50% glycerol in PBS. The cells were imaged by using Nikon Eclipse 80i fluorescence microscope (Nikon). Expression level of vimentin was quantitated by measuring mean fluorescence intensity from at least 50 cells in 10 random HPF of each sample using NIS-Elements D V.4.11 software (Nikon).

Effects of si-Vimentin vs. si-Control on Activities of the COM-Treated Exosomes on Effector Immune/Inflammatory Cells

After COM treatment, exosomes derived from the si-Control-transfected and si-Vimentin-transfected macrophages were isolated. Thereafter, 30 μg of these intact exosomes were incubated with U937 monocytes, Jurkat T-cells, and macrophages (2×10^5 cells/well) for 24 h and the effector cells were subjected to evaluation of their migratory and phagocytic activities as aforementioned.

Effects of COM-Treated Exosomes and si-Vimentin on Proinflammatory Cytokine Production in the Effector Immune/Inflammatory Cells

To evaluate effects of COM-treated exosomes and si-Vimentin on proinflammatorty cytokine production in the effector immune/inflammatory cells, U937 monocytes (2×10^5 cells/well) were incubated with 30 μg intact exosomes derived from the non-transfected untreated macrophages (controlled exosomes), si-Control-transfected COM-treated macrophages, and si-Vimentin-transfected COM-treated macrophages for 24 h. The culture supernatant was collected, clarified by centrifugation at 300 *g*, and then subjected to indirect ELISA to measure level of IL-8, one of the proinflammatory cytokines produced by the effector immune/inflammatory cells. The sample preparation and ELISA protocols were similar to those used for ELISA measurement of IL-1β as described above (except for primary antibody that was rabbit polyclonal anti-IL-8 antibody (Santa Cruz Biotechnology) instead).

Statistical Analysis

Statistical analyses were performed using SPSS software version 13.0 (SPSS; Chicago, IL, USA). Comparisons between two sets of data (e.g., controlled exosome vs. COM-treated exosome) were performed by unpaired Student's *t*-test, whereas multiple comparisons were performed by one-way ANOVA with Tukey's *post hoc* test. *P*-values less than 0.05 were considered statistically significant.

RESULTS

Morphological and Marker Confirmation

Macrophage exosomes were isolated by microfiltration and differential centrifugation. Their morphology was examined using

the negative staining method and visualized by TEM. The results showed membrane-bounded, spherical shape vesicles with a size range of 50–80 nm (**Figure 1A**), consistent with the typical morphology and size of exosomes reported previously (28). In addition, Western blotting was performed to confirm the expression of exosomal markers. The data showed that levels of HSP70, Rab5, and Rab7, all of which are the typical exosomal markers, were enriched in the exosome purified fraction as compared to the whole supernatant (**Figures 1B–D**), indicating that isolation of macrophage exosomes was successful.

Significantly Altered Proteins in Macrophage Exosomes after Exposure to COM Crystals

Macrophages were treated with or without 100 μg/ml COM crystals for 16 h and their exosomal proteins were then subjected to comparative proteome analysis using 2-DE-based proteomics approach ($n = 5$ gels/group; a total of 10 gels were analyzed). Deep Purple fluorescence protein staining and Image Master 2D Platinum software (GE healthcare) with high stringent criteria for protein spot detection revealed approximately 150–200 protein spots in each 2-D gel (**Figure 2**). Spot matching, quantitative intensity analysis and statistics revealed six significantly altered protein spots in exosomes derived from COM-treated macrophages (COM-treated exosomes) as compared to the controls (**Figure 2**). These significantly altered proteins were then successfully identified by nanoLC-ESI-ETD MS/MS analyses (**Figure 2**), including L-plastin, coronin-like protein, pyruvate kinase, actin-related protein 3 (Arp3), HSP90β, and vimentin (**Table 1**). All these identified proteins were classified based on their main biological processes and immunological functions using UniProt Knowledgebase (UniProtKB) (http://www.uniprot.org), which is the central hub for collection of functional information of proteins. For biological processes, these included actin filament bundle assembly, actin cytoskeleton organization, ATP biosynthesis processes, actin nucleation, cellular response to unfolded proteins, and intermediate filament organization (**Table 2**). For immunological functions, most of the identified proteins were involved mainly in immune response, including T-cell activation, T-cell homeostasis, Fc-gamma (Fcγ) receptor pathway mediated phagocytosis, interferon-γ (IFN-γ) regulation, and cell migration and movement (**Table 2**).

Validation of the Proteome Data by Western Blotting

Western blot analysis was performed to validate the proteome data of two selected representative proteins with decreased and increased levels, respectively. The data demonstrated that the decreased level of HSP90β and increased level of vimentin in COM-treated exosomes as determined by 2-DE-based proteome analysis could be confirmed by Western blot analysis using Rab5, an exosomal marker, as the loading control to normalize (**Figure 3**).

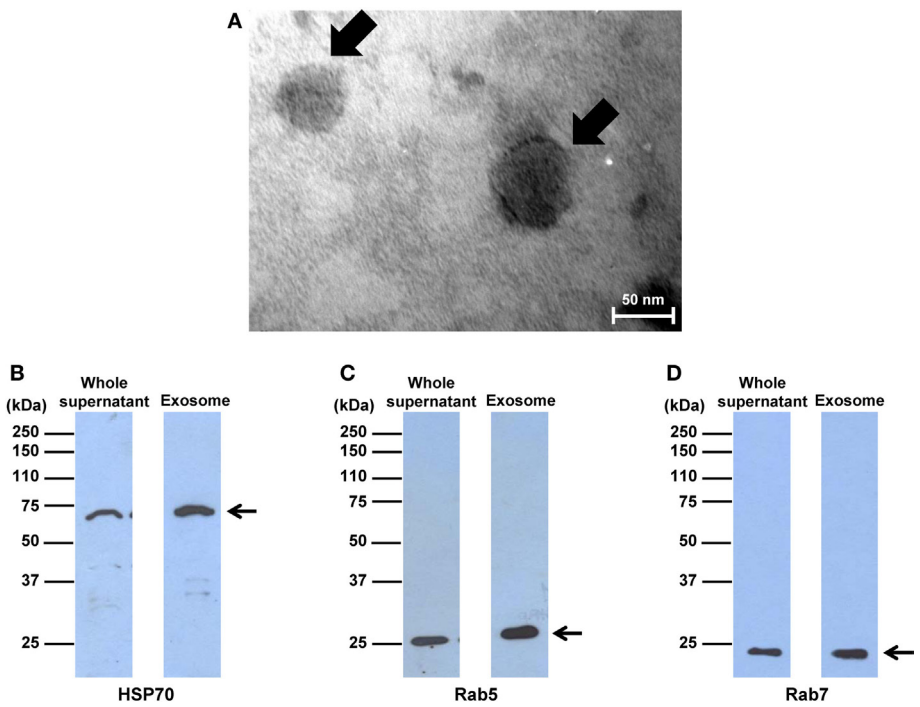

FIGURE 1 | Morphology and markers of exosomes isolated from macrophages. **(A)** Exosomes were isolated from macrophages, negatively stained with uranyl acetate, and imaged by transmission electron microscopy. The arrow indicates typical spherical shape of exosomes at original magnification of 250,000×. **(B–D)** Western blot analyses of exosomal markers, including heat shock protein 70, Rab5, and Rab7, in the whole supernatant compared to the exosome purified fraction (with an equal amount of total protein loaded in each lane). Note that these are the cropped images of the original blots, which are fully shown as Figure S1 in Supplementary Material.

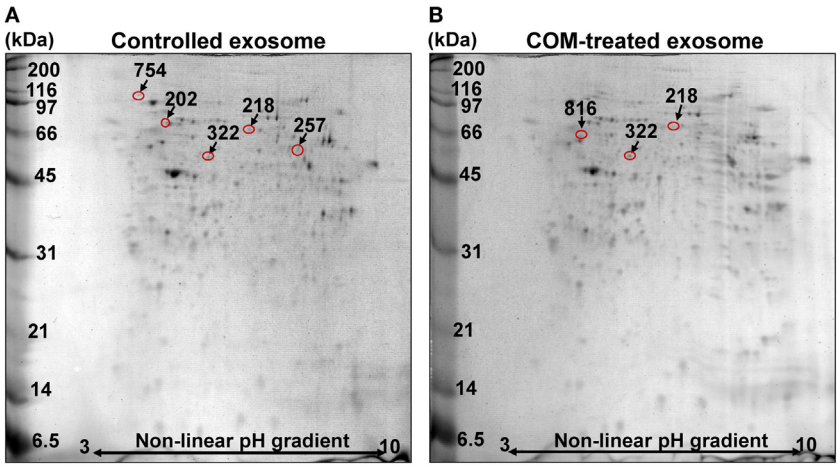

FIGURE 2 | 2-D proteome map of differentially expressed proteins. **(A)** Representative 2-D map of the controlled macrophage exosomes. **(B)** Representative 2-D map of exosomes derived from the calcium oxalate monohydrate (COM)-treated macrophages (COM-treated exosomes). Deep Purple fluorescence protein staining, $n = 5$ gels/group, a total of 10 gels were analyzed. The differentially expressed proteins are labeled with numbers that correspond to those indicated in **Tables 1** and **2**.

Effects of COM Crystals on Inflammasome Activation

To evaluate the inflammatory response induced by COM crystal treatment, activation of inflammasome was evaluated by measuring level of IL-1β, one of the markers of inflammasome activation, in culture supernatants of the COM-treated vs. controlled macrophages. ELISA revealed significant increase in IL-1β production in the COM-treated macrophages, suggesting that inflammasome was activated by COM crystal treatment (**Figure 4**).

Effects of COM-Treated vs. Controlled Exosomes on Monocyte and T-Cell Migration

Because most of the altered proteins were involved in immune response and vimentin (one of the proteins involving in cell migration/movement) was markedly increased in the COM-treated exosomes, we thus speculated that the COM-treated exosomes might affect migration of monocytes and T-cells. Our hypothesis was addressed by evaluation of the effects of COM-treated vs. controlled exosomes on monocyte and T-cell migration. The migration assay was performed using transwell and numbers of the migrated monocytes and T-cells were counted after incubation with these differential exosomes for 24 h. The results showed marked increases in numbers of migrating monocytes (**Figures 5A,B**) and T-cells (**Figures 6A,B**) after induction with COM-treated exosomes as compared to the controlled exosomes.

Effects of COM-Treated vs. Controlled Exosomes on Monocyte and T-Cell Activation

Activation of monocytes and T-cells was evaluated by measuring CD11b-positive monocytes and CD69-positive T-cells, respectively. Flow cytometric analysis revealed that number of the CD11b-positive monocytes was significantly increased (**Figures 5C,D**), whereas that of the CD69-positive cells was significantly decreased (**Figures 6C,D**) by the COM-treated exosomes.

Effects of COM-Treated vs. Controlled Exosomes on Macrophage Phagocytic Activity

Because Arp3, a protein involving in Fcγ receptor pathway mediated phagocytosis, was significantly increased in COM-treated exosomes, we thus hypothesized that the COM-treated exosomes might affect macrophage phagocytic activity. Our hypothesis was addressed by evaluation of the effects of COM-treated vs. controlled exosomes on macrophage phagocytic activity. The results showed that number of the phagocytic cells and phagocytic index of macrophages were significantly increased after the cells were exposed to the COM-treated exosomes as compared to the controlled exosomes (**Figure 7**).

Effects of si-Vimentin vs. si-Control on Activities of the COM-Treated Exosomes on Effector Immune/Inflammatory Cells

To validate functional relevance of the COM-treated exosomes in immune response, vimentin whose level was significantly increased in the COM-treated exosomes was knocked down by siRNA technique. The efficacy of siRNA targeting on vimentin (si-Vimentin) was confirmed by immunofluorescence staining, which showed markedly decreased level of vimentin in the si-Vimentin-transfected COM-treated macrophages as compared to the si-Control-transfected COM-treated macrophages (**Figure 8**).

Exosomes derived from these si-Vimentin-transfected COM-treated and si-Control-transfected COM-treated macrophages were then isolated and subjected to functional assays

TABLE 1 | Summary of significantly altered proteins in macrophage exosomes after exposure to 100 μg/ml COM crystals for 16 h.

Spot no.	Protein name	NCBI ID	MS/MS identification scores	%Cov	No. of distinct/total matched peptides	p/	MW (kDa)	Intensity (mean ± SEM)		Ratio (COM-treated/ controlled)	*P*-value
								Controlled exosome	COM-treated exosome		
202	L-plastin	gi|62898171	1,215	36	24/37	5.20	70.79	0.1702 ± 0.0724	0.0000 ± 0.0000	0.00	0.047
218	Coronin-like protein	gi|5902134	361	19	10/11	6.25	51.68	0.2537 ± 0.0697	0.0629 ± 0.0562	0.25	0.046
257	Pyruvate kinase isozymes M1/M2 isoform 2	gi|488544468	462	17	11/11	7.96	58.43	0.1466 ± 0.0634	0.0000 ± 0.0000	0.00	0.046
322	Actin-related protein 3 isoform 1	gi|5031573	512	22	10/12	5.61	47.80	0.3521 ± 0.0297	0.5521 ± 0.0452	1.57	0.006
754	HSP90-beta	gi|306891	87	11	9/9	4.97	85.58	0.2632 ± 0.0743	0.0000 ± 0.0000	0.00	0.008
816	Vimentin	gi|340219	730	39	20/22	5.03	53.74	0.0000 ± 0.0000	1.1192 ± 0.3448	#DIV/0	0.043

%Cov = %Sequence coverage [(number of the matched residues/total number of residues in the entire sequence) × 100%].

#DIV/0 = Divided by zero.

NCBI, National Center for Biotechnology Information.

to evaluate migratory and phagocytic activities of the effector immune/inflammatory cells. The data showed that the COM-treated exosomes derived from the si-Vimentin-transfected macrophages caused significant decreases in migratory activities of both monocytes and T-cells as compared to the COM-treated exosomes derived from the si-Control-transfected macrophages (**Figure 9**). In addition, macrophages incubated with the COM-treated exosomes derived from the si-Vimentin-transfected cells had significantly fewer numbers of phagocytic cells and less phagocytic index than when they were incubated with the COM-treated exosomes derived from the si-Control-transfected cells (**Figure 10**).

Effects of COM-Treated Exosomes and si-Vimentin on Proinflammatory Cytokine Production in the Effector Immune/ Inflammatory Cells

To evaluate effects of COM-treated exosomes and si-Vimentin on proinflammatory cytokine production in the effector immune/ inflammatory cells, ELISA was performed to measure level of IL-8, one of the proinflammatory cytokines, produced from U937 monocytes incubated with exosomes derived from the non-transfected untreated macrophages (controlled exosomes), si-Control-transfected COM-treated macrophages, and si-Vimentin-transfected COM-treated macrophages. The data revealed significantly increased level of IL-8 produced by the cells incubated with the COM-treated exosomes derived from the si-Control-transfected macrophages, whereas si-Vimentin successfully restored IL-8 to the basal level (comparable to the cells incubated with the controlled exosomes) (**Figure 11**).

DISCUSSION

Exosomes are originated from the internalized vesicles *via* endocytosis that subsequently form multivesicular bodies (MVB) (29). They are secreted to extracellular milieu *via* exocytosis pathway by fusing MVB with plasma membranes (30). Exosomes contain several types of biomolecules, including mRNAs, microRNAs, proteins and lipids, which reflect their diverse biological functions (31). From their origination, exosomes are commonly enriched with proteins associated with MVB biogenesis, transport and fusion (30). In addition, they are also enriched with intregrins (CD81 and CD82), tetraspanins (CD9 and CD63), chaperones (HSP70 and HSP90), and major histocompatibility complex class I and class II (32). For intercellular communications, exosomes shuttle their biomolecules to the target cells by three major mechanisms, including receptor–ligand interaction, direct fusion with plasma membranes, and endocytosis (30).

Macrophage exosomes have been demonstrated to possess immune functions in several diseases, including host–pathogen interactions and cancers (30). For host–pathogen interactions, *in vitro* studies have shown that macrophages with intracellular pathogens secrete greater amounts of exosomes as compared to the uninfected cells. Exosomes derived from these infected macrophages activate naive macrophages through tumor

TABLE 2 | Biological process and immunological function of the significantly altered proteins in COM-treated exosomes.

Spot no.	Protein name	Biological process	Immunological function	Alteration in COM-treated exosomes
202	L-plastin	Actin filament bundle assembly	T-cell activation involved in immune response	Decreased
218	Coronin-like protein	Actin cytoskeleton organization	T-cell homeostasis	Decreased
257	Pyruvate kinase isozymes M1/M2 isoform 2	ATP biosynthesis process	–	Decreased
322	Actin-related protein 3 isoform 1	Actin nucleation	Fcγ receptor pathway mediated phagocytosis	Increased
754	HSP90-beta	Cellular response to unfold proteins	IFN-γ regulation	Decreased
816	Vimentin	Intermediate filament organization	Cell migration and movement	Increased

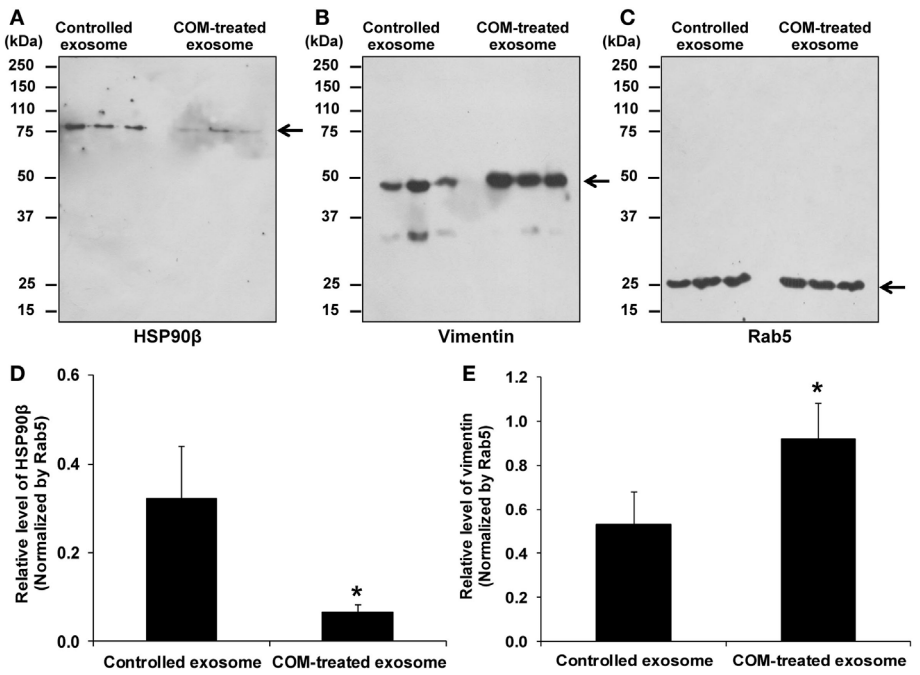

FIGURE 3 | Validation of the proteome data by Western blot analysis. **(A)** The decreased level of HSP90β in exosomes derived from the COM-treated macrophages (COM-treated exosomes). **(B)** The increased level of vimentin in the COM-treated exosomes. **(C)** Rab5 served as the loading control. **(D)** Normalized level of HSP90β. **(E)** Normalized level of vimentin. Each bar represents mean ± SD of the data obtained from three independent biological replicates. *$P < 0.05$ vs. controlled exosomes.

necrosis factor-α and IL-12, and subsequently recruit monocytes and neutrophils into the inflammatory sites (33, 34). In cancers, macrophage-derived exosomes can promote cancer cell invasion and metastasis. The proteome data has demonstrated that these exosomes have increased levels of matrix metalloproteinase (MMP) and cathepsins, which can cleave extracellular matrix facilitating tumor dissemination (35).

In kidney stone disease, infiltration of macrophages in the renal interstitium can promote chronic inflammation, leading to chronic kidney disease (1–3). Macrophages secrete several types of biomolecules in response to CaOx crystals deposited in renal interstitium, including ROS, chemokines, proinflammatory cytokines, and fibrogenic factors that subsequently stimulate the inflammatory processes and provoke tubulointerstitial damage (10–12). These secretory products may also play important autocrine and/or paracrine roles in the renal interstitial milieu. In addition, interstitial CaOx crystal deposition can then activate mononuclear phagocytes (i.e., dendritic cells and macrophages) to secret IL-1β through NLRP3/ASC/caspase-1-dependent pathway, causing renal inflammation in kidney stone disease (15). These findings indicate that CaOx crystals are also involved in activation of inflammasome, the multiprotein complex that plays crucial role in innate immunity (15). Likewise, infection and cellular stress can enhance inflammasome activation in the activated macrophages as indicated by redistribution and spatial organization of ASC (apoptotic speck-like protein containing a CARD) to the cytoplasm, followed by assembly of inflammasome components, including Nod-like receptors (NLR) and caspase-1 in the perinuclear space, which is necessary for inflammasome function such as maturation of IL-1β and IL-18 for further inflammatory signaling. In contrast, primary localization of ASC and caspase-1 in the nucleus is commonly observed in the resting monocytes/macrophages (36). Consistent with the previous reports, we demonstrated herein that COM crystals could

induce inflammasome activation in macrophages, leading to the increased level of IL-1β, one of the markers for inflammasome activation, in culture supernatant (**Figure 4**). In addition, we have demonstrated for the first time that COM crystals could induce changes in proteins expressed in exosomes isolated from macrophages and these altered exosomal proteins were involved in several immune functions (**Figure 2**; **Tables 1** and **2**).

Vimentin is the most abundant intermediate filament that stabilizes cellular architecture (37). In immune cells, vimentin can be secreted from the activated monocytes, macrophages, and neutrophils and is responsible for activating cell migration, proinflammatory signaling, and oxidative burst (38). In cancers, exosomes derived from macrophages can induce cytoskeletal rearrangement by transferring vimentin-containing exosomes, which further stimulate metastasis of the cancer cells through Wnt signaling pathway (39, 40). Herein, our proteome data showed that vimentin was markedly increased in the COM-treated exosomes that could be confirmed by Western blot analysis. Note that vimentin band at low molecular mass (approximately 30 kDa) was observed in some samples, especially in the controlled exosomes (**Figure 3B**). In monocyte-derived macrophages, it was possible that vimentin could be degraded during sample processing or cleaved by proteases and then secreted during differentiation process (41). Alternatively, it could be the protein kinase C-dependent phosphorylated form of vimentin that was secreted by activated macrophages (38).

From the proteome data, we hypothesized that the COM-treated exosomes might promote migratory activity of other immune cells in the renal interstitium. Accordingly, migration assay was performed to evaluate migratory activities of monocytes and T-cells exposed to COM-treated vs. controlled exosomes. The functional data confirmed that the COM-treated exosomes dramatically enhanced monocyte and T-cell migration (**Figures 5A,B** and **6A,B**). Monocytes are important responder cells in the renal interstitium to develop chronic inflammation in kidney stone disease (42, 43). Under inflammatory response, monocytes are stimulated to enhance their immune functions. Our functional data clearly demonstrated the activation of monocytes by COM-treated exosomes as evidenced by an increase of CD11b, which is a marker for monocyte activation

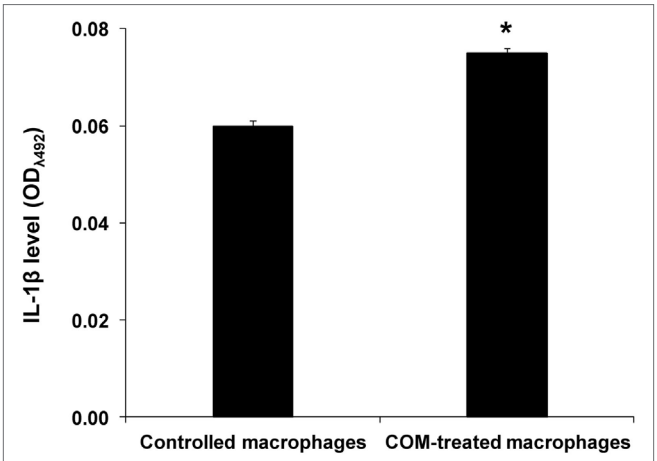

FIGURE 4 | Effects of calcium oxalate monohydrate (COM) crystals on inflammasome activation. Interelukin-1β level was measured by ELISA in culture supernatants of macrophages with or without COM crystal treatment. Each bar represents mean ± SD of the data obtained from three independent biological replicates. *$P < 0.05$ vs. control.

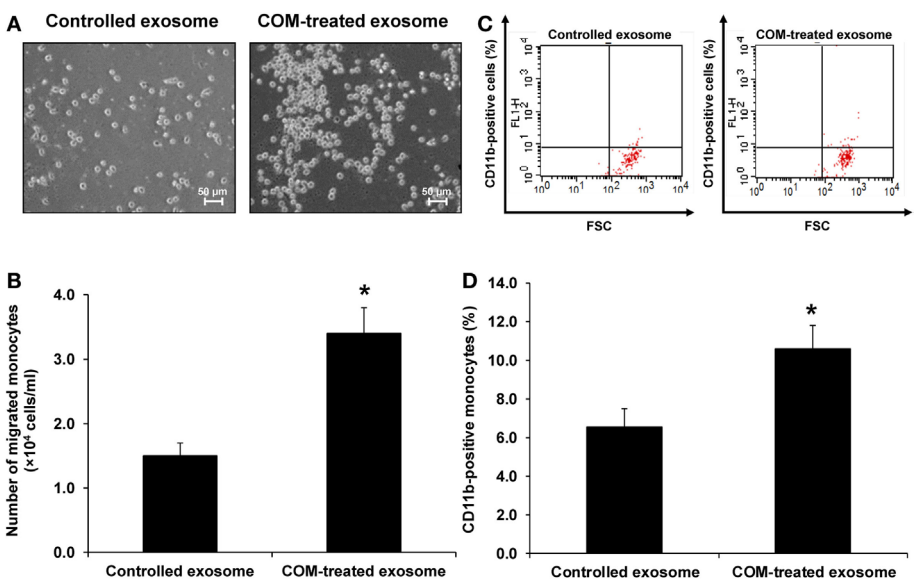

FIGURE 5 | Effects of calcium oxalate monohydrate (COM)-treated vs. controlled exosomes on monocyte migration and activation. **(A)** The migrated monocytes at the lower chamber of transwell were examined and imaged using an inverted phase-contrast light microscope with an original magnification of 200×. **(B)** The migrated monocytes were counted from at least 10 low-power fields (LPF). **(C)** The representative dot plot of flow cytometric data in each group to quantitate the CD11b-positive migrated monocytes (FSC, forward scatter, indicating cell size). **(D)** The percentage the CD11b-positive cells. Each bar represents mean ± SD of the data obtained from three independent biological replicates. *$P < 0.05$ vs. controlled exosomes.

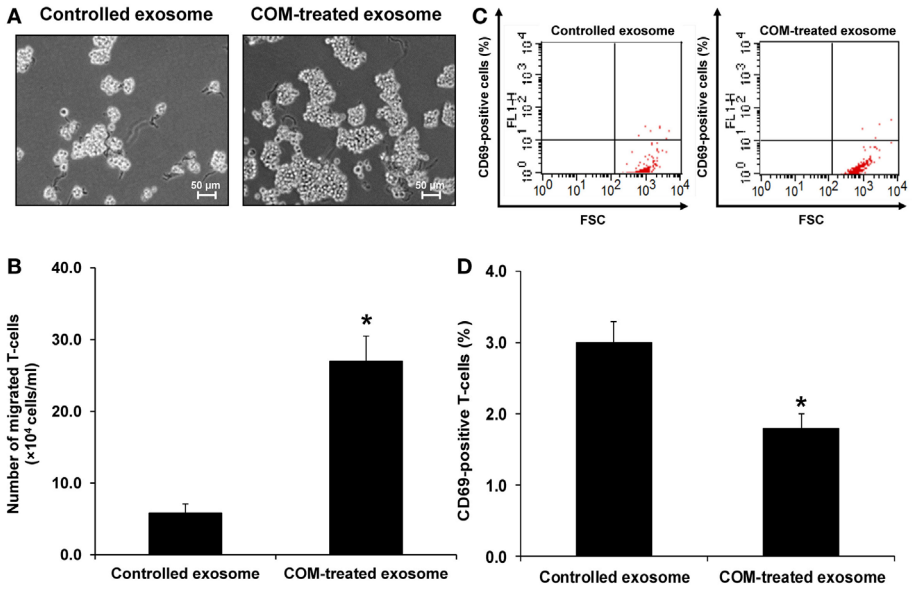

FIGURE 6 | Effects of calcium oxalate monohydrate (COM)-treated vs. controlled exosomes on T-cell migration and activation. **(A)** The migrated T-cells at the lower chamber of transwell were examined and imaged using an inverted phase-contrast light microscope with an original magnification of 200×. **(B)** The migrated T-cells were counted from at least 10 low-power fields (LPF). **(C)** The representative dot plot of flow cytometric data in each group to quantitate the CD69-positive migrated T-cells (FSC, forward scatter, indicating cell size). **(D)** The percentage the CD69-positive cells. Each bar represents mean ± SD of the data obtained from three independent biological replicates. *$P < 0.05$ vs. controlled exosomes.

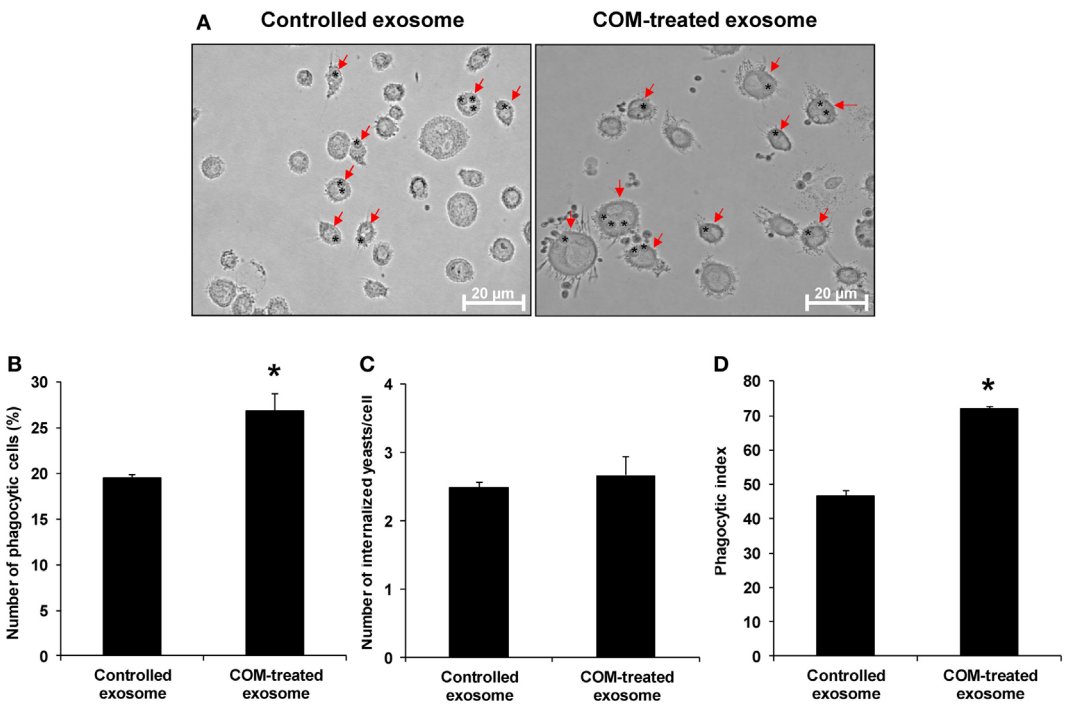

FIGURE 7 | Effects of calcium oxalate monohydrate (COM)-treated vs. controlled exosomes on macrophage phagocytic activity. Macrophages were incubated with intact controlled exosomes or COM-treated exosomes for 24 h followed by incubation with *Saccharomyces cerevisiae* for 1 h. **(A)** The phagocytic cells (indicated with arrows), representing macrophages with at least one internalized yeast (indicated with asterisks), were examined under an inverted phase-contrast light microscope with the original magnification of 400×. Phagocytic activities were calculated from at least 10 high-power fields to determine percentage of the phagocytic cells **(B)**, number of the internalize yeasts per cell **(C)**, and phagocytic index **(D)** (see formulas in Section "Materials and Methods"). Each bar represents mean ± SD of the data obtained from three independent biological replicates. *$P < 0.05$ vs. controlled exosomes.

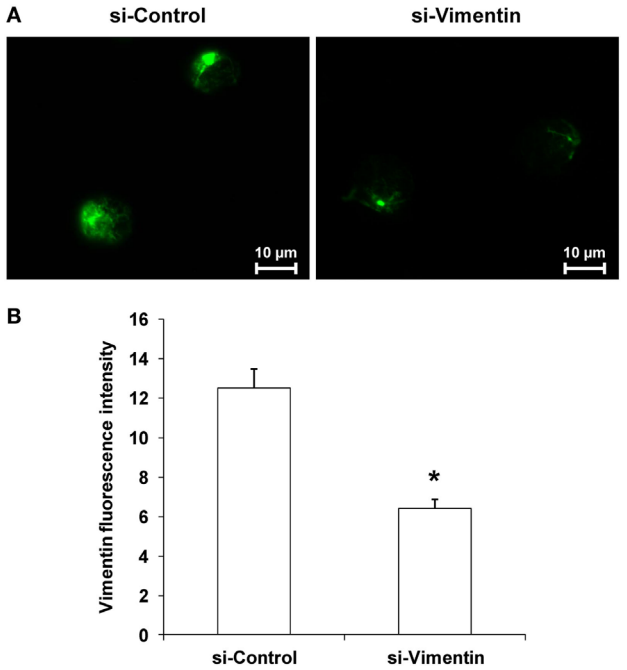

FIGURE 8 | Efficacy of knockdown of vimentin by small-interfering RNA (siRNA). **(A)** Immunofluorescence staining of vimentin in the siRNA targeting on vimentin-transfected vs. si-Control-transfected macrophages after calcium oxalate monohydrate treatment. **(B)** Mean fluorescence intensity of vimentin was measured from at least 10 high-power fields. Each bar represents mean ± SD of the data obtained from three independent biological replicates. *$P < 0.05$ vs. si-Control.

(44), on their surfaces (**Figures 5C,D**). In contrast, we found the decreases of L-plastin and coronin-like protein in the COM-treated exosomes. L-plastin is the actin-bundling protein that is exclusively found in leukocytes, i.e., macrophages, lymphocytes, neutrophils, and other granulocytes (40, 45). This protein consists of two tandem repeated actin-binding domains, which are responsible for F-actin bundling and rearrangement (46). Interestingly, L-plastin has been reported to specifically induce T-lymphocyte activation (47). Likewise, coronin-like protein is an actin and microtubule binding protein that plays pivotal role in T-cell activation (48). Their decreases implicated a reduction of T-cell activation. Our functional data clearly showed the significant decrease of CD69, a marker for T-cell activation (49), on surfaces of T-cells exposed to the COM-treated exosomes confirming that T-cell activation was reduced by the COM-treated exosomes (**Figures 6C,D**).

Furthermore, we also observed significant increase in level of Arp3 isoform1 in the COM-treated exosomes. Arp3 is a member of Arp2/3 complex, which is localized on cell surfaces and is essential for filopodia and lamellipodia structure (50). Arp2/3 complex is important for cell motility and phagosome formation that are the critical steps for phagocytic activity of phagocytes (51). Our functional data showed clear evidence that the COM-treated exosomes had an autocrine function by activation of phagocytic activity of macrophages (**Figure 7**). Therefore, the increased level of Arp 3 in the COM-treated exosomes might be responsible for such autocrine effect.

Finally, to further confirm the functional relevance of our proteome findings in immune response, vimentin was knocked down by siRNA technique. The data have confirmed that macrophage

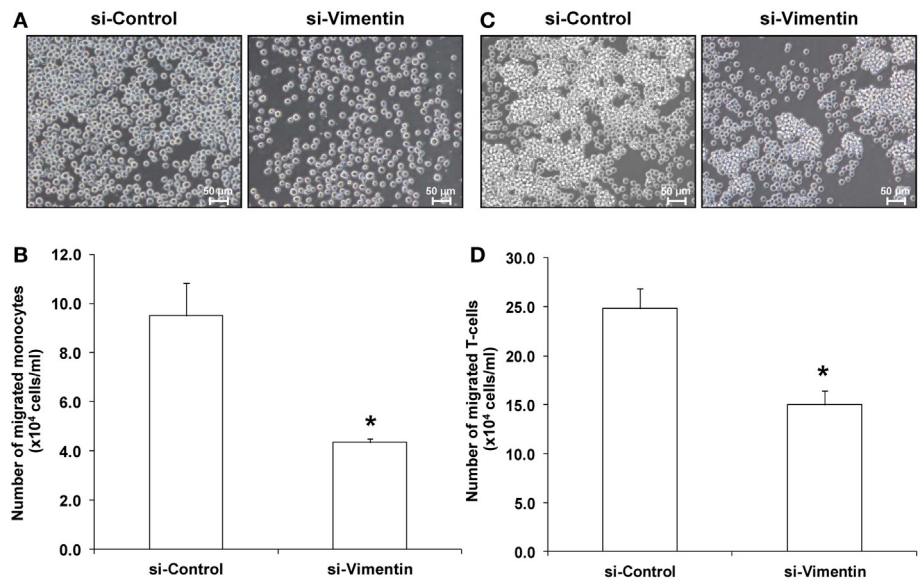

FIGURE 9 | Effects of small-interfering RNA targeting on vimentin vs. si-Control on activities of the calcium oxalate monohydrate-treated exosomes on monocyte and T-cell migration. This experiment was performed using transwell similar to that of the non-transfected cells. The migrated monocytes **(A)** and T-cells **(C)** at the lower chamber of transwell were examined and imaged using an inverted phase-contrast light microscope with an original magnification of 200×. The migrated monocytes **(B)** and T-cells **(D)** were counted from at least 10 low-power fields. Each bar represents mean ± SD of the data obtained from three independent biological replicates. *$P < 0.05$ vs. si-Control.

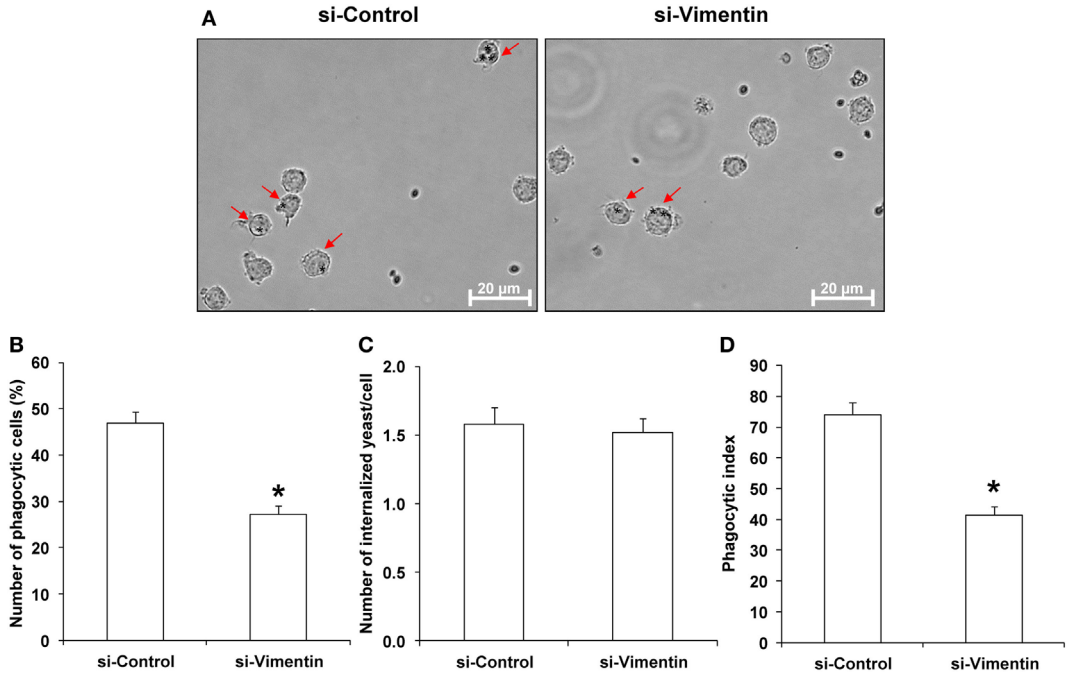

FIGURE 10 | Effects of small-interfering RNA targeting on vimentin (si-Vimentin) vs. si-Control on activities of the calcium oxalate monohydrate (COM)-treated exosomes on macrophage phagocytic activity. Macrophages were incubated with intact exosomes derived from si-Control-transfected COM-treated or si-Vimentin-transfected COM-treated macrophages for 24 h followed by incubation with *Saccharomyces cerevisiae* for 1 h. **(A)** The phagocytic cells (indicated with arrows), representing macrophages with at least one internalized yeast (indicated with asterisks), were examined under an inverted phase-contrast light microscope with the original magnification of 400×. Phagocytic activities were calculated from at least 10 high-power fields to determine percentage of the phagocytic cells **(B)**, number of the internalize yeasts per cell **(C)**, and phagocytic index **(D)** (see formulas in Section "Materials and Methods"). Each bar represents mean ± SD of the data obtained from three independent biological replicates. *$P < 0.05$ vs. si-Control.

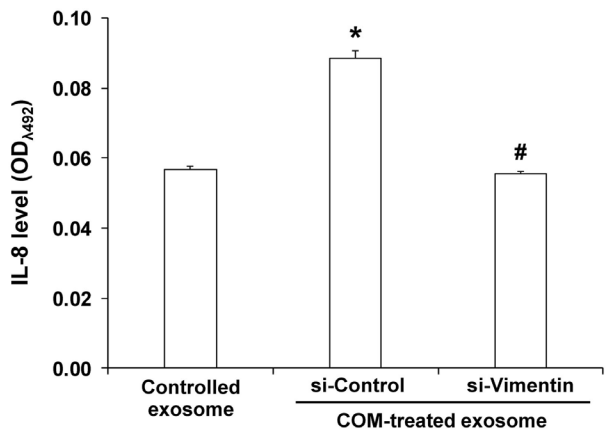

FIGURE 11 | Effects of calcium oxalate monohydrate (COM)-treated exosomes and small-interfering RNA targeting on vimentin (si-Vimentin) on proinflammatory cytokine production in the effector immune/inflammatory cells. U937 monocytes were incubated with intact exosomes derived from the non-transfected untreated (controlled exosome), si-Control-transfected COM-treated, or si-Vimentin-transfected COM-treated macrophages for 24 h. The culture supernatants were collected and subjected to indirect ELISA to measure level of interleukin-8, one of the proinflammatory cytokines produced by the effector immune/inflammatory cells. Each bar represents mean ± SD of the data obtained from three independent biological replicates. *$P < 0.05$ vs. controlled exosome; #$P < 0.05$ vs. si-Control-transfected COM-treated exosome.

exosomal vimentin played significant roles in immune response to COM crystals and were involved in proinflammatory cytokine production, monocyte and T-cell migration, and phagocytic activity of macrophages (**Figures 9–11**). Regarding its role in immune response, a recent study has revealed that vimentin can be secreted by activated macrophages in response to either pro- or anti-inflammatory cytokines. In response to pathogens, secreted vimentin has been implicated in producing oxidative metabolites that are essential for effective bacterial killing by the activated macrophages (38). In addition, vimentin has been reported as a chemoattractant for monocyte migration, consistent to our findings. Interestingly, truncated vimentin generated by leukolysin (also known as MMP25) can enhance phagocytic activity of macrophages (52). These findings support the role of the exosomal vimentin in recruitment of immune cells and enhancement of phagocytic activity of macrophages observed in our study. Nevertheless, the knowledge on biological roles of extracellular vimentin in immune function is currently limited. Therefore, molecular mechanisms of exosomal vimentin in immunology deserve further investigations.

Although this study was quite convincing to clarify significant immune functions of the COM-treated exosomes related to inflammatory response in kidney stone disease, some technical limitations should be mentioned. First, using the 2-DE-based proteomics approach, a relatively small number of altered proteins were identified. Additionally, some of the identified altered

proteins were detectable only in one group, but were under the detectability limit in the other group by using this approach (**Table 1**). Actually, they were not really absent in such group as in cases of HSP90β and vimentin, which could not be detected by 2-DE in the COM-treated and controlled exosomes, respectively, whereas they were detectable in both groups by Western blotting but with significant changes in their levels (**Figure 3**). Moreover, 2-DE-based approach has another limitation in resolving membrane or highly hydrophobic proteins, which are the major constituents on exosomal surfaces. Therefore, using gel-free and other more sensitive proteomics approaches would overcome such limitations and yield a wider image of significant impact of macrophage exosomes in pathogenic mechanisms of kidney stone disease.

Second, there was a difference in number of migrated monocytes induced by exosomes derived from the COM-treated macrophages in the former experiment (**Figure 5B**) as compared to that induced by exosomes derived from the si-Control-transfected COM-treated macrophages in the latter to validate the functional relevance of macrophage exosomal vimentin in the immune response to COM crystals (**Figure 9B**). This difference was most likely due to inter-assay variations (particularly from different batches of U937 cell aliquots used and different lots of PMA employed for macrophage derivatization). Nevertheless, each of these experiments had its own corresponding control. Therefore, the functional relevance of macrophage exosomes should not be hampered by these common variations. Similar phenomenon was observed for the percentage of phagocytic cells induced by exosomes derived from the COM-treated macrophages in the former experiment (**Figure 7B**) as compared to that induced by exosomes derived from the si-Control-transfected COM-treated macrophages in the latter (**Figure 10B**). However, the consistency in phagocytic index in both sets of experiments on different occasions (**Figures 7D** and **10D**, respectively) might be able to strengthen our claim.

Finally, it should be noted that only vimentin was selected for functional validation of the immunological roles of macrophage exosomes in response to COM crystals by si-RNA technique. Other altered proteins reported in **Tables 1** and **2** might also play significant roles in such immune response as well. Manipulation of their expression (by knockdown and/or overexpression methods) would provide more lines of evidence to convince the crucial roles of macrophage exosomes in progressive interstitial inflammation in kidney stone pathogenic mechanisms.

In summary, we have reported herein changes in macrophage exosomal proteins after exposure to COM crystals. These altered exosomal proteins were involved mainly in immune response with possible autocrine and/or paracrine effects. Specifically, the COM-treated exosomes induced proinflammatory cytokine production, increased monocyte and T-cell migration, and promoted monocyte activation while reduced T-cell activation. In addition, the COM-treated exosomes enhanced phagocytic activity of macrophages. Moreover, our present study has demonstrated for the first time that the macrophage exosomal vimentin played significant roles in the immune response to COM crystals, although the significant roles of other exosomal proteins could not be entirely excluded. Taken together, these findings provided some implications to the immune response during kidney stone pathogenesis *via* exosomal pathway of macrophages after exposure to COM crystals.

AUTHOR CONTRIBUTIONS

NS, RK, AN, and VT designed research. NS, RK, and AN performed experiments. NS, RK, AN, and VT analyzed data. All authors wrote, reviewed, and approved the manuscript.

ACKNOWLEDGMENTS

We are grateful to Arada Vinaiphat and Supaporn Khamchun for their technical assistance. This study was supported by Mahidol University research grant and the Thailand Research Fund (IRN60W0004 and IRG5980006). NS is supported by the Royal Golden Jubilee PhD Program (PHD/0182/2554).

SUPPLEMENTARY MATERIAL

The Supplementary Material for this article can be found online at http://www.frontiersin.org/articles/10.3389/fimmu.2018.00316/full#supplementary-material.

REFERENCES

1. de Water R, Noordermeer C, Houtsmuller AB, Nigg AL, Stijnen T, Schroder FH, et al. Role of macrophages in nephrolithiasis in rats: an analysis of the renal interstitium. *Am J Kidney Dis* (2000) 36:615–25. doi:10.1053/ajkd.2000.16203
2. Okada A, Yasui T, Fujii Y, Niimi K, Hamamoto S, Hirose M, et al. Renal macrophage migration and crystal phagocytosis via inflammatory-related gene expression during kidney stone formation and elimination in mice: detection by association analysis of stone-related gene expression and microstructural observation. *J Bone Miner Res* (2010) 25:2701–11. doi:10.1002/jbmr.158
3. Singhto N, Sintiprungrat K, Thongboonkerd V. Alterations in macrophage cellular proteome induced by calcium oxalate crystals: the association of HSP90 and F-actin is important for phagosome formation. *J Proteome Res* (2013) 12:3561–72. doi:10.1021/pr4004097
4. Schubert G. Stone analysis. *Urol Res* (2006) 34:146–50. doi:10.1007/s00240-005-0028-y
5. Sheng X, Ward MD, Wesson JA. Crystal surface adhesion explains the pathological activity of calcium oxalate hydrates in kidney stone formation. *J Am Soc Nephrol* (2005) 16:1904–8. doi:10.1681/ASN.2005040400
6. Elliot S, Goldsmith P, Knepper M, Haughey M, Olson B. Urinary excretion of aquaporin-2 in humans: a potential marker of collecting duct responsiveness to vasopressin. *J Am Soc Nephrol* (1996) 7:403–9.
7. Tomazic BB, Nancollas GH. The dissolution of calcium oxalate kidney stones. A kinetic study. *J Urol* (1982) 128:205–8. doi:10.1016/S0022-5347(17)52819-0
8. Wang T, Thurgood LA, Grover PK, Ryall RL. A comparison of the binding of urinary calcium oxalate monohydrate and dihydrate crystals to human kidney cells in urine. *BJU Int* (2010) 106:1768–74. doi:10.1111/j.1464-410X.2010.09258.x
9. Vinaiphat A, Aluksanasuwan S, Manissorn J, Sutthimethakorn S, Thongboonkerd V. Response of renal tubular cells to differential types and doses of calcium oxalate crystals: integrative proteome network analysis and functional investigations. *Proteomics* (2017) 17:15–6. doi:10.1002/pmic.201700192

10. Khan SR. Reactive oxygen species as the molecular modulators of calcium oxalate kidney stone formation: evidence from clinical and experimental investigations. *J Urol* (2013) 189:803–11. doi:10.1016/j.juro.2012.05.078
11. de Water R, Leenen PJ, Noordermeer C, Nigg AL, Houtsmuller AB, Kok DJ, et al. Cytokine production induced by binding and processing of calcium oxalate crystals in cultured macrophages. *Am J Kidney Dis* (2001) 38:331–8. doi:10.1053/ajkd.2001.26098
12. Kanlaya R, Sintiprungrat K, Thongboonkerd V. Secreted products of macrophages exposed to calcium oxalate crystals induce epithelial mesenchymal transition of renal tubular cells via RhoA-dependent TGF-beta1 pathway. *Cell Biochem Biophys* (2013) 67:1207–15. doi:10.1007/s12013-013-9639-z
13. Anders HJ, Suarez-Alvarez B, Grigorescu M, Foresto-Neto O, Steiger S, Desai J, et al. The macrophage phenotype and inflammasome component NLRP3 contributes to nephrocalcinosis-related chronic kidney disease independent from IL-1-mediated tissue injury. *Kidney Int* (2018). doi:10.1016/j.kint.2017.09.022
14. Mulay SR, Anders HJ. Crystal nephropathies: mechanisms of crystal-induced kidney injury. *Nat Rev Nephrol* (2017) 13:226–40. doi:10.1038/nrneph.2017.10
15. Mulay SR, Kulkarni OP, Rupanagudi KV, Migliorini A, Darisipudi MN, Vilaysane A, et al. Calcium oxalate crystals induce renal inflammation by NLRP3-mediated IL-1beta secretion. *J Clin Invest* (2013) 123:236–46. doi:10.1172/JCI63679
16. Mulay SR, Evan A, Anders HJ. Molecular mechanisms of crystal-related kidney inflammation and injury. Implications for cholesterol embolism, crystalline nephropathies and kidney stone disease. *Nephrol Dial Transplant* (2014) 29:507–14. doi:10.1093/ndt/gft248
17. Kusmartsev S, Dominguez-Gutierrez PR, Canales BK, Bird VG, Vieweg J, Khan SR. Calcium oxalate stone fragment and crystal phagocytosis by human macrophages. *J Urol* (2016) 195:1143–51. doi:10.1016/j.juro.2015.11.048
18. Tamura M, Aizawa R, Hori M, Ozaki H. Progressive renal dysfunction and macrophage infiltration in interstitial fibrosis in an adenine-induced tubulointerstitial nephritis mouse model. *Histochem Cell Biol* (2009) 131:483–90. doi:10.1007/s00418-009-0557-5
19. Yang M, Chen J, Su F, Yu B, Su F, Lin L, et al. Microvesicles secreted by macrophages shuttle invasion-potentiating microRNAs into breast cancer cells. *Mol Cancer* (2011) 10:117. doi:10.1186/1476-4598-10-117
20. Thongboonkerd V, Semangoen T, Chutipongtanate S. Factors determining types and morphologies of calcium oxalate crystals: molar concentrations, buffering, pH, stirring and temperature. *Clin Chim Acta* (2006) 367:120–31. doi:10.1016/j.cca.2005.11.033
21. Thongboonkerd V, Semangoen T, Sinchaikul S, Chen ST. Proteomic analysis of calcium oxalate monohydrate crystal-induced cytotoxicity in distal renal tubular cells. *J Proteome Res* (2008) 7:4689–700. doi:10.1021/pr8002408
22. Sintiprungrat K, Singhto N, Sinchaikul S, Chen ST, Thongboonkerd V. Alterations in cellular proteome and secretome upon differentiation from monocyte to macrophage by treatment with phorbol myristate acetate: insights into biological processes. *J Proteomics* (2010) 73:602–18. doi:10.1016/j.jprot.2009.08.001
23. Ngai HH, Sit WH, Jiang PP, Xu RJ, Wan JM, Thongboonkerd V. Serial changes in urinary proteome profile of membranous nephropathy: implications for pathophysiology and biomarker discovery. *J Proteome Res* (2006) 5:3038–47. doi:10.1021/pr060122b
24. Thongboonkerd V, Klein JB, Arthur JM. Proteomic identification of a large complement of rat urinary proteins. *Nephron Exp Nephrol* (2003) 95:e69–78. doi:10.1159/000073674
25. Thongboonkerd V, Klein JB, Pierce WM, Jevans AW, Arthur JM. Sodium loading changes urinary excretion: a proteomic analysis. *Am J Physiol Renal Physiol* (2003) 284:F1155–63. doi:10.1152/ajprenal.00140.2002
26. Tavichakorntrakool R, Boonsiri P, Prasongwatana V, Lulitanond A, Wongkham C, Thongboonkerd V. Differential colony size, cell length, and cellular proteome of *Escherichia coli* isolated from urine vs. stone nidus of kidney stone patients. *Clin Chim Acta* (2017) 466:112–9. doi:10.1016/j.cca.2016.12.018
27. Amimanan P, Tavichakorntrakool R, Fong-ngern K, Sribenjalux P, Lulitanond A, Prasongwatana V, et al. Elongation factor Tu on *Escherichia coli* isolated from urine of kidney stone patients promotes calcium oxalate crystal growth and aggregation. *Sci Rep* (2017) 7:2953. doi:10.1038/s41598-017-03213-x
28. Thery C, Amigorena S, Raposo G, Clayton A. Isolation and characterization of exosomes from cell culture supernatants and biological fluids. *Curr Protoc Cell Biol* (2006) 3:3.22. doi:10.1002/0471143030.cb0322s30
29. Keller S, Sanderson MP, Stoeck A, Altevogt P. Exosomes: from biogenesis and secretion to biological function. *Immunol Lett* (2006) 107:102–8. doi:10.1016/j.imlet.2006.09.005
30. Bobrie A, Colombo M, Raposo G, Thery C. Exosome secretion: molecular mechanisms and roles in immune responses. *Traffic* (2011) 12:1659–68. doi:10.1111/j.1600-0854.2011.01225.x
31. Vlassov AV, Magdaleno S, Setterquist R, Conrad R. Exosomes: current knowledge of their composition, biological functions, and diagnostic and therapeutic potentials. *Biochim Biophys Acta* (2012) 1820:940–8. doi:10.1016/j.bbagen.2012.03.017
32. McDonald MK, Tian Y, Qureshi RA, Gormley M, Ertel A, Gao R, et al. Functional significance of macrophage-derived exosomes in inflammation and pain. *Pain* (2014) 155:1527–39. doi:10.1016/j.pain.2014.04.029
33. Bhatnagar S, Shinagawa K, Castellino FJ, Schorey JS. Exosomes released from macrophages infected with intracellular pathogens stimulate a proinflammatory response in vitro and in vivo. *Blood* (2007) 110:3234–44. doi:10.1182/blood-2007-03-079152
34. Singh PP, Smith VL, Karakousis PC, Schorey JS. Exosomes isolated from mycobacteria-infected mice or cultured macrophages can recruit and activate immune cells in vitro and in vivo. *J Immunol* (2012) 189:777–85. doi:10.4049/jimmunol.1103638
35. Zhu Y, Chen X, Pan Q, Wang Y, Su S, Jiang C, et al. A comprehensive proteomics analysis reveals a secretory path- and status-dependent signature of exosomes released from tumor-associated macrophages. *J Proteome Res* (2015) 14:4319–31. doi:10.1021/acs.jproteome.5b00770
36. Bryan NB, Dorfleutner A, Rojanasakul Y, Stehlik C. Activation of inflammasomes requires intracellular redistribution of the apoptotic speck-like protein containing a caspase recruitment domain. *J Immunol* (2009) 182:3173–82. doi:10.4049/jimmunol.0802367
37. Toivola DM, Tao GZ, Habtezion A, Liao J, Omary MB. Cellular integrity plus: organelle-related and protein-targeting functions of intermediate filaments. *Trends Cell Biol* (2005) 15:608–17. doi:10.1016/j.tcb.2005.09.004
38. Mor-Vaknin N, Punturieri A, Sitwala K, Markovitz DM. Vimentin is secreted by activated macrophages. *Nat Cell Biol* (2003) 5:59–63. doi:10.1038/ncb898
39. Greening DW, Gopal SK, Mathias RA, Liu L, Sheng J, Zhu HJ, et al. Emerging roles of exosomes during epithelial-mesenchymal transition and cancer progression. *Semin Cell Dev Biol* (2015) 40:60–71. doi:10.1016/j.semcdb.2015.02.008
40. Evans JG, Correia I, Krasavina O, Watson N, Matsudaira P. Macrophage podosomes assemble at the leading lamella by growth and fragmentation. *J Cell Biol* (2003) 161:697–705. doi:10.1083/jcb.200212037
41. Honke K, Wada Y. Regulation of vimentin expression and protease-mediated vimentin degradation during differentiation of human monocytic leukemia cells. *Jpn J Cancer Res* (1997) 88:484–91. doi:10.1111/j.1349-7006.1997.tb00407.x
42. de Water R, Noordermeer C, van der Kwast TH, Nizze H, Boeve ER, Kok DJ, et al. Calcium oxalate nephrolithiasis: effect of renal crystal deposition on the cellular composition of the renal interstitium. *Am J Kidney Dis* (1999) 33:761–71. doi:10.1016/S0272-6386(99)70231-3
43. Umekawa T, Iguchi M, Uemura H, Khan SR. Oxalate ions and calcium oxalate crystal-induced up-regulation of osteopontin and monocyte chemoattractant protein-1 in renal fibroblasts. *BJU Int* (2006) 98:656–60. doi:10.1111/j.1464-410X.2006.06334.x
44. Strauss-Ayali D, Conrad SM, Mosser DM. Monocyte subpopulations and their differentiation patterns during infection. *J Leukoc Biol* (2007) 82:244–52. doi:10.1189/jlb.0307191
45. Shinomiya H. Plastin family of actin-bundling proteins: its functions in leukocytes, neurons, intestines, and cancer. *Int J Cell Biol* (2012) 2012:213492. doi:10.1155/2012/213492
46. Namba Y, Ito M, Zu Y, Shigesada K, Maruyama K. Human T cell L-plastin bundles actin filaments in a calcium-dependent manner. *J Biochem* (1992) 112:503–7. doi:10.1093/oxfordjournals.jbchem.a123929
47. Wabnitz GH, Kocher T, Lohneis P, Stober C, Konstandin MH, Funk B, et al. Costimulation induced phosphorylation of L-plastin facilitates surface transport of the T cell activation molecules CD69 and CD25. *Eur J Immunol* (2007) 37:649–62. doi:10.1002/eji.200636320

48. Nal B, Carroll P, Mohr E, Verthuy C, Da Silva MI, Gayet O, et al. Coronin-1 expression in T lymphocytes: insights into protein function during T cell development and activation. *Int Immunol* (2004) 16:231–40. doi:10.1093/intimm/dxh022
49. Ziegler SF, Ramsdell F, Alderson MR. The activation antigen CD69. *Stem Cells* (1994) 12:456–65. doi:10.1002/stem.5530120502
50. Welch MD, DePace AH, Verma S, Iwamatsu A, Mitchison TJ. The human Arp2/3 complex is composed of evolutionarily conserved subunits and is localized to cellular regions of dynamic actin filament assembly. *J Cell Biol* (1997) 138:375–84. doi:10.1083/jcb.138.2.375
51. Hurst IR, Zuo J, Jiang J, Holliday LS. Actin-related protein 2/3 complex is required for actin ring formation. *J Bone Miner Res* (2004) 19:499–506. doi:10.1359/JBMR.0301238
52. Starr AE, Bellac CL, Dufour A, Goebeler V, Overall CM. Biochemical characterization and N-terminomics analysis of leukolysin, the membrane-type 6 matrix metalloprotease (MMP25): chemokine and vimentin cleavages enhance cell migration and macrophage phagocytic activities. *J Biol Chem* (2012) 287:13382–95. doi:10.1074/jbc.M111.314179

Conflict of Interest Statement: The authors declare that the research was conducted in the absence of any commercial or financial relationships that could be construed as a potential conflict of interest.

frontiers in Immunology

ORIGINAL RESEARCH
published: 18 June 2018
doi: 10.3389/fimmu.2018.01358

Hodgkin Lymphoma-Derived Extracellular Vesicles Change the Secretome of Fibroblasts Toward a CAF Phenotype

Bastian Dörsam[1†], Teresa Bösl[2†], Katrin S. Reiners[2], Sabine Barnert[3], Rolf Schubert[3], Olga Shatnyeva[2], Paola Zigrino[4], Andreas Engert[2], Hinrich P. Hansen[2] and Elke Pogge von Strandmann[1,2]*

[1] Clinic for Hematology, Oncology and Immunology, Experimental Tumor Research, Center for Tumor Biology and Immunology, Philipps University, Marburg, Germany, [2] Department of Internal Medicine, University Hospital of Cologne, Cologne, Germany, [3] Department of Pharmaceutical Technology and Biopharmacy, Albert-Ludwigs-University, Freiburg, Germany, [4] Department of Dermatology, University Hospital of Cologne, Cologne, Germany

OPEN ACCESS

Edited by:
Christopher Gregory, University of Edinburgh, United Kingdom

Reviewed by:
Daniel Lambert, University of Sheffield, United Kingdom
Andrew Devitt, Aston University, United Kingdom

***Correspondence:**
Elke Pogge von Strandmann
poggevon@staff.uni-marburg.de

†Shared first authors.

Specialty section:
This article was submitted to Immunological Tolerance and Regulation, a section of the journal Frontiers in Immunology

Received: *29 January 2018*
Accepted: *31 May 2018*
Published: *18 June 2018*

Citation:
Dörsam B, Bösl T, Reiners KS, Barnert S, Schubert R, Shatnyeva O, Zigrino P, Engert A, Hansen HP and von Strandmann EP (2018) Hodgkin Lymphoma-Derived Extracellular Vesicles Change the Secretome of Fibroblasts Toward a CAF Phenotype. Front. Immunol. 9:1358. doi: 10.3389/fimmu.2018.01358

Secretion of extracellular vesicles (EVs) is a ubiquitous mechanism of intercellular communication based on the exchange of effector molecules, such as growth factors, cytokines, and nucleic acids. Recent studies identified tumor-derived EVs as central players in tumor progression and the establishment of the tumor microenvironment (TME). However, studies on EVs from classical Hodgkin lymphoma (cHL) are limited. The growth of malignant Hodgkin and Reed–Sternberg (HRS) cells depends on the TME, which is actively shaped by a complex interaction of HRS cells and stromal cells, such as fibroblasts and immune cells. HRS cells secrete cytokines and angiogenic factors thus recruiting and inducing the proliferation of surrounding cells to finally deploy an immunosuppressive TME. In this study, we aimed to investigate the role of tumor cell-derived EVs within this complex scenario. We observed that EVs collected from Hodgkin lymphoma (HL) cells were internalized by fibroblasts and triggered their migration capacity. EV-treated fibroblasts were characterized by an inflammatory phenotype and an upregulation of alpha-smooth muscle actin (α-SMA), a marker of cancer-associated fibroblasts. Analysis of the secretome of EV-treated fibroblast revealed an enhanced release of pro-inflammatory cytokines (e.g., IL-1α, IL-6, and TNF-α), growth factors (G-CSF and GM-CSF), and pro-angiogenic factors such as VEGF. These soluble factors are known to promote HL progression. In line, ingenuity pathway analysis identified inflammatory pathways, including TNF-α/NF-κB-signaling, as key factors directing the EV-dependent phenotype changes in fibroblasts. Confirming the *in vitro* data, we demonstrated that EVs promote α-SMA expression in fibroblasts and the expression of proangiogenic factors using a xenograft HL model. Collectively, we demonstrate that HL EVs alter the phenotype of fibroblasts to support tumor growth, and thus shed light on the role of EVs for the establishment of the tumor-promoting TME in HL.

Keywords: Hodgkin lymphoma, extracellular vesicles, tumor microenvironment, cancer-associated fibroblasts, NF-κB-signaling

INTRODUCTION

Hodgkin lymphoma (HL) is a rare cancer usually arising in the lymph nodes, which was initially described by Thomas Hodgkin (1). Mainly, two distinct entities are described for HL, the classical Hodgkin lymphoma (cHL) accounting for 95% of all cases, and a rare nodular lymphocyte predominant HL form (2).

A unique characteristic of classical HL is that the malignant Hodgkin and Reed–Sternberg cells (HRS cells) account for only 1% of the tumor tissue, which is composed of a massive infiltrate of reactive cells (lymphocytes, fibroblasts, and cells of the innate immune system) (3). Typically, HRS cells are surrounded by impaired T cells, forming a T cell rosette, which impedes a direct interaction with other cells. Thus, crosstalk *via* soluble factors and a complex network of chemokine/cytokine interactions facilitates the establishment of a tumor-supportive environment (4). HRS cells usually arise from mature B cells but undergo a severe alteration during progression to malignant cells concomitant with loss of characteristic markers for B cells/cells of the hematopoietic system (5). The events involved in genesis of malignant HRS cells are partially understood; however, the most frequent changes result in consecutive activation of the NF-κB-signaling pathway and deregulation of other pathways, including JAK/STAT, MAPK/ERK, NOTCH1, and PI3K/AKT. Although HRS cells are considered the master regulator of the inflammatory response in the lymphoid tissue of HL, survival of the few malignant cells is likely dependent on the tumor microenvironment (TME) and interaction with non-malignant cells (3). The HL-specific TME is constituted of many different cell types, including immune cells, such as lymphocytes, plasma cells, neutrophils, eosinophils, and mast cells as well as fibroblasts. Expression of a variety of cytokines and chemokines facilitate the attraction of immune cells and the establishment of this tumor-promoting milieu and, therefore, has been extensively studied in the past years (6, 7). HL cells exploit different mechanisms to escape from immune surveillance, including the inhibition of effector cells, e.g., *via* secretion of immune suppressive molecules, such as TARC, MICA, and BAG6, ligands for receptors (CCR4, NKG2D, NKp30, respectively) expressed on a subset of T cells and NK cells (8–11).

Recently, the relevance of extracellular vesicles (EVs) for the intercellular crosstalk and the establishment of a tumor-promoting microenvironment was raised in several studies (12, 13).

Extracellular vesicles are a central part of intercellular communication allowing cells to interact with close and distant cells *via* the delivery of signal molecules. In detail, EVs play a crucial role in the diverse interactions in the tumor-supportive ME. The smallest EV-subpopulation with a diameter of 50–150 nm is commonly referred to as exosomes, which are generated *via* the endocytic pathway and carry parent cell-specific molecules. These molecules include proteins, DNA, noncoding RNAs, and miRNAs/mRNAs (13). The chaperone HSP70 and tetraspanins CD9, CD63, and CD81 are present on EV-subpopulations and commonly used as markers (14).

Here, we investigate the EV-mediated interplay of HL cells and fibroblast. In detail, we report that HL cells and fibroblasts interact in a bi-directional manner, changing migratory properties and, most interestingly, encouraging the transition of healthy fibroblasts to a CAF phenotype concomitant with alteration of their inflammatory secretome.

MATERIALS AND METHODS

Cell Culture

The human HL cell line KM-H2 (Deutsche Sammlung von Mikroorganismen und Zellkulturen) as well as the human primary fibroblast cell line HDF_n (American Type Culture Collection) were maintained in DMEM GlutaMAX or RPMI 1640 (Thermo Fisher Scientific) supplemented with 10% fetal calf serum (FCS) and antibiotics (100 U/ml penicillin and 100 µg/ml streptomycin) at 37°C with 5% CO_2.

Isolation of EVs and Quantification of EV Protein Cargo

Cells were cultivated in EV-depleted medium for 48 h followed by EV-isolation *via* sequential ultracentrifugation as previously described (15). In brief, supernatants were centrifuged for 10 min at 300 × *g*, 10 min at 3,000 × *g*, and 30 min at 10,000 × *g*. Subsequently, the supernatant of the 10,000 × *g* fraction was centrifuged for 90 min at 100,000 × *g* and the obtained pellet washed with PBS at the same speed for 90 min. After resuspension of the pellet in PBS, protein content was determined using the BCA protein assay kit (Thermo Scientific) and a SpectraMax M4 (Molecular Devices). Samples were stored at −80°C for further analysis.

EV-Depletion of Medium and Cultivation of Cells With Isolated EVs

Extracellular vesicles were removed from the medium by ultracentifugation (90 min at 100,000 *g*). The pellet containing EVs was carefully discarded. Cells were cultivated in EV-depleted medium with purified EVs as indicated.

Nanoparticle Tracking Analysis (NTA)

Number and size distribution of isolated EVs were estimated by the means of NTA. EVs were diluted 1:1,000 with PBS (Biochrom). Five repeated measurements of 60 s with an infusion rate of 40 were recorded consecutively and analyzed using a Nanosight NS300 with the NTA 3.0 software (Malvern Instruments).

Flow Cytometry

Adherent cells were harvested using Accutase (Life Technologies). For flow cytometric assessment, cells were stained with different concentrations of DiO (AAT Bioquest) for 5 min at 37°C. Isolated vesicles were processed for flow cytometry as described: 100 µg (≈1×10^9) EVs were coupled to 1×10^5 4.5 µm polystyrene beads (Polysciences) in PBS over night at 4°C for assessment of surface proteins (15). After blocking with 2% bovine serum albumin (BSA) for 1 h at 25°C under shaking, molecules of interest were either probed with labeled Annexin V, respectively a labeled primary PE-labeled antibody against CD30 (BioLegend, 333906, 1:100) or primary antibodies against CD9 (BioLegend, 312102, 1:100), CD63 (BioLegend, 353013, 1:100), or CD81 (BioLegend, 349501, 1:100), and a secondary goat anti-mouse-PE antibody (BioLegend, 405705, 1:100). Antibody incubation was performed

for 30 min on ice under exclusion of light in FACS buffer (PBS with 0.2% BSA, 0.2% sodium azide). Samples were analyzed with a FACS Calibur (Becton Dickinson).

Electron Microscopy

Extracellular vesicles were isolated from the supernatant of KM-H2 cells and resuspened in PBS. 3 µl of the EV solution was transferred onto a copper grid (Quantifoil S7/2 Cu 400 mesh, carbon films; Quantifoil Micro Tools). After removal of excess liquid, the copper grid was snap-frozen by immersion into liquid ethane. Samples were analyzed with a transmission electron microscope (Leo 912 Ω-mega) at −174°C. The device was operated at 120 kV and images recorded with a 6,300- to 12,500-fold magnification.

SDS-PAGE and Immunoblot Analysis

Adherent cells were harvested with Accutase and whole cell lysates of the cell pellet prepared using a buffer containing 50 mM Tris pH 8.0, 150 mM NaCl, 0.5% Triton X-100, 0.5% sodium deoxycholate, protease, and phosphatase inhibitors (Roche). 100 µl of the buffer was used to lyse 1×10^6 cells for 5 min under rotation at room temperature (RT). Subsequently, the samples were centrifuged at 14,000 *g* for 10 min at 4°C, the pellet removed and the lysate stored at −20°C if it was not processed directly upon preparation. Protein content was determined using the BCA protein assay kit (Thermo Fisher Scientific). 20 µg of protein per sample were heated in Laemmli sample buffer to 96°C for 10 min and subjected on a 10% SDS-PAGE. After separation, proteins were transferred to a 0.2 µm nitrocellulose membrane (GE Healthcare) with a wet blot chamber (BioRad). After blocking with 5% non-fat dry milk in TBS-T (137 mM NaCl, 50 mM Tris–Cl, 0.05% Tween-20, pH 7.4), the membrane was probed with the desired primary antibodies against β-Actin (Abcam, ab6276, 1:15,000), CD9 (Santa Cruz Biotechnology, sc-13118, 1:100), CD63 (Invitrogen, 10628D, 1:500), or CD81 (BioLegend, 349501, 1:500) for 2 h at RT and then washed three times with TBS-T. Incubation with the appropriate horseradish peroxidase-conjugated secondary antibody (Cell Signaling Technology, 7076, 1:2,500) was performed for 1 h at RT. Proteins were detected *via* enhanced chemiluminescence using Pierce ECL Western Blotting Substrate (Thermo Fisher Scientific).

Immunofluorescence

The phenotype switch of fibroblasts after exposure to EVs (scratch assay) was analyzed by probing α-SMA as a marker for activated fibroblasts. Cells were grown on cover slips and fixed with 4% paraformaldehyde for 15 min at RT, washed thrice with PBS, and permeabilized with 1% Triton X-100 in PBS for 30 min at RT. Subsequently, washed cells were blocked with 10% FCS and 0.2% Tween-20 in PBS for 30 min at RT and incubated with a FITC-conjugated α-SMA antibody (Sigma-Aldrich, F3777, 1:250) for 1 h at RT under exclusion of light. Nuclei were stained with 1 µg/ml DAPI (Roche). Cover slips were mounted on microscope slides using VECTASHIELD Antifade Mounting Medium for Fluorescence (VECTAMicroscopic analysis was performed using an Olympus IX51 with the imaging software CellSens).

Extracellular vesicles were visualized by staining of parental HL cells with 1 µM DiO for 5 min at 37°C prior to seeding. DiO-positive (DiO^+) vesicles were harvested *via* sequential ultracentrifugation. 100 µg/ml DiO^+ EVs were added to fibroblast cell growing on cover slips for 2 days. Cells were processed in the way described above. The plasma membrane of fibroblasts was stained with CellMask Deep Red Plasma Membrane Stain [Invitrogen according to the manufacturer's protocol and the nuclear dye Hoechst 33342 (Sigma-Aldrich, B2261, 1:5,000)]. Followed by washing with PBS, internalization of EVs by target cells was evaluated with the confocal microscope Leica TCS SP8.

Cell Viability Assay (XTT Assay)

The impact of HL EVs isolated from KM-H2 cell culture on the proliferation of HDF_n cells and *vice versa* was probed using the XTT assay (AppliChem). 6×10^3 KM-H2 or 1×10^5 HDF_n cells per well were seeded on a 96-well plate. Cells were incubated with the amount of EVs and time period indicated in the according figure. The XTT staining solution was prepared according to the manufacturer's protocol, 50 µl staining solution added to each well containing 100 µl growth medium, and incubated for 2 h at 37°C. Absorbance was then measured with an Infinite M1000 microplate reader (Tecan) at a wave length of 475 and 660 nm as reference.

Migration Assays

Migration of HL cells was studied in a 24-well Boyden chamber with 8.0 µm pores (Falcon/Fisher Scientific). 1×10^6 HL cells were transferred into the upper compartment, while crude fibroblast supernatant or medium (with serum, EV depleted) containing 100 µg/ml EVs were placed in the lower compartment. According to the NTA data, a protein concentration of 100 µg/ml corresponds to about 1×10^9 Hodgkin cell-derived EVs/ml. Migrated cells were counted after an incubation time of 26 h.

The scratch assay was performed to monitor the migration of fibroblasts. 1.5×10^5 HDF_n cells/well were seeded in a 24-well Falcon plate. The cell layer was impaired with a scratch and 100 µg/ml HL EVs or medium added. For every condition, cells were seeded in triplicates and two spots per well were monitored with images being recorded in an interval of 15 min for 24 h. For analysis, the scratch width was determined with ImageJ (National Institutes of Health) after 0, 3, 12, and 21 h, wound closure was calculated with the following formula:

$$\%\text{wound closure} = 1 - \left(\frac{\text{scratch width} t_{x\text{h}}}{\text{scratch width} t_{0\text{h}}} \right) \times 100.$$

Directed migration was studied with a chemotaxis assay performed in Neuroprobe ChemoTx plates. Migration of Calcein AM (MoBiTe)-labeled HDF_n cells toward 40 µg/ml, 150 mg/ml HL EVs or medium (triplicates), was assessed after 2 h *via* fluorescence detection with an Infinite M1000 microplate reader (Tecan).

Cytokine Array

Chemokines/cytokines in the supernatant of fibroblast cells were quantified using the Human Cytokine Array/Chemokine Array 64-Plex from Eve Technologies and a Bio-Plex200 (BioRad) according to the manufacturer's instructions.

Analysis of Proteomic Data *via* Ingenuity Pathway Analysis (IPA)

Pathway analysis of proteomics data from HL EVs [part of proteomics data were published (16); full list see Table S1 in Supplementary Material] was performed using the IPA tool from QIAGEN (IPA Summer Release 2015, QIAGEN Bioinformatics).

Protein cargo of EVs isolated from the supernatant of the HL cell line KM-H2 was analyzed *via* mass spectroscopy as previously described by our group (16). In brief: the EV proteins were separated with the help of a 10% SDS-PAGE, the lanes subsequently extracted from the gel, reduced (5 mM dithiothreitol, 25 min at 56°C), alkylated (14 mM iodoacetamide, 30 min at RT under exclusion of light), and then digested with trypsin (Promega). Samples were analyzed using an LTQ Velos Orbitrap mass spectrometer (Thermo Fisher Scientific) paired with LC–MS/MS (EASY-nLC system, Proxeon Biosystem). Separated by a 2–90% acetonitrile gradient in 0.1% formic acid, using a PicoFrit Column (20 cm, ID75 µm, 5 µm particle size, New objective) followed. Finally, the full scan MS spectra (m/z 300–2,000) were checked in the Orbitrap analyzer. Peak lists (msf) were created using Proteome Discoverer version 1.3 (Thermo Fisher Scientific) with a Sequest search engine. The obtained search data were further checked with the software ScaffoldQ + version 3.3.1.

In the context of this study, the results found with the Human Cytokine Array/Chemokine Array 64-Plex Eve Technologies and pre-existing proteomics data (Table S1 in Supplementary Material) were merged in an IPA analysis.

Mouse Xenograft Model

1×10^7 HDF_n cells and 1×10^7 KM-H2 cells were mixed in 100 µl PBS and the cell suspension injected subcutaneously into the lower flank of female NOD scid gamma (NSG) mice (Charles River) to establish tumors. Mice received 50 µg DiO-labeled KM-H2 EVs in 100 µl PBS ($n = 4$) or vehicle control ($n = 4$) *via* intravenous injection into the tail vein at day 2, 4, and 7 after transplantation of tumor cells. Formation of tumors was checked periodically, and tumor volume calculated using the formula (length × width × height)/2. Animals were sacrificed at day 30 and tumor tissue processed for analysis.

Processing and Histopathology of Tumor Tissue

Upon resection, tumor tissue was snap-frozen in optimal-cutting-temperature compound (Tissue-Tek O.C.T., Sakura Finetek) and sectioned at 5 µm using a HM560 microtome (Thermo Fisher Scientific). Tumor sections were air dried for at least 4 h at RT and stored at −80°C. Hematoxylin and eosin (H&E) staining of cryo-sections was performed for histopathological evaluation of tumor tissue sections were first stained with hematoxylin solution, rinsed with water, and stained with Eosin G solution. Excess dye was cleansed away, the stained sections embedded in GLC Mounting Medium (Sakura Finetek) and sealed with a cover slip. Samples were analyzed with a Keyence Microscope BZ-9000 and the BZ-II Viewer.

Isolation of Single Cells From Tumor Tissue and Flow Cytometry

Snap-frozen tumor tissue was wet with PBS and kept on ice, chopped with a scalpel and carefully pushed through the mesh of a cell strainer. The cells were re-suspended in 10 ml RPMI 1640 cell culture medium and the suspension overlaid with 20 ml human Ficoll–Paque density gradient medium (GE Healthcare) in a reaction tube. After centrifugation at 2,000 rpm for 20 min at RT (deceleration without brake), the cells were transferred in a fresh tube and washed with PBS for 5 min at 1,200 rpm and pellet resuspended in 1 ml RPMI 1640 and kept on ice. Isolated tumor cells were counted and equal amounts per tumor probed with an APC-conjugated mouse anti-human CD30 antibody (BioLegend, 333909, 1:100) for 30 min on ice and then analyzed *via* flow cytometry as described above.

Immunohistochemistry

Cryo-sections of tumor tissue were fixed with 1% PFA for 15 min at RT, blocked and permeabilized with 10% normal goat serum and 0.2% Triton X-100 in PBS for 30 min, washed three times with PBS, and subsequently probed with the following primary antibodies: CD30 [clone Ki-4 (17)], CD31 (BD Bioscience, 557355, 1:1,000), and α-SMA conjugated with Cy3 (Sigma-Aldrich, C6198, 1:200). Microscopy slides were incubated with the primary antibody over night at 4°C and then washed in PBS, followed by washing three times with PBS and incubation with the appropriate secondary antibody for 45 min at RT: goat anti-mouse-AF594 (Molecular Probes, A11032, 1:1,000) or goat anti-rat-AF594 (Molecular Probes, A11007, 1:1,000). After washing thrice with PBS, nuclei were stained with DAPI (1 µg/ml). Finally, stained sections were embedded in GLC Mounting Medium and sealed with a cover slip. Samples were analyzed using a Keyence Microscope BZ-9000 and the BZ-II Viewer.

Statistical Analysis

Experiments were performed independently and at least in three biological replicates, if not stated otherwise. Results obtained from representative experiments are shown. Data are presented as mean + SEM and were analyzed using GraphPad Prism6 software. Statistical significance was calculated as indicated in the figure legends.

Study Approval

This study was carried out in accordance with § 8 Abs. 1 des Tierschutzgesetzes (animal welfare law of the German Federal Government) and the protocol was approved by the local authorities [Landesamt für Natur, Umwelt und Verbraucherschutz (LANUV), State Northrhine-Westfalia].

RESULTS

HL-Derived Vesicles Display Prime Characteristics of EVs

Initially, we isolated EVs from the supernatant of healthy fibroblasts and the HL cell line KM-H2 by the means of differential ultracentrifugation (18, 19). NTA of the samples revealed a size

distribution of the particles characteristic for small EVs, the so-called exosomes. Representative size distribution plots presented in **Figure 1A** confirm a mode size of about 130 nm for fibroblast-derived EVs and HL EVs, thus, being in the range typical for EVs obtained from the 100,000 × *g* fraction. The electron microscopy picture shows purified EVs from HL cells (KM-H2)

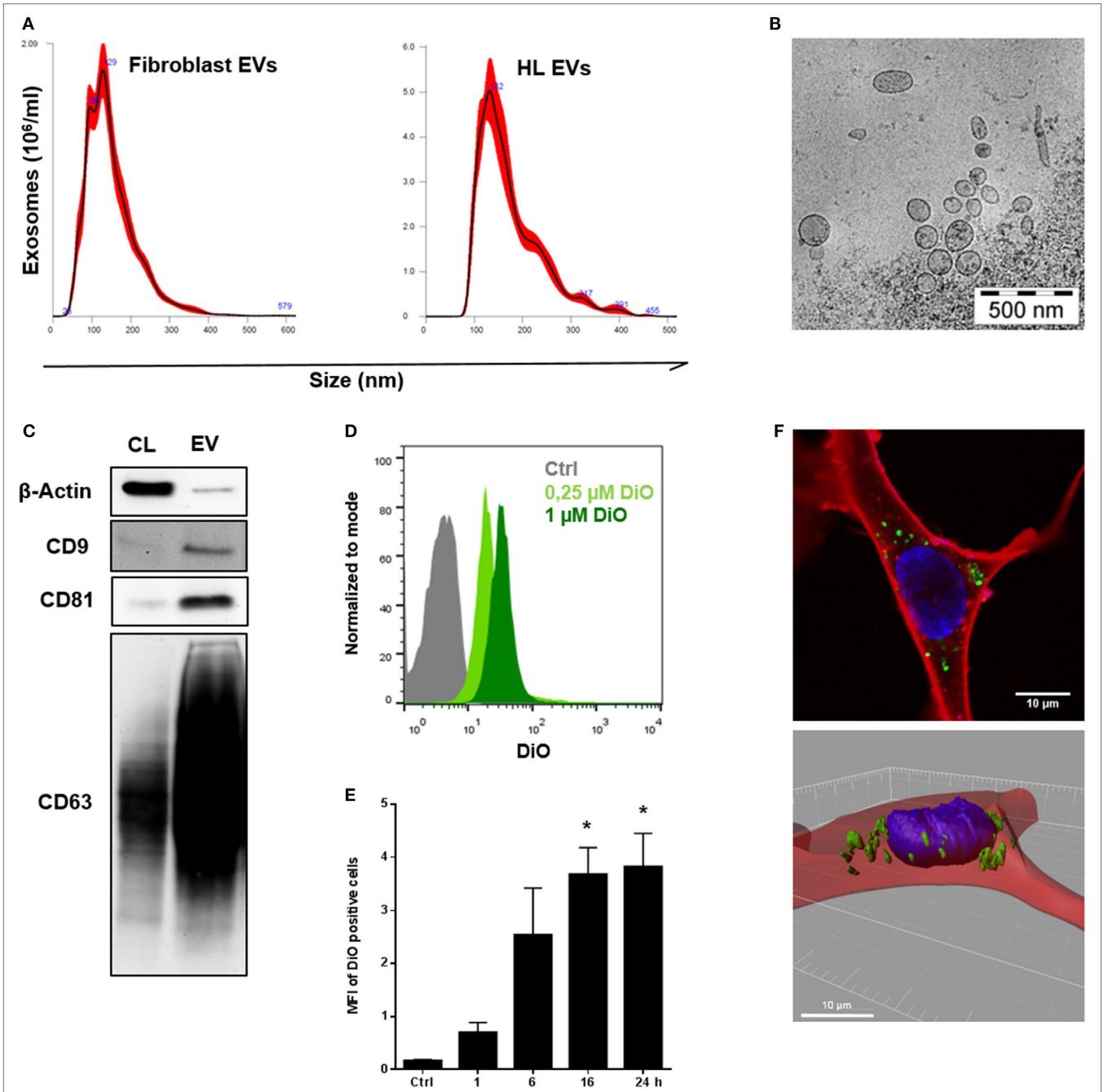

FIGURE 1 | Characterization and internalization of tumor-derived extracellular vesicles (EVs) by fibroblast cells *in vitro*. **(A)** Size distribution of fibroblast EVs (performed once) or Hodgkin lymphoma (HL) EVs (representative experiment, $n = 3$), measured by nanoparticle tracking analysis. **(B)** Electron microscopic image of purified HL EVs ($n = 1$). **(C)** Western blot analysis of exosome markers on HL-derived EVs. Cell lysate of HL cells served as control. Presented is one of three independent experiments. **(D)** Flow cytometry of beads coupled HL EVs which was collected from unstained cells (Ctrl) or from DiO-stained cells (0.25 or 1 µM DiO, $n = 1$). Normalization to mode: events are normalized in a scale with 100 being maximum (FlowJo v10). **(E)** Internalization of DiO-labeled HL EVs by fibroblasts assessed *via* flow cytometry at different time points as indicated. Fibroblast cells were incubated with 100 µg DiO^+-EVs or DiO-negative EVs as negative control in the presence of EV-depleted medium. Statistical significance was calculated with one-way ANOVA and Tukey's multiple comparisons test (mean + SEM of three biological replicates; $^*p \geq 0.05$). **(F)** Visualization of EV-uptake into fibroblasts *via* immunofluorescence: cytoplasm was stained with Cell Mask Deep Red (red), nuclei with Hoechst and HL-derived EVs with DiO (green). Upper picture shows a recipient cell with internalized HL EVs. Bottom picture depicts a three-dimensional view.

ranging from sizes between 70 and 200 nm (**Figure 1B**). For further characterization of the EVs, Western blot analysis and flow cytometry were used to identify the proposed markers for EVs of the 100,000 × *g* fraction CD9, CD81, and CD63 (14) on the surface of HL EVs. Western blot analysis confirmed a strong abundance of CD9, CD81, and CD63 on HL EVs (**Figure 1C**), which could also be confirmed *via* flow cytometry (Figure S1A in Supplementary Material). Moreover, FACS bead assay affirmed the presence of phosphatidylserine and the HL cell marker CD30 on the vesicles, confirming their descent from HL cells (Figure S1B in Supplementary Material).

Tumor Cell-Derived EVs Are Internalized by Fibroblasts

Next, HL cells were treated with the lipophilic dye DiO (Figure S1C in Supplementary Material). Under these conditions, cells release DiO-stained EVs, which allows to monitor their internalization by fibroblasts. Subsequently, DiO^+ EVs were purified from cell culture supernatant (**Figure 1D**). Fibroblasts were challenged with DiO^+ EVs for different time points as indicated. Flow cytometric analysis revealed a time-dependent binding and/or uptake of DiO^+ EVs by fibroblasts resulting in DiO-labeling of the recipient cells reaching a maximum after 16 h (**Figure 1E**). The observed interaction of EVs and fibroblasts was elucidated in more detail by means of confocal microscopy. To this end, fibroblasts were exposed to DiO^+-EVs for 48 h as described before, but nuclei were stained with Hoechst (blue) and the CellMask Deep Red (red) directly prior to confocal microscopy. **Figure 1F** (upper picture) shows a representative image of a fibroblast with loaded HL EVs (green). Three-dimensional depiction of the fibroblast from a *z*-axis-series of pictures through the cell (Figure S1D in Supplementary Material) allowed exact determination of the position of internalized DiO^+-EVs in the analyzed cell (**Figure 1F**, lower picture). Thus, internalization of HL EVs by fibroblasts was confirmed. However, it is conceivable that even binding of EVs to fibroblasts may contribute to phenotypic changes and signal transduction.

EVs of HL Cells and Fibroblasts Interact in a Bi-Directional Manner to Enhance Motility and Facilitate Directed Migration

Within the TME, both malignant and non-malignant cells interact to prepare a favorable surrounding for the tumor. We aimed to dissect the role of vesicular factors in these bi-directional communication processes with main focus on the impact of EVs from HL cells on the motility and migration of fibroblasts and *vice versa*. Initially, we measured the proliferation of HDF_n cells co-cultivated with HL EVs and conversely KM-H2 cells co-cultivated with HDF_n EVs. Results of the XTT assays did not show any relevant differences in cell proliferation in presence or absence of EVs for both tested cell lines (Figures S3C,D in Supplementary Material) suggesting that the proliferation is not affected by internalized EVs. Next, we studied the role of fibroblast-derived EVs using a transwell approach. Of note, the mobility of HL cells was significantly increased by crude fibroblast supernatant, containing all secreted molecules and vesicles, and by purified fibroblast EVs, compared to control cells incubated with medium (**Figure 2A**). The mobility of HL cells was slightly higher, but not significantly increased, after incubation with the supernatant in comparison to purified fibroblast EVs, implying that also soluble factors in the supernatant might influence tumor cell mobility. The bi-directional cross-talk of HL EVs on fibroblasts was investigated by means of the so-called scratch assay in which the wound closure of a fibroblast cell monolayer was tested in presence or absence of HL EVs (21 h). The experiment confirms a significant enhancement of wound closure/directed migration of fibroblasts in response to HL EVs (**Figure 2B**). Chemotaxis plays a central role in directed migration of cells. To this end, the influence of HL EVs on the directed migration of fibroblasts was tested with Neuroprobe ChemoTx plates in which cells can migrate through a membrane toward an attractant. Statistical evaluation in **Figure 2C** confirms a dose-dependent attraction of fibroblasts by HL EVs. In conclusion, we demonstrated that the bi-directional communication of HL cells and stromal cells/fibroblasts *via* EVs impacts on the motility of HL cells and facilitates the directed migration of fibroblasts.

HL-Derived EVs Promote Transition of Healthy Fibroblasts to a Cancer-Associated Phenotype

Given the evidence for internalization of HL EVs by fibroblasts and their positive effect on the migration, we set out to investigate the effects of HL EVs on the phenotype of fibroblasts. Therefore, we combined the scratch assay as described before with immunofluorescence to evaluate the abundance of alpha-smooth muscle actin protein (α-SMA), a commonly used marker for cancer-associated fibroblasts (CAFs) (20). Representative pictures in **Figure 2D** indicate a higher number of α-SMA positive cells upon exposure to HL EVs, pointing to their activation toward a CAF phenotype. Of note, treatment with TGF-β as a positive control (Figure S2A in Supplementary Material, lower panel) did not provoke a higher ratio of α-SMA positive fibroblasts. This might reflect the herterogenicity of the HDF_n cells since α-SMA is, besides being expressed in CAFs, the most significant marker for myofibroblasts (21). This observation is in line with the work of Koumas and colleagues in which TGF-β induced expression of α-SMA was observed in a part of the assessed fibroblast population only (22).

Transition of fibroblasts into a CAF phenotype is characterized by alterations in gene expression affecting different cellular pathways including the cell's secretome (20), which was further studied using a 64-Plex Chemokine Array. Fibroblasts were exposed to HL EVs or medium for 24 h and their secretome in the presence or absence of EVs was analyzed. 19 of the 64 assayed chemokines/cytokines showed significantly altered levels in the supernatant of fibroblasts treated with HL EVs demonstrating that the phenotypical change correlates with modulation of the release of soluble factors (**Figure 2E**; Figure S2 in Supplementary Material). Of note, secretion of the chemokines and cytokines is known as a critical factor in HL pathogenesis (23) and disease relevant molecules such as TNF-α are enhanced in presence of HL EVs with highest significance. Besides of that, a group of

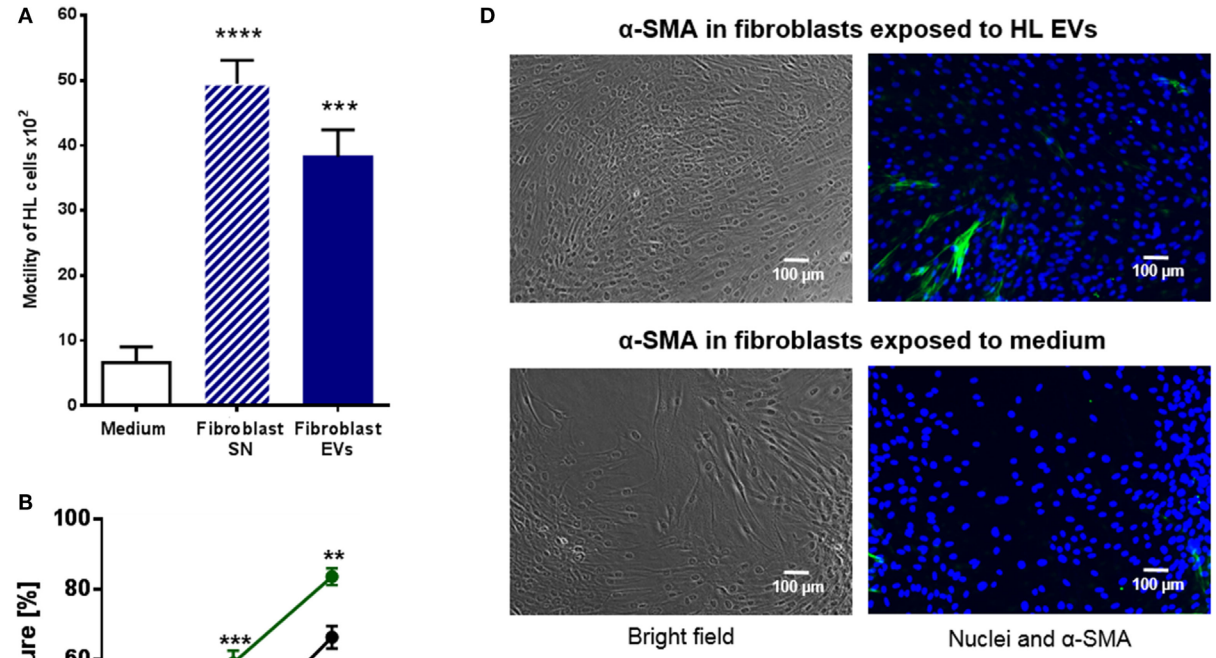

E

Human Cytokine Array/Chemokine Array Targets							
6CKine (CCL-21)	FGF-2	IFN-γ	IL-1RA	IL-3	IP-10 (CXCL-10)	MIP-1α (CCL-3)	TARC (CCL-17)
BCA-1 (CXCL-13)	Flt-3L	IL-10	IL-1α	IL-33	*LIF*	MIP-1β (CCL-4)	*TGF-α*
CTACK (CCL-27)	CX3CL1	IL-12 (P40)	IL-1β	IL-4	*MCP-1 (CCL-2)*	PDGF-AA	TNF-α
EGF	G-CSF (CSF3)	IL-12 (P70)	IL-2	IL-5	MCP-2 (CCL-8)	PDGF-AB/BB	TNF-β
ENA-78 (CXCL-5)	GM-CSF (CFS2)	IL-13	IL-20	IL-6	MCP-3 (CCL-7)	RANTES (CCL-5)	TPO (MPL ligand)
Eotaxin-1 (CCL-11)	GRO pan (CXCL-1)	IL-15	IL-21	*IL-7*	MCP-4 (CCL-13)	sCD40L	TRAIL (TNFSF-10)
Eotaxin-2 (CCL-24)	I-309 (CCL-1)	IL-16	IL-23	IL-8	MDC (ADAM11)	SCF (KIT ligand)	TSLP
Eotaxin-3 (CCL-26)	IFN-α2	IL-17A	IL-28A	IL-9	MIP-1d (CCL-15)	SDF-1α+β (CXCL-12)	VEGF

FIGURE 2 | Extracellular vesicles (EVs) promote migration of Hodgkin lymphoma (HL) cells and HL EVs can alter the phenotype of fibroblast cells. **(A)** Transwell migration assay (8 µm pores): HL cells were exposed to supernatant from fibroblast cells or EVs for 26 h. Statistical significance was calculated with one-way ANOVA and Tukey's multiple comparisons test (presented is mean + SEM, four biological replicates; ***$p \geq 0.001$; ****$p \geq 0.0001$). **(B)** Scratch assay: 24 h wound closure of fibroblast cells exposed to HL EVs (green) or medium (black). Student's *t*-test was performed to check for significant differences between both treatments (mean ± SEM, $n = 3$; *$p \geq 0.05$; **$p \geq 0.01$). **(C)** Chemotaxis assay: migration of labeled fibroblast cells through Neuroprobe ChemoTx plates (5 µm pores) exposed to medium, 40 or 150 µg/ml HL EVs. Statistical assessment was performed with one-way ANOVA and Tukey's multiple comparisons test (data are presented as mean + SEM, $n = 4$; *$p \geq 0.05$; **$p \geq 0.01$). **(D)** Exemplary bright field and fluorescence pictures of a scratch assay after 24 h exposure of fibroblasts to 100 µg/ml (≈1×10^9 EVs/ml) HL EVs or medium. Nuclei stained with DAPI (blue), fibroblast cells with α-SMA (green). This experiment was performed in three independent replicates. **(E)** Human 64-Plex chemokine array: quantification of chemokines/cytokines after 24 h in the supernatant of fibroblasts in presence or absence of HL EVs. Not detected cytokines/chemokines are depicted in italic letters; abundant factors are in bold; enhanced expression is highlighted in green, whereas red boxes indicate lower expression after exposure to HL EVs. Statistical differences in abundance of chemokines/cytokine were determined using Student's *t*-test (three independent replicates).

chemotactic cytokines (e.g., ENA-78, GRO pan) were measurable in higher levels as well as the pro-inflammatory NF-κB-induced cytokines IL-1α and IL-6. This was in line with a higher abundance of growth factors (G-CSF, GM-CSF) and angiogenesis stimulating factors (VEGF). All of these cytokines/chemokines are important for the establishment of a tumor-favorable environment in HL. Strikingly, most of the altered targets are part of the signaling network of the inflammatory master key regulator NF-κB, a driver pathway in HL (4, 24, 25). In line, IPA (Qiagen) of HL-EV proteomics data from our previous studies (16) (Table S1 in Supplementary Material) merged with the results from the Cytokine array (**Figure 2E**; Figure S2B in Supplementary Material) revealed inflammatory pathways, including TNF-α/NF-κB-signaling, as key factors directing the EV-dependent phenotype changes in fibroblasts. The core analysis of altered cytokines/chemokines unraveled a key role for the inflammatory mediators STAT3, IFNγ, TNF-α and the involvement of TOLL-like receptor-, reactive oxygen species-, and NF-κB-signaling (Figure S4 in Supplementary Material).

Vice versa, ROS signaling and NF-κB-signaling pathways popped up upon IPA of the proteins identified by mass spectrometry of HL EV protein cargo isolated from the supernatant of KM-H2 cells. These results point to a central role of the TNF-α/NF-κB axis in HL EV-mediated alteration in recipient fibroblast.

HL EVs Promote a CAF Phenotype and Vascularization in a Xenograft Model

To investigate the *in vivo* impact of HL EVs on fibroblasts, we applied a HL xenograft model with KM-H2 cells to immunodeficient NSG mice. Fibroblasts and HL cells (1:1) were subcutaneously transplanted into the lower flank of NSG mice (age 141 days). Animals of the treatment group received an intravenous injection of 50 µg DiO^+ HL EVs at day 22, 25, 27, and 28, animals of the control group were injected with PBS. Necropsy was performed at the end of the experiment and tumor growth was monitored as soon as tumors were visible. Both groups showed a comparable tumor growth/volume in this model (**Figure 3A**). **Figure 3B** shows representative overview and detail pictures of tumor sections stained with H&E from EV-treated mice and control animals. In accordance with the comparable tumor growth, tumors of both groups showed a similar histology and similar staining of nuclei (blue), cytoplasm and the extracellular matrix (pink). Flow cytometry revealed a high abundance of CD30-positive cells in tumor tissue of EV-treated and control animals (**Figure 3C**). After we successfully confirmed the growth of human HL cells in immunodeficient NSG mice, the effect of HL-derived EVs on the migration of fibroblasts and the induction of a CAF phenotype was investigated. **Figure 3E** shows statistical evaluation of α-SMA levels in tumor tissue sections (Figure S3A in Supplementary Material) of both groups with the number of α-SMA-positive fibroblasts being 2.93-fold higher in the EV-treated group. Moreover, the angiogenesis marker CD31 was increased in the tumor tissue of EV-treated animals pointing to a higher vascularization (1.74-fold increase) in tumors of EV-treated mice (**Figure 3F**; Figure S3B in Supplementary Material). Of note, we could observe the DiO^+ HL EVs in sections of paraffin-embedded tumor tissue *via* immunofluorescence (**Figure 3D**). Collectively, we successfully established human HL tumors in immunodeficient NSG mice and, moreover, found evidence for alteration of the phenotypes of fibroblasts in the TME toward an activated CAF phenotype. Histological analysis of tumor tissue revealed higher vascularization in tumor tissue caused by the administered HL-derived EVs.

Altogether, HL EVs have shown to modulate cellular activities and are able to re-program the phenotype in fibroblasts promoting a suitable TME for tumor growth and progression.

DISCUSSION

Bi-directional communication between malignant cells and the cells composing the TME is critical for tumor growth, progression, and metastasis. This is of particular importance in HL since few malignant cells interact with a large number of stroma cells to establish a tumor-supportive environment (7).

Here, we provide evidence that HL cell-derived EVs modulate the TME by re-programming or educating fibroblasts to promote a tumor supporting environment.

This conclusion is based on the observation that fibroblast internalize HL EVs (1) causing an increased migration capacity of the recipient cells (2), which was associated with the induced release of cytokines/chemokines relevant for HL tumor progression (3).

Fibroblasts found in association with HL cells (so-called HL-AF for HL-activated fibroblasts) (7) release growth factors and cytokines, such as TGF-β or IL-6 into the surrounding malignant tissue to support tumor growth and maintenance (26). However, the mechanisms underlying the transformation from healthy fibroblasts to HL-AF are not fully understood (27). One of the factors involved is IL-7 released by HL cells which triggers IL-6 production in fibroblasts (28). Moreover, HL cells release IL-13, TNF-α, and TGF-β thereby promoting fibroblast proliferation (29).

In this work, we present first evidence that tumor cell-derived EVs are also able to shape the phenotype of fibroblasts. A contribution of both soluble and vesicular components was demonstrated: the crude cell supernatant, the soluble fraction, and purified vesicles were able to educate fibroblasts toward a tumor-promoting phenotype. These findings complement data demonstrating that the EV-dependent cell-cell communication between distant cells in HL involves CD30-expressing HL EVs. CD30 is a receptor of the TNF receptor superfamily and responsible for constitutive NF-κB-signaling in HL cells, which contributes to HL pathogenesis. It was shown that CD30-HL EVs are guided by a network of protrusions to CD30L-positive granulocytes and neutrophils to induce the release of IL-8, which triggers angiogenesis (16). In line with our findings, Giannoni and colleagues reported a crucial role of carcinoma-derived vesicular IL-6 in the activation of fibroblasts (30). Vesicular activators of the NF-κB-signaling pathway (e.g., TNF-α and TGF-β) secreted by prostate cancer cells trigger the differentiation of fibroblasts into CAFs, promote stemness, and angiogesis (31, 32). These data suggest that EVs play a fundamental role in the organization of the TME.

Factors that were released by fibroblasts in response to EV-treatment include numerous molecules that shape the

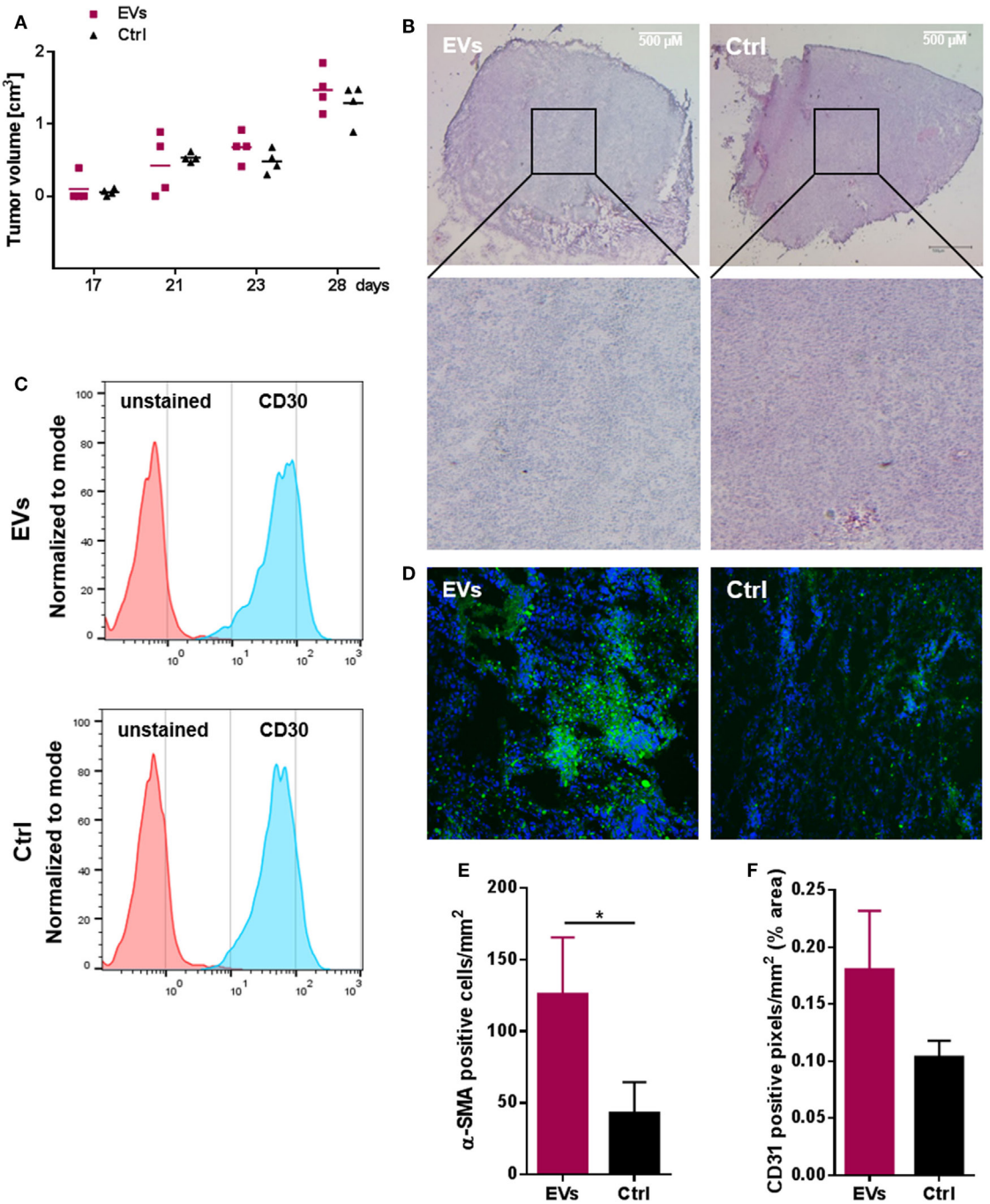

FIGURE 3 | Hodgkin lymphoma (HL) xenograft model. 1×10^7 HDF_n + 1×10^7 KM-H2 cells were subcutaneously transplanted into NOD scid gamma mice (age 141 days). Treatment group ($n = 4$ animals) received an i.v. injection of HL extracellular vesicles (EVs) administered *via* the tail vein at day 22, 25, 27, and 28, animals of the control group ($n = 4$ animals) were injected with PBS. Necropsy was performed on day 30. **(A)** Tumor growth in EV-treated and control animals; tumor volume was assessed as tumors were detectable ($n = 4$ animals per group). **(B)** Representative hematoxylin and eosin stainings of tumor tissue cryo-sections (25× magnification) from EV-treated (EVs) or control (Ctrl) animals (four animals per group were analyzed). **(C)** Abundance of CD30 on cells of four resected tumors analyzed by flow cytometry. **(D)** DiO-positive tumor cells after internalization of labeled HL EVs ($n = 4$). **(E)** Number of α-SMA positive cells and **(F)** cells expressing the vascularization marker CD31 in tumor sections of both groups assessed microscopically and quantified using ImageJ software (http://rsb.info.nih.gov/ij) (Student's *t*-test of $n \geq 3$ samples presented as mean + SEM; $^*p \geq 0.05$).

TME and the associated non-malignant cells (Figure S2 in Supplementary Material). Among these is TARC, a chemokine which binds to the chemokine receptor CCR4 expressed on malignant cells, regulatory T cells, and Th2 cells that are enriched in tumor tissue. Thus, TARC promotes the inflammatory HL TME (33). Of note, enhanced TARC serum levels correlate with

a bad prognosis for HL patients and is proposed as a possible biomarker for disease (10). Furthermore, secretion of growth factors (G-CSF, GM-CSF) and angiogenesis stimulating factors (VEGF), which is induced in EV-treated fibroblasts, is known to promote a tumor-supportive environment in hematological and solid tumors (34–37).

In line with this study, it was reported that EVs collected from chronic lymphocytic leukemia (CLL) transfer their molecular cargo to stromal cells to induce a phenotype corresponding to CAFs resulting in increased angiogenesis and the release of pro-survival chemokines/cytokines (38). The molecular basis of these pro-inflammatory, tumor supporting EV-mediated activation is only partly defined. One critical factor seems to be the protein S100-A9 which activates the NF-κB pathway during CLL progression in CLL cells in an autocrine loop (39). Another recent study showed that tumor cell-derived EVs are able to trigger TGF-β-dependent fibroblast-differentiation toward a phenotype which supports angiogenesis and tumor growth (40). However, the molecular basis for the activity of EVs which shape the TME is complex and remains to be investigated in more detail. Mass spectrometry of HL EVs isolated from the supernatant of KM-H2 cells revealed mTOR-signaling, protein ubiquitination, ROS signaling and NF-κB-signaling as prominent canonical pathways. These results suggest the involvement of TNF-α/NF-κB pathways in the functionality of HL EV, and this is one of the most relevant tumor drivers involved in the pathobiology of Hodgkin's disease (3, 41).

A relevant and immunocompetent mouse model for HL is not available; hence, we used a xenograft model to confirm that HL EVs can modulate the tumor microenvironment. Treatment of animals with HL EVs after transplantation of HL cells and fibroblast cells did not influence tumor growth compared to the control group, which did not receive EVs. Potential growth differences are probably not detectable in this fast-developing tumor model, at least in the absence of an immune system. However, the induction of the CAF marker α-SMA could be observed in tumor tissue of animals receiving HL EVs and this was associated with higher blood vessel formation. Of note, we could detect DiO^+ HL EVs in sections of paraffin-embedded tumor tissue *via* immunofluorescence indicating an accumulation of tumor-derived vesicles at the tumor site.

Taken together, we provide evidence for a model of bi-directional cross-talk *via* EVs and soluble factors between HL cells and non-malignant stromal cells both *in vitro* and *in vivo*. Within this network, HL EVs shape the phenotype of fibroblasts, skewing their phenotype to a cancer-associated cell state and leading to changes in the secretome of fibroblasts (**Figure 4**). We propose that a deregulated NF-κB pathway in HRS cells critically contributes to HL EV function, since a NF-κB signature was identified in HL EV samples, using IPA. Alteration of NF-κB-signaling pathways in fibroblasts mediated by signal molecules in HL EV-cargo should be addressed in future studies in more detail. In this study, we identified potential players including IL-1α, IL-6, TNF-α, and VEGF. A better understanding of the complex interactions in HL and the extended knowledge about the role of EVs in that context might aid to develop novel therapeutic tools to fight cancer.

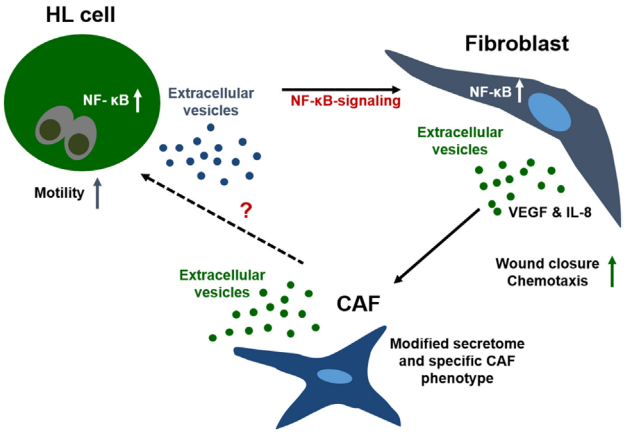

FIGURE 4 | Interaction of fibroblasts and Hodgkin lymphoma (HL) cells in the tumor microenvironment. Communication of the few malignant cells in HL with fibroblasts is crucial for survival of the tumor cells. Due to the spatial distance between the cells, direct cell–cell interaction is not the first-line communication mechanism. Interaction of both cell types is facilitated by soluble and vesicular factors, e.g., chemokines/cytokines, which enhance motility and migration of cells. Further, HL extracellular vesicles shape the phenotype of fibroblasts, skewing the cells to a cancer-associated cell state concomitant with alteration of their secretome. Our results suggest a strong involvement of the TNF-α/NF-κB axis in this process.

ETHICS STATEMENT

This study was carried out in accordance with § 8 Abs. 1 des Tierschutzgesetzes and the protocol was approved by the local authorities [Landesamt für Natur, Umwelt und Verbraucherschutz (LANUV), State Northrhine-Westfalia].

AUTHOR CONTRIBUTIONS

ES, HH, and AE: designed research and analyzed data. TB, KR, SB, RS, OS, and PZ: performed research. ES, BD, and KR wrote the paper.

ACKNOWLEDGMENTS

The authors thank Mrs. Gisela Schön and Mr. Jan Zamek (Cologne) for excellent technical assistance.

FUNDING

This study was supported by research grants of the Wilhelm Sander Stiftung (grant 2015.145.1 to ES) and the University Medical Center Giessen and Marburg (UKGM, grant 12/2017MR to ES).

SUPPLEMENTARY MATERIAL

The Supplementary Material for this article can be found online at https://www.frontiersin.org/articles/10.3389/fimmu.2018.01358/full#supplementary-material.

FIGURE S1 | **(A)** Representative histograms of flow cytometric analysis of exosome markers **(B)** as well as phosphatidylserine and the Hodgkin lymphoma (HL) marker CD30 on HL-derived extracellular vesicles (EVs) (line) compared to isotype control (solid blot). The in **(A,B)** presented FACS analysis was performed in three independent experiments. **(C)** Flow cytometric evaluation of HL cells stained with 0.25 or 1 µm DiO compared to unstained cells (Ctrl). **(D)** EV-uptake in fibroblasts cells studied *via* IF: cytoplasm was stained with cell mask deep red (red), nuclei with Hoechst and HL-derived EVs with DiO (green). Depicted are three representative pictures from upper, middle, and bottom section of a fibroblast.

FIGURE S2 | **(A)** Representative bright field and fluorescence pictures of a scratch assay after 24 h exposure of fibroblasts to 100 µg/ml Hodgkin lymphoma (HL) extracellular vesicles (EVs), medium or 5 ng/ml TGF-β as a positive control. Nuclei are depicted in blue and abundance of α-SMA in green. Microscopic assessment of α-SMA was performed for all three independent scratch assays summarized in **Figure 2B**. **(B)** Statistical evaluation of the Human 64-Plex Chemokine Array. Abundance of chemokines/cytokines after 24 h in the supernatant of fibroblasts under influence of HL EVs compared to cells incubated with normal medium (white bars: decrease, black bars: increase). Statistical differences were determined with a Student's *t*-test (mean + SEM of three independent replicates; $*p \geq 0.05$; $**p \geq 0.01$; $***p \geq 0.001$; $****p \geq 0.0001$).

FIGURE S3 | Representative pictures of tumor tissue sections of EV-treated animals and control animals stained for **(A)** α-SMA or **(B)** CD31 (red), nuclei were stained with DAPI (blue). Staining was performed for four animals per group. **(C)** Cell proliferation (XTT assay) of HDF_n cells treated with 100 or 200 µg/ml KM-H2 extracellular vesicles (EVs) for the indicated time periods and **(D)** KM-H2 cells exposed to 100 or 200 µg/ml HDF_n EVs over the indicated time course. Depicted is one experiment per cell line. The red numbers display a decrease of cell proliferation compared to the PBS-treated control, whereas green numbers express an increase of proliferation after exposure to EVs. Absorbance was measured at 475 nm with 660 nm as reference wave length.

FIGURE S4 | Pathway analysis of proteomics data obtained from analysis of Hodgkin lymphoma extracellular vesicles using the ingenuity pathway analysis (IPA) tool from QIAGEN (IPA Summer Release 2015, QIAGEN Bioinformatics).

VIDEO S1 | Scratch assay to monitor the migration of fibroblasts in presence of HL EVs.

VIDEO S2 | Scratch assay to monitor the migration of fibroblasts in absence of HL EVs.

REFERENCES

1. Hodgkin T. On some morbid appearances of the absorbent glands and spleen. *Med Chir Trans* (1832) 17:68–114. doi:10.1177/095952873201700106
2. DeVita VT, Costa J. Toward a personalized treatment of Hodgkin's disease. *N Engl J Med* (2010) 362:942–3. doi:10.1056/NEJMe0912481
3. Küppers R, Engert A, Hansmann M-L. Hodgkin lymphoma. *J Clin Invest* (2012) 122:3439–47. doi:10.1172/JCI61245
4. Aldinucci D, Gloghini A, Pinto A, de Filippi R, Carbone A. The classical Hodgkin's lymphoma microenvironment and its role in promoting tumour growth and immune escape. *J Pathol* (2010) 221:248–63. doi:10.1002/path.2711
5. Tzankov A, Zimpfer A, Pehrs A-C, Lugli A, Went P, Maurer R, et al. Expression of B-cell markers in classical Hodgkin lymphoma: a tissue microarray analysis of 330 cases. *Mod Pathol* (2003) 16:1141–7. doi:10.1097/01.MP.0000093627.51090.3F
6. Steidl C, Connors JM, Gascoyne RD. Molecular pathogenesis of Hodgkin's lymphoma: increasing evidence of the importance of the microenvironment. *J Clin Oncol* (2011) 29:1812–26. doi:10.1200/JCO.2010.32.8401
7. Aldinucci D, Celegato M, Casagrande N. Microenvironmental interactions in classical Hodgkin lymphoma and their role in promoting tumor growth, immune escape and drug resistance. *Cancer Lett* (2016) 380:243–52. doi:10.1016/j.canlet.2015.10.007
8. Zocchi MR, Catellani S, Canevali P, Tavella S, Garuti A, Villaggio B, et al. High ERp5/ADAM10 expression in lymph node microenvironment and impaired NKG2D ligands recognition in Hodgkin lymphomas. *Blood* (2012) 119:1479–89. doi:10.1182/blood-2011-07-370841
9. Reiners KS, Topolar D, Henke A, Simhadri VR, Kessler J, Sauer M, et al. Soluble ligands for NK cell receptors promote evasion of chronic lymphocytic leukemia cells from NK cell anti-tumor activity. *Blood* (2013) 121:3658–65. doi:10.1182/blood-2013-01-476606
10. Sauer M, Plütschow A, Jachimowicz RD, Kleefisch D, Reiners KS, Ponader S, et al. Baseline serum TARC levels predict therapy outcome in patients with Hodgkin lymphoma. *Am J Hematol* (2013) 88:113–5. doi:10.1002/ajh.23361
11. Zocchi MR, Camodeca C, Nuti E, Rossello A, Venè R, Tosetti F, et al. ADAM10 new selective inhibitors reduce NKG2D ligand release sensitizing Hodgkin lymphoma cells to NKG2D-mediated killing. *Oncoimmunology* (2016) 5:e1123367. doi:10.1080/2162402X.2015.1123367
12. Ruivo CF, Adem B, Silva M, Melo SA. The biology of cancer exosomes: insights and new perspectives. *Cancer Res* (2017) 77(23):6480–8. doi:10.1158/0008-5472.CAN-17-0994
13. Dörsam B, Reiners KS, von Strandmann EP. Cancer-derived extracellular vesicles: friend and foe of tumour immunosurveillance. *Philos Trans R Soc Lond B Biol Sci* (2018) 373. doi:10.1098/rstb.2016.0481
14. Kowal J, Arras G, Colombo M, Jouve M, Morath JP, Primdal-Bengtson B, et al. Proteomic comparison defines novel markers to characterize heterogeneous populations of extracellular vesicle subtypes. *Proc Natl Acad Sci U S A* (2016) 113:E968–77. doi:10.1073/pnas.1521230113
15. Simhadri VR, Reiners KS, Hansen HP, Topolar D, Simhadri VL, Nohroudi K, et al. Dendritic cells release HLA-B-associated transcript-3 positive exosomes to regulate natural killer function. *PLoS One* (2008) 3:e3377. doi:10.1371/journal.pone.0003377
16. Hansen HP, Engels H-M, Dams M, Paes Leme AF, Pauletti BA, Simhadri VL, et al. Protrusion-guided extracellular vesicles mediate CD30 trans-signalling in the microenvironment of Hodgkin's lymphoma. *J Pathol* (2014) 232:405–14. doi:10.1002/path.4306
17. Horn-Lohrens O, Tiemann M, Lange H, Kobarg J, Hafner M, Hansen H, et al. Shedding of the soluble form of CD30 from the Hodgkin-analogous cell line L540 is strongly inhibited by a new CD30-specific antibody (Ki-4). *Int J Cancer* (1995) 60:539–44. doi:10.1002/ijc.2910600419
18. Théry C, Amigorena S, Raposo G, Clayton A. Isolation and characterization of exosomes from cell culture supernatants and biological fluids. *Curr Protoc Cell Biol* (2006) Chapter 3:Unit3.22. doi:10.1002/0471143030.cb0322s30
19. Livshits MA, Livshts MA, Khomyakova E, Evtushenko EG, Lazarev VN, Kulemin NA, et al. Isolation of exosomes by differential centrifugation: theoretical analysis of a commonly used protocol. *Sci Rep* (2015) 5:17319. doi:10.1038/srep17319
20. Augsten M. Cancer-associated fibroblasts as another polarized cell type of the tumor microenvironment. *Front Oncol* (2014) 4:820. doi:10.3389/fonc.2014.00062
21. Goldberg MT, Han Y-P, Yan C, Shaw MC, Garner WL. TNF-alpha suppresses alpha-smooth muscle actin expression in human dermal fibroblasts: an implication for abnormal wound healing. *J Invest Dermatol* (2007) 127:2645–55. doi:10.1038/sj.jid.5700890
22. Koumas L, Smith TJ, Feldon S, Blumberg N, Phipps RP. Thy-1 expression in human fibroblast subsets defines myofibroblastic or lipofibroblastic phenotypes. *Am J Pathol* (2003) 163:1291–300. doi:10.1016/S0002-9440(10)63488-8
23. Hsu PL, Hsu SM. Production of tumor necrosis factor-alpha and lymphotoxin by cells of Hodgkin's neoplastic cell lines HDLM-1 and KM-H2. *Am J Pathol* (1989) 135:735–45.
24. Jost PJ, Ruland J. Aberrant NF-kappaB signaling in lymphoma: mechanisms, consequences, and therapeutic implications. *Blood* (2007) 109:2700–7. doi:10.1182/blood-2006-07-025809
25. Weniger MA, Küppers R. NF-κB deregulation in Hodgkin lymphoma. *Semin Cancer Biol* (2016) 39:32–9. doi:10.1016/j.semcancer.2016.05.001
26. Jia C-C, Wang T-T, Liu W, Fu B-S, Hua X, Wang G-Y, et al. Cancer-associated fibroblasts from hepatocellular carcinoma promote malignant cell proliferation by HGF secretion. *PLoS One* (2013) 8:e63243. doi:10.1371/journal.pone.0063243
27. Kalluri R, Zeisberg M. Fibroblasts in cancer. *Nat Rev Cancer* (2006) 6:392–401. doi:10.1038/nrc1877
28. Cattaruzza L, Gloghini A, Olivo K, Di Francia R, Lorenzon D, de Filippi R, et al. Functional coexpression of interleukin (IL)-7 and its receptor (IL-7R) on Hodgkin and Reed-Sternberg cells: involvement of IL-7 in tumor cell growth

and microenvironmental interactions of Hodgkin's lymphoma. *Int J Cancer* (2009) 125:1092–101. doi:10.1002/ijc.24389
29. Aldinucci D, Lorenzon D, Olivo K, Rapanà B, Gattei V. Interactions between tissue fibroblasts in lymph nodes and Hodgkin/Reed-Sternberg cells. *Leuk Lymphoma* (2004) 45:1731–9. doi:10.1080/10428190410001683633
30. Giannoni E, Bianchini F, Masieri L, Serni S, Torre E, Calorini L, et al. Reciprocal activation of prostate cancer cells and cancer-associated fibroblasts stimulates epithelial-mesenchymal transition and cancer stemness. *Cancer Res* (2010) 70:6945–56. doi:10.1158/0008-5472.CAN-10-0785
31. Fiaschi T, Giannoni E, Taddei ML, Cirri P, Marini A, Pintus G, et al. Carbonic anhydrase IX from cancer-associated fibroblasts drives epithelial-mesenchymal transition in prostate carcinoma cells. *Cell Cycle* (2013) 12:1791–801. doi:10.4161/cc.24902
32. Ramteke A, Ting H, Agarwal C, Mateen S, Somasagara R, Hussain A, et al. Exosomes secreted under hypoxia enhance invasiveness and stemness of prostate cancer cells by targeting adherens junction molecules. *Mol Carcinog* (2015) 54:554–65. doi:10.1002/mc.22124
33. Küppers R. The biology of Hodgkin's lymphoma. *Nat Rev Cancer* (2009) 9:15–27. doi:10.1038/nrc2542
34. Aguayo A, Kantarjian H, Manshouri T, Gidel C, Estey E, Thomas D, et al. Angiogenesis in acute and chronic leukemias and myelodysplastic syndromes. *Blood* (2000) 96:2240–5.
35. Peinado H, Alečković M, Lavotshkin S, Matei I, Costa-Silva B, Moreno-Bueno G, et al. Melanoma exosomes educate bone marrow progenitor cells toward a pro-metastatic phenotype through MET. *Nat Med* (2012) 18:883–91. doi:10.1038/nm.2753
36. Costa-Silva B, Aiello NM, Ocean AJ, Singh S, Zhang H, Thakur BK, et al. Pancreatic cancer exosomes initiate pre-metastatic niche formation in the liver. *Nat Cell Biol* (2015) 17:816–26. doi:10.1038/ncb3169
37. Yang J, Li W, He X, Zhang G, Yue L, Chai Y. VEGF overexpression is a valuable prognostic factor for non-Hodgkin's lymphoma evidence from a systemic meta-analysis. *Dis Markers* (2015) 2015:786790. doi:10.1155/2015/786790
38. Paggetti J, Haderk F, Seiffert M, Janji B, Distler U, Ammerlaan W, et al. Exosomes released by chronic lymphocytic leukemia cells induce the transition of stromal cells into cancer-associated fibroblasts. *Blood* (2015) 126:1106–17. doi:10.1182/blood-2014-12-618025
39. Prieto D, Sotelo N, Seija N, Sernbo S, Abreu C, Durán R, et al. S100-A9 protein in exosomes from chronic lymphocytic leukemia cells promotes NF-κB activity during disease progression. *Blood* (2017) 130:777–88. doi:10.1182/blood-2017-02-769851
40. Webber JP, Spary LK, Sanders AJ, Chowdhury R, Jiang WG, Steadman R, et al. Differentiation of tumour-promoting stromal myofibroblasts by cancer exosomes. *Oncogene* (2015) 34:290–302. doi:10.1038/onc.2013.560
41. Jundt F, Anagnostopoulos I, Bommert K, Emmerich F, Müller G, Foss HD, et al. Hodgkin/Reed-Sternberg cells induce fibroblasts to secrete eotaxin, a potent chemoattractant for T cells and eosinophils. *Blood* (1999) 94:2065–71.

Conflict of Interest Statement: The authors declare that the research was conducted in the absence of any commercial or financial relationships that could be construed as a potential conflict of interest.

frontiers in Immunology

ORIGINAL RESEARCH
published: 05 November 2018
doi: 10.3389/fimmu.2018.02481

Tumor-Derived Microvesicles Enhance Cross-Processing Ability of Clinical Grade Dendritic Cells

*Marco Dionisi[1†], Claudia De Archangelis[1†], Federico Battisti[1], Hassan Rahimi Koshkaki[1], Francesca Belleudi[2], Ilaria Grazia Zizzari[1], Ilary Ruscito[1,3], Christian Albano[1], Alessandra Di Filippo[1], Maria Rosaria Torrisi[2,4], Pierluigi Benedetti Panici[5], Chiara Napoletano[1], Marianna Nuti[1] and Aurelia Rughetti[1]**

[1] Department of Experimental Medicine, "Sapienza" University of Rome, Rome, Italy, [2] Department of Clinical and Molecular Medicine, Laboratory affiliated to Istituto Pasteur Italia - Fondazione Cenci Bolognetti, "Sapienza" University of Rome, Rome, Italy, [3] European Competence Center for Ovarian Cancer, Department of Gynecology, Campus Virchow Klinikum, Charité - Universitätsmedizin Berlin, Corporate Member of Freie Universität Berlin, Humboldt-Universität zu Berlin, Berlin Institute of Health, Berlin, Germany, [4] U.O.C. Genetica medica e Diagnostica cellulare avanzata, S. Andrea University Hospital, Rome, Italy, [5] Department of Gynecology-Obstetrics and Urology, "Sapienza" University of Rome, Rome, Italy

OPEN ACCESS

Edited by:
Ivan Poon,
La Trobe University, Australia

Reviewed by:
Daniel Benitez-Ribas,
Hospital Clínic de Barcelona, Spain
Monisha Samuel,
La Trobe University, Australia

***Correspondence:**
Aurelia Rughetti
aurelia.rughetti@uniroma1.it

[†]These authors have contributed equally to this work

Specialty section:
This article was submitted to Immunological Tolerance and Regulation, a section of the journal Frontiers in Immunology

Received: *31 March 2018*
Accepted: *08 October 2018*
Published: *05 November 2018*

Citation:
Dionisi M, De Archangelis C, Battisti F, Rahimi Koshkaki H, Belleudi F, Zizzari IG, Ruscito I, Albano C, Di Filippo A, Torrisi MR, Benedetti Panici P, Napoletano C, Nuti M and Rughetti A (2018) Tumor-Derived Microvesicles Enhance Cross-Processing Ability of Clinical Grade Dendritic Cells. Front. Immunol. 9:2481. doi: 10.3389/fimmu.2018.02481

Tumor cells release extracellular microvesicles (MVs) in the microenvironment to deliver biological signals to neighboring cells as well as to cells in distant tissues. Tumor-derived MVs appear to play contradictory role promoting both immunosuppression and tumor growth and both evoking tumor specific immune response. Recent evidences indicate that tumor-derived MVs can positively impact Dendritic Cells (DCs) immunogenicity by reprogramming DC antigen processing machinery and intracellular signaling pathways, thus promoting anti-tumor response. DCs are considered pivot cells of the immune system due to their exclusive ability to coordinate the innate and acquired immune responses, cross-present exogenous antigens, and prime naïve T cells. DCs are required for the induction and maintenance of long-lasting anti-tumor immunity and their exploitation has been extensively investigated for the design of anti-tumor vaccines. However, the clinical grade culture conditions that are required to generate DCs for therapeutic use can strongly affect their functions. Here, we investigated the immunomodulatory impact of MVs carrying the MUC1 tumor glycoantigen (MVs_{MUC1}) as immunogen formulation on clinical grade DCs grown in X-VIVO 15 (X-DCs). Results indicated that X-DCs displayed reduced performance of the antigen processing machinery in term of diminished phagocytosis and acidification of the phagosomal compartment suggesting an altered immunogenicity of clinical grade DCs. Pulsing DCs with MVs_{MUC1} restored phagosomal alkalinization, triggering ROS increase. This was not observed when a soluble MUC1 protein was employed (rMUC1). Concurrently, MVs_{MUC1} internalization by X-DCs allowed MUC1 cross-processing. Most importantly, MVs_{MUC1} pulsed DCs activated IFNγ response mediated by MUC1 specific $CD8^+$ T cells. These results strongly support the employment of tumor-derived MVs as immunogen platforms for the implementation of DC-based vaccines.

Keywords: dendritic cells, DC vaccine, microvesicles, cancer immunotherapy, antigen processing, phagosome, tumor antigens, MUC1

INTRODUCTION

Dendritic Cells (DCs) are antigen presenting cells (APCs) crucial for the promotion and maintenance of the anti-tumor immune response due to their ability to coordinate innate and adaptive immune response and to activate T cells inducing immune memory (1, 2). DCs are equipped with a variety of receptors able to sense tissue and cellular damage; they are endowed with an unique and powerful antigen processing machinery that enable them to crossprocess and present antigens; lastly, they display a complex pattern of costimulatory/inhibitory receptors/ligands that regulate interactions with effector immune cells (3). These biological features empower DCs to perform T cell cross priming thus activating both $CD4^+$ and $CD8^+$ T cells (4, 5).

Indeed, the exploitation of DCs in order to activate, redirect and boost the immune response against the tumor is one of the first strategies foreseen for anti-cancer immunotherapeutic purposes (6–8). Among the different biological and experimental parameters that have to be considered in the design of DC-based vaccines, antigen selection and modality of antigen loading are key points that still require to be improved to obtain an optimal DC vaccine (9). Optimization of immunogen formulation is also crucial to compensate those biological changes that characterized DCs grown in clinical grade culture conditions and that could affect the overall immunostimulatory ability of DCs (10, 11).

Recently, cell-derived extracellular microvesicles (MVs) have been regarded as an interesting option for the formulation of DC-based vaccines.

Release of MVs is an inter-cellular communication modality that allows the delivery of molecular signals into the microenvironment triggering metabolic reprogramming of the acceptor cells even in distant tissue districts, overcoming cell-to-cell contact (12, 13). Distinct MV subsets are shed by each cell and are heterogeneous for biogenesis, size, and molecular cargo components (14).

During tumor transformation, MVs released by the transforming cells exert apparently contradictory effects on host immune response. Tumor MVs have been show to promote tumor growth, modulate matrix components and trigger immunosuppression thus leading to invasion and metastasis (15–17). On the other hand, it is clear that tumor MVs can activate and promote long lasting anti-tumor immune responses (18–20). In mouse models tumor-derived MVs have been shown to be optimal immunogens for immunotherapeutic vaccination both in prophylactic and therapeutic settings (21). In addition, the immunogenity of tumor MVs appeared to be superior to the one of soluble antigens since they trigger a more efficient anti-tumor immune response than soluble antigens (22). Recent evidences suggest that immunogenicity of tumor-derived MVs observed *in vivo* may be also dependent by the antigenic and molecular signals that tumor MVs convey to DCs. Tumor-derived MVs are source of tumor antigen repertoire and have been shown to reprogram DC antigen processing and signaling pathways, resulting in increased DC immunogenicity (23–26).

In this work, we investigated whether MV based immune formulations could restore the biological performance of DCs differentiated in X-VIVO 15 serum free medium (X-DCs). Results indicated that X-DCs displayed a reduced performance of the antigen processing machinery as compared to standard DCs (S-DCs) i.e. reduced phagocytosis and acidification of the phagosomal compartment.

The antigen processing ability of both X-DCs and S-DCs was evaluated employing two distinct formulations of the MUC1 tumor glycoantigen: a soluble recombinant MUC1 glycoprotein (rMUC1) and tumor-derived MVs carrying MUC1 (MVs_{MUC1}), isolated from the MUC1 transfected DG75 cell line (27). Results indicated that only MVs_{MUC1} up-take restored the phagosomal alkalinization of X-DCs and this event was dependent by the modulation of the phagosomal radical oxigen species. Moreover, MUC1 cross-processing to HLA class I compartment was still occurring in X-DCs upon MV pulsing and IFNγ response mediated by MUC1 specific $CD8^+$T cells could be triggered by MVs_{MUC1} pulsed DCs. These results strongly suggest that the employment of MVs as immunogens for DC-based vaccine may contribute to restore the functionality of antigen processing machinery in clinical grade DCs, besides transferring the entire antigenic *repertoire* of tumor cells. Also, these evidences support further exploitation of MVs based formulation as off the shelf/cell free-immunogens for the implementation of DC-based vaccines.

MATERIALS AND METHODS

Recombinant MUC1 Glycoprotein (rMUC1)

rMUC1 was produced by CHO-K1 cells (ATCC CRL-9618) transfected with a MUC1-murine-IgG2a fusion cDNA construct containing 16 MUC1 tandem repeats. The secreted MUC1-IgG was highly sialylated due to the translational modifications occurring in CHO-K1 cells. The rMUC1 glycoprotein was purified from cell culture supernatant by anion exchange chromatography after cleavage of the Fc portion by enterokinase treatment (28).

Dendritic Cell Generation

Dendritic cells were generated as previously described (29). Briefly, Peripheral Blood Mononuclear Cells (PBMCs) were isolated from buffy coat of healthy donors, by Ficoll-Hypaque gradient (Lympholite-H, Canada) (Policlinico Umberto I Ethics Committee- Protocol nr. 4214/2016; written informed consent was obtained from the subjects in accordance with Declaration of Helsinki). $CD14^+$ monocytes were isolated from PBMCs by immunoselection kit (StemCell Technologies Inc., CA, USA) and cultured with RPMI 1640 (Sigma-Aldrich, MO, USA) complemented with 10% Fetal Bovine Serum (FBS; Euroclone, Italy) (S-DCs) or in clinical grade X-VIVO 15 culture medium (X-DCs) (Lonza, Switzerland) in the presence of 500 UI/mL of GM-CSF and 2,000 UI/mL of IL-4 (R&D Systems, USA) (day 0 and 2). Immature DCs (iDCs) grown in X-VIVO 15 were indicated as X-DCs, while iDCs grown in the presence of FBS were indicated as S-DCs. Cells were maintained in a humidified atmosphere at 37°C and 5% CO_2 (HERAcell 150, AHSI, Italy). At day 5, iDCs were matured (mDCs) by adding rhIL-1β (1,000 UI/mL−10 ng/mL), IL-6 (1,000 UI/mL−10 ng/mL), TNF-α (465 UI/mL−10 ng/mL) and prostaglandin E_2 (1 μg/mL) (all from R&D Systems, USA) for 16 h.

mDCs grown in the presence of RPMI + 10% FBS or X-VIVO 15 were employed only for $CD8^+$T cells activation and ELISpot assay. Immature X-DCs and S-DCs were employed for all the other experiments.

Cell Lines

DG75 cell line and MUC1-DG75–transfected cells were cultured as previously described in RPMI + 10% FBS (Euroclone) without or with neomycin (1 mg/mL; Invitrogen, CA, USA), respectively (27). Before MVs production, MUC1-DG75 cells were analyzed for the expression of MUC1 by flow cytometry (see below).

Flow Cytometry

DC phenotype staining was performed using the following antibodies directly conjugated with fluorescein isothiocyanate (FITC) or phycoerythrin (PE): IgG_1-FITC and IgG_1-PE as isotype controls (both from Biolegend); anti-HLAII-DR-FITC, anti-CD86-FITC, anti-CD83-PE (all from BD Biosciences), anti-CD40-PE, anti-CD14-PE, and anti-CCR7-FITC (all from Biolegend). DCs (2×10^5 cells/50μL sample) were incubated with conjugated MoAb (according to the manufacturer's recommendation) for 30 min at room temperature (RT). After washing (in 2 mL of PBS w/o Mg^{++} and Ca^{++}, centrifuged at 250 × g for 5 min), cell pellet was resuspended in PBS (100 μL); at least 1×10^4 events were evaluated using a FACSCanto II flow cytometer running FACSDiva data acquisition and analysis software (Becton Dickinson).

To evaluate MUC1 expressed by MUC1-DG75 cells, 1×10^5 cells were incubated with MoAb Ma552 (1:40; Monosan, Netherlands, 50 μL/sample) for 30 min at RT and binding revealed with FITC-conjugated anti-mouse antibody (1:600; Jackson-Immunoresearch Laboratories, PA, USA). MoAb MOPC21 (1:100; Sigma-Aldrich, 50 μL/sample) was employed as isotype control.

MV Purification

MVs were purified from cell culture supernatant of MUC1-DG75 (MVs_{MUC1}) or DG75 cells (MVs_{DG75}) (23). To generate MVs, cells were cultured 3.5×10^5 cells/mL in RPMI 1640 (Sigma-Aldrich) complemented with 2% FBS (Euroclone) for 48 h. Supernatant (70 mL/tube) underwent to serial centrifugation steps at 4°C (250 × g for 10 min, 550 × g for 30 min, 1,500 × g for 30 min) (Allegra™ 6R Centrifuges, Beckman Coulter, USA). Then supernatant was ultracentrifuged at 10,000 × g for 30 min at 4°C. Following transfer in fresh tube, the supernatant was ultracentrifuged at 100,000 × g for 1 h at 4°C (Type 35 rotor, Beckman Coulter, USA). Following the last ultracentrifugation step, supernatant was discarded and the final pellet containing MVs was gently resuspended in PBS w/o Mg^{++} and Ca^{++} (100 μL/pellet), aliquoted and stored at −20°C. Protein concentration was measured by Bradford assay (Bio-Rad Laboratories, USA). An average of 0. 95 μg/μL of MVs_{MUC1} and 0.91 μg/μL of MVs_{DG75} was obtained.

MV Characterization

Size determination of MVs_{MUC1} was performed by Nanoparticle Tracking Analysis (NTA) technology (30). MVs were thawed on ice and diluted in PBS between 1:500 and 1:20,000 to achieve the optimal number of MVs/mL. Three videos (30 s each) were recorded for each sample loading, employing the NanoSight NS300 instrument (Malvern Instruments Ltd, Malvern, UK). Measurements were performed employing the NTA 2.3 analytical software. Results were shown as the average of the three recordings.

MUC1 expression on MVs_{MUC1} was evaluated by flow cytometry. MVs_{MUC1} (5 μg/sample) were incubated with the anti-MUC1 MoAb Ma552 (Monosan) (1:100 for 30 min, 50 μL/sample, RT). After washing in PBS w/o Mg^{++} and Ca^{++}(1 mL/sample, 30 min at 13,000 rpm, RT), MVs_{MUC1} were incubated with FITC-conjugated anti-mouse antibody (1:600; Jackson-Immunoresearch Laboratories, 50 μL/sample). MoAb MOPC21 (1:100; Sigma-Aldrich) was employed as isotype control. To exclude background noise, flow cytometry analysis was performed setting the lowest Forward Scatter Threshold [300] and the highest FSC/SSC voltage. A total of 30,000 events were acquired with low flow rate, using a FACSCanto II flow cytometer running FACSDiva data acquisition and analysis software (Becton Dickinson).

Western Blot

MVs_{DG75}, MVs_{MUC1} and extract of DG75-MUC1 cell line (obtained by freeze and thaw method) (30 μg for sample) were separated on 4–12% SDS-PAGE (95V, 220 mA for 90 min at RT) and blotted onto nitrocellulose transfer membrane (Schleicher und Schuell, DE). Prestained protein ladder (10 μL) by Nippon Genetics Europe GmbH was used. After blocking (5% BSA in PBS), membranes were incubated with anti-MUC1 MoAb Ma552 (1:100, 1 h at RT; Monosan), followed by anti-mouse Fc peroxidase-conjugated antibody (1:20,000; 1 h at RT;Jackson ImmunoResearch, USA). Protein bands were detected with enhanced chemiluminescence reagents (ECL Western Blotting Detection; Amersham Biosciences, UK).

Measurement of DC Phagosomal pH

DC phagosomal pH was measured as previously described (23). Briefly, immature DCs were pulsed (10^6 cells/100 μL) for 30 min at 37°C in CO_2-indipendent medium (Gibco-Life Technologies, UK) with 3 μm microbeads (Polysciences Inc., USA) coupled with FITC (1 mg/mL) (pH sensitive, Sigma-Aldrich) and FluoProbes 647 (1 mg/mL) (pH insensitive, Interchim, France). After extensive washing in cold PBS w/o Mg^{++} and $Ca^{++}$to remove not internalized microbeads, cells were incubated at 37°C ("chase") at different time points (10, 20, 30, 60, and 120 min) in CO_2-indipendent medium and immediately analyzed by flow cytometry (FACSCanto II, FACSDiva software, Becton Dickinson). A FL1(FITC)/FL4(FluoProbes 647) gate selective for cells that had phagocytosed only one microbead was employed. Values of the ratio between the Mean Fluorescence Intensity (MFI) of FL1(FITC)/FL4(FluoProbes 647) were compared with a standard curve obtained by suspending DCs that had phagocytosed beads, in CO_2-independent medium at a fixed pH (ranging from pH 5.5 to pH 8) containing 0.1% Triton X-100 (Bio-Rad Laboratories, Inc., Italy).

The effect of MUC1 based immunogens on phagosomal pH of X-DCs was analyzed by pulsing the immature X-DC samples (10^6 cells/100 μL) for 30 min at 37°C in CO_2-indipendent

medium (Gibco-Life Technologies) with rMUC1 glycoprotein (20 μg/mL) and MVs_{MUC1} (500 μg/mL). Then, the DCs samples were processed as above described. To block NADPH oxidase 2 (NOX2) activity, 10 μM Diphenyleneiodonium chloride (DPI, Sigma-Aldrich) was added to DCs 30 min before MVs pulsing and it was maintained throughout the experiment in each solution the DCs were suspended in.

Phagocytosis Assay

To evaluate phagocytosis capability, DCs (10^6 cells/100 μL) were pulsed with 3 μm microbeads (Polysciences Inc., USA) coupled with FluoProbes 647 (ROS insensitive, Interchim) for 30 min at 37°C in the growth medium. The samples were then extensively washed in cold PBS to remove not internalized microbeads. The cells were resuspended in growth medium (10^6 cells/100 μL) and kept at 37°C for 1 h. After washing in cold PBS, samples were analyzed (at least 2×10^5 events) by flow cytometry employing FACScanto II (Becton Dickinson). As control, cells were also kept at 4°C on wet ice to block phagocytosis capability. Phagocytosis was indicated as the percentage of fluorescence positive cells subtracted of the fluorescence signal associated to the corresponding control sample.

Immunofluorescence Microscopy

iDCs (both S-DCs and X-DCs) (10^6 cells/100 μL) were incubated with rMUC1 glycoprotein (20 μg) or MVs_{MUC1} (500 μg/mL) in growth medium for 2 h or 12 h at 37°C, 5% CO_2. At the end of incubation, iDCs were washed twice in PBS and were cytospun (8×10^4 cells/sample) and fixed with cold acetone/methanol (1:1; Carlo Erba Reagents, Italy). iDCs were incubated in humid chamber with the anti-MUC1 MoAb Ma552 (1:20, Monosan) for 45 min at RT, washed in PBS (5 min in orbital shaker, 3 times), followed by FITC-conjugated goat anti-mouse $F(ab)_2$ for 30 min at RT (1:100). Both dilutions were performed in PBS. MUC1 positive cells were counted (30 fields) for each experimental condition and percentage was expressed as ratio between positive and total cell in the field. Three independent experiments were evaluated.

To study MUC1 cross-processing, the iDCs (both S-DCs and X-DCs) (10^6 cells/100 μL) were incubated with rMUC1 or MVs_{MUC1} for 12 h as above described. iDCs were then washed and stained for MUC1 expression as above. After PBS rinse (3 times, 5 min, orbital shaker), block of aspecific sites was performed by 15 min incubation with Superblock reagent (50 μL sample/slide). Following removal of the blocking solution, the iDCs were then incubated with MoAbs anti-HLAII-DR (L243 clone, 100 μL of neat supernatant) or rabbit polyclonal antibody anti-calreticulin (1:50; Stressgene, USA) (45 min, RT in the dark) to visualized HLA class II and I compartments, respectively. After washing (PBS, 3 times, 5 min, orbital shaker), samples were then incubated with Texas red–conjugated goat anti-mouse or anti-rabbit antibody, respectively (1:200, 30 min in the dark; Jackson ImmunoResearch, USA).

Fluorescence signals were visualized with an Axiovert 200 inverted microscope (Zeiss, Germany); cells were scanned in a series of 0.5 μm sequential sections with an ApoTome System (Zeiss) and images were all acquired by the digital camera Axio CAM MRm (Zeiss). Image analysis was performed by the Axiovision software (Zeiss) and a reconstruction of a selection of three central optical sections was shown in each figure. Quantitative analysis of the extent of colocalization of fluorescence signals was performed using the Axiovision software (Zeiss). The mean ± SE percent of colocalization was calculated analyzing a minimum of 30 cells for each treatment randomly taken from three independent experiments.

$MUC1^+$ $CD8^+$ T Cell Enrichment and IFNγ ELISpot

$MUC1^+$ $CD8^+$ T cell enrichment and IFNγ ELISpot were performed as previously described (23). Briefly, PBMCs of a MUC1 vaccinated ovarian cancer patient (open-label phase I/II safety clinical peptide vaccination trial (31), approved by Policlinico Umberto I Ethics Committee and Italian National Institute of Health/protocol no. LITRM/DIMIGE05/01; Ethical Committee Protocol nr. 1454/2008) were isolated by Ficoll/Hypaque density gradient. Written informed consent was obtained from the subjects in accordance with Declaration of Helsinki. $CD8^+$ T cells were purified by $CD8^+$ positive immunoselection kit (Stemcell Technologies, USA) and kept in RPMI + 5% FBS at 37°, 5% CO_2. The $CD8^-$ cell fraction (4×10^6 cell/mL) was incubated overnight (o/n) with 50 μg/mL of $MUC1_{159-167}$ peptide (SAPDNRPAL) (ClinAlfa, Switzerland) and 5 μg/mL β2-microglobulin (Sigma Aldrich) in RPMI + 1% FBS, at 37°, 5% CO_2. The $MUC1_{159-167}$ peptide specifically binds HLAI-A2 groove (31). The following day, $CD8^-$ cells were irradiated (30 Gy) and plated with autologous $CD8^+$ T cells (1:1; 2×10^6 total cells/mL) in RPMI + 5% FBS, supplemented with IL-2 (50 UI/mL, Peprotech, USA) and IL-7 (1,000 UI/mL; R&D System).

After 7 day of co-culture, freshly isolated and MUC1-pulsed autologous PBMCs (generated as above described) were irradiated and added to the culture (1:1), with IL-2 (50 UI/mL, Peprotech, USA) and IL-7 (1,000 UI/mL; R&D System). At the same time, autologous $CD14^+$ cells were immunoselected (Stemcell Technologies, USA) and cultured in RPMI + 10% FBS or X-VIVO 15 in the presence of GM-CSF (500 UI/mL) and IL-4 (2,000 UI/mL) (day 0 and 2). At day 5, iDCs (1×10^5 cells/100 μL) were pulsed o/n with MVs_{MUC1} (500 μg/mL), MVs_{DG75} (500 μg/mL) or [$MUC1_{159-167}$ peptide with β2-microglobulin] (50 and 5 μg/mL, respectively). After 2 h pulsing, the DC samples were matured with cytokine cocktail, o/n. Following maturation, mDCs were washed in PBS and added to $MUC1^+$ enriched $CD8^+$ T cells (1:5, respectively), previously expanded in culture and purified by immunoselection to remove cell debris. Pulsed mDCs/T cells were plated (1×10^5 T cells/2×10^4 DCs/200 μL /well) in duplicate onto the anti-IFNγ-precoated (1:200; BD Biosciences) ELISpot plate (MultiScreen, Merck, Germany), o/n. Unpulsed DCs + T cells were also plated at the same concentration. IFNγ cytokine release was detected with biotinylated anti-IFNγ antibody (1:250, 2 h; BD Biosciences), revealed with streptavidin-alkaline phosphatase (BD Biosciences) (1:1,000, 100 μL /well, 1 h) and chromogen

substrate (SIGMA FAST BCIP/NBT, Sigma). Spots were counted using the ImmunoSpot Image Analyzer (Aelvis, Germany).

The average values of the experimental conditions [(DCs + $MUC1_{159-167}$) + $CD8^+$T cells] and [(DCs + MVs_{MUC1}) + $CD8^+$T cells] were subtracted of the average values of the background samples [unpulsed DCs + $CD8^+$T cells] and [(DC + MVs_{DG75}) + $CD8^+$T cells], respectively.

Statistical Analysis

Statistics was performed using GraphPad Prism software, version 6 (GraphPad Software, Inc., USA). Results were expressed as mean values ± SD. *p*-values were calculated using Student's *t*-test when comparing two groups of continuous variables. Significance level was defined as *p*-value <0.05 ($^*p < 0.05$; $^{**}p < 0.01$; $^{***}p < 0.005$).

RESULTS

Dendritic Cells for Clinical Use Display a Less Efficient Antigen Processing Phagosomal Machinery

Serum-free culture conditions employed for generating DCs for anti-tumor vaccination can alter DC phenotype, modifying to some extent their immunogenicity (8, 10, 32). Indeed, DCs grown in the serum free X-VIVO 15 medium (X-DCs) acquired a spindle-like morphology, quite distinct from the one observed in DCs grown in RPMI in the presence of FBS (S-DCs) (**Figures 1Ab,a** respectively). Results from the phenotypic analysis performed by flow cytometry, showed that at the immature stage, X-DCs expressed significant higher levels of the maturative marker CCR7 chemokine receptor ($p < 0.05$) (**Figure 1B**). CD14 expression was slightly higher although not significant in immature X-DCs, while no significant change in the expression of other markers was observed between the two DC cultures.

Following maturation, in both DC cultures the activation markers were upregulated, although with a different intensity. Mature X-DCs displayed a reduced expression of CD40 costimulatory molecule ($p < 0.05$) as compared to mature S-DCs, as well as a trend in the reduction of CD86 and CD83 costimulatory molecules could be observed. These changes were accompanied by the significant increase of CD14 in mature X-DCs vs. mature S-DCs ($p < 0.05$). Again a trend in a more pronounced expression of CCR7 marker was still maintained in mature X-DCs (**Figure 1B**).

Phagocytosis is a crucial biological function of immature DCs and it is a key step for the antigen loading of DCs for cancer vaccines. Phagocytic activity of both immature S-DCs and X-DCs was evaluated by flow cytometry, following the uptake of 3 μm microbeads, conjugated with FluoProbes 647, fluorochrome not affected by changes in pH. After 1 h incubation at 37°C, phagocytosis of X-DCs was significantly reduced as compared to S-DCs ($p < 0.01$) (**Figure 1C**). Phagosomal activity in DCs is specifically dependent on a mild alkalinization, differently from what is observed in other antigen presenting cells (APCs) such as macrophages.

Kinetic of phagosomal pH in both immature X-DCs and S-DCs was followed by flow cytometry. As shown in **Figure 1D**, S-DCs presented a neutral phagosomal pH (7.01 pH) that significantly increased after 2 h chase (7.35 pH) ($p < 0.05$).

X-DCs differently behaved: phagosomal pH of X-DCs was significantly lower than S-DCs both at 10 min and 120 min chase ($p < 0.001$). Furthermore, in X-DCs phagosomal pH appeared to decrease during the chase, although not significantly.

These results suggest that clinical grade DCs have a phenotype and a biological behavior that appears to remain at a more immature stage with a more acid phagosomal compartment as compared to standard S-DCs. This feature could contribute to reduce antigen cross-processing efficiency of clinical grade DCs.

DC Uptake of the Tumor Associated MUC1 Antigen Carried by MVs Increases Antigen Internalization and Induces Phagosomal Alkalinization

We have recently shown that MV up-take by DCs allows cross-presentation of the MUC1 tumor glycoantigen by triggering a faster alkalinization of DC phagosomal compartment (23). We therefore evaluated whether MV uptake could similarly impact phagosomal pH in the clinical grade X-DCs.

MVs were isolated from the supernatant of MUC1-DG75 cell line (MVs_{MUC1}). MV size characterization by Nanoparticles Tracking Analysis (NTA) indicated that MVs_{MUC1} were heterogeneous for size: 3 main vesicle populations could be identified with a size corresponding to 105, 175, and 285 nm (**Figure 2A**). The MUC1 tumor glycoantigen was a molecular cargo component of the MVs_{MUC1} as characterized by flow cytometry (**Figure 2B**) and Western blot analysis confirmed the presence of the MUC1 antigen (**Figure 2C**). A soluble recombinant form of MUC1 glycoprotein (rMUC1) was also employed. The rMUC1 had a glycosylation profile (high level of sialylation), similar to the MUC1 carried by MVs_{MUC1} as defined by pattern reactivity of MoAbs specific for distinct MUC1 glycoforms (27).

To evaluate whether phagosomal compartment was differentially modulated by the up-take of the two distinct MUC1 immunogens, X-DCs were pulsed with MVs_{MUC1} and the soluble rMUC1 glycoprotein for 30 min (37°C) and then with FITC/FP647-coupled beads and pH kinetic was followed for 2 h. Results indicated that MVs_{MUC1} significantly increased the phagosomal pH of X-DCs within the first 60 min (reaching 7.05 pH at 20 min) as compared to unpulsed X-DCs ($p < 0.05$), then decreasing and reaching the same values of unpulsed X-DCs at the end of chase. Uptake of soluble rMUC1 glycoprotein did not modify the acidic phagosomal microenvironment of X-iDCs (**Figure 3A**). To investigate whether the phagosomal pH increase observed in clinical grade X-DCs after MVs up-take was accompanied also by modulation of ROS molecules, MVs-uptake effects were studied in X-DC pretreated with DPI as shown in **Figure 3B**. DPI treatment of X-DCs significantly decreased phagosomal pH of X-DCs during the chase ($p < 0.05$). When DPI treated X-DCs were pulsed with MVs_{MUC1} ([X-DCs + DPI] +

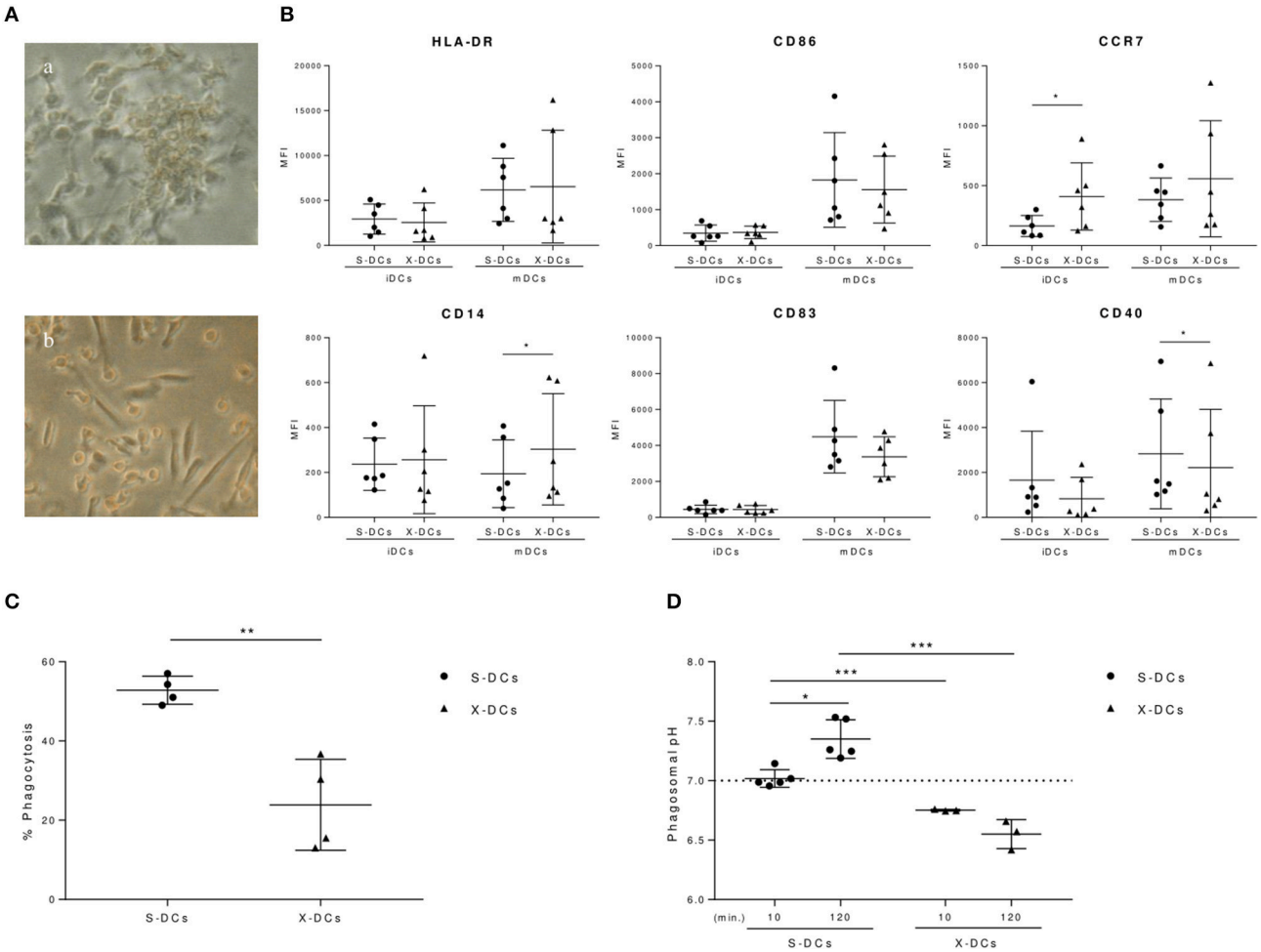

FIGURE 1 | Clinical grade DCs display different biological features compared to standard S-DCs**. (A)** Morphological differences of DCs grown in RPMI + 10%FBS (S-DCs) and in X-VIVO 15 (X-DCs) (a,b, respectively) visualized by phase contrast inverted microscope (ZEISS West Germany IM35, 3,2X). **(B)** Flow cytometry analysis of immature and mature DCs (iDCs and mDCs, respectively) grown in FBS-RPMI or X-VIVO 15 after 6 day culture in the presence of GM-CSF, IL-4. iDCs were matured with IL-6, IL-1β, PGE-2, and TNF-α on day 5. IgG_1 PE and FITC were used as isotype controls and employed to evaluate fluorescence signal background and set the gate. Results were shown as value of Mean Fluorescence Intensity (MFI) of each phenotypic marker subtracted of the corresponded negative control MFI value and depicted as scatter plot (black circle for S-DCs; black triangles for X-DCs). Statistically significant differences between S-DCs vs X-DCs were indicated (*$p < 0.05$). **(C)** Phagocytosis of S-DCs and X-DCs was evaluated at 1 h from the internalization of 3 μm FITC/FluoProbes 647 coupled beads by flow cytometry (FACSCanto II, FACSDiva software, BD Biosciences). Results were plotted as percentage of positive cells of experimental samples subtracted of the percentage of positive cells of corresponding cell samples kept at 4°C for 1 h (black circle for S-DCs; black triangles for X-DCs). **(D)** Phagosomal pH of clinical grade X-DCs (three donor, black triangles), is compared to the S-DCs (five donors, black circles) at 10 min and 120 min of chase. Average of the results of each experiment is plotted as black line. Dashed line indicates the pH neutrality value (pH 7). Significance between samples was evaluated by Student's *t* test. (*$p < 0.05$; **$p < 0.01$, *** $p < 0.005$).

MVs_{MUC1}) the phagosomal pH significantly increased in the first 60 min of chase ($p < 0.05$), although remaining lower than untreated X-DCs. These results indicated that up-take of MVs_{MUC1} also modulated antigen processing machinery of X-DCs by inducing alkalinization of the phagosomal microenvironment. The antigenic transfer of MUC1 was also investigated evaluating the percentage of MUC1 positive DCs following incubation with both MVs_{MUC1} and both rMUC1 by immunofluorescence studies, at 2 h and 12 h of incubation at 37°C (**Figure 3C**).

At 2 h pulsing, the percentage of X-DCs that had internalized MVs_{MUC1} was lower than the corresponding S-DCs ($p < 0.05$). A similar trend in decrease was also observed when the soluble rMUC1 was employed as immunogen. At 12 h of pulsing this difference was enhanced: the percentage of MUC1 positive X-DCs was much lower than MUC1 positive S-DCs for both MVs_{MUC1} and rMUC1 glycoprotein ($p < 0.01$ and $p < 0.005$, respectively). Interestingly, MUC1 antigenic transfer to X-DCs appeared to be more efficient when mediated by MVs_{MUC1} than the rMUC1 at 12h ($p < 0.01$). These results suggest that MVs_{MUC1} may be more efficient in antigenic transfer than the soluble rMUC1 glycoprotein, despite the fact that the intracellular availability of the MUC1 antigen is strongly reduced in X-DCs as compared to S-DCs.

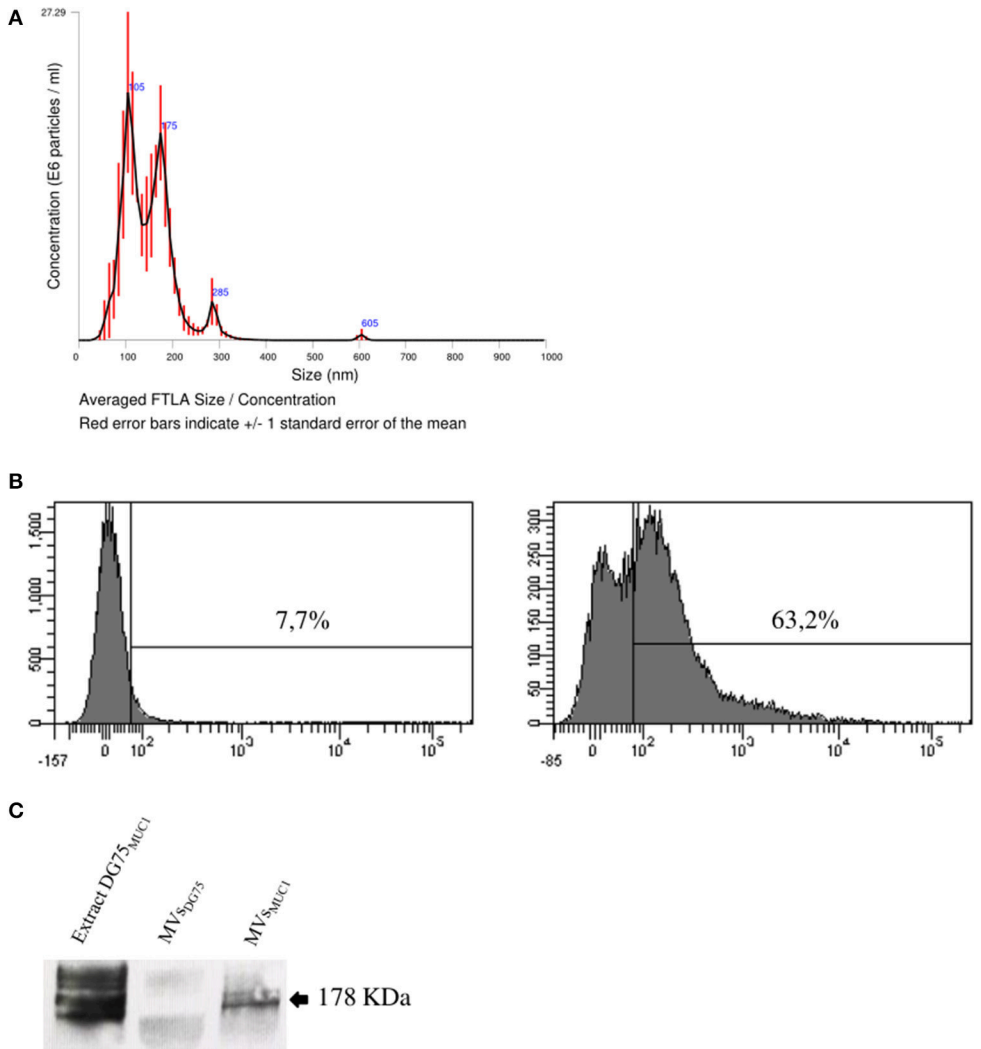

FIGURE 2 | Characterization of tumor-derived microvesicles (MVs_{MUC1}). **(A)** Size measurement of MVs shed by the MUC1-transfected DG75 lymphoblastoid cell line (MVs_{MUC1}) using Nanosight NS300 that employs Nanoparticles Tracking Analysis (NTA) technology. Results are plotted as graph; *y-axis*: concentration of particles; *x-axis*: size of particles in nanometer. The black curve is obtained by the merge of three independent measurements for each MV sample. **(B)** MUC1 expression in MVs_{MUC1} by flow cytometry. MoAb MOPC21 was employed as isotype control (left). MUC1 expression was detected employing the MoAb Ma552 (right). **(C)** Western Blot analysis to detect MUC1 in MVs_{DG75}, MVs_{MUC1} and MUC1-DG75 cell extracts (30 μg/sample) employing the MoAb Ma552. The extract of MUC1-DG75 cell line was used as positive control.

Tumor-Derived MVs Mediate MUC1 Antigen Cross-Processing in Clinical Grade DCs and Activation of MUC1 Specific $CD8^+$ T Cells

Clinical grade DCs seems to show some "macrophages-like" features such as acid phagosomal pH and high ROS content in their phagosomal compartment (data not shown). We wanted to investigate further if this could affect their ability to cross-process tumor associated antigens (TAA). Both X-DCs and S-DCs were pulsed with MVs_{MUC1} and the rMUC1 soluble glycoprotein and intracellular distribution of the MUC1 antigen was observed by immunofluorescence, after 12 h.

In S-DCs pulsed with MVs_{MUC1} (**Figure 4A**, row 1 and 2), MUC1 colocalized with calreticulin, marker of HLA class I compartment (38%) (**Figure 4A**, row 1), while scarce colocalization with HLA-DR, marker of HLA class II compartment (5%) was found (**Figure 4A**, row 2). When rMUC1 was employed to pulse S-DCs, low colocalization for both calreticulin and HLAII-DR compartment markers was found (<18%) (**Figure 4B**, row 1 and 2). These results confirmed previous observations indicating that only MUC1 supplied to DCs as cargo of MVs were routed to $calreticulin^+$ compartment (27).

In X-DCs, following up-take of both immunogens, MUC1 colocalization was increased HLAII-DR positive compartment

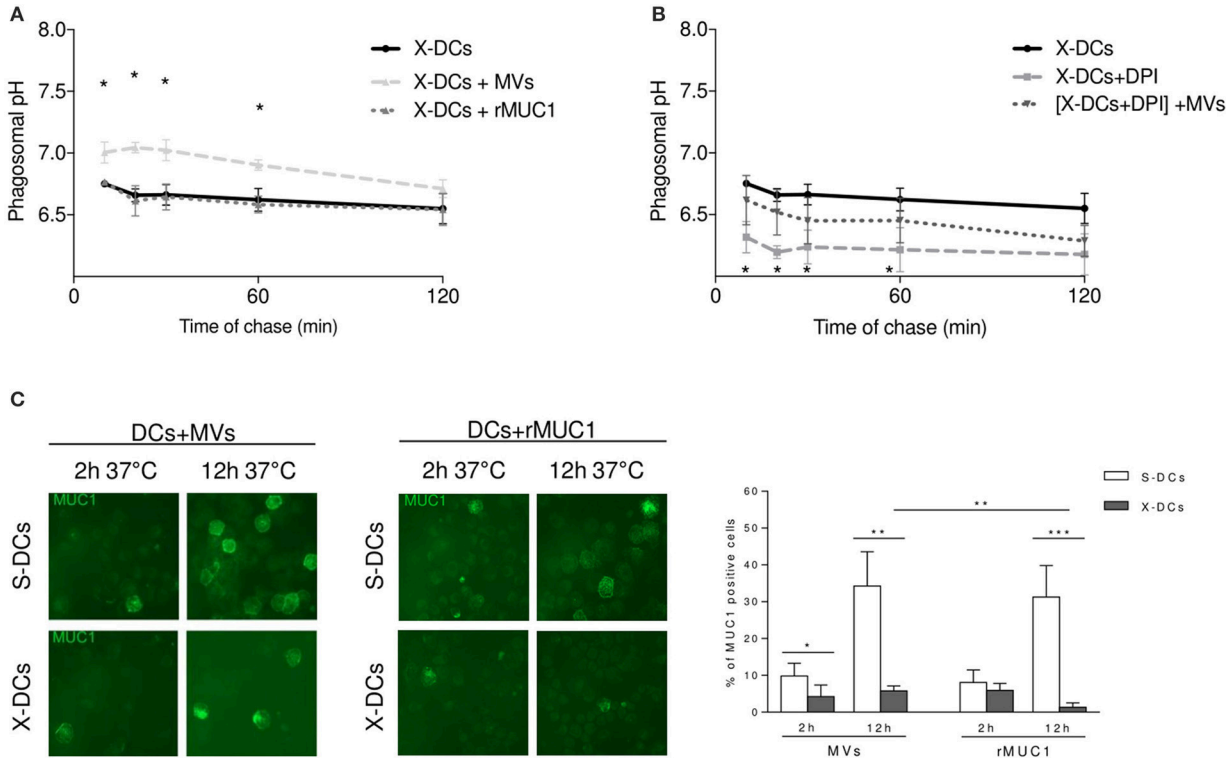

FIGURE 3 | Tumor-derived MVs_{MUC1} efficiently increase X-DC phagosomal pH and transfer MUC1 antigen to X-DCs. **(A)** Kinetic of phagosomal pH (10–120 min chase) of X-DCs, pulsed with soluble rMUC1 or with MVs_{MUC1}. Following MVs_{MUC1} uptake, phagosomal pH of X-DCs (light gray dashed line) was significantly increased in the first 60 min of chase ($p < 0.05$) as compared to unpulsed X-DCs (black continuous line). Soluble rMUC1 protein uptake did not alter phagosomal pH of X-DCs (dark gray dashed line). The average ± SD of three independent experiments (3 different donors) was shown. *$p < 0.05$. **(B)** Phagosomal pH measurement in X-DCs in the presence of 10 μM Diphenyleneiodonium chloride (DPI), NOX2 inhibitor, without or with MVs_{MUC1}. DPI treatment decreased pH compared to untreated X-DCs (light gray dashed line vs. black continuous line, respectively). In [DPI-treated X-DCs + MVs_{MUC1}] (black dotted line) phagosomal pH was partially restored. The difference between [DPI treated X-DCs] and [DPI-treated X-DCs + MVs_{MUC1}] was significant for the first 60 min of chase ($p < 0.05$). Values are mean ± SD of three independent experiments. *$p < 0.05$; **$p < 0.01$, ***$p < 0.005$. **(C)** MUC1 expression in DCs following pulsing with rMUC1 glycoprotein or MVs_{MUC1}. S-DCs (first row) and X-DCs grown in X-VIVO 15 (second row) were visualized by immunofluorescence staining after 2 and 12 h incubation, employing the anti-MUC1 MoAb Ma552 (green). The average ± SD of percentage of positive cells (evaluated by counting 30 fields for each experimental condition, three independent experiments) was shown as histograms (White: S-DCs; gray: X-DCs). Uptake by X-DCs was significantly decreased as compared to S-DCs. Within the X-DCs, MVs_{MUC1} uptake was higher than the soluble rMUC1 ($p < 0.01$). *$p < 0.05$; **$p < 0.01$, ***$p < 0.005$.

as compared to S-DCs ($p < 0.01$ for MVs_{MUC1} and $p < 0.05$ for rMUC1). In particular, MUC1 colocalized with HLAII-DR molecules in dots, close to the plasma membrane in X-DCs pulsed with MVs_{MUC1} (**Figure 4A**, row 4) as well as rMUC1 (**Figure 4B**, row 4). Interestingly, in X-DCs, colocalization of MUC1 with calreticulin positive compartment was observed only when X-DCs were pulsed with MVs_{MUC1}, although at a lower extent of the corresponding S-DCs ($p < 0.05$). rMUC1 did not appear to colocalize significantly with calreticulin marker in X-DCs.

These results showed that while the soluble rMUC1 was mainly found in association with HLAII-DR, MVs_{MUC1} could be up-taken and cross-processed in HLA class I and II compartments by clinical grade X-DCs, although this was reduced compared to S-DCs.

To investigate whether the reduced cross-processing of MVs_{MUC1} in X-DCs was still sufficient to activate MUC1 specific T cell responses, $CD8^+$ T cells were isolated by immunomagnetic selection from PBMCs of an ovarian cancer patient, previously vaccinated with the HLAI-A2 restricted $MUC1_{159-167}$ peptide (31). MUC1 specific $CD8^+$ T cells were expanded *in vitro* by a two round stimulation with autologous PBMCs pulsed with the $MUC1_{159-167}$ peptide.

At the end of the culture, T cell activation was evaluated as IFNγ release in ELISpot assay (**Figure 4C**). The MUC1 enriched $CD8^+$ T cells were stimulated by autologous X-DCs or S-DCs, loaded with immunogenic $MUC1_{159-167}$ peptide or pulsed with $MVs_{MUC1.}$ T cells stimulated by unpulsed DCs or DCs pulsed with MVs_{DG75} (MVs from untransfected DG75 cells) were employed as background controls (for MUC1 peptide loaded and MVs_{MUC1} pulsed DCs, respectively). As shown in **Figure 4C**, X-DCs were less efficient as stimulator of IFNγ T-cell mediated response, independently by the MUC1 immunogen employed. MVs_{MUC1} appeared to perform better as immunogen than the exogenous $MUC1_{159-167}$ peptide. In particular in [X-DCs+ MVs_{MUC1}] induced a similar T response to [S-DCs + $MUC1_{159-167}$], suggesting that the MUC1 carried by MVs could be processed and cross-presented to T cells also by X-DCs, whose

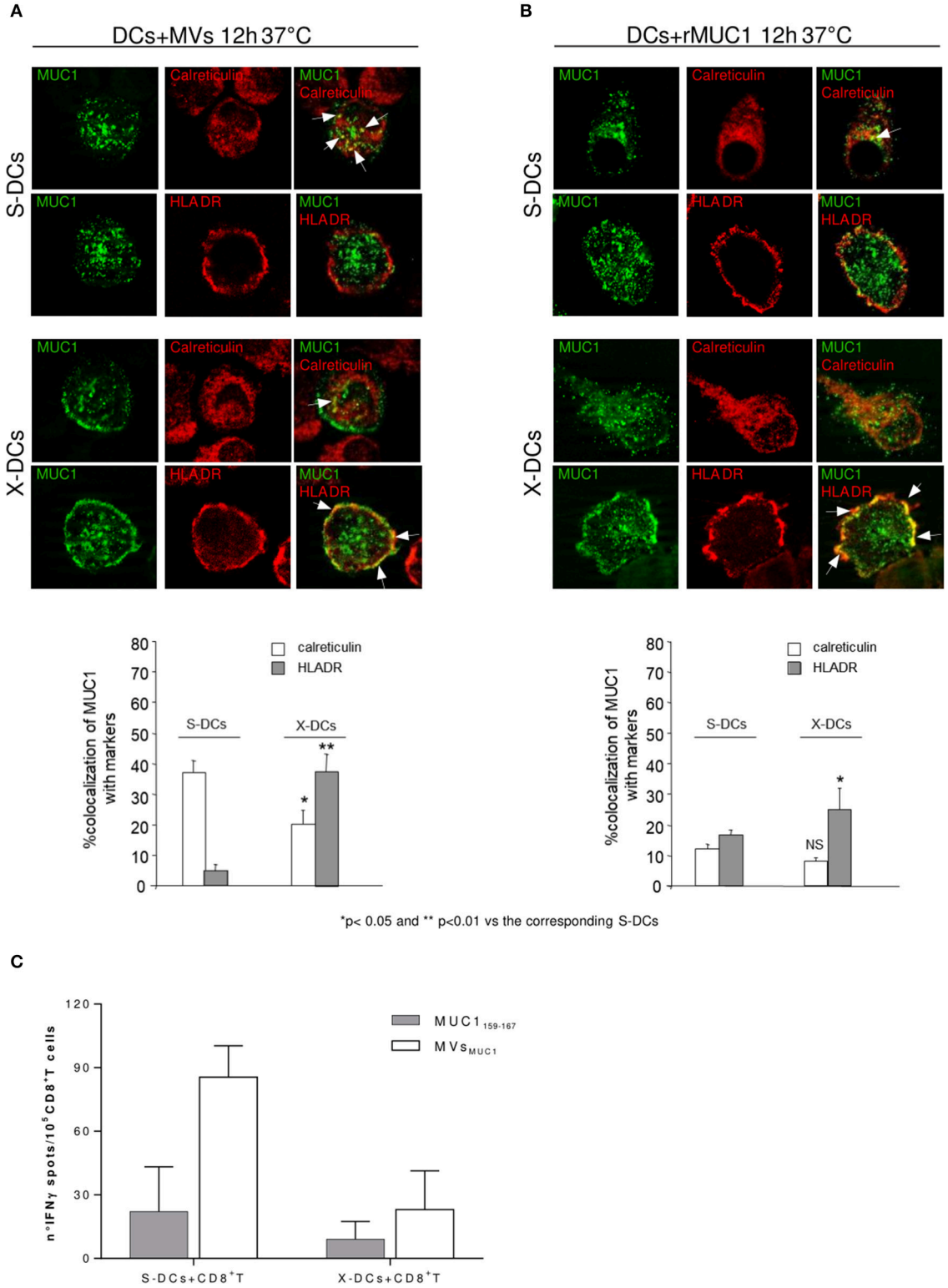

FIGURE 4 | Clinical Grade DCs maintain the ability to cross-process antigen, when MUC1 is carried by MVs and to activate MUC1 specific $CD8^+$ T cells. Intracellular localization of MUC1 carried by MVs_{MUC1} **(A)** or as soluble rMUC1 glycoform **(B)** in S-DCs (first and second row) and in X-DCs (third and fourth row) were visualized by immunofluorescence staining after 12 h of internalization employing the anti-MUC1 MoAb Ma552 (green) combined with antibodies specific for distinct intracellular compartment markers (red). In particular: anti-calreticulin polyclonal rabbit antibody, [calreticulin ER resident protein, employed as marker for HLA class I compartment] (first and third rows) and anti-HLAII-DR for HLA-II compartment (second and fourth rows). The percentage of colocalization (yellow) was calculated

(Continued)

FIGURE 4 | analyzing a minimum of 30 cells for each treatment randomly taken from three independent experiments. Results are expressed as mean values ± SE in histograms. Magnification, x63; Bar, 10 mm. $^{**}p < 0.01$ and $^{*}p < 0.05$ for X-DCs vs. the corresponding S-DCs pulsed with MVs_{MUC1} or rMUC1. **(C)** ELISpot assay to evaluate the IFNγ production by enriched MUC1-specific $CD8^+$ T cells obtained from an ovarian cancer patient in response to mature S-DCs (left) or X-DCs (right) loaded with $MUC1_{159-167}$ peptide (white histogram) or pulsed with MVs_{MUC1} (grey histogram). The average values of the experimental samples [(DCs + $MUC1_{159-167}$) + $CD8^+$T cells] and [(DC + MVs_{MUC1}) + $CD8^+$T cells] were subtracted of the corresponding background samples i.e., [unpulsed DCs + $CD8^+$T cells] and [(DCs + MVs_{DG75}) + $CD8^+$T cells], respectively. Results were expressed as mean values ± SD of duplicates.

processing and presentation abilities were dampened by culture conditions.

DISCUSSION

One of the critical key point in designing DCs-based antitumor vaccines is the choice of antigen formulation: the ideal immunogen should deliver a broad repertoire of TAAs combined to activatory signals in order to potentiate immunostimulatory capability of DCs. This strategy would reduce the possibility of immune escape and overcome HLA haplotype restriction that is a real limit for the peptide based DCs approach (33).

There is a compelling need to search for optimal immunogen formulations to efficaciously target and load DCs with antigens, and at the same time to activate them for improving anti-tumor DCs performance. Nowadays, that immune checkpoint blockade allows to clinically reverse the immune exhaustion, DC-based vaccines are being reassessed as a powerful approach to activate/maintain the unleashed antitumor memory T cell responses in order to control tumor disease progression (9, 34).

Cell released MVs display biological characteristics that make them as optimal candidate as immunogen platform able to simultaneously deliver multiple tumor antigens and immunostimulatory signals to DCs (35). Tumor-derived MVs can enhance the immunogenicity of soluble antigen (21, 22) and induce $CD8^+$ T-cell responses in *in vitro* human studies toward tumor antigens (36). Delivery of the tumor antigens by MVs also modulate cross-presentation of those tumor glycosylated antigens such as MUC1 that are thought to induce only a tolerogenic $CD4^+$ T cell response, although being relevant for tumor targeting (27). Furthermore, tumor-derived MVs have been shown to activate DCs *in vivo* by delivering tumor DNA triggering intracellular signaling cGAS/STING pathway resulting in potent anti-tumor responses (24–26).

In this study, we provide evidences that clinical grade culture conditions hamper DC immunogenicity by reducing phagocytosis and inducing a macrophage like feature of the phagosomal compartment i.e., strong acidification, besides altering DCs phenotype. We showed that tumor-derived MVs carrying the MUC1 tumor glycoantigen employed as immunogen, restored phagosomal pH close to neutrality, allowing cross-presentation of the tumor associated MUC1 glycoantigen and the activation of MUC1 specific $CD8^+$ T cell response.

Culture conditions are critical for DC differentiation process from progenitor cells. It has described that *ex-vivo* DCs for clinical use are less immunogenic, because of a reduced expression of HLA and costimulatory molecules. Addition of human serum (autologous or pooled) to implement clinical grade DC performance appears to hamper cytokine production and reduce migratory capacity of DCs (37, 38). Indeed, the high plasticity of DCs, that enable them to quickly sense *in vivo stimuli*, can become a critical point in formulating experimental protocols for *ex-vivo* DC cultures (8). DCs generated in X-VIVO 15 serum free medium (X-DCs) displayed a spindle-like morphology and a distinct ability to respond to maturative pro-inflammatory cytokines than S-DCs (DCs grown in RPMI+10%FBS). Previous work had shown that DCs culture in X-VIVO 15 performed poorly in phenotype and cytokine secretion (10). Despite optimization of the culture protocol (anticipating cytokine re-addition during the culture; Napoletano C, unpublished), X-DCs still performed differently compare to S-DCs. Immature X-DCs had increased expression of the maturative CCR7 marker, while following maturation, CD14 marker was still maintained ($p < 0.05$). Also mature X-DCs showed a lower upregulation of costimulatory molecules than S-DCs.

This phenotype is associated to a reduced phagocytosis of immature X-DCs that usually is a functional feature of the mature DCs. This aspect can be quite relevant for the up-take of immunogens that are based on protein or particulated-based antigens. Most interestingly, the phagosomal machinery appeared to be modified by clinical grade culture conditions. X-DCs displayed a significant acidification of the phagosomal compartment that was maintained during the time following 3 μm beads phagocytosis, while phagosomal pH of S-DCs was close to neutrality and increased during the incubation time following 3 μm bead internalization.

Phagosome is a crucial compartment for the ability of DCs to cross-present antigens: it is considered a central hub for the cell where molecular cargos are docked and then sorted to other intracellular compartments of the cell (39). The cross-processing ability of DCs is finely tuned by a mild alkalinization of the phagosomal compartment. Induction of $CD8^+$ T cells was obtained only by priming with monocyte-derived DCs with alkaline phagosomal pH, while macrophages, with an acid phagosomal pH, did not cross-process antigen (40). In mouse models, $CD8^+$ DCs with a higher cross-processing ability showed an alkaline phagosomal pH (41). It has been hypothesized that alkaline pH delays protein degradation thus increasing the antigen amount available for cytoplasmic transportation and HLA-I association (39, 42, 43).

The results obtained suggest that X-DCs possess phagosomal machinery with strong similarities to macrophages, that quickly degrades the antigen thus favoring HLAII presentation and the induction of $CD4^+$ T cells. Thus, the reduced ability to

internalize the antigen combined to the increased efficiency in antigen degradation would imply a reduced immunogenicity of the DC vaccine designed. To investigate if this was the case, we employed two MUC1 based immunogens forms: a soluble rMUC1 glycoprotein, produced in CHO-K1 cells and MVs_{MUC1}, tumor-derived MVs carrying the MUC1 antigen purified from a MUC1 stable transfected cell line. Size characterization by NTA indicated that vesicles were heterogenous and biochemical characterization of cell markers (data not shown) indicated that the prevalence of MVs_{MUC1} derived from plasma membrane exocytic pathways. Indeed, after 12 h pulsing, X-DCs showed a striking significant reduction of intracellular MUC1 distribution than S-DCs, for both the immunogens employed (MVs_{MUC1}: $p < 0.01$; rMUC1: $p < 0.005$), strongly suggesting that the reduced up-take and the acidic compartment of X-DCs hasten degradation of MUC1 antigen.

We have recently shown that uptake of tumor-derived MVs exerts an immunostimulatory effect on antigen presentation by DCs, inducing a faster alkalinization of phagosomal compartment thus allowing cross-presentation of the MUC1 tumor glycosylated antigen (23). This mechanism could be of great relevance for shaping the immunogenicity of glycosylated tumor antigens.

We then asked whether, tumor-derived MVs could be a suitable immunogen formulation to counteract the phagosomal alkalinization and restore a pH value close to neutrality.

Uptake of MVs_{MUC1} by X-DCs significantly restored the phagosomal pH of X-DCs to neutrality in the first 60 min chase. This metabolic event is also supported by the observation that following pulsing of X-DCs with MVs_{MUC1}, intracellular MUC1 distribution is significantly higher ($p < 0.01$) than X-DCs pulsed with rMUC1, thus suggesting that protein degradation has been lessened. Phagosomal pH is strictly dependent by Radical Oxigen Species (ROS) level produced in the phagosome by the combined and dynamically regulated function of NADPH oxidase 2 (NOX2) and VATPase (41, 44).

Indeed, MVs_{MUC1} uptake contributes to phagosomal ROS increase, as shown by NOX2 blocking experiments with the DPI inhibitor. However, other metabolic pathways triggered by MV uptake could be involved in the fine tuning of phagosomal ROS balance and pH regulation.

Most important, MVs_{MUC1} internalization allowed MUC1 cross-processing by X-DCs, despite these cells displayed a "macrophage-like" phagosomal compartment. After 12 h from MV internalization, in X-DCs MUC1 colocalized with HLA class II compartment (39%), but also with the calreticulin marker employed as HLA class I compartment (21%). In S-DCs MUC1 colocalization was prevalent with the calreticulin$^+$ compartment (38%), as expected. The rMUC1 soluble glycoprotein was sorted exclusively in HLAII compartment both in S-DCs and in X-DCs. In DCs, cross-processing of soluble antigens occurs by distinct mechanisms: the "cytosolic" and "vacuolar" pathways. In the former, the internalized antigen sorted into the phagosome, then translocates in the cytosol where proteasome degradation occurs and proteolitic peptides are loaded by TAP dependent mechanism in the ER where the association to MHCI occurs. In the vacuolar pathway, exogenous antigens are degraded in the endosome, loading endosome resident MHCI molecules (39, 45). The co-localization of MUC1 with the ER marker calreticulin, and the detection of MUC1 in the cytosolic fraction of MVs_{MUC1} pulsed DCs previously shown (27), clearly suggested that the cytosolic pathway was involved in the MUC1 cross-processing mediated by MVs delivery, although the vacuolar pathway could not be excluded. These intracellular events resulted in cross-presentation of the MUC1 antigen since X-DCs pulsed with MVs_{MUC1} were able to activate CD8$^+$ T cells specific for the HLA-A2 restricted $MUC1_{159-167}$ epitope, although with a lower efficiency than S-DCs, as expected.

Thus, delivery of antigenic cargo through MVs appeared to be a possible strategy to empower antigen presenting ability of DCs for clinical use.

Tumor-derived MVs immunogenicity could be possibly enhanced by mean of genetic and biochemical interventions with the ultimate goal to generate an off the shelf/cell free immunogen (46, 47). Induced genome instability of tumor cells could increase the amount of novel neoantigens that elicit strong immune response (48), thus increasing the antigenic cargo of the released MVs. Also, modulation of glycosylation is an appealing option to harness MVs immunogenicity (49). So far, glycosylation is regarded as a complex and finely tuned signaling code among cells and microenvironment, not just a "default cell décor" (50). DCs are endowed of specific receptor, C-type lectin, recognizing selectively the distinct glycan moieties (51). By specific and selective ligand receptor interaction, glycan *repertoire* shapes immunogenicity of the antigens by modulating their internalization and at the same time triggering activatory/inhibitory signals to the DCs (52–54). Selective genome editing strategies allow to control glycan synthesis, thus obtaining cells (and therefore MVs) with the desired glycan profile and defined immunoregulatory properties (55).

In summary, we have investigated the immunomodulatory impact of tumor-derived MVs carrying MUC1 as immunogen in clinical grade culture condition DCs. Results indicate that optimization of the MUC1 antigen cross-processing could be induced upon tumor derived MVs_{MUC1} internalization in clinical grade X-DCs, despite their acidic phagosomal compartment, that is a feature of macrophage cells. This effect appears to be dependent by metabolic changes triggered by phagosomal ROS increase and alkalinization. Furthermore, MVs_{MUC1} pulsed DCs could stimulate MUC1 specific CD8$^+$ T cells to produce IFNγ response. We believe these results to further support the exploitation of tumor-derived MVs as optimal immunogens for DC-based anti-cancer vaccine.

AUTHOR CONTRIBUTIONS

All authors contributed with their specific expertise to study design, data collection, analysis, and interpretation of results and to critically evaluate and approve the manuscript prior publication. AR designed and supervised the study and wrote the manuscript. FeB and CN developed the methodology for phagosomal pH and ROS detection and performed DC studies. MD and CDA were responsible for cell and DC culture, phagosomal pH measurments, ROS detection in DC phagosome, flow cytometry analysis. HRK,

IGZ, and IR performed microvesicles production, isolation and biochemical characterization. ADF performed flow cytometry analysis of cell and microvesicles. MRT and FrB were responsible for the immunofluorescence studies. CA performed $MUC1^+$ $CD8^+$ T cell enrichment and IFNγ ELISpot, together to HRK. PBP provided cancer patient blood samples and clinical information. MN provided valuable support for the study design and interpretation of results.

FUNDING

This study was supported by Sapienza University of Rome [Grant RM116154D8CAD997 to AR; C26A15HYMX (CN); RG11715C7D85000E (MN)]. Also, the study was partially supported by AIRC (IG17432 to MN and IG15858 to MT).

ACKNOWLEDGMENTS

The authors are most grateful to the EU project QLK3-CT-2002-02010 team for the rMUC1 glycoprotein, to Prof. P. Trivedi (Sapienza, University of Rome, Italy) for providing the DG75 cell line and to Mr. M. Cristiani for his helpful collaboration. The authors acknowledge Mr. F. Castagna during his Bachelor training and are particularly grateful to Dr. Caterina Gori (IRCCS L. Spallanzani, Rome, Italy) for support and advice throughout the project.

REFERENCES

1. Pulendran B. The varieties of immunological experience: of pathogens, stress, and dendritic cells. *Annu Rev Immunol.* (2015) 33:563–606. doi: 10.1146/annurev-immunol-020711-075049
2. Qian C, Cao X. Dendritic cells in the regulation of immunity and inflammation. *Semin Immunol.* (2018) 35:3–11. doi: 10.1016/j.smim.2017.12.002
3. Pardoll DM. The blockade of immune checkpoints in cancer immunotherapy. *Nat Rev Cancer* (2012) 12:252–64. doi: 10.1038/nrc3239
4. Kurts C, S Robinson BW, Knolle PA. Cross-priming in health and disease. *Nat Rev Immunol.* (2010) 10:403–14. doi: 10.1038/nri2780
5. Sánchez-Paulete AR, Teijeira A, Cueto FJ, Garasa S, Pérez-Gracia JL, Sánchez-Arráez A, Sancho D, Melero I. Antigen cross-presentation and T-cell cross-priming in cancer immunology and immunotherapy. *Ann Oncol.* (2017) 28:xii44–55. doi: 10.1093/annonc/mdx237
6. Steinman RM. Dendritic cells *in vivo:* a key target for a new vaccine science. *Immunity* (2008) 29:319–24. doi: 10.1016/j.immuni.2008.08.001
7. Bryant CE, Sutherland S, Kong B, Papadimitrious MS, Fromm PD, Hart DNJ. Dendritic cells as cancer therapeutics. *Semin Cell Dev Biol.* (2018) doi: 10.1016/j.semcdb.2018.02.015
8. Santos PM, Butterfield LH. Dendritic cell–based cancer vaccines. *J Immunol.* (2018) 200:443–9. doi: 10.4049/jimmunol.1701024
9. Saxena M, Bhardwaj N. Re-emergence of dendritic cell vaccines for cancer treatment. *Trends Cancer* (2018) 4:119–37. doi: 10.1016/j.trecan.2017.12.007
10. Napoletano C, Pinto D, Bellati F, Taurino F, Rahimi H, Tomao F, et al. A comparative analysis of serum and serum-free media for generation of clinical grade DCs. *J Immunother* (2007) 30:567–76. doi: 10.1097/CJI.0b013e318046f396
11. Kalantari T, Kamali-Sarvestani E, Ciric B, Karimi MH, Kalantari M, Faridar A, et al., Generation of immunogenic and tolerogenic clinical-grade dendritic cells. *Immunol Res.* (2011) 51:153–60. doi: 10.1007/s12026-011-8255-5
12. Tkach M, Théry C. Communication by extracellular vesicles: where we are and where we need to go. *Cell* (2016) 164:1226–32. doi: 10.1016/j.cell.2016.01.043
13. van Niel G, D'Angelo G, Raposo G. Shedding light on the cell biology of extracellular vesicles. *Nat Rev Mol Cell Biol.* (2018) 19:213–28. doi: 10.1038/nrm.2017.125
14. Sedgwick AE, D'Souza-Schorey C. The biology of extracellular microvesicles. *Traffic* (2018) 19:319–27. doi: 10.1111/tra.12558
15. Maia J, Caja S, Strano Moraes MC, Couto N, Costa-Silva B. Exosome-based cell-cell communication in the tumor microenvironment. *Front Cell Dev Biol.* (2018) 6:18. doi: 10.3389/FCELL.2018.00018
16. Nabet BY, Qiu Y, Shabason JE, Wu TJ, Yoon T, Kim BC, et al. Exosome RNA unshielding couples stromal activation to pattern recognition receptor signaling in cancer. *Cell* (2017) 170:352–366.e13. doi: 10.1016/j.cell.2017.06.031
17. Naito Y, Yoshioka Y, Yamamoto Y, Ochiya T. How cancer cells dictate their microenvironment: present roles of extracellular vesicles. *Cell Mol Life Sci.* (2017) 74:697–713. doi: 10.1007/s00018-016-2346-3
18. Andre F, Schartz NE, Movassagh M, Flament C, Pautier P, Morice P, et al. Malignant effusions and immunogenic tumour-derived exosomes. *Lancet* (2002) 360:295–305. doi: 10.1016/S0140-6736(02)09552-1
19. Bu N, Wu H, Sun B, Zhang G, Zhan S, Zhang R, et al. Exosome-loaded dendritic cells elicit tumor-specific CD8+ cytotoxic T cells in patients with glioma. *J Neurooncol.* (2011) 104:659–67. doi: 10.1007/s11060-011-0537-1
20. Menay F, Herschlik L, De Toro J, Cocozza F, Tsacalian R, Gravisaco MJ, et al. Exosomes isolated from ascites of T-cell lymphoma-bearing mice expressing surface CD24 and HSP-90 induce a tumor-specific immune response. *Front Immunol.* (2017) 8:286. doi: 10.3389/fimmu.2017.00286
21. Gu X, Erb U, Büchler MW, Zöller M. Improved vaccine efficacy of tumor exosome compared to tumor lysate loaded dendritic cells in mice. *Int J Cancer* (2015) 136:E74–84. doi: 10.1002/ijc.29100
22. Zeelenberg IS, Ostrowski M, Krumeich S, Bobrie A, Jancic C, Boissonnas A, et al. Targeting tumor antigens to secreted membrane vesicles *in vivo* induces efficient antitumor immune responses. *Cancer Res.* (2008) 68:1228–35. doi: 10.1158/0008-5472.CAN-07-3163
23. Battisti F, Napoletano C, Koshkaki HR, Belleudi F, Zizzari IG, Ruscito I, et al. Tumor-derived microvesicles modulate antigen cross-processing via reactive oxygen species-mediated alkalinization of phagosomal compartment in dendritic cells. *Front Immunol.* (2017) 8:1–14. doi: 10.3389/fimmu.2017.01179
24. Zhang H, Tang K, Zhang Y, Ma R, Ma J, Li Y, et al. Cell-free Tumor microparticle vaccines stimulate dendritic cells via cGAS/STING signaling. *Cancer Immunol Res.* (2015) 3:196–205. doi: 10.1158/2326-6066.CIR-14-0177
25. Kitai Y, Kawasaki T, Sueyoshi T, Kobiyama K, Ishii KJ, Zou J, et al. DNA-containing exosomes derived from cancer cells treated with topotecan activate a STING-Dependent pathway and reinforce antitumor immunity. *J Immunol.* (2017) 198:1649–59. doi: 10.4049/jimmunol.1601694
26. Diamond JM, Vanpouille-Box C, Spada S, Rudqvist N-P, Chapman J, Ueberheide B, et al. Exosomes shuttle TREX1-sensitive IFN-stimulatory dsDNA from irradiated cancer cells to dendritic cells. *Cancer Immunol Res.* (2018) 6: 910–20. doi: 10.1158/2326-6066.CIR-17-0581
27. Rughetti A, Rahimi H, Belleudi F, Napoletano C, Battisti F, Zizzari IG, et al. Microvesicle cargo of tumor-associated MUC1 to dendritic cells allows cross-presentation and speci fi c carbohydrate processing. *Cancer Immunol Res.* (2014) 2:177–86. doi: 10.1158/2326-6066.CIR-13-0112-T
28. Rughetti A, Pellicciotta I, Biffoni M, Bäckström M, Link T, Bennet EP, et al. Recombinant tumor-associated MUC1 glycoprotein impairs the differentiation and function of dendritic cells. *J Immunol.* (2005) 174:7764–72. doi: 10.4049/jimmunol.174.12.7764
29. Napoletano C, Mattiucci S, Colantoni A, Battisti F, Zizzari IG, Rahimi H, et al. *Anisakis pegreffii* impacts differentiation and function of human dendritic cells. *Parasite Immunol* (2018) 40:e12527. doi: 10.1111/pim.12527
30. Dragovic RA, Gardiner C, Brooks AS, Tannetta DS, Ferguson DJP, Hole P, et al. Sizing and phenotyping of cellular vesicles using nanoparticle

tracking analysis. *Nanomed Nanotechnol Biol Med.* (2011) 7:780–8. doi: 10.1016/j.nano.2011.04.003
31. Antonilli M, Rahimi H, Visconti V, Napoletano C, Ruscito I, Zizzari IG, et al. Triple peptide vaccination as consolidation treatment in women affected by ovarian and breast cancer: clinical and immunological data of a phase I/II clinical trial. *Int J Oncol.* (2016) 48:1369–78. doi: 10.3892/ijo.2016.3386
32. Peng JC, Thomas R, Nielsen LK. Generation and maturation of dendritic cells for clinical application under serum-free conditions. *J Immunother* (2005) 28:599–609. doi: 10.1097/01.cji.0000175491.21099.04
33. Constantino J, Gomes C, Falcão A, Cruz MT, Neves BM. Antitumor dendritic cell-based vaccines: lessons from 20 years of clinical trials and future perspectives. *Transl Res.* (2016) 168:74–95. doi: 10.1016/j.trsl.2015.07.008
34. Palucka AK, Coussens LM. The basis of oncoimmunology. *Cell* (2016) 164:1233–47. doi: 10.1016/j.cell.2016.01.049
35. Zhang H, Huang B. Tumor cell-derived microparticles: a new form of cancer vaccine. *Oncoimmunology* (2015) 4:8–10. doi: 10.1080/2162402X.2015.1017704
36. Napoletano C, Rughetti A, Landi R, Pinto D, Bellati F, Rahimi H, et al. Immunogenicity of allo-vesicle carrying erbb2 tumor antigen for dendritic cell-based anti-tumor immunotherapy. *Int J Immunopathol Pharmacol.* (2009) 22:647–58. doi: 10.1177/039463200902200310
37. Kolanowski STHM, Sritharan L, Lissenberg-Thunnissen SN, Van Schijndel GMW, Van Ham SM, Brinke A Ten. Comparison of media and serum supplementation for generation of monophosphoryl lipid A/interferon-γ-matured type I dendritic cells for immunotherapy. *Cytotherapy* (2014) 16:826–34. doi: 10.1016/j.jcyt.2013.12.005
38. da Silva Simoneti G, Saad STO, Gilli SCO. An efficient protocol for the generation of monocyte derived dendritic cells using serum-free media for clinical applications in post remission AML patients. *Ann Clin Lab Sci.* (2014) Spring; 44:180–8. Available online at: www.annclinlabsci.org
39. Alloatti A, Kotsias F, Magalhaes JG, Amigorena S. Dendritic cell maturation and cross-presentation: timing matters! *Immunol Rev.* (2016) 272:97–108. doi: 10.1111/imr.12432
40. Mantegazza AR, Savina A, Vermeulen M, Pérez L, Geffner J, Hermine O, et al. NADPH oxidase controls phagosomal pH and antigen cross-presentation in human dendritic cells. *Blood* (2008) 112:4712–22. doi: 10.1182/blood-2008-01-134791
41. Savina A, Peres A, Cebrian I, Carmo N, Moita C, Hacohen N, et al. The small GTPase Rac2 controls phagosomal alkalinization and antigen crosspresentation selectively in CD8+ dendritic cells. *Immunity* (2009) 30:544–55. doi: 10.1016/j.immuni.2009.01.013
42. van Montfoort N, Camps MG, Khan S, Filippov DV, Weterings JJ, Griffith JM, et al. Antigen storage compartments in mature dendritic cells facilitate prolonged cytotoxic T lymphocyte cross-priming capacity. *Proc Natl Acad Sci USA.* (2009) 106:6730–5. doi: 10.1073/pnas.0900969106
43. Delamarre L, Pack M, Chang H, Mellman I, Trombetta ES. Differential lysosomal proteolysis in antigen-presenting cells determines antigen fate. *Science* (2005) 307:1630–4. doi: 10.1126/science.1108003
44. Kotsias F, Hoffmann E, Amigorena S, Savina A. Reactive oxygen species production in the phagosome: impact on antigen presentation in dendritic cells. *Antioxid Redox Signal.* (2013) 18:714–29. doi: 10.1089/ars.2012.4557
45. Embgenbroich M, Burgdorf S. Current concepts of antigen cross-presentation. *Front Immunol.* (2018) 9:1643. doi: 10.3389/fimmu.2018.01643
46. Yang Y, Hong Y, Cho E, Kim GB, Kim I-S. Extracellular vesicles as a platform for membrane-associated therapeutic protein delivery. *J Extracell Vesicles* (2018) 7:1440131. doi: 10.1080/20013078.2018.1440131
47. Roy S, Hochberg FH, Jones PS. Extracellular vesicles: the growth as diagnostics and therapeutics; a survey. *J Extracell Vesicles* (2018) 7:1438720. doi: 10.1080/20013078.2018.1438720
48. Efremova M, Finotello F, Rieder D, Trajanoski Z. Neoantigens generated by individual mutations and their role in cancer immunity and immunotherapy. *Front Immunol.* (2017) 8:1679. doi: 10.3389/fimmu.2017.01679
49. Williams C, Royo F, Aizpurua-Olaizola O, Pazos R, Boons G-J, Reichardt N-C, et al. Glycosylation of extracellular vesicles: current knowledge, tools and clinical perspectives. *J Extracell Vesicles* (2018) 7:1442985. doi: 10.1080/20013078.2018.1442985
50. Gabius H-J. The sugar code: why glycans are so important. *Biosystems* (2018) 164:102–11. doi: 10.1016/j.biosystems.2017.07.003
51. Brown GD, Willment JA, Whitehead L. C-type lectins in immunity and homeostasis. *Nat Rev Immunol* (2018) 18:374–89. doi: 10.1038/s41577-018-0004-8
52. de Oliveira Figueiroa E, Albuquerque da Cunha CR, Albuquerque PBS, de Paula RA, Aranda-Souza MA, Alves MS, et al. Lectin-carbohydrate interactions: implications for the development of new anticancer agents. *Curr Med Chem.* (2017) 24:3667–80. doi: 10.2174/0929867324666170523110400
53. Zizzari IG, Martufi P, Battisti F, Rahimi H. The macrophage galactose-type C-Type Lectin (MGL) modulates regulatory T cell functions. *PLoS ONE* (2015) 10:e0132617. doi: 10.1371/journal.pone.0132617
54. Rodríguez E, Schetters STT, Van Kooyk Y. The tumour glyco-code as a novel immune checkpoint for immunotherapy. *Nat Rev Immunol.* (2018) 18:204–11. doi: 10.1038/nri.2018.3
55. Steentoft C, Bennett EP, Schjoldager KT-BG, Vakhrushev SY, Wandall HH, Clausen H. Precision genome editing: a small revolution for glycobiology. *Glycobiology* (2014) 24:663–80. doi: 10.1093/glycob/cwu046

Conflict of Interest Statement: The authors declare that the research was conducted in the absence of any commercial or financial relationships that could be construed as a potential conflict of interest.

frontiers in Immunology

PERSPECTIVE
published: 23 May 2018
doi: 10.3389/fimmu.2018.01111

Apoptotic Tumor Cell-Derived Extracellular Vesicles as Important Regulators of the Onco-Regenerative Niche

Christopher D. Gregory and Ian Dransfield*

Medical Research Council Centre for Inflammation Research at the University of Edinburgh, The Queen's Medical Research Institute, Edinburgh, United Kingdom

Cells undergoing apoptosis produce heterogeneous populations of membrane delimited extracellular vesicles (Apo-EVs) which vary not only in size—from tens of nanometers to several microns—but also in molecular composition and cargo. Apo-EVs carry a variety of potentially biologically active components, including small molecules, proteins, and nucleic acids. Larger forms of Apo-EVs, commonly termed "apoptotic bodies," can carry organelles, such as mitochondria and nuclear fragments. Molecules displayed on the surface of extracellular vesicles (EVs) can contribute substantially to their size, as well as their functions. Thus far, relatively little is known of the functional significance of Apo-EVs apart from their roles in fragmentation of dying cells and indicated immunomodulatory activities. Here, we discuss EV production by dying tumor cells and consider the possible roles of Apo-EVs in a cell death-driven sector of the tumor microenvironment known as the onco-regenerative niche (ORN). We propose that tumor-derived Apo-EVs are significant vehicles of the ORN, functioning as critical intercellular communicators that activate oncogenic tissue repair and regeneration pathways. We highlight important outstanding questions and suggest that Apo-EVs may harbor novel therapeutic targets.

Keywords: extracellular vesicles, apoptosis, inflammation and cancer, tumor microenvironment, angiogenesis, tissue repair and regeneration, macrophage activation, tumor biology

OPEN ACCESS

Edited by:
Shohei Hori,
The University of Tokyo, Japan

Reviewed by:
Ai Kotani,
Tokai University Isehara Hospital, Japan
Naohiro Seo,
Mie University, Japan

****Correspondence:***
Christopher D. Gregory
chris.gregory@ed.ac.uk

Specialty section:
This article was submitted to Immunological Tolerance and Regulation, a section of the journal Frontiers in Immunology

Received: *07 March 2018*
Accepted: *03 May 2018*
Published: *23 May 2018*

Citation:
Gregory CD and Dransfield I (2018) Apoptotic Tumor Cell-Derived Extracellular Vesicles as Important Regulators of the Onco-Regenerative Niche. Front. Immunol. 9:1111. doi: 10.3389/fimmu.2018.01111

INTRODUCTION: APOPTOSIS, AND THE ONCO-REGENERATIVE NICHE (ORN)

In addition to its activities in developmental sculpting and adult tissue involution, apoptosis is renowned for its capacity to regulate tissue turnover and homeostasis in which, simplistically, the expansion of cell populations is balanced by regulated cell death (and *vice versa*). In cancer, this balance between cell gain and cell loss becomes dysregulated, resulting in accumulation of tumor cells and net growth of neoplastic tissues (**Figure 1**). By effecting controlled cell deletion, apoptosis imposes a brake on oncogenesis, a logical concept that has long been proven and is widely accepted. Indeed, inhibition of the tumor suppressor function of apoptosis led to the categorization of a new class of oncogenes—*BCL2* being the prototypic member—that could promote cell survival through suppression of apoptosis and thereby impose an oncogenic imbalance on the cell birth/cell death equation (1). Furthermore, the apoptosis effector protease, caspase-8, is mutated in multiple cancer types and the survival pathway PI3K/Akt/mTOR is dysregulated frequently in tumors (2). By contrast,

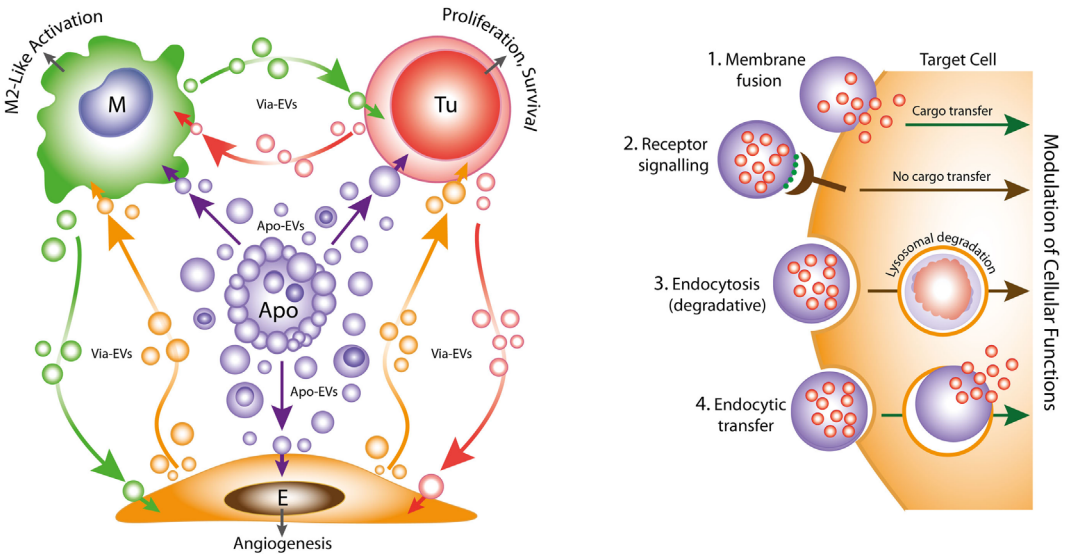

FIGURE 1 | Left: oncogenic extracellular vesicle (EV) networks in the onco-regenerative niche (ORN). Schematic representation of the ORN illustrating the potential roles of Apo-EVs from dying tumor cells (Apo) in providing oncogenic signals to neighboring cells in the niche, exemplified by macrophages (M), viable tumor cells (Tu), and endothelial cells (E). We propose that Apo-EVs target such cells and modulate cellular functions, including macrophage polarization toward a reparative phenotype (M2-like activation state), promotion of tumor cell survival and proliferation, and angiogenesis. EVs from viable cells (Via-EVs) of tumor and stromal cell origin also seem likely to participate in these processes. Right: mechanisms of cell targeting and modulation by (Apo)-EVs. Examples of possible modes of interaction of Apo-EVs with target cells that may lead to modulation of cellular functions with or without transfer of intact EV cargoes (biologically active cargoes represented by small red circles). 1. Membrane fusion (receptor-dependent or -independent) permits transfer of EV cargoes to cytosolic locations. 2. Docking of EVs through receptor–ligand interaction may activate intracellular signaling pathways in the absence of cargo transfer. Ligands such as phosphatidylserine (PtdSer) (green) exposed at EV surfaces may interact directly or indirectly with target cell receptors (examples in the case of PtdSer including BAI1, TIM-4, Stabilin 2, Axl, Mer, as well as integrins αvβ3 and αvβ5). 3. Endocytic pathways (including phagocytosis) resulting in lysosomal degradation of cargoes are also likely to modulate cellular functions such as through metabolite supply and *via* receptor ligation. 4. Putative endocytic uptake of EVs without lysosomal degradation. We propose that Apo-EV cargoes are transferred intact to multiple intracellular compartments *via* this type of pathway.

pro-apoptotic regulators such as p53 and BIM (3) among others have firmly established tumor-suppressive roles for apoptosis. For these and other reasons, the capacity to evade apoptosis has become a well-accepted hallmark of cancer (4).

However, set opposite its tumor suppressor functions, the apoptosis machinery can endow dying cells with the ability to stimulate proliferation of neighboring cells, either as part of developmental programmes or in tissue repair and regeneration in adult tissues (5–9). High levels of apoptosis are commonly associated with poor prognosis in multiple cancer types (10–17) and expression of pro-apoptotic effector molecules such as active Caspase-3 and Bax can correlate with aggressive disease (18, 19). Furthermore, low-level activation of the apoptosis programme can promote genomic instability and oncogenic transformation (20).

Emerging evidence suggests strongly that both constitutive and therapy-induced apoptosis can engender pro-oncogenic responses that enhance tumor growth and cause post-therapeutic relapse (21–24). In this scenario, tumor-cell apoptosis itself promotes imbalance in the cell birth/cell death equation that ultimately favors net tumor growth. Such regenerative effects of apoptosis in the context of the tumor microenvironment led one of us to propose recently the concept of the ORN: a tumor-promoting network of tumor cells, stromal cells, and immune cells which, together with associated extracellular components, including EVs, soluble factors and matrix molecules, is orchestrated by tumor-cell apoptosis (**Figure 1**) (25, 26). We speculate that pervasive apoptotic tumor cell-derived signals in the ORN provide important pathways for tumor growth, metastasis and to post-therapeutic relapse. Here, we consider the potential roles of apoptotic tumor cell-derived EVs in providing such signals.

APO-EVs AND APOPTOTIC BODIES

It is becoming increasingly clear that EVs are important intercellular communication vehicles in the tumor microenvironment, shuttling an array of biologically active molecules reciprocally between tumor and non-tumor cells, modulating the development of primary tumors and metastases. We propose that Apo-EVs—as well as EVs generated in viable cells responding to their apoptotic neighbors—are important elements of the ORN (**Figure 1**). EV production is a well-established hallmark of apoptosis, as is surface blebbing (zeiosis) of the plasma membrane in cells responding to apoptosis stimuli. Blebs may be important precursors to Apo-EVs, but it remains unclear to what extent the process of surface blebbing is related mechanistically to the production of Apo-EVs. Here, we use the term "Apo-EV" to encompass all classes of subcellular vesicles produced as a consequence of apoptosis. These include small (~50–1,000 nm) as well as larger vesicles (1 to several microns in diameter), often

referred to as "apoptotic bodies," which harbor caspase-modified autoantigens, nuclear remnants containing condensed chromatin, and well-defined organelles, such as mitochondria and endoplasmic reticulum. Among the smaller vesicles are likely to be exosomes of endosomal pathway origin and budding plasma membrane EVs also known as microvesicles or ectosomes (27). As with all EVs, the size of Apo-EVs matters—not only in relation to what molecular and organelle cargoes can be carried but also with respect to the specific contribution of molecular cargoes, such as cell surface proteins, to overall EV size (**Figure 2**). While Apo-EVs are undoubtedly heterogeneous both in size and content (28), the underlying causes of this heterogeneity remain obscure.

APO-EV PRODUCTION MECHANISMS

During apoptosis, caspase-dependent cleavage, and activation of Rho-activated kinase, ROCK I alters actomyosin contractility, resulting in membrane blebbing (30). Blebbing occurs independently of altered K^+ and Cl^- channel activity that results in increased K^+ permeability and the reduction of cell volume that accompanies apoptosis. Instead, bleb formation occurs as a consequence of detachment of the plasma membrane from the actin cortex and increased hydrostatic pressure generated by the actomyosin system (31). As a consequence, there is rapid local influx of cytosolic material and "ballooning" of the membrane, resulting in bleb enlargement. Although cytoskeletal proteins are lacking in newly formed blebs, as blebbing progresses, there is reassembly of the cortical cytoskeleton underneath the membrane. Treatment of cells with the ROCK inhibitor Y-27632 reduces both the formation of apoptotic bodies and the capacity for apoptotic-cell clearance (32). Formation of small Apo-EVs may also be regulated through similar ROCK-dependent mechanisms (33), as are EVs generated by a variety of tumor cell types (34).

It has been widely assumed that the plasma membrane of apoptotic cells, apoptotic blebs, and Apo-EVs are molecularly homogeneous, displaying broadly similar changes, such as phosphatidylserine (PtdSer) exposure. However, there is evidence that apoptotic bodies exhibit loss of membrane integrity that allows limited molecular exchange (35), which may allow selective release of molecules that are able to modulate innate inflammatory mechanisms. Protein release from apoptotic bodies, particularly of nucleosomal histones, was reduced following inhibition of activity of either ROCK or myosin ATPase (35). Loss of membrane permeability may be phased as apoptosis progresses, prior to the catastrophic loss of membrane integrity during secondary necrosis. Formation of Apo-EVs and gradual loss of membrane permeability could represent a mechanism to provide transient protection of proteins from local proteolytic degradation and/or clearance, potentially allowing signals relating to cellular demise to be disseminated distally, for example to other parts of the tumor microenvironment and to metastatic sites.

Studies of the recognition and phagocytosis of apoptotic cells have revealed potentially contrasting roles for membrane blebbing and the formation of apoptotic bodies. Formation of apoptotic blebs may promote phagocytosis of apoptotic cells. Compromised apoptotic cell uptake following inhibition of blebbing (36) could be partially reversed by addition of the PtdSer opsonin, MFG-E8. Other phospholipid binding proteins such as C1q have been demonstrated to bind avidly to apoptotic blebs and C1q binds to neuronal blebs, acting to augment phagocytosis by microglia (37). ROCK-dependent high-density opsonization of apoptotic blebs could generate a topology that promotes phagocyte recognition, providing an explanation for why low-level PtdSer exposure is not sufficient to signal phagocytosis of viable cells. Thus, membrane blebbing likely facilitates maintenance of self-tolerance and suppression of antitumor immunity

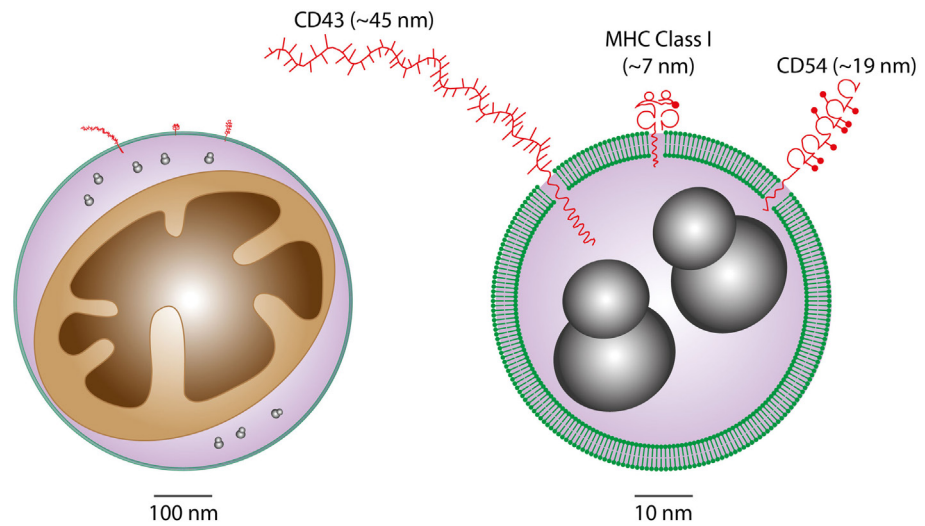

FIGURE 2 | Considerations of vesicular cargoes in relation to extracellular vesicle (EV) sizes. Schematic representations of Apo-EVs of ~500 nm (left) and 50 nm (right) are shown with delimiting lipid bilayer (green), a small mitochondrion (brown), ribosomes (gray), and examples of surface proteins all drawn approximately to scale. Note the significant potential impact of surface molecule size on total vesicle size in the case of small vesicles displaying relatively large surface molecules [measurement and representation of cell surface proteins adapted from Ref. (29)].

through direct effects on apoptotic cell clearance. Other phenomena related to vesiculation during apoptosis have also been noted recently. Following the description of apoptopodia—fine protuberances from apoptotic cells that appear to be involved in the release of larger varieties of Apo-EVs (>1 μm) (38)—EV production from certain apoptotic cell types has been observed to involve fragmentation of membrane protrusions resembling beads on a string (39). While the significance of these observations has not been fully elucidated, they provide clues as to the molecular events underlying the production of Apo-EVs and their cargo loading preferences. Intriguingly, Apo-EVs produced from beaded apoptopodia were found to be depleted of nuclear components including histones and nuclear DNA (39) that are well-known constituents of apoptotic bodies (40).

CARGOES AND FUNCTIONAL ACTIVITIES

While EVs ostensibly of non-apoptotic cell origins have been the subject of intense research in cancer biology in recent years, the biology of Apo-EVs remains less clear. Following on from seminal work showing that glioblastoma EVs carry RNA and protein cargoes having tumor growth-promoting properties and utility as diagnostic biomarkers (41), a wealth of evidence now implicates EVs in regulating tumor growth and metastatic spread through control of angiogenesis, drug resistance, and antitumor immunity. Furthermore, the roles of EVs in intercellular communication in the tumor microenvironment are becoming better defined. Taking some recent examples, in murine melanoma, tumor cell-derived exosomes have been reported to promote the accumulation of pro-tumor macrophages *via* their ability to educate mesenchymal stromal cells which, like tumor-associated macrophages, are able to promote malignant disease *via* multiple modes, including growth factor production, suppression of antitumor immunity and angiogenesis (42). EVs from circulating tumor cells are also generated under conditions of shear flow. These EVs may play important roles in establishing the metastatic niche in the lung through interaction with the lung vasculature and rapidly accumulating myeloid cells (which phagocytose them) (43). It is noteworthy that EVs provide an intercellular signaling mechanism to transfer drug resistance to susceptible cells. For example, transfer of resistance to the multi-receptor tyrosine kinase inhibitor drug, Sunitinib can be achieved by a long, non-coding RNA (lncARSA) which acts by competing for binding to mir-34 and mir-449 to promote AXL and c-MET expression in renal cell carcinoma cells by carriage in exosomes and transfer to susceptible cells, thereby propagating resistance (44). Intriguingly, EVs isolated from cancer-associated fibroblasts are able to alter the metabolic profile of pancreatic tumor cells that interact with, and internalize them (45). Metabolic reprogramming by EVs involved inhibition of oxidative phosphorylation by mitochondria resulting in promotion of glycolysis and glutamine-dependent reductive carboxylation (46) in the recipient tumor cells. Furthermore, EVs were found to be capable of transferring multiple metabolic constituents including amino acids, lipids, citrate, and pyruvate among others, to tumor cells endowing them with the capacity to grow in nutrient-deficient media *in vitro* (45). These results strongly support the notion that EVs in the tumor microenvironment provide tumor cells with critical metabolic signals and constituents which permit growth of tumor clones under conditions of stress such as hypoxia and nutrient deprivation.

The extent to which Apo-EVs—including the larger variety, apoptotic bodies—can perform similarly diverse functions to their non-apoptotic counterparts awaits detailed clarification. However, several studies would tend to suggest that Apo-EVs represent far more than biological "waste disposal" units. We support the definition of Apo-EVs as those EVs, regardless of size or cargo, that are produced as a consequence of activation of the apoptosis effector machinery (such as executioner caspase activation) and that ultimately results in cell death. Thus, active Apo-EV production presages cell death and a major challenge for the allocation of functional properties to Apo-EVs specifically will be their discrimination from EVs produced by cells activated by other (for example, stress) pathways, including those en route to apoptosis. Like all EVs, Apo-EVs are overtly heterogeneous as illustrated by their size profile alone, which, ranges from around 30 nm to several microns (47, 48). To what extent size of Apo-EVs relates to functional properties is largely unknown, although small EVs (30–100 nm, which the authors termed "exosome-like") produced by vascular endothelial cells downstream of caspase-3 activation were found to be distinct from their larger counterparts (microvesicles and apoptotic bodies) both in cargo composition and biological function (48). Vascular endothelial cell-derived apoptotic bodies carry histones and other nuclear proteins as well as abundant markers of organelles including mitochondria, endoplasmic reticulum, and ribosomes (48), confirming observations of apoptotic body cargoes in other systems. By contrast, the exosome-like EVs were found to be enriched in lysosomal, basement membrane and extracellular matrix proteins (48). Intriguingly, certain hallmark proteins of exosomes, including TSG101, CD9, and CD81, were missing from the exosome-like EVs whereas others, notably fibronectin, syntenin and translationally controlled tumor protein (TCTP) were present. Critically, exosome-like EVs were found to be immunogenic, in contrast to apoptotic bodies (48), confirming the presumption that the latter, as major remnants of apoptotic cells, are generally tolerogenic.

These recent studies extend earlier investigations demonstrating the segregation of nuclear components into granular and vesicular structures and extrusion from the cell in EV-like structures and apoptotic bodies (49–54). Strikingly, DNA and RNA from apoptotic cells have been described as segregating into non-overlapping vesicular entities, adding to the complexity of Apo-EV heterogeneity. It is well established that the blebs of apoptotic cell surfaces harbor antigens of common significance in autoimmune disease, including the ribonucleoproteins La and Ro and nucleosomal DNA (55). The immunogenicity of exosome-like EVs from apoptotic endothelial cells adds a further dimension to this phenomenon. Thus, the C-terminal fragment (LG3) of the basement membrane component Perlecan carried by the exosome-like EVs is highly immunogenic and may be responsible for the production of autoantibodies that can severely compromise successful renal transplantation (48). Substantial further investigations are warranted in order to clarify the differential

capacity of apoptotic cells and their derived vesicles to modulate tolerance and immunity.

Besides immuno-regulatory properties, Apo-EVs have additional functional attributes based, like other EV classes, on their ability to transfer bioactive molecules to "target" cells. For example, apoptotic bodies (1–4 μm) derived from mature endothelial cells have been shown to stimulate the proliferation and differentiation of circulating endothelial progenitor cells (56). Indeed, Apo-EVs of endothelial cell origin carry a variety of biologically active components in addition to the aforementioned immunogenic Perlecan LG3, including TCTP, which can inhibit apoptosis in vascular smooth muscle cells (57). Apo-EVs may also allow the transfer of intact organelles between cells. In this context, it is noteworthy that mitochondrial transfer *via* EVs may represent an important response to stressful conditions as exemplified by the transfer of intact mitochondria from astrocytes to neurons in order to provide survival signals during the ischemic conditions of stroke (58). One of the most intriguing cargoes of Apo-EVs is genomic DNA since it has been shown that apoptotic bodies are able to mediate the horizontal transfer of DNA between somatic cells. While the details of the modes of transfer and fundamental roles of Apo-EVs (versus the remnants of apoptotic cells) have not been studied, DNA from apoptotic cells can undoubtedly be transferred to neighboring cells including tumor cells, endothelial cells, fibroblasts, and macrophages leading to apoptotic cell-derived gene expression in the recipient cells. In normal physiology, cells are protected by a DNA damage response requiring DNAse II, Chk2, and p53/p21, and deficiency in p53 and p21 can ultimately render murine embryonic fibroblasts oncogenic following transfer of DNA from apoptotic cells harboring c-myc or H-Ras oncogenes in combination with a drug resistance gene (59–61). These results have significant implications not only for genomic stability and heterogeneity of tumor cells but also for the acquisition of aberrant DNA by non-tumor cell components of the ORN, notably endothelial cells, macrophages and fibroblasts, all of which have known capacity to engulf apoptotic cells and bodies. Such genetic changes in the ORN could provide important pro-oncogenic signals even if the resultant "exogenous" gene expression is transient.

CONCLUSION AND FUTURE PERSPECTIVES

While it is clear that the breakdown of apoptotic cells into membrane-bounded fragments of broad size ranges varies between different cell types, the full extent of the functional properties of Apo-EVs remains unknown. It has been reported that formation of "bite-sized" apoptotic bodies can aid in the phagocytic clearance of dying cells (36). This may be important for the apoptotic-cell clearance processes of so-called non-professional (i.e., non-macrophage) phagocytes. However, macrophages and other phagocytes have overt capacity to engulf whole apoptotic cells rapidly (62). We propose that the most important function of Apo-EVs in the context of cancer is the propagation of intercellular signals of fundamental importance to the ORN. Understanding their modes of interaction with recipient cells, their mechanisms of internalization and intracellular processing will be crucial to understanding fully the physiological and pathological attributes of Apo-EVs. To date, virtually nothing is known of these processes, although it may be expected that some clearance/engulfment mechanisms of apoptotic cells and Apo-EVs will prove to share molecular components (**Figure 1**). It is noteworthy in this context that PtdSer exposed on EVs is involved in their uptake by target cells expressing PtdSer receptors such as TIM-4, known for phagocytosis of apoptotic cells (63). A critical question is whether endocytosed or phagocytosed Apo-EV cargo is necessarily degraded by lysosomes, as is generally assumed. Thus, the targeting mechanisms of Apo-EVs along with the destinies of their cargoes require detailed clarification.

Pro-inflammatory extracellular vesicles (EVs) are produced by macrophages responding to ATP *via* P2X7 receptors. It has been reported recently that this results in NLPR3 inflammasome activation in human macrophages, which consequently undergo vesicle-mediated unconventional secretion of IL-1β (64). Conversely, alveolar macrophage-derived EVs have been shown to suppress airway inflammation (65). Thus, the vesicular intercommunication that results from tissue damage is likely to involve a varied mix of vesicle populations, including pro- and anti-inflammatory, derived not only from dying cells but also from their responsive neighbors or recruited phagocytes (**Figure 1**). Since the ORN represents a sector of the tumor microenvironment engaged in dysregulated, cell death-driven tissue repair and regeneration, it seems likely that the intercellular communications so achieved by EVs of the ORN will prove to overlap with those in healing or chronic wounds. Future work aimed at identifying the underlying mechanisms may yield novel molecular targets for both cancer and wound treatments.

AUTHOR CONTRIBUTIONS

Both authors planned and co-wrote the manuscript.

FUNDING

The authors' research is funded by Bloodwise and the Medical Research Council (UK).

REFERENCES

1. Korsmeyer SJ. Bcl-2 initiates a new category of oncogenes: regulators of cell death. *Blood* (1992) 80:879–86.
2. Westhoff MA, Marschall N, Debatin KM. Novel approaches to apoptosis-inducing therapies. *Adv Exp Med Biol* (2016) 930:173–204. doi:10.1007/978-3-319-39406-0_8
3. Delbridge AR, Pang SH, Vandenberg CJ, Grabow S, Aubrey BJ, Tai L, et al. RAG-induced DNA lesions activate proapoptotic BIM to suppress lymphomagenesis in p53-deficient mice. *J Exp Med* (2016) 213(10):2039–48. doi:10.1084/jem.20150477
4. Hanahan D, Weinberg RA. The hallmarks of cancer. *Cell* (2000) 100:57–70. doi:10.1016/S0092-8674(00)81683-9
5. Bergmann A, Steller H. Apoptosis, stem cells, and tissue regeneration. *Sci Signal* (2010) 3:re8. doi:10.1126/scisignal.3145re8
6. Vriz S, Reiter S, Galliot B. Cell death: a program to regenerate. *Curr Top Dev Biol* (2014) 108:121–51. doi:10.1016/B978-0-12-391498-9.00002-4

7. Fuchs Y, Steller H. Live to die another way: modes of programmed cell death and the signals emanating from dying cells. *Nat Rev Mol Cell Biol* (2015) 16:329–44. doi:10.1038/nrm3999
8. Perez-Garijo A, Steller H. Spreading the word: non-autonomous effects of apoptosis during development, regeneration and disease. *Development* (2015) 142:3253–62. doi:10.1242/dev.127878
9. Dabrowska C, Li M, Fan Y. Apoptotic caspases in promoting cancer: implications from their roles in development and tissue homeostasis. *Adv Exp Med Biol* (2016) 930:89–112. doi:10.1007/978-3-319-39406-0_4
10. Leoncini L, Del Vecchio MT, Megha T, Barbini P, Galieni P, Pileri S, et al. Correlations between apoptotic and proliferative indices in malignant non-Hodgkin's lymphomas. *Am J Pathol* (1993) 142:755–63.
11. Tormanen U, Eerola AK, Rainio P, Vahakangas K, Soini Y, Sormunen R, et al. Enhanced apoptosis predicts shortened survival in non-small cell lung carcinoma. *Cancer Res* (1995) 55:5595–602.
12. Stammler G, Sauerbrey A, Zintl F, Volm M. Apoptotic index, Fas and bcl-2 in initial and relapsed childhood acute lymphoblastic leukaemia. *Apoptosis* (1997) 2:377–83. doi:10.1023/A:1026405707823
13. Symmans WF, Cangiarella JF, Symmans PJ, Cohen JM, Yee HT, Bennett G, et al. Apoptotic index from fine needle aspiration cytology as a criterion to predict histologic grade of non-Hodgkin's lymphoma. *Acta Cytol* (2000) 44:194–204. doi:10.1159/000326360
14. Dworakowska D, Jassem E, Jassem J, Karmolinski A, Dworakowski R, Wirth T, et al. Clinical significance of apoptotic index in non-small cell lung cancer: correlation with p53, mdm2, pRb and p21WAF1/CIP1 protein expression. *J Cancer Res Clin Oncol* (2005) 131:617–23. doi:10.1007/s00432-005-0010-7
15. Hilska M, Collan YU, VJ OL, Kossi J, Hirsimaki P, Laato M, et al. The significance of tumor markers for proliferation and apoptosis in predicting survival in colorectal cancer. *Dis Colon Rectum* (2005) 48:2197–208. doi:10.1007/s10350-005-0202-x
16. Sun B, Sun Y, Wang J, Zhao X, Wang X, Hao X. Extent, relationship and prognostic significance of apoptosis and cell proliferation in synovial sarcoma. *Eur J Cancer Prev* (2006) 15:258–65. doi:10.1097/01.cej.0000198896.02185.68
17. Boder J, Abdalla F, Elfagieh M, Buhmeida A, Collan Y. Apoptotic activity in Libyan breast cancer. *World J Surg Oncol* (2012) 10:102. doi:10.1186/1477-7819-10-102
18. Hu Q, Peng J, Liu W, He X, Cui L, Chen X, et al. Elevated cleaved caspase-3 is associated with shortened overall survival in several cancer types. *Int J Clin Exp Pathol* (2014) 7:5057–70.
19. Bairey O, Zimra Y, Shaklai M, Okon E, Rabizadeh E. Bcl-2, Bcl-X, Bax, and Bak expression in short- and long-lived patients with diffuse large B-cell lymphomas. *Clin Cancer Res* (1999) 5:2860–6.
20. Ichim G, Lopez J, Ahmed SU, Muthalagu N, Giampazolias E, Delgado ME, et al. Limited mitochondrial permeabilization causes DNA damage and genomic instability in the absence of cell death. *Mol Cell* (2015) 57:860–72. doi:10.1016/j.molcel.2015.01.018
21. Li F, Huang Q, Chen J, Peng Y, Roop DR, Bedford JS, et al. Apoptotic cells activate the "phoenix rising" pathway to promote wound healing and tissue regeneration. *Sci Signal* (2010) 3:ra13. doi:10.1126/scisignal.2000634
22. Huang Q, Li F, Liu X, Li W, Shi W, Liu FF, et al. Caspase 3-mediated stimulation of tumor cell repopulation during cancer radiotherapy. *Nat Med* (2011) 17:860–6. doi:10.1038/nm.2385
23. Ford CA, Petrova S, Pound JD, Voss JJ, Melville L, Paterson M, et al. Oncogenic properties of apoptotic tumor cells in aggressive B cell lymphoma. *Curr Biol* (2015) 25:577–88. doi:10.1016/j.cub.2014.12.059
24. Lauber K, Herrmann M. Tumor biology: with a little help from my dying friends. *Curr Biol* (2015) 25:R198–201. doi:10.1016/j.cub.2015.01.040
25. Gregory CD, Ford CA, Voss JJ. Microenvironmental effects of cell death in malignant disease. *Adv Exp Med Biol* (2016) 930:51–88. doi:10.1007/978-3-319-39406-0_3
26. Gregory CD, Paterson M. An apoptosis-driven 'onco-regenerative niche': roles of tumour-associated macrophages and extracellular vesicles. *Philos Trans R Soc Lond B Biol Sci* (2018) 373:1–9. doi:10.1098/rstb.2017.0003
27. Lynch C, Panagopoulou M, Gregory CD. Extracellular vesicles arising from apoptotic cells in tumors: roles in cancer pathogenesis and potential clinical applications. *Front Immunol* (2017) 8:1174. doi:10.3389/fimmu.2017.01174
28. Turiak L, Misjak P, Szabo TG, Aradi B, Paloczi K, Ozohanics O, et al. Proteomic characterization of thymocyte-derived microvesicles and apoptotic bodies in BALB/c mice. *J Proteomics* (2011) 74:2025–33. doi:10.1016/j.jprot.2011.05.023
29. Barclay AN, Brown M, Law SKA, McKnight A, Tomlinson M, van der Merwe PA. *The Leucocyte Antigen Factsbook*. London: Academic Press (1997).
30. Coleman ML, Sahai EA, Yeo M, Bosch M, Dewar A, Olson MF. Membrane blebbing during apoptosis results from caspase-mediated activation of ROCK I. *Nat Cell Biol* (2001) 3:339–45. doi:10.1038/35070009
31. Charras GT, Yarrow JC, Horton MA, Mahadevan L, Mitchison TJ. Non-equilibration of hydrostatic pressure in blebbing cells. *Nature* (2005) 435:365–9. doi:10.1038/nature03550
32. Orlando KA, Stone NL, Pittman RN. Rho kinase regulates fragmentation and phagocytosis of apoptotic cells. *Exp Cell Res* (2006) 312:5–15. doi:10.1016/j.yexcr.2005.09.012
33. Sapet C, Simoncini S, Loriod B, Puthier D, Sampol J, Nguyen C, et al. Thrombin-induced endothelial microparticle generation: identification of a novel pathway involving ROCK-II activation by caspase-2. *Blood* (2006) 108:1868–76. doi:10.1182/blood-2006-04-014175
34. Li B, Antonyak MA, Zhang J, Cerione RA. RhoA triggers a specific signaling pathway that generates transforming microvesicles in cancer cells. *Oncogene* (2012) 31:4740–9. doi:10.1038/onc.2011.636
35. Wickman GR, Julian L, Mardilovich K, Schumacher S, Munro J, Rath N, et al. Blebs produced by actin-myosin contraction during apoptosis release damage-associated molecular pattern proteins before secondary necrosis occurs. *Cell Death Differ* (2013) 20:1293–305. doi:10.1038/cdd.2013.69
36. Orlando KA, Pittman RN. Rho kinase regulates phagocytosis, surface expression of GlcNAc, and Golgi fragmentation of apoptotic PC12 cells. *Exp Cell Res* (2006) 312:3298–311. doi:10.1016/j.yexcr.2005.09.012
37. Fraser DA, Pisalyaput K, Tenner AJ. C1q enhances microglial clearance of apoptotic neurons and neuronal blebs, and modulates subsequent inflammatory cytokine production. *J Neurochem* (2010) 112:733–43. doi:10.1111/j.1471-4159.2009.06494.x
38. Poon IK, Chiu YH, Armstrong AJ, Kinchen JM, Juncadella IJ, Bayliss DA, et al. Unexpected link between an antibiotic, pannexin channels and apoptosis. *Nature* (2014) 507:329–34. doi:10.1038/nature13147
39. Atkin-Smith GK, Tixeira R, Paone S, Mathivanan S, Collins C, Liem M, et al. A novel mechanism of generating extracellular vesicles during apoptosis via a beads-on-a-string membrane structure. *Nat Commun* (2015) 6:7439. doi:10.1038/ncomms8439
40. Wickman G, Julian L, Olson MF. How apoptotic cells aid in the removal of their own cold dead bodies. *Cell Death Differ* (2012) 19:735–42. doi:10.1038/cdd.2012.25
41. Skog J, Wurdinger T, van Rijn S, Meijer DH, Gainche L, Sena-Esteves M, et al. Glioblastoma microvesicles transport RNA and proteins that promote tumour growth and provide diagnostic biomarkers. *Nat Cell Biol* (2008) 10:1470–6. doi:10.1038/ncb1800
42. Lin LY, Du LM, Cao K, Huang Y, Yu PF, Zhang LY, et al. Tumour cell-derived exosomes endow mesenchymal stromal cells with tumour-promotion capabilities. *Oncogene* (2016) 35(46):6038–42. doi:10.1038/onc.2016.131
43. Headley MB, Bins A, Nip A, Roberts EW, Looney MR, Gerard A, et al. Visualization of immediate immune responses to pioneer metastatic cells in the lung. *Nature* (2016) 531:513–7. doi:10.1038/nature16985
44. Qu L, Ding J, Chen C, Wu ZJ, Liu B, Gao Y, et al. Exosome-transmitted lncARSR promotes sunitinib resistance in renal cancer by acting as a competing endogenous RNA. *Cancer Cell* (2016) 29:653–68. doi:10.1016/j.ccell.2016.03.004
45. Zhao H, Yang L, Baddour J, Achreja A, Bernard V, Moss T, et al. Tumor microenvironment derived exosomes pleiotropically modulate cancer cell metabolism. *Elife* (2016) 5:e10250. doi:10.7554/eLife.10250
46. Mullen AR, Wheaton WW, Jin ES, Chen PH, Sullivan LB, Cheng T, et al. Reductive carboxylation supports growth in tumour cells with defective mitochondria. *Nature* (2011) 481:385–8. doi:10.1038/nature10642
47. Akers JC, Gonda D, Kim R, Carter BS, Chen CC. Biogenesis of extracellular vesicles (EV): exosomes, microvesicles, retrovirus-like vesicles, and apoptotic bodies. *J Neurooncol* (2013) 113:1–11. doi:10.1007/s11060-013-1084-8
48. Dieude M, Bell C, Turgeon J, Beillevaire D, Pomerleau L, Yang B, et al. The 20S proteasome core, active within apoptotic exosome-like vesicles, induces autoantibody production and accelerates rejection. *Sci Transl Med* (2015) 7:318ra200. doi:10.1126/scitranslmed.aac9816

49. Balaj L, Lessard R, Dai L, Cho YJ, Pomeroy SL, Breakefield XO, et al. Tumour microvesicles contain retrotransposon elements and amplified oncogene sequences. *Nat Commun* (2011) 2:180. doi:10.1038/ncomms1180
50. Halicka HD, Bedner E, Darzynkiewicz Z. Segregation of RNA and separate packaging of DNA and RNA in apoptotic bodies during apoptosis. *Exp Cell Res* (2000) 260:248–56. doi:10.1006/excr.2000.5027
51. Biggiogera M, Bottone MG, Pellicciari C. Nuclear RNA is extruded from apoptotic cells. *J Histochem Cytochem* (1998) 46:999–1005. doi:10.1177/002215549804600903
52. Biggiogera M, Bottone MG, Martin TE, Uchiumi T, Pellicciari C. Still immunodetectable nuclear RNPs are extruded from the cytoplasm of spontaneously apoptotic thymocytes. *Exp Cell Res* (1997) 234:512–20. doi:10.1006/excr.1997.3657
53. Biggiogera M, Bottone MG, Pellicciari C. Nuclear ribonucleoprotein-containing structures undergo severe rearrangement during spontaneous thymocyte apoptosis. A morphological study by electron microscopy. *Histochem Cell Biol* (1997) 107:331–6. doi:10.1007/s004180050118
54. Scovassi AI, Bottone MG, Biggiogera M, Pellicciari C. Dynamic relocation of nuclear proteins during the execution phase of apoptosis. *Biochem Pharmacol* (2008) 76:1440–50. doi:10.1016/j.bcp.2008.06.005
55. Casciola-Rosen LA, Anhalt G, Rosen A. Autoantigens targeted in systemic lupus erythematosus are clustered in two populations of surface structures on apoptotic keratinocytes. *J Exp Med* (1994) 179:1317–30. doi:10.1084/jem.179.4.1317
56. Hristov M, Erl W, Linder S, Weber PC. Apoptotic bodies from endothelial cells enhance the number and initiate the differentiation of human endothelial progenitor cells in vitro. *Blood* (2004) 104:2761–6. doi:10.1182/blood-2003-10-3614
57. Sirois I, Raymond MA, Brassard N, Cailhier JF, Fedjaev M, Hamelin K, et al. Caspase-3-dependent export of TCTP: a novel pathway for antiapoptotic intercellular communication. *Cell Death Differ* (2011) 18:549–62. doi:10.1038/cdd.2010.126
58. Hayakawa K, Esposito E, Wang X, Terasaki Y, Liu Y, Xing C, et al. Transfer of mitochondria from astrocytes to neurons after stroke. *Nature* (2016) 535:551–5. doi:10.1038/nature18928
59. Holmgren L, Szeles A, Rajnavolgyi E, Folkman J, Klein G, Ernberg I, et al. Horizontal transfer of DNA by the uptake of apoptotic bodies. *Blood* (1999) 93:3956–63.
60. Bergsmedh A, Szeles A, Henriksson M, Bratt A, Folkman MJ, Spetz AL, et al. Horizontal transfer of oncogenes by uptake of apoptotic bodies. *Proc Natl Acad Sci U S A* (2001) 98:6407–11. doi:10.1073/pnas.101129998
61. Bergsmedh A, Ehnfors J, Kawane K, Motoyama N, Nagata S, Holmgren L. DNase II and the Chk2 DNA damage pathway form a genetic barrier blocking replication of horizontally transferred DNA. *Mol Cancer Res* (2006) 4:187–95. doi:10.1158/1541-7786.MCR-05-0262
62. Savill J. The innate immune system: recognition of apoptotic cells. In: Gregory CD, editor. *Apoptosis and the Immune Response*. New York: Wiley-Liss (1995). p. 341–69.
63. French KC, Antonyak MA, Cerione RA. Extracellular vesicle docking at the cellular port: extracellular vesicle binding and uptake. *Semin Cell Dev Biol* (2017) 67:48–55. doi:10.1016/j.semcdb.2017.01.002
64. Valimaki E, Cypryk W, Virkanen J, Nurmi K, Turunen PM, Eklund KK, et al. Calpain activity is essential for atp-driven unconventional vesicle-mediated protein secretion and inflammasome activation in human macrophages. *J Immunol* (2016) 197(8):3315–25. doi:10.4049/jimmunol.1501840
65. Han CZ, Juncadella IJ, Kinchen JM, Buckley MW, Klibanov AL, Dryden K, et al. Macrophages redirect phagocytosis by non-professional phagocytes and influence inflammation. *Nature* (2016) 539:570–4. doi:10.1038/nature20141

Conflict of Interest Statement: The authors declare that the research was conducted in the absence of any commercial or financial relationships that could be construed as a potential conflict of interest.

frontiers in Immunology

REVIEW
published: 07 May 2018
doi: 10.3389/fimmu.2018.00957

Tumor-Derived Apoptotic Vesicles: With Death They Do Part

*Morad-Remy Muhsin-Sharafaldine and Alexander D. McLellan**

Department of Microbiology and Immunology, University of Otago, Dunedin, New Zealand

Tumor cells release lipid particles known as extracellular vesicles (EV) that contribute to cancer metastasis, to the immune response, and to thrombosis. When tumors are exposed to radiation or chemotherapy, apoptotic vesicles (ApoVs) are released in abundance as the plasma membrane delaminates from the cytoskeleton. Recent studies have suggested that ApoVs are distinct from the EVs released from living cells, such as exosomes or microvesicles. Depending on their treatment conditions, tumor-released ApoV have been suggested to either enhance or suppress anti-cancer immunity. In addition, tumor-derived ApoV possess procoagulant activity that could increase the thrombotic state in cancer patients undergoing chemotherapy or radiotherapy. Since ApoVs are one of the least appreciated type of EVs, we focus in this review on the distinctive characterization of tumor ApoVs and their proposed mechanistic effects on cancer immunity, coagulation, and metastasis.

Keywords: extracellular vesicles, apoptotic vesicles, membrane blebs, chemotherapy, thrombosis

OPEN ACCESS

Edited by:
Ivan Poon,
La Trobe University,
Australia

Reviewed by:
Rong Xu,
La Trobe University,
Australia
Muriel Moser,
Free University of Brussels,
Belgium

***Correspondence:**
Alexander D. McLellan
alex.mclellan@otago.ac.nz

Specialty section:
This article was submitted to Immunological Tolerance and Regulation, a section of the journal Frontiers in Immunology

Received: *30 January 2018*
Accepted: *17 April 2018*
Published: *07 May 2018*

Citation:
Muhsin-Sharafaldine M-R and McLellan AD (2018) Tumor-Derived Apoptotic Vesicles: With Death They Do Part. Front. Immunol. 9:957. doi: 10.3389/fimmu.2018.00957

INTRODUCTION

The term extracellular vesicle (EV) describes membrane particles released from eukaryote cells, as well as prokaryote microorganisms (1). It is now evident that EV plays important roles in multiple biological systems involved in the control of homeostasis of the organism. For example, intercellular signaling is mediated by EV in processes, such as bone calcification, immune tolerance and activation, neuron-glia communication, wound repair, and hemostasis (2–7). Furthermore, EVs have been implicated in pathological conditions, such as viral and prion transfer, cardiovascular disease, thrombosis, autoimmune diseases (e.g., rheumatoid arthritis and multiple sclerosis), sickle cell anemia, and cancer (8–14).

Extracellular vesicle can be isolated *via* differential and/or density gradient centrifugation based on their relative size and density. Depending on their parental cell type and their cellular site of origin, EVs differ in terms of size, composition, density, and other biochemical and structural properties (15, 16). Exosomes, one of the smallest EV, are released from a large spectrum of living cells and range from 40–100 nm in diameter [isolated at sedimentation speeds of $\geq$100,000 $\times$ *g*; Ref. (17)]. While the differentiation or activation state of primary cells is critical for exosome release (18), Wolfers et al. have shown that murine and human tumor cell lines constitutively release exosomes (19). After their discovery by electron microscopy in 1981 (20), numerous studies have shown that exosomes may function as intercellular messengers in a diverse range of roles controlling cellular physiology and pathology (5, 19, 21–24).

Living cells also secrete larger, membrane-derived EV known as microvesicles (MV). These were first described by Chargaff and West in 1946 and were later characterized as a predominant procoagulant product of degranulating platelets (25, 26). MVs range in size (0.1–2 μm in diameter) and have been shown to be constitutively released by tumor cells potentially carrying oncogenes (27).

In addition, "migratory benign cells-derived EV" structures, termed migrasomes (≤3 μm), that harbor internal EV, have also recently been described (28). Tumor-derived EV (100–500 nm) that transport epidermal growth factor receptor variant III, overexpressed in the parental human U373 astrocytoma tumor cell line have been referred to as "oncosomes" (29). Other studies that have used this term and verified the tumor origin of "oncosomes" due to other oncogenic cargo (30–33). However, it is still not clear from the original (29), or clarified definitions (34), if oncosomes contain "oncogenes" (i.e., transforming nucleic acids), "oncogenic receptors" (oncogene products; i.e., epidermal growth factor receptor variant III polypeptide), or whether this terminology merely reflect their functional transforming ability (transfer of oncogenic activity). Since the term oncosomes originates from a single cell line studied (29), the size range, cargo, or morphological features cannot yet be extrapolated to other tumor cells. Moreover, oncosomes have yet to be included in the ISEV guidelines (35, 36).

During apoptosis, cellular contents are packaged into apoptotic blebs (0.03–5 μm) for clearance with minimal perturbation/inflammation to the surrounding tissues (15, 37). The term "apoptotic bodies" usually refers to the larger (1–5 μm) bleb fraction (38, 39) that may contain a proportion of nuclear content and are released when the plasma membrane delaminates from the cytoskeleton (37). Due to their variable size range, apoptotic blebs are isolated at different sedimentation speeds [1,000–110,000 × *g*; Ref. (15, 40–43)]. An obvious problem with definition occurs when studies isolate smaller apoptotic blebs at high speeds (≥100,000 × *g*); resulting in likely contamination with exosomes due to the similar sedimentation forces used in the isolation of these two EV sub-types. However, contaminating exosomes will have distinguishable markers (discussed later) that could be utilized to enhance apoptotic vesicles (ApoVs) purity. In addition, there is no consensus regarding the nomenclature for the smaller fraction of apoptotic blebs (0.03–1 μm). For example, the terms apoptotic microparticles, small ApoVs, and even apoptotic bodies have been used to define the smaller apoptotic blebs (15, 40, 44, 45). For this reason, the term ApoVs will be used in this review to describe lipid encapsulated EV released from dying (apoptotic) cells.

Extracellular vesicles are becoming increasingly studied due to their release by cancer cells and their reported influence on the immune system, metastasis, angiogenesis, and coagulation (46–49). Although tumor-derived ApoVs are released in relative abundance following chemotherapeutic treatment, as compared to exosomes and MV (12, 47), limited research has been directed toward ApoV. Here, we will focus on the ApoV and their functional implications in cancer, the immune system, and coagulation.

CELL DEATH: A GENERAL OVERVIEW

At present, at least six cellular processes leading to cellular death have been described: mitotic catastrophe, senescence, necrosis, necroptosis, autophagy, and apoptosis (50, 51). However, it is unclear whether the six cellular death mechanisms are strictly independent, or if they all eventually overlap to some degree.

During eukaryotic cell division (mitosis), DNA-damaging agents cause cells to lose or gain a single chromosome (an aneuploid state) that, if left unchecked, could lead to severe genomic instability (52, 53). This may result in irreversible damage and death of the aberrant dividing cell in a manner known as mitotic catastrophe (51, 53). Prior to the discovery of mitotic catastrophe, Hayflick et al. showed that normal cells eventually cease to divide *in vitro* despite the availability of favorable conditions for cell growth (54). This inflammatory death mechanism, defined as senescence, is now known to be triggered by several signals such as DNA damage or shortened/dysfunctional telomeres (38, 50, 51, 55, 56). Necrosis is the uncontrolled breakdown of the cell membrane and consequent release of intracellular contents and proinflammatory molecules into the extracellular matrix (57, 58). Several pathological conditions, such as infection, ischemia, or inflammation can cause necrosis and that is generally characterized by cellular swelling and organelle degradation (57, 59). Necrosis can be triggered in a controlled manner, a process known as necroptosis, and driven by receptor-interacting protein kinase 1, 3, and pseudokinase mixed lineage kinase domain-like (60, 61). Autophagy is triggered when redundant or unwanted proteins are excessively targeted for degradation by the cell's proteolytic mechanisms (50). One of the main mediators of autophagy is ubiquitin, often leading to degradation within proteasomes (50, 62, 63). Apart from apoptosis, autophagy and necrosis are the only other types of cell death that are characterized by membrane blebbing (50, 58, 64).

Apoptosis is a highly controlled process and is activated *via* two main pathways: the extrinsic (or receptor) pathway is characterized by the binding of a ligand to a death receptor of a cell (65). Activation of these death receptors by their ligands may lead to the assembly of the Fas-associated death domain and caspase-8 (66). Apoptosis is orchestrated *via* the activation of a (usually inactive) cytoplasmic family of proteins known as caspases (67–69). The activation of one may lead to the activation of another and thus initiate apoptosis in a cascade fashion. Hence, within the extrinsic pathway, recruited, activated caspase-8 cleaves caspase-3 which will cleave other caspases, eventually leading to apoptosis (69, 70). The other pathway, known as the intrinsic pathway, also converges at caspase-3 (67). However, the intrinsic (or mitochondrial) pathway is usually triggered *via* stress signals that may lead the mitochondrion to the leakage of proapoptotic factors, including cytochrome c, into the cytoplasm (67, 69, 70). This results in the formation/activation of several protein complexes including caspase-9 which then cleaves caspase-3 leading to downstream disassembly of cellular components (70). One of the main features of apoptosis is the formation and release of membrane blebs or ApoV (71). One advantage of the apoptotic process is that proteins and nucleic acids, that would otherwise trigger an immune response, are packaged within these apoptotic blebs for rapid clearance by the immune system (72, 73). On the other hand, materials that act as autoantigens may also be packaged into apoptotic blebs (45).

GENERAL MECHANISMS OF EV FORMATION

The mechanism of EV release is tightly regulated and differs between exosomes, MV, and ApoV (**Figure 1**). The exosomal machinery begins with the cell membrane invaginating inwards toward the intracellular matrix by endocytosis, forming an endosome (74). This early endosome is formed by the aid of proteins such as Ras-related in the brain GTPases and soluble *N*-ethylmaleimide-sensitive factor attachment protein receptor proteins (75). In later stages, further invagination of the endosome leads to the formation of intraluminal vesicles (ILV) and this late endosome is now referred to as a multivesicular body (MVB) (38, 76). Although their specific role remains unclear, tetraspanins, the endosomal sorting complexes required for transport (ESCRT) complexes, and ALG-2-interacting protein X, are involved in ILV formation (15). The excision of ILV into MVB requires ESCRT-III proteins, such as vacuolar protein sorting-associated protein 20, 24, and Snf7 (77). MVB can then either be targeted for degradation/recycling or may fuse with the cell membrane releasing ILV known as exosomes (15, 38, 74). Alternatively, lipid-metabolizing enzymes, such as neutral sphingomyelinase and phospholipase D2, can drive the formation of MVB and ILV in an ESCRT-independent manner (78, 79). However, it remains unknown how ESCRT and lipid-metabolizing enzymes cooperate to induce exosome formation (78).

Cells also release EV through the direct outward membrane budding and depending on the state of the cell, the EV is termed MV or ApoV. Initially, the shedding mechanism of MV or ApoV is thought to begin with the influx of calcium into activated or dying cells, respectively, resulting in the activation of calcium-dependent proteases, such as calpain and gelsolin (38, 80, 84, 85). This leads to the disruption of the membrane cytoskeleton, exposure of phosphatidylserine (PS), and initial formation of membrane protrusions (81, 85). ADP-ribosylation factor-6 initiates a signaling cascade eventually activating the Rho-associated

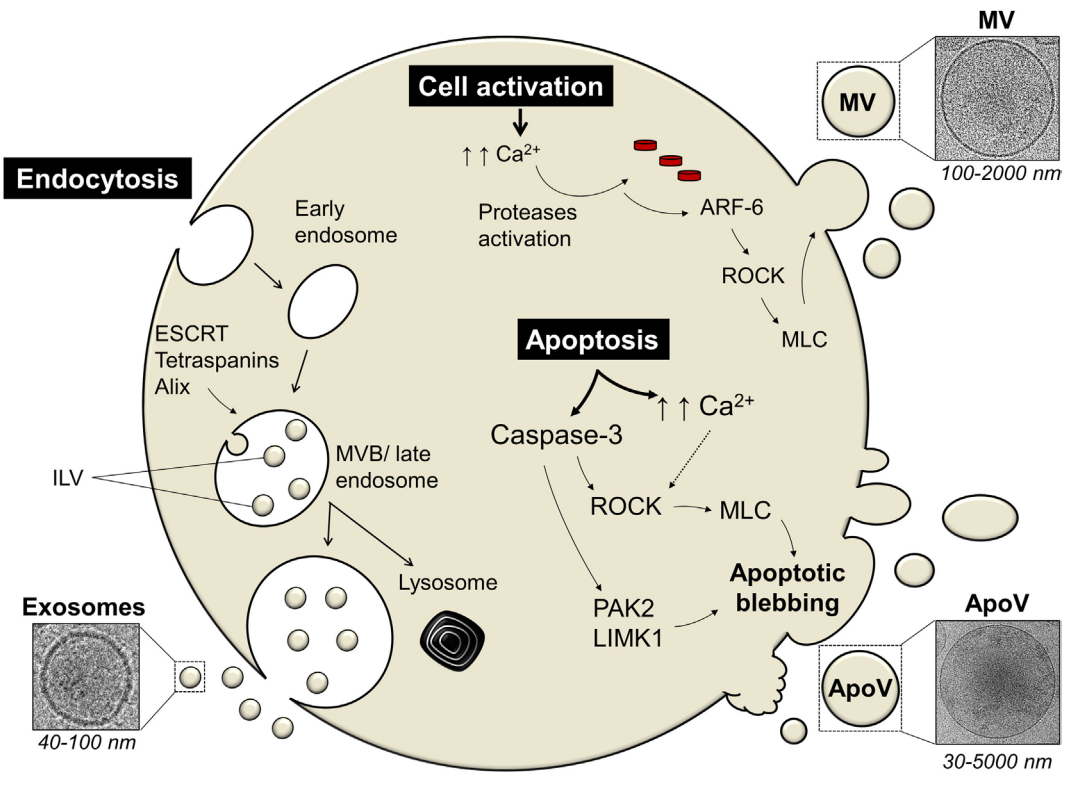

FIGURE 1 | The mechanism of extracellular vesicles (EVs) release differs among different types of EV. Exosomes are secreted *via* the endosomal pathway, starting with the inward invagination of the cell membrane forming an early endosome. In later stages, further invagination of the endosome leads to the formation of intraluminal vesicles (ILV) and this late endosome is now referred to as a multivesicular body [MVB; Ref. (38, 76)]. The MVB can either be targeted for cellular destruction/recycling by lysosomes or it may fuse with the cell membrane thus releasing ILV as exosomes. Proteins involved in exosomal machinery include the endosomal sorting complexes required for transport (ESCRT), tetraspanins (such as CD9), ALG-2-interacting protein X (Alix), and tumor susceptibility gene 101 [TSG101; Ref. (74)]. Microvesicles (MV) and apoptotic vesicles (ApoV) are secreted *via* the direct outward budding of the cell membrane. Cellular activation or apoptosis results in an increased influx of calcium ions (Ca^{2+}) which triggers proteases, such as calpain or gelsolin (80). These activated proteases lead to cytoskeletal disruption. ADP-ribosylation factor-6 (ARF-6) initiates a signaling cascade eventually activating the Rho-associated protein kinase (ROCK) signaling pathway which in turn activates myosin light-chain (MLC) kinases that activates and phosphorylates MLC that would initiate blebbing eventually leading to ApoV/MV release (81, 82). Apoptosis initiation also activates apoptotic enzymes known as caspases. Caspase-3 can cleave ROCK transforming it into a constitutive truncated form which then enhances the phosphorylation and activation of MLC that leads to ApoV shedding (83). Caspase-3-mediated blebbing can also act on other blebbing-mediated proteins, such as LIM domain kinase 1 (LIMK1) or p21-activated kinase (PAK2); reviewed in Ref. (71).

protein kinase (ROCK) signaling pathway which in turn activates myosin light-chain (MLC) kinases that activates and phosphorylates MLC (38, 82, 86). The cell membrane then begins to bleb due to increased hydrostatic pressure following MLC-driven actomyosin contractions (87). Eventually ApoV or MV is released (81, 82). The mechanism of MV/ApoV scission remains unclear. However, it has been shown that vacuolar protein sorting four participates in the scission of T cell-derived MV (88). No incision proteins have yet been identified in ApoV release. One could speculate that the budding off of ApoV may resemble the mechanism of ILV excision. It has been hypothesized; however, that ApoV may simply break-off due to shear force under flow conditions and/or interaction of a recipient phagocyte "pinching" off ApoV (71).

Despite the mechanistic similarities between ApoV and MV, the apoptotic cell passes through a three-step apoptotic disassembly process to finally release ApoV [reviewed in Ref. (71)]. One major pathway of apoptosis is orchestrated *via* the activation of cytoplasmic caspases (67–69). Sequential activation of caspases leads to dismantling and repackaging of cellular and nuclear content caspase-3 (69, 70). The blebbing of the apoptotic cell marks the first step of apoptotic disassembly and is linked to caspase-3 (83, 89, 90). There is evidence that caspase-3 can cleave ROCK-1 transforming it into a constitutive truncated form which then enhances the phosphorylation and activation of MLC (89–91). Caspase-3 can also act on other blebbing-mediated proteins, such as LIM domain kinase 1 or p21-activated kinase (92, 93). The blebbing cell then moves to stage two whereby membrane protrusions form *via* microtubule spikes and/or long string-like constructs known as apoptopodia (94, 95). Finally, the apoptotic cell fragments, and the formed ApoV, detached from the membrane protrusions and are released.

MOLECULAR PROFILE OF EV

The composition of EV largely depends on the type and differentiation state of the parental cell. Currently, differential ultracentrifugation is the most common technique to isolate EV. Exosomes are isolated using $\geq$100,000 $\times$ *g* along with pore filtration to remove larger EV fractions (21, 23). However, it has proved difficult to isolate the larger MV or ApoV, and to obtain a pure EV preparation as ApoV or MV purified from identical centrifugation speeds may cross-contaminate due to spontaneous cell death or MV release (47). Despite these limitations, various proteins, DNA, RNA, and lipid profiles have been identified to assist in the phenotyping of MV and ApoV (23, 47, 96–98). Current methodology for protein detection in EV includes western blotting, flow cytometry, and mass spectrometry (24, 47). It is now clear that many of the proteins enriched in EV are involved in EV formation or trafficking (3). Despite the different types of EV, there are well-documented markers that are commonly shared among EV fractions (24). Cluster of differentiation 147 (CD147), for example, is consistently observed to be enriched in tumor-derived EV (47, 99, 100). Acting as an Extracellular Matrix Metalloproteinase Inducer as a main role, CD147 is thus also referred to as "EMMPRIN." Once matrix metalloproteinases (such as MMP1, MMP2, and MMP11) are induced by CD147, the enzymes help to break the extracellular matrix thus aiding in the proliferation of tumor cells (101–103). With a family of at least 30 proteins, tetraspanins levels are also elevated in EV (104–106). However, recent studies have shown the expression level of the tetraspanin CD9 is lower in ApoV compared to exosomes or MV (47, 96, 99, 107). Tetraspanins are glycoproteins suspected to be involved in cell motility, adhesion, and proliferation, and are known to complex with integrins (108, 109). It is, therefore, not surprising that adhesion molecules, such as integrins are also detected in EV (23, 47, 96, 99). Despite all the efforts, there has not been a stand-alone protein marker for ApoV that can distinguish them from other EV types (47, 96).

Interestingly, the DNA-associated proteins, histones, were assumed to be exclusive ApoV markers (46). Despite this, a proteomic study of dendritic cells (DC)-derived exosomes by Théry et al. detected histones in exosomes (15). They hypothesized that their presence may be due to the spontaneous DC apoptosis, contaminating the DC-derived exosome preparations with disintegrating nuclear material. However, it is now appreciated that histones localize within the cytoplasm, as well as the nucleus (110), and histones within exosomes and ApoV have been widely documented (45, 47, 111). Since EV contain nucleic acids, including RNA, it is likely that histones in EV act as chaperones for nucleic acids (46, 112). It has been proposed that the presence of RNA in exosomes may be due to the fact that MVB contain RNA-induced silencing complexes (113–115) where there is a direct interaction between histones and RNA (113). A study by Müller et al. suggests that the histone H3 modification is necessary for exosome release (116). Furthermore, glioma-derived EVs have been known to carry mRNA, micro RNA, and proteins that contribute to tumor growth (112, 117). The uptake of glioma-derived MV, containing oncogenic epidermal growth factor receptor, by endothelial cells have been known to greatly alter the nature of the endothelial cells in a manner that elevates tumor angiogenesis (117). However, a recent study revealed that there is a clear difference in the RNA profile between ApoV, MV, and exosomes, highlighting that ribosomal RNA and smaller RNA is highest in ApoV (118). Previous studies have identified that the RNA content in EV is reflective of the RNA content of the cell of origin (115, 119). Since DNA fragmentation is a feature of apoptosis, it was no surprise that DNA fragments have been detected in ApoV (120, 121). These DNA fragments can be transferred to recipient cells and reused when ApoVs are engulfed by phagocytes (121).

The exposure of PS on the outer leaflet of EV membranes is a common feature among EV (7, 21, 122). PS is a membrane aminophospholipid that is actively kept within the intracellular level (inner leaflet) of a living cell by the (predicted) ATP-dependent membrane lipid transporters known as flippases (123–125). Simultaneously, the other group of (predicted) lipid transporters, floppases, transports choline- and amino-phospholipids toward the outer membrane leaflet (126). The rate of floppase activity is usually 10 times slower compared to flippase (127). However, during apoptosis or cell activation, flippase is believed to be inhibited and different lipid transporters, scramblases, are activated (128–130). Unlike the other two lipid transporters, scramblases are calcium-dependent and ATP-independent (123, 131). The activity of scramblase transporters moves all major classes of phospholipids back and forth, thereby destroying the

phospholipid asymmetry orchestrated by flippases and floppases (128). The presence of PS at the extracellular leaflet by scramblases is a key marker of apoptosis and is particularly enriched in ApoV (47, 96, 123).

Since EV originate from the cell membrane, they are expected to carry various cellular surface glycoproteins and glycolipids [commonly known as glycans; Ref. (132)]. Most studies have focused on exosomes for glycan profile, and demonstrate a complex and varying glycan content depending on the cell of origin (133–137). The use of plant-derived carbohydrate-binding proteins (lectins) and mass spectrometry has been an integral part of glycan profiling (136–139). Glycomic analysis remains challenging; however, due to the lack of specific glycan ligands and the fact that a large number of low molecular weight carbohydrate molecules are the building blocks of various molecular structures (140). Thus, the glycomic profiles of EV remain refractory to analysis and, therefore, a major hurdle to laboratories studying the molecular composition of EV. Nevertheless, studies have shown that the glycans detected in EV participate in protein trafficking, attachment, and EV uptake by recipient cells (134, 136, 141–144). The glycome of mammalian cells-derived EV shows consistency in terms of lectin interactions suggesting the presence of *N*-acetylglucosamine as an integral component of most EV glycans (140).

The surface of EV is negatively charged partially due to the heavy sialylation of surface glycans (47, 49, 138, 145–147). Increase in sialylation is also a common feature of tumor cells along with other proteins such as the superfamily tetraspanins (148, 149). It remains to be determined if this anionic-rich surface due to sialylation dictates the function of EV. Nevertheless, EVs have a sialic acid-rich surface and EV bind to the sialic-acid binding lectin CD169 (47, 49, 138). Interestingly, CD169 has a low (mM) affinity to sialic acids and thus only heavily sialylated structures (such as tumor-derived EV) are able to bind avidly to $CD169^+$ macrophages (150). Moreover, CD169 binds to α2,6 and α2,3 sialic acids of EV but prefers the latter [discussed later in Ref. (47, 49)].

ApoV AND THE IMMUNE SYSTEM

Tumor antigens can be captured by antigen-presenting cells (APC) *via* direct cell-to-cell contact with living or apoptotic cells (151), heat-shock-associated and soluble proteins, or tumor-EV (19, 152–155). Tumor antigens captured by APC activate CD4 helper and cytotoxic lymphocyte-driven immune responses for tumor regression (156–159). Previous reports indicate that EVs display major histocompatibility complex 1 (MHC-I) and MHC-II on their surface and theoretically should be capable of antigen-presenting function (4, 81, 160). However, cross-presentation of apoptotic cell and EV-associated antigens are more often observed *in vivo*, rather than direct antigen presentation by the vesicles themselves (19, 161–163). Dendritic cells (DCs) appear to be the major APC subset able to efficiently present antigens derived from apoptotic cells to stimulate both MHC-II and MHC-I-restricted CD4 and CD8 T cell responses (162). Exploiting the ability of DC-derived exosomes to eradicate established tumors due to the expression of MHC-I and -II on the surface of the exosomes (164) can be useful for exosome-based vaccine therapy. Heat-shock proteins have been detected in exosomes (23, 99), and have been reported by Srivastava's group to participate in immunogenic action *via* their interaction with APC (165).

Paradoxically, studies regarding apoptotic cell-associated antigens have either identified them as immunosuppressive (166–168) or immunostimulatory (169–171), depending on the experimental setting. Recent studies suggest that tumor-derived ApoV can downregulate the immunostimulatory effect of antigen-specific DC *in vivo* (47, 167). There is evidence that the immunosuppressive effect of apoptotic cells and ApoV is caused by the transforming growth factor β1 [TGF-β1; Ref. (167, 172, 173)]. PS participates in the immunosuppression by ApoV through the induction of TGF-β from tissue-resident macrophages (174). Interestingly, the same study showed that TGF-β was not released when apoptotic cells failed to express PS (174). A recent study also highlights that the culture content of chemotherapy-treated tumor cells (floating dead cells, supernatant, and potentially ApoV) promotes primary tumor growth (175). The study also showed that this tumorigenic effect was caused by macrophages releasing proinflammatory cytokines known to promote tumor growth, and was PS-dependent (175).

In contrast, exposure of DC to murine myeloid cell-derived ApoV resulted in DC maturation and the secretion of proinflammatory cytokines (176). Leukemic-derived ApoV can elicit DC-driven CD8 T cell activation (177) and the immunization of antigen-pulsed tumor-derived ApoV alone elicits a significant CD8-mediated and anti-cancer immune response in mice (47). In addition, compared to MV or exosomes, tumor-derived ApoV afforded the highest anti-tumor protection against a specific antigen, *via* unknown mechanisms (99). Intriguingly, ApoV elicited the highest protection despite containing the lowest level of tumor antigen (ovalbumin), as compared to MV and exosomes (99). Despite its documented role in immunosuppression (174, 175), PS may also act as an immune stimulant and, therefore, it is possible that PS enrichment on the surface of ApoV could be responsible for their superior immunogenic activity. Hoffman et al. identified that apoptotic cell clearance is enhanced by PS-receptor mediated micropinocytosis [a regulated form of endocytosis for solute molecules and antigens; Ref. (178, 179)]. The pathway is highly active among APC such as macrophages and DC (179). Moreover, it was shown that blocking PS on MV (by annexin V) disables their uptake by target cells (29).

For apoptotic cells and their ApoV to be efficiently cleared by phagocytes, their exposed PS functions as an "eat-me" signal to phagocytes (71, 178). First, PS binds to annexin V which in turn is recognized by phagocytes (123, 180). However, PS is also a known ligand for other receptors, such as β2-glycoprotein I (181), Mer receptor tyrosine kinase (182), lectin-like oxidized low density lipoprotein-receptor 1 (183), and PS-receptor (184), all of which are known to promote apoptotic cell clearance (182, 184–186). For example, PS-receptor-deficient mice died due to accumulation of uncleared apoptotic cells in lung alveoli (184). A sufficient threshold of PS exposure is necessary for phagocytic clearance. Borisenko et al. have measured phagocytosis of live, apoptotic, and live with the inclusion of exogenous PS (187). Their study concluded that phagocytosis is directly proportional to PS levels. Thus, PS exposure is a critical factor for the clearance of apoptotic materials. Although PS and its receptors are critical for phagocytic

recognition, the Albert group have demonstrated that integrin subunits $\alpha_V\beta3$ and $\alpha_V\beta5$ on macrophages and DCs, respectively, participate in phagocytic clearance of apoptotic cells, but these studies did not investigate a possible involvement of PS in the phagocytic process (162, 188). Furthermore, oxidation levels on apoptotic cells and ApoV create a binding site for thrombospondin and the complement protein C3b, which are in turn recognized by phagocytes (38, 189, 190). CD44-deficiency has been shown to impair apoptotic cell clearance in the lungs (191). This coincides with our study that showed that ApoV express higher CD44 than MV and exosomes (99). The fact that apoptotic cells and their ApoVs are efficiently recognized by the immune system opens a potential use of ApoV for vaccination against cancer. Indeed, PS exposure is seen in all EV (38, 46, 99, 192), and PS participates in the uptake of exogenous antigens (29, 193). However, the slight increase of PS levels on ApoV (96, 99), above that observed for MV and exosomes could still be the threshold necessary to induce a superior immune response. There have been several clinical trials for cancer treatments using exosome-borne tumor antigens, but with poor outcome (194–197). Nevertheless, since immune cells efficiently recognize antigens on ApoV (47, 170, 177, 198), ApoVs remain of interest for cancer immunotherapy.

ApoV can act as immunostimulatory or immunosuppressive. This greatly highlights our lack of understanding of the complexity of ApoV interactions with the immune system. Adding to the complexity of our understanding, *in vitro*-generated ApoV is not immediately engulfed, as would be expected to happen *in vivo*. Therefore, the results of *in vitro* studies may not always reflect the true *in vivo* situation. Unfortunately, there are limited studies regarding tumor-derived ApoV and their implications for cancer and the immune system. Because tumor-derived ApoVs are strongly thrombotic (see below), this makes it difficult to conduct immune activation studies utilizing systemic application of ApoV regarding of tumor-derived ApoV (48, 99).

COULD CD169 BE THE GATE FOR EV-DRIVEN LYMPH NODE METASTASIS?

One of the most important events of tumor metastasis is the migration of tumor cells from the primary site to the draining lymph node [LN; Ref. (199)]. Invading tumor cells eventually spread to other LNs in a sequential fashion starting and ending from the closest (draining) to most distal LN, respectively (200). In fact, there is convincing evidence that draining LNs are the best prognostic estimators for the status of the entire lymphatic nodal system (201). Within the subcapsular sinus (SCS) of LN, macrophages are the first to be exposed to antigens and have a role in presenting the captured antigens to APC, including B cells (202). Hood et al. have demonstrated that B16F10-derived exosomes accumulate in and prepare the draining lymph node for tumor invasion (203). This mechanism is often termed "seed and soil" in metastasis, where tumor-derived EVs are regarded as "seeds" preparing a particular site (the soil) for tumor cell invasion (204, 205). The studies suggest that tumor-derived EVs facilitate invasion by enhancing angiogenesis and immunosuppression *in situ* (22, 203, 206). Interestingly, a macrophage-restricted receptor known as sialoadhesin (CD169; Siglec-1) is abundantly expressed on the surface of macrophages within the SCS of LN, marginal zones of the spleen, and liver [Kupffer cells; Ref. (49)]. CD169 is a member of the sialic-acid binding Ig-like lectin family of proteins; this enriched level of CD169 expression allows these $CD169^+$ macrophages to bind to glycoproteins bearing terminal sialic acids (207). Depending on the experimental setting, $CD169^+$ macrophages mediate a tolerogenic or immunogenic response to self-antigens, infection, and tumor models (208–212).

Several studies that deplete the entire $CD169^+$ macrophage population (using diphtheria toxin or clodronate liposomes) indicate that the function of $CD169^+$ macrophages is immunogenic (213–216). In cancer, the Tanaka group's $CD169^+$ macrophage depletion model showed that the cells have a critical role in the anti-cancer effect (212). Interestingly, they show that upon immunization with dead tumor cells, $CD169^+$ macrophages cross-present tumor antigens to $CD8^+$ T cells thereby mediating a cytotoxic-mediated anti-cancer immune response. Consistent with these findings, Pucci et al. showed that tumor spread is significantly reduced when tumor-derived EV are captured by CD169 (209). The results showed that CD169 poses a physical barrier to block tumor-derived EV interactions with LN B cells preventing pro-metastatic humoral immunity (209).

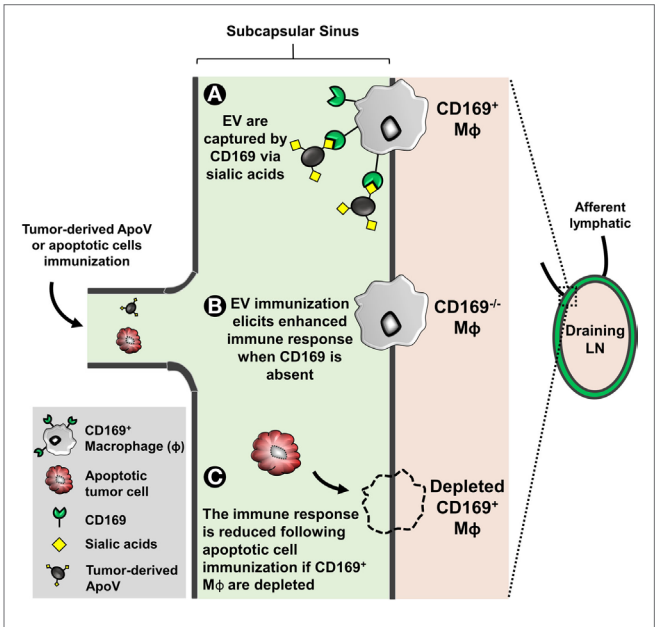

FIGURE 2 | The subcapsular sinus of lymph nodes (LN) is rich in macrophages expressing the surface molecule CD169. EVs are enriched in surface sialylated ligands. **(A)** $CD169^+$ macrophages can bind to these EV in a sialic acid-dependent manner. CD169 binds to α2,6 and α2,3 sialic acids but prefers the latter (47, 49). **(B)** EL4 (thymoma)-derived apoptotic vesicle (ApoV) immunization, $CD169^{-/-}$ mice elicit a significant enhanced cytotoxic response (47). The invasion of tumor cells from the primary site to the draining LN is unaffected by CD169 (217). However, the direct implication of EV and tumor metastasis with respect to CD169 remains unknown. **(C)** When depleted, $CD169^+$ macrophages have a critical role in the anti-cancer effect (212). $CD169^+$ macrophages cross-present tumor antigens from dead tumor cells to $CD8^+$ T cells thereby mediating a cytotoxic-mediated anti-cancer immune response.

The function of the high surface sialylated state of EV remains unclear, however, studies have identified that CD169$^+$ macrophages exclusively capture EV in a CD169-sialic acid-dependent manner (47, 49). EV-immunized CD169-deficient mice display a significant elevated immunogenicity, suggesting that the function of the CD169 receptor itself may be immunoinhibitory [**Figure 2**; Ref. (47, 49)]. However, our recent study suggested that progression of primary tumor growth and LN metastasis was not significantly associated with CD169 expression in mice (217). Despite this, the direct implication of CD169 capture of EV (the "seed") and CD169 (the "soil" receptor) in tumor metastasis has not been extensively investigated. Since cancer patients have an increased level of circulating tumor-derived EV bearing pro-metastatic factors highlights the urgency to further explore the role of the tumor EV receptor CD169 in cancer progression.

TUMOR-DERIVED ApoV AND COAGULATION

Thrombosis is a pathophysiological condition characterized by localized clotting of the blood within a blood vessel leading to a blockage of blood flow (218, 219). In venous thromboembolism (VTE), the wall of the endothelium remains intact but may transform from an anticoagulant to a procoagulant surface (218, 219). Cancer patients have a fourfold increased risk of developing VTE (220, 221). Strikingly, this risk is increased to more than sixfold when the patients are receiving chemotherapy (221, 222). The risk of VTE depends on the cancer type and stage as well as the type of anti-cancer drug administered, which may alter the hemostatic state in patients (223, 224). Tamoxifen, gemcitabine, and platinum-based compounds, for example, are known to lower the levels of circulating anticoagulants (225–228). In contrast, thalidomide treatment for leukemia does not increase the risk of VTE unless combined with other drugs (229, 230). In general, solid tumors pose a greater risk of VTE and worsened prognosis as compared to lymphomas (231). It is now evident that the leading cause of death in cancer patients receiving chemotherapy is VTE (223, 224).

The shedding of procoagulant EV from human cancer cells was first reported in 1981 (232). In the later decades, tissue factor (TF; CD142) and PS exposure were identified as the main procoagulant components of EV (233). TF expression in tumor cells is linked to the mutations in p53 and phosphatase and tensin homolog PTEN (234), resulting in dysregulation of TF expression which may be upregulated 10^5-fold compared to non-malignant counterparts (235). TF is an integral membrane protein with a MW of approximately 45 kDa. TF is not only present on the surface of most non-hematopoietic tumors but is also present in EVs released from these tumor cells (47, 48, 99, 235–238). Although the majority of procoagulant TF is vesicle associated, an alternatively spliced soluble form of TF acts independently of FVII to stimulate angiogenesis (239, 240). Moreover, the cytoplasmic domain of TF is involved in signaling events that promote tumor metastasis, further demonstrating that TF displays pro-metastatic function independent of FVII (241).

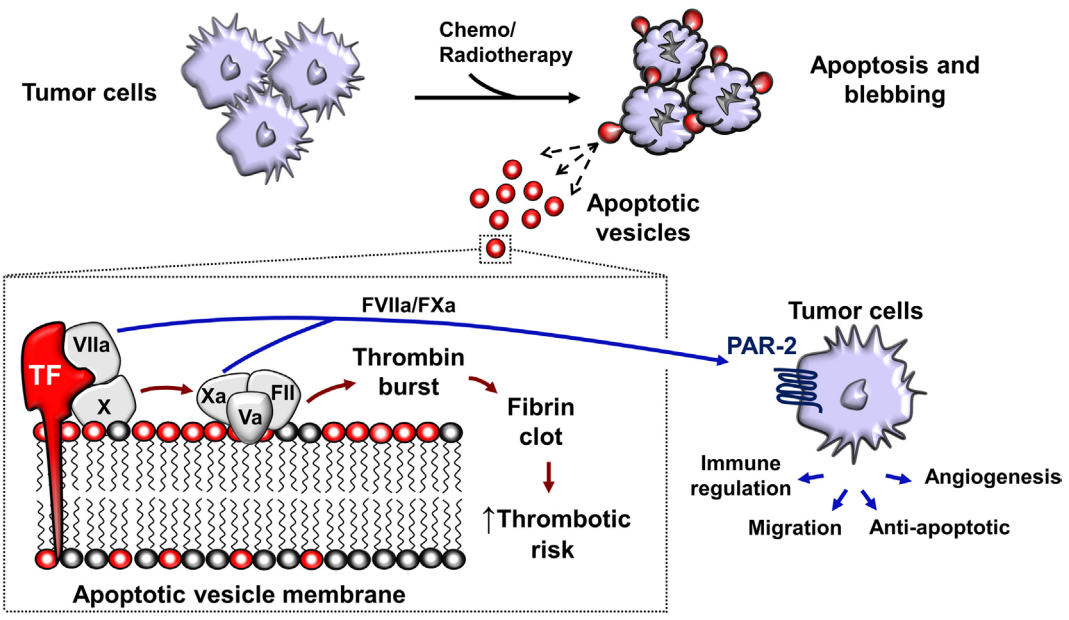

FIGURE 3 | Chemotherapy or radiotherapy-exposed tumor cells may initiate apoptosis and trigger the release apoptotic vesicles (ApoV). Tumor-derived ApoVs express tissue factor (TF) and harbor an anionic-rich surface due to phosphatidylserine (PS) exposure. TF/PS procoagulant complex binds with activated factor VII (FVIIa) and activates the extrinsic coagulation cascade that eventually leads to a fibrin clot. *In vitro,* tumor-derived ApoV are significantly more procoagulant than MV, exosomes, or their cell of origin (47, 48, 99). FVIIa and FXa also cleaves protease-activated receptor-2 (PAR-2) present on the surface of tumor cells (250–252). This results in signal transduction events important in angiogenesis that enhances tumor blood supply and tumor cell growth (234). ApoVs are, therefore, a potential source of increasing the risk of thrombosis and metastasis in cancer patients undergoing chemotherapy.

The association of tumor-derived EV and thrombotic risk is now well-appreciated (193, 233, 242–244). Cancer patients have a significantly higher number of circulating EV compared to healthy controls (243–245). For example, pancreatic cancer patients undergoing chemotherapy are known to possess elevated levels of TF-bearing EV, thus increasing the risk of VTE (246). This phenomenon was observed by Zwicker et al. when they concluded that TF-bearing EVs were associated with VTE in cancer patients (244). Since VTE risk is increased by chemotherapy, this implicates tumor-derived ApoV released from dying tumor cells (**Figure 3**). Although the levels of detected EV in chemotherapy patients are increased, it remains difficult to determine their identity as either tumor, leukocyte, platelet, or endothelial-derived particles. In addition, there is a vast overlap between tumor-derived exosomes, MV, and ApoV with respect to their size, lipid compositions, surface markers, morphology, and functional behavior (21, 96, 99). *In vitro* assays indicate that tumor-derived ApoV are significantly procoagulant in a TF/PS-dependent manner (48, 99, 247). The predisposition to VTE observed in cancer patients may be due to the close association of tumor with the extensive networks of vasculature, allowing the direct interaction of tumor-derived EV with blood-borne coagulation factors. However, the depth of the contribution of local release of tumor EV to the systemic hypercoagulable state observed in cancer patients remains to be elucidated (220, 222, 248, 249).

The presence of TF on ApoV may contribute to metastasis, since TF-mediated coagulation aids cancer progression (241, 253). In 1995, Bromberg et al. were the first to demonstrate a coagulation-independent role for metastasis by TF through mutation of a TF region required for the initiation of coagulation (241). Interestingly, despite the dramatically lower ability of the extracellular mutant to initiate coagulation, metastasis still occurred. This coagulation-independent effect was likely due to the additional function of TF in the activation of the protease-activated receptor-2 (PAR-2), present on the surface of tumor cells (250–252). TF binds to and activates factor VII, activated factor VII (FVIIa) cleaves PAR-2, resulting in signal transduction events important in angiogenesis that enhances tumor blood supply and tumor cell growth (234). Later studies suggested that the formation of the TF:FVIIa complex was necessary to induce metastasis *via* the inhibition of apoptosis, promoting cell adhesion, and angiogenesis (254–256). TF expression on tumor cells has been widely implicated in triggering thrombotic events in cancer patients (236). With the possibility that metastatic tumor cells may upregulate TF up to ~1,000-fold compared to non-metastatic cells (235), TF can be considered as a potent pro-metastatic molecule present on solid and myeloid leukemia-derived ApoV (47, 48).

CONCLUSION

Despite the current advances in the field, much remains to be identified about ApoV and their composition, immune clearance, and their implications in cancer and coagulation. Furthermore, it remains unclear if tumor-derived ApoV generated by varying apoptotic agents possess distinct molecular, or morphological, or functional differences. There is greater need to improve on the isolation methods of EV to enhance their purity and decrease any co-contamination between different subtypes. Since ApoV suppress or stimulate an immune response, then they can potentially be used to treat autoimmunity or cancer, respectively. As for the latter, the immunogenic nature of ApoV opens the possibility to exploit their molecular composition for clinical utility as prophylactic and therapeutic cancer vaccines.

AUTHOR CONTRIBUTIONS

MM-S wrote the bulk of the review and made the figures. AM contributed to planning, scientific input, and editing of the manuscript.

FUNDING

This work cited from our laboratory was funded by a University of Otago Research Grant and the Otago Medical Research Foundation.

REFERENCES

1. Jang SC, Kim SR, Yoon YJ, Park KS, Kim JH, Lee J, et al. In vivo kinetic biodistribution of nano-sized outer membrane vesicles derived from bacteria. *Small* (2015) 11(4):456–61. doi:10.1002/smll.201401803
2. Anderson HC. Vesicles associated with calcification in the matrix of epiphyseal cartilage. *J Cell Biol* (1969) 41(1):59–72. doi:10.1083/jcb.41.1.59
3. Robbins PD, Morelli AE. Regulation of immune responses by extracellular vesicles. *Nat Rev Immunol* (2014) 14(3):195–208. doi:10.1038/nri3622
4. Raposo G, Nijman HW, Stoorvogel W, Liejendekker R, Harding CV, Melief CJ, et al. B lymphocytes secrete antigen-presenting vesicles. *J Exp Med* (1996) 183(3):1161–72. doi:10.1084/jem.183.3.1161
5. Frühbeis C, Fröhlich D, Kuo WP, Krämer-Albers E-M. Extracellular vesicles as mediators of neuron-glia communication. *Front Cell Neurosci* (2013) 7:182. doi:10.3389/fncel.2013.00182
6. Sonnemann KJ, Bement WM. Wound repair: toward understanding and integration of single-cell and multicellular wound responses. *Annu Rev Cell Dev Biol* (2011) 27:237. doi:10.1146/annurev-cellbio-092910-154251
7. Heijnen HF, Schiel AE, Fijnheer R, Geuze HJ, Sixma JJ. Activated platelets release two types of membrane vesicles: microvesicles by surface shedding and exosomes derived from exocytosis of multivesicular bodies and alpha-granules. *Blood* (1999) 94(11):3791–9.
8. Robertson C, Booth SA, Beniac DR, Coulthart MB, Booth TF, McNicol A. Cellular prion protein is released on exosomes from activated platelets. *Blood* (2006) 107(10):3907–11. doi:10.1182/blood-2005-02-0802
9. Gould SJ, Booth AM, Hildreth JE. The Trojan exosome hypothesis. *Proc Natl Acad Sci U S A* (2003) 100(19):10592–7. doi:10.1073/pnas.1831413100
10. VanWijk MJ, VanBavel E, Sturk A, Nieuwland R. Microparticles in cardiovascular diseases. *Cardiovasc Res* (2003) 59(2):277–87. doi:10.1016/S0008-6363(03)00367-5
11. Furie B, Furie BC. Role of platelet P-selectin and microparticle PSGL-1 in thrombus formation. *Trends Mol Med* (2004) 10(4):171–8. doi:10.1016/j.molmed.2004.02.008
12. Distler JH, Pisetsky DS, Huber LC, Kalden JR, Gay S, Distler O. Microparticles as regulators of inflammation: novel players of cellular crosstalk in the rheumatic diseases. *Arthritis Rheum* (2005) 52(11):3337–48. doi:10.1002/art.21350
13. Simak J, Gelderman MP, Yu H, Wright V, Baird AE. Circulating endothelial microparticles in acute ischemic stroke: a link to severity, lesion volume and outcome. *J Thromb Haemost* (2006) 4(6):1296–302. doi:10.1111/j.1538-7836.2006.01911.x

14. Lima LG, Chammas R, Monteiro RQ, Moreira ME, Barcinski MA. Tumor-derived microvesicles modulate the establishment of metastatic melanoma in a phosphatidylserine-dependent manner. *Cancer Lett* (2009) 283(2):168–75. doi:10.1016/j.canlet.2009.03.041
15. Théry C, Boussac M, Véron P, Ricciardi-Castagnoli P, Raposo G, Garin J, et al. Proteomic analysis of dendritic cell-derived exosomes: a secreted subcellular compartment distinct from apoptotic vesicles. *J Immunol* (2001) 166(12):7309–18. doi:10.4049/jimmunol.166.12.7309
16. Thery C, Zitvogel L, Amigorena S. Exosomes: composition, biogenesis and function. *Nat Rev Immunol* (2002) 2(8):569–79. doi:10.1038/nri855
17. Taylor DD, Akyol S, Gercel-Taylor C. Pregnancy-associated exosomes and their modulation of T cell signaling. *J Immunol* (2006) 176(3):1534–42. doi:10.4049/jimmunol.176.3.1534
18. McLellan AD. Exosome release by primary B cells. *Crit Rev Immunol* (2009) 29(3):203–17. doi:10.1615/CritRevImmunol.v29.i3.20
19. Wolfers J, Lozier A, Raposo G, Regnault A, Thery C, Masurier C, et al. Tumor-derived exosomes are a source of shared tumor rejection antigens for CTL cross-priming. *Nat Med* (2001) 7(3):297–303. doi:10.1038/85438
20. Trams EG, Lauter CJ, Salem N Jr, Heine U. Exfoliation of membrane ecto-enzymes in the form of micro-vesicles. *Biochim Biophys Acta* (1981) 645(1):63–70. doi:10.1016/0005-2736(81)90512-5
21. Thery C, Ostrowski M, Segura E. Membrane vesicles as conveyors of immune responses. *Nat Rev Immunol* (2009) 9(8):581–93. doi:10.1038/nri2567
22. Taylor DD, Gercel-Taylor C. Tumour-derived exosomes and their role in cancer-associated T-cell signalling defects. *Br J Cancer* (2005) 92(2):305–11. doi:10.1038/sj.bjc.6602316
23. Théry C, Regnault A, Garin J, Wolfers J, Zitvogel L, Ricciardi-Castagnoli P, et al. Molecular characterization of dendritic cell-derived exosomes. Selective accumulation of the heat shock protein Hsc73. *J Cell Biol* (1999) 147(3):599–610. doi:10.1083/jcb.147.3.599
24. Raposo G, Stoorvogel W. Extracellular vesicles: exosomes, microvesicles, and friends. *J Cell Biol* (2013) 200(4):373–83. doi:10.1083/jcb.201211138
25. Wolf P. The nature and significance of platelet products in human plasma. *Br J Haematol* (1967) 13(3):269–88. doi:10.1111/j.1365-2141.1967.tb08741.x
26. Chargaff E, West R. The biological significance of the thromboplastic protein of blood. *J Biol Chem* (1946) 166(1):189–97.
27. Smalley DM, Sheman NE, Nelson K, Theodorescu D. Isolation and identification of potential urinary microparticle biomarkers of bladder cancer. *J Proteome Res* (2008) 7(5):2088–96. doi:10.1021/pr700775x
28. Ma L, Li Y, Peng J, Wu D, Zhao X, Cui Y, et al. Discovery of the migrasome, an organelle mediating release of cytoplasmic contents during cell migration. *Cell Res* (2015) 25(1):24–38. doi:10.1038/cr.2014.135
29. Al-Nedawi K, Meehan B, Micallef J, Lhotak V, May L, Guha A, et al. Intercellular transfer of the oncogenic receptor EGFRvIII by microvesicles derived from tumour cells. *Nat Cell Biol* (2008) 10(5):619–24. doi:10.1038/ncb1725
30. Di Vizio D, Kim J, Hager MH, Morello M, Yang W, Lafargue CJ, et al. Oncosome formation in prostate cancer: association with a region of frequent chromosomal deletion in metastatic disease. *Cancer Res* (2009) 69(13):5601–9. doi:10.1158/0008-5472.CAN-08-3860
31. Di Vizio D, Morello M, Dudley AC, Schow PW, Adam RM, Morley S, et al. Large oncosomes in human prostate cancer tissues and in the circulation of mice with metastatic disease. *Am J Pathol* (2012) 181(5):1573–84. doi:10.1016/j.ajpath.2012.07.030
32. Tatischeff I. Cell-derived extracellular vesicles open new perspectives for cancer research. *Cancer Res Front* (2015) 1(2):208–24. doi:10.17980/2015.208
33. Zappulli V, Friis KP, Fitzpatrick Z, Maguire CA, Breakefield XO. Extracellular vesicles and intercellular communication within the nervous system. *J Clin Invest* (2016) 126(4):1198–207. doi:10.1172/JCI81134
34. Meehan B, Rak J, Di Vizio D. Oncosomes – large and small: what are they, where they came from? *J Extracell Vesicles* (2016) 5:1–2. doi:10.3402/jev.v5.33109
35. Lötvall J, Hill AF, Hochberg F, Buzás EI, Di Vizio D, Gardiner C, et al. Minimal experimental requirements for definition of extracellular vesicles and their functions: a position statement from the international society for extracellular vesicles. *J Extracell Vesicles* (2014) 3:26913. doi:10.3402/jev.v3.26913
36. Coumans FAW, Brisson AR, Buzas EI, Dignat-George F, Drees EEE, El-Andaloussi S, et al. Methodological guidelines to study extracellular vesicles. *Circ Res* (2017) 120(10):1632–48. doi:10.1161/CIRCRESAHA.117.309417
37. Wickman G, Julian L, Olson MF. How apoptotic cells aid in the removal of their own cold dead bodies. *Cell Death Differ* (2012) 19(5):735–42. doi:10.1038/cdd.2012.25
38. Akers JC, Gonda D, Kim R, Carter BS, Chen CC. Biogenesis of extracellular vesicles (EV): exosomes, microvesicles, retrovirus-like vesicles, and apoptotic bodies. *J Neurooncol* (2013) 113(1):1–11. doi:10.1007/s11060-013-1084-8
39. Hristov M, Erl W, Linder S, Weber PC. Apoptotic bodies from endothelial cells enhance the number and initiate the differentiation of human endothelial progenitor cells in vitro. *Blood* (2004) 104(9):2761–6. doi:10.1182/blood-2003-10-3614
40. Bhatnagar S, Schorey JS. Exosomes released from infected macrophages contain *Mycobacterium avium* glycopeptidolipids and are proinflammatory. *J Biol Chem* (2007) 282(35):25779–89. doi:10.1074/jbc.M702277200
41. Orozco AF, Jorgez CJ, Horne C, Marquez-Do DA, Chapman MR, Rodgers JR, et al. Membrane protected apoptotic trophoblast microparticles contain nucleic acids: relevance to preeclampsia. *Am J Pathol* (2008) 173(6):1595–608. doi:10.2353/ajpath.2008.080414
42. Litvack ML, Post M, Palaniyar N. IgM promotes the clearance of small particles and apoptotic microparticles by macrophages. *PLoS One* (2011) 6(3):e17223. doi:10.1371/journal.pone.0017223
43. Atkin-Smith GK, Paone S, Zanker DJ, Duan M, Phan TK, Chen W, et al. Isolation of cell type-specific apoptotic bodies by fluorescence-activated cell sorting. *Sci Rep* (2017) 7:39846. doi:10.1038/srep39846
44. Reich CF III, Pisetsky DS. The content of DNA and RNA in microparticles released by Jurkat and HL-60 cells undergoing in vitro apoptosis. *Exp Cell Res* (2009) 315(5):760–8. doi:10.1016/j.yexcr.2008.12.014
45. Schiller M, Bekeredjian-Ding I, Heyder P, Blank N, Ho AD, Lorenz HM. Autoantigens are translocated into small apoptotic bodies during early stages of apoptosis. *Cell Death Differ* (2007) 15(1):183–91. doi:10.1038/sj.cdd.4402239
46. Gyorgy B, Szabo TG, Pasztoi M, Pal Z, Misjak P, Aradi B, et al. Membrane vesicles, current state-of-the-art: emerging role of extracellular vesicles. *Cell Mol Life Sci* (2011) 68(16):2667–88. doi:10.1007/s00018-011-0689-3
47. Black LV, Saunderson SC, Coutinho FP, Muhsin-Sharafaldine MR, Damani TT, Dunn AC, et al. The CD169 sialoadhesin molecule mediates cytotoxic T-cell responses to tumour apoptotic vesicles. *Immunol Cell Biol* (2016) 94(5):430–8. doi:10.1038/icb.2015.111
48. Muhsin-Sharafaldine MR, Kennedy BR, Saunderson SC, Buchanan CR, Dunn AC, Faed JM, et al. Mechanistic insight into the procoagulant activity of tumor-derived apoptotic vesicles. *Biochim Biophys Acta* (2017) 1861(2):286–95. doi:10.1016/j.bbagen.2016.11.020
49. Saunderson SC, Dunn AC, Crocker PR, McLellan AD. CD169 mediates the capture of exosomes in spleen and lymph node. *Blood* (2014) 123(2):208–16. doi:10.1182/blood-2013-03-489732
50. Okada H, Mak TW. Pathways of apoptotic and non-apoptotic death in tumour cells. *Nat Rev Cancer* (2004) 4(8):592–603. doi:10.1038/nrc1412
51. Ricci MS, Zong W-X. Chemotherapeutic approaches for targeting cell death pathways. *Oncologist* (2006) 11(4):342–57. doi:10.1634/theoncologist.11-4-342
52. Holland AJ, Cleveland DW. Boveri revisited: chromosomal instability, aneuploidy and tumorigenesis. *Nat Rev Mol Cell Biol* (2009) 10(7):478–87. doi:10.1038/nrm2718
53. Vitale I, Galluzzi L, Castedo M, Kroemer G. Mitotic catastrophe: a mechanism for avoiding genomic instability. *Nat Rev Mol Cell Biol* (2011) 12(6):385–92. doi:10.1038/nrm3115
54. Hayflick L. The limited in vitro lifetime of human diploid cell strains. *Exp Cell Res* (1965) 37(3):614–36. doi:10.1016/0014-4827(65)90211-9
55. Campisi J, d'Adda di Fagagna F. Cellular senescence: when bad things happen to good cells. *Nat Rev Mol Cell Biol* (2007) 8(9):729–40. doi:10.1038/nrm2233
56. Vallejo AN, Weyand CM, Goronzy JJ. T-cell senescence: a culprit of immune abnormalities in chronic inflammation and persistent infection. *Trends Mol Med* (2004) 10(3):119–24. doi:10.1016/j.molmed.2004.01.002
57. Majno G, Joris I. Apoptosis, oncosis, and necrosis. An overview of cell death. *Am J Pathol* (1995) 146(1):3–15.
58. Edinger AL, Thompson CB. Death by design: apoptosis, necrosis and autophagy. *Curr Opin Cell Biol* (2004) 16(6):663–9. doi:10.1016/j.ceb.2004.09.011
59. Proskuryakov SY, Gabai V, Konoplyannikov A. Necrosis is an active and controlled form of programmed cell death. *Biochemistry (Mosc)* (2002) 67(4):387–408. doi:10.1023/A:1015289521275

60. Hitomi J, Christofferson DE, Ng A, Yao J, Degterev A, Xavier RJ, et al. Identification of a molecular signaling network that regulates a cellular necrotic cell death pathway. *Cell* (2008) 135(7):1311–23. doi:10.1016/j.cell.2008.10.044
61. Yoon S, Kovalenko A, Bogdanov K, Wallach D. MLKL, the protein that mediates necroptosis, also regulates endosomal trafficking and extracellular vesicle generation. *Immunity* (2017) 47(1):51–65.e7. doi:10.1016/j.immuni.2017.06.001
62. Kirkin V, McEwan DG, Novak I, Dikic I. A role for ubiquitin in selective autophagy. *Mol Cell* (2009) 34(3):259–69. doi:10.1016/j.molcel.2009.04.026
63. Bursch W, Hochegger K, Torok L, Marian B, Ellinger A, Hermann RS. Autophagic and apoptotic types of programmed cell death exhibit different fates of cytoskeletal filaments. *J Cell Sci* (2000) 113(7):1189–98.
64. Barros LF, Kanaseki T, Sabirov R, Morishima S, Castro J, Bittner CX, et al. Apoptotic and necrotic blebs in epithelial cells display similar neck diameters but different kinase dependency. *Cell Death Differ* (2003) 10:687. doi:10.1038/sj.cdd.4401236
65. Fulda S, Debatin KM. Extrinsic versus intrinsic apoptosis pathways in anticancer chemotherapy. *Oncogene* (2006) 25(34):4798–811. doi:10.1038/sj.onc.1209608
66. Rytömaa M, Martins LM, Downward J. Involvement of FADD and caspase-8 signalling in detachment-induced apoptosis. *Curr Biol* (1999) 9(18):1043–S2. doi:10.1016/S0960-9822(99)80454-0
67. Cohen GM. Caspases: the executioners of apoptosis. *Biochem J* (1997) 326 (Pt 1):1–16. doi:10.1042/bj3260001
68. Thornberry NA, Lazebnik Y. Caspases: enemies within. *Science* (1998) 281(5381):1312–6. doi:10.1126/science.281.5381.1312
69. Grütter MG. Caspases: key players in programmed cell death. *Curr Opin Struct Biol* (2000) 10(6):649–55. doi:10.1016/S0959-440X(00)00146-9
70. Mehmet H. Apoptosis: caspases find a new place to hide. *Nature* (2000) 403(6765):29–30. doi:10.1038/47377
71. Atkin-Smith GK, Poon IKH. Disassembly of the dying: mechanisms and functions. *Trends Cell Biol* (2017) 27(2):151–62. doi:10.1016/j.tcb.2016.08.011
72. Savill J, Gregory C, Haslett C. Eat me or die. *Science* (2003) 302(5650):1516–7. doi:10.1126/science.1092533
73. Kerr JFR, Wyllie AH, Currie AR. Apoptosis: a basic biological phenomenon with wide-ranging implications in tissue kinetics. *Br J Cancer* (1972) 26(4):239–57. doi:10.1038/bjc.1972.33
74. Bobrie A, Colombo M, Raposo G, Théry C. Exosome secretion: molecular mechanisms and roles in immune responses. *Traffic* (2011) 12(12):1659–68. doi:10.1111/j.1600-0854.2011.01225.x
75. Bock JB, Matern HT, Peden AA, Scheller RH. A genomic perspective on membrane compartment organization. *Nature* (2001) 409:839. doi:10.1038/35057024
76. van Deurs B, Holm PK, Kayser L, Sandvig K, Hansen SH. Multivesicular bodies in HEp-2 cells are maturing endosomes. *Eur J Cell Biol* (1993) 61(2):208–24.
77. Wollert T, Wunder C, Lippincott-Schwartz J, Hurley JH. Membrane scission by the ESCRT-III complex. *Nature* (2009) 458:172. doi:10.1038/nature07836
78. Xu R, Greening DW, Zhu HJ, Takahashi N, Simpson RJ. Extracellular vesicle isolation and characterization: toward clinical application. *J Clin Invest* (2016) 126(4):1152–62. doi:10.1172/JCI81129
79. Trajkovic K, Hsu C, Chiantia S, Rajendran L, Wenzel D, Wieland F, et al. Ceramide triggers budding of exosome vesicles into multivesicular endosomes. *Science* (2008) 319(5867):1244–7. doi:10.1126/science.1153124
80. Miyoshi H, Umeshita K, Sakon M, Imajoh-Ohmi S, Fujitani K, Gotoh M, et al. Calpain activation in plasma membrane bleb formation during tert-butyl hydroperoxide-induced rat hepatocyte injury. *Gastroenterology* (1996) 110(6):1897–904. doi:10.1053/gast.1996.v110.pm8964416
81. Muralidharan-Chari V, Clancy J, Plou C, Romao M, Chavrier P, Raposo G, et al. ARF6-regulated shedding of tumor cell-derived plasma membrane microvesicles. *Curr Biol* (2009) 19(22):1875–85. doi:10.1016/j.cub.2009.09.059
82. Schlienger S, Campbell S, Claing A. ARF1 regulates the Rho/MLC pathway to control EGF-dependent breast cancer cell invasion. *Mol Biol Cell* (2014) 25(1):17–29. doi:10.1091/mbc.E13-06-0335
83. Sebbagh M, Renvoizé C, Hamelin J, Riché N, Bertoglio J, Bréard J. Caspase-3-mediated cleavage of ROCK I induces MLC phosphorylation and apoptotic membrane blebbing. *Nat Cell Biol* (2001) 3:346. doi:10.1038/35070019
84. Khorchid A, Ikura M. How calpain is activated by calcium. *Nat Struct Mol Biol* (2002) 9(4):239–41. doi:10.1038/nsb0402-239
85. Pasquet JM, Dachary-Prigent J, Nurden AT. Calcium influx is a determining factor of calpain activation and microparticle formation in platelets. *Eur J Biochem* (1996) 239(3):647–54. doi:10.1111/j.1432-1033.1996.0647u.x
86. Kawaguchi K, Saito K, Asami H, Ohta Y. ADP ribosylation factor 6 (Arf6) Acts through FilGAP protein to down-regulate Rac protein and regulates plasma membrane blebbing. *J Biol Chem* (2014) 289(14):9675–82. doi:10.1074/jbc.M113.546051
87. Charras GT, Yarrow JC, Horton MA, Mahadevan L, Mitchison T. Non-equilibration of hydrostatic pressure in blebbing cells. *Nature* (2005) 435(7040):365–9. doi:10.1038/nature03550
88. Choudhuri K, Llodrá J, Roth EW, Tsai J, Gordo S, Wucherpfennig KW, et al. Polarized release of T-cell-receptor-enriched microvesicles at the immunological synapse. *Nature* (2014) 507:118. doi:10.1038/nature12951
89. Mills JC, Stone NL, Erhardt J, Pittman RN. Apoptotic membrane blebbing is regulated by myosin light chain phosphorylation. *J Cell Biol* (1998) 140(3):627–36. doi:10.1083/jcb.140.3.627
90. Leverrier Y, Ridley AJ. Apoptosis: caspases orchestrate the ROCKn' bleb. *Nat Cell Biol* (2001) 3:E91. doi:10.1038/35070151
91. Coleman ML, Sahai EA, Yeo M, Bosch M, Dewar A, Olson MF. Membrane blebbing during apoptosis results from caspase-mediated activation of ROCK I. *Nat Cell Biol* (2001) 3(4):339–45. doi:10.1038/35070009
92. Tomiyoshi G, Horita Y, Nishita M, Ohashi K, Mizuno K. Caspase-mediated cleavage and activation of LIM-kinase 1 and its role in apoptotic membrane blebbing. *Genes Cells* (2004) 9(6):591–600. doi:10.1111/j.1356-9597.2004.00745.x
93. Rudel T, Bokoch GM. Membrane and morphological changes in apoptotic cells regulated by caspase-mediated activation of PAK2. *Science* (1997) 276(5318):1571–4. doi:10.1126/science.276.5318.1571
94. Moss DK, Betin VM, Malesinski SD, Lane JD. A novel role for microtubules in apoptotic chromatin dynamics and cellular fragmentation. *J Cell Sci* (2006) 119(11):2362–74. doi:10.1242/jcs.02959
95. Poon IKH, Chiu Y-H, Armstrong AJ, Kinchen JM, Juncadella IJ, Bayliss DA, et al. Unexpected link between an antibiotic, pannexin channels and apoptosis. *Nature* (2014) 507:329. doi:10.1038/nature13147
96. Osteikoetxea X, Balogh A, Szabo-Taylor K, Nemeth A, Szabo TG, Paloczi K, et al. Improved characterization of EV preparations based on protein to lipid ratio and lipid properties. *PLoS One* (2015) 10(3):e0121184. doi:10.1371/journal.pone.0121184
97. Thakur BK, Zhang H, Becker A, Matei I, Huang Y, Costa-Silva B, et al. Double-stranded DNA in exosomes: a novel biomarker in cancer detection. *Cell Res* (2014) 24:766. doi:10.1038/cr.2014.44
98. Ratajczak MZ, Ratajczak J. Horizontal transfer of RNA and proteins between cells by extracellular microvesicles: 14 years later. *Clin Transl Med* (2016) 5(1):7. doi:10.1186/s40169-016-0087-4
99. Muhsin-Sharafaldine MR, Saunderson SC, Dunn AC, Faed JM, Kleffmann T, McLellan AD. Procoagulant and immunogenic properties of melanoma exosomes, microvesicles and apoptotic vesicles. *Oncotarget* (2016) 7(35):56279–94. doi:10.18632/oncotarget.10783
100. Millimaggi D, Mari M, D'Ascenzo S, Carosa E, Jannini EA, Zucker S, et al. Tumor vesicle-associated CD147 modulates the angiogenic capability of endothelial cells. *Neoplasia* (2007) 9(4):349–57. doi:10.1593/neo.07133
101. Zucker S, Hymowitz M, Conner C, Zarrabi HM, Hurewitz AN, Matrisian L, et al. Measurement of matrix metalloproteinases and tissue inhibitors of metalloproteinases in blood and tissues: clinical and experimental applications. *Ann N Y Acad Sci* (1999) 878(1):212–27. doi:10.1111/j.1749-6632.1999.tb07687.x
102. Zucker S, Hymowitz M, Rollo EE, Mann R, Conner CE, Cao J, et al. Tumorigenic potential of extracellular matrix metalloproteinase inducer. *Am J Pathol* (2001) 158(6):1921–8. doi:10.1016/S0002-9440(10)64660-3
103. Voigt H, Vetter-Kauczok CS, Schrama D, Hofmann UB, Becker JC, Houben R. CD147 impacts angiogenesis and metastasis formation. *Cancer Invest* (2009) 27(3):329–33. doi:10.1080/07357900802392675
104. Andreu Z, Yáñez-Mó M. Tetraspanins in extracellular vesicle formation and function. *Front Immunol* (2014) 5:442. doi:10.3389/fimmu.2014.00442
105. Hemler ME. Tetraspanin proteins mediate cellular penetration, invasion, and fusion events and define a novel type of membrane microdomain. *Annu Rev Cell Dev Biol* (2003) 19(1):397–422. doi:10.1146/annurev.cellbio.19.111301.153609

106. Zöller M. Tetraspanins: push and pull in suppressing and promoting metastasis. *Nat Rev Cancer* (2009) 9(1):40–55. doi:10.1038/nrc2543
107. Mathivanan S, Simpson RJ. ExoCarta: a compendium of exosomal proteins and RNA. *Proteomics* (2009) 9(21):4997–5000. doi:10.1002/pmic.200900351
108. Hemler ME. Tetraspanin proteins promote multiple cancer stages. *Nat Rev Cancer* (2014) 14(1):49–60. doi:10.1038/nrc3640
109. Berditchevski F. Complexes of tetraspanins with integrins: more than meets the eye. *J Cell Sci* (2001) 114(23):4143–51.
110. Burgess RJ, Zhang Z. Histone chaperones in nucleosome assembly and human disease. *Nat Struct Mol Biol* (2013) 20(1):14–22. doi:10.1038/nsmb.2461
111. Kowal J, Arras G, Colombo M, Jouve M, Morath JP, Primdal-Bengtson B, et al. Proteomic comparison defines novel markers to characterize heterogeneous populations of extracellular vesicle subtypes. *Proc Natl Acad Sci U S A* (2016) 113(8):E968–77. doi:10.1073/pnas.1521230113
112. Skog J, Wurdinger T, van Rijn S, Meijer DH, Gainche L, Curry WT, et al. Glioblastoma microvesicles transport RNA and proteins that promote tumour growth and provide diagnostic biomarkers. *Nat Cell Biol* (2008) 10(12):1470–6. doi:10.1038/ncb1800
113. Palma J, Yaddanapudi SC, Pigati L, Havens MA, Jeong S, Weiner GA, et al. MicroRNAs are exported from malignant cells in customized particles. *Nucleic Acids Res* (2012) 40(18):9125–38. doi:10.1093/nar/gks656
114. Gibbings DJ, Ciaudo C, Erhardt M, Voinnet O. Multivesicular bodies associate with components of miRNA effector complexes and modulate miRNA activity. *Nat Cell Biol* (2009) 11(9):1143–9. doi:10.1038/ncb1929
115. Valadi H, Ekström K, Bossios A, Sjöstrand M, Lee JJ, Lötvall JO. Exosome-mediated transfer of mRNAs and microRNAs is a novel mechanism of genetic exchange between cells. *Nat Cell Biol* (2007) 9:654–9. doi:10.1038/ncb1596
116. Müller G, Schneider M, Gassenhuber J, Wied S. Release of exosomes and microvesicles harbouring specific RNAs and glycosylphosphatidylinositol-anchored proteins from rat and human adipocytes is controlled by histone methylation. *Am J Mol Biol* (2012) 2(3):187–209. doi:10.4236/ajmb.2012.23020
117. Al-Nedawi K, Meehan B, Rak J. Microvesicles: messengers and mediators of tumor progression. *Cell Cycle* (2009) 8(13):2014–8. doi:10.4161/cc.8.13.8988
118. Crescitelli R, Lässer C, Szabó TG, Kittel A, Eldh M, Dianzani I, et al. Distinct RNA profiles in subpopulations of extracellular vesicles: apoptotic bodies, microvesicles and exosomes. *J Extracell Vesicles* (2013) 2(1):20677. doi:10.3402/jev.v2i0.20677
119. Nolte-'t Hoen EN, Buermans HP, Waasdorp M, Stoorvogel W, Wauben MH, 't Hoen PA. Deep sequencing of RNA from immune cell-derived vesicles uncovers the selective incorporation of small non-coding RNA biotypes with potential regulatory functions. *Nucleic Acids Res* (2012) 40(18):9272–85. doi:10.1093/nar/gks658
120. Halicka HD, Bedner E, Darzynkiewicz Z. Segregation of RNA and separate packaging of DNA and RNA in apoptotic bodies during apoptosis. *Exp Cell Res* (2000) 260(2):248–56. doi:10.1006/excr.2000.5027
121. Holmgren L, Szeles A, Rajnavölgyi E, Folkman J, Klein G, Ernberg I, et al. Horizontal transfer of DNA by the uptake of apoptotic bodies. *Blood* (1999) 93(11):3956–63.
122. Freyssinet JM. Cellular microparticles: what are they bad or good for? *J Thromb Haemost* (2003) 1(7):1655–62. doi:10.1046/j.1538-7836.2003.00309.x
123. Balasubramanian K, Mirnikjoo B, Schroit AJ. Regulated externalization of phosphatidylserine at the cell surface: implications for apoptosis. *J Biol Chem* (2007) 282(25):18357–64. doi:10.1074/jbc.M700202200
124. Daleke DL. Phospholipid flippases. *J Biol Chem* (2007) 282(2):821–5. doi:10.1074/jbc.R600035200
125. Segawa K, Kurata S, Yanagihashi Y, Brummelkamp TR, Matsuda F, Nagata S. Caspase-mediated cleavage of phospholipid flippase for apoptotic phosphatidylserine exposure. *Science* (2014) 344(6188):1164–8. doi:10.1126/science.1252809
126. Groen A, Romero MR, Kunne C, Hoosdally SJ, Dixon PH, Wooding C, et al. Complementary functions of the flippase ATP8B1 and the floppase ABCB4 in maintaining canalicular membrane integrity. *Gastroenterology* (2011) 141(5):1927–37.e1–4. doi:10.1053/j.gastro.2011.07.042
127. Bitbol M, Devaux PF. Measurement of outward translocation of phospholipids across human erythrocyte membrane. *Proc Natl Acad Sci U S A* (1988) 85(18):6783–7. doi:10.1073/pnas.85.18.6783
128. Hankins HM, Baldridge RD, Xu P, Graham TR. Role of flippases, scramblases and transfer proteins in phosphatidylserine subcellular distribution. *Traffic* (2015) 16(1):35–47. doi:10.1111/tra.12233
129. Zhou Q, Zhao J, Stout JG, Luhm RA, Wiedmer T, Sims PJ. Molecular cloning of human plasma membrane phospholipid scramblase a protein mediating transbilayer movement of plasma membrane phospholipids. *J Biol Chem* (1997) 272(29):18240–4. doi:10.1074/jbc.272.29.18240
130. Suzuki J, Umeda M, Sims PJ, Nagata S. Calcium-dependent phospholipid scrambling by TMEM16F. *Nature* (2010) 468(7325):834–8. doi:10.1038/nature09583
131. Suzuki J, Denning DP, Imanishi E, Horvitz HR, Nagata S. Xk-related protein 8 and CED-8 promote phosphatidylserine exposure in apoptotic cells. *Science* (2013) 341(6144):403–6. doi:10.1126/science.1236758
132. Varki A, Lowe JB. Chapter 6: Biological roles of glycans. In: Varki A, Cummings RD, Esko JD, editors. *Essentials of Glycobiology*. 2nd edition. Cold Spring Harbor (NY): Cold Spring Harbor Laboratory Press (2009). Available from: https://www.ncbi.nlm.nih.gov/books/NBK1897/
133. Zonneveld MI, Brisson AR, van Herwijnen MJC, Tan S, van de Lest CHA, Redegeld FA, et al. Recovery of extracellular vesicles from human breast milk is influenced by sample collection and vesicle isolation procedures. *J Extracell Vesicles* (2014) 3(1):24215. doi:10.3402/jev.v3.24215
134. Echevarria J, Royo F, Pazos R, Salazar L, Falcon-Perez JM, Reichardt N-C. Microarray-based identification of lectins for the purification of human urinary extracellular vesicles directly from urine samples. *Chembiochem* (2014) 15(11):1621–6. doi:10.1002/cbic.201402058
135. da Silva RP, Heiss C, Black I, Azadi P, Gerlach JQ, Travassos LR, et al. Extracellular vesicles from *Paracoccidioides* pathogenic species transport polysaccharide and expose ligands for DC-SIGN receptors. *Sci Rep* (2015) 5:14213. doi:10.1038/srep14213
136. Gerlach JQ, Krüger A, Gallogly S, Hanley SA, Hogan MC, Ward CJ, et al. Surface glycosylation profiles of urine extracellular vesicles. *PLoS One* (2013) 8(9):e74801. doi:10.1371/journal.pone.0074801
137. Krishnamoorthy L, Bess JW Jr, Preston AB, Nagashima K, Mahal LK. HIV-1 and microvesicles from T cells share a common glycome, arguing for a common origin. *Nat Chem Biol* (2009) 5:244. doi:10.1038/nchembio.151
138. Batista BS, Eng WS, Pilobello KT, Hendricks-Muñoz KD, Mahal LK. Identification of a conserved glycan signature for microvesicles. *J Proteome Res* (2011) 10(10):4624–33. doi:10.1021/pr200434y
139. Gupta G, Surolia A, Sampathkumar S-G. Lectin microarrays for glycomic analysis. *OMICS* (2010) 14(4):419–36. doi:10.1089/omi.2009.0150
140. Gerlach JQ, Griffin MD. Getting to know the extracellular vesicle glycome. *Mol Biosyst* (2016) 12(4):1071–81. doi:10.1039/c5mb00835b
141. Wang S, Cesca F, Loers G, Schweizer M, Buck F, Benfenati F, et al. Synapsin I is an oligomannose-carrying glycoprotein, acts as an oligomannose-binding lectin, and promotes neurite outgrowth and neuronal survival when released via glia-derived exosomes. *J Neurosci* (2011) 31(20):7275–90. doi:10.1523/JNEUROSCI.6476-10.2011
142. Shimoda A, Tahara Y, Sawada S-I, Sasaki Y, Akiyoshi K. Glycan profiling analysis using evanescent-field fluorescence-assisted lectin array: importance of sugar recognition for cellular uptake of exosomes from mesenchymal stem cells. *Biochem Biophys Res Commun* (2017) 491(3):701–7. doi:10.1016/j.bbrc.2017.07.126
143. Barrès C, Blanc L, Bette-Bobillo P, André S, Mamoun R, Gabius H-J, et al. Galectin-5 is bound onto the surface of rat reticulocyte exosomes and modulates vesicle uptake by macrophages. *Blood* (2010) 115(3):696–705. doi:10.1182/blood-2009-07-231449
144. Hogan MC, Manganelli L, Woollard JR, Masyuk AI, Masyuk TV, Tammachote R, et al. Characterization of PKD protein-positive exosome-like vesicles. *J Am Soc Nephrol* (2009) 20(2):278–88. doi:10.1681/ASN.2008060564
145. Gomes J, Gomes-Alves P, Carvalho S, Peixoto C, Alves P, Altevogt P, et al. Extracellular vesicles from ovarian carcinoma cells display specific glycosignatures. *Biomolecules* (2015) 5(3):1741. doi:10.3390/biom5031741
146. Takanori A, Kei K, Nami H, Masashi K, Takanori I. Evaluation of desialylation effect on zeta potential of extracellular vesicles secreted from human prostate cancer cells by on-chip microcapillary electrophoresis. *Jpn J App Phys* (2014) 53(6S):06JL1. doi:10.7567/JJAP.53.06JL01
147. Escrevente C, Grammel N, Kandzia S, Zeiser J, Tranfield EM, Conradt HS, et al. Sialoglycoproteins and N-glycans from secreted exosomes of ovarian

carcinoma cells. *PLoS One* (2013) 8(10):e78631. doi:10.1371/journal.pone.0078631
148. Wang P-H. Altered glycosylation in cancer: sialic acids and sialyltransferases. *J Cancer Mol* (2005) 1(2):73–81. doi:10.29685/JCM.200512.0001
149. Ashman LK, Zöller M. Tetraspanins in cancer. In: Berditchevski F, Rubinstein E, editor. *Tetraspanins. Proteins and Cell Regulation*, vol 9. Dordrecht: Springer (2013). p. 257–98.
150. Crocker PR, Vinson M, Kelm S, Drickamer K. Molecular analysis of sialoside binding to sialoadhesin by NMR and site-directed mutagenesis. *Biochem J* (1999) 341(Pt 2):355–61. doi:10.1042/bj3410355
151. Matheoud D, Baey C, Vimeux L, Tempez A, Valente M, Louche P, et al. Dendritic cells crosspresent antigens from live B16 cells more efficiently than from apoptotic cells and protect from melanoma in a therapeutic model. *PLoS One* (2011) 6(4):e19104. doi:10.1371/journal.pone.0019104
152. Harshyne LA, Watkins SC, Gambotto A, Barratt-Boyes SM. Dendritic cells acquire antigens from live cells for cross-presentation to CTL. *J Immunol* (2001) 166(6):3717–23. doi:10.4049/jimmunol.166.6.3717
153. Zeelenberg IS, van Maren WWC, Boissonnas A, Van Hout-Kuijer MA, Den Brok MHMGM, Wagenaars JAL, et al. Antigen localization controls T cell-mediated tumor immunity. *J Immunol* (2011) 187(3):1281–8. doi:10.4049/jimmunol.1003905
154. Basu S, Binder RJ, Ramalingam T, Srivastava PK. CD91 is a common receptor for heat shock proteins gp96, hsp90, hsp70, and calreticulin. *Immunity* (2001) 14(3):303–13. doi:10.1016/S1074-7613(01)00111-X
155. Valenti R, Huber V, Iero M, Filipazzi P, Parmiani G, Rivoltini L. Tumor-released microvesicles as vehicles of immunosuppression. *Cancer Res* (2007) 67(7):2912–5. doi:10.1158/0008-5472.CAN-07-0520
156. Mitchell DA, Nair SK, Gilboa E. Dendritic cell/macrophage precursors capture exogenous antigen for MHC class I presentation by dendritic cells. *Eur J Immunol* (1998) 28(6):1923–33. doi:10.1002/(SICI)1521-4141(199806)28:06<1923::AID-IMMU1923>3.0.CO;2-9
157. Knuth A, Wölfel T, Klehmann E, Boon T, Meyer zum Büschenfelde KH. Cytolytic T-cell clones against an autologous human melanoma: specificity study and definition of three antigens by immunoselection. *Proc Natl Acad Sci U S A* (1989) 86(8):2804–8. doi:10.1073/pnas.86.8.2804
158. Heiser A, Coleman D, Dannull J, Yancey D, Maurice MA, Lallas CD, et al. Autologous dendritic cells transfected with prostate-specific antigen RNA stimulate CTL responses against metastatic prostate tumors. *J Clin Invest* (2002) 109(3):409–17. doi:10.1172/JCI0214364
159. Ludewig B, Ochsenbein AF, Odermatt B, Paulin D, Hengartner H, Zinkernagel RM. Immunotherapy with dendritic cells directed against tumor antigens shared with normal host cells results in severe autoimmune disease. *J Exp Med* (2000) 191(5):795–804. doi:10.1084/jem.191.5.795
160. Winau F, Weber S, Sad S, de Diego J, Hoops SL, Breiden B, et al. Apoptotic vesicles crossprime CD8 T cells and protect against tuberculosis. *Immunity* (2006) 24(1):105–17. doi:10.1016/j.immuni.2005.12.001
161. Saunderson SC, McLellan AD. Role of lymphocyte subsets in the immune response to primary B cell–derived exosomes. *J Immunol* (2017) 199(7):2225–35. doi:10.4049/jimmunol.1601537
162. Albert ML, Sauter B, Bhardwaj N. Dendritic cells acquire antigen from apoptotic cells and induce class I-restricted CTLs. *Nature* (1998) 392(6671):86–9. doi:10.1038/32183
163. Heusermann W, Hean J, Trojer D, Steib E, von Bueren S, Graff-Meyer A, et al. Exosomes surf on filopodia to enter cells at endocytic hot spots, traffic within endosomes, and are targeted to the ER. *J Cell Biol* (2016) 213(2):173–84. doi:10.1083/jcb.201506084
164. Zitvogel L, Regnault A, Lozier A, Wolfers J, Flament C, Tenza D, et al. Eradication of established murine tumors using a novel cell-free vaccine: dendritic cell derived exosomes. *Nat Med* (1998) 4(5):594–600. doi:10.1038/nm0598-594
165. Srivastava P. Interaction of heat shock proteins with peptides and antigen presenting cells: chaperoning of the innate and adaptive immune responses. *Annu Rev Immunol* (2002) 20:395–425. doi:10.1146/annurev.immunol.20.100301.064801
166. Voll RE, Herrmann M, Roth EA, Stach C, Kalden JR, Girkontaite I. Immunosuppressive effects of apoptotic cells. *Nature* (1997) 390(6658):350–1. doi:10.1038/37022
167. Xie Y, Bai O, Yuan J, Chibbar R, Slattery K, Wei Y, et al. Tumor apoptotic bodies inhibit CTL responses and antitumor immunity via membrane-bound transforming growth factor-β1 inducing CD8+ T-cell anergy and CD4+ Tr1 cell responses. *Cancer Res* (2009) 69(19):7756–66. doi:10.1158/0008-5472.CAN-09-0496
168. Wermeling F, Chen Y, Pikkarainen T, Scheynius A, Winqvist O, Izui S, et al. Class A scavenger receptors regulate tolerance against apoptotic cells, and autoantibodies against these receptors are predictive of systemic lupus. *J Exp Med* (2007) 204(10):2259–65. doi:10.1084/jem.20070600
169. Obeid M, Tesniere A, Ghiringhelli F, Fimia GM, Apetoh L, Perfettini J-L, et al. Calreticulin exposure dictates the immunogenicity of cancer cell death. *Nat Med* (2007) 13(1):54–61. doi:10.1038/nm1523
170. Bellone M, Iezzi G, Rovere P, Galati G, Ronchetti A, Protti MP, et al. Processing of engulfed apoptotic bodies yields T cell epitopes. *J Immunol* (1997) 159(11):5391–9.
171. Apetoh L, Tesniere A, Ghiringhelli F, Kroemer G, Zitvogel L. Molecular interactions between dying tumor cells and the innate immune system determine the efficacy of conventional anticancer therapies. *Cancer Res* (2008) 68(11):4026–30. doi:10.1158/0008-5472.CAN-08-0427
172. Chen H, Tritton TR, Kenny N, Absher M, Chiu JF. Tamoxifen induces TGF-β1 activity and apoptosis of human MCF-7 breast cancer cells in vitro. *J Cell Biochem* (1996) 61(1):9–17. doi:10.1002/(SICI)1097-4644(19960401)61:1<9::AID-JCB2>3.0.CO;2-Z
173. Fadok VA, Bratton DL, Konowal A, Freed PW, Westcott JY, Henson PM. Macrophages that have ingested apoptotic cells in vitro inhibit proinflammatory cytokine production through autocrine/paracrine mechanisms involving TGF-beta, PGE2, and PAF. *J Clin Invest* (1998) 101(4):890. doi:10.1172/JCI1112
174. Huynh M-LN, Fadok VA, Henson PM. Phosphatidylserine-dependent ingestion of apoptotic cells promotes TGF-β1 secretion and the resolution of inflammation. *J Clin Invest* (2002) 109(1):41. doi:10.1172/JCI0211638
175. Sulciner ML, Serhan CN, Gilligan MM, Mudge DK, Chang J, Gartung A, et al. Resolvins suppress tumor growth and enhance cancer therapy. *J Exp Med* (2017) 215(1):115–140. doi:10.1084/jem.20170681
176. Fransen JH, Hilbrands LB, Ruben J, Stoffels M, Adema GJ, van der Vlag J, et al. Mouse dendritic cells matured by ingestion of apoptotic blebs induce T cells to produce interleukin-17. *Arthritis Rheum* (2009) 60(8):2304–13. doi:10.1002/art.24719
177. Ruben JM, van den Ancker W, Bontkes HJ, Westers TM, Hooijberg E, Ossenkoppele GJ, et al. Apoptotic blebs from leukemic cells as a preferred source of tumor-associated antigen for dendritic cell-based vaccines. *Cancer Immunol Immunother* (2014) 63(4):335–45. doi:10.1007/s00262-013-1515-6
178. Hoffmann PR, deCathelineau AM, Ogden CA, Leverrier Y, Bratton DL, Daleke DL, et al. Phosphatidylserine (PS) induces PS receptor-mediated macropinocytosis and promotes clearance of apoptotic cells. *J Cell Biol* (2001) 155(4):649–59. doi:10.1083/jcb.200108080
179. Lim JP, Gleeson PA. Macropinocytosis: an endocytic pathway for internalising large gulps. *Immunol Cell Biol* (2011) 89(8):836–43. doi:10.1038/icb.2011.20
180. Martínez MC, Freyssinet J-M. Deciphering the plasma membrane hallmarks of apoptotic cells: phosphatidylserine transverse redistribution and calcium entry. *BMC Cell Biol* (2001) 2(1):20. doi:10.1186/1471-2121-2-20
181. Balasubramanian K, Chandra J, Schroit AJ. Immune clearance of phosphatidylserine-expressing cells by phagocytes: the role of β2-glycoprotein i in macrophage recognition. *J Biol Chem* (1997) 272(49):31113–7. doi:10.1074/jbc.272.49.31113
182. Scott RS, McMahon EJ, Pop SM, Reap EA, Caricchio R, Cohen PL, et al. Phagocytosis and clearance of apoptotic cells is mediated by MER. *Nature* (2001) 411(6834):207–11. doi:10.1038/35079659
183. Sambrano GR, Steinberg D. Recognition of oxidatively damaged and apoptotic cells by an oxidized low density lipoprotein receptor on mouse peritoneal macrophages: role of membrane phosphatidylserine. *Proc Natl Acad Sci U S A* (1995) 92(5):1396–400. doi:10.1073/pnas.92.5.1396
184. Li MO, Sarkisian MR, Mehal WZ, Rakic P, Flavell RA. Phosphatidylserine receptor is required for clearance of apoptotic cells. *Science* (2003) 302(5650):1560–3. doi:10.1126/science.1087621
185. Oka K, Sawamura T, Kikuta K-I, Itokawa S, Kume N, Kita T, et al. Lectin-like oxidized low-density lipoprotein receptor 1 mediates phagocytosis of aged/apoptotic cells in endothelial cells. *Proc Natl Acad Sci U S A* (1998) 95(16):9535–40. doi:10.1073/pnas.95.16.9535

186. Maiti SN, Balasubramanian K, Ramoth JA, Schroit AJ. β-2-glycoprotein 1-dependent macrophage uptake of apoptotic cells binding to lipoprotein receptor-related protein receptor family members. *J Biol Chem* (2008) 283(7):3761–6. doi:10.1074/jbc.M704990200
187. Borisenko GG, Matsura T, Liu S-X, Tyurin VA, Jianfei J, Serinkan FB, et al. Macrophage recognition of externalized phosphatidylserine and phagocytosis of apoptotic Jurkat cells—existence of a threshold. *Arch Biochem Biophys* (2003) 413(1):41–52. doi:10.1016/S0003-9861(03)00083-3
188. Albert ML, Kim J-I, Birge RB. [alpha]v[beta]5 integrin recruits the CrkII-Dock180-Rac1 complex for phagocytosis of apoptotic cells. *Nat Cell Biol* (2000) 2:899. doi:10.1038/35046549
189. Takizawa F, Tsuji S, Nagasawa S. Enhancement of macrophage phagocytosis upon iC3b deposition on apoptotic cells. *FEBS Lett* (1996) 397(2–3):269–72. doi:10.1016/S0014-5793(96)01197-0
190. Friedl P, Vischer P, Freyberg M. The role of thrombospondin-1 in apoptosis. *Cell Mol Life Sci* (2002) 59(8):1347–57. doi:10.1007/s00018-002-8512-9
191. Teder P, Vandivier RW, Jiang D, Liang J, Cohn L, Puré E, et al. Resolution of lung inflammation by CD44. *Science* (2002) 296(5565):155–8. doi:10.1126/science.1069659
192. Segawa K, Nagata S. An apoptotic "eat me" signal: phosphatidylserine exposure. *Trends Cell Biol* (2015) 25(11):639–50. doi:10.1016/j.tcb.2015.08.003
193. Del Conde I, Shrimpton CN, Thiagarajan P, Lopez JA. Tissue-factor-bearing microvesicles arise from lipid rafts and fuse with activated platelets to initiate coagulation. *Blood* (2005) 106(5):1604–11. doi:10.1182/blood-2004-03-1095
194. Escudier B, Dorval T, Chaput N, André F, Caby M-P, Novault S, et al. Vaccination of metastatic melanoma patients with autologous dendritic cell (DC) derived-exosomes: results of the first phase I clinical trial. *J Transl Med* (2005) 3(1):10. doi:10.1186/1479-5876-3-10
195. Viaud S, Terme M, Flament C, Taieb J, Andre F, Novault S, et al. Dendritic cell-derived exosomes promote natural killer cell activation and proliferation: a role for NKG2D ligands and IL-15Ralpha. *PLoS One* (2009) 4(3):e4942. doi:10.1371/journal.pone.0004942
196. Dai S, Wei D, Wu Z, Zhou X, Wei X, Huang H, et al. Phase I clinical trial of autologous ascites-derived exosomes combined with GM-CSF for colorectal cancer. *Mol Ther* (2008) 16(4):782–90. doi:10.1038/mt.2008.1
197. Besse B, Charrier M, Lapierre V, Dansin E, Lantz O, Planchard D, et al. Dendritic cell-derived exosomes as maintenance immunotherapy after first line chemotherapy in NSCLC. *Oncoimmunology* (2016) 5(4):e1071008. doi:10.1080/2162402X.2015.1071008
198. Kokhaei P, Choudhury A, Mahdian R, Lundin J, Moshfegh A, Osterborg A, et al. Apoptotic tumor cells are superior to tumor cell lysate, and tumor cell RNA in induction of autologous T cell response in B-CLL. *Leukemia* (2004) 18(11):1810–5. doi:10.1038/sj.leu.2403517
199. Carter BA, Jensen RA, Simpson JF, Page DL. Benign transport of breast epithelium into axillary lymph nodes after biopsy. *Am J Clin Pathol* (2000) 113(2):259–65. doi:10.1309/7EF8-F1W7-YVNT-H8H5
200. Van Trappen PO, Pepper MS. Lymphatic dissemination of tumour cells and the formation of micrometastases. *Lancet Oncol* (2002) 3(1):44–52. doi:10.1016/S1470-2045(01)00621-0
201. Murray CA, Leong WL, McCready DR, Ghazarian DM. Histopathological patterns of melanoma metastases in sentinel lymph nodes. *J Clin Pathol* (2004) 57(1):64–7. doi:10.1136/jcp.57.1.64
202. Gray EE, Friend S, Suzuki K, Phan TG, Cyster JG. Subcapsular sinus macrophage fragmentation and CD169+ bleb acquisition by closely associated IL-17-committed innate-like lymphocytes. *PLoS One* (2012) 7(6):e38258. doi:10.1371/journal.pone.0038258
203. Hood JL, San RS, Wickline SA. Exosomes released by melanoma cells prepare sentinel lymph nodes for tumor metastasis. *Cancer Res* (2011) 71(11):3792–801. doi:10.1158/0008-5472.CAN-10-4455
204. Kaplan RN, Rafii S, Lyden D. Preparing the "soil": the premetastatic niche. *Cancer Res* (2006) 66(23):11089–93. doi:10.1158/0008-5472.CAN-06-2407
205. Psaila B, Lyden D. The metastatic niche: adapting the foreign soil. *Nat Rev Cancer* (2009) 9(4):285–93. doi:10.1038/nrc2621
206. Hood JL, Pan H, Lanza GM, Wickline SA. Consortium for translational research in advanced I, nanomedicine. Paracrine induction of endothelium by tumor exosomes. *Lab Invest* (2009) 89(11):1317–28. doi:10.1038/labinvest.2009.94
207. O'Neill ASG, van den Berg TK, Mullen GED. Sialoadhesin – a macrophage-restricted marker of immunoregulation and inflammation. *Immunology* (2013) 138(3):198–207. doi:10.1111/imm.12042
208. Bernhard CA, Ried C, Kochanek S, Brocker T. CD169+ macrophages are sufficient for priming of CTLs with specificities left out by cross-priming dendritic cells. *Proc Natl Acad Sci U S A* (2015) 112(17):5461–6. doi:10.1073/pnas.1423356112
209. Pucci F, Garris C, Lai CP, Newton A, Pfirschke C, Engblom C, et al. SCS macrophages suppress melanoma by restricting tumor-derived vesicle-B cell interactions. *Science* (2016) 352(6282):242–6. doi:10.1126/science.aaf1328
210. Iannacone M, Moseman EA, Tonti E, Bosurgi L, Junt T, Henrickson SE, et al. Subcapsular sinus macrophages prevent CNS invasion on peripheral infection with a neurotropic virus. *Nature* (2010) 465(7301):1079–83. doi:10.1038/nature09118
211. Ravishankar B, Shinde R, Liu H, Chaudhary K, Bradley J, Lemos HP, et al. Marginal zone CD169+ macrophages coordinate apoptotic cell-driven cellular recruitment and tolerance. *Proc Natl Acad Sci U S A* (2014) 111(11):4215–20. doi:10.1073/pnas.1320924111
212. Asano K, Nabeyama A, Miyake Y, Qiu C-H, Kurita A, Tomura M, et al. CD169-Positive macrophages dominate antitumor immunity by crosspresenting dead cell-associated antigens. *Immunity* (2011) 34(1):85–95. doi:10.1016/j.immuni.2010.12.011
213. Chow A, Huggins M, Ahmed J, Hashimoto D, Lucas D, Kunisaki Y, et al. CD169(+) macrophages provide a niche promoting erythropoiesis under homeostasis, myeloablation and in JAK2V617F-induced polycythemia vera. *Nat Med* (2013) 19(4):429–36. doi:10.1038/nm.3057
214. Barral P, Polzella P, Bruckbauer A, van Rooijen N, Besra GS, Cerundolo V, et al. CD169(+) macrophages present lipid antigens to mediate early activation of invariant nkt cells in lymph nodes. *Nat Immunol* (2010) 11(4):303–12. doi:10.1038/ni.1853
215. Junt T, Moseman EA, Iannacone M, Massberg S, Lang PA, Boes M, et al. Subcapsular sinus macrophages in lymph nodes clear lymph-borne viruses and present them to antiviral B cells. *Nature* (2007) 450(7166):110–4. doi:10.1038/nature06287
216. Kawasaki N, Vela JL, Nycholat CM, Rademacher C, Khurana A, van Rooijen N, et al. Targeted delivery of lipid antigen to macrophages via the CD169/sialoadhesin endocytic pathway induces robust invariant natural killer T cell activation. *Proc Natl Acad Sci U S A* (2013) 110(19):7826–31. doi:10.1073/pnas.1219888110
217. Muhsin-Sharafaldine MR, Saunderson SC, Dunn AC, McLellan AD. Melanoma growth and lymph node metastasis is independent of host CD169 expression. *Biochem Biophys Res Commun* (2017) 486(4):965–70. doi:10.1016/j.bbrc.2017.03.138
218. Mackman N. Triggers, targets and treatments for thrombosis. *Nature* (2008) 451(7181):914–8. doi:10.1038/nature06797
219. Rosendaal FR. Venous thrombosis: a multicausal disease. *Lancet* (1999) 353(9159):1167–73. doi:10.1016/S0140-6736(98)10266-0
220. Khorana AA, Francis CW, Culakova E, Kuderer NM, Lyman GH. Thromboembolism is a leading cause of death in cancer patients receiving outpatient chemotherapy. *J Thromb Haemost* (2007) 5(3):632–4. doi:10.1111/j.1538-7836.2007.02374.x
221. Ornstein DL, Zacharski LR. Cancer, thrombosis, and anticoagulants. *Curr Opin Pulm Med* (2000) 6(4):301–8. doi:10.1097/00063198-200007000-00009
222. Heit JA, Silverstein MD, Mohr DN, Petterson TM, O'Fallon WM, Melton LJ III. Risk factors for deep vein thrombosis and pulmonary embolism: a population-based case-control study. *Arch Intern Med* (2000) 160(6):809–15. doi:10.1001/archinte.160.6.809
223. Ashrani AA, Rajkumar SV. Chemotherapy-associated thrombosis. *Cancer Treat Res* (2009) 148:181–206. doi:10.1007/978-0-387-79962-9_11
224. Haddad TC, Greeno EW. Chemotherapy-induced thrombosis. *Thromb Res* (2006) 118(5):555–68. doi:10.1016/j.thromres.2005.10.015
225. Mannucci PM, Bettega DD, Chantarangkul VV, Tripodi AA, Sacchini VV, Veronesi UU. Effect of tamoxifen on measurements of hemostasis in healthy women. *Arch Intern Med* (1996) 156(16):1806–10. doi:10.1001/archinte.1996.00440150056006
226. Pemberton K, Melissari E, Kakkar V. The influence of tamoxifen in vivo on the main natural anticoagulants and fibrinolysis. *Blood Coagul Fibrinolysis* (1993) 4(6):935–42. doi:10.1097/00001721-199312000-00011

227. Verso M, Agnelli G, Barni S, Gasparini G, LaBianca R. A modified Khorana risk assessment score for venous thromboembolism in cancer patients receiving chemotherapy: the Protecht score. *Intern Emerg Med* (2012) 7(3):291–2. doi:10.1007/s11739-012-0784-y
228. Roselli M, Ferroni P, Riondino S, Mariotti S, Laudisi A, Vergati M, et al. Impact of chemotherapy on activated protein C-dependent thrombin generation–association with VTE occurrence. *Int J Cancer* (2013) 133(5):1253–8. doi:10.1002/ijc.28104
229. Rajkumar SV, Blood E, Vesole D, Fonseca R, Greipp PR; Eastern Cooperative Oncology Group. Phase III clinical trial of thalidomide plus dexamethasone compared with dexamethasone alone in newly diagnosed multiple myeloma: a clinical trial coordinated by the eastern cooperative oncology group. *J Clin Oncol* (2006) 24(3):431–6. doi:10.1200/JCO.2005.03.0221
230. Rajkumar SV, Hayman S, Gertz MA, Dispenzieri A, Lacy MQ, Greipp PR, et al. Combination therapy with thalidomide plus dexamethasone for newly diagnosed myeloma. *J Clin Oncol* (2002) 20(21):4319–23. doi:10.1200/JCO.2002.02.116
231. Sørensen HT, Mellemkjaer L, Olsen JH, Baron JA. Prognosis of cancers associated with venous thromboembolism. *N Engl J Med* (2000) 343(25):1846–50. doi:10.1056/NEJM200012213432504
232. Dvorak HF, Quay SC, Orenstein NS, Dvorak AM, Hahn P, Bitzer AM, et al. Tumor shedding and coagulation. *Science* (1981) 212(4497):923–4. doi:10.1126/science.7195067
233. Date K, Hall J, Greenman J, Maraveyas A, Madden LA. Tumour and microparticle tissue factor expression and cancer thrombosis. *Thromb Res* (2013) 131(2):109–15. doi:10.1016/j.thromres.2012.11.013
234. van den Berg YW, Osanto S, Reitsma PH, Versteeg HH. The relationship between tissue factor and cancer progression: insights from bench and bedside. *Blood* (2012) 119(4):924–32. doi:10.1182/blood-2011-06-317685
235. Mueller BM, Reisfeld RA, Edgington TS, Ruf W. Expression of tissue factor by melanoma cells promotes efficient hematogenous metastasis. *Proc Natl Acad Sci U S A* (1992) 89(24):11832–6. doi:10.1073/pnas.89.24.11832
236. Geddings JE, Mackman N. Tumor-derived tissue factor-positive microparticles and venous thrombosis in cancer patients. *Blood* (2013) 122(11):1873–80. doi:10.1182/blood-2013-04-460139
237. Rickles FR, Patierno S, Fernandez PM. Tissue factor, thrombin, and cancer. *Chest* (2003) 124(3 Suppl):58S–68S. doi:10.1378/chest.124.3_suppl.58S
238. Ueno T, Toi M, Koike M, Nakamura S, Tominaga T. Tissue factor expression in breast cancer tissues: its correlation with prognosis and plasma concentration. *Br J Cancer* (2000) 83:164. doi:10.1054/bjoc.2000.1272
239. van den Berg YW, van den Hengel LG, Myers HR, Ayachi O, Jordanova E, Ruf W, et al. Alternatively spliced tissue factor induces angiogenesis through integrin ligation. *Proc Natl Acad Sci U S A* (2009) 106(46):19497–502. doi:10.1073/pnas.0905325106
240. Hobbs JE, Zakarija A, Cundiff DL, Doll JA, Hymen E, Cornwell M, et al. Alternatively spliced human tissue factor promotes tumor growth and angiogenesis in a pancreatic cancer tumor model. *Thromb Res* (2007) 120(Suppl 2):S13–21. doi:10.1016/S0049-3848(07)70126-3
241. Bromberg ME, Konigsberg WH, Madison JF, Pawashe A, Garen A. Tissue factor promotes melanoma metastasis by a pathway independent of blood coagulation. *Proc Natl Acad Sci U S A* (1995) 92(18):8205–9. doi:10.1073/pnas.92.18.8205
242. Lechner D, Weltermann A. Chemotherapy-induced thrombosis: a role for microparticles and tissue factor? *Semin Thromb Hemost* (2008) 34(2):199–203. doi:10.1055/s-2008-1079261
243. Tesselaar MET, Romijn FPHTM, Van Der Linden IK, Bertina RM, Osanto S. Microparticle-associated tissue factor activity in cancer patients with and without thrombosis. *J Thromb Haemost* (2009) 7(8):1421–3. doi:10.1111/j.1538-7836.2009.03504.x
244. Zwicker JI, Liebman HA, Neuberg D, Lacroix R, Bauer KA, Furie BC, et al. Tumor-derived tissue factor–bearing microparticles are associated with venous thromboembolic events in malignancy. *Clin Cancer Res* (2009) 15(22):6830–40. doi:10.1158/1078-0432.CCR-09-0371
245. Thaler J, Ay C, Weinstabl H, Dunkler D, Simanek R, Vormittag R, et al. Circulating procoagulant microparticles in cancer patients. *Ann Hematol* (2011) 90(4):447–53. doi:10.1007/s00277-010-1111-1
246. Echrish H, Madden L, Greenman J, Maraveyas A. PO-84 expression of tissue factor (TF) and growth factor receptors on pancreatic cell lines: correlation with TF activity and cell invasion. *Thromb Res* (2010) 125:S188–9. doi:10.1016/S0049-3848(10)70134-1
247. Davila M, Amirkhosravi A, Coll E, Desai H, Robles L, Colon J, et al. Tissue factor-bearing microparticles derived from tumor cells: impact on coagulation activation. *J Thromb Haemost* (2008) 6(9):1517–24. doi:10.1111/j.1538-7836.2008.02987.x
248. Blom JW, Vanderschoot JP, Oostindier MJ, Osanto S, van der Meer FJ, Rosendaal FR. Incidence of venous thrombosis in a large cohort of 66,329 cancer patients: results of a record linkage study. *J Thromb Haemost* (2006) 4(3):529–35. doi:10.1111/j.1538-7836.2006.01804.x
249. Huang H, Korn JR, Mallick R, Friedman M, Nichols C, Menzin J. Incidence of venous thromboembolism among chemotherapy-treated patients with lung cancer and its association with mortality: a retrospective database study. *J Thromb Thrombolysis* (2012) 34(4):446–56. doi:10.1007/s11239-012-0741-7
250. Darmoul D, Marie J, Devaud H, Gratio V, Laburthe M. Initiation of human colon cancer cell proliferation by trypsin acting at protease-activated receptor-2. *Br J Cancer* (2001) 85(5):772–9. doi:10.1054/bjoc.2001.1976
251. Massi D, Naldini A, Ardinghi C, Carraro F, Franchi A, Paglierani M, et al. Expression of protease-activated receptors 1 and 2 in melanocytic nevi and malignant melanoma. *Hum Pathol* (2005) 36(6):676–85. doi:10.1016/j.humpath.2005.04.008
252. Ge L, Shenoy SK, Lefkowitz RJ, DeFea K. Constitutive protease-activated receptor-2-mediated migration of MDA MB-231 breast cancer cells requires both β-arrestin-1 and-2. *J Biol Chem* (2004) 279(53):55419–24. doi:10.1074/jbc.M410312200
253. Bromberg ME, Sundaram R, Homer RJ, Garen A, Konigsberg WH. Role of tissue factor in metastasis: functions of the cytoplasmic and extracellular domains of the molecule. *Thromb Haemost* (1999) 82(1):88–92. doi:10.1055/s-0037-1614634
254. Hembrough TA, Swartz GM, Papathanassiu A, Vlasuk GP, Rote WE, Green SJ, et al. Tissue factor/factor VIIa inhibitors block angiogenesis and tumor growth through a nonhemostatic mechanism. *Cancer Res* (2003) 63(11):2997–3000.
255. Sorensen BB, Rao LV, Tornehave D, Gammeltoft S, Petersen LC. Antiapoptotic effect of coagulation factor VIIa. *Blood* (2003) 102(5):1708–15. doi:10.1182/blood-2003-01-0157
256. Ott I, Fischer EG, Miyagi Y, Mueller BM, Ruf W. A role for tissue factor in cell adhesion and migration mediated by interaction with actin-binding protein 280. *J Cell Biol* (1998) 140(5):1241–53. doi:10.1083/jcb.140.5.1241

Conflict of Interest Statement: The authors declare that the research was conducted in the absence of any commercial or financial relationships that could be construed as a potential conflict of interest.

The reviewer RX and handling Editor declared their shared affiliation.

frontiers in Immunology

MINI REVIEW
published: 28 June 2018
doi: 10.3389/fimmu.2018.01486

Apoptotic Cell-Derived Extracellular Vesicles: More Than Just Debris

*Sarah Caruso and Ivan K. H. Poon**

Department of Biochemistry and Genetics, La Trobe Institute for Molecular Science, La Trobe University, Melbourne, VIC, Australia

The many functions of extracellular vesicles (EVs) like exosomes and microvesicles released from healthy cells have been well characterized, particularly in relation to their roles in immune modulation. Apoptotic bodies, a major class of EV released as a product of apoptotic cell disassembly, and other types of EVs released from dying cells are also becoming recognized as key players in this emerging field. There is now increasing evidence to suggest that EVs produced during apoptosis have important immune regulatory roles, a concept relevant across different disease settings including autoimmunity, cancer, and infection. Therefore, this review focuses on how the formation of EVs during apoptosis could be a key mechanism of immune modulation by dying cells.

OPEN ACCESS

Edited by:
Luis Graca,
Universidade de Lisboa, Portugal

Reviewed by:
Jeffrey Louis Curtis,
University of Michigan, United States
Bruce Milne Hall,
University of New South Wales, Australia

***Correspondence:**
Ivan K. H. Poon
i.poon@latrobe.edu.au

Specialty section:
This article was submitted to Immunological Tolerance and Regulation, a section of the journal Frontiers in Immunology

Received: *28 February 2018*
Accepted: *14 June 2018*
Published: *28 June 2018*

Citation:
Caruso S and Poon IKH (2018) Apoptotic Cell-Derived Extracellular Vesicles: More Than Just Debris. Front. Immunol. 9:1486. doi: 10.3389/fimmu.2018.01486

Keywords: apoptotic bodies, apoptotic microvesicles, extracellular vesicles, immunomodulation, apoptosis

IMMUNE REGULATION BY EXTRACELLULAR VESICLES (EVs)

There are three main types of EVs formed by a cell, namely exosomes, microvesicles, and apoptotic bodies (ApoBDs). These three types of EVs vary in size, content, and mechanism of formation (**Figure 1**) (1). To date, exosomes and microvesicles generated from healthy cells are more extensively characterized and the formation of these EVs is key in mediating intercellular communication and immune regulation. Exosomes and microvesicles have been shown to play an important role in processes including antigen presentation, immune suppression, antitumor immunity, and autoimmunity. This has been the subject of many reviews, highlighting how EVs modulate immune responses by a myriad of mechanisms (2–5). Of particular interest is how the contents of exosomes and microvesicles enable them to regulate immune cell functions. Notably, these EVs can exhibit immune activating or immune suppressing properties depending on the specific circumstances. For example, exosomes have been shown to either activate or dampen the overall cytokine response through regulation of gene expression in monocytes and release of soluble cytokine receptors, respectively (6, 7). Exosomes derived from dendritic cells, B lymphocytes, and tumor cells have also been shown to regulate immunological memory through the surface expression of antigen-presenting MHC I and MHC II molecules, and subsequently eliciting T cell activation and maturation (8–12). Exosomes can also play a role in cross-presentation pathways and have been shown to promote dendritic cell activation and maturation (12). Furthermore, microvesicles can modulate immune responses by transporting cytokines such as IL-1β (13) and proinflammatory microRNAs (14).

Both exosomes and microvesicles are generally described as EVs released from healthy cells, however, dying cells can also release a variety of EVs, broadly known as apoptotic cell-derived EVs (ApoEVs) (**Figure 1**) (1, 15, 16). Subtypes of ApoEVs include large membrane-bound vesicles like ApoBDs (15, 17) or smaller apoptotic microvesicles (ApoMVs) (18, 19), both of which are described in detail below. While it has been well established that EVs can exhibit immunomodulatory effects, most studies have focused on EVs released from healthy cells, with EVs released from dying cells largely understudied. Nevertheless, a number of studies have suggested that ApoEVs have similar

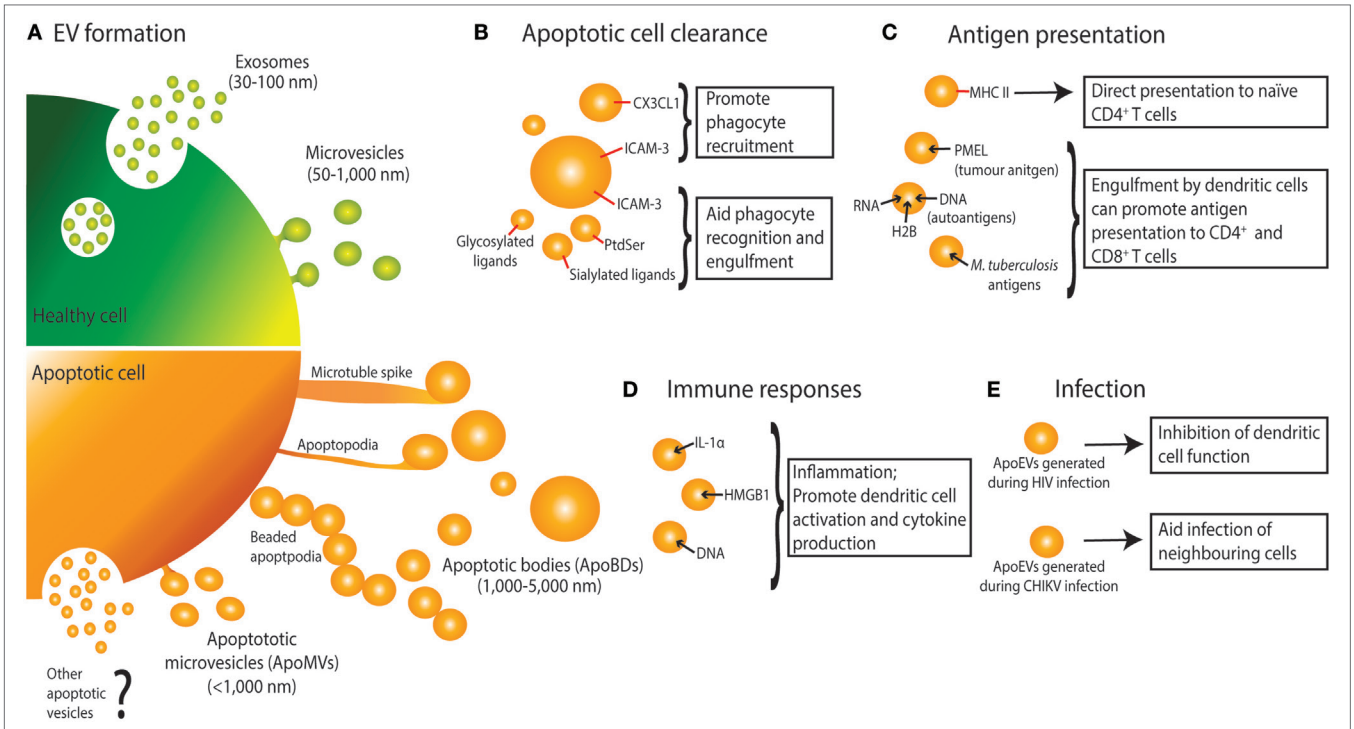

FIGURE 1 | Extracellular vesicle (EV) formation and immune functions of apoptotic cell-derived EVs (ApoEVs). **(A)** Healthy cells form two main types of EV, namely exosomes that are release *via* exocytosis of multivesicular bodies, and microvesicles that are shed from the plasma membrane. During apoptosis, dying cells can also release ApoEVs. Apoptotic cells can undergo morphological changes including membrane blebbing, thin membrane protrusion formation (microtubule spikes, apoptopodia, and beaded-apoptopodia), and generation of distinct apoptotic bodies (ApoBDs). Apoptotic cells can also release EVs that are similar in size as microvesicles (ApoMVs), however, it is unclear if ApoMVs are generated *via* the same mechanism as microvesicles from healthy cells. Whether apoptotic cells can generate vesicles that are similar to exosomes is undetermined. **(B)** ApoEVs can harbor "find-me" signals (e.g., CX3CL1 and ICAM-3) to attract phagocytic cells, as well as "eat-me" signals [e.g., ICAM-3, phosphatidylserine (PtdSer), and sialylated and glycosylated ligands] to promote uptake by phagocytes. **(C)** ApoEVs have MHC II molecules on their surface, which is essential for direct antigen presentation to naïve $CD4^+$ T cells and activation of immunological memory. ApoEVs can also carry antigen to professional antigen-presenting cells (e.g., dendritic cells). Antigens carried by ApoEVs include autoantigens, tumor antigens, and microbial antigens. **(D)** ApoEVs can promote inflammation by transporting proinflammatory cytokines such as IL-1α and damage-associated molecular patterns including DNA and HMGB1. **(E)** ApoEVs can aid HIV infection by inhibiting dendritic cell activation. Chikungunya virus (CHIKV) can hijack ApoEVs to propagate infection to neighboring cells.

functional importance as EVs released from healthy cells. ApoEV formation has two key proposed functions: (a) aiding apoptotic cell clearance and (b) means of intercellular communication, both of which have implications in immune regulation. Many cells in the body are constantly undergoing apoptosis, and while a large portion of these are healthy cells undergoing normal turnover, apoptosis also occurs in many immunological and disease settings including inflammation, infection, autoimmunity, and cancer (20–23). Here, we discuss how ApoEVs may act as an immunomodulatory mechanism for apoptotic cells.

GENERATION OF EVs DURING APOPTOSIS

As first described by Kerr et al., during apoptosis a cell undergoes a series of morphological changes resulting in the dismantling of the dying cell (17). Recently, disassembly of the apoptotic cell is categorized into three distinct morphological steps, namely apoptotic membrane blebbing, thin membrane protrusion formation, and ultimately generation of ApoBDs that are generally defined as 1–5 μm in diameter (15, 17) (**Figure 1**). While less is known about the mechanisms driving the formation of ApoBDs compared to other types of EVs, recent studies suggest that it is a highly regulated process and has been reviewed in detail (15, 16, 24). Besides ApoBDs, cells can also release smaller EVs such as ApoMVs (<1 μm in diameter) during the progression of apoptosis, possibly through membrane budding (18, 19, 25, 26). However, molecular regulators of ApoMVs formation are not well defined.

It is important to note that in the literature there are striking discrepancies in the characterization and isolation of ApoEVs (27, 28). Aside from size, currently there are no well-defined criteria to distinguish ApoBDs from other ApoEVs, in particular ApoMVs. Although proteomic studies comparing these ApoEV subtypes have been performed (25, 26), clear standard for the characterization and purification of ApoEV subtypes is lacking (highlighted in **Table 1**). These discrepancies make it difficult to draw accurate conclusions regarding the functions of ApoEVs and caution should be taken when interpreting data involving ApoEVs. Taking these limitations into consideration, here we use

TABLE 1 | Variation in nomenclature and isolation/characterization methods in articles describing the immunomodulatory properties of ApoEVs.

Author and year	Reference	Nomenclature used by the authors	Summary of main findings	Isolation/characterization method	ApoEV subtype (ApoBDs, ApoMVs, or unclear[a])
Segundo et al. (1999)	(39)	Apoptotic blebs	Cell-depleted supernatant from apoptotic B cells stimulated macrophage chemotaxis. When the supernatant was passed through a 0.1 μm filter this effect was lost, suggesting larger vesicles are responsible for the observed effect	Centrifugation at 300 *g* to remove cells, followed by 100,000 *g* spin to collect vesicles. Purity of cell-depleted supernatant validated by microscopy	Mix of ApoMVs and ApoBDs
Thery et al. (2001)	(25)	ApoMVs	Proteomics analysis of exosomes and apoptotic vesicles was performed and showed differential enrichment of proteins between each vesicle type. Total vesicle number increased in the apoptotic samples	Isolation of ApoEVs by differential centrifugation (300, 1,200, 10,000, and 110,000 *g*). Vesicles were further characterized by flow cytometry and exposure of surface PtdSer monitored	Mix of ApoBDs and ApoMVs
Schaible et al. (2003)	(57)	Apoptotic vesicles	Apoptotic vesicles from tuberculosis-infected macrophages transferred bacterial antigen to dendritic cells. After engulfment of these apoptotic vesicles, dendritic cells could then crossprime $CD8^+$ T cells	Isolation of ApoEVs by differential centrifugation (800, 1,800, 25,000, and 100,000 *g*). Size of vesicles used not described	Unclear
Distler et al. (2005)	(43)	Microparticles	Engulfment of ApoEVs by macrophages induced macrophage apoptosis and the release of microparticles	Centrifugation at 1,500 *g* to remove cells, followed by 100,000 *g* spin to collect vesicles. Vesicles further characterized by flow cytometry	Mix of ApoMVs and ApoBDs
Winau et al. (2006)	(58)	Apoptotic vesicles	Vaccination with apoptotic vesicles protected mice against tuberculosis infection	Isolation of ApoEVs by differential centrifugation (800, 1,800, 25,000, and 100,000 *g*). Size of vesicles validated by EM (approximately 500 nm)	Unclear, likely ApoMVs
Schiller et al. (2008)	(53)	ApoBDs	Autoantigens such as H2B and DNA, RNA were distributed into ApoBDs from lymphoblasts, which were subsequently engulfed by monocyte-derived phagocytes. Lymphoblasts showed an increase in vesicle formation during apoptosis	Centrifugation at 300 *g* to remove cells, and the supernatant passed through a 1.2 μm filter, followed by 100,000 *g* spin to collect vesicle. Large ApoBDs may be excluded. Vesicle size determined by EM (approximate 500 nm)	Mix of ApoMVs and some ApoBDs
Truman et al. (2008)	(37)	Apoptotic microparticles	CX3CL1/fractalkine released as vesicle-associated signal from apoptotic B lymphocytes	Cell-free supernatant was used (procedure not described). Vesicles were further characterized by flow cytometry and exposure of surface PtdSer monitored	Unclear
Fransen et al. (2009)	(36)	Apoptotic blebs	Apoptotic blebs were engulfed more efficiently than apoptotic cells by dendritic cells. Only the blebs but not the apoptotic cells induced dendritic cell maturation and IL-6 release	Apoptotic cells were centrifuged at 1,550 *g* (this pellet is likely to contain large ApoBDs). Supernatant were centrifuged at 15,700 *g* to isolate "apoptotic blebs." No vesicle size validation described	Mix of ApoMVs and ApoBDs
Reich and Pisetsky (2009)	(52)	Microparticles	Microparticles contained DNA and RNA that antibodies could access	Centrifugation at 400 *g* to remove cells, and the supernatant passed through a 1.2 μm filter. Small ApoBDs may be included. No vesicle size validation described	Mix of ApoMVs and some ApoBDs
Berda-Haddad et al. (2011)	(42)	ApoBDs, microparticles	ApoBDs but not microparticles contained IL-1α and induced neutrophil infiltration *in vivo*	Centrifugation at 300 *g* to remove apoptotic cells, followed by 4,500 and 75,000 *g* spin to collect vesicles. Apoptotic supernatant was analyzed by flow cytometry, and different sized beads were used to identify 1–3 μm events (ApoBDs) and 0.5–1 μm events (microparticles)	ApoBDs and ApoMVs
Krejbich-Trotot et al. (2011)	(71)	Apoptotic blebs	Infection of HeLa cells with Chikungunya virus induced apoptosis and infection of neighboring cells. Blocking blebbing and apoptotic bleb formation decreased infection of neighboring cells	Analyzed vesicle function using inhibitors of membrane blebbing (ROCK1 inhibitors and actin polymerization inhibitors). Vesicle size not determined	ApoBDs, possibly ApoMVs
Bilyy et al. (2012)	(50)	Subcellular membranous particle (scMP)	Glycosylated ligands were detected on the surface of scMP, which acted as an "eat-me" signal for macrophages	Procedure for isolating scMP and vesicle size validation not described. scMP population monitored by flow cytometry	Unclear

(*Continued*)

TABLE 1 | Continued

Author and year	Reference	Nomenclature used by the authors	Summary of main findings	Isolation/characterization method	ApoEV subtype (ApoBDs, ApoMVs, or unclear[a])
Farinacci et al. (2012)	(56)	Apoptotic vesicles	Apoptotic vesicles from tuberculosis-infected macrophages activated dendritic cells following engulfment and subsequently primed $CD4^+$ and $CD8^+$ T cells	Isolation of ApoEVs by differential centrifugation (800, 1,800, 25,000, and 100,000 *g*). Vesicle size determined by EM (40–250 nm)	ApoMVs
Frleta et al. (2012)	(70)	Apoptotic microparticles	HIV infection induced the production of apoptotic microparticles that could suppress the ability of dendritic cells to prime CD8 T cells	Centrifugation at 400 *g* to remove cells, and the supernatant ultracentrifuged at 100,000 *g*. Vesicles were further characterized by flow cytometry and exposure of surface PtdSer monitored. Vesicle size determined by EM (0.1–1 μm)	ApoMVs and possibly some ApoBDs
Schiller et al. (2012)	(19)	Apoptotic cell-derived membrane microparticles (AdMPs)	Apoptotic microparticles stimulated dose-dependent IFN-α production from plasmacytoid dendritic cells, whereas supernatants from viable or necrotic cells had no effects	Centrifugation at 500 *g* to remove cells, and the supernatant passed through a 1.2 μm filter followed by 100,000 *g* spin to collect vesicles. Small ApoBDs may be included. Vesicles further characterized by flow cytometry	Mix of ApoMVs and some ApoBDs
Torr et al. (2012)	(40)	Apoptotic microparticles	ICAM-3 was lost from the surface of apoptotic cells with the formation of ICAM-3-associated apoptotic microparticles. These vesicles promoted macrophage recruitment, while vesicles from ICAM-3 deficient cells were less effective	Centrifugation at 350 *g* to remove apoptotic cells, and the supernatant was used. Vesicle size determined by dynamic light scattering (average 200 nm in diameter, much smaller than expected based on the isolation procedure)	Mix of ApoMVs and ApoBDs
Fehr et al. (2013)	(63)	Apoptotic cell-derived membrane vesicles, apoptotic blebs	Apoptotic blebs increased expression of dendritic cell activation markers, but decreased MHC II on dendritic cells. Apoptotic blebs-treated dendritic cells failed to induce T cell proliferation	Centrifugation at 500 *g* to remove cells, and the supernatant passed through a 1.2 μm filter. Small ApoBDs may be included. Vesicles further characterized by flow cytometry	Mix of ApoMVs and some ApoBDs
Schiller et al. (2013)	(69)	Apoptotic cell-derived membraneous vesicles (ACMVs)	HMGB1 detected in vesicles generated during apoptosis	Centrifugation at 500 *g* to remove cells, and the supernatant passed through a 1.2 μm filter followed by 100,000 *g* spin to collect vesicles. Small ApoBDs may be included. Vesicles further characterized by flow cytometry	Mix of ApoMVs and some ApoBDs
Eguchi et al. (2015)	(41)	Microparticles	Adipocyte microparticles promoted monocyte chemotaxis both *in vitro* and *in vivo*	The supernatant following centrifugation at 2,000 *g* was used. Exposure of surface PtdSer on vesicles monitored by flow cytometry	Mix of ApoMVs and ApoBDs
Niessen et al. (2015)	(44)	AdMPs	Uptake of apoptotic microparticles by macrophages promoted the release of proinflammatory cytokines IL-6, IL-8, and TNFα	Centrifugation at 500 *g* to remove cells, and the supernatant passed through a 1.2 μm filter followed by 100,000 *g* spin. Small ApoBDs may be included. Size of vesicles used not described	Mix of ApoMVs and some ApoBDs
Zirngibl et al. (2015)	(54)	ACMVs	Autoantigen histone H2B was shown to be loaded into apoptotic vesicles in a cytoskeleton-dependent manner	Monitored apoptotic vesicles by microscopy and classified into small (<1 μm), medium (1–3 μm), or large (>3 μm) vesicles	N/A
Black et al. (2016)	(51)	Apoptotic vesicles	CD169 (macrophage adhesin molecule) on apoptotic vesicles suppressed dendritic cell-mediated cytotoxic T cell response	Isolation of ApoEVs by differential centrifugation (25,000 *g* pellet). Sucrose gradient was used to separate ApoEVs from non-apoptotic material (only used fractions with β-actin). Vesicle size determined by CryoEM (35–814 nm)	ApoMVs
Muhsin-Sharafaldine et al. (2016)	(66)	Apoptotic vesicles, MVs	Apoptotic vesicles were able to activate naïve T cells and stimulate immunological memory *via* vesicle-associated MHC/antigen complex	Centrifugation at 450 and 3,200 *g* to remove cells, followed by a 25,000 *g* spin. Sucrose gradient was used to separate ApoEVs, microparticles, and exosomes. Vesicle size determined by CryoEM and dynamic light scattering (103–816 nm)	ApoMVs

(*Continued*)

TABLE 1 | Continued

Author and year	Reference	Nomenclature used by the authors	Summary of main findings	Isolation/characterization method	ApoEV subtype (ApoBDs, ApoMVs, or unclear[a])
Sisirak et al. (2016)	(64)	Apoptotic microparticles	DNA contained in apoptotic microparticles was shown to be antigenic when not digested by DNase1L3 and could contribute to an SLE-like condition	Centrifugation at 1,500 rpm to remove cells, followed by 22,000 *g* spin to collect vesicles from apoptotic cells generated *in vitro*. Centrifugation at 2,000 *g* to remove cells, followed by 22,000 *g* spin to collect vesicles from plasma. Vesicles further characterized by flow cytometry and exposure of surface PtdSer monitored	Mix of ApoBDs and ApoMVs
Ainola et al. (2017)	(18)	ApoBDs, apoptotic particles, apoptotic microparticles	Noted an increase in vesicles formation (ApoBDs and microparticles) when HeLa cells were exposed to apoptotic stimuli. These vesicles mediated autoantigen transfer to plasmacytoid dendritic cells, resulting in proinflammatory cytokine production. Highlighted differences between subtypes of vesicles generated during apoptosis	Isolation of ApoEVs by differential centrifugation at 357 *g* (cell pellet), 1,400 *g* (ApoBDs), 16,000 *g* (ApoBDs and microvesicles), and 100,000 *g* (microvesicles). ApoEVs were further characterized by flow cytometry, ApoBDs (1–4 μm), and ApoMVs (0.1–1 μm), based on sizing beads. Authors commented on size overlap and how complete separation is not possible	ApoBDs, ApoMVs, mix of ApoBDs and ApoMVs
Tucher et al. (2018)	(26)	Apoptotic cell-released large EVs and small EVs	Noted an increase in large EVs (200–1,000 nm) being released from T cells following the induction of apoptosis. Performed proteomic analysis on different EV subsets and identified several proteins that may be specific to T cell ApoEVs	Centrifugation at 300 *g* to remove cells, supernatant passed through a 1.2 μm filter. Further centrifugation at 10,000 *g* to pellet large EVs followed by 100,000 *g* to pellet small EVs. Vesicle size distribution determined by nanoparticle tracking analysis	Mix of ApoMVs and some ApoBDs

[a]*Where there was no indication from the purification procedure if the ApoEVs used were ApoMVs (50–1,000 nm) or ApoBDs (1,000–5,000 nm).*

ApoMVs, apoptotic microvesicles; ApoBDs, apoptotic bodies; ApoEVs, apoptotic cell-derived EVs; PtdSer, phosphatidylserine; EVs, extracellular vesicles; SLE, systemic lupus erythematous.

the general term ApoEVs where it is unclear which subtype of ApoEVs is presented in a given study, and ApoBDs and ApoMVs to describe vesicles predominantly >1–5 μm and <1 μm in diameter, respectively.

ApoEVs AID REMOVAL OF DYING CELLS

It has been well established that apoptotic cells coordinate a number of intercellular signals to aid in their detection and removal, and these signals are critical to ensure the immunologically silent characteristic of apoptosis (22, 29). Defective apoptotic cell clearance has been identified as a key contributing factor to autoimmune disease, whereby cells that are unable to be cleared efficiently eventually undergo secondary necrosis and release potentially damaging proinflammatory contents and autoantigens (30–32). There has been mounting evidence suggesting that the release of ApoEVs during apoptosis can promote clearance of apoptotic material, with the mechanism underpinning this process discussed below (33–36).

"Find-Me" Signals in Association With ApoEVs

For efficient apoptotic cell clearance, the recruitment of phagocytic cells toward the site of cell death is essential. To this end, apoptotic cells can release molecular factors known as "find-me" signals to attract phagocytes. Traditional "find-me" signals include the release soluble factors such as ATP, UTP, CX3CL1/fractalkine, and lysophosphatidylcholine (21, 22, 37, 38). However, there is also evidence of ApoEV-associated "find-me" signals being released from apoptotic cells.

While few studies elucidated the specific molecules involved in ApoEV-mediated recruitment of phagocytes, they have demonstrated ApoEVs to exhibit chemoattractive properties (39–41). Nevertheless, the "find-me" signal CX3CL1/fractalkine was found to be released from apoptotic B lymphocytes in association with ApoMVs (37) and the chemoattractive molecule ICAM-3 was associated with ApoEVs generated from apoptotic lymphoma cells (40). It is interesting to note that ApoEVs appear to have preferential recruitment of macrophages but not neutrophils (41). Such selective recruitment of different phagocytes by ApoEVs may be related to the subtype of ApoEVs being released by the apoptotic cell, in which one study comparing endothelial cell-derived ApoEVs of different size showed that only larger ApoEVs (1–3 μm in diameter, corresponding to ApoBDs) promoted neutrophil migration, whereas smaller EVs (<1 μm, corresponding to ApoMVs) could not (42). It is worth noting that this phenomenon has been observed *in vitro* as well as *in vivo*, where intraperitoneal administration of ApoBDs in a mouse model stimulated neutrophil infiltration (42). Thus, different subtype of ApoEVs may have distinct functions in apoptotic cell clearance.

ApoEV Formation Promotes Engulfment

Besides attracting phagocytes, formation of ApoEVs, in particular cell fragmentation into ApoBDs has been suggested to enhance removal of apoptotic material, an effect probably attributed to

the size of ApoBDs being smaller bite-size pieces that can easily be engulfed by phagocytes. Supporting this concept, it has been shown that dendritic cells can more readily engulf smaller ApoBDs than whole apoptotic cells (16, 36). Furthermore, cells undergoing apoptotic cell disassembly and therefore producing ApoEVs are more efficiently engulfed by macrophages (33, 43, 44).

It should be noted that exposure of "eat-me" signals, such as phosphatidylserine (PtdSer), on apoptotic cells label them for clearance by phagocytes (22, 45). Likewise, ApoEVs can also expose "eat-me" signals like PtdSer on their surface and be recognized by macrophages for removal *via* phagocytic receptors such as CD36 (43, 46–49). Interestingly, ApoEVs can also expose ICAM-3, and specific sialylated and glycosylated ligands on its surface to trigger recognition and engulfment by macrophages (40, 50, 51).

ApoEVs AS KEY REGULATORS OF ANTIGEN PRESENTATION

An important immunomodulatory property of EVs is their ability to aid antigen presentation, a fundamental process for adaptive immunity. As mentioned above, EVs like exosomes have been shown to mediate antigen presentation *via* direct and cross-presentation mechanisms (8–12). Similarly, ApoEVs can also regulate antigen presentation *via* these mechanisms in a number of disease settings including autoimmunity (18, 52–54), antimicrobial immune responses (55–58), and organ/transplant rejection (59). Direct antigen presentation involves the vesicle carrying surface MHC molecules in complex with antigenic peptide to directly interact with naïve T cells (60). ApoEVs generated from dendritic cells and B16-F1 melanoma cells carried MHC II molecules suggesting the potential of ApoEVs to activate $CD4^+$ T cells (61). Alternatively, cross-presentation relies on the vesicle transporting the antigen to professional antigen-presenting cells, in particular dendritic cells, for antigen processing and presentation to $CD8^+$ T cells (62). In one study, ApoEVs generated from *Mycobacterium tuberculosis*-infected mouse macrophages were found to transfer bacterial-derived antigens to dendritic cells, and subsequently activate naïve $CD8^+$ T cells (57). Furthermore, engulfment of ApoEVs by dendritic cells has also been shown to modulate their antigen-presenting capabilities. ApoEVs generated from lymphoblasts were found to suppress immune responses by downregulating MHC II molecules on dendritic cells (63).

While the mechanisms underpinning the ability of ApoEVs to modulate antigen presentation are diverse, it is clear that ApoEVs can contribute to the development of autoimmunity, and establishment of antitumor and antimicrobial immunity by regulating the antigen presentation process, as discussed further in detail below.

ApoEVs as Mediators of Autoimmunity

As discussed above, impaired clearance of dying cells is a major factor contributing to the development of autoantibodies in autoimmune conditions (30–32). Although the formation of ApoEVs has been shown to promote apoptotic cell clearance (36, 40, 43, 51) and thus limiting the release on intracellular antigenic and proinflammatory contents, ApoEVs formation has also been proposed as a mechanism of facilitating the transport of autoantigens to antigen-presenting cells and drive autoimmunity. In particular, ApoEVs have been implicated in the development of systemic lupus erythematous (SLE), whereby autoantigens such as histone H2B can be translocated into ApoEVs during the early stages of apoptosis in HeLa cells *via* a microtubule driven mechanism (54). Lymphoblast-derived ApoEVs containing histone were also more readily engulfed by monocyte-derived phagocytes (53). Furthermore, ApoEV-associated autoantigens like DNA can bind directly to antinuclear antibodies (52, 64), a common feature of autoimmune conditions (65). In addition to autoantigens associated with SLE, Sjögren's syndrome nuclear autoantigens, such as hy1-RNA, are also detectable in both ApoMVs and ApoBDs generated from epithelial cells and can be transferred to dendritic cells *via* these ApoEVs (18).

Promoting Antitumor Immunity Through ApoEVs

With most cancer treatments focusing on inducing apoptosis in tumor cells, it becomes important to consider how the release of ApoEVs from dying tumor cells will impact the immune response toward the tumor. Recently, it has been shown that ApoMVs derived from tumorigenic apoptotic melanoma cells can promote antitumor immunity, in which mice immunized with ApoMVs generated from B16-F1 cells following doxorubicin treatment were protected against subsequent tumor challenges (61). Importantly, the tumor antigen PMEL was also found in ApoMVs (66), supporting the concept that ApoMVs can facilitate the transport of tumor antigens to antigen-presenting cells to promote antitumor immunity. It is interesting to note that despite ApoMVs having a relatively lower quantity of the tumor antigen PMEL as compared to other EVs like exosomes, the antitumor protective effect of ApoMV immunization was greater (61), suggesting that ApoMVs may aid antigen presentation *via* a different mechanism as other EVs and were able to promote a more robust antitumor immune response. As discussed earlier, "eat-me" signals such as PtdSer are present on ApoEVs (43, 46). Interestingly, another "eat-me" signal, calreticulin, that are exposed on certain apoptotic tumor cells can play a key role in promoting antitumor immunity through dendritic cells (23, 48, 67, 68). Therefore, it would be of interest to determine whether calreticulin is present on ApoEVs and whether exposure of calreticulin is important for ApoEV-mediated antitumor immunity.

Establishing Antimicrobial Immunity Through ApoEVs

In addition to the presentation of self-antigens, it is important to note that under conditions where infected cells undergo apoptosis, the resultant ApoEVs may also harbor antigens from the infectious agent. The transfer of microbial-derived antigens *via* ApoEVs to antigen presentation cells like dendritic cells have been shown to provide a protective effect for the host. For example, ApoEVs released from apoptotic macrophages infected with the *M. tuberculosis* can be engulfed by peripheral monocyte-derived and splenic dendritic cells, which could subsequently

activate the engulfing dendritic cells to prime naïve $CD4^+$ or $CD8^+$ T cells (56–58). Significantly, ApoEVs generated from *M. tuberculosis*-infected cells were able to be used to vaccinate naïve animals and provided protection against tuberculosis infection, highlighting the potential use of ApoEVs as vaccines (58). While these studies focus on tuberculosis infection, ApoEVs could play an important role in regulating antimicrobial immunity against other pathogens, however, these remain underexplored.

ApoEVs MODULATE IMMUNE CELL RESPONSES

In addition to antigens, ApoEVs can harbor a variety of biomolecules that could directly modulate immune cells, most commonly *via* vesicle-associated cytokines or damage-associated molecular patterns (DAMPs), which could drive inflammation and dictate the immune cell responses. For example, proinflammatory cytokine IL-1α was detected in ApoBDs but not ApoMVs generated from endothelial cells induced to undergo apoptosis by prothrombic and hypoxic conditions *in vitro* (42). In a mouse model, administration of these endothelial cell-derived ApoBDs into the peritoneal cavity was able to induce production of neutrophil chemokines and promote neutrophil infiltration to drive sterile inflammation (42). Furthermore, an increase in IFN-α production by plasmacytoid dendritic cells in response to DNA in lymphoblast-derived ApoMVs was comparatively more pronounced than DNA isolated from whole cells (19). In this case, vesicle-associated DAMPs were responsible in promoting dendritic cell maturation, with the potential to promote damaging inflammation and possibly autoimmune conditions (19, 53). Besides DNA, other DAMPs such as HMGB1 can also be found in ApoEVs derived from peripheral blood mononuclear cells and T cells (26, 69).

HIJACKING ApoEVs DURING VIRAL INFECTIONS

The potential protective effects of ApoEVs in infection was discussed earlier, however, ApoEVs have also been implicated in facilitating the spread of infection *via* two different mechanisms. First, ApoEVs generated from infected cells could modulate the immune response and makes it favorable for the progression of infection. ApoMVs generated during HIV infection were able to modulate the dendritic cells response *via* binding to the CD44 receptor, resulting in decrease cytokine production from dendritic cells and inhibition of their ability to prime T cells or natural killer cells (70). Second, ApoEVs could directly aid viral propagation by mediating the transfer of infectious virions to neighboring cells. Chikungunya virus was shown to induce apoptosis and the formation of ApoBDs in infected HeLa cells and blocking ApoBD formation by targeting the apoptotic cell disassembly process pharmacologically limited infection spreading to neighboring cells (71). Thus, although the formation of ApoEVs by infected cells could be beneficial for the host by facilitating the antigen presentation process, certain viruses may hijack ApoEVs to aid viral propagation.

CONCLUSION

Overall, there is compelling evidence to support the importance of ApoEVs in immune modulation, and ApoEVs can play a significant role across many aspects of immunity and disease settings. Therefore, ApoEVs are more than just debris or by-products of apoptosis and should be considered as a key mechanism for apoptotic cells to communicate with surrounding cells. The ability of ApoEVs to either activate or dampen immune responses demonstrates the fine balance between the beneficial effects of ApoEV generation and the potentially damaging implications. However, as highlighted in this review, there are marked discrepancies in the characterization and isolation of ApoEVs, making it difficult to accurately define their functions. To progress the field, it is critical to identify suitable criteria to distinguish different subtypes of ApoEVs and develop better experimental systems to modulate ApoEV formation under physiologically relevant conditions.

AUTHOR CONTRIBUTIONS

All authors listed have made a substantial, direct, and intellectual contribution to the work and approved it for publication.

FUNDING

This work was supported by grants from the National Health & Medical Research Council of Australia (GNT1125033 and GNT1140187) and Australian Research Council (DP170103790) to Ivan K. H. Poon.

REFERENCES

1. Akers JC, Gonda D, Kim R, Carter BS, Chen CC. Biogenesis of extracellular vesicles (EV): exosomes, microvesicles, retrovirus-like vesicles, and apoptotic bodies. *J Neurooncol* (2013) 113(1):1–11. doi:10.1007/s11060-013-1084-8
2. Robbins PD, Morelli AE. Regulation of immune responses by extracellular vesicles. *Nat Rev Immunol* (2014) 14(3):195–208. doi:10.1038/nri3622
3. Buzas EI, Gyorgy B, Nagy G, Falus A, Gay S. Emerging role of extracellular vesicles in inflammatory diseases. *Nat Rev Rheumatol* (2014) 10(6):356–64. doi:10.1038/nrrheum.2014.19
4. Thery C, Ostrowski M, Segura E. Membrane vesicles as conveyors of immune responses. *Nat Rev Immunol* (2009) 9(8):581–93. doi:10.1038/nri2567
5. Meckes DG Jr, Raab-Traub N. Microvesicles and viral infection. *J Virol* (2011) 85(24):12844–54. doi:10.1128/JVI.05853-11
6. Bretz NP, Ridinger J, Rupp AK, Rimbach K, Keller S, Rupp C, et al. Body fluid exosomes promote secretion of inflammatory cytokines in monocytic cells via toll-like receptor signaling. *J Biol Chem* (2013) 288(51):36691–702. doi:10.1074/jbc.M113.512806
7. Hawari FI, Rouhani FN, Cui X, Yu ZX, Buckley C, Kaler M, et al. Release of full-length 55-kDa TNF receptor 1 in exosome-like vesicles: a mechanism for generation of soluble cytokine receptors. *Proc Natl Acad Sci U S A* (2004) 101(5):1297–302. doi:10.1073/pnas.0307981100
8. Muller L, Mitsuhashi M, Simms P, Gooding WE, Whiteside TL. Tumor-derived exosomes regulate expression of immune function-related genes in human T cell subsets. *Sci Rep* (2016) 6:20254. doi:10.1038/srep20254
9. Qazi KR, Gehrmann U, Domange Jordo E, Karlsson MC, Gabrielsson S. Antigen-loaded exosomes alone induce Th1-type memory through a B-cell-dependent mechanism. *Blood* (2009) 113(12):2673–83. doi:10.1182/blood-2008-04-153536

10. Raposo G, Nijman HW, Stoorvogel W, Liejendekker R, Harding CV, Melief CJ, et al. B lymphocytes secrete antigen-presenting vesicles. *J Exp Med* (1996) 183(3):1161–72. doi:10.1084/jem.183.3.1161
11. Sprent J. Direct stimulation of naive T cells by antigen-presenting cell vesicles. *Blood Cells Mol Dis* (2005) 35(1):17–20. doi:10.1016/j.bcmd.2005.04.004
12. Giri PK, Schorey JS. Exosomes derived from *M. bovis* BCG infected macrophages activate antigen-specific CD4+ and CD8+ T cells in vitro and in vivo. *PLoS One* (2008) 3(6):e2461. doi:10.1371/journal.pone.0002461
13. MacKenzie A, Wilson HL, Kiss-Toth E, Dower SK, North RA, Surprenant A. Rapid secretion of interleukin-1beta by microvesicle shedding. *Immunity* (2001) 15(5):825–35. doi:10.1016/S1074-7613(01)00229-1
14. Diehl P, Fricke A, Sander L, Stamm J, Bassler N, Htun N, et al. Microparticles: major transport vehicles for distinct microRNAs in circulation. *Cardiovasc Res* (2012) 93(4):633–44. doi:10.1093/cvr/cvs007
15. Atkin-Smith GK, Tixeira R, Paone S, Mathivanan S, Collins C, Liem M, et al. A novel mechanism of generating extracellular vesicles during apoptosis via a beads-on-a-string membrane structure. *Nat Commun* (2015) 6:7439. doi:10.1038/ncomms8439
16. Poon IKH, Chiu Y-H, Armstrong AJ, Kinchen JM I, Juncadella J, Bayliss DA, et al. Unexpected link between an antibiotic, pannexin channels and apoptosis. *Nature* (2014) 507(7492):329–34. doi:10.1038/nature13147
17. Kerr JF, Wyllie AH, Currie AR. Apoptosis: a basic biological phenomenon with wide-ranging implications in tissue kinetics. *Br J Cancer* (1972) 26(4):239–57. doi:10.1038/bjc.1972.33
18. Ainola M, Porola P, Takakubo Y, Przybyla B, Kouri VP, Tolvanen TA, et al. Activation of plasmacytoid dendritic cells by apoptotic particles – mechanism for the loss of immunologic tolerance in Sjogren's syndrome. *Clin Exp Immunol* (2017) 191(3):301–310. doi:10.1111/cei.13077
19. Schiller M, Parcina M, Heyder P, Foermer S, Ostrop J, Leo A, et al. Induction of type I IFN is a physiological immune reaction to apoptotic cell-derived membrane microparticles. *J Immunol* (2012) 189(4):1747–56. doi:10.4049/jimmunol.1100631
20. Ferguson TA, Herndon J, Elzey B, Griffith TS, Schoenberger S, Green DR. Uptake of apoptotic antigen-coupled cells by lymphoid dendritic cells and cross-priming of CD8(+) T cells produce active immune unresponsiveness. *J Immunol* (2002) 168(11):5589–95. doi:10.4049/jimmunol.168.11.5589
21. Hochreiter-Hufford A, Ravichandran KS. Clearing the dead: apoptotic cell sensing, recognition, engulfment, and digestion. *Cold Spring Harb Perspect Biol* (2013) 5(1):a008748. doi:10.1101/cshperspect.a008748
22. Poon IK, Lucas CD, Rossi AG, Ravichandran KS. Apoptotic cell clearance: basic biology and therapeutic potential. *Nat Rev Immunol* (2014) 14(3):166–80. doi:10.1038/nri3607
23. Zitvogel L, Kepp O, Kroemer G. Decoding cell death signals in inflammation and immunity. *Cell* (2010) 140(6):798–804. doi:10.1016/j.cell.2010.02.015
24. Atkin-Smith GK, Poon IK. Disassembly of the dying: mechanisms and functions. *Trends Cell Biol* (2016) 27(2):151–62. doi:10.1016/j.tcb.2016.08.011
25. Thery C, Boussac M, Veron P, Ricciardi-Castagnoli P, Raposo G, Garin J, et al. Proteomic analysis of dendritic cell-derived exosomes: a secreted subcellular compartment distinct from apoptotic vesicles. *J Immunol* (2001) 166(12):7309–18. doi:10.4049/jimmunol.166.12.7309
26. Tucher C, Bode K, Schiller P, Classen L, Birr C, Souto-Carneiro MM, et al. Extracellular vesicle subtypes released from activated or apoptotic T-lymphocytes carry a specific and stimulus-dependent protein Cargo. *Front Immunol* (2018) 9:534. doi:10.3389/fimmu.2018.00534
27. Tixeira R, Caruso S, Paone S, Baxter AA, Atkin-Smith GK, Hulett MD, et al. Defining the morphologic features and products of cell disassembly during apoptosis. *Apoptosis* (2017) 22(3):475–7. doi:10.1007/s10495-017-1345-7
28. Lynch C, Panagopoulou M, Gregory CD. Extracellular vesicles arising from apoptotic cells in tumors: roles in cancer pathogenesis and potential clinical applications. *Front Immunol* (2017) 8:1174. doi:10.3389/fimmu.2017.01174
29. Wickman G, Julian L, Olson MF. How apoptotic cells aid in the removal of their own cold dead bodies. *Cell Death Differ* (2012) 19(5):735–42. doi:10.1038/cdd.2012.25
30. Nagata S, Hanayama R, Kawane K. Autoimmunity and the clearance of dead cells. *Cell* (2010) 140(5):619–30. doi:10.1016/j.cell.2010.02.014
31. Baumann I, Kolowos W, Voll RE, Manger B, Gaipl U, Neuhuber WL, et al. Impaired uptake of apoptotic cells into tingible body macrophages in germinal centers of patients with systemic lupus erythematosus. *Arthritis Rheum* (2002) 46(1):191–201. doi:10.1002/1529-0131(200201)46:1<191::AID-ART10027>3.0.CO;2-K
32. Gaipl US, Munoz LE, Grossmayer G, Lauber K, Franz S, Sarter K, et al. Clearance deficiency and systemic lupus erythematosus (SLE). *J Autoimmun* (2007) 28(2–3):114–21. doi:10.1016/j.jaut.2007.02.005
33. Witasp E, Uthaisang W, Elenstrom-Magnusson C, Hanayama R, Tanaka M, Nagata S, et al. Bridge over troubled water: milk fat globule epidermal growth factor 8 promotes human monocyte-derived macrophage clearance of non-blebbing phosphatidylserine-positive target cells. *Cell Death Differ* (2007) 14(5):1063–5. doi:10.1038/sj.cdd.4402096
34. Moss DK, Betin VM, Malesinski SD, Lane JD. A novel role for microtubules in apoptotic chromatin dynamics and cellular fragmentation. *J Cell Sci* (2006) 119(Pt 11):2362–74. doi:10.1242/jcs.02959
35. Casares N, Pequignot MO, Tesniere A, Ghiringhelli F, Roux S, Chaput N, et al. Caspase-dependent immunogenicity of doxorubicin-induced tumor cell death. *J Exp Med* (2005) 202(12):1691–701. doi:10.1084/jem.20050915
36. Fransen JH, Hilbrands LB, Ruben J, Stoffels M, Adema GJ, van der Vlag J, et al. Mouse dendritic cells matured by ingestion of apoptotic blebs induce T cells to produce interleukin-17. *Arthritis Rheum* (2009) 60(8):2304–13. doi:10.1002/art.24719
37. Truman LA, Ford CA, Pasikowska M, Pound JD, Wilkinson SJ I, Dumitriu E, et al. CX3CL1/fractalkine is released from apoptotic lymphocytes to stimulate macrophage chemotaxis. *Blood* (2008) 112(13):5026–36. doi:10.1182/blood-2008-06-162404
38. Lauber K, Bohn E, Krober SM, Xiao YJ, Blumenthal SG, Lindemann RK, et al. Apoptotic cells induce migration of phagocytes via caspase-3-mediated release of a lipid attraction signal. *Cell* (2003) 113(6):717–30. doi:10.1016/S0092-8674(03)00422-7
39. Segundo C, Medina F, Rodriguez C, Martinez-Palencia R, Leyva-Cobian F, Brieva JA. Surface molecule loss and bleb formation by human germinal center B cells undergoing apoptosis: role of apoptotic blebs in monocyte chemotaxis. *Blood* (1999) 94(3):1012–20.
40. Torr EE, Gardner DH, Thomas L, Goodall DM, Bielemeier A, Willetts R, et al. Apoptotic cell-derived ICAM-3 promotes both macrophage chemoattraction to and tethering of apoptotic cells. *Cell Death Differ* (2012) 19(4):671–9. doi:10.1038/cdd.2011.167
41. Eguchi A, Mulya A, Lazic M, Radhakrishnan D, Berk MP, Povero D, et al. Microparticles release by adipocytes act as "find-me" signals to promote macrophage migration. *PLoS One* (2015) 10(4):e0123110. doi:10.1371/journal.pone.0123110
42. Berda-Haddad Y, Robert S, Salers P, Zekraoui L, Farnarier C, Dinarello CA, et al. Sterile inflammation of endothelial cell-derived apoptotic bodies is mediated by interleukin-1alpha. *Proc Natl Acad Sci U S A* (2011) 108(51):20684–9. doi:10.1073/pnas.1116848108
43. Distler JH, Huber LC, Hueber AJ, Reich CF III, Gay S, Distler O, et al. The release of microparticles by apoptotic cells and their effects on macrophages. *Apoptosis* (2005) 10(4):731–41. doi:10.1007/s10495-005-2941-5
44. Niessen A, Heyder P, Krienke S, Blank N, Tykocinski LO, Lorenz HM, et al. Apoptotic-cell-derived membrane microparticles and IFN-alpha induce an inflammatory immune response. *J Cell Sci* (2015) 128(14):2443–53. doi:10.1242/jcs.162735
45. Ravichandran KS, Lorenz U. Engulfment of apoptotic cells: signals for a good meal. *Nat Rev Immunol* (2007) 7(12):964–74. doi:10.1038/nri2214
46. Jiang L, Tixeira R, Caruso S, Atkin-Smith GK, Baxter AA, Paone S, et al. Monitoring the progression of cell death and the disassembly of dying cells by flow cytometry. *Nat Protoc* (2016) 11(4):655–63. doi:10.1038/nprot.2016.028
47. Fadok VA, Voelker DR, Campbell PA, Cohen JJ, Bratton DL, Henson PM. Exposure of phosphatidylserine on the surface of apoptotic lymphocytes triggers specific recognition and removal by macrophages. *J Immunol* (1992) 148(7):2207–16.
48. Verhoven B, Schlegel RA, Williamson P. Mechanisms of phosphatidylserine exposure, a phagocyte recognition signal, on apoptotic T lymphocytes. *J Exp Med* (1995) 182(5):1597–601. doi:10.1084/jem.182.5.1597
49. Fadok VA, Warner ML, Bratton DL, Henson PM. CD36 is required for phagocytosis of apoptotic cells by human macrophages that use either a phosphatidylserine receptor or the vitronectin receptor (alpha v beta 3). *J Immunol* (1998) 161(11):6250–7.
50. Bilyy RO, Shkandina T, Tomin A, Munoz LE, Franz S, Antonyuk V, et al. Macrophages discriminate glycosylation patterns of apoptotic cell-derived microparticles. *J Biol Chem* (2012) 287(1):496–503. doi:10.1074/jbc.M111.273144

51. Black LV, Saunderson SC, Coutinho FP, Muhsin-Sharafaldine MR, Damani TT, Dunn AC, et al. The CD169 sialoadhesin molecule mediates cytotoxic T-cell responses to tumour apoptotic vesicles. *Immunol Cell Biol* (2016) 94(5):430–8. doi:10.1038/icb.2015.111
52. Reich CF III, Pisetsky DS. The content of DNA and RNA in microparticles released by Jurkat and HL-60 cells undergoing in vitro apoptosis. *Exp Cell Res* (2009) 315(5):760–8. doi:10.1016/j.yexcr.2008.12.014
53. Schiller M, Bekeredjian-Ding I, Heyder P, Blank N, Ho AD, Lorenz HM. Autoantigens are translocated into small apoptotic bodies during early stages of apoptosis. *Cell Death Differ* (2008) 15(1):183–91. doi:10.1038/sj.cdd.4402239
54. Zirngibl M, Furnrohr BG, Janko C, Munoz LE, Voll RE, Gregory CD, et al. Loading of nuclear autoantigens prototypically recognized by systemic lupus erythematosus sera into late apoptotic vesicles requires intact microtubules and myosin light chain kinase activity. *Clin Exp Immunol* (2015) 179(1):39–49. doi:10.1111/cei.12342
55. DeSantis CE, Lin CC, Mariotto AB, Siegel RL, Stein KD, Kramer JL, et al. Cancer treatment and survivorship statistics, 2014. *CA Cancer J Clin* (2014) 64(4):252–71. doi:10.3322/caac.21235
56. Farinacci M, Weber S, Kaufmann SH. The recombinant tuberculosis vaccine rBCG DeltaureC:hly(+) induces apoptotic vesicles for improved priming of CD4(+) and CD8(+) T cells. *Vaccine* (2012) 30(52):7608–14. doi:10.1016/j.vaccine.2012.10.031
57. Schaible UE, Winau F, Sieling PA, Fischer K, Collins HL, Hagens K, et al. Apoptosis facilitates antigen presentation to T lymphocytes through MHC-I and CD1 in tuberculosis. *Nat Med* (2003) 9(8):1039–46. doi:10.1038/nm906
58. Winau F, Weber S, Sad S, de Diego J, Hoops SL, Breiden B, et al. Apoptotic vesicles crossprime CD8 T cells and protect against tuberculosis. *Immunity* (2006) 24(1):105–17. doi:10.1016/j.immuni.2005.12.001
59. Dieude M, Bell C, Turgeon J, Beillevaire D, Pomerleau L, Yang B, et al. The 20S proteasome core, active within apoptotic exosome-like vesicles, induces autoantibody production and accelerates rejection. *Sci Transl Med* (2015) 7(318):318ra200. doi:10.1126/scitranslmed.aac9816
60. Braciale TJ, Morrison LA, Sweetser MT, Sambrook J, Gething MJ, Braciale VL. Antigen presentation pathways to class I and class II MHC-restricted T lymphocytes. *Immunol Rev* (1987) 98:95–114. doi:10.1111/j.1600-065X.1987.tb00521.x
61. Muhsin-Sharafaldine MR, Saunderson SC, Dunn AC, Faed JM, Kleffmann T, McLellan AD. Procoagulant and immunogenic properties of melanoma exosomes, microvesicles and apoptotic vesicles. *Oncotarget* (2016) 7(35):56279–94. doi:10.18632/oncotarget.10783
62. Joffre OP, Segura E, Savina A, Amigorena S. Cross-presentation by dendritic cells. *Nat Rev Immunol* (2012) 12(8):557–69. doi:10.1038/nri3254
63. Fehr EM, Spoerl S, Heyder P, Herrmann M, Bekeredjian-Ding I, Blank N, et al. Apoptotic-cell-derived membrane vesicles induce an alternative maturation of human dendritic cells which is disturbed in SLE. *J Autoimmun* (2013) 40:86–95. doi:10.1016/j.jaut.2012.08.003
64. Sisirak V, Sally B, D'Agati V, Martinez-Ortiz W, Ozcakar ZB, David J, et al. Digestion of chromatin in apoptotic cell microparticles prevents autoimmunity. *Cell* (2016) 166(1):88–101. doi:10.1016/j.cell.2016.05.034
65. Munoz LE, Janko C, Schulze C, Schorn C, Sarter K, Schett G, et al. Autoimmunity and chronic inflammation – two clearance-related steps in the etiopathogenesis of SLE. *Autoimmun Rev* (2010) 10(1):38–42. doi:10.1016/j.autrev.2010.08.015
66. Muhsin-Sharafaldine MR, Kennedy BR, Saunderson SC, Buchanan CR, Dunn AC, Faed JM, et al. Procoagulant properties of tumor apoptotic vesicles. *Biochim Biophys Acta* (2016) 7(35):56279–94. doi:10.1016/j.bbagen.2016.11.020
67. Garg AD, Krysko DV, Verfaillie T, Kaczmarek A, Ferreira GB, Marysael T, et al. A novel pathway combining calreticulin exposure and ATP secretion in immunogenic cancer cell death. *EMBO J* (2012) 31(5):1062–79. doi:10.1038/emboj.2011.497
68. Gardai SJ, McPhillips KA, Frasch SC, Janssen WJ, Starefeldt A, Murphy-Ullrich JE, et al. Cell-surface calreticulin initiates clearance of viable or apoptotic cells through trans-activation of LRP on the phagocyte. *Cell* (2005) 123(2):321–34. doi:10.1016/j.cell.2005.08.032
69. Schiller M, Heyder P, Ziegler S, Niessen A, Classen L, Lauffer A, et al. During apoptosis HMGB1 is translocated into apoptotic cell-derived membranous vesicles. *Autoimmunity* (2013) 46(5):342–6. doi:10.3109/08916934.2012.750302
70. Frleta D, Ochoa CE, Kramer HB, Khan SA, Stacey AR, Borrow P, et al. HIV-1 infection-induced apoptotic microparticles inhibit human DCs via CD44. *J Clin Invest* (2012) 122(12):4685–97. doi:10.1172/JCI64439
71. Krejbich-Trotot P, Denizot M, Hoarau JJ, Jaffar-Bandjee MC, Das T, Gasque P. Chikungunya virus mobilizes the apoptotic machinery to invade host cell defenses. *FASEB J* (2011) 25(1):314–25. doi:10.1096/fj.10-164178

Conflict of Interest Statement: The authors declare that the research was conducted in the absence of any commercial or financial relationships that could be construed as a potential conflict of interest.

frontiers in Immunology

ORIGINAL RESEARCH
published: 02 July 2018
doi: 10.3389/fimmu.2018.01466

Helicobacter pylori Outer Membrane Vesicle Size Determines Their Mechanisms of Host Cell Entry and Protein Content

Lorinda Turner[1†], Natalie J. Bitto[2,3], David L. Steer[4], Camden Lo[5], Kimberley D'Costa[1], Georg Ramm[6,7], Mitch Shambrook[3,8], Andrew F. Hill[3,8], Richard L. Ferrero[1,9] and Maria Kaparakis-Liaskos[1,2,3†]*

[1] Centre for Innate Immunity and Infectious Diseases, Hudson Institute of Medical Research, Clayton, Melbourne, VIC, Australia, [2] Department of Physiology, Anatomy and Microbiology, School of Life Sciences, La Trobe University, Melbourne, VIC, Australia, [3] Research Centre for Extracellular Vesicles, School of Molecular Sciences, La Trobe University, Melbourne, VIC, Australia, [4] Monash University, Clayton, VIC, Australia, [5] Monash Micro Imaging, Monash University, Clayton, VIC, Australia, [6] Monash Biomedical Proteomics Facility, Monash University, Clayton, VIC, Australia, [7] Department of Biochemistry and Molecular Biology, Monash University, Melbourne, VIC, Australia, [8] La Trobe Institute for Molecular Sciences, La Trobe University, Melbourne, VIC, Australia, [9] Department of Microbiology, Biomedicine Discovery Institute, Monash University, Melbourne, VIC, Australia

Gram-negative pathogens ubiquitously shed outer membrane vesicles (OMVs) that play a central role in initiating and regulating pathogenesis in the host. Due to their highly inflammatory nature, OMVs are extensively being examined for their role in mediating disease in addition to their applications in innovative vaccines. A key mechanism whereby OMVs mediate inflammation and disease progression is dependent on their ability to enter host cells. Currently, the role of OMV size on determining their mechanism of cellular entry and their protein composition remains unknown. In this study, we examined the mechanisms whereby OMV size regulates their mode of entry into epithelial cells, in addition to their protein cargo and composition. We identified that a heterogeneous sized population of *Helicobacter pylori* OMVs entered epithelial cells *via* macropinocytosis, clathrin, and caveolin-dependent endocytosis. However, smaller OMVs ranging from 20 to 100 nm in size preferentially entered host cells *via* caveolin-mediated endocytosis. Whereas larger OMVs ranging between 90 and 450 nm in size entered host epithelial cells *via* macropinocytosis and endocytosis. Most importantly, we identified the previously unknown contribution that OMV size has on determining their protein content, as fewer and less diverse bacterial proteins were contained within small OMVs compared to larger OMVs. Collectively, these findings identify the importance of OMV size in determining the mechanisms of OMV entry into host cells, in addition to regulating their protein cargo, composition, and subsequent immunogenicity. These findings have significant implications in broadening our understanding of the bacterial regulation of virulence determinants and immunogenic proteins associated with OMVs, their role in mediating pathogenesis and in refining the design and development of OMV-based vaccines.

Keywords: bacterial membrane vesicles, endocytosis, macropinocytosis, pathogenesis, proteomics, outer membrane vesicles, size

OPEN ACCESS

Edited by:
Herman Waldmann, University of Oxford, United Kingdom

Reviewed by:
Kevin Maloy, University of Oxford, United Kingdom
Alfonso Pompella, Università degli Studi di Pisa, Italy

***Correspondence:**
Maria Kaparakis-Liaskos
m.liaskos@latrobe.edu.au

***Present address:**
Lorinda Turner, Department of Medicine, University of Cambridge, Cambridge, United Kingdom; Maria Kaparakis-Liaskos, Department of Physiology, Anatomy and Microbiology, School of Life Sciences, La Trobe University, Melbourne, VIC, Australia

Specialty section:
This article was submitted to Immunological Tolerance and Regulation, a section of the journal Frontiers in Immunology

Received: *12 March 2018*
Accepted: *12 June 2018*
Published: *02 July 2018*

Citation:
Turner L, Bitto NJ, Steer DL, Lo C, D'Costa K, Ramm G, Shambrook M, Hill AF, Ferrero RL and Kaparakis-Liaskos M (2018) Helicobacter pylori Outer Membrane Vesicle Size Determines Their Mechanisms of Host Cell Entry and Protein Content. Front. Immunol. 9:1466. doi: 10.3389/fimmu.2018.01466

INTRODUCTION

Gram-negative bacteria ubiquitously shed vesicles known as outer membrane vesicles (OMVs) during their normal growth [reviewed in Ref. (1, 2)]. OMVs are spherical, bi-layered membrane vesicles ranging from approximately 20 to 350 nm in size, and their release occurs naturally both *in vitro* and *in vivo*. The importance of OMV production during the natural course of infection and in pathogenesis has been highlighted by the identification of OMVs within infected host tissues, including the gastric mucosa of *Helicobacter pylori* infected individuals (3), as well as in the cerebrospinal fluid and sera of patients with meningococcal infection (4). In addition, the ability of OMVs produced by commensal bacteria to prevent diseases such as experimental colitis has been reported (5), further broadening the role of OMVs in disease and gut homeostasis.

Outer membrane vesicles from a range of bacteria have been identified to have a similar protein (6–8) and lipid (9) composition to the outer membranes of their parent bacterium. Specifically, OMVs may contain inner and outer membrane proteins, periplasmic proteins (10), lipopolysaccharide (LPS) (10), peptidoglycan (PG) (11), DNA (12–14), and toxins (3, 15–18). As the protein composition of OMVs is highly similar to that of their parent bacterium, their use and development as innovative vaccines is being extensively examined (19–27). Therefore, due to the similarity of OMVs to their parent bacterium and their highly immunogenic nature, OMV-based vaccines are currently being developed and licensed for human use [reviewed in Ref. (27, 28)].

As OMVs contain many pathogenic proteins originating from their parent bacterium, they are extremely effective at initiating and regulating pro-inflammatory responses in the host. For example, OMVs from the Gram-negative pathogens *H. pylori*, *Neisseria*, *Pseudomonas*, *Campylobacter*, and *Vibrio* induce the secretion of interleukin-8 (IL-8) by non-phagocytic epithelial cells (11, 29–31). The ability of OMVs to initiate and mediate a pro-inflammatory response in host epithelial cells is largely dependent upon their uptake and entry into host cells. There are numerous reported mechanisms, whereby OMVs enter non-phagocytic epithelial cells to mediate inflammation in the host. These include lipid-raft-dependent (11, 32–35), or lipid-raft-independent mechanisms (29), in addition to the requirement for endocytosis (32, 34, 36–38) or macropinocytosis (33). However, to date, the contribution of OMV size on determining the mechanism of OMV entry into non-phagocytic epithelial cells, in addition to determining their protein composition has not been examined and is the focus of this work.

In this study, we characterized the mechanisms whereby *H. pylori* OMV size regulates their route of endocytic entry into non-phagocytic epithelial cells, in addition to regulating their protein content. Our findings revealed that a heterogeneous sized population of OMVs entered human epithelial cells *via* macropinocytosis, caveolin, and clathrin-dependent endocytosis. We identified the previously unknown contribution of OMV size on determining the mechanism of entry into host cells. Specifically, we found that smaller *H. pylori* OMVs ranging from 20 to 100 nm in size entered epithelial cells *via* macropinocytosis, clathrin, and caveolin-dependent endocytosis, and that inhibition of caveolin had the greatest reduction in small OMV entry into host cells. However, the entry of larger OMVs into epithelial cells was inhibited by all mechanisms of endocytosis and did not appear to display a bias for entry *via* any particular mechanism. Most importantly, we determined that OMV size predetermines the protein composition of OMVs, as larger OMVs contain a greater number and wider range of proteins when compared to smaller OMVs. Collectively these findings are the first to report that OMV size plays a role in the mechanisms of host cell entry and their protein content and composition. These findings have major implications for understanding the role of OMVs in mediating bacterial pathogenesis and facilitating their design and development as innovative vaccines.

MATERIALS AND METHODS

Bacterial Strains and OMV Purification

Helicobacter pylori 251 *cag*PAI (11) was cultured using Horse Blood Agar medium (Blood Agar Base No2, Oxoid) or in Brain Heart Infusion broth (Becton Dickinson, USA), supplemented with 0.6% (w/v) β-cyclodextrin (Sigma-Aldrich, USA) by shaking at 120 rpm. Cultures were grown at 37°C under microaerobic conditions. *H. pylori* OMVs were purified from log phase cultures as described previously (11). In brief, bacteria were pelleted from overnight cultures by centrifugation at 2,500 × *g* for 20 min. Supernatants were subsequently filtered using a 0.22 μm PES filter and OMVs were pelleted from these supernatants by ultracentrifugation (100,000 × *g*, 2 h, 4°C). The resulting OMV pellets were resuspended in PBS and protein concentrations determined by the Bradford Protein Assay (Bio-Rad, USA).

Separation of OMVs by Size Using Sucrose Gradient Purification

Outer membrane vesicle preparations in 6 ml were layered onto discontinuous sucrose gradients, consisting of 12.5 ml 25% (w/v) sucrose, 15.5 ml 42% (w/v) sucrose, and 5 ml 56% (w/v) sucrose and subjected to ultracentrifugation (100,000 × *g*, 16 h, 4°C) (11). Thirteen fractions (3 ml each) were collected, washed with PBS to remove any remaining sucrose, and concentrated to a final volume of 500 μl using Amicon YM-10 columns (Millipore, Ireland).

Fluorescent Labeling of OMVs

Outer membrane vesicles (2 mg/ml) were labeled with 1% (v/v) 3,3′-dioctadecyloxacarbocyanine perchlorate (DiO; Molecular Probes, USA) for 20 min at 37°C (39). Excess dye was removed by washing OMVs three times with PBS using a 10 kDa MWCO filtration column (Amicon).

Cell Culture

Human gastric adenocarcinoma (AGS) and human embryonic kidney (HEK293) cells were routinely cultured using RPMI or DMEM respectively, supplemented with 10% (v/v) fetal calf serum (FCS). Cells were seeded at a density of 1×10^5 cells per ml in 12- or 24-well plate for 24 h. For IL-8 secretion studies, cells were co-cultured with heterogeneous, sucrose purified small or large OMVs (50 μg/ml) for 24 h. IL-8 in cultured supernatants

was quantified using the BD OptEIA human IL-8 ELISA kit as per the manufacturer's instructions (BD Biosciences, USA).

Chemical Inhibition of OMV Entry into Epithelial Cells

Inhibition of OMV entry was performed using chemical inhibitors of endocytosis (all from Sigma-Aldrich, USA) at the following concentrations, as described previously (40): cytochalasin D (2 μM), dynasore monohydrate (10 μM), nocodazole (3.3 μM), valinomycin (10 μM), or chlorpromazine (15 μg/ml) (29). AGS or HEK293 cells were pre-treated with inhibitors for 30 min. The cells were subsequently washed twice and the media replaced prior to incubation with 50 μg/ml of OMVs for 4 or 16 h for fluorescence analysis and 24 h to quantify IL-8 production by ELISA.

Cytotoxicity Assay

AGS or HEK293 cells were treated with endocytosis inhibitors or 0.5% (w/v) sodium azide (41) for 30 min. Cells were then washed and media replaced for 4 h. Cellular cytotoxicity was measured using the CellTiter-Glo® assay (Promega, USA), according to the manufacturer's instructions. Luminescence was measured using a FLUOstar OPTIMA (BMG Labtech, Australia).

siRNA Knockdown and qRT-PCR

siRNA knockdown and validation of knockdown was performed as previously described (39). In brief, AGS cells were transfected with two pre-designed and inventoried siRNAs at a final concentration of 10 nM, using Lipofectamine 2000 (Invitrogen). The siRNA sequences used were: *PAK1* (s10019, s10021), *DNM2* (s4212, s4213), *CAV1* (s2447, s2448), and *CLTC* (s477, s475) (Ambion, Applied Biosystems). As a control, cells were transfected with control siRNA (Qiagen, VIC, Australia). To determine the effectiveness of siRNA knockdown, RNA was isolated from siRNA transfected AGS cells using the Purelink RNA mini kit (Life Technologies) and reverse transcribed into cDNA using Superscript III and oligo (dT) primers (Life Technologies). Gene silencing was assessed by TaqMan qRT-PCR using validated FAM labeled *PAK1* (Hs00945621_m1), *DNM2* (Hs00974698_m1), *CAV1* (Hs00971716_m1), and *CLTC* (Hs00964504_m1) primers (all from Ambion, Applied Biosystems), and 18S rRNA FAM labeled primer sets (assay, ID 4319413E, Applied Biosystems). Assays were performed in triplicate using MicroAmp Optical 384-well reaction plate (Applied Biosystems). Target gene cDNA concentrations for each sample were determined using the standard curve and normalized to 18S rRNA expression.

Flow Cytometry

The effectiveness of trypan blue quenching of OMV-associated DiO fluorescence was examined by flow cytometry. AGS cells were incubated with DiO labeled OMVs for 4 h prior to permeabilization with 0.01% (v/v) Triton-X for 10 min, or not permeabilized. Fluorescence was quenched with trypan blue (0.025% final concentration). Cells were washed once and resuspended in DPBS (Gibco, Invitrogen, NY, USA) containing 2% (v/v) FCS and analyzed by flow cytometry using BD FACS CANTO II and BD FACS Diva software v6.0. A total of 6×10^4 cells were counted for each condition. Data were analyzed using FlowJo version 7.6.

Fluorescence Microscopy

AGS cells were seeded onto glass coverslips in 12-well plate (Becton Dickinson Labware, NJ, USA) and cultured overnight. Cells were pre-treated with inhibitors for 30 min, washed twice and media replaced, prior to co-culture with 50 μg/ml of DiO labeled OMVs for 4 or 16 h as indicated. Effectiveness of trypan blue quenching of DiO fluorescence was examined by permeabilization of cells with 0.01% (v/v) Triton-X for 10 min, prior to addition of trypan blue. For all other experiments, extracellular fluorescence was quenched using 0.025% (v/v) trypan blue (Sigma Chemical Co., MO, USA) (29), prior to washing three times with PBS and fixing with 4% (v/v) formaldehyde (Merck, Darmstadt, Germany) for 20 min. Nuclei were stained with 4′,6-diamidino-2-phenylindole, dilactate (DAPI; Molecular Probes, OR, USA), and mounted in Dako Fluorescent mounting medium (Dako North America Inc., CA, USA). To confirm the effectiveness of chemical inhibition, cells were pre-treated with inhibitors followed by the addition of either pHRODO red conjugated human transferrin (hTf; 16.7 μg/ml) (42) or FITC conjugated Dextran, 70 kDa (Dex70; 2.5 mg/ml) (43), for 4 h. Extracellular fluorescence was quenched with trypan blue and cells were fixed and mounted as described previously. Images were acquired on an Applied Precision Instruments DeltaVision deconvolution microscope using a 40 × 1.35NA oil objective at 512 × 512 × 14 bit per channel. Z-stacks (10–15 μm) at 0.2 μm per slice were acquired and deconvolved based on the point spread function of the system. Images were analyzed by Imaris (v7.1.0 Bitplane AG), where the average intensity density of OMV fluorescence was derived by measuring the sum intensity of OMV fluorescence multiplied by the OMV volume, then averaged across cells in the field of view. These arbitrary intensity density units were then normalized to OMV alone groups and expressed as average signal density. For inhibition analysis, the means of each condition were determined for three-independent experiments and plotted as average signal density.

Examination of OMVs by Transmission Electron Microscopy and NanoSight

Outer membrane vesicle samples were prepared for electron microscopy as described previously (44). Grids were viewed using a Hitachi H-7500 transmission electron microscope at 70 K × view and images captured using Digital micrograph™ 1.71.38 (Gatan Inc.). Image analysis was performed using ImageJ v1.47n. OMV size was determined using NanoSight NTA 3.2 (Malvern Instruments, UK). NanoSight particle tracking analysis was performed using heterogeneous OMVs in addition to sucrose gradient purified OMVs obtained from fractions 6 and 12. Fractions were washed with 10 ml DPBS (Gibco) using 10 kDa MWCO filtration columns (Amicon). Fractions 6 and 12 of a sucrose gradient without OMVs was also washed with 10 ml DPBS and used as a blank for NanoSight analysis of their corresponding fraction, while DPBS was used as a blank for heterogeneous OMVs. NanoSight particle analysis was performed in 60 s reads in triplicate, with the gain set to 10, focus to −112,

and camera level 8. Background from the corresponding blank samples was subtracted from each sample read and the average of the three reads was calculated and plotted as particle size versus number of particles per ml.

Proteomic Analysis of OMVs

Proteomic analysis of OMVs was performed as described previously (44), using a pool of three biological OMV replicates. In brief, heterogeneous or fractionated OMV preparations (10 μg) were separated using Novex® 10–20% Tris-Glycine gels (Life Technologies, CA, USA). Proteins contained within OMVs were visualized by staining with Coomassie Blue (Expedeon Ltd., Cambridgeshire, UK). For proteomic analyses, OMV preparations (6 μg) were reduced in 2.5 mM DTT followed by alkylation with 10 mM iodoacetamide and then 0.5 μg trypsin in 20 mM. Ammonium bicarbonate was added and the samples were incubated at 37°C overnight. Tryptic digests were analyzed by LC–MS/MS using the QExactive mass spectrometer (Thermo Scientific, Bremen, Germany) coupled online with an RSLC nano HPLC (Ultimate 3000, Thermo Scientific, Bremen, Germany) as previously described (44). Peptides were selected for MS/MS analysis in Full MS/dd-MS^2 (TopN) mode with the following parameter settings: TopN 10, resolution 17500, MSMS AGC target 1e5, 60 ms Max IT, NCE 27, and 3 *m/z* isolation window. Underfill ratio was set at 10% and dynamic exclusion was set to 15 s. Data were processed using Proteome Discoverer V1.4 (Thermo Fisher Scientific) and searched against a custom database downloaded from the National Centre for Biotechnology Information ftp site using the MS Amanda search engine. The following search parameters were used: missed cleavages, 1; peptide mass tolerance, ±15 ppm; peptide fragment tolerance, ±0.2 Da; peptide charge, 2+, 3+, and 4+; static modifications, carbamidomethyl; and dynamic modification, oxidation (Met). Low and medium confidence peptides were filtered with at least 0.02 FDR (high confidence).

Statistical Analysis

Error bars indicate the mean ± SEM. Fluorescence microscopy experiments were analyzed by One-Way Analysis of Variance (ANOVA) followed by Dunnett's *post hoc* test. IL-8 responses were analyzed using ANOVA and compared to OMV non-treated group. Statistical analyses were performed using Prism software. Differences were considered significant when $^{*}P < 0.05$, $^{**}P < 0.01$, $^{***}P < 0.001$, $^{****}P < 0.0001$.

RESULTS

A Heterogeneous Population of *H. pylori* OMVs Enter Host Cells by Micropinocytosis, Clathrin, and Caveolin-Dependent Endocytosis to Induce the Production of IL-8

Outer membrane vesicles enter non-phagocytic human epithelial cells to subsequently mediate a pro-inflammatory innate immune response. In this study, we sought to elucidate the mechanisms used by *H. pylori* OMVs to enter human epithelial cells and subsequently induce the production of IL-8. To do this, we initially blocked the clathrin, caveolin, or micropinocytosis pathways in both human gastric (AGS) and embryonic kidney (HEK293) cells using chemical inhibitors. We subsequently confirmed the viability of AGS and HEK293 cells post treatment with each chemical inhibitor, in addition to the inhibitors effectiveness (Figure S1 in Supplementary Material). To do this, both AGS and HEK293 cells were treated for 30 min with either: cytochalasin D or nocodazole, to block macropinocytosis, dynasore monohydrate to inhibit dynamin-dependent endocytosis which is utilized by both clathrin and caveolin-mediated entry, or valinomycin to block clathrin-mediated endocytosis (45). The viability of inhibitor-treated and control AGS and HEK293 cells was determined using the CellTiter-Glo assay (Figures S1A,B in Supplementary Material). Both AGS and HEK293 cells remained viable 4 h post treatment with each of the specific inhibitors of the macropinocytosis or endocytosis pathways, compared to azide control cells (Figure S1 in Supplementary Material). The specificity and effectiveness of each of the endocytosis inhibitors was next confirmed. To do this, AGS cells were pre-treated with each of the inhibitors prior to incubation with fluorescently labeled control compounds known to enter host cells via specific pathways. We found that the entry of fluorescently labeled human transferrin, which enters host cells specifically *via* clathrin-mediated endocytosis (42), was markedly reduced in cells pre-treated with dynasore or valinomycin as expected, to comparable levels as the positive control chlorpromazine (Figure S2A in Supplementary Material). Similarly, treatment of AGS cells with cytochalasin D reduced the internalization of micropinocytosis-dependent dextran70 into cells, and treatment with nocodazole resulted in a slight reduction of Dex70 into host cells (Figure S2B in Supplementary Material). Collectively, these findings confirmed the viability of both AGS and HEK cells post treatment with each inhibitor, and the effectiveness of each inhibitor in our assays.

We next sought to elucidate the endocytic mechanisms utilized by fluorescently labeled *H. pylori* OMV to enter host cells. However, this required us to ensure that we could remove any extracellular OMV-associated fluorescence from our analysis by quenching using the cell impermeant dye trypan blue. The effectiveness of trypan blue quenching of extracellular OMV-associated fluorescence was determined using AGS cells that had been cultured with DiO labeled *H. pylori* OMVs, then permeabilized using Triton-X and treated with trypan blue. Effective quenching of fluorescence was confirmed and quantified using both confocal microscopy and flow cytometry. We found that there was a slight reduction in extracellular fluorescence when OMV-stimulated AGS cells were incubated with trypan blue compared to stimulated cells that were not treated with trypan blue (Figure S3E in Supplementary Material). This suggests that there were very few extracellular OMVs present post incubation and subsequent sample preparation for analysis by flow cytometry. We also showed that OMV-stimulated AGS cells that were permeabilized and treated with trypan blue had negligible detectable fluorescence, compared with OMV-stimulated control cells (Figure S3 in Supplementary Material).

Using these validated inhibitors of endocytosis and micropinocytosis pathways, we examined the endocytic mechanisms utilized by a fluorescently labeled heterogeneous population of *H. pylori* OMVs to enter host cells. AGS cells were pre-treated with each inhibitor prior to the addition of a heterogeneous population of fluorescently labeled OMVs and any extracellular fluorescence associated with OMVs was quenched using the cell impermeant dye trypan blue. The addition of fluorescently labeled OMVs to AGS cells pre-treated with inhibitors of endocytosis revealed that the transient inhibition of micropinocytosis, clathrin, caveolin, and dynamin-dependent endocytosis in AGS cells significantly reduced the amount of OMV-associated intracellular fluorescence, compared to untreated cells stimulated with OMVs (**Figures 1A,B**). We found that inhibition of dynamin had the greatest effect in reducing OMV entry into AGS cells ($P > 0.001$). Also, dynamin had a greater effect of inhibiting OMV entry into host cells when compared to valinomycin ($P < 0.001$) and nocodazole ($P < 0.05$). These findings indicate that a heterogeneous population of *H. pylori* OMVs enters AGS cells *via* all pathways of micropinocytosis and endocytosis, and with inhibition of dynamin having the greatest effect on reducing OMV entry into epithelial cells.

We next confirmed the ability of a heterogeneous population of *H. pylori* OMVs to enter AGS cells *via* multiple pathways of endocytosis, with a preferential use for dynamin-mediated entry using siRNA. To do this, we used siRNA to knockdown macropinocytosis, clathrin, or caveolin-mediated endocytosis in AGS cells prior to the stimulation of these cells with fluorescently labeled OMVs (**Figure 1C**). As a control, AGS cells were transfected with control siRNA. The efficiency of siRNA knockdown of each endocytosis or micropinocytosis pathway in AGS cells was confirmed only using qRT-PCR (Figure S4 in Supplementary Material). AGS cells in which micropinocytosis, clathrin, or caveolin-dependent endocytosis pathways were knocked down had a significant reduction in intracellular OMV-associated fluorescence compared to siRNA control cells stimulated with OMVs (**Figure 1C**). In particular, siRNA inhibition of caveolin and dynamin had the greatest effects at inhibiting OMV entry ($P < 0.001$) when compared to control siRNA stimulated cells, thus confirming our findings using chemical inhibition (**Figure 1A**), Furthermore, siRNA inhibition of caveolin and dynamin had the greatest effect of inhibiting OMV entry into AGS cells when compared to siRNA inhibition of clathrin and micropinocytosis ($P < 0.05$). Collectively, these findings identify that a heterogeneous population of OMVs enter AGS cells *via* micropinocytosis, clathrin, and caveolin-mediated endocytosis, with a preference for dynamin-dependent and caveolin-mediated endocytosis.

Numerous studies have reported that the internalization of OMVs into non-phagocytic epithelial cells results in the production of the pro-inflammatory cytokine, IL-8 (11, 39, 46). Therefore, we investigated if the inhibition of OMV entry into host cells *via* micropinocytosis and endocytosis also reduced IL-8 production by AGS and HEK293 cells. Pre-treatment of AGS cells with each of the chemical inhibitors significantly reduced IL-8 production in response to OMV stimulation (**Figure 1D**, $P < 0.001$). Similarly, inhibition of endocytosis and micropinocytosis pathways inhibited IL-8 production by HEK293 cells in response to OMV stimulation (Figure S5 in Supplementary Material). Collectively, these findings demonstrate that inhibition of each of these pathways significantly reduces OMV-mediated IL-8 responses in host cells.

OMVs Size Determines Their Mechanism of Entry Into Host Cells

We next investigated the unknown role of OMV size on regulating the route of entry into host epithelial cells. To do this, we used

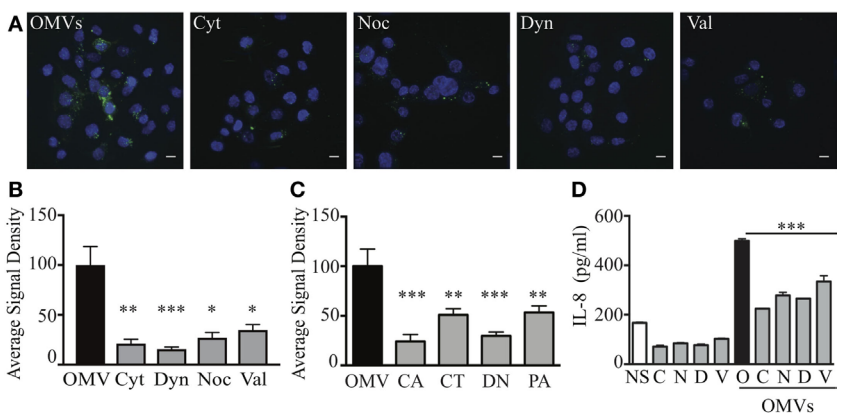

FIGURE 1 | Heterogeneous sized outer membrane vesicles (OMVs) enter host cells *via* macropinocytosis, clathrin, caveolin, and dynamin-dependent endocytosis. **(A,B)** AGS cells were treated with cytochalasin D (Cyt), nocodazole (Noc), dynasore (Dyn), valinomycin (Val), or left untreated (OMV), prior to co-culture with DiO (green) labeled heterogeneous populations of OMVs. Nuclear DNA was stained with DAPI (blue) to allow enumeration of cells. Extracellular fluorescence was quenched with trypan blue. **(C)** The average signal density of internalized green fluorescent OMVs (OMVs) into cells pre-treated with siRNAs to specifically inhibit caveolin (CA), clathrin (CT), dynamin (DN), or macropinocytosis (PA) was measured and normalized to OMV alone group treated with control siRNA. **(D)** IL-8 production in AGS cells that were non-stimulated (NS, open bars), stimulated with OMVs alone as a control (black bar), or pre-treated with chemical inhibitors cytochalasin D (C), nocodazole (N), dynasore (D), valinomycin (V) (gray bars) prior to co-culture with OMVs. Data are represented as mean ± SEM of three replicate experiments. Line indicates statistical significance compared to OMV control group. Images are representative of three-independent experiments in which >100 cells were counted per treatment **(A)**, or pooled from three-independent experiments **(B–D)**. Error bars indicate ±SEM of >100 cells. $^{*}P < 0.05$, $^{**}P < 0.01$, $^{***}P < 0.001$.

sucrose gradient ultracentrifugation to separate a heterogeneous population of *H. pylori* OMVs ranging from 20 to 500 nm in size into two main populations, differing in both size and density (11). Analysis of the initial heterogeneous population using NanoSight Tracking Analysis revealed that approximately 96% of OMVs contained within the heterogeneous population were greater than 100 nm in diameter, with only 4% of OMVs being less than 100 nm in diameter (data not shown). Using sucrose density separation, OMVs were purified from fractions 6 and 12, which we have previously reported to contain small or large OMVs, respectively (11). The size of OMVs contained within fractions 6 and 12 were determined using NanoSight Tracking Analysis and were visualized using transmission electron microscopy (**Figure 2**). NanoSight analysis revealed that fraction 6 contained OMVs ranging between 20 and 100 nm in size, whereas OMVs purified from fraction 12 ranged from 90 to 450 nm in diameter (**Figures 2C,D**). Furthermore, there were multiple sized populations contained both within fractions 6 and 12 OMVs indicating that there is heterogeneity in the size of OMVs contained within these fractions (**Figures 2C,D**).

We next determined whether OMV size may define the mechanism of entry into non-phagocytic host cells. To do this, OMVs from the small fraction (fraction 6) or large fraction (fraction 12) were added to AGS cells in which the micropinocytosis, clathrin, or caveolin-mediated endocytosis pathways were knocked down using siRNA. The number of internalized OMVs was subsequently quantified using confocal microscopy (**Figure 3**). Our findings revealed that although small OMVs could enter AGS cells *via* all pathways of micropinocytosis and endocytosis, they predominantly entered *via* caveolin-dependent endocytosis with the greatest efficiency ($P < 0.0001$, all compared to control OMVs) (**Figure 3A**). Comparison of OMV entry between all siRNA knockdown groups revealed that caveolin had the greatest effect at inhibiting entry of small OMVs into AGS cells compared to clathrin and dynamin ($P < 0.01$, $P < 0.05$, respectively).

In comparison, larger OMVs entered AGS cells *via* all pathways of micropinocytosis and endocytosis when compared to OMV control group (**Figure 3B**). Further comparisons between siRNA knockdown groups revealed that clathrin and dynamin had a greater effect at inhibiting the entry of large OMVs into AGS cells compared to caveolin and macropinocytosis [$P < 0.01$ dynamin Vs. macropinocytosis (PAK), $P < 0.05$ for all other analyses]. Collectively, these findings identify that although small and large OMVs enter host cells *via* all pathways of endocytosis, OMV size does determine their efficiency to enter host cells as caveolin has the greatest role in mediating entry of smaller OMVs into AGS cells. Also, larger OMVs may have a preference for clathrin and dynamin-mediated entry into host cells.

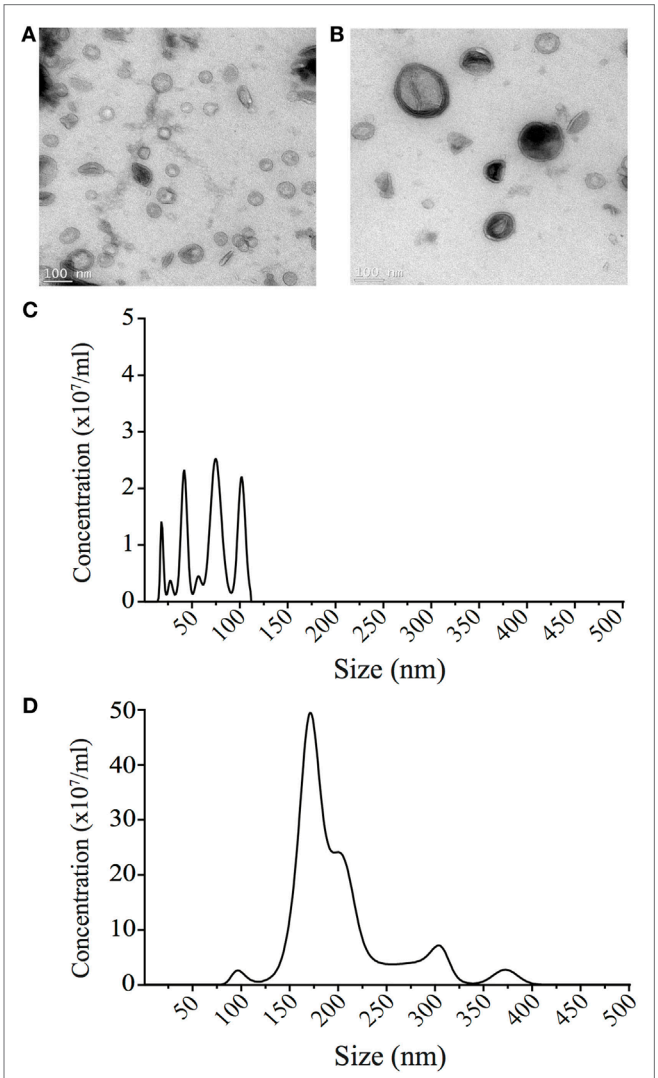

FIGURE 2 | Small and large outer membrane vesicle (OMV) populations purified from a heterogeneous population of OMVs using sucrose gradient purification. **(A)** Transmission electron micrographs of small OMVs present in fraction 6 and **(B)** larger OMVs present in fraction 12. Scale bar represents 100 nm. **(C)** The sizes (nm) of OMVs found within fraction 6 containing small OMVs were determined using NanoSight Tracking Analysis and revealed four populations of OMVs ranging from 20 to 100 nm in size. **(D)** The size (nm) of OMVs found within fraction 12 containing larger OMVs was determined using NanoSight Tracking Analysis. Multiple populations of OMVs were contained within fraction 12, that ranged from 90 to 400 nm in size.

OMV Size Determines Their Protein Content

Although bacteria may selectively package protein cargo into OMVs (27, 47, 48), the role of OMV size on regulating protein content and composition has not been investigated. Therefore, we sought to determine if *H. pylori* OMV size regulated their protein composition and cargo. For this, we initially examined small (fraction 6), large (fraction 12), and heterogeneous *H. pylori* OMV populations by SDS-PAGE (**Figure 4A**). We identified that the smaller *H. pylori* OMVs found within fraction 6 contained fewer proteins, compared to both larger OMVs contained within fraction 12 and the heterogeneous population of parent OMVs (**Figure 4A**). These findings support our previous preliminary findings identifying that fewer proteins were contained within smaller OMVs (11).

We further elucidated the role of OMV size on protein composition by performing detailed LC–MS/MS proteomic analysis of equivalent protein concentrations of small and large OMVs. LC–MS/MS proteomic analysis revealed that only a total of 28

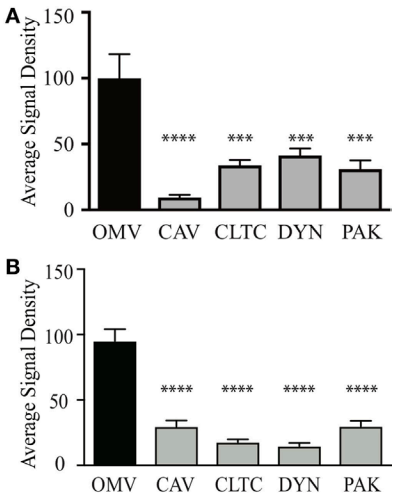

FIGURE 3 | Outer membrane vesicle (OMV) size determines their route of entry into epithelial cells. The average signal density of internalized small **(A)** or large **(B)** green fluorescent (OMVs) into AGS cells pre-treated with siRNAs to specifically inhibit clathrin (CTLC), caveolin (CAV), dynamin (DYN), or macropinocytosis (PAK) was measured and normalized to OMV alone group treated with control siRNA. Data are pooled from three-independent experiments in which >100 AGS cells were counted per treatment. Error bars indicate ± SEM of >100 cells. ***$P < 0.001$, ****$P < 0.0001$.

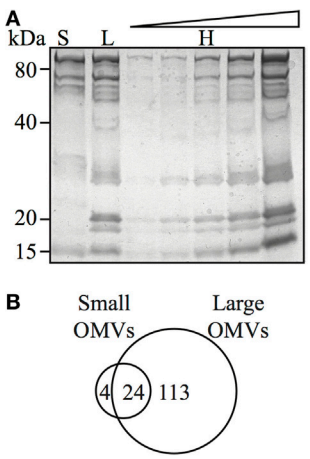

FIGURE 4 | Outer membrane vesicle (OMV) size determines their protein content and composition. **(A)** Coomassie blue-stained polyacrylamide gel showing protein profiles of small (S), large (L), and heterogeneous (H) OMVs, the latter loaded in increasing concentration. **(B)** Venn diagram of proteins detected within small and large OMVs. A total of 137 proteins were detected in large OMVs and 28 proteins were detected in small OMVs. There were 24 proteins found in both large and small OMV populations.

H. pylori-specific proteins were contained within small OMVs isolated from fraction 6, compared with a total of 137 proteins contained within the large OMVs of fraction 12 (**Figure 4B**; Tables S1 and S2 in Supplementary Material, respectively). Of all of the proteins identified within both small and large OMVs, 113 were unique to large OMVs, 4 proteins were unique to small OMVs, and 24 proteins were common to both sized OMV preparations (**Figure 4B**). Interestingly, proteins associated with *H. pylori* survival or virulence were common to both small and large OMVs, including: urease A and B subunits, neutrophil activating protein, vacuolating cytotoxin (VacA), and the porin HopA (**Table 1**). Larger OMVs contained many of the known *H. pylori* adhesins, such as SabA, BabA, iron-regulated proteins, the Hop family of outer membrane proteins and numerous flagella basal and hook proteins (Table S2 in Supplementary Material). These proteins were absent in smaller OMVs (Table S1 in Supplementary Material). The four proteins exclusively contained within small OMVs were predominately associated with metabolism, and not virulence or adhesion (Table S1 in Supplementary Material). Collectively, this proteomic analysis revealed that larger OMVs contain significantly more proteins compared to smaller OMVs, and that most of the *H. pylori* adhesins are associated within larger OMVs purified from fraction 12. Furthermore, both small and large populations of OMVs contained many known virulence determinants, suggesting that both small and large sized OMVs play a role in mediating pathogenesis in the host.

DISCUSSION

Outer membrane vesicles are produced by all Gram-negative bacteria as part of their normal growth and have been reported to play a role in pathogenesis, bacterial cell communication, and biofilm formation [reviewed in Ref. (1)]. Furthermore, due to the highly inflammatory nature of OMVs, and their ability to harbor a range of bacterial proteins and immunogenic epitopes, they are extensively being developed as novel vaccine technology suitable for human and animal use [reviewed in Ref. (27)]. One of the key mechanisms whereby OMVs from various bacteria mediate an inflammatory response in the host is due to their ability to enter non-phagocytic host cells resulting in the production of pro-inflammatory cytokines (11, 29, 32, 33, 35–38, 49). Despite the numerous extensive studies investigating the mechanisms of OMV entry into host cells, the role of OMV size on mediating their mechanism of cellular entry and protein composition has not been determined.

The overall aim of this study was to elucidate the role of OMV size on determining their route of entry into non-phagocytic epithelial cells, in addition to defining their protein cargo and composition. To do this, we first examined the mode of entry of a heterogeneous population of *H. pylori* OMVs into host epithelial cells. Using chemical inhibition of the three main pathways of endocytosis: macropinocytosis, clathrin, and caveolin-mediated endocytosis, we found that a heterogeneous population of OMVs entered non-phagocytic human epithelial cells *via* all mechanisms of endocytosis and micropinocytosis, with chemical inhibition of dynamin-mediated endocytosis having the greatest effect in limiting OMV cellular entry (**Figures 1A,B**). These findings were validated by performing siRNA studies in which we confirmed the level of knockdown using qRT-PCR, but not at the protein level. Using siRNA to knockdown all three pathways of cellular entry, we confirmed our findings that OMVs entered host cells *via* micropinocytosis, clathrin, and cavolin-dependent endocytosis with inhibition of caveolin and dynamin

TABLE 1 | *Helicobacter pylori* proteins common in both small and large outer membrane vesicles (OMVs) (fractions 6 and 12).

Description	Gene	Score	Coverage	Score	Coverage
	No.	Small OMVs	Small OMVs	Large OMVs	Large OMVs
Outer membrane proteins					
Outer membrane protein HopA (Omp6)	HP0229	125.13	2.90	12,690.51	17.18
Thioredoxin	HP1548	166.95	14.42	1,183.40	34.62
Peptidoglycan-associated lipoprotein precursor (Omp18)	HP1125	205.39	10.61	1,809.68	17.88
Metabolism					
Urease subunit alpha	HP0073	13,062.19	56.72	68.49	8.40
Gamma-glutamyltranspeptidase	HP1118	693.31	5.82	7,237.48	16.93
Urease subunit beta	HP0072	26,367.78	52.55	2,594.83	14.76
Iron(III) ABC transporter periplasmic iron-binding protein (CeuE)	HP1562	363.55	7.21	6,586.97	37.24
Carbonic anhydrase	HP1186	1,372.04	18.81	5,111.16	34.65
Catalase-like protein	HP0485	123.63	4.14	3,216.80	30.89
Iron(III) ABC transporter periplasmic iron-binding protein (CeuE)	HP1561	140.59	2.99	2,559.96	18.21
Catalase	HP0875	7,584.68	47.13	26,552.56	54.26
Post translational modification, protein turnover, chaperones					
Chaperonin GroEL	HP0010	5,672.37	35.35	373.71	4.58
Bifunctional methionine sulfoxide reductase A/B protein	HP0224	1,826.54	14.48	12,539.26	31.20
Serine protease (HtrA)	HP1019	141.34	2.48	6,565.50	25.51
Alkyl hydroperoxide reductase (TsaA)	HP1563	503.19	5.56	413.07	14.65
Other					
Neutrophil activating protein (NapA) (bacterioferritin)	HP0243	4,741.96	38.19	376.22	16.67
Hypothetical protein HP0231	HP0231	400.83	3.77	8,592.37	38.49
Hypothetical protein HP0305	HP0305	142.05	5.98	2,442.19	38.04
Hypothetical protein HP1454	HP1454	234.35	4.95	9,609.87	35.64
Hypothetical protein HP0129	HP0129	293.54	7.09	3,695.28	24.82
Hypothetical protein HP0721	HP0721	683.38	18.42	6681.98	19.08
Vacuolating cytotoxin (VacA)	HP0887	1,510.21	3.33	7,883.58	15.89
Neuraminyllactose-binding hemagglutinin homolog (HpaA)	HP0410	227.63	4.82	4,096.93	14.86
Hypothetical protein HP1286	HP1286	613.71	11.54	4,171.54	17.58

having the greatest effects (**Figure 1C**). When examining the effect of inhibition of macropinocytosis, clathrin, and caveolin-dependent endocytosis on OMV-induced IL-8 responses, we discovered that all three pathways of cellular entry contributed to IL-8 production in response to OMV stimulation. This is the first report identifying that a small reduction in OMV cellular entry may have a profound effect on the level of the resulting host inflammatory response.

Particle size is known to play a role in determining the mechanism of endocytosis of lipid particles or latex beads into host cells (50, 51). In our previous study, we identified that OMVs less than 100 nm in diameter induced higher levels of NF-κB activity than larger OMVs, suggesting that these smaller OMVs may be more efficient at entering host epithelial cells and initiating pro-inflammatory responses (11). To determine the role of OMV size in host cell entry, we used our previously reported method to separate OMVs according to size and density (11). Using this method, we separated a heterogeneous population of *H. pylori* OMVs into two populations that were enriched for either small OMVs, up to approximately 100 nm in size, or large OMVs ranging between 90 and 400 nm (**Figure 2**). Using siRNA to limit OMV entry *via* micropinocytosis, clathrin, or caveolin-mediated endocytosis, we determined that small OMVs entered host cells *via* all three mechanisms (**Figure 3**) with a preference for caveolin-mediated entry. Whereas, siRNA studies determined that a population of larger OMVs entered host cells *via* all three mechanisms of endocytosis examined, and clathrin and dynamin may have the greatest effect at mediating entry (**Figure 3**). Collectively, these findings suggest that OMV size may regulate the route of entry into host cells, and that smaller OMVs preferentially enter non-phagocytic epithelial cells *via* caveolin (**Figure 3**). Previous studies have indicated that there are multiple mechanisms whereby bacterial OMVs can enter host cells. For example, Kesty et al. showed that enterotoxigenic *Escherichia coli* OMVs interacted with host cell caveolin, and that inhibition of clathrin-mediated endocytosis had no effect on vesicle uptake (32). However, clathrin-mediated endocytosis was reported by others to be required for internalization of *H. pylori* OMVs into host cells (29). Furthermore, there is some discrepancy in the literature regarding the specific mechanisms whereby OMVs from the same pathogen enter non-phagocytic host cells, and, therefore, the precise mode of OMV entry into host cells remains unclear. Based on our findings, we suggest that determining the size of OMVs contained within an OMV preparation is vital and may account for the differences seen in the modes of OMV entry between research groups.

In addition, this study identified a previously unknown role of OMV size in regulating OMV protein cargo composition. Specifically, proteomic analyses of small and large OMVs revealed that smaller OMVs contained significantly fewer proteins within them, compared to larger OMVs. Moreover, we showed that larger *H. pylori* OMVs contained bacterial adhesion proteins that

were absent from smaller OMVs, which may facilitate their entry into host cells *via* receptor-mediated endocytosis. We identified 24 proteins common to both small and large OMVs; these were mostly proteins associated with virulence, including the vacuolating toxin (VacA), demonstrating a potential pathogenic role for OMVs of various sizes. An earlier study reported that OMVs containing VacA were less dependent on clathrin for entry, when compared with VacA negative OMVs, indicating that toxin containing OMVs may enter host cells by more than one mechanism (29). To our knowledge, no studies have been performed regarding the amount of VacA toxin associated with OMVs from different strains of *H. pylori*, or OMVs of different sizes, and it is plausible that different sized OMVs may contain varying amounts of toxin, which may also facilitate their entry *via* receptor-mediated endocytosis. This finding that variation in OMV size and cargo composition may regulate the mechanism of OMV-mediated endocytosis used to enter host cells warrants further investigation and forms the basis of future studies.

Collectively, our findings identify that OMV size has a key role in regulating both the route of OMV entry into host cells and their protein cargo composition. These findings highlight an important issue within the OMV field, being the importance of defining the size and composition of OMVs when determining their route of cellular entry and subsequent biological functions, as variability in OMV size and composition may alter the experimental outcomes. We propose variations in OMV size may be a reason for the discrepancies in the mechanisms of OMV host cell entry reported by various groups when examining OMVs from the same organisms, in addition to discrepancies in proteomic data. Therefore, we conclude that OMV size predetermines their route of cellular entry and their cargo composition. These findings have fundamental and significant implications that should be considered when examining the role of OMVs in pathogenesis, their protein content, and ultimately their use as vaccines against bacterial infections in humans. Further research elucidating the mechanisms whereby OMV size and composition regulates the mechanism(s) of OMV entry is vital to further develop OMVs as innovative vaccine technology, in addition to understanding their contribution to pathogenesis in the host.

AUTHOR CONTRIBUTIONS

LT, NB, DS, CL, KD, GR, and MK-L performed the research. MS, AH, and RF provided reagents and advice. LT, NB, and MK-L wrote the manuscript.

FUNDING

This project was supported by Discovery grants from the Australian Research Council (MK-L DP110104165; RF, DP120104911), the La Trobe University RFA Understanding Diseases Grant (MK-L), the Victorian State Government Operational Infrastructure Scheme, the MHTP Imaging Research Platform, the LIMS Flow cytometry facility and the LIMS BioImaging Facility (La Trobe University). MK-L is an inaugural veski Inspiring Women Fellow. RF is a National Health and Medical Research Council Senior Research Fellow (APP1079904). LT was funded by an Australian Postgraduate Award and a Monash University Faculty of Medicine, Nursing and Health Sciences Excellence Award.

SUPPLEMENTARY MATERIAL

The Supplementary Material for this article can be found online at https://www.frontiersin.org/articles/10.3389/fimmu.2018.01466/full#supplementary-material.

REFERENCES

1. Kaparakis-Liaskos M, Ferrero RL. Immune modulation by bacterial outer membrane vesicles. *Nat Rev Immunol* (2015) 15:375–87. doi:10.1038/nri3837
2. Schwechheimer C, Kuehn MJ. Outer-membrane vesicles from gram-negative bacteria: biogenesis and functions. *Nat Rev Microbiol* (2015) 13:605–19. doi:10.1038/nrmicro3525
3. Fiocca R, Necchi V, Sommi P, Ricci V, Telford J, Cover TL, et al. Release of *Helicobacter pylori* vacuolating cytotoxin by both a specific secretion pathway and budding of outer membrane vesicles. Uptake of released toxin and vesicles by gastric epithelium. *J Pathol* (1999) 188:220–6. doi:10.1002/(SICI)1096-9896(199906)188:2<220::AID-PATH307>3.0.CO;2-C
4. Brandtzaeg P, Bryn K, Kierulf P, Ovstebø R, Namork E, Aase B, et al. Meningococcal endotoxin in lethal septic shock plasma studied by gas chromatography, mass-spectrometry, ultracentrifugation, and electron microscopy. *J Clin Invest* (1992) 89:816–23. doi:10.1172/JCI115660
5. Shen Y, Giardino Torchia ML, Lawson GW, Karp CL, Ashwell JD, Mazmanian SK. Outer membrane vesicles of a human commensal mediate immune regulation and disease protection. *Cell Host Microbe* (2012) 12:509–20. doi:10.1016/j.chom.2012.08.004
6. Williams JN, Skipp PJ, Humphries HE, Christodoulides M, O'connor CD, Heckels JE. Proteomic analysis of outer membranes and vesicles from wild-type serogroup B *Neisseria meningitidis* and a lipopolysaccharide-deficient mutant. *Infect Immun* (2007) 75:1364–72. doi:10.1128/IAI.01424-06
7. Mullaney E, Brown P, Smith S, Botting A, Yamaoka Y, Terres A, et al. Proteomic and functional characterisation of the outer membrane vesicles from the gastric pathogen *Helicobacter pylori*. *Proteomics Clin Appl* (2009) 3:785–96. doi:10.1002/prca.200800192
8. Olofsson A, Vallström A, Petzold K, Tegtmeyer N, Schleucher J, Carlsson S, et al. Biochemical and functional characterization of *Helicobacter pylori* vesicles. *Mol Microbiol* (2010) 77:1539–55. doi:10.1111/j.1365-2958.2010.07307.x
9. Beveridge TJ. Structures of gram-negative cell walls and their derived membrane vesicles. *J Bacteriol* (1999) 181:4725–33.
10. Beveridge TJ, Kadurugamuwa JL. Periplasm, periplasmic spaces, and their relation to bacterial wall structure: novel secretion of selected periplasmic proteins from *Pseudomonas aeruginosa*. *Microb Drug Resist* (1996) 2:1–8. doi:10.1089/mdr.1996.2.1
11. Kaparakis M, Turnbull L, Carneiro L, Firth S, Coleman HA, Parkington HC, et al. Bacterial membrane vesicles deliver peptidoglycan to NOD1 in epithelial cells. *Cell Microbiol* (2010) 12:372–85. doi:10.1111/j.1462-5822.2009.01404.x
12. Dorward D, Garon C, Judd R. Export and intercellular transfer of DNA via membrane blebs of *Neisseria gonorrhoeae*. *J Bacteriol* (1989) 171:2499–505. doi:10.1128/jb.171.8.4196-4201.1989
13. Kadurugamuwa J, Beveridge T. Virulence factors are released from *Pseudomonas aeruginosa* in association with membrane vesicles during normal growth and exposure to gentamicin: a novel mechanism of enzyme secretion. *J Bacteriol* (1995) 177:3998–4008. doi:10.1128/jb.177.14.3998-4008.1995
14. Renelli M, Matias V, Lo R, Beveridge TJ. DNA-containing membrane vesicles of *Pseudomonas aeruginosa* PAO1 and their genetic transformation potential. *Microbiology* (2004) 150:2161–9. doi:10.1099/mic.0.26841-0
15. Horstman A, Kuehn M. Enterotoxigenic *Escherichia coli* secretes active heat-labile enterotoxin via outer membrane vesicles. *J Biol Chem* (2000) 275:12489–96. doi:10.1074/jbc.275.17.12489

16. Clavin Kouokam J, Wai SN, Fallman M, Dobrindt U, Hacker J, Uhkin BE. Active necrotizing factor 1 associated with outer membrane vesicles from uropathogenic *Escherichia coli*. *Infect Immun* (2006) 74:2022–30. doi:10.1128/IAI.74.4.2022-2030.2006
17. Chitcholtan K, Hampton M, Keenan J. Outer membrane vesicles enhance the carcinogenic potential of *Helicobacter pylori*. *Carcinogenesis* (2008) 29:2400–5. doi:10.1093/carcin/bgn218
18. Lindmark B, Rompikuntal PK, Vaitkevicius K, Song T, Mizunoe Y, Uhlin BE, et al. Outer membrane vesicle-mediated release of cytolethal distending toxin (CDT) from *Campylobacter jejuni*. *BMC Microbiol* (2009) 9:220. doi:10.1186/1471-2180-9-220
19. Haneberg B, Dalseg R, Wedege E, Høiby EA, Haugen IL, Oftung F, et al. Intranasal administration of a meningococcal outer membrane vesicle vaccine induces persistent local mucosal antibodies and serum antibodies with strong bactericidal activity in humans. *Infect Immun* (1998) 66:1334–41.
20. Keenan J, Oliaro J, Domigan N, Potter H, Aitken G, Allardyce R, et al. Immune response to an 18-kilodalton outer membrane antigen identifies lipoprotein 20 as a *Helicobacter pylori* vaccine candidate. *Infect Immun* (2000) 68:3337–43. doi:10.1128/IAI.68.6.3337-3343.2000
21. Keenan J, Rijpkema SG, Durrani Z, Roake J. Differences in immunogenicity and protection in mice and guinea pigs following intranasal immunization with *Helicobacter pylori* outer membrane antigens. *FEMS Immunol Med Microbiol* (2003) 36:199–205. doi:10.1016/S0928-8244(03)00091-9
22. Alaniz RC, Deatherage BL, Lara JC, Cookson BT. Membrane vesicles are immunogenic facsimiles of *Salmonella typhimuirum* that potently activate dendritic cells, prime B and T cell responses, and stimulate protective immunity *in vivo*. *J Immunol* (2007) 179:7692–701. doi:10.4049/jimmunol.179.11.7692
23. Roberts R, Moreno G, Bottero D, Gaillard ME, Fingermann M, Graieb A, et al. Outer membrane vesicles as acellular vaccine against pertussis. *Vaccine* (2008) 26:4639–46. doi:10.1016/j.vaccine.2008.07.004
24. Schild S, Nelson E, Camilli A. Immunization with *Vibrio cholerae* outer membrane vesicles induces protective immunity in mice. *Infect Immun* (2008) 76:4554–63. doi:10.1128/IAI.00532-08
25. Ito AY, Néri S, Machado MSS, Tunes CF, De Gaspari EN. Homologous prime-boost strategy in neonate mice using *Neisseria lactamica*. *Vaccine* (2009) 27:3422–8. doi:10.1016/j.vaccine.2009.01.114
26. Roier S, Leitner DR, Iwashkiw J, Schild-Prufert K, Feldman MF, Krohne G, et al. Intranasal immunization with nontypeable *Haemophilus influenzae* outer membrane vesicles induces cross-protective immunity in mice. *PLoS One* (2012) 7:e42664. doi:10.1371/journal.pone.0042664
27. Bitto NJ, Kaparakis-Liaskos M. The therapeutic benefit of bacterial membrane vesicles. *Int J Mol Sci* (2017) 18:1287–301. doi:10.3390/ijms18061287
28. Pathirana RD, Kaparakis-Liaskos M. Bacterial membrane vesicles: biogenesis, immune regulation and pathogenesis. *Cell Microbiol* (2016) 18:1518–24. doi:10.1111/cmi.12658
29. Parker H, Chitcholtan K, Hampton MB, Keenan JI. Uptake of *Helicobacter pylori* outer membrane vesicles by gastric epithelial cells. *Infect Immun* (2010) 78:5054–61. doi:10.1128/IAI.00299-10
30. Bielig H, Dongre M, Zurek B, Wai SN, Kufer TA. A role for quorum sensing in regulating innate immune responses mediated by *Vibrio cholerae* outer membrane vesicles (OMVs). *Gut Microbes* (2011) 2:274–9. doi:10.4161/gmic.2.5.18091
31. Chatterjee D, Chaudhuri K. *Vibrio cholerae* O395 outer membrane vesicles modulate intestinal epithelial cells in a NOD1 protein-dependent manner and induce dendritic cell-mediated Th2/Th17 cell responses. *J Biol Chem* (2013) 288:4299–309. doi:10.1074/jbc.M112.408302
32. Kesty N, Mson K, Reedy M, Miller S, Kuehn M. Enterotoxigenic *Escherichia coli* vesicles target toxin delivery into mammalian cells. *EMBO J* (2004) 23:4538–49. doi:10.1038/sj.emboj.7600471
33. Bomberger JM, Maceachran DP, Coutermarsh BA, Ye S, O'toole GA, Stanton BA. Long-distance delivery of bacterial virulence factors by *Pseudomonas aeruginosa* outer membrane vesicles. *PLoS Pathog* (2009) 5:e1000382. doi:10.1371/journal.ppat.1000382
34. Furuta N, Tsuda K, Omori H, Yoshimori T, Yoshimura F, Amano A. *Porphorymonas gingivalis* outer membrane vesicles enter human epithelial cells via an endocytic pathway and are sorted into lysosomal compartments. *Infect Immun* (2009) 77:4187–96. doi:10.1128/IAI.00009-09
35. Elmi A, Watson E, Sandu P, Gundogdu O, Mills DC, Inglis NF, et al. *Campylobacter jejuni* outer membrane vesicles play an important role in bacterial interactions with human intestinal epithelial cells. *Infect Immun* (2012) 80:4089–98. doi:10.1128/IAI.00161-12
36. Furuta N, Takeuchi H, Amano A. Entry of *Porphyromonas gingivalis* outer membrane vesicles into epithelial cells causes cellular functional impairment. *Infect Immun* (2009) 77:4761–70. doi:10.1128/IAI.00841-09
37. Schaar V, De Vries SPW, Perez Vidakovics MLA, Bootsma HJ, Larsson L, Hermans PWM, et al. Multicomponent *Moraxella catarrhalis* outer membrane vesicles induce an inflammatory response and are internalized by human epithelial cells. *Cell Microbiol* (2011) 13(3):432–49. doi:10.1111/j.1462-5822.2010.01546.x
38. Chatterjee D, Chaudhuri K. Association of cholera toxin with *Vibrio cholerae* outer membrane vesicles which are internalized by human intestinal epithelial cells. *FEBS Lett* (2011) 585:1357–62. doi:10.1016/j.febslet.2011.04.017
39. Irving AT, Mimuro H, Kufer TA, Lo C, Wheeler R, Turner LJ, et al. The immune receptor NOD1 and kinase RIP2 interact with bacterial peptidoglycan on early endosomes to promote autophagy and inflammatory signaling. *Cell Host Microbe* (2014) 15:623–35. doi:10.1016/j.chom.2014.04.001
40. Lee J, Tattoli I, Wojtal KA, Vavricka SR, Philpott DJ, Girardin SE. pH-dependent internalization of muramyl peptides from early endosomes enables Nod1 and Nod2 signaling. *J Biol Chem* (2009) 284:23818–29. doi:10.1074/jbc.M109.033670
41. Weyermann J, Lochmann D, Zimmer A. A practical note on the use of cytotoxicity assays. *Int J Pharm* (2005) 288:369–76. doi:10.1016/j.ijpharm.2004.09.018
42. Vercauteren D, Vandenbroucke RE, Jones AT, Rejman J, Demeester J, De Smedt SC, et al. The use of inhibitors to study endocytic pathways of gene carriers: optimization and pitfalls. *Mol Ther* (2010) 18:561–9. doi:10.1038/mt.2009.281
43. Falcone S, Cocucci E, Podini P, Kirchhausen T, Clementi E, Meldolesi J. Macropinocytosis: regulated coordination of endocytic and exocytic membrane traffic events. *J Cell Sci* (2006) 119:4758–69. doi:10.1242/jcs.03238
44. Turner L, Praszkier J, Hutton ML, Steer D, Ramm G, Kaparakis-Liaskos M, et al. Increased outer membrane vesicle formation in a *Helicobacter pylori* tolB mutant. *Helicobacter* (2015) 20:269–83. doi:10.1111/hel.12196
45. Irurzun A, Carrasco L. Entry of poliovirus into cells is blocked by valinomycin and concanamycin A. *Biochemistry* (2001) 40:3589–600. doi:10.1021/bi002069p
46. Ismail S, Hampton MB, Keenan JI. *Helicobacter pylori* outer membrane vesicles modulate proliferation and interleukin-8 production by gastric epithelial cells. *Infect Immun* (2003) 71:5670–5. doi:10.1128/IAI.71.10.5670-5675.2003
47. Haurat MF, Aduse-Opoku J, Rangarajan M, Dorobantu L, Gray MR, Curtis MA, et al. Selective sorting of cargo proteins into bacterial membrane vesicles. *J Biol Chem* (2011) 286:1269–76. doi:10.1074/jbc.M110.185744
48. Elhenawy W, Bording-Jorgensen M, Valguarnera E, Haurat MF, Wine E, Feldman MF. LPS remodeling triggers formation of outer membrane vesicles in *Salmonella*. *mBio* (2016) 7(4):e00940-16. doi:10.1128/mBio.00940-16
49. Tsuda K, Amano A, Umebayashi K, Inaba H, Nakagawa I, Nakanishi Y, et al. Molecular dissection of internalization of *Porphyromonas gingivalis* by cells using fluorescent beads coated with bacterial membrane vesicle. *Cell Struct Funct* (2005) 30:81–91. doi:10.1247/csf.30.81
50. Brewer JM, Pollock KGJ, Tetley L, Russell DG. Vesicle size influences the trafficking, processing, and presentation of antigens in lipid vesicles. *J Immunol* (2004) 173:6143–50. doi:10.4049/jimmunol.173.10.6143
51. Rejman J, Oberle V, Zuhorn IS, Hoekstra D. Size-dependent internalization of particles via the pathways of clathrin- and caveolae-mediated endocytosis. *Biochem J* (2004) 377:159–69. doi:10.1042/bj20031253

Conflict of Interest Statement: The authors declare that the research was conducted in the absence of any commercial or financial relationships that could be construed as a potential conflict of interest.

The reviewer KM and the handling Editor declared their shared affiliation.

frontiers in Immunology

ORIGINAL RESEARCH
published: 30 April 2018
doi: 10.3389/fimmu.2018.00850

Hookworm Secreted Extracellular Vesicles Interact With Host Cells and Prevent Inducible Colitis in Mice

Ramon M. Eichenberger[1], Stephanie Ryan[1], Linda Jones[1], Geraldine Buitrago[1], Ramona Polster[1], Marcela Montes de Oca[2], Jennifer Zuvelek[3], Paul R. Giacomin[1], Lindsay A. Dent[4], Christian R. Engwerda[2], Matthew A. Field[1,5], Javier Sotillo[1] and Alex Loukas[1]**

[1] Centre for Biodiscovery and Molecular Development of Therapeutics, Australian Institute of Tropical Health and Medicine, James Cook University, Cairns, QLD, Australia, [2] Immunology and Infection Laboratory, QIMR Berghofer Medical Research Institute, Brisbane, QLD, Australia, [3] Pathology Queensland Cairns Laboratory, Queensland Health, Cairns, QLD, Australia, [4] School of Biological Sciences, University of Adelaide, Adelaide, SA, Australia, [5] Department of Immunology, John Curtin School of Medical Research, Australian National University, Canberra, ACT, Australia

OPEN ACCESS

Edited by:
Ivan Poon,
La Trobe University,
Australia

Reviewed by:
Lauren A. Zenewicz,
University of Oklahoma Health Sciences Center, United States
Kristin Tarbell,
Amgen, United States

***Correspondence:**
Javier Sotillo
javier.sotillo@jcu.edu.au;
Alex Loukas
alex.loukas@jcu.edu.au

Specialty section:
This article was submitted to Immunological Tolerance and Regulation, a section of the journal Frontiers in Immunology

Received: 30 January 2018
Accepted: 06 April 2018
Published: 30 April 2018

Citation:
Eichenberger RM, Ryan S, Jones L, Buitrago G, Polster R, Montes de Oca M, Zuvelek J, Giacomin PR, Dent LA, Engwerda CR, Field MA, Sotillo J and Loukas A (2018) Hookworm Secreted Extracellular Vesicles Interact With Host Cells and Prevent Inducible Colitis in Mice. Front. Immunol. 9:850. doi: 10.3389/fimmu.2018.00850

Gastrointestinal (GI) parasites, hookworms in particular, have evolved to cause minimal harm to their hosts, allowing them to establish chronic infections. This is mediated by creating an immunoregulatory environment. Indeed, hookworms are such potent suppressors of inflammation that they have been used in clinical trials to treat inflammatory bowel diseases (IBD) and celiac disease. Since the recent description of helminths (worms) secreting extracellular vesicles (EVs), exosome-like EVs from different helminths have been characterized and their salient roles in parasite–host interactions have been highlighted. Here, we analyze EVs from the rodent parasite *Nippostrongylus brasiliensis,* which has been used as a model for human hookworm infection. *N. brasiliensis* EVs (*Nb*-EVs) are actively internalized by mouse gut organoids, indicating a role in driving parasitism. We used proteomics and RNA-Seq to profile the molecular composition of *Nb*-EVs. We identified 81 proteins, including proteins frequently present in exosomes (like tetraspanin, enolase, 14-3-3 protein, and heat shock proteins), and 27 sperm-coating protein-like extracellular proteins. RNA-Seq analysis revealed 52 miRNA species, many of which putatively map to mouse genes involved in regulation of inflammation. To determine whether GI nematode EVs had immunomodulatory properties, we assessed their potential to suppress GI inflammation in a mouse model of inducible chemical colitis. EVs from *N. brasiliensis* but not those from the whipworm *Trichuris muris* or control vesicles from grapes protected against colitic inflammation in the gut of mice that received a single intraperitoneal injection of EVs. Key cytokines associated with colitic pathology (IL-6, IL-1β, IFNγ, and IL-17a) were significantly suppressed in colon tissues from EV-treated mice. By contrast, high levels of the anti-inflammatory cytokine IL-10 were detected in *Nb*-EV-treated mice. Proteins and miRNAs contained within helminth EVs hold great potential application in development of drugs to treat helminth infections as well as chronic non-infectious diseases resulting from a dysregulated immune system, such as IBD.

Keywords: nematode, colitis, immunomodulation, parasite–host interaction, miRNA, proteomics, exosome, extracellular vesicles

INTRODUCTION

Parasitic helminths (worms) modify the immune system of their host to avoid immune ejection, a strategy which promotes their long-term survival and results in chronic infection (1), but also has a bystander effect by protecting against the onset of inflammatory disorders that result from a dysregulated immune response (2). Hookworms, blood-feeding intestinal nematode parasites, are particularly adept at manipulating the immune systems of their mammalian hosts (3). Hookworm infection is one of the major human ailments affecting approximately 600 million people worldwide (4, 5). When hookworms first encounter a mammalian host, they release a suite of molecules referred to as excretory/secretory products (ESP), a mixture of proteins, carbohydrates, and lipids that represent the primary interface between hookworms and their hosts. In helminth parasites, the ES proteins orchestrate a wide range of activities crucial for their survival and propagation, including penetration of the host dermis, tissue invasion, feeding, reproduction, and evasion of the host immune system (3, 6, 7).

Nippostrongylus brasiliensis is a nematode of mice and rats, although it does infect a number of other rodent species (8). Because of its similarities to the life cycle of hookworm species (e.g., *Ancylostoma* spp., and *Necator americanus*), this species is often referred as the "rat hookworm" and has been frequently used as a model to study the immunobiology of human hookworm infections (9–13).

Following the migration of infective larvae (L3) through rodent tissues, *N. brasiliensis* triggers a highly polarized T helper type 2 (Th2) response in the skin, lungs, and intestinal mucosa (13), characteristics present also in human hookworm infections, including CD4+ T cell-dependent IgE production, eosinophilia, mastocytosis, and mucus production (3). Furthermore, hookworm infections are characterized by the generation of an immune-regulatory environment with the anti-inflammatory cytokines IL-10 and TGFβ, and regulatory T cells, type 2 innate lymphoid cells, tolerogenic dendritic cells, and M2 macrophages to prevent potentially dangerous pathology (14, 15).

Because of the exquisite immunomodulatory capacity of helminths, helminth therapy is under investigation for the treatment of inflammatory diseases, and has shown promise in both clinical trials and studies in animals with a range of inflammatory diseases, such as celiac disease, asthma, multiple sclerosis, and inflammatory bowel diseases (IBD) (16–20). Different research groups—including us—have demonstrated that the immunomodulatory environment induced by hookworms can be attributed to their secreted products (7, 21–25).

There is emerging evidence of the release of extracellular vesicles (EVs) during helminth infections—which correspond to a sub-fraction of the ESP—playing important roles in both parasite–parasite communications as well as in parasite–host interactions (26, 27). Nematode roundworm EVs can suppress potentially dangerous type 2 innate responses and eosinophilia and generate a regulatory and/or suppressive immune state that is beneficial for the parasite's long-term survival (28). EVs have also been reported from platyhelminth flatworms (29, 30): schistosome EVs impact macrophage differentiation (31), and liver fluke EVs are internalized by human cholangiocytes and promote cell proliferation and potentially contribute to the development of liver cancer (32).

It was demonstrated that hookworm ESP mitigate colitis in different mouse models (21–23), and at least one recombinant ESP protein has been shown to possess anti-colitic properties (33). Here, we characterize the protein- and miRNA-cargo of secreted EVs from the hookworm-like nematode *N. brasiliensis*, show that these EVs are internalized by cells in murine gastrointestinal (GI) tract organoids, and evaluate their immunomodulatory properties in experimentally induced murine colitis. We then compared the data to that generated with EVs from a distantly related intestinal nematode, the whipworm *Trichuris muris* (*Tm*), and discuss the outcomes in terms of the immunobiology of these two major human helminth infections. This study conveys novel insights into the roles of nematode EVs and reveals potential applications of an entirely new generation of therapeutics to treat inflammatory disorders.

MATERIALS AND METHODS

Parasite Material, Isolation of ESP, and EV Purification

Excretory/secretory products were collected from adult *N. brasiliensis* and *Tm* parasites, and EVs were purified. Exosome-like vesicles from grapes ("grapeosomes") were purified and used as a negative purification and vesicle control.

Nippostrongylus brasiliensis was maintained in Sprague–Dawley rats (Animal Resources Centre, Perth, WA, Australia) as previously described (10). Infective L3 were prepared from 2-week rat fecal cultures. Adult worms were recovered from small intestines on day 8 post infection following subcutaneous injection of 3,000 infective L3. Adult worms were washed in PBS containing 5× antibiotic/antimycotic (AA; Sigma-Aldrich, St. Louis, MO, USA) and cultured in 24-well plates (500 worms/well) for 7 days in RPMI containing 1× AA and 1× GlutaMAX™ supplement (Gibco, Thermo Fisher, Waltham, MA, USA) at 37°C and 5% CO_2. The media obtained during the first 4 h after parasite culturing was discarded. ESP were collected daily, subjected to sequential differential centrifugation at 500, 2,000, and 4,000 *g* for 30 min each to remove eggs and parasite debris. For the isolation of ES products, media was concentrated using a 10 kDa spin concentrator (Merck Millipore, Billerica, MA, USA) and stored at 1.0 mg/ml in PBS at −80°C until used.

Trichuris muris parasites were obtained from genetically susceptible B10.BR mice (Animal Resources Centre) infected with 200 *Tm* eggs. Adult worms were harvested from the cecum of infected mice 5 weeks after infection, washed in PBS containing 5× AA and cultured in 6-well plates for 5 days in RPMI containing 1× AA, at 37°C and 5% CO_2. Each well contained ~500 worms in 4.5 ml media. Further processing was similar to that described herein for ESP from *N. brasiliensis*. Dead worms were removed and ES products were collected daily.

We chose exosomes derived from grapes as a control for our animal studies because they served as a non-mammalian source of EVs that are capable of being internalised by mouse organoid cells and protect against dextran sulfate sodium-induced

colitis (34). Grapeosomes were purified from commercially purchased grapes (*Vitis vinifera* "Thompson seedless") according to Ju et al. (34) with some modifications. Peeled grapes were minced and filtered through a 21 µm nylon mesh (Scrynel, Lanz-Anliker, Rohrbach, Switzerland) and 0.22 µm Steritop® Membrane (GP Millipore Express®PLUS, Merck) and further processed as described herein for parasite ESP.

For the isolation of EVs, the media obtained after differential centrifugation was processed as described previously (30). Briefly, concentrated ESP were centrifuged for 45 min at 15,000 *g* to remove larger vesicles. A MLS-50 rotor (Beckman Coulter, Brea, CA, USA) was used to ultracentrifuge the supernatant for 3 h at 120,000 *g*. Supernatant resulting from this centrifugation corresponds to vesicle-depleted ESP (protein fraction). The resultant pellet was resuspended in 70 µl of PBS and subjected to Optiprep® density gradient (ODG) separation. 1 ml of 40, 20, 10, and 5% iodixanol solutions prepared in 0.25 M sucrose, 10 mM Tris–HCl, pH 7.2, were layered in decreasing density in an ultracentrifuge tube, and the 70 µl containing the resuspended EVs was added to the top layer and ultracentrifuged at 120,000 *g* for 18 h at 4°C. 70 µl of PBS was added to the control tube prepared as described above. A total of 12 fractions were recovered from the ODG, and the excess Optiprep® solution was removed by buffer exchanging with 8 ml of PBS containing 1× EDTA-free protease inhibitor cocktail (Santa Cruz, Dallas, TX, USA) using a 10 kDa spin concentrator. The absorbance (340 nm) was measured in each of the fractions and density was calculated using a standard curve with known standards. The protein concentration of all fractions was measured using a Pierce BCA Protein Assay Kit (Thermo Fisher). All fractions were kept at −80°C until use.

Size and Concentration Analysis of EVs

The size distribution and particle concentration of fractions recovered after ODG were measured using tunable resistive pulse sensing (TRPS) by qNano (Izon, Christchurch, New Zealand) following the manufacturer's instructions for working with smaller range nanopores. Voltage and pressure values were set to optimize the signal to ensure high sensitivity. A nanopore NP100 was used for all fractions analyzed except for the grape vesicles, where a NP150 was used. Calibration was performed using CP100 carboxylated polystyrene calibration particles (Izon) at a 1:1,000 dilution. Samples were diluted 1:5 and applied to the nanopore. The size and concentration of particles were determined using the software provided by Izon (version 3.2). Protein concentration was measured in all fractions, and EV purity determined as described previously (35).

Proteomic Analysis

For the proteomic analysis of EVs from *N. brasiliensis*, 50 µg of protein of the ODG fractions with a density of 1.06–1.10 g/ml (fractions 7–9) were loaded on a 12% SDS-PAGE gel and electrophoresed at 100 V until the protein marker reached 2/3 of the total run length (approximately for 1.5 h). Each lane was sliced into 10 pieces, which were subjected to trypsin digestion as described previously (12). The final digest supernatant was removed from the gel slices, and residual peptides were removed from the gel slices by washing three times with 0.1% trifluoroacetic acid for 45 min at 37°C. Peptide samples were combined into 5 tubes per lane, resulting in total 15 samples for mass spectrometry analysis. Samples were desalted and concentrated using Zip-Tip® and kept at −80°C until use.

Samples were reconstituted in 10 µl of 5% formic acid. Six microliters of sample was injected onto a 50 mm 300 µm C18 trap column (Agilent Technologies, Santa Clara, CA, USA) and desalted for 5 min at 30 µl/min using 0.1% formic acid (aq). Peptides were then eluted onto an analytical nano HPLC column (150 mm × 75 µm 300SBC18, 3.5 µm, Agilent Technologies) at a flow rate of 300 nl/min and separated using a 95 min gradient of 1–40% buffer B (90/10 acetonitrile/0.1% formic acid) followed by a steeper gradient of 40–80% buffer B in 5 min. The mass spectrometer (ABSCIEX 5600+) operated in information-dependent acquisition mode, in which a 1-s TOF MS scan from 350–1,400 *m/z* was performed, and for product ion ms/ms 80–1,400 *m/z* ions observed in the TOF-MS scan exceeding a threshold of 100 counts and a charge state of +2 to +5 were set to trigger the acquisition of product ion. Analyst 1.6.1 (ABSCIEX) software was used for data acquisition and analysis.

For the analysis of the EV mass spectrometry data, a database was built using the *N. brasiliensis* genome (PRJEB511) with the common repository of adventitious proteins (cRAP[1]) appended to it. Database search was performed using Mascot Versions 2.4 (Matrix Science Ltd., London, UK) and X!Tandem, MS-GF+, OMSSA, and Tide search engines using SearchGUI (36). The same parameters were used as described in Ref. (37).

The mass spectrometry proteomics data have been deposited in the ProteomeXchange Consortium *via* the PRIDE partner repository with the dataset identifiers PXD009165 and 10.6019/PXD009165. A final list of parasite-specific proteins resulted by combining the different fractions and removing hits for common contaminants from the cRAP database, considering only proteins containing at least two validated unique peptides matching *N. brasiliensis* gene models. Proteins were functionally classified according to Gene Ontology categories using the software Blast2GO basic version 4.0.7 (38). Putative signal peptides and transmembrane domain(s) were predicted using the programs CD-Search tool (39) and SignalP (40). Structural comparison of proteomic datasets was performed by all-vs-all blast in NCBI Blast + executables (v2.7.1).

miRNA Analysis

Biological replicates of *N. brasiliensis* EVs (*Nb*-EVs) obtained from three different batches of worms were used. ODG fractions with a density between 1.07 and 1.09 (fractions containing pure EV samples after TRPS analysis) were pooled and excess Optiprep® solution was removed by buffer exchanging. miRNA was extracted using the mirVana™ miRNA Isolation Kit (Thermo Fisher) according to the manufacturer's instructions. RNA was eluted over two fractions of 50 µl each and stored at −80°C until analyzed.

The RNA quality, yield, and size of total and small RNAs were analyzed using capillary electrophoresis (Agilent 2100 Bioanalyzer, Agilent Technologies). miRNA was prepared for sequencing using a QIAseq™ miRNA library preparation

[1]http://www.thegpm.org/crap/ (Accessed: April 5, 2017).

kit(Qiagen, Hilden, Germany) according to the manufacturer's instructions. RNA-Seq was performed on a NextSeq 500 (Illumina, single-end 75-bp SR mid output run, up to 130M reads per sample). Quality control, library preparation, and sequencing were performed at the Ramaciotti Centre for Genomics at the University of New South Wales. The data have been deposited in NCBI's Gene Expression Omnibus under GEO series accession number GSE111478.

The miRDeep2 package (41) was used to identify known and putative novel miRNAs present in all miRNA replicates. As there are no *N. brasiliensis* miRNAs available in miRBase release 21 (42), the miRNAs from the nematodes *Ascaris suum*, *Brugia malayi*, *Caenorhabditis elegans*, *Caenorhabditis brenneri*, *Caenorhabditis briggsae*, *Caenorhabditis remanei*, *Haemonchus contortus*, *Pristionchus pacificus*, *Panagrellus redivivus*, and *Strongyloides ratti* were utilized as a training set for the algorithm. Only miRNA sequences commonly identified in all replicates were included for further analyses. The interaction between miRNA and murine host genes was predicted using the miRanda algorithm 3.3a (43). Input 3'UTR from the *Mus musculus* GRCm38.p5 assembly was retrieved from the Ensembl database release 86 and combined with the murine 3′UTRs from the rodent database in the UTRdb release 11 (44, 45). The software was run with strict 5' seed pairing, energy threshold of −20 kcal/mol and default settings for gap open and gap extend penalties. Interacting hits were filtered by conservative cutoff values for pairing scores (>155) and matches (>80%). The resulting gene list was classified by the Panther classification system[2] using pathway classification (46) and curated by the reactome pathway database[3] (47). miRNA host target interactions to individual genes in cytokine pathways (PantherDB P00010, P00031, P00034, P00035, P00036, P00052, P00053, and P00054) of *Nb*-EV miRNAs, *Tm*-EV miRNAs (37), and shared homologs were linked and illustrated by the package "alluvial" v0.1-2 in R v3.3.2 (48).

Exosome Uptake in Murine Small Intestinal (SI) Organoids (Mini-Guts)

Murine SI organoids were produced from intestinal crypts of a female C57 Bl6/J mouse according to previous reports (49) with some modifications. Briefly, murine SI crypts were dissociated with Gentle Cell Dissociation reagent (Stemcell Technology Inc., Vancouver, BC, Canada). Approximately 500 crypts were seeded in 50 µl of Matrigel (Corning Inc., New York, NY, USA) in a 24-well plate and cultured in Intesticult Organoid Growth Medium (Stemcell Technology Inc.).

Imaging was performed as described in Eichenberger et al. (37) with minor modifications. Briefly, to investigate internalization of EVs in the SI epithelium layer, 30–50 million PKH26 (Sigma-Aldrich) -labeled EVs in 3–5 µl were injected into the central lumen of individual organoids and cultured for 3 h at 37 and 4°C, respectively. Washed organoids were fixed and autofluorescence was quenched with 50 mM NH_4Cl in PBS (for 30 min at RT) and 100 mM glycine in PBS (for 5 min). Cell nuclei were stained with Hoechst dye (Invitrogen, Carlsbad, CA, USA) and images were visualized on a laser scanning confocal microscope (Zeiss 780 NLO, Zeiss, Oberkochen, Germany). Confocal image deconvolution was performed in ImageJ using the plugins "Diffraction PSF 3D" for PSF calculation and "DeconvolutionLab" with the Tikhonov–Miller algorithm for 2D deconvolution (50).

Experimental Model of Colitis

To assess the prophylactic impact of *N. brasiliensis* secreted products on experimental colitis in mice, we used the 2,4,6-trinitrobenzene sulfonic acid (TNBS; Sigma-Aldrich) method of acute inducible colitis. Weight-matched (18.86–21.31 g) 6-week-old male BALB/c mice were purchased from Animal Resources Centre, assessed for health and placed at random in groups of five animals per cage. All the experiments were repeated with the same number of mice in each group, resulting in independent duplicate experiments using the same groups. Mice were maintained at the JCU animal facility (Cairns campus) under normal conditions of regulated temperature (22°C) and lighting (12 h light/dark cycle) with free access to pelleted food and water in accordance with Australian animal rights and regulation standards.

One day prior to the induction of colitis, 20 µg of the test compounds in 200 µl PBS per mouse were administered intraperitoneal to 5 mice per group, whereas in a first approach 6 different groups were included in the study: (1) healthy naïve mice; (2) PBS (colitis control); (3) *Nb*-EVs; (4) *N. brasiliensis* ESP; (5) *N. brasiliensis* vesicle-depleted ESP (protein fraction); and (6) grapeosomes (vesicle and purification control). The experiment was repeated in an independent duplicate experiment (resulting in a total of 10 mice per group). *Tm* EVs and *Tm* vesicle-depleted ESP were evaluated in another, repeated experiment only.

TNBS colitis was induced as described earlier (33, 51). Animals were monitored daily for clinical signs including weight loss, piloerection, mobility, and fecal consistency/bleeding. An overall cumulative clinical score included weight loss (increase = 0; no weight loss = 1; loss = 2), piloerection (absent = 0; mild = 1; severe = 2), feces (normal = 0; mild diarrhea = 1; bloody, liquid, or unable to defecate after 5 min = 2), and mobility (normal = 0; lethargic = 1; motionless, sickly = 2). Clinical monitoring was performed by the same person at similar time points in a blinded manner (unaware of the groups). At day 3, mice were euthanized and the colon (from cecum to rectum) was removed and macroscopically assessed for colitis by scoring (absent = 0; mild = 1; moderate = 2; severe = 3) for the independent parameters of adhesions, ulceration, colonic thickening, and mucosal edema. Colon length was recorded, and 0.5–1 cm colon pieces were removed for *ex vivo* culturing for the measurement of tissue cytokine production and histological assessment of inflammatory infiltration. Tissue pieces for culturing were weighed to normalize cytokine data.

Colonic tissue was cultured in complete media (RPMI 1640, 10% heat-inactivated FCS, 1% HEPES, 100 U of penicillin/ml, 100 µg of streptomycin/ml, and 2 mM/l –glutamine; all reagents sourced from Invitrogen) for 24 h and supernatant was subsequently used to quantify levels of the cytokines IL-1β, IL-6, IL-10, IL17-a, IFN-γ, and TGFβ. Cytokine levels were measured by ELISA using Ready-Set-Go kits (Invitrogen) according to the

[2]http://pantherdb.org/ (Accessed: December 7, 2017).
[3]www.reactome.org (Accessed: December 7, 2017).

manufacturer's instructions, and a POLARstar Omega spectrophotometer (BMG Labtech, Thermo Fisher).

Tissue for histology was placed in formalin to fix tissue then transferred to 70% ethanol for storage and transport. Tissue was embedded in paraffin and sectioned longitudinally for histology. Slides were stained with hematoxylin and eosin (H&E). Tissue processing and staining was performed at the Cairns Hospital pathology laboratory. Inflammatory infiltrate was determined by the scoring method described in Hong et al. (52).

Results from the duplicate experiments were combined for statistical analysis. Statistical analyses were performed using GraphPad Prism (version 7.03). Comparisons were made between the sample treatment with TNBS groups and the PBS + TNBS group; p values of <0.05 were considered significant. When two groups were compared, a Mann–Whitney (unpaired, non-parametric) U-test was applied. All data are representative of at least two experiments (total $n = 10$ mice; with 5 mice/experimental group).

RESULTS

N. brasiliensis Secretes EVs That Are Internalized by Host Cells

In 12 ODG fractions from concentrated and purified *N. brasiliensis* ESP, we purified vesicles in a size range of 60–160 nm (mean 95 ± 37.3 nm), which were most abundant in fractions 7–10 (density of 1.06–1.11 g/ml) as detected by qNano TRPS (**Figure 1**). *Nb*-EVs were verified by proteomic analysis, revealing several proteins which are frequently present in mammalian exosomes ("EV-markers"), including tetraspanin (NBR_0001199101), enolase (NBR_0001176401), 14-3-3 protein (NBR_0000671101), heat shock protein 70 (HSP70; NBR_0000494801), histones, and structural/cytoskeletal proteins (Table S1 in Supplementary Material). It has been demonstrated that EVs from *Tm* are actively internalized by murine intestinal cells within colonic organoids (37). We assessed whether murine host intestinal cells internalized *Nb*-EVs using murine small intestine (the site of residence of the adult worm) organoids, comprised of the complete census of progenitors and differentiated cells from the SI epithelial tissue growing in cell culture. We observed internalization of *Nb*-EVs by organoid cells cultured at 37°C but not at 4°C when cells were metabolically inactive and endocytosis was inhibited (**Figure 2**). Confocal microscopy images revealed that fluorescently labeled EVs were detected inside the cells with a cytoplasmic location within the donut-shaped organoid epithelial layer.

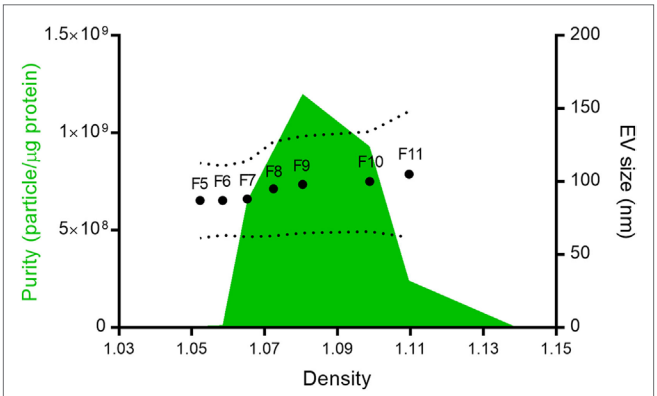

FIGURE 1 | *Nippostrongylus brasiliensis* secreted extracellular vesicles (EVs). Mean particle size (dots), size range (dotted line), and purity (green area) of the different fractions isolated after Optiprep® density gradient centrifugation. Despite protein being detected in all fractions, only vesicles from fractions 5–11 (F5–F11) could be quantified by tunable resistive pulse sensing. The purity of the different fractions was calculated according to Webber and Clayton (35).

N. brasiliensis but Not *Tm* EVs Protect Mice Against Chemically Induced Colitis

The immunomodulatory properties of EVs from two distinct soil transmitted nematodes (rodent hookworm *N. brasiliensis* and whipworm *Tm*) were explored in experimental colitis. The chemically (TNBS)-induced mouse model of colitis is T-cell mediated and skewed toward a mixed Th1/Th2 immune response and induces transmural inflammation in the gut with clinical features similar to human ulcerative colitis (53). Interestingly, only secreted proteins and vesicles from *Nippostronglylus* (ESP, EVs, and vesicle-depleted ESP) showed efficacy in preventing colitis signs and symptoms, whereas purified fractions from *Tm* did not confer significant protection (**Figure 3**; Figure S1 in Supplementary Material).

Induction of intestinal inflammation resulted in a 15–20% weight loss in the PBS-treated colitis control group over the course of the study (**Figure 3A**). Mice from all groups initially lost weight, whereas *Nb*-EV-treated mice recovered most of their initial weight by the end of the experiment (on day 3). In comparison to the naïve healthy control mice, colon length was significantly decreased in the colitis group ($p < 0.001$), while *Nb*-EV-treated mice remained unaffected by the administration of TNBS.

Macroscopic analysis of the colons revealed a significant reduction of tissue inflammation in animals treated with *Nippostrongylus* secreted fractions as seen by significant longer colons, fewer adhesions, absence of mucosal edema and colon wall thickening, and no ulceration (Figure S2 in Supplementary Material), reflected by significantly improved clinical and pathological scores

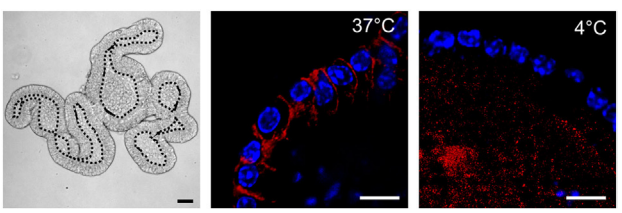

FIGURE 2 | *Nippostrongylus brasiliensis* extracellular vesicles (EVs) are internalized by murine small intestinal (SI) organoid cells. Representative laser scanning confocal microscopy images (Zeiss 780 NLO) of PKH26-labeled EVs (red) at 37 and 4°C (metabolically inactive cells). EVs are internalized by cells within organoids at 37°C 3 h after particle-injection into the organoid central lumen (corresponding to the luminal side of the gut). Hoechst dye (blue) was used to label cell nuclei. Left panel demonstrates a bright field image (Zeiss AxioImager M1 ApoTome) of the tissue architecture of a murine SI organoid. Central lumen of the organoids is separated by the dotted line from the epithelial cell layer. Bar corresponds to 10 µm.

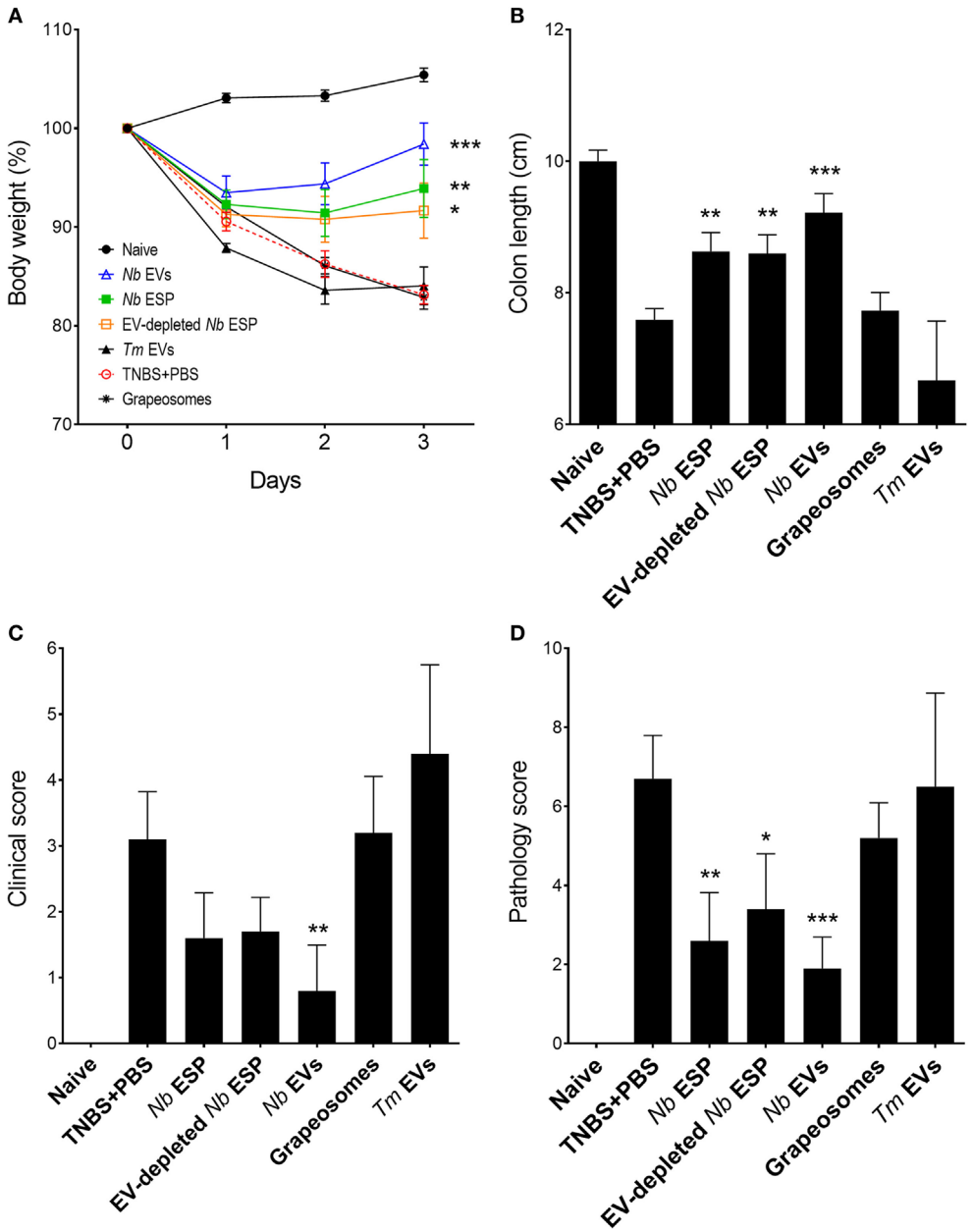

FIGURE 3 | Protective effects of *Nippostrongylus brasiliensis* secreted fractions in experimental colitis. Mice received a single intraperitoneal injection of 20 µg protein in PBS 1 day prior to intrarectal administration of 2.5 mg of TNBS in 50% ethanol. **(A)** Body weight was recorded daily for the indicated groups. **(B)** Colon length measured after euthanasia at the end of the experiment (day 3). **(C)** Clinical examination and scoring of mice on day 3, including weight loss, piloerection, feces consistency, and mobility of mice from normal to severely affected (0–3). **(D)** After euthanasia, colons were visually scored by presence of adhesions, edema, mucosal wall thickening, and ulceration from absent to severe (high) on a scale of 0–3. Data show mean ± SEM of pooled data from two independent trials ($n = 10$ mice/group). Groups were compared to the PBS + TNBS (colitis) control group by Mann–Whitney *U*-test. $^{*}p < 0.05$; $^{**}p < 0.01$; $^{***}p < 0.001$. Data for *Trichuris muris* (*Tm*) extracellular vesicles (EVs) were analyzed in a separate independent experiment (see Figure S1 in Supplementary Material) and included only for representation.

(**Figures 3C,D**). Unlike *Nb*-EV-treated mice, histology (H&E staining) of distal colon sections from the PBS group showed mucosal erosion and epithelial hyperplasia, pronounced cellular infiltration in the lamina propria and intraepithelial compartments, evidence of edema and ulceration, and loss of healthy goblet cells (**Figure 4B**). Scoring of histological sections for overall pathology illustrated that *Nb*-EV-treated mice had significantly reduced histopathology ($p = 0.004$) (**Figures 4C,D**), displaying an overall mucosal architecture similar to that of naïve healthy control mice (**Figures 4A,D**).

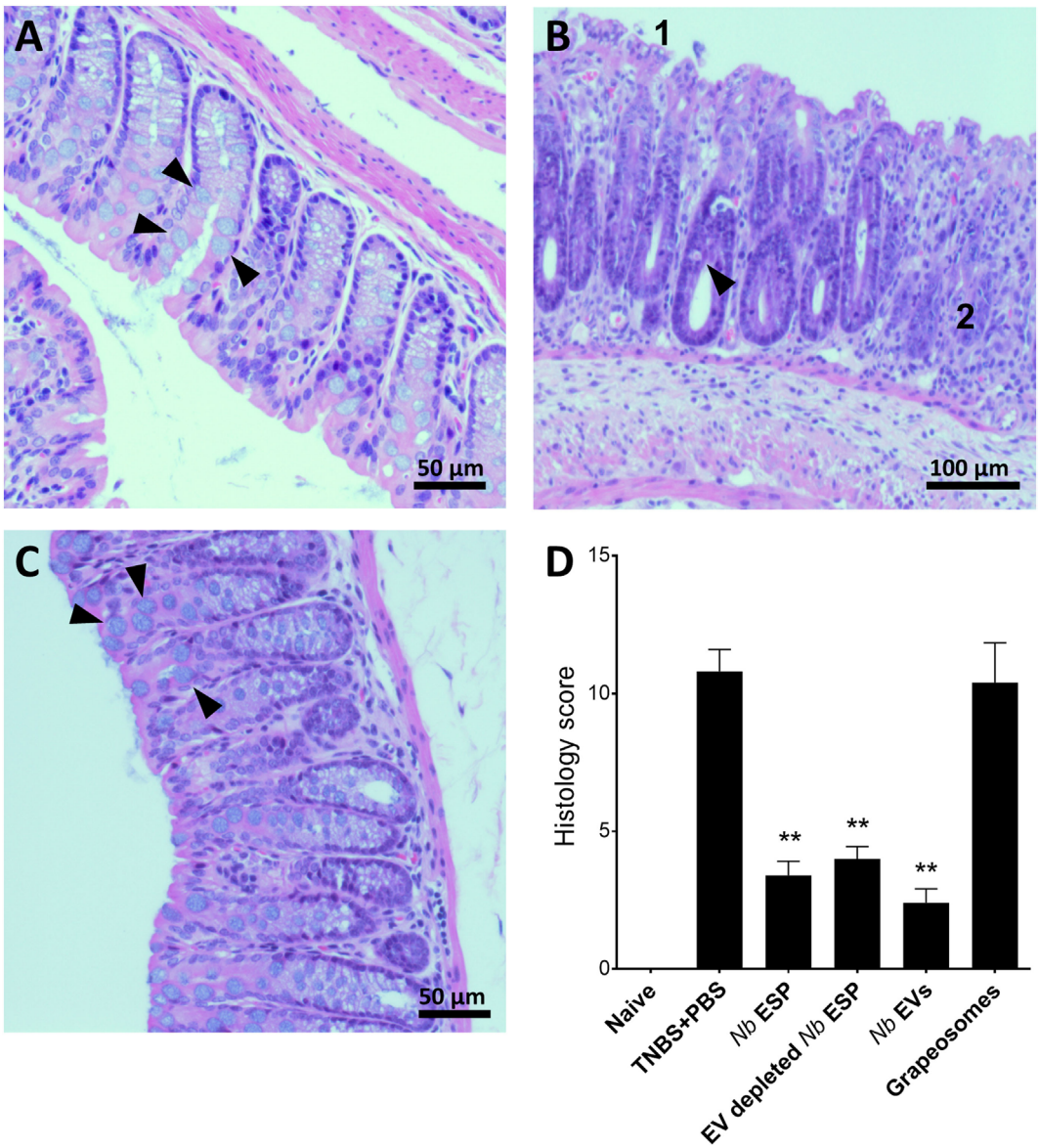

FIGURE 4 | *Nippostrongylus brasiliensis* extracellular vesicles (EVs) protect from TNBS-induced histopathology. Representative photomicrographs of hematoxylin and eosin stained colonic tissue sections. A representative section from the distal colon (~1 cm) was fixed in 4% paraformaldehyde for histological observations. **(A)** Healthy naïve control mouse; **(B)** PBS-treated colitis control; **(C)** *N. brasiliensis* EV-treated mouse. Arrows point to normal goblet cells **(A,C)** and goblet cell destruction **(B)**. (1) Tissue erosion and (2) cellular infiltrates and overall tissue hyperplasia. **(D)** Histological scoring of histopathology. Statistical analyses were performed by pooling data from groups of mice from two independent but reproducible experiments (n = 10 mice/group). Error bars represent mean ± SEM. Groups were statistically compared to the PBS + TNBS (colitis) control group (**$p < 0.01$).

Compared to other tested fractions from *Nippostrongylus*, *Nb*-EVs generally had the best scores in all of the tested parameters (weight loss, colon length, clinical-, macroscopic-, and histological score), although without statistical differences between the fractions. The purification method or the presence of vesicles itself did not have an impact on intestinal inflammation, as the grapeosomes-treated group showed severe inflammation post-TNBS administration, similar to that observed for the PBS + TNBS control group.

Nb-EVs Promote Immune Regulation in Colonic Tissue Which Is Different From That Induced by Soluble ESP Proteins

To address the impact of *Nippostrongylus* secreted molecules on the production of cytokines at the site of inflammation, colons of mice exposed to TNBS were cultured and cytokine secretion was analyzed by ELISA (**Figure 5**). Mice treated with any *Nippostrongylus* secretory product prior to administration of TNBS showed a significant reduction in the levels of the

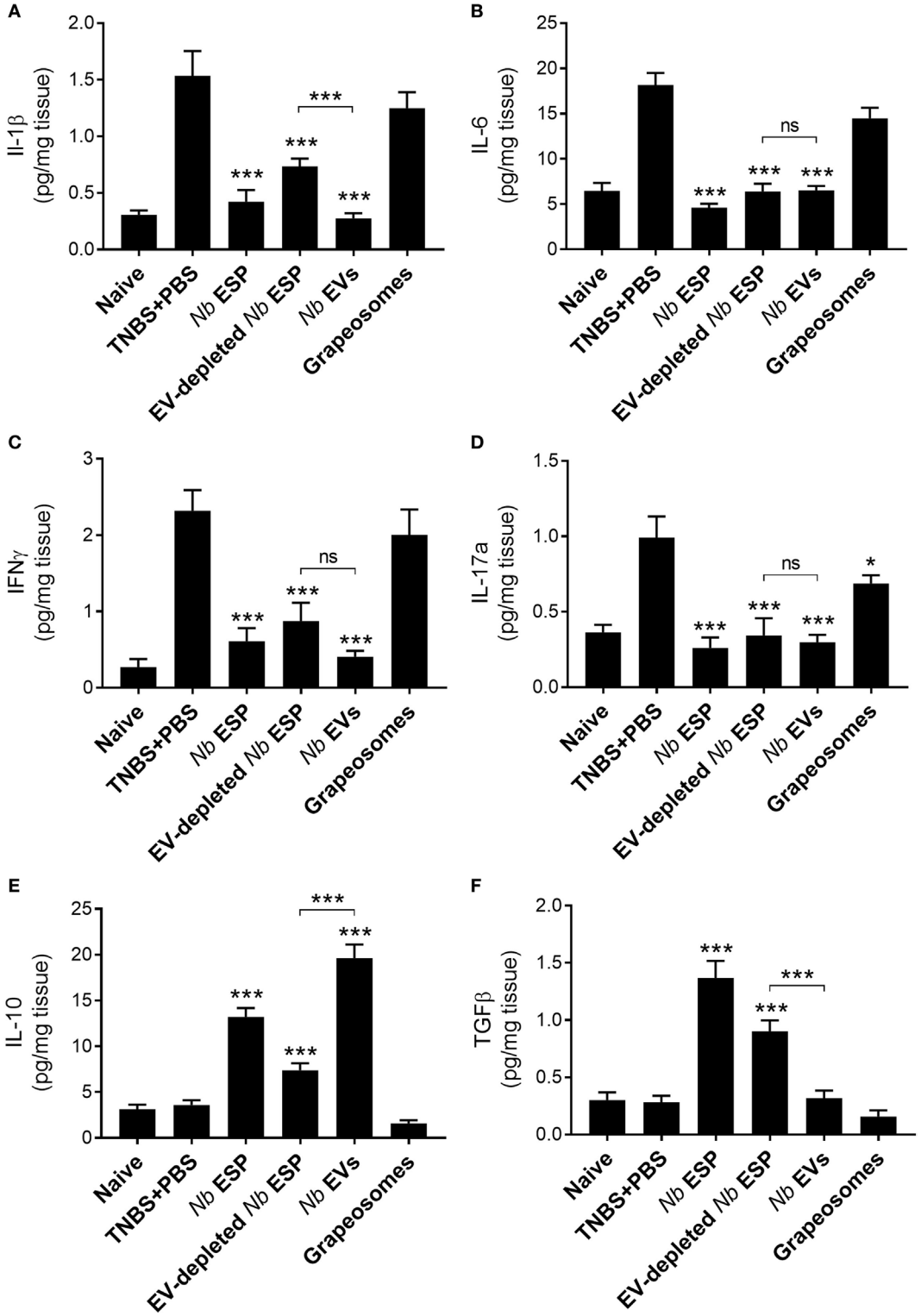

FIGURE 5 | *Nippostrongylus brasiliensis* extracellular vesicles (EVs) suppress colonic inflammatory cytokine production and promote IL-10 secretion in mice. Cytokine profile of cultured colon tissue of healthy naïve mice, mice treated with *N. brasiliensis* secreted products, PBS colitis control and grape-vesicle (grapeosomes) control mice. **(A)** IL-1β; **(B)** IL-6; **(C)** IFNγ; **(D)** IL-17a; **(E)**; IL-10; and **(F)** TGFβ. All groups were compared to the PBS + TNBS (colitis) control group; the *N. brasiliensis* secreted protein group (EV-depleted) was also compared with the purified vesicles group (bracket). All comparisons were performed using a Mann–Whitney *U*-test. $^{*}p < 0.05$; $^{**}p < 0.01$; $^{***}p < 0.001$. Error bars represent mean ± SEM.

pro-inflammatory cytokines IL-1β, IL-6, IL-17a, and IFNγ, and the levels were—except for IL-1β in the secreted protein fraction—similar to those of naïve healthy control mice. By contrast, only the levels of the anti-inflammatory cytokine IL-10 was increased in the *Nb*-EV-treated group, which was significantly higher ($p < 0.001$) than that of mice treated with secreted proteins only. In comparison, the levels of TGFβ in the *Nb*-EV group were not significantly different from the healthy naïve mice or the PBS-treated group.

Nb-EVs Contain Helminth-Specific Proteins and miRNA Cargo With Putative Immunomodulatory Properties

Purified *Nb*-EVs were digested with trypsin and analyzed by LC-MS/MS, resulting in a list of 81 proteins for *Nb*-EVs (Table S1 in Supplementary Material). Next to the proteomic "EV-markers" ($n = 8$) and structural proteins ($n = 7$) mentioned previously, the most abundant *Nb*-EV proteins ($n = 27$, 33.3%) were sperm-coating protein (SCP)-like extracellular proteins, also called SCP/Tpx-1/Ag5/PR-1/Sc7 domain containing proteins (SCP/TAPS), of which a high proportion (9 of 27) belonged to the helminth-specific *Ancylostoma*-secreted protein family (ASP; syn. activation-associated proteins). Furthermore, the dataset contains proteinases ($n = 10$), hypothetical proteins ($n = 8$), membrane-bound enzymes and transport proteins ($n = 5$), chaperones other than HSP70 ($n = 2$), and other metabolic enzymes ($n = 13$). In 53 (65.4%) of the 81 proteins, a signal peptide was absent (Table S1 in Supplementary Material), which is characteristic for EV proteins as a class of non-classically secreted particles.

Despite the differences between the two nematode EV populations in their immunological protection against colitis, their proteomic cargo share high sequence- and functional homology, including the abundantly represented SCP/TAPS proteins. Proteins unique for the *Nb*-EV dataset consist of seven uncharacterized hypothetical proteins, three apyrase isoforms—which are catalysts for the hydrolysis of ATP to yield AMP and inorganic phosphate—and a saposin protein (Table S2 in Supplementary Material).

By sequencing and screening biological triplicates for miRNA cargo in *Nb*-EVs using the Illumina NextSeq platform and downstream analyses, we identified 52 miRNAs commonly present in all datasets, 47 of which have close homologs to 31 other nematode miRNAs (**Figure 6**).

Potential interactions of *N. brasiliensis* miRNAs with murine host genes were explored by computational target prediction. The 52 nematode EV-miRNAs were predicted to interact with 2,093 unique 3′UTR binding sites of the mouse genome assembly (Table S3 in Supplementary Material). Associated annotated coding genes were grouped according to signaling, metabolic, and disease pathways (Figure S3 in Supplementary Material). Interestingly, immune system-related gene networks were predicted to be targeted by 30 of the 52 detected miRNAs, of which 23 directly affect cytokine signaling networks—including the most abundant nbr-miR-ev49 (**Figure 6**; Table S4 in Supplementary Material).

Given that *Nb*-EVs but not *Tm*-EVs protected against inducible colitis in mice, we compared the vesicular miRNA cargo of these two nematodes. When we compared the miRNA component of *Nb*- and *Tm*-EVs, we found only 26 Nbr_miRs to be homologous to *Tm*-EV miRNAs, some of which are isomiRs (**Figure 6**). Of these, 13 shared miRNAs were predicted to target gene networks involved in the immune system (10 of which targeted cytokine gene networks). We further analyzed the miRNA host gene target prediction for specific interactions with genes involved in pro- and anti-inflammatory cytokine responses based on the miRanda algorithm (Figure S4 in Supplementary Material). This global cursory analysis of host gene interactions by nematode EVs points to a strong regulation of cytokine gene networks through parasite miRNAs. The analysis illustrates that EV-miRNAs from both nematodes interact with pro- and anti-inflammatory host genes. Overall, however, there are more cytokine genes targeted by EV miRNAs that are unique to *N. brasiliensis* ($n = 29$) than by EV miRNAs that are unique to *Tm* ($n = 17$). Prediction analyses unfortunately are not able to demonstrate the fate of the targeted gene (i.e., upregulated vs. downregulated expression).

DISCUSSION

Immune evasion is a common strategy of parasitic helminths to survive and reproduce within a hostile environment, while neutralizing immune pathways that would otherwise expel them and resetting the thresholds of immune reactivity (15). Hookworms have evolved to establish chronic infections while inducing minimal pathology to the host when present in small numbers (3). They achieve this state of mutual tolerance by promoting regulatory immune circuits *via* expansion of various regulatory and tolerogenic immune cell subsets (3, 15). Hookworms drive a "modified Th2" immune response, including typical Th2 cytokines (IL-4, IL-5, IL-9, and IL-13) but also the regulatory cytokines IL-10 and TGF-β. In hookworm-infected humans at least, the skewing of the immune response enables the parasite to survive for long periods, despite the presence of a robust, albeit non-sterilizing immune response (54–56). Hookworms and humans have instead coevolved to reach an immunological *status quo*, where Th2 responses likely keep worm burdens in check (so as not to overwhelm and ultimately kill the host), but regulatory responses ensure that at least some worms survive and reproduce over many years.

The immunoregulatory prowess of hookworms has been highlighted in clinical trials for IBD (57) and celiac disease (20). Using animal models of inflammatory diseases, we and others have shown using *N. brasiliensis* (58) and *Ancylostoma* sp. (21–23, 25) that injection of ESP alone mimics the immune phenotype of the worm infection and is sufficient to suppress inflammation in numerous models of autoimmunity and allergy. Until now, identification of bioactive hookworm ESP molecules has placed emphasis on the protein moieties (25, 33, 59), and other molecular entities have been ignored.

As we show herein, a major component of ESP from hookworms and other helminths is EVs. These parasite EVs have been shown to deposit their payloads consisting of proteins, nucleic acids, lipids, and metabolites into host cells where at least some of them exert their immunomodulatory properties (27, 28). Here, we demonstrate that *N. brasiliensis*, which is frequently used as

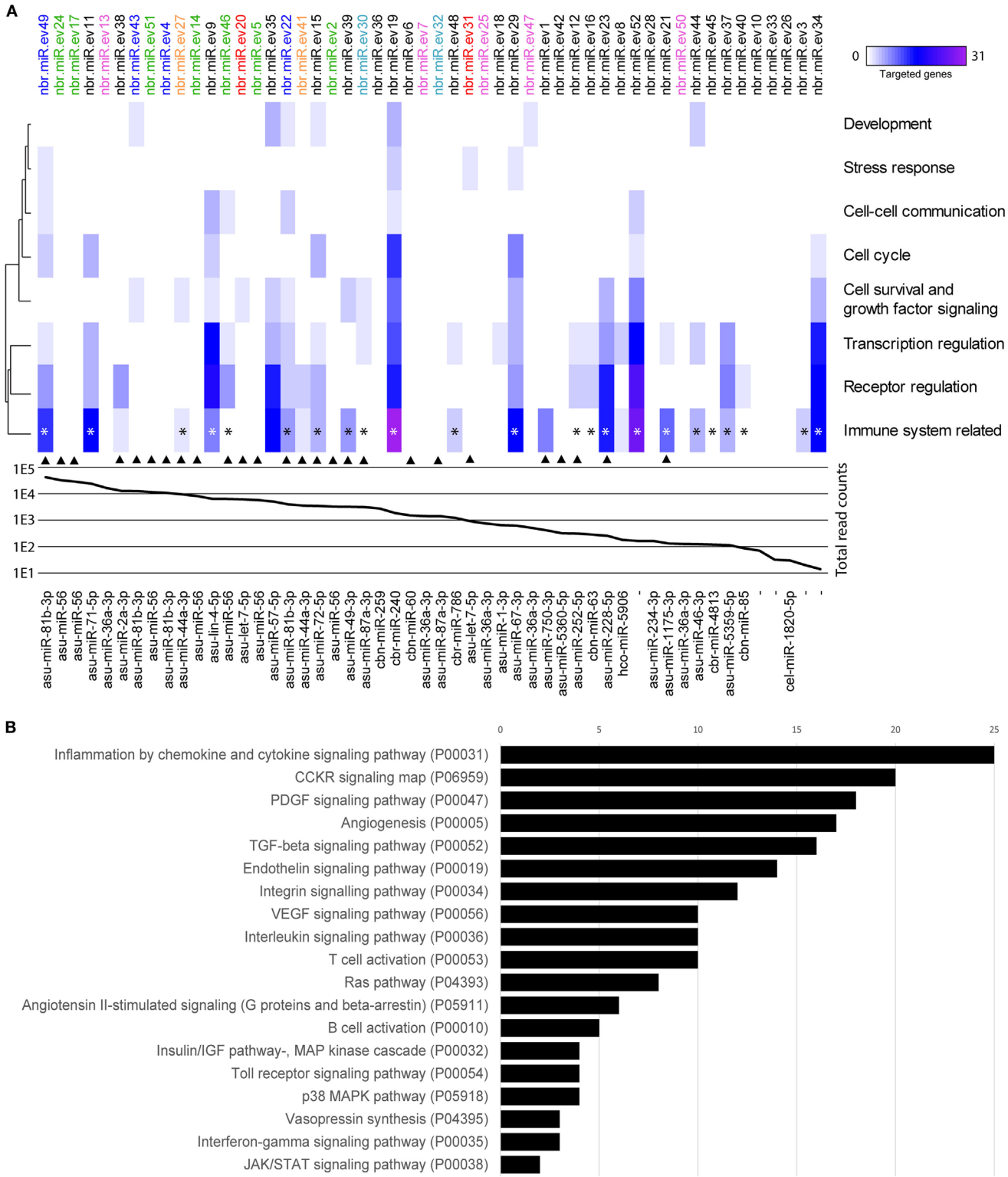

FIGURE 6 | miRNAs of *Nippostrongylus brasiliensis* extracellular vesicles (EVs) are predicted to interact with different murine host gene networks. **(A)** Functional map of *N. brasiliensis* EV miRNAs and their target murine host genes categorized by PantherDB signaling pathway analysis (heat map corresponds to individual targeted genes in the murine host). Top axis shows the 52 identified miRNAs (termed as nbr-miR-ev#). IsomiRs are indicated in color. Graph represents the abundance (mean read counts from three biological replicates). Bottom axis shows their closest homologs (*de novo* transcripts are left empty). Homologs to miRNAs found in *Trichuris muris* EVs are marked by an arrow [according to Eichenberger et al. (37)]. * indicates miRNAs targeting genes involved in cytokine networks. **(B)** Total number of targeted gene networks identified by PantherDB categories classified as "immune system related." Data are available in Table S3 in Supplementary Material.

a model for human hookworm infection, secretes exosome-like EVs that possess immunoregulatory molecules.

Extracellular vesicles from the trematode *Opisthorchis viverrini* and the nematodes *Brugia malayi*, *Heligmosomoides polygyrus*, and *Tm* are internalized by host cells (32, 37, 60, 61). Similarly, *Nb*-EVs interact with murine cells, as demonstrated by the uptake of stained EVs *in vitro* in murine SI organoids. Similar to *Tm*, the cellular interaction seems to be non-specific, and all cell types found within the organoids (mainly absorptive enterocytes, goblet cells, enteroendocrine cells, Paneth cells, and Lgr5+ stem cells) contained fluorescently labeled EVs. One drawback of this groundbreaking organoid culture system (62) is the lack of immune cells. Hence, further studies are needed to explore the specific impact of parasite EVs on host immune cells, particularly T cells (e.g., intraepithelial lymphocytes) and antigen-presenting cells.

To evaluate the immunomodulatory properties of nematode EVs, we induced T cell-dependent acute colitis in mice. In this model, TNBS haptenizes the colonic microbiota, which then translocates across the ethanol-disrupted gut epithelium and elicits a mixed Th1/Th2 immune response, and induces transmural inflammation in the gut with clinical, morphological, and histopathological features similar to those of human IBD (63). Our results indicate that EVs from *Nippostrongylus* (*Nb*-EVs) protected against intestinal inflammation, whereas EVs from *Tm* did not. This finding is somewhat surprising, given that *Trichuris* spp. have coevolved with their hosts to establish chronic infections. A major difference in the biology of these two GI helminths is the life cycle—hookworm infect the host by skin penetration followed by a refined systemic migration through the vasculature of the lungs en route to the small bowel whereupon they bury their anterior ends in the sub-mucosa and feed on extravasated blood; whipworms, however, have a direct oral infection route and feed on (and burrow into) the epithelial layer.

Prophylactic treatment of mice prior to administration of TNBS with *Nb*-EVs, "complete" ESP, or the EV-depleted soluble protein fraction, resulted in suppression of pro-inflammatory cytokines IFN-γ, IL-6, IL-17a, and IL-1β. IL-10 has a protective role against colitic inflammation (64). Furthermore, genetic-linkage analysis of patients with colitis revealed distinct mutations in the IL-10 gene, demonstrating a central role for this cytokine in the negative feedback necessary to maintain mucosal homeostasis (65, 66). As seen previously with "complete" *Ancylostoma caninum* (dog hookworm) ESP treatment in TNBS colitis (21), *Nb*-EVs promoted the production of IL-10, suggesting a potential mechanism of systemic regulation of inflammation. By contrast, TGF-β was found to be elevated only in mice which were treated with secreted proteins (ESP or vesicle-depleted fraction) and not EVs. Nevertheless, these groups displaying elevated TGF-β levels, although significantly protected against some parameters of colitis, generally displayed lower levels of protection compared with EV-treated mice. TGF-β is responsible for suppression of gut inflammation and enhancing barrier function, and it promotes the induction of functional Tregs from naive CD4+ T-cell precursors (67, 68). Hence, nematode immune evasion strategies rely most probably on a finely tuned cocktail of soluble and vesicular molecules to regulate host immunity.

The EV proteomes of both *N. brasiliensis* and *Tm* are replete with SCP/TAPS proteins. This family of proteins is abundantly expressed by parasitic nematodes and trematodes (69). Their roles are still mostly unknown, but in hookworms they have been suggested to play roles in larval skin penetration (70), in the transition from the free-living to parasitic stages (71), and modulation of the immune response (72, 73). Despite the significantly greater ability of hookworm EVs compared with whipworms EVs to suppress TNBS-induced inflammation, SCP/TAPS proteins were over-represented in both EV populations.

An emerging mechanism of parasite-driven immune modulation is *via* the transfer of genetic information between host and parasite. To this end, we identified 52 *N. brasiliensis* miRNAs, including five novel miRNAs without homology to other nematode miRNAs deposited in the reference database. miRNAs are considered as regulators of the immune response by targeting host immune cell mRNAs for degradation or translational repression (74). *N. brasiliensis* miRNAs that putatively regulate expression of mouse genes involved in specific gene networks and cellular pathways were identified. Our *in silico* prediction analysis of murine host gene interactions of miRNAs points toward a strong involvement of parasite miRNAs in regulation/modulation of the host immune system. Although there were few homologies with recently published *Tm* EV miRNA datasets (37, 75), the *N. brasiliensis* miRNAs seem to target immunological networks more specifically *via* a greater abundance and redundancy of several isomiRs. The prediction resulted in a potential 2,093 unique interactions with mouse transcripts. Although it is known that target-predictions bear a high false-positive rate, it provides insights into the most highly rated interaction networks. Correspondingly, the most affected pathway was "cytokine and chemokine signaling" (P00031 in PatherDB). The located genes encoded mostly chemokine receptors and downstream signaling molecules (data not shown but mined from Table S3 in Supplementary Material). Interestingly, pathway analysis indicated that *Nb*-EV miRNAs mapped to interleukin-networks, notably IL-6 receptor and IL-6 signal transducers, IL-17 receptor genes, and IL-21. We also identified single hits with interactions to the Th2 cytokines IL-13 and IL-33, many of which showed altered expression in EV-treated mice after TNBS administration. Furthermore, targeting of the IFNγ- (P00035) and TFGβ- (P00052) signaling pathways was noted. Overall, our analysis of putatively targeted host genes illustrates that EV-miRNAs from nematodes interact with pro- and anti-inflammatory pathways. Interestingly, *Tm*-EV miRNAs seem to primarily target pathways that function downstream of cytokine receptor engagement, such as signal transduction (e.g., IRAK2/4) and transcription factors (e.g., STAT1, NFATs, and SMADs), while *Nb*-EV miRNAs directly target cytokine and cytokine receptor transcripts. However, *in vivo* experiments with miRNAs (separated from other EV components such as proteins) are needed to confirm the *in silico* predictions.

Although not explored herein, regulation of angiogenesis and wound-repair mechanisms (e.g., vascular endothelial growth factor; P00056) were frequently targeted by *Nb*-EV miRNAs. Given that miRNAs, in addition to their well-studied repressive function, can act with certain context-dependent factors to stabilize and increase translation of targets by both transcriptional

and posttranscriptional mechanisms (76), a role for worm EVs in healing and vascularizing the wounds it causes when feeding is plausible (77).

In summary, *Nb*-EVs induced protection against intestinal inflammation while EVs from an unrelated source (grapes) did not. By contrast, EVs from the whipworm *Tm* did not induce protection against acute colitis. Administration of *Nb*-EVs to mice induced a unique cytokine profile compared to that induced by soluble ESP proteins; *Nb*-EVs promoted significantly greater levels of IL-10 secretion in the colon compared to soluble EV-depleted ES products, and this finding might be due to miRNAs contained within the EVs. Our findings provide insight into the immunobiology of hookworm EVs, and show for the first time that helminth EVs suppress colitis and likely harbor therapeutic molecules for the treatment of inflammatory bowel and other autoimmune diseases.

ETHICS STATEMENT

The study was approved by the James Cook University (JCU) Animal Ethics Committee (A2180, A2213, and A2300). Animals were maintained at the JCU animal house (Cairns campus) under normal conditions of regulated temperature and lighting (12 h light/dark cycle) with free access to pelleted food and water. Mice and rats were kept in cages in compliance with the Australian Code of Practice for the Care and Use of Animals for Scientific Purposes.

AUTHOR CONTRIBUTIONS

RE, JS, and AL conceived and designed the study. RE performed most of the experiments. SR, LJ, RP, GB, and JS assisted in the *in vivo* experiments and analyses. MO and CE facilitated imaging. JZ performed sample histology. PG and LD propagated animal model and *in vivo* studies. MF provided bioinformatics assistance and support. RE and AL wrote the manuscript. All authors proofed the manuscript.

ACKNOWLEDGMENTS

We thank staff in the AITHM Cairns and Townsville animal facility, with special thanks to Dr. S. Rowarth, A. Susianto, and L. Finn for animal husbandry, and staff in the QIMR Flow Cytometry and Microscopy Facility, with special thanks to Dr. N. Waterhouse, and Dr. T. H. Nguyen for technical assistance.

FUNDING

This work was supported by a program grant from the National Health and Medical Research Council (NHMRC) [program grant number 1037304] and a Senior Principal Research fellowship from NHMRC to AL. RE was supported by an "Early Postdoc Mobility" fellowship (P2ZHP3_161693) from the Swiss National Science Foundation. The funders had no role in study design, data collection and analysis, decision to publish, or preparation of the manuscript.

SUPPLEMENTARY MATERIAL

The Supplementary Material for this article can be found online at https://www.frontiersin.org/articles/10.3389/fimmu.2018.00850/full#supplementary-material.

FIGURE S1 | Effects of *Trichuris muris* secreted fractions in experimental colitis. Mice received a single intraperitoneal injection of 20 µg protein in PBS 1 day prior to intrarectal administration of 2.5 mg of TNBS in 50% ethanol. Data display daily recorded body weight, final clinical examination, colon length, and colon pathology after euthanasia.

FIGURE S2 | Representative images of mouse colons from all the groups examined in the experimental colitis model.

FIGURE S3 | Prediction of *Nippostrongylus brasiliensis* extracellular vesicle (EV) miRNA target interactions to murine host genes. Functional map of *N. brasiliensis* EV miRNAs and their target murine host genes categorized by PantherDB signaling, metabolic, disease, and other pathways. Heat map corresponds to individual targeted genes in the murine host.

FIGURE S4 | Alluvial diagram depicting interactions between nematode EV miRNAs and mouse host cytokine gene targets. *Nippostrongylus brasiliensis* (*Nb*)-EV miRNAs (green), *Trichuris muris* (*Tm*)-EV miRNAs (pink), and shared homologs (orange) are presented. Links are colored according to canonical pro- (red) and anti-inflammatory (blue) responses.

TABLE S1 | Proteomic analysis of extracellular vesicles (EVs) secreted by *Nippostrongylus brasiliensis*. Details of the identification of the proteins present in the EVs secreted by *N. brasiliensis* using X!Tandem, Tide, MS-GF+ and OMSSA. All proteins are shown, including contaminants.

TABLE S2 | Structural (all-vs-all blast) and functional (Blast2GO) comparison of *Nippostrongylus brasiliensis*- and *Trichuris muris*-EV proteomes.

TABLE S3 | Data description on predicted *Nippostrongylus brasiliensis* miRNA–host target interactions. Table showing the 52 miRNAs identified in the *N. brasiliensis* extracellular vesicles and their 3′UTR predicted binding sites in the mouse genome.

TABLE S4 | Pathway analysis and parsing of *Nippostrongylus brasiliensis* EV miRNAs and their target murine host genes categorized by PantherDB pathways.

REFERENCES

1. van Riet E, Hartgers FC, Yazdanbakhsh M. Chronic helminth infections induce immunomodulation: consequences and mechanisms. *Immunobiology* (2007) 212(6):475–90. doi:10.1016/j.imbio.2007.03.009
2. McSorley HJ, Hewitson JP, Maizels RM. Immunomodulation by helminth parasites: defining mechanisms and mediators. *Int J Parasitol* (2013) 43(3–4):301–10. doi:10.1016/j.ijpara.2012.11.011
3. Loukas A, Hotez PJ, Diemert D, Yazdanbakhsh M, McCarthy JS, Correa-Oliveira R, et al. Hookworm infection. *Nat Rev Dis Primers* (2016) 2:16088. doi:10.1038/nrdp.2016.88
4. Fenwick A. The global burden of neglected tropical diseases. *Public Health* (2012) 126(3):233–6. doi:10.1016/j.puhe.2011.11.015
5. Pullan RL, Smith JL, Jasrasaria R, Brooker SJ. Global numbers of infection and disease burden of soil transmitted helminth infections in 2010. *Parasit Vectors* (2014) 7:37. doi:10.1186/1756-3305-7-37
6. Mulvenna J, Hamilton B, Nagaraj SH, Smyth D, Loukas A, Gorman JJ. Proteomics analysis of the excretory/secretory component of the blood-feeding stage of the hookworm, *Ancylostoma caninum*. *Mol Cell Proteomics* (2009) 8(1):109–21. doi:10.1074/mcp.M800206-MCP200
7. Maizels RM, McSorley HJ. Regulation of the host immune system by helminth parasites. *J Allergy Clin Immunol* (2016) 138(3):666–75. doi:10.1016/j.jaci.2016.07.007
8. Kassai T, Redl P. PGE1 without effect on *Nippostrongylus brasiliensis*. *Int J Parasitol* (1982) 12(4):243. doi:10.1016/0020-7519(82)90024-8
9. Dent LA, Daly CM, Mayrhofer G, Zimmerman T, Hallett A, Bignold LP, et al. Interleukin-5 transgenic mice show enhanced resistance to primary infections

with *Nippostrongylus brasiliensis* but not primary infections with *Toxocara canis*. *Infect Immun* (1999) 67(2):989–93.
10. Giacomin PR, Gordon DL, Botto M, Daha MR, Sanderson SD, Taylor SM, et al. The role of complement in innate, adaptive and eosinophil-dependent immunity to the nematode *Nippostrongylus brasiliensis*. *Mol Immunol* (2008) 45(2):446–55. doi:10.1016/j.molimm.2007.05.029
11. Knott ML, Matthaei KI, Foster PS, Dent LA. The roles of eotaxin and the STAT6 signalling pathway in eosinophil recruitment and host resistance to the nematodes *Nippostrongylus brasiliensis* and *Heligmosomoides bakeri*. *Mol Immunol* (2009) 46(13):2714–22. doi:10.1016/j.molimm.2009.05.016
12. Sotillo J, Sanchez-Flores A, Cantacessi C, Harcus Y, Pickering D, Bouchery T, et al. Secreted proteomes of different developmental stages of the gastrointestinal nematode *Nippostrongylus brasiliensis*. *Mol Cell Proteomics* (2014) 13(10):2736–51. doi:10.1074/mcp.M114.038950
13. Nair MG, Herbert DR. Immune polarization by hookworms: taking cues from T helper type 2, type 2 innate lymphoid cells and alternatively activated macrophages. *Immunology* (2016) 148(2):115–24. doi:10.1111/imm.12601
14. Hewitson JP, Grainger JR, Maizels RM. Helminth immunoregulation: the role of parasite secreted proteins in modulating host immunity. *Mol Biochem Parasitol* (2009) 167(1):1–11. doi:10.1016/j.molbiopara.2009.04.008
15. McSorley HJ, Maizels RM. Helminth infections and host immune regulation. *Clin Microbiol Rev* (2012) 25(4):585–608. doi:10.1128/CMR.05040-11
16. Summers RW, Elliott DE, Urban JF Jr, Thompson RA, Weinstock JV. *Trichuris suis* therapy for active ulcerative colitis: a randomized controlled trial. *Gastroenterology* (2005) 128(4):825–32. doi:10.1053/j.gastro.2005.01.005
17. Croese J, O'Neil J, Masson J, Cooke S, Melrose W, Pritchard D, et al. A proof of concept study establishing *Necator americanus* in Crohn's patients and reservoir donors. *Gut* (2006) 55(1):136–7. doi:10.1136/gut.2005.079129
18. Feary JR, Venn AJ, Mortimer K, Brown AP, Hooi D, Falcone FH, et al. Experimental hookworm infection: a randomized placebo-controlled trial in asthma. *Clin Exp Allergy* (2010) 40(2):299–306. doi:10.1111/j.1365-2222.2009.03433.x
19. Fleming JO. Helminth therapy and multiple sclerosis. *Int J Parasitol* (2013) 43(3–4):259–74. doi:10.1016/j.ijpara.2012.10.025
20. Croese J, Giacomin P, Navarro S, Clouston A, McCann L, Dougall A, et al. Experimental hookworm infection and gluten microchallenge promote tolerance in celiac disease. *J Allergy Clin Immunol* (2015) 135(2):508–16. doi:10.1016/j.jaci.2014.07.022
21. Ruyssers NE, De Winter BY, De Man JG, Loukas A, Pearson MS, Weinstock JV, et al. Therapeutic potential of helminth soluble proteins in TNBS-induced colitis in mice. *Inflamm Bowel Dis* (2009) 15(4):491–500. doi:10.1002/ibd.20787
22. Cancado GG, Fiuza JA, de Paiva NC, Lemos Lde C, Ricci ND, Gazzinelli-Guimaraes PH, et al. Hookworm products ameliorate dextran sodium sulfate-induced colitis in BALB/c mice. *Inflamm Bowel Dis* (2011) 17(11):2275–86. doi:10.1002/ibd.21629
23. Ferreira I, Smyth D, Gaze S, Aziz A, Giacomin P, Ruyssers N, et al. Hookworm excretory/secretory products induce interleukin-4 (IL-4)+ IL-10+ CD4+ T cell responses and suppress pathology in a mouse model of colitis. *Infect Immun* (2013) 81(6):2104–11. doi:10.1128/IAI.00563-12
24. Mosconi I, Dubey LK, Volpe B, Esser-von Bieren J, Zaiss MM, Lebon L, et al. Parasite proximity drives the expansion of regulatory T cells in Peyer's patches following intestinal helminth infection. *Infect Immun* (2015) 83(9):3657–65. doi:10.1128/IAI.00266-15
25. Navarro S, Pickering DA, Ferreira IB, Jones L, Ryan S, Troy S, et al. Hookworm recombinant protein promotes regulatory T cell responses that suppress experimental asthma. *Sci Transl Med* (2016) 8(362):362ra143. doi:10.1126/scitranslmed.aaf8807
26. Marcilla A, Trelis M, Cortes A, Sotillo J, Cantalapiedra F, Minguez MT, et al. Extracellular vesicles from parasitic helminths contain specific excretory/secretory proteins and are internalized in intestinal host cells. *PLoS One* (2012) 7(9):e45974. doi:10.1371/journal.pone.0045974
27. Coakley G, Maizels RM, Buck AH. Exosomes and other extracellular vesicles: the new communicators in parasite infections. *Trends Parasitol* (2015) 31(10):477–89. doi:10.1016/j.pt.2015.06.009
28. Buck AH, Coakley G, Simbari F, McSorley HJ, Quintana JF, Le Bihan T, et al. Exosomes secreted by nematode parasites transfer small RNAs to mammalian cells and modulate innate immunity. *Nat Commun* (2014) 5:5488. doi:10.1038/ncomms6488
29. Nowacki FC, Swain MT, Klychnikov OI, Niazi U, Ivens A, Quintana JF, et al. Protein and small non-coding RNA-enriched extracellular vesicles are released by the pathogenic blood fluke *Schistosoma mansoni*. *J Extracell Vesicles* (2015) 4:28665. doi:10.3402/jev.v4.28665
30. Sotillo J, Pearson M, Potriquet J, Becker L, Pickering D, Mulvenna J, et al. Extracellular vesicles secreted by *Schistosoma mansoni* contain protein vaccine candidates. *Int J Parasitol* (2016) 46(1):1–5. doi:10.1016/j.ijpara.2015.09.002
31. Wang L, Li Z, Shen J, Liu Z, Liang J, Wu X, et al. Exosome-like vesicles derived by *Schistosoma japonicum* adult worms mediates M1 type immune-activity of macrophage. *Parasitol Res* (2015) 114(5):1865–73. doi:10.1007/s00436-015-4373-7
32. Chaiyadet S, Sotillo J, Smout M, Cantacessi C, Jones MK, Johnson MS, et al. Carcinogenic liver fluke secretes extracellular vesicles that promote cholangiocytes to adopt a tumorigenic phenotype. *J Infect Dis* (2015) 212(10):1636–45. doi:10.1093/infdis/jiv291
33. Ferreira IB, Pickering DA, Troy S, Croese J, Loukas A, Navarro S. Suppression of inflammation and tissue damage by a hookworm recombinant protein in experimental colitis. *Clin Transl Immunology* (2017) 6(10):e157. doi:10.1038/cti.2017.42
34. Ju S, Mu J, Dokland T, Zhuang X, Wang Q, Jiang H, et al. Grape exosome-like nanoparticles induce intestinal stem cells and protect mice from DSS-induced colitis. *Mol Ther* (2013) 21(7):1345–57. doi:10.1038/mt.2013.64
35. Webber J, Clayton A. How pure are your vesicles? *J Extracell Vesicles* (2013) 2:19861. doi:10.3402/jev.v2i0.19861
36. Vaudel M, Barsnes H, Berven FS, Sickmann A, Martens L. SearchGUI: an open-source graphical user interface for simultaneous OMSSA and X!Tandem searches. *Proteomics* (2011) 11(5):996–9. doi:10.1002/pmic.201000595
37. Eichenberger RM, Talukder MH, Field MA, Wangchuk P, Giacomin P, Loukas A, et al. Characterization of *Trichuris muris* secreted proteins and extracellular vesicles provides new insights into host–parasite communication. *J Extracell Vesicles* (2018) 7(1):1428004. doi:10.1080/20013078.2018.1428004
38. Gotz S, Garcia-Gomez JM, Terol J, Williams TD, Nagaraj SH, Nueda MJ, et al. High-throughput functional annotation and data mining with the Blast2GO suite. *Nucleic Acids Res* (2008) 36(10):3420–35. doi:10.1093/nar/gkn176
39. Marchler-Bauer A, Lu S, Anderson JB, Chitsaz F, Derbyshire MK, DeWeese-Scott C, et al. CDD: a conserved domain database for the functional annotation of proteins. *Nucleic Acids Res* (2011) 39(Database issue):D225–9. doi:10.1093/nar/gkq1189
40. Petersen TN, Brunak S, von Heijne G, Nielsen H. SignalP 4.0: discriminating signal peptides from transmembrane regions. *Nat Methods* (2011) 8(10):785–6. doi:10.1038/nmeth.1701
41. Friedlander MR, Mackowiak SD, Li N, Chen W, Rajewsky N. miRDeep2 accurately identifies known and hundreds of novel microRNA genes in seven animal clades. *Nucleic Acids Res* (2012) 40(1):37–52. doi:10.1093/nar/gkr688
42. Kozomara A, Griffiths-Jones S. miRBase: annotating high confidence microRNAs using deep sequencing data. *Nucleic Acids Res* (2014) 42(Database issue):D68–73. doi:10.1093/nar/gkt1181
43. Enright AJ, John B, Gaul U, Tuschl T, Sander C, Marks DS. MicroRNA targets in *Drosophila*. *Genome Biol* (2003) 5(1):R1. doi:10.1186/gb-2003-5-1-r1
44. Grillo G, Turi A, Licciulli F, Mignone F, Liuni S, Banfi S, et al. UTRdb and UTRsite (RELEASE 2010): a collection of sequences and regulatory motifs of the untranslated regions of eukaryotic mRNAs. *Nucleic Acids Res* (2010) 38(Database issue):D75–80. doi:10.1093/nar/gkp902
45. Yates A, Akanni W, Amode MR, Barrell D, Billis K, Carvalho-Silva D, et al. Ensembl 2016. *Nucleic Acids Res* (2016) 44(D1):D710–6. doi:10.1093/nar/gkv1157
46. Mi H, Huang X, Muruganujan A, Tang H, Mills C, Kang D, et al. PANTHER version 11: expanded annotation data from gene ontology and reactome pathways, and data analysis tool enhancements. *Nucleic Acids Res* (2016) 45(D1):D183–9. doi:10.1093/nar/gkw1138
47. Fabregat A, Sidiropoulos K, Garapati P, Gillespie M, Hausmann K, Haw R, et al. The reactome pathway knowledgebase. *Nucleic Acids Res* (2016) 44(D1):D481–7. doi:10.1093/nar/gkv1351
48. R Development Core Team. *R: A Language and Environment for Statistical Computing*. Vienna, Austria: R Foundation for Statistical Computing (2010).
49. Sato T, Stange DE, Ferrante M, Vries RG, Van Es JH, Van den Brink S, et al. Long-term expansion of epithelial organoids from human colon, adenoma,

adenocarcinoma, and Barrett's epithelium. *Gastroenterology* (2011) 141(5): 1762–72. doi:10.1053/j.gastro.2011.07.050
50. Sage D, Donati L, Soulez F, Fortun D, Schmit G, Seitz A, et al. DeconvolutionLab2: an open-source software for deconvolution microscopy. *Methods* (2017) 115:28–41. doi:10.1016/j.ymeth.2016.12.015
51. Wangchuk P, Navarro S, Shepherd C, Keller PA, Pyne SG, Loukas A. Diterpenoid alkaloids of *Aconitum laciniatum* and mitigation of inflammation by 14-O-acetylneoline in a murine model of ulcerative colitis. *Sci Rep* (2015) 5:12845. doi:10.1038/srep12845
52. Hong T, Yang Z, Lv CF, Zhang Y. Suppressive effect of berberine on experimental dextran sulfate sodium-induced colitis. *Immunopharmacol Immunotoxicol* (2012) 34(3):391–7. doi:10.3109/08923973.2011.609887
53. Kiesler P, Fuss IJ, Strober W. Experimental models of inflammatory bowel diseases. *Cell Mol Gastroenterol Hepatol* (2015) 1(2):154–70. doi:10.1016/j.jcmgh.2015.01.006
54. Loukas A, Constant SL, Bethony JM. Immunobiology of hookworm infection. *FEMS Immunol Med Microbiol* (2005) 43(2):115–24. doi:10.1016/j.femsim.2004.11.006
55. McSorley HJ, Loukas A. The immunology of human hookworm infections. *Parasite Immunol* (2010) 32(8):549–59. doi:10.1111/j.1365-3024.2010.01224.x
56. Geiger SM, Alexander ND, Fujiwara RT, Brooker S, Cundill B, Diemert DJ, et al. *Necator americanus* and helminth co-infections: further down-modulation of hookworm-specific type 1 immune responses. *PLoS Negl Trop Dis* (2011) 5(9):e1280. doi:10.1371/journal.pntd.0001280
57. Croese J, Wood MJ, Melrose W, Speare R. Allergy controls the population density of *Necator americanus* in the small intestine. *Gastroenterology* (2006) 131(2):402–9. doi:10.1053/j.gastro.2006.05.019
58. Trujillo-Vargas CM, Werner-Klein M, Wohlleben G, Polte T, Hansen G, Ehlers S, et al. Helminth-derived products inhibit the development of allergic responses in mice. *Am J Respir Crit Care Med* (2007) 175(4):336–44. doi:10.1164/rccm.200601-054OC
59. Moyle M, Foster DL, McGrath DE, Brown SM, Laroche Y, De Meutter J, et al. A hookworm glycoprotein that inhibits neutrophil function is a ligand of the integrin CD11b/CD18. *J Biol Chem* (1994) 269(13):10008–15.
60. Zamanian M, Fraser LM, Agbedanu PN, Harischandra H, Moorhead AR, Day TA, et al. Release of small RNA-containing exosome-like vesicles from the human filarial parasite *Brugia malayi*. *PLoS Negl Trop Dis* (2015) 9(9):e0004069. doi:10.1371/journal.pntd.0004069
61. Coakley G, McCaskill JL, Borger JG, Simbari F, Robertson E, Millar M, et al. Extracellular vesicles from a helminth parasite suppress macrophage activation and constitute an effective vaccine for protective immunity. *Cell Rep* (2017) 19(8):1545–57. doi:10.1016/j.celrep.2017.05.001
62. Eisenstein M. Organoids: the body builders. *Nat Methods* (2018) 15:19. doi:10.1038/nmeth.4538
63. Wirtz S, Neufert C, Weigmann B, Neurath MF. Chemically induced mouse models of intestinal inflammation. *Nat Protoc* (2007) 2(3):541–6. doi:10.1038/nprot.2007.41
64. Li B, Alli R, Vogel P, Geiger TL. IL-10 modulates DSS-induced colitis through a macrophage-ROS-NO axis. *Mucosal Immunol* (2014) 7(4):869–78. doi:10.1038/mi.2013.103
65. Glocker EO, Kotlarz D, Boztug K, Gertz EM, Schaffer AA, Noyan F, et al. Inflammatory bowel disease and mutations affecting the interleukin-10 receptor. *N Engl J Med* (2009) 361(21):2033–45. doi:10.1056/NEJMoa0907206
66. Kotlarz D, Beier R, Murugan D, Diestelhorst J, Jensen O, Boztug K, et al. Loss of interleukin-10 signaling and infantile inflammatory bowel disease: implications for diagnosis and therapy. *Gastroenterology* (2012) 143(2):347–55. doi:10.1053/j.gastro.2012.04.045
67. Becker C, Fantini MC, Schramm C, Lehr HA, Wirtz S, Nikolaev A, et al. TGF-beta suppresses tumor progression in colon cancer by inhibition of IL-6 trans-signaling. *Immunity* (2004) 21(4):491–501. doi:10.1016/j.immuni.2004.07.020
68. Fu S, Zhang N, Yopp AC, Chen D, Mao M, Chen D, et al. TGF-beta induces Foxp3 + T-regulatory cells from CD4+ CD25- precursors. *Am J Transplant* (2004) 4(10):1614–27. doi:10.1111/j.1600-6143.2004.00566.x
69. Cantacessi C, Gasser RB. SCP/TAPS proteins in helminths – where to from now? *Mol Cell Probes* (2012) 26(1):54–9. doi:10.1016/j.mcp.2011.10.001
70. Wu XJ, Sabat G, Brown JF, Zhang M, Taft A, Peterson N, et al. Proteomic analysis of *Schistosoma mansoni* proteins released during in vitro miracidium-to-sporocyst transformation. *Mol Biochem Parasitol* (2009) 164(1):32–44. doi:10.1016/j.molbiopara.2008.11.005
71. Moser JM, Freitas T, Arasu P, Gibson G. Gene expression profiles associated with the transition to parasitism in *Ancylostoma caninum* larvae. *Mol Biochem Parasitol* (2005) 143(1):39–48. doi:10.1016/j.molbiopara.2005.04.012
72. Chen J, Hu X, He S, Wang L, Hu D, Wang X, et al. Expression and immune response analysis of *Schistosoma japonicum* VAL-1, a homologue of vespid venom allergens. *Parasitol Res* (2010) 106(6):1413–8. doi:10.1007/s00436-010-1817-y
73. Tribolet L, Cantacessi C, Pickering DA, Navarro S, Doolan DL, Trieu A, et al. Probing of a human proteome microarray with a recombinant pathogen protein reveals a novel mechanism by which hookworms suppress B-cell receptor signaling. *J Infect Dis* (2015) 211(3):416–25. doi:10.1093/infdis/jiu451
74. Coakley G, Buck AH, Maizels RM. Host parasite communications-messages from helminths for the immune system: parasite communication and cell-cell interactions. *Mol Biochem Parasitol* (2016) 208(1):33–40. doi:10.1016/j.molbiopara.2016.06.003
75. Tritten L, Tam M, Vargas M, Jardim A, Stevenson MM, Keiser J, et al. Excretory/secretory products from the gastrointestinal nematode *Trichuris muris*. *Exp Parasitol* (2017) 178:30–6. doi:10.1016/j.exppara.2017.05.003
76. Maute RL, Dalla-Favera R, Basso K. RNAs with multiple personalities. *Wiley Interdiscip Rev RNA* (2014) 5(1):1–13. doi:10.1002/wrna.1193
77. Gause WC, Wynn TA, Allen JE. Type 2 immunity and wound healing: evolutionary refinement of adaptive immunity by helminths. *Nat Rev Immunol* (2013) 13(8):607–14. doi:10.1038/nri3476

Conflict of Interest Statement: The authors declare that this research was conducted in the absence of any commercial or financial relationships that could be construed as a potential conflict of interest.

frontiers in Immunology

METHODS
published: 24 May 2018
doi: 10.3389/fimmu.2018.01011

Monitoring Extracellular Vesicle Cargo Active Uptake by Imaging Flow Cytometry

Yifat Ofir-Birin[1], Paula Abou karam[1], Ariel Rudik[1], Tal Giladi[1], Ziv Porat[2] and Neta Regev-Rudzki[1]**

[1] Department of Biomolecular Sciences, Faculty of Biochemistry, Weizmann Institute of Science, Rehovot, Israel, [2] Flow Cytometry Unit, Life Sciences Core Facilities, Weizmann Institute of Science, Rehovot, Israel

Extracellular vesicles are essential for long distance cell–cell communication. They function as carriers of different compounds, including proteins, lipids and nucleic acids. Pathogens, like malaria parasites (*Plasmodium falciparum*, *Pf*), excel in employing vesicle release to mediate cell communication in diverse processes, particularly in manipulating the host response. Establishing research tools to study the interface between pathogen-derived vesicles and their host recipient cells will greatly benefit the scientific community. Here, we present an imaging flow cytometry (IFC) method for monitoring the uptake of malaria-derived vesicles by host immune cells. By staining different cargo components, we were able to directly track the cargo's internalization over time and measure the kinetics of its delivery. Impressively, we demonstrate that this method can be used to specifically monitor the translocation of a specific protein within the cellular milieu upon internalization of parasitic cargo; namely, we were able to visually observe how uptaken parasitic *Pf*-DNA cargo leads to translocation of transcription factor IRF3 from the cytosol to the nucleus within the recipient immune cell. Our findings demonstrate that our method can be used to study cellular dynamics upon vesicle uptake in different host–pathogen and pathogen–pathogen systems.

Keywords: extracellular vesicles, imaging flow cytometry, malaria, *Plasmodium falciparum*, vesicle uptake

OPEN ACCESS

Edited by:
Maria Kaparakis-Liaskos, La Trobe University, Australia

Reviewed by:
Pawel R. Kiela, University of Arizona, United States
Lianjun Zhang, Université de Lausanne, Switzerland

***Correspondence:**
Ziv Porat
ziv.porat@weizmann.ac.il;
Neta Regev-Rudzki
neta.regev-rudzki@weizmann.ac.il

Specialty section:
This article was submitted to Immunological Tolerance and Regulation, a section of the journal Frontiers in Immunology

Received: *30 January 2018*
Accepted: *23 April 2018*
Published: *24 May 2018*

Citation:
Ofir-Birin Y, Abou karam P, Rudik A, Giladi T, Porat Z and Regev-Rudzki N (2018) Monitoring Extracellular Vesicle Cargo Active Uptake by Imaging Flow Cytometry. Front. Immunol. 9:1011. doi: 10.3389/fimmu.2018.01011

INTRODUCTION

Extracellular vesicles (EVs) are membrane-surrounded structures that are secreted by cells into the intercellular environment. EVs shuttle lipids, proteins, RNA, DNA, and other metabolites between cells and tissues. They diverge into two main subgroups according to their cellular origin: microvesicles (200–1,000 nm in diameter) are shed from the plasma membrane, whereas exosomes, which are smaller in size (40–200 nm in diameter) originate from the endosome as intraluminal vesicles enclosed within multivesicular bodies (1–3). Over the past decade, it has become clear that most, if not all, organisms utilize this evolutionary conserved mechanism for cell-to-cell communication within and between populations [reviewed in Ref. (4–6)]. A key element in this communication process is EV uptake by recipient cells, which generally includes endocytosis, phagocytosis, and micropinocytosis [reviewed in Ref. (7)]. Although several pathways have been suggested, the specific molecular events that regulate EV translocation and uptake by target cells remain almost entirely unknown. Therefore, there is a need to develop new techniques to study these events.

Pathogens, in particular, have found EVs to be a useful tool for evading and manipulating the immune response, ultimately succeeding in infecting new susceptible hosts (4, 8–10). Parasites,

for instance, are known for their remarkable ability to avoid the host immune system, yet in many cases the mechanisms that underlie these processes are still unknown. *Plasmodium falciparum* (*Pf*), one of the most deadly species of *Plasmodium*, causes malaria in humans. Recent studies have revealed that the intracellular malaria parasites secrete EVs from the host cell to deliver multiple components that promote cell communication (11–16). Importunately, it was shown that parasitic EV-DNA is transferred into the host cytosol, where it is detected by the STING-dependent cytosolic DNA sensing pathway to modulate host gene induction from a distance. Upon sensing *Pf*-EV-DNA in the cytoplasm, the protein STING becomes active and prompts a chain of events that includes the phosphorylation of kinase TBK1 and transcription factor IRF3. Phosphorylated IRF3 (pIRF3) then enters the nucleus to induce the transcription of genes, including type I IFN genes (16).

Since EVs harbor promising clinical applications (2, 17) both as diagnostic tools and as a drug delivery mechanism (18), high-throughput technologies for detecting EVs in a population-based manner are warranted (19, 20). Such demands for advanced and robust tools have led to adaptations of large-scale imaging approaches, including imaging flow cytometry (IFC) (21–23).

Imaging flow cytometry combines the speed and high-throughput of conventional flow cytometry with the information-rich imagery of microscopy. These distinct abilities enable IFC to rapidly acquire high-quality multispectral images (24–26). This technique allows the measurement not only of fluorescence levels, but also of the pixel distribution and cellular localization, such as distinguishing between homogenous and speckled staining and the co-localization of different markers, respectively. When using conventional flow cytometry, the detection of individual EVs is often misleading due to their nano-size, which falls within the range of electronic noise. IFC overcomes this drawback, since the ability to measure single pixel intensities enables it to even detect fluorescent particles that are smaller than the diffraction limit (23, 24, 27–29).

Here, we demonstrate that IFC can be used as an accurate large-scale method for tracking the dynamics of the uptake of individual types of cargo components (RNA, proteins, and lipids). We further utilized the system of activated IRF3 translocation as a platform for demonstrating the capability of IFC to specifically monitor protein translocation within target cells. Using IFC, we were able to determine the kinetics of the translocation of pIRF3 from the cytosol into the nucleus following insertion of *Pf*-DNA cargo (24 h analysis).

This powerful approach paves the way not only to measuring the process of vesicle internalization by different recipient cells, but also to directly studying activated protein movement and, thus, further investigating related cellular signaling events.

METHOD

Parasite Line and Culture

The NF54 parasite line was obtained from the Malaria Research Reference Reagent Resource Center (MR4). Parasites were maintained in culture in O+ or A+ erythrocytes at 4% hematocrit in RPMI-HEPES supplemented with 0.5% (w/v) AlbumaxII (Invitrogen) as previously described (30).

EV Isolation and Fluorescence Staining

Extracellular vesicles were isolated from the NF54 strain in a high parasitemia (approximately 8%) of *Pf*-infected red blood cells (RBCs) culture using a Beckman OPTIMA90X ultracentrifuge with a TI70 rotor, as previously described (31). The pellet was resuspended in $PBS^{-/-}$, and the purified EVs were stained according to the manufacturer's protocol with slight modifications, as described below. We used several fluorescent stains for the different vesicle compounds: thiazole orange (TO) (Sigma Aldrich) for RNA-cargo, Ghost Dye UV (GO) (Tonbo bioscience) for protein cargo, and DiI, DiD, or DiO (Thermo Fisher Scientific) for lipid cargo. For the double-staining assay, EVs were stained using a combination of DiI and GO; DiD and GO; DiD and TO; or TO and GO. The stains were incubated with EVs at a 1 µl/ml ratio at 37°C for 30 min. Labeled vesicles were then washed in ice-cold PBS and precipitated again in an ultracentrifuge at 37k RPM over night. Next, the vesicle pellet was washed and resuspended in $PBS^{-/-}$, and the size and concentration of the labeled vesicles were measured by NanoSight ns300 with the associated laser (32).

EV Uptake Into Monocytes

Monocyte cells of the THP-1 cell line were cultured (33) overnight in RPMI1640+ L-glutamine (Biological Industries Ltd., Beit Ha'Emek, Israel) and 10% FBS (Biological Industries Ltd., Beit Ha'Emek, Israel). Prior to the vesicle treatment, cells were washed in $PBS^{-/-}$, resuspended in RPMI1640+ (Biological Industries Ltd., Beit Ha'Emek, Israel) and plated in 6-well plate, ~$1.5*10^6$ cells per well. For EV comparative uptake measurements, THP-1 cells were incubated with an increased relative volume amount of labeled *P. falciparum* infected RBC- derived EVs (0, 10, 50, and 100%) for 5 min before being fixated in 4% PFA for 30 min on ice, washed in PBS and analyzed by IFC (see below).

IRF3 Translocation Analysis

THP-1 cells were transfected with *P. falciparum* genomic DNA for 5 or 24 h, as was previously done (16). Following transfection, cells were fixed and permeabilized with 4% PFA and 2% sucrose at 4°C for 30 min. Fixated cells were washed and blocked with filtered 5% BSA in PBS for 1 h. Primary antibodies, human IRF3 (Cell signaling #11904 1:200 dilution in 5% BSA PBS) and human pIRF3 (Cell signaling #29047 1:50 dilution in 5% BSA PBS) were incubated overnight and washed three times, for 10 min each time, with 5% BSA PBS. Secondary antibody AlexaFluor®488 anti-rabbit antibody (Life technology, 1:200 dilution in 5% BSA PBS) and Hoechst (H6024 SIGMA) were incubated for 30 min and then washed three times, for 10 min each time, with 5% BSA PBS and resuspended in PBS (−/−) before being imaged by IFC (see below).

Multispectral IFC Analysis

Cells or individual EVs were imaged using a multispectral IFC (ImageStreamX mark II, Amnis Corp., Seattle, WA, USA, Part of MERCK-EMD Millipore). To obtain kinetic measurements, THP-1 cells were kept on ice and EVs stained with TO were added. Samples were immediately introduced into the instrument and

the acquisition started approximately 90–150 s afterward. In the direct EV uptake measurements, EVs were labeled and ~$1.5*10^8$ EVs were imaged using IFC. The ImageStreamX uses calibration beads that are 3 μm. To exclude these beads from the acquisition, objects were gated according to their area and intensity of the side scatter channel (Ch06) and the uniform bead population was easily identified and eliminated. At least 5×10^4 cells were collected from each sample and data were analyzed using the manufacturer's image analysis software (IDEAS 6.2; Amnis Corp.). Images were compensated for fluorescent dye overlap by using single-stain controls. THP1 cells were gated for single cells, using the area and aspect-ratio features, and for focused cells using the Gradient RMS feature, as previously described (22). Cropped cells were further eliminated by plotting the cell area of the bright field image against the Centroid X feature (the number of pixels in the horizontal axis from the left corner of the image to the center of the cell mask). EV internalization was evaluated using several features, including the intensity (the sum of the background − subtracted pixel values within the masked area of the image) and max pixel (the largest value of the background − subtracted pixel). For IRF3 nuclear translocation, cells were also gated for DNA positive cells according to the area and intensity of the DNA staining, and cell doublets were further eliminated by plotting the area Vs. the aspect ratio of the nuclear staining. The co-localization of IRF3 with the nuclear image (Hoechst) was calculated using the Similarity feature (log transformed Pearson's Correlation Coefficient between the two images). Values above 1.5 indicate co-localization.

Monitoring THP-1 Cell Survival Following Uptake of *Pf*-Derived EVs

THP-1 cells were cultivated as described in the EV uptake subsection. ~$1*10^6$ THP-1 cells were incubated with $50*10^6$ EVs for 5 min. The cells were then washed and seeded in 6-well plate and monitored for 72 h, live and dead cells were counted and the media changed every 24 h. The viability was tested using trypan blue (Sigma Aldrich).

RESULTS

Monitoring *Pf*-Derived EV-Stained Cargo by IFC

To better characterize the interactions of *Pf*-derived vesicles with host immune target cells, we established an EV uptake assay and were able to fluorescently track labeled vesicles. Since EVs contain proteins, RNA, and lipids, we used different fluorescent stains to specifically label each cargo component in the EVs derived from *Pf*-infected RBCs. TO was used for vesicle RNA, DiI, DiD, and DiO stains for lipids, and Ghost dye for vesicle membrane proteins (**Figure 1A**). Vesicles imaged with IFC exhibited a clear signal of individual vesicles for each of these cargo-component stains (**Figure 1A**). The right insert in **Figure 1A** shows an example of the percentage of RNA (TO)-positive EVs, gated according to unlabeled samples. A Nanosight nc300 particle detector was used to confirm the purity of vesicle production and the fluorescence intensity of the EV population (Figure S1 in Supplementary Material).

Next, we performed a subsequent uptake assay into monocytes (THP-1 cells). Using the different fluorescent stains, we were able to monitor the uptake of RNA, protein, and lipid components within the host immune cells (monocytes) by IFC (**Figure 1B**). The right insert in **Figure 1B** shows the percentage of monocytes positive for TO-labeled EVs, gated according to unlabeled samples. While we were able to track the uptake signal of transferred RNA and proteins during the first 40 min of the analysis, the lipid cargo signal was detectable within monocytes only for a very short time period at the start of the incubation period (<5 min). The rapid reduction in the lipid signal may imply that membrane fusion is involved in the uptake mechanism. The internalization of the EVs, however, could be detected only under physiological condition at 37°C and not at 4°C (Figure S3 in Supplementary Material), similar to what was previously shown (16).

Detecting EV Double-Stained Components Using IFC: An Indication of the Internalization of the Entire Vesicle Into the Host Cells

Detecting and quantifying EVs by IFC have been previously described (12, 23, 24, 27–29, 34, 35). However, due to their small size, detection of individual EVs using bright field only is very limited, as the pixel size is 0.3 μm using the 60× lens. Detection by light scattering using conventional flow cytometry is also limited. Although we can detect sub-micron polystyrene beads, lipid-based vesicles have a lower refractive index than beads (less than 1.4, compared to 1.6 for beads). This results in lower light scattering, placing the signal within the range of background noise. Therefore, to facilitate their detection, fluorescence labeling is needed.

To increase cargo detection confidence, we generated double-stained vesicles by co-labeling different components (RNA, proteins, and lipids). Purified *Pf*-infected RBC-derived EVs were co-stained using four different combinations; for instance, co-staining RNA and lipids (**Figure 2A**). Individual vesicles imaged using IFC were positive for the double-staining (**Figure 2A**), validating the detection of vesicles containing different molecular components.

We further measured the uptake of the co-stained vesicles within recipient monocytes following 5 min of incubation (**Figure 2B**). The window of detection within the first 5 min of uptake sufficed to detect the double-staining signals of the different components and these were co-localized in the cell area. The fact that we could detect the different cargo components at the same area (co-localized) within less than 5 min of uptake implies that the entire vesicle is, in fact, inserted into the host cell rather than being fused to the cell's surface.

To verify that indeed the increase in fluorescence intensity is due to EV uptake and not due to auto-fluorescence or dyes aggregates, we incubated THP-1 recipient cells with increasing concentrations of stained EVs and quantified their uptake. As expected, the signal received from the recipient cells increased in line with the amount of vesicles present (**Figure 3**). This was not a result of dye aggregates, as this increase was not seen when dyes were added to PBS alone, vesicle-free (data not shown). The percentage of THP1 cells positive for TO-labeled EVs was

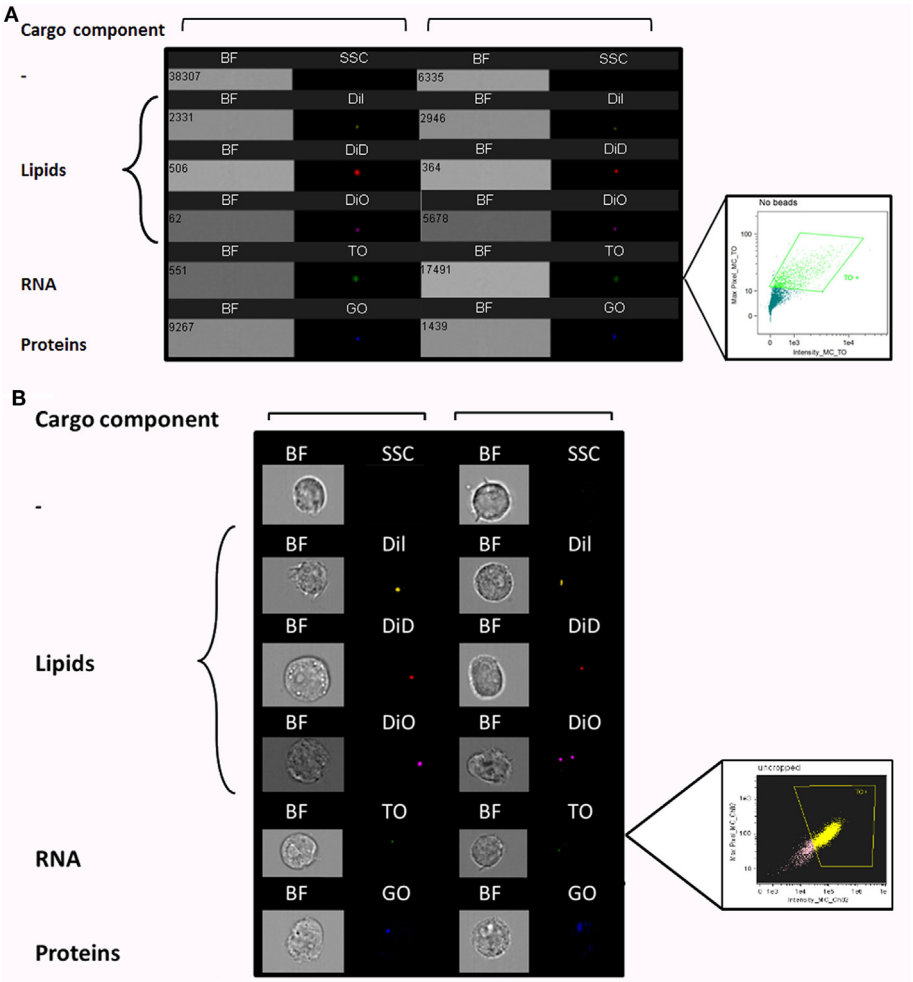

FIGURE 1 | Visualization of *Plasmodium falciparum* (*Pf*)-derived extracellular vesicles (EVs) by imaging flow cytometry (IFC). **(A)** Visualization of single-stained *Pf*-derived EVs by IFC. *Pf*-derived EVs stained with lipid (DiI, DiD, and DiO), RNA [thiazole orange (TO)], or protein (GO) dyes. Insert shows percentage of TO-positive EVs (43%), gated according to unlabeled EVs. Representative results from at least three experiments are shown. Abbreviations: BF, bright field; SSC, side scatter. **(B)** Internalization (uptake) of *Pf*-derived EVs into monocytes as visualized by IFC. EVs were stained with lipid (DiI, DiD, and DiO), RNA (TO), or protein (GO) dyes and then $7.5*10^7$ dyed EVs were introduced into $1.5*10^6$ THP-1 cells for 5 min. The cells were fixated as described in Section "Method" and vesicle uptake was imaged using IFC. EVs are detected as spots inside recipient cells. Insert shows percentage of EV-positive cells (72.5%), gated according to unlabeled EVs. Representative results from at least three experiments are shown. Abbreviations: BF, bright field; SSC, side scatters.

gated according to THP1 cells incubated with unlabeled EVs (**Figure 1B**).

Imaging flow cytometry can detect fluorescently labeled EVs even at sub-resolution range, since bright enough fluorescence can fill more than one pixel and enable sample detection. Additional removal of artifacts can be done by verifying that the two fluorescent channels co-localize to the same object (**Figure 2A**), which is not possible in conventional flow cytometry. This demonstrates that IFC can be a useful technique for studying the dynamics of cargo distribution within the cell upon uptake. Specifically, since the EV population originating from the same cells is often heterogeneous, this can lead to diversified uptake mechanisms of target cells and, as a result, can affect cargo destination. Therefore, IFC can be adapted not just to detect cargo internalization, but also to explore the nature of the EV uptake and the internal localization of components.

Monitoring the Kinetics of the Uptake Into the Host of the RNA Contained in *Pf*-Derived Vesicles

To understand the *Pf*-EV-cargo's function in the host target cells, it would be valuable to analyze the kinetics of cargo uptake into target cells. Since we could only detect the lipid signal during the first 5 min of incubation with recipient cells, we examined whether it is possible to explore the uptake kinetics cargo components within the recipient cells over time. This was achieved by establishing a vesicle-uptake kinetics assay. RNA-labeled EVs were added to live THP1 cells and the derived signal was read continuously (after a 90–150 Sec loading time) by IFC for 45 min. A trend line was calculated by the statistical software R, using the "ggplot2" package (36). The smoothing method used was a generalized additive model, which is the package's default

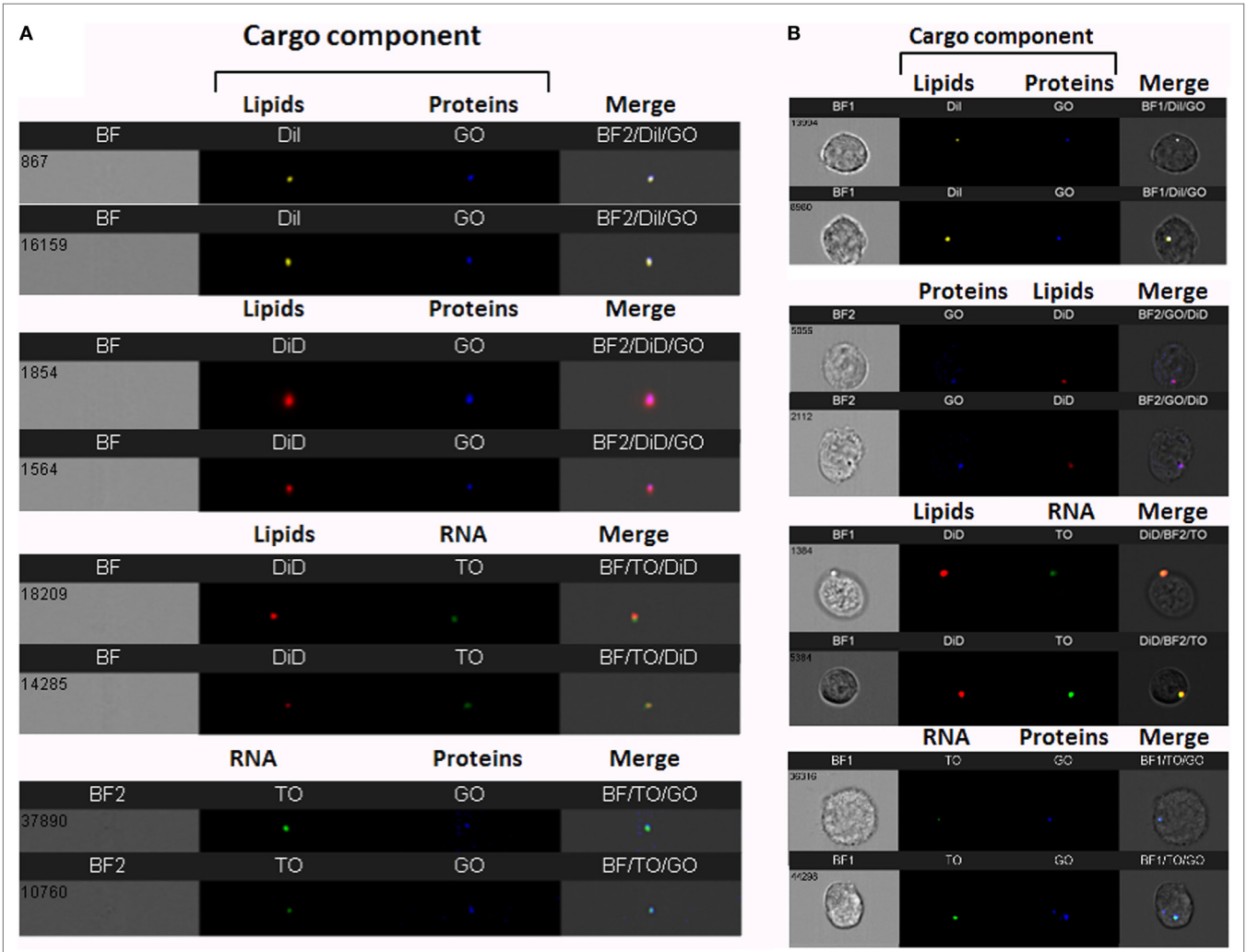

FIGURE 2 | Visualization of double-stained *Plasmodium falciparum* (*Pf*)-derived extracellular vesicles (EVs) by imaging flow cytometry (IFC). **(A)** IFC analysis of double-stained *Pf*-derived EVs. *Pf*-derived EVs co-labeled with different combinations of two stains: for lipids (DiI, DiD, or DiO), RNA [thiazole orange (TO)], and proteins (GO). Representative results from at least three experiments are shown. Abbreviations: BF, bright field; SSC, side scatter **(B)** Uptake assay of *Pf*-derived EVs into monocytes (THP-1). IFC imaging of *Pf*-derived EVs labeled with two stains for lipids (DiI, DiD, or DiO) and/or RNA (TO) and/or proteins (GO) uptaken into THP-1 cells as described in the Section "Method." Representative results from at least three experiments are shown. Abbreviations: BF, bright field; SSC, side scatter.

for $n > 1{,}000$. The results were compared with the acquisition of unlabeled EVs (**Figure 4A**). As demonstrated, the transferred RNA signal intensity in the cells increased over time, indicating progressive uptake of *Pf*-labeled EVs within monocytes (**Figure 4B**). Remarkably, the EVs uptake into monocytes occurs rapidly; 10 min after co-incubation most of the monocytes (>90%) stained positive for RNA-cargo (TO dye). Notably, no growth effects were observed within recipient monocytes as compared to control cells during the 72 h post EV uptake (Figure S2 in Supplementary Material).

Monitoring the IRF3 Translocation to the Nucleus Following *Pf* gDNA Internalization Into Host Monocytes

Previously, we showed that, upon internalization of *Pf* DNA-harboring EVs into host monocytes, the parasitic DNA cargo prompts STING-dependent DNA sensing response. The protein STING subsequently activates kinase TBK1, which phosphorylates the transcription factor IRF3, causing IRF3 to translocate to the nucleus and induce STING-dependent gene expression (16). The ability to track the translocation of proteins within host cells upon pathogen EV uptake could be a useful tool for determining their function and the resultant alteration in signaling pathways within the host cell. We used IFC to test whether it is possible to measure the translocation of transcription factor IRF3 from the cytosol to the nucleus upon insertion of *Pf*-DNA cargo into host cells. For that, monocytes were transfected with *Pf*-genomic DNA that mimics the internalization of parasitic DNA into host monocytes by EVs as described in a previous study (16). Using a specific antibody against the phosphorylated form of IRF3 (pIRF3), we demonstrated that the intensity of the activated form, pIRF3, progressively increased upon the internalization of the cargo (*Pf*-DNA); after 24 h, the majority of pIRF3 was

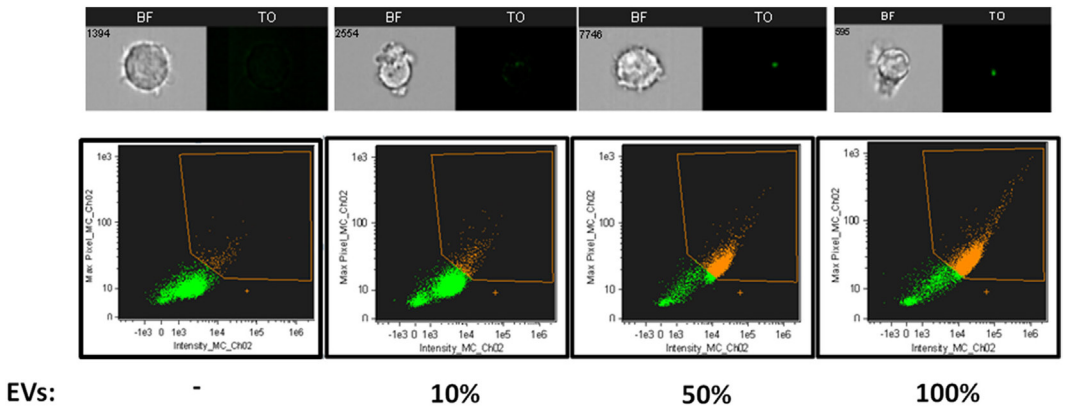

FIGURE 3 | Relative *Plasmodium falciparum* (*Pf*)-derived extracellular vesicles (EV) uptake into monocytes. Relative amounts of EVs (100, 50, 10, and 0%) were stained using the same amount of [thiazole orange (TO)] dye. THP-1 cells were incubated with RNA (TO)-labeled EVs for 5 min before being fixated and imaged by imaging flow cytometry. Graphs show the percentage of TO-labeled EV-positive cells, gated according to unlabeled EVs. Representative results from experiments out of three are shown. Abbreviation: BF, bright field.

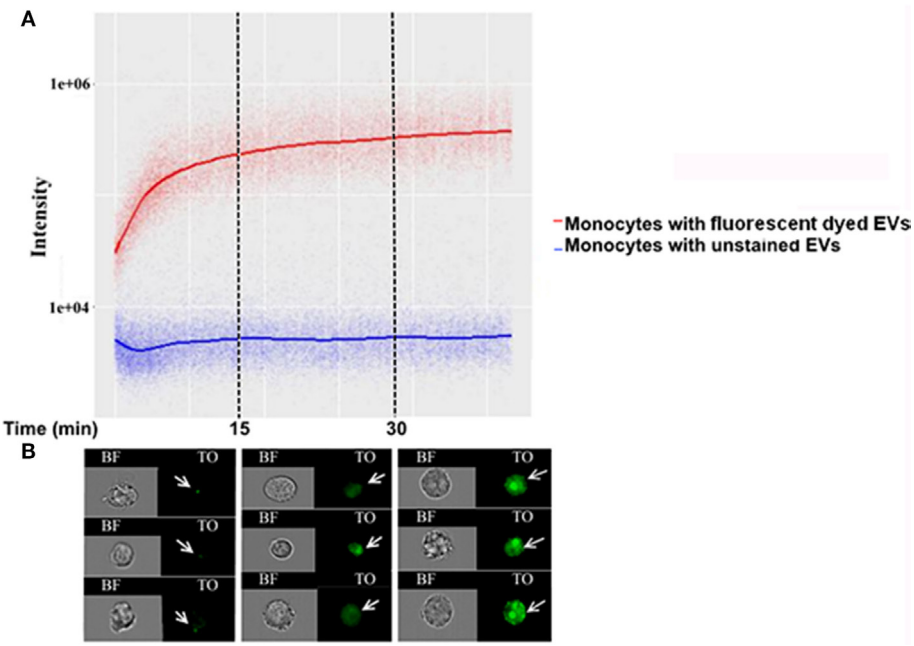

FIGURE 4 | Kinetics measurement of *Plasmodium falciparum* (*Pf*)-extracellular vesicles (EV) uptake into monocytes using imaging flow cytometry (IFC). *Pf*-derived EVs were labeled by thiazole orange (TO), and their uptake into THP-1 cells was measured for 45 min. **(A)** Graph representing the signal modification in TO intensity that was detected over time originating from monocyte recipient cells. Representative results from three independent experiments are shown. **(B)** Signal detected by IFC from three representative recipient cells from each of the three time groups. Within the first 15 min, the EV signal appears as clear spots inside the cells (I), followed by the signal spreading inside the cell area for up to 30 min from EV internalization (II–III).

localized in the nucleus (**Figure 5A** bottom panel). As seen in **Figure 5A**, upper panel, these results were confirmed by using a primary antibody against IRF3 itself; a positive signal appeared in the nucleus over the course of the 24 h following cargo insertion, indicating the alteration within recipient immune cells and the migration of the transcription factor from the cytosol to the nucleus. Thus, using IFC to track the outcome of *Pf*-EV uptake by host cells may help to reveal the nature of the EV's role in malaria pathogenesis.

DISCUSSION

The need for establishing high-throughput EV population characterization methods led us to adapt existing approaches, such as

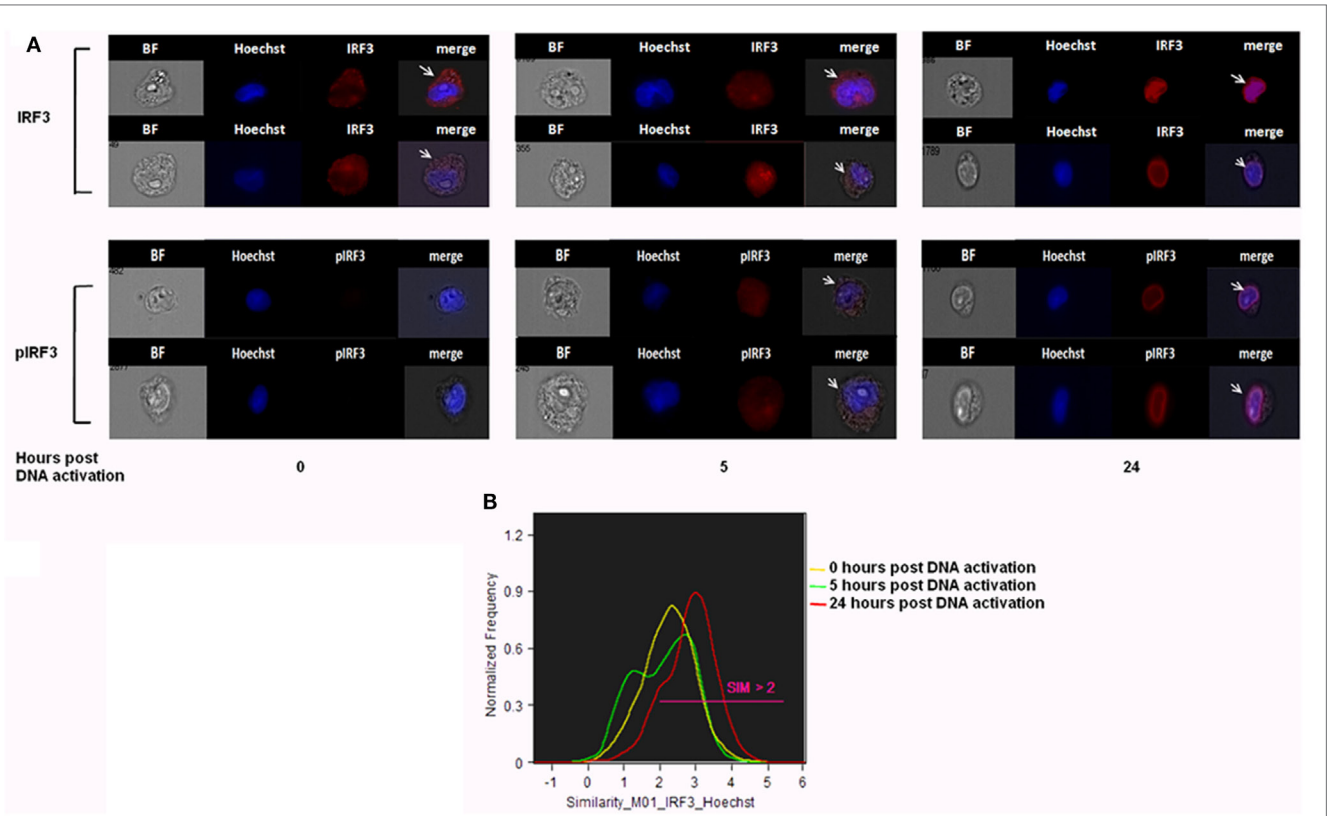

FIGURE 5 | IRF3 and phosphorylated IRF3 (pIRF3) translocation into the nucleus upon *Plasmodium falciparum* (*Pf*)-genomic DNA intake by recipient host monocytes. **(A)** THP-1 cells were transfected with *Pf* gDNA for 5 or 24 h. Cells were next fixated and labeled with Hoechst (DNA dye), IRF3 (upper panel), or pIRF3 (bottom panel) antibodies, imaged and analyzed by imaging flow cytometry at different time points. Representative results from at least three experiments are shown $n = 2*10^5$. **(B)** Similarity values between the IRF3 and nuclear image. Values over 1.5 are considered as co-localization. Representative results from at least three experiments are shown. *T*-test ($p < 0.001$) analysis for similarity values between 24 h and not treated and between 24 and 5 h was performed.

flow cytometry and IFC, for the benefit of the vesicles research field. Measurements using conventional fluorescence microscopy are challenging due to EV fluid dispersal and limited analysis and quantification tools. Conversely, in conventional flow cytometry, objects are measured according to their light scattering and fluorescence intensity, thus limiting the sensitivity for small, dim particles, such as EVs. Reaching a higher dynamic range, lower noise, and a higher quantum yield can be achieved in IFC by using a CCD camera instead of photomultiplier tubes (22–24, 26). In addition, IFC operates in a time delay integration mode, which increases the exposure time from microseconds to milliseconds, further enhancing sensitivity (22–24, 26). By exploiting the 60×, high numerical aperture (NA = 0.9) lens, we reached a high degree of light gathering and sensitivity. When using this lens, the core width is set to 7 μm, making it narrow enough to keep most of the acquired objects in focus. Thus, the combination of precise fluidics and a highly sensitive CCD camera, in addition to careful gating with visual inspection, facilitates the accurate detection of low intensity, small size objects, and making IFC a powerful tool for sensitive, accurate, statistically robust analysis of EVs (24, 27, 28). We also directed our efforts to calibrating the EVs' double-stain so as to increase the validity of the experimental results. The end results of our efforts was an advanced method for following simultaneously the delivery of different cargo components into recipient cells, which we validated by visually following the internalization of malaria parasitic EVs.

The advantage of the IFC method is that it can be used to study EV uptake in any system, eliminating the need for specific antibodies, but necessitating dependence on non-specific staining (e.g., for RNA, proteins, or lipids). Recent works have indeed successfully used IFC to demonstrate [and a single fluorescent stain (35)] the uptake of vesicles and to characterize the properties of vesicles (24, 28, 29, 34, 35). One study used specific antigens to explore vesicles in blood (37), while another displayed the ability to monitor vesicle adherence in whole blood in a competitive uptake assay (21). Using specific fluorescent-antibodies, the latter study found that vesicles adhere preferentially to monocytes, which supports directed EV targeting. Yet, the mechanisms by which pathogen-derived vesicles are uptaken by target host cells has remained, thus far, mostly elusive.

Applying the advanced IFC method we developed to the study of malaria parasitic EVs, we successfully isolated EVs derived from *Pf*-infected RBCs and demonstrated their rapid integration (less than 5 min) into human monocytes (**Figures 1B**, **2B**, **3** and **4**). Using IFC, we exhibit a robust kinetic assay for measuring cargo internalization during uptake and monitoring

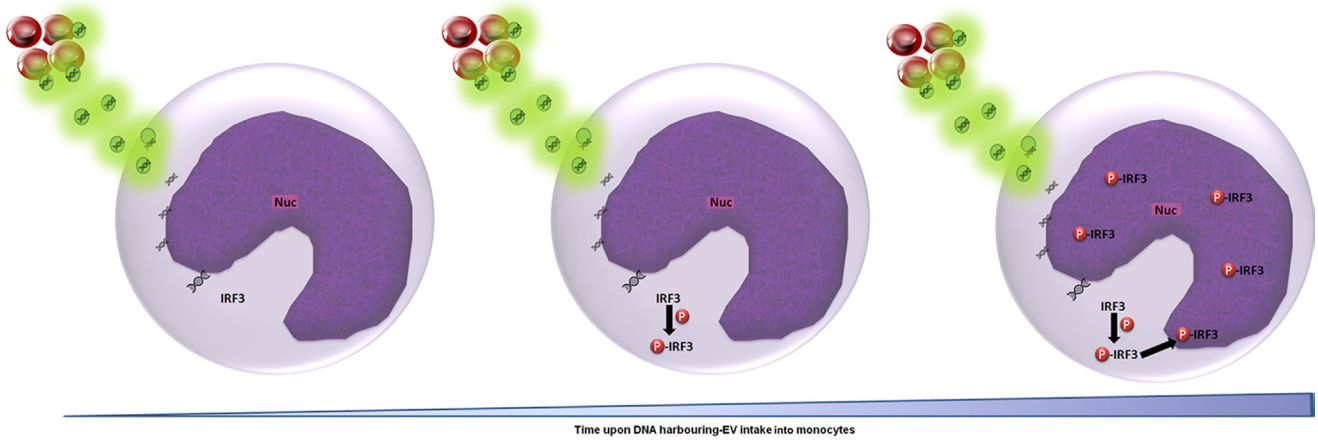

FIGURE 6 | Schematic representation of the cascade of events upon *Plasmodium falciparum* (*Pf*)-gDNA intake by host monocytes. In non-activated monocytes, transcription factor IRF3 is localized in the cytoplasm. Upon *Pf*, DNA cargo internalization into the cytoplasm, IRF3 undergoes phosphorylation and is translocated into the nucleus to induce the cellular immune response (from left to right). Abbreviation: Nuc, nucleus.

the molecular effect of *Pf*-EV cargo internalization into host target cells. We also demonstrated the powerful ability of IFC to directly track the migration of a host transcription factor (IRF3) within the cellular environment once the protein becomes activated due to parasitic cargo internalization (**Figures 5** and **6**; a schematic illustration). The statistical strength of a robust analysis of thousands of recipient cells increases the physiological feasibility of these occurrences. Characterizing the EV content by different dyes, tracking the kinetics of EV uptake into target cells and, finally, tracking the activation of the specific factors within target cells may shed light on the EVs' function in host–pathogen communication and, hence, demonstrate the usefulness of IFC as a robust tool to study EV uptake and cargo dynamics.

Such means will open up additional research directions into the cellular alterations of host proteins upon the uptake of pathogen-derived EVs. Therefore, IFC could generally improve our knowledge on EV uptake mechanisms and shed additional light on other EV functions.

AUTHOR CONTRIBUTIONS

YO-B, NR-R, and ZP designed the experiments and wrote the paper. YO-B established EV uptake monitoring assay by IFC. YO-B, PK, AR, and TG performed the experiments.

FUNDING

We wish to acknowledge Dr. Ron Rotkopf for the statistical analysis. We thank Malaria Research Reference Reagent Resource Center (MR4) for their generous supply of parasite strains. This research was supported by a Weizmann Institute Staff Scientist Grant for ZP. The research of NR-R is supported by the Benoziyo Endowment Fund for the Advancement of Science, the Jeanne and Joseph Nissim Foundation for Life Sciences Research and the Samuel M. Soref and Helene K. Soref Foundation. NR-R is the incumbent of the Enid Barden and Aaron J. Jade President's Development Chair for New Scientists in Memory of Cantor John Y. Jade. NR-R is grateful for the support from the European Research Council (ERC) under the European Union's Horizon 2020 research and innovation program (grant agreement No 757743), and the Israel Science Foundation (ISF) (619/16 and119034).

SUPPLEMENTARY MATERIAL

The Supplementary Material for this article can be found online at https://www.frontiersin.org/articles/10.3389/fimmu.2018.01011/full#supplementary-material.

FIGURE S1 | *Plasmodium falciparum* (Pf)-derived extracellular vesicles (EVs) characterization by NTA Nanosight. *Pf*-derived EVs analyzed by Nanosight NS300 (Malvern) for size distribution and particle concentration. The graphs represent the mean of 6*60 s measurements by Nanosight NS300. EV concertation is $3.4*10^7 \pm 1.7*10^7$ and the diameter mean is 91 nm. Representative results from at least three experiments are shown.

FIGURE S2 | THP-1 cell growth following uptake of *Plasmodium falciparum* (Pf)-derived extracellular vesicles (EVs). *Pf*-derived EVs were introduced to THP-1 cells for 5 min, and then washed. **(A)** Cell viability tests. This experiment is a representative of three biological repeats. SD and *T*-test analysis ($p \geq 0.1$). Representative results from at least three experiments are shown. **(B)** Percentage of dead cells was measured using trypan blue. This experiment is a representative of three biological repeats. SD and *T*-test analysis ($p \geq 0.1$).

FIGURE S3 | *Pf*-EV intake by monocytes at different temperatures. THP-1 cells were incubated with RNA (TO)-labeled *Pf*-EVs at 37 or 4°C for 5 min. Cells were then washed with ice-cold PBS (–/–) and imaged by imaging flow cytometry. Graphs show TO-labeled positive cells (yellow), gated according to unlabeled cells. At 37°C 37.5% of the cells were positive to TO signal, at 4°C 1.06% of the cells were positive to TO. Abbreviations: TO, thiazole Orange; Pf, *Plasmodium falciparum*; EV, extracellular vesicle.

REFERENCES

1. Conde-Vancells J, Rodriguez-Suarez E, Embade N, Gil D, Matthiesen R, Valle M, et al. Characterization and comprehensive proteome profiling of exosomes secreted by hepatocytes. *J Proteome Res* (2008) 7:5157–66. doi:10.1021/pr8004887
2. van der Pol E, Böing AN, Harrison P, Sturk A, Nieuwland R. Classification, functions, and clinical relevance of extracellular vesicles. *Pharmacol Rev* (2012) 64:676–705. doi:10.1124/pr.112.005983
3. van der Pol E, Coumans FAW, Grootemaat AE, Gardiner C, Sargent IL, Harrison P, et al. Particle size distribution of exosomes and microvesicles determined by transmission electron microscopy, flow cytometry, nanoparticle tracking analysis, and resistive pulse sensing. *J Thromb Haemost* (2014) 12:1182–92. doi:10.1111/jth.12602
4. Montaner S, Galiano A, Trelis M, Martin-Jaular L, del Portillo HA, Bernal D, et al. The role of extracellular vesicles in modulating the host immune response during parasitic infections. *Front Immunol* (2014) 5:433. doi:10.3389/fimmu.2014.00433
5. Ofir-Birin Y, Heidenreich M, Regev-Rudzki N. Pathogen-derived extracellular vesicles coordinate social behaviour and host manipulation. *Semin Cell Dev Biol* (2017) 67:83–90. doi:10.1016/j.semcdb.2017.03.004
6. Schorey JS, Cheng Y, Singh PP, Smith VL. Exosomes and other extracellular vesicles in host-pathogen interactions. *EMBO Rep* (2015) 16:24–43. doi:10.15252/embr.201439363
7. Mulcahy LA, Pink RC, Carter DRF. Routes and mechanisms of extracellular vesicle uptake. *J Extracell Vesicles* (2014) 3:1–14. doi:10.3402/jev.v3.24641
8. Baglio SR, van Eijndhoven MAJ, Koppers-Lalic D, Berenguer J, Lougheed SM, Gibbs S, et al. Sensing of latent EBV infection through exosomal transfer of 5′pppRNA. *Proc Natl Acad Sci U S A* (2016) 113(5):E587–96. doi:10.1073/pnas.1518130113
9. Pathirana RD, Kaparakis-Liaskos M. Bacterial membrane vesicles: biogenesis, immune regulation and pathogenesis. *Cell Microbiol* (2016) 18:1518–24. doi:10.1111/cmi.12658
10. Pegtel DM, van de Garde MDB, Middeldorp JM. Viral miRNAs exploiting the endosomal-exosomal pathway for intercellular cross-talk and immune evasion. *Biochim Biophys Acta* (2011) 1809:715–21. doi:10.1016/j.bbagrm.2011.08.002
11. Couper KN, Barnes T, Hafalla JCR, Combes V, Ryffel B, Secher T, et al. Parasite-derived plasma microparticles contribute significantly to malaria infection-induced inflammation through potent macrophage stimulation. *PLoS Pathog* (2010) 6:e1000744. doi:10.1371/journal.ppat.1000744
12. Mantel PY, Hoang AN, Goldowitz I, Potashnikova D, Hamza B, Vorobjev I, et al. Malaria-infected erythrocyte-derived microvesicles mediate cellular communication within the parasite population and with the host immune system. *Cell Host Microbe* (2013) 13:521–34. doi:10.1016/j.chom.2013.04.009
13. Mantel P-Y, Hjelmqvist D, Walch M, Kharoubi-Hess S, Nilsson S, Ravel D, et al. Infected erythrocyte-derived extracellular vesicles alter vascular function via regulatory Ago2-miRNA complexes in malaria. *Nat Commun* (2016) 7:12727. doi:10.1038/ncomms12727
14. Martin-Jaular L, Nakayasu ES, Ferrer M, Almeida IC, del Portillo HA. Exosomes from *Plasmodium yoelii*-infected reticulocytes protect mice from lethal infections. *PLoS One* (2011) 6:e26588. doi:10.1371/journal.pone.0026588
15. Regev-Rudzki N, Wilson DW, Carvalho TG, Sisquella X, Coleman BM, Rug M, et al. Cell-cell communication between malaria-infected red blood cells via exosome-like vesicles. *Cell* (2013) 153:1120–33. doi:10.1016/j.cell.2013.04.029
16. Sisquella X, Ofir-Birin Y, Pimentel MA, Cheng L, Abou Karam P, Sampaio NG, et al. Malaria parasite DNA-harbouring vesicles activate cytosolic immune sensors. *Nat Commun* (2017) 8:1985. doi:10.1038/s41467-017-02083-1
17. Xu R, Greening DW, Zhu H-J, Takahashi N, Simpson RJ. Extracellular vesicle isolation and characterization: toward clinical application. *J Clin Invest* (2016) 126:1152–62. doi:10.1172/JCI81129
18. Revenfeld ALS, Baek R, Nielsen MH, Stensballe A, Varming K, Jørgensen M. Diagnostic and prognostic potential of extracellular vesicles in peripheral blood. *Clin Ther* (2014) 36:830–46. doi:10.1016/j.clinthera.2014.05.008
19. Grasso L, Wyss R, Weidenauer L, Thampi A, Demurtas D, Prudent M, et al. Molecular screening of cancer-derived exosomes by surface plasmon resonance spectroscopy. *Anal Bioanal Chem* (2015) 407:5425–32. doi:10.1007/s00216-015-8711-5
20. Wyss R, Grasso L, Wolf C, Grosse W, Demurtas D, Vogel H. Molecular and dimensional profiling of highly purified extracellular vesicles by fluorescence fluctuation spectroscopy. *Anal Chem* (2014) 86:7229–33. doi:10.1021/ac501801m
21. Fendl B, Weiss R, Fischer MB, Spittler A, Weber V. Characterization of extracellular vesicles in whole blood: Influence of pre-analytical parameters and visualization of vesicle-cell interactions using imaging flow cytometry. *Biochem Biophys Res Commun* (2016) 478:168–73. doi:10.1016/j.bbrc.2016.07.073
22. George TC, Fanning SL, Fitzgeral-Bocarsly P, Medeiros RB, Highfill S, Shimizu Y, et al. Quantitative measurement of nuclear translocation events using similarity analysis of multispectral cellular images obtained in flow. *J Immunol Methods* (2006) 311:117–29. doi:10.1016/j.jim.2006.01.018
23. Lannigan J, Erdbruegger U. Imaging flow cytometry for the characterization of extracellular vesicles. *Methods* (2016) 112:55–67. doi:10.1016/j.ymeth.2016.09.018
24. Erdbrügger U, Rudy CK, Etter ME, Dryden KA, Yeager M, Klibanov AL, et al. Imaging flow cytometry elucidates limitations of microparticle analysis by conventional flow cytometry. *Cytom Part A* (2014) 85:756–70. doi:10.1002/cyto.a.22494
25. Filby A, Day W, Purewal S, Martinez-Martin N. The analysis of cell cycle, proliferation, and asymmetric cell division by imaging flow cytometry. *Methods Mol Biol* (2016) 1389:71–95. doi:10.1007/978-1-4939-3302-0_5
26. Ortyn WE, Hall BE, George TC, Frost K, Basiji DA, Perry DJ, et al. Sensitivity measurement and compensation in spectral imaging. *Cytom Part A* (2006) 69:852–62. doi:10.1002/cyto.a.20306
27. Barteneva NS, Fasler-Kan E, Bernimoulin M, Stern JNH, Ponomarev ED, Duckett L, et al. Circulating microparticles: square the circle. *BMC Cell Biol* (2013) 14:23. doi:10.1186/1471-2121-14-23
28. Clark RT. Imaging flow cytometry enhances particle detection sensitivity for extracellular vesicle analysis. *Nat Methods* (2015) 12:i–ii. doi:10.1038/nmeth.f.380
29. Vallhov H, Gutzeit C, Johansson SM, Nagy N, Paul M, Li Q, et al. Exosomes containing glycoprotein 350 released by EBV-transformed B cells selectively target B cells through CD21 and block EBV infection in vitro. *J Immunol* (2011) 186:73–82. doi:10.4049/jimmunol.1001145
30. Trager W, Jensen JB. Human malaria parasites in continuous culture. *Science* (1976) 193:673–5. doi:10.1126/science.781840
31. Coleman BM, Hanssen E, Lawson VA, Hill AF. Prion-infected cells regulate the release of exosomes with distinct ultrastructural features. *FASEB J* (2012) 26:4160–73. doi:10.1096/fj.11-202077
32. Dragovic RA, Gardiner C, Brooks AS, Tannetta DS, Ferguson DJP, Hole P, et al. Sizing and phenotyping of cellular vesicles using nanoparticle tracking analysis. *Nanomedicine* (2011) 7:780–8. doi:10.1016/j.nano.2011.04.003
33. Unterholzner L, Keating SE, Baran M, Horan KA, Jensen SB, Sharma S, et al. IFI16 is an innate immune sensor for intracellular DNA. *Nat Immunol* (2010) 11:997–1004. doi:10.1038/ni.1932
34. Barteneva NS, Fasler-Kan E, Vorobjev IA. Imaging flow cytometry: coping with heterogeneity in biological systems. *J Histochem Cytochem* (2012) 60:723–33. doi:10.1369/0022155412453052
35. Franzen CA, Simms PE, Van Huis AF, Foreman KE, Kuo PC, Gupta GN. Characterization of uptake and internalization of exosomes by bladder cancer cells. *Biomed Res Int* (2014) 2014:619829. doi:10.1155/2014/619829
36. Wickham H. Elegant graphics for data analysis. *Media* (2009) 35:211. doi:10.1007/978-0-387-98141-3
37. Headland SE, Jones HR, D'Sa ASV, Perretti M, Norling LV. Cutting-edge analysis of extracellular microparticles using ImageStream(X) imaging flow cytometry. *Sci Rep* (2014) 4:5237. doi:10.1038/srep05237

Conflict of Interest Statement: The authors declare that the research was conducted in the absence of any commercial or financial relationships that could be construed as a potential conflict of interest.

Advantages of publishing in Frontiers

OPEN ACCESS
Articles are free to read for greatest visibility and readership

FAST PUBLICATION
Around 90 days from submission to decision

HIGH QUALITY PEER-REVIEW
Rigorous, collaborative, and constructive peer-review

TRANSPARENT PEER-REVIEW
Editors and reviewers acknowledged by name on published articles

Frontiers
Avenue du Tribunal-Fédéral 34
1005 Lausanne | Switzerland

Visit us: www.frontiersin.org
Contact us: info@frontiersin.org | +41 21 510 17 00

REPRODUCIBILITY OF RESEARCH
Support open data and methods to enhance research reproducibility

DIGITAL PUBLISHING
Articles designed for optimal readership across devices

FOLLOW US
@frontiersin

IMPACT METRICS
Advanced article metrics track visibility across digital media

EXTENSIVE PROMOTION
Marketing and promotion of impactful research

LOOP RESEARCH NETWORK
Our network increases your article's readership